Dissertation zur Erlangung des Doktorgrades
der Fakultät für Chemie und Pharmazie
der Ludwig-Maximilians-Universität München

Synthesis and characterization of new 1*N* and 2*N*-substituted tetrazoles applicable for Energetic Coordination Compounds and assessment of candidates for HMX and TNT replacement

Moritz Alexander Kofen

aus

Starnberg, Deutschland

2022

Erklärung

Diese Dissertation wurde im Sinne von § 7 der Promotionsordnung vom 28. November 2011 von Herrn Professor Dr. Thomas M. Klapötke betreut.

Eidesstattliche Versicherung

Diese Dissertation wurde eigenständig und ohne unerlaubte Hilfsmittel erarbeitet.

München, den 05.09.2022

Moritz Alexander Kofen

Dissertation eingereicht am:	07.09.2022
1. Gutachter:	Prof. Dr. Thomas M. Klapötke
2. Gutachter:	Prof. Dr. Konstantin Karaghiosoff
Mündliche Prüfung am:	25.10.2022

Danksagung

Zuallererst gilt mein größter Dank meinem Doktorvater Herrn Prof. Dr. Thomas M. Klapötke, für die Möglichkeit als Teil seines Arbeitskreises zu promovieren und für seine finanziellen Zuwendungen und damit finanzierte Forschung der letzten Jahre. Durch Ihre unermüdliche Betreuung und ungeheure Freiheit der Forschung waren Sie ein Pfeiler meiner Arbeit. Ebenfalls danke ich Ihnen für Ihre außerordentliche Hilfsbereitschaft und Unterstützung bei Problemen jeglicher Art. Nicht zu vergessen ist ebenfalls Ihr großzügiger Freiraum für Besuche unterschiedlicher Konferenzen und Symposien, die es ermöglicht haben, den eignen wissenschaftlichen Horizont zu erweitern. Zuletzt danke ich Ihnen für ihre Großzügigkeit zur Teilnahme an externen Weiterbildungen und Zertifizierungskursen.

Bei Herrn Prof. Dr. Konstantin Karaghiosoff bedanke ich mich zuerst für die Anfertigung des Zweitgutachtens. Daneben bedanke ich mich für die Möglichkeit als Teil des IT-Teams eine wichtige Aufgabe im Arbeitskreis übernehmen zu können. Natürlich gilt dir mein persönlicher Dank für etliche Gespräche, die mit deiner lockeren und freundschaftlichen Art, ein fester Bestandteil für die angenehme Arbeitsatmosphäre im Arbeitskreis sind. Natürlich bin ich dir außerordentlich dankbar für deine Bereitschaft, dein Wissen über NMR und Messungen von Einkristallen jederzeit zu teilen. Ich hoffe, dass auch in Zukunft weitere Doktoranden, Masteranden, Bacheloranden sowie Studenten von dir lernen dürfen und du weiterhin mit Elan und Freude die Universitätsgemeinschaft bereicherst.

Des Weiteren bedanke ich mich bei Prof. Dr. Silvija Maric, Prof. Dr. Hans-Christian Böttcher, Prof. Dr. Andreas Kornath und Prof. Dr. Lena Daumann für ihre Bereitschaft Teil des Prüfungskomitees zu sein.

Ein außerordentlicher Dank gebührt Herrn Dr. Jörg Stierstorfer, der die letzten Jahre eine hervorragende Betreuung für diese Dissertation geleistet hat. Durch unzählige Diskussionen und Ideen zur Themenfindung hast du substanziell zu dieser Dissertation beigetragen. Gerade durch die Vielzahl deiner Ideen hat man deine Leidenschaft für Chemie gespürt und es war ein leichtes sich davon anstecken zu lassen. Neben der chemischen Arbeit warst du aber auch eine sehr große Hilfe bei der Zusammenstellung und Anfertigung von Publikationen, sowie bei dem Lösen von problematischen Kristallstrukturen. Durch dein kritisches Feedback hast du maßgeblichen zur Qualitätssteigerung der Publikationen beigetragen. Durch deine Geduld etliche Versionen immer wieder Korrektur zu lesen, hast du mir beigebracht gute wissenschaftliche Arbeiten zu schreiben. Fehlen darf auch nicht der Dank für die Korrektur dieser Arbeit und den Input zur Gestaltung von (farbigen) Bildern. Einer meiner größten Erfolge war mit Sicherheit das Erstellen der letzten Figure 1, die dir auf Anhieb gefallen hat.

Ein nicht geringerer Dank gilt Frau Irene Scheckenbach, der guten Seele dieses Arbeitskreises. Ohne Ihre ausdauernde und stets freundliche Person würde der Alltag im Arbeitskreis bei weitem nicht so rund laufen. Vor allem konnte man sich immer auf Sie verlassen, wenn es um bürokratische und/oder organisatorische Angelegenheiten ging.

Weiterhin ist ein nahezu unermesslicher Teil dieser Doktorarbeit die Kollegen und Kolleginnen, sowie die ehemaligen Mitglieder dieses einzigartigen Arbeitskreises. Durch die außerordentlich harmonische Atmosphäre ist der Arbeitsalltag zu jeder Zeit angenehm und man freut sich auf jeden neuen Tag mit diesen Kollegen. Natürlich sorgen auch die etlichen Gespräche in der Kaffeeküche, beim Mittagessen oder im Seminar für eine anregende Atmosphäre. So manches Gespräch in den Abendstunden ist gar so anregend, dass die Erforschung der Auswirkung von verantwortungsvollem Genuss ethanolischer Mischungen am nächsten Morgen bereits ein gemeinsames Paper füllen könnte. Niemals vergessen werde ich die etlichen gemeinsamen Freizeitaktivitäten von Skifahren, Saalfesten, Fußballturnieren, Paintballmatches, Biertastings, Wiesnbesuche, das Wochenende in Prag, sowie etliche Trockeneis-Schnappi-Bomben und Nerf-Gun Battles (natürlich nicht in den Laboren). All dies hat zu einem sehr angenehmen Arbeitsalltag geführt und ist das was den Arbeitskreis, neben der hervorragenden Forschung eines Jeden, zu dem macht was er ist. Vor allem bin ich dankbar, dass ich ein Teil dieser Gruppe sein durfte und die Kollegen mitunter als Freunde bezeichnen kann. Besonders bedanken möchte ich mich hier bei Alexander Harter, Maximilian Benz, Elena Reinhardt, Jasmin Lechner, Tobias Lenz, Marcus Lommel, Lukas Bauer, Jan Willy Cremers, Christian Riedelsheimer, Michael Gruhne, Simon Endraß, Alexander Schweiger, Veronika Fuchs, Andreas Neuer, Alicia Dufter, Maurus Völkl, Dr. Michael Voggenreiter, Dr. Cornelia Unger, Dr. Dominik Dosch und Dr. Ivan Gospodinov – vielen Dank das ihr zu einer außerordentlichen Zeit beigetragen habt. Abseits der Forschung und den Diskussionen über wissenschaftliche Themen seid ihr mit sehr ans Herz gewachsen! Natürlich gilt das auch für die Mitglieder der „Subgroup" Karaghiosoff, Alexander Gisnapp, Jonathan Tietze, Dr. Christin Kirst und Dr. Marco Reichel, die genauso der Gruppendynamik beigetragen haben wie jeder andere.

Danken möchte ich ebenfalls meinen Bacheloranden und F-Praktikanten, David Cermak, Dominik Werhahn, Clemens Kaußler, Laszlo Schmidt, Christoph Kremser und Alexander Wiegand, ohne deren außerordentliche Hilfe die ganzen anstehenden Arbeiten nicht zu schaffen gewesen wären. Neben eurer hervorragenden chemischen Arbeit waren auch die Stunden abseits des Labors eine Bereicherung. Ich wünsche euch alles Gute für eure wissenschaftliche und berufliche Karriere.

Besonderer Dank gebührt Dr. Maximilian „Wurzy" Wurzenberger der als mein Laborkollege immer Geduld und Nervenstärke bewiesen hat, wenn mal wieder etwas „nicht so funktioniert hat" und natürlich für die Betreuung meiner Masterarbeit. Auch wenn ich die Komplexe erst nach meiner Masterarbeit aufgegriffen habe, warst du hier eine unglaublich große Hilfe und deine Anleitung hat mir gezeigt, wie vielseitig dieses Gebiet sein kann. Daneben danke ich dir für die ansonsten ruhige und entspannte Atmosphäre im Labor, und die etlichen Gespräche über Chemie, aber auch um die Möglichkeit sich mit dir über alle nur denkbaren Themen unterhalten zu können. Der gleiche Dank gebührt auch Marcus Lommel, der als Wurzys Nachfolger dessen ruhige Art und damit die angenehme Laboratmosphäre weiterführt. Natürlich gilt dir mein Dank für die unglaublich gute Spotify Playlist und das Korrekturlesen von Teilen dieser Arbeit.

Des Weiteren gilt mein Dank Maximilian Benz der die Arbeit für uns gemeinsamen Industrieprojekt sehr angenehm und produktiv macht, auch wenn sein Mikrophon meistens aus heiterem Himmel bei den Meetings nicht funktionieren wollte.

Unserem CTA Stefan Huber möchte ich für seine Hilfe und motivierten Arbeit im IT-Team danken, vor allem dafür, dass du mir hier meistens den Rücken freihältst. Natürlich danke ich dir auch für deine Hilfe bei technischen Problemen, die zuverlässige Organisation von Chemikalien sowie sonstigem Labormaterialien und die netten Pläuschchen, die stets zur Erheiterung beigetragen haben.

Dr. Peter Meyer danke ich für die Messung etlicher Einkristalle die an unserem Gerät nicht möglich gewesen waren, sowie die Hilfe bei besonderen Problemstrukturen.

Ein unendlich großer Dank gebührt meiner Familie, besonders meinen Eltern Wolfgang und Ingrid, sowie meinen Stiefeltern Barbara und Joseph. Ohne eure Unterstützung, Geduld und motivierenden, aber auch kritisierenden Gesprächen, wäre diese Arbeit nicht zu dem geworden was sie wäre – und ich nicht zu der Person, die ich heute bin! Natürlich danke ich auch meiner Schwester Tina und meinem Schwager Jacob, die immer ein offenes Ohr für mich haben und unsere

Familie nun sogar um drei unbeschreibliche Neffen und Nichten erweitert haben. Last but not least gilt mein Dank auch meiner Freundin Magdalena. Ohne dich wären die letzten zwei Jahre nicht so liebevoll und lebenswert gewesen, ich möchte keine Sekunde davon missen. Vor allem bin ich dir unendlich dankbar dafür, dass du immer für mich da bist und mich täglich dazu motivierst eine bessere Version meiner Selbst zu werden, für mich und für uns.

1 Introduction

1.1 A Brief History of Explosives

In the history of humankind, few substances had a more pronounced and lasting effect on the development as a society than energetic materials. While early energetic materials mainly consisted of mixtures of substances, which are now referred to as gunpowder or propellants, the most significant breakthrough was the invention of new synthetic access to nitric acid by *Glauber* in the 17th century.[1] Due to the discovery of vast amounts of sodium nitrate (*Chile Salpeter*[2]), nitric acid and potassium nitrate were soon commercially available in the early 19th century. This commercial abundance led to the discovery of nitroglycerin (NG, Figure 1) by *Sobrero*[3] and the enhancement by *Nobel*[4] to the less sensitive mixture dynamite (nitroglycerin and diatomaceous earth, "Kieselguhr"). Later, different mixtures such as gelignite (nitroglycerin, nitrocellulose (NC), and other stabilizers such as camphor, similar: cordite or ballistite) were quickly established in civilian uses such as mining or construction as well as in firearms. Significantly, the application of dynamite substituted raw manpower in industrial projects like setting up large railway systems, the first steps toward modern logistics.[5] Ultimately, the industrial synthesis of nitrate salts or nitric acid became a priority for chemists in the early 20th century, which peaked with the development of the *Haber-Bosch* process[6], which provided enough ammonia to produce nitric acid according to the *Ostwald* process[7] economically. While this was peak synthetic chemistry, worthy of the Nobel prize, and still used in modern society, previous chemists had already reported compounds showing explosive behavior, yet they did not fully understand it. Fulminating gold (lat. *fulminare* = "to cause lightning") was reported as early as 1585 by *Schwaertzer*[8], which despite being suggested by its name, is not containing any fulminate anions. It took chemists nearly exactly 300 years and several uncontrolled explosions and injuries until, in 1886, *Raschig*[8] proposed a heterogenous mixture of more than one compound for fulminating gold - meanwhile, *E. Howard* was the first to synthesize mercury fulminate (MF, Figure 1), even though he wasn't sure about the composition.[9] He quenched a reaction mixture of mercury and concentrated nitric acid onto an ethanolic solution, forming grey and highly explosive solids. Later, it turned out he was the first to report a synthetic procedure for MF, representing one of the first synthetic explosives. Nearly 60 years later, *Alfred Nobel* invented the blasting caps filled with mercury fulminate, revolutionizing the explosive technology of his time.[4] This invention was able to carry on even into modern days energetic materials applications receiving only minor changes. The biggest is the replacement of

MF with lead azide[3] (LA) or lead styphnate[10] (LS) (Figure 1), owing to the high toxicity of mercury fulminate. Due to the large number of synthesized explosives within the 19th and 20th centuries, a classification of the substances is urgently needed.

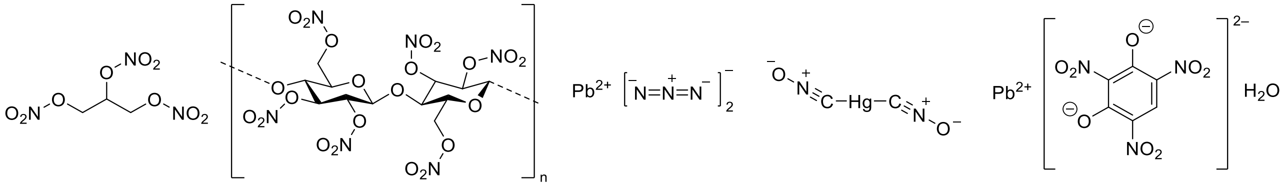

Nitroglycerin, NG **Nitrocellulose, NC** **Lead azide, LA** **Mercury fulminate, MF** **Lead styphnate, LS**

Figure 1. Overview of the molecular structures of historically important explosives.

1.2 Classification of Energetic Materials

The investigation of energetic materials is accompanied by several classifications that aim to categorize and sort the enormous number of known materials. It is possible to sort energetic materials according to their detonation velocity, detonation pressure, and their chemical composition. However, the most straightforward approach classifies them regarding their application (Figure 2).

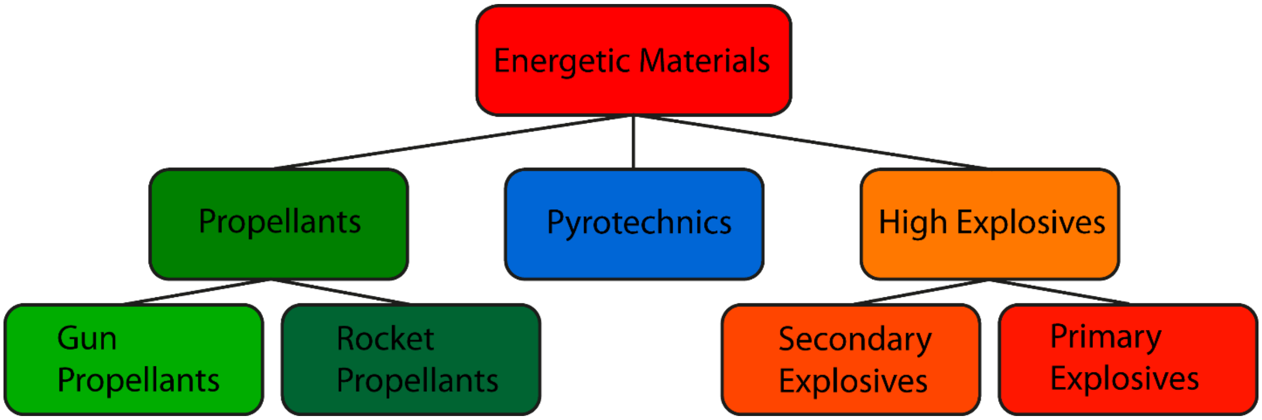

Figure 2. Classification of Energetic Materials according to their application.

Accordingly, propellants, pyrotechnics, and high explosive (HE) are the three main domains of energetic materials, which are further divided into sub-classes. Independent of their classification, energetic materials are required to fulfill different criteria depending on the application. While a broad range of applications is generally possible, some requirements are common to all three classes of energetics, that are their sensitivities toward external stimuli such as impact (IS), friction (FS), and electrostatic discharge (ESD) as well as their performance. The term "performance" is ultimately a matter of application as it includes values such as the detonation velocity (*D*), detonation pressure (*P_{CJ}*), or the volume of gaseous products (*V_0*) and several additional factors, which are essential to various applications.

1.2.1 Propellants and Pyrotechnics

Propellants and Pyrotechnics are two classes of energetic materials that should exhibit a deflagration upon ignition, defined by an exothermic chemical reaction in which the expansion of the reaction front is slower than the velocity of sound in the combustion material.[3] Additionally, compounds within this category are most often required to be as insensitive as possible, ideally completely insensitive toward impact (IS > 40 J) and friction (FS > 360 N). Pyrotechnics cover many applications, like the generation of light, heat, and sound. On the contrary, propellants are designed to produce a large number of gaseous products to perform mechanical work in the form of propelling an object. Further, they are divided into gun and rocket propellants. Gun propellants are intended to accelerate a projectile by a short impulse and most commonly are applied as single, double and triple-base propellants, consisting of nitrocellulose, nitroguanidine (NQ), and nitroglycerine. Rocket propellants can be divided into liquid and solid propellants, applying either heterogeneous or homogeneous mixtures of solid ammonium perchlorate (AP) and aluminum or liquid propellants. An example of a liquid propellant is a mixture of unsymmetrical 1,1-dimethylhydrazine (UDMH) and red fuming nitric acid (RFNA) or nitrogen tetraoxide, which react hypergolic upon contact.

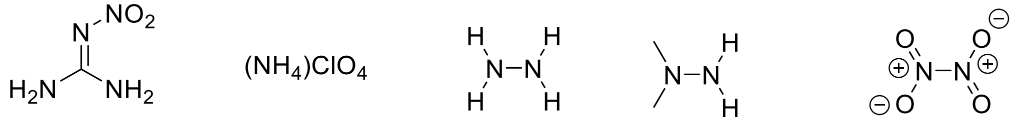

NQ **AP** **Hydrazine** **UDMH** **nitrogen tetraoxide**

Figure 3. Commonly used gun and rocket propellants.

Common to all kinds of pyrotechnics and propellants is the combination of individual fuel and oxidizer to generate the desired energetic material. The only exceptions are mono rocket propellants and single-base gun propellants, which either include fuel and oxidizer within the molecular structure like in NC (gun propellant) or contain chemical materials that exothermically decompose when contacted with a catalyst (e.g., hydrazine and hydrogen peroxide). The most important parameter of propellants is their specific impulse, which describes the change of impulse, thrust F, per mass ejected.[3]

$$I_{sp} = \frac{dp}{dm} = \frac{F}{\frac{dm}{dt}}$$

Equation 1. Specific impulse as the thrust (F) per mass ejected over time.

1.2.2 High explosives

Primary Explosives. The class of high explosives subdivides into secondary and primary explosives. Such compounds are typically used for destructive work for military or civil applications. Generally, primary explosives are substances that can be initiated by a simple initiating impulse (SII) and are required to generate a shock wave which transfers to less sensitive explosives. Therefore, primaries must show a rapid so-called deflagration to detonation transition (DDT).[11] As the velocity of reaction front expansion can accelerate during a self-sustained deflagration of an energetic material, a velocity equal to or faster than the speed of sound in the combustion material may be reached, at which the deflagration traverse into a detonation. Typical SIIs applied to set off primary explosives include electric sparks, flame, heat, impact, or friction and are most commonly applied via a non-explosive device. A distinction between primary and secondary explosives is most often according to the speed of DDT, which is significantly higher for primary explosives. Additionally, primary explosives typically exhibit very high sensitivities toward impact (≤ 4 J), friction (≤ 10 N), and electrostatic discharge (≤ 20 mJ). Contrary to their high sensitivity and ability to produce a shockwave, primary explosives normally exhibit an overall low performance, typically reaching detonation velocities around 5000–6000 m s^{-1}. However, the detonation velocity is not a critical parameter of primary explosives, as can be seen with LA (5300 m s^{-1}) and LS (4900 m s^{-1}).[3] In addition to the direct use of primary explosives, they are often included in priming mixtures to assure error-free ignition of the pyrotechnical mixtures to produce heat, flame, or sound.[11] Even though only small amounts of primary explosives are typically applied in an energetic device, their impact on the health of the user and the environment is not negligible, especially when containing heavy metals. Therefore, new heavy metal-free candidates are investigated due to the recognition of the high toxicity of lead[3] and other heavy metal-containing salts. A prominent replacement (Figure 4) is 2-diazo-4,6-dinitrophenolat (DDNP) which is already introduced to several commercially available products.[12] Additional candidates (Figure 4) are copper(I) 5-nitrotetrazolate (DBX-1[13]), potassium 2,4-dinitrobenzofuroxane (KDNBF[14]), and potassium 1,1'-dinitramino-5,5'bistetrazolate (K_2DNABT[15]), which are salts of far less toxic metals.[11]

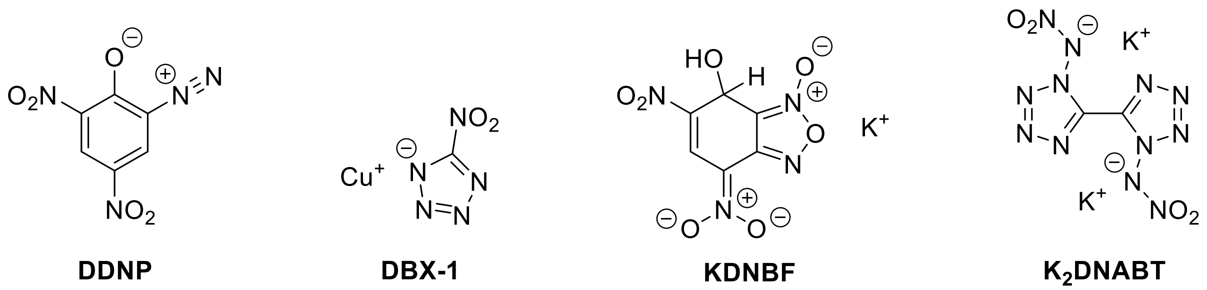

Figure 4. Possible replacements for lead azide and lead styphnate.

Especially, K_2DNABT is an extremely dangerous material to handle, even on a small scale. Like typical primary explosives, it exhibits high impact (< 1 J) and friction (< 0.1 N) sensitivities but combines those with the performance (8330 m s^{-1}) of a secondary explosive.[16]

Secondary Explosives. Compounds from the subclass of secondary explosives are typically distinguished from primary explosives by a slower DDT and the missing detonation capability when being initiated by an SII. The initiation of secondary explosives is, therefore, typically possible by a shock wave produced by a primary explosive. Additionally, secondary explosives are the main charge of a detonation device and are thus required to be less sensitive toward external stimuli (IS $\geq$ 4 J, FS $\geq$ 80 N, ESD $\geq$ 100 mJ) while exhibiting a drastically higher performance than primary explosives. Also, there are several characteristic parameters for secondary explosives, foremost the detonation velocity D [m s^{-1}], detonation pressure P [kbar], and the heat of explosion Q [kJ kg^{-1}]. Owing to the wide range of properties, some compounds are typically referred to as "high performance" secondary explosives (Figure 5), such as hexogen (RDX[14]), octogen (HMX[14]), hexanitroisowurtzitan (CL-20[17]), and dihydroxylammonium-5,5′-bistetrazolyl-1,1′-diolat (TKX-50[18]). These compounds exhibit detonation velocities between 8800 m s^{-1} (RDX) and 9698 m s^{-1} (TKX-50). On the other hand, there are commonly applied compounds with drastically lower performance, such as 2,4,6-trinitrotoluene (TNT), which exhibits a detonation velocity of 6900 m s^{-1}. These compounds are used owing to a specific property, which is its melting point for TNT, which offers the possibility to produce melt-cast formulations. This is especially useful, as normally no material is used as a pure substance, but it is always combined in a mixture of several compounds.

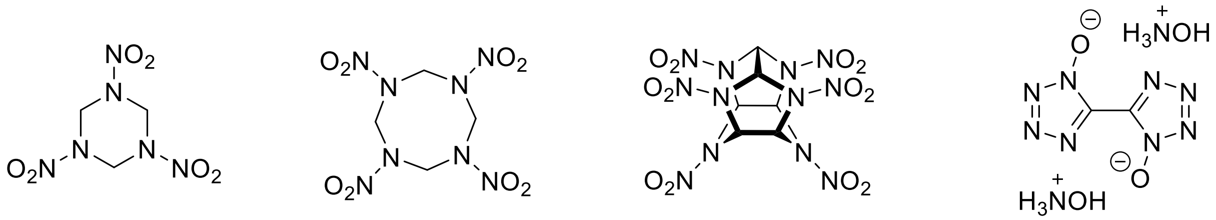

Figure 5. Molecular structure of high-performing secondary explosives.

The second example of an often-included compound in formulations is 3-nitro-1,2,4-triazol-5-on (NTO), which acts as a *desensitizer*, reducing the sensitivity of a formulation while not drastically decreasing the performance.[19] The third kind of secondary explosives is the family of highly thermal stable compounds, such as hexanitrostilben (HNS[20]) and 2,6-bis(pikrylamino)-3,5-dinitropyridin (PYX[21]), being low performing (≤ 7700 m s^{-1}) but necessary for application at high ambient temperatures, such as deep mining. The last kind of secondary explosives, booster explosives, is represented by its most prominent example, pentaerythritol tetranitrate (PETN). This compound is included in several military applications, such as in *Semtex*, where it is mixed and phlegmatized with silicone oils. In its application as a booster explosive, it can be used to transfer the initial shockwave of a primary explosive, ultimately ensuring a better initiation of the main charge's secondary explosive.

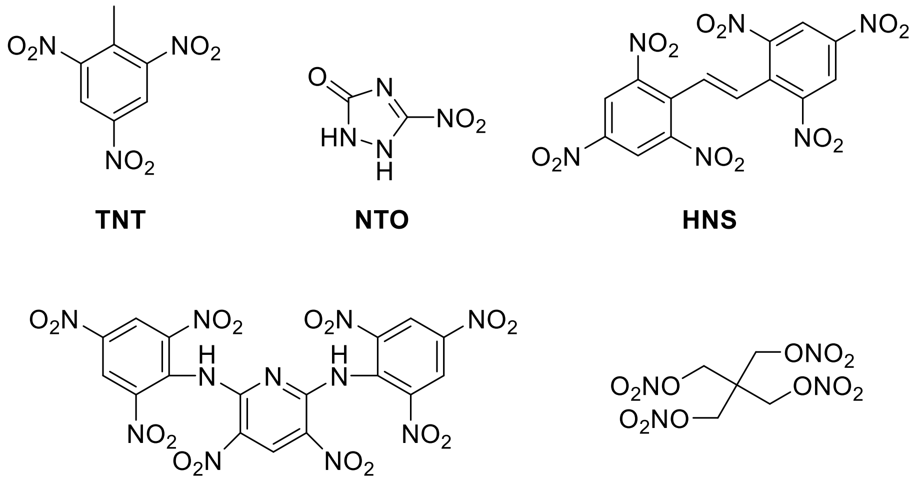

Figure 6. Molecular structures of TNT, NTO, HNS, PYX, and PETN.

Comparing the structural motives of all previously shown secondary explosives makes it common for nearly all compounds to include nitro groups to obtain their explosive properties. The only exception thus far is TKX-50, based on an oxidized 5,5'-bistetrazole scaffold, making it the first representative of the class of nitrogen-rich heterocycles.

1.3 Nitrogen rich Heterocycles

Due to the influence of nitro- or nitrate-containing explosives on the living organism and the environment, research has begun shifting toward searching for compounds with comparable properties and lower toxicity. This was also initiated with the introduction of the **R**egistration, **E**valuation, **A**uthorization, and **R**estriction of **Ch**emicals regulation (REACH) introduced by the European Union in 2007.[22] This regulation prohibits certain chemicals within the European Union and introduces a candidate list of chemicals of high concern, which may be included in the list of prohibited chemicals in the future. Therefore, *Thomas M. Klapötke et al.* search for less toxic energetic materials, focusing on nitrogen-rich compounds. Generally, introducing high nitrogen content into a molecule drastically increases the enthalpy of formation. Upon exothermic decomposition, these compounds decompose with the formation of N-N triple bonds in N_2. The significantly higher bond energy of N-N triple bonds over N-N single or double bonds (Figure 7) releases an enormous amount of energy upon combustion or detonation.

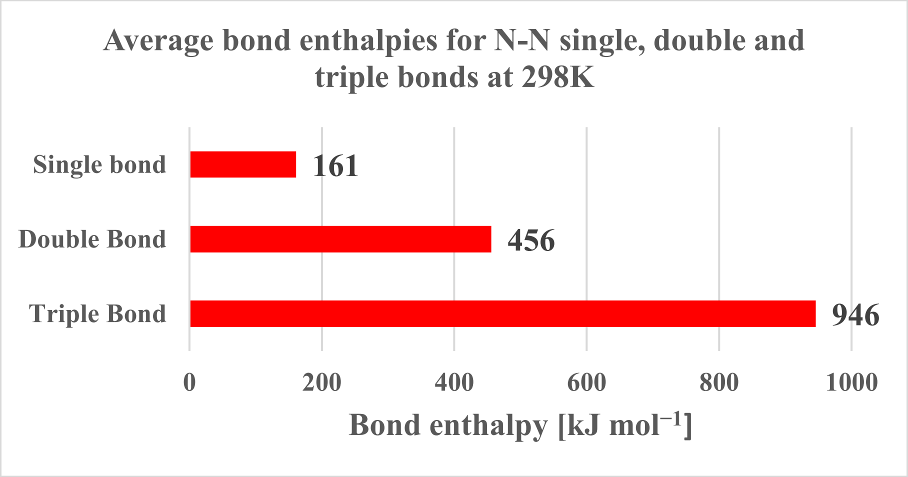

Figure 7. Average bond enthalpy of N-N single, double, and triple bonds.

Besides the prominent TKX-50, compounds of this kind are most often based on the chemistry of azoles, ranging from 1*H*-pyrrole to 1*H*-pentazole (Figure 8). The advantage of the azole scaffolds is their high enthalpy of formations, especially for 1*H*-tetrazole and 1*H*-pentazole. These backbones dramatically increase the endothermicity of the resulting energetic compound, and thus high performances can be assumed. While 1*H*-pentazole exhibits a drastically high enthalpy of formation, its poor synthetical accessibility and instability explain the lack of pentazole employing energetic compounds. Some pentazole derivatives are still reported, the first being 1-Phenyl-pentazole[23] by *Huisgen et al.*, where the pentazole scaffold is stabilized by aryl functional groups and is thus far away from being an energetic compound. Next in line of the azoles is 1*H*-tetrazole, which combines a still high enthalpy of formation (4794 kJ kg^{-1}) with good synthetical access, and it is therefore not surprising that two of the most promising compounds, DBX-1, and TKX-50, are based on this scaffold.

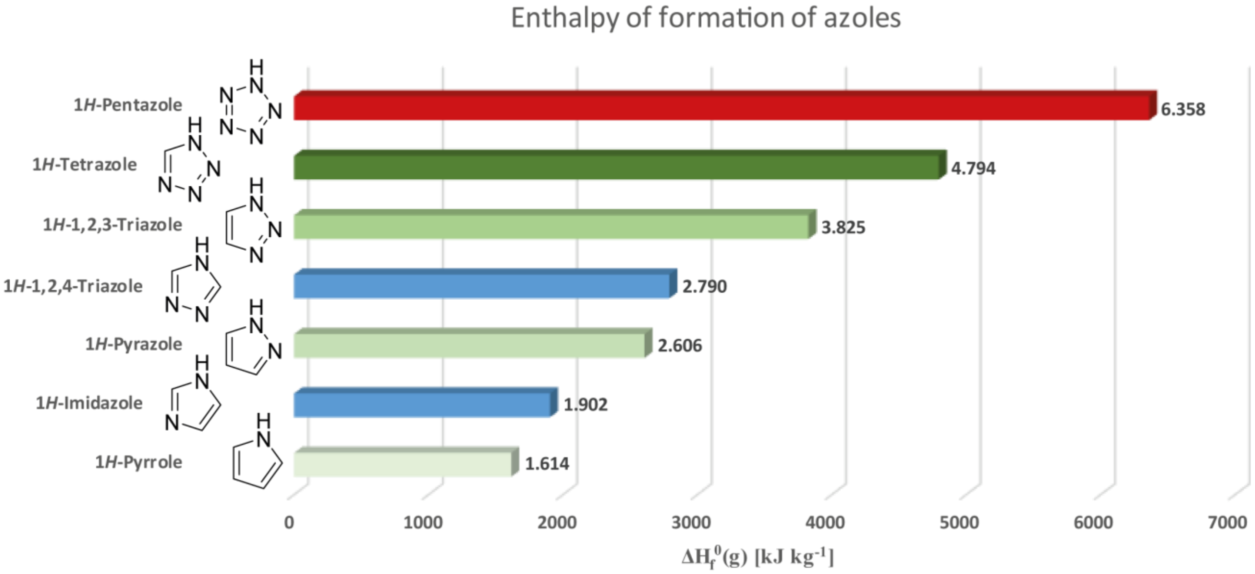

Figure 8. Molecular structures of azole and their respective enthalpy of formation.

Since tetrazole derivatives often exhibit high sensitivities toward external stimuli[24], there are also numerous promising compounds based on the triazole and pyrazole scaffolds, including 7-amino-2,3,6-trinitropyrazolo[5,1-*c*][1,2,4]triazine (PTX)[25], dihydroxylammonium 3,3′-dinitro-5,5′-bis-1,2,4-triazole-1,1-diolate (MAD-X1)[26], and bis(3,4,5-trinitropyrazolyl)-methane (BTNPM)[27]. While there are also several imidazole derivatives reported[28], partially being considerable explosives, their lack in enthalpy of formation limits the research interest in imidazoles and pyrroles as energetic materials. Most often, such compounds are discussed in the context of pharmaceutical applications.[29] An unusual explosive for its time is (2-(5-cyanotetrazolato)pentaamine cobalt(III) perchlorate (CP), first reported in the late 1960s, it was applied in low-voltage detonators since 1979[30] as a replacement for toxic LA and LS. Due to the restriction of dicyanamide as the precursor of 5-cyanotetrazole by the Environmental Protection Agency (EPA)[31], the application of CP was soon discontinued. Nonetheless, CP is one of the first representatives of Energetic Coordination Compounds (ECCs).

1.4 Energetic Coordination Compounds

A quite similar but more powerful representative is tetraamine-*cis*-bis-(5-nitro-2*H*-tetrazolato-N^2) cobalt(III) perchlorate (BNCP)[32], which is also an ECC exhibiting a fast DDT after an SII. BNCP was also one of the first compounds capable of being initiated by a laser, launching the investigation of several ECCs toward their laser ignitability, like for 5-hydrazino-1*H*-tetrazole mercury(II) perchlorate (HTMP)[33], and even led to the reevaluation of copper(II) chlorate complexes as laser ignitable primary explosives.[34] The basic approach toward ECCs combines transition metals (e.g., Cu, Zn, Ni, and Ag) with energetic ligands and oxidizing (e.g., ClO_4^-, ClO_3^-, and NO_3^-), reducing (N_3^-) or nitroaromatic (e.g., picrate, and styphnate) anions (Figure 9). Most metals and anions are introduced as their respective salts, while most often, the applied ligands need elaborate synthesis, as they usually are not commercially available. Nonetheless, this offers a nearly infinite number of possible combinations, which allows fine-tuning of the energetic properties according to the intended application and represents the main advantage of ECCs.

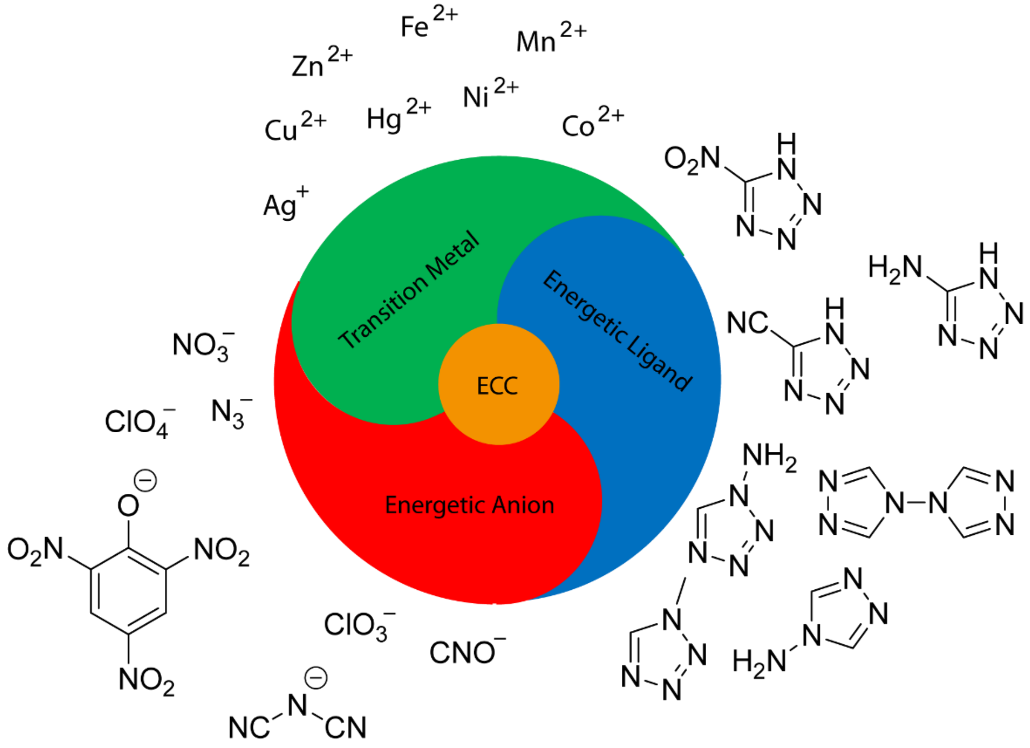

Figure 9. Concept of ECCs, combining metal cations, energetic ligands and energetic anions with representatives of each component.

Due to the many combinations, it is possible to stabilize extremely sensitive materials, like silver(I) fulminate or copper(II) azide, or achieve sensitizing of usually insensitive non-energetic salts.[34-

35] This is feasible by choosing between the anions mentioned above to increase or decrease the energy of the resulting ECC. Especially the selection of ligands with unique properties (Figure 10), like a bridging effect between metal centers (1,1-DTM[36]), high enthalpies of formation (AET[24b] and APT[37]), or a high oxygen balance (1-NET[38]) can introduce different characteristics to the resulting ECC. Despite some outliers, ECCs often exhibit the characteristic property of a primary explosive, which is the fast transition from an SII to a detonation. Therefore, the main goal of ECC formation is to tune properties toward a possible replacement of lead azide and lead styphnate, which are still used despite their long-known drawbacks. Quite recently, research shifted toward investigating ECCs as burn rate modifiers, and some are even discussed as representatives of metal-organic frameworks (MOFs) as solid-state hypergolic fuels for the next generations of rocket motors.[39]

1.5 Motivation and Objectives

The investigation and quest for energetic materials as replacements for lead azide (LA) and lead styphnate (LS) resulted in the synthesis of several new promising compounds. Yet, LA and LS are still the most used primary explosives for military and civil applications, even though health concerns derive from the uptake of lead. In addition, both substances have been included in the REACH Candidate List of Substances of Very High Concern for Authorization, therefore a ban on both substances can be expected soon. By applying the concept of ECCs, several promising compounds have already been synthesized and investigated. Extensive efforts on synthesizing new ligands for ECCs, is most often based on the 1*H*-tetrazole scaffold. Some of the most promising examples (AET, and APT) of ligands previously investigated in our working group are depicted in Figure 10.

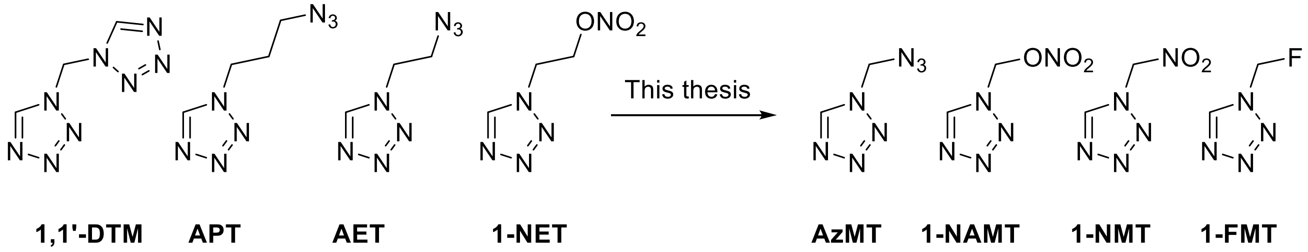

Figure 10. Molecular structures of the typical nitrogen rich ligands APT AET, 1-NET together with some ligands of this thesis.

Likewise, the introduction of alkyl bridged explosophores (e.g., azides, nitrates, or nitro groups) to the basic tetrazole backbone, proved to be highly desirable for the design of novel ligands. Most of these compounds exhibit high enthalpies of formation, good oxygen balances, high densities, and most importantly, lack any acidic functionalities. As such, they are ideal ligands and have proven to yield high-performing ECCs.[24b, 37-38] Nonetheless, most ligands incorporate either ethylene- or propylene-bridges, while only a very limited number of compounds include a methylene-moiety. Therefore, the first part of this thesis focuses on the introduction of a methylene bridging functionality to the 1*H*-tetrazole backbone and achieving further functionalization of this bridging moiety. Special focus is put on the introduction of the oxidizing functional groups $-ONO_2$, and $-NO_2$, as well as the introduction of the $-N_3$ and -F moiety to extend the series of *N*-(azidoalkyl)-tetrazoles by its smallest possible representative. All compounds are extensively characterized and to extend the general understanding of energetic coordination compounds, several ECCs were developed, including the novel tetrazole derivatives as ligands. Due to the success of TKX-50 as an explosive, an outlier part of this thesis investigates the chemistry of 1-hydroxytetrazole, which represents the smaller brother of the TKX-50 backbone, 5,5'-bistetrazol-1,1'-diol.

The second part of this thesis is in cooperation with an industry partner and focuses on the two topics of HMX and TNT replacement, by assessing and reevaluating the properties of literature known compounds. This research topic was brought to us by our partner in order to have alternatives for HMX and TNT in case they should be affected by the REACH regulation in the future. Therefore, after extensive literature searches scanning for possible candidates for each topic, a priority list of compounds to be synthesized and analyzed is found together with the industry partner. Thereby, compounds with a high chance of replacing HMX or TNT have to exhibit several criteria, given by the industry, which are summarized in table 1 (HMX) and table 2 (TNT).

Table 1. Properties and specifications for the research on an HMX replacement.

Properties	Specifications
Detonation velocity (m s^{-1})	> 9100
Density (g cm^{-3})	> 1.9
Impact sensitivity (J)	> 5
Friction sensitivity (N)	> 120
Electric spark (mJ)	> 700 mJ
Decomposition T (°C)	> 200
Synthesis	Economic process: synthesis step, process time, cost of raw materials
Toxicity	REACH compliant

Table 2. Properties and specifications for the research on a TNT replacement.

Properties	Specifications
Detonation velocity (m s^{-1})	> 7600
Density (g cm^{-3})	> 1.76
Melting Point [°C]	< 110
Decomposition T (°C)	> 180
Sensitivities	Not higher than PETN (4 J, 80 N)
Synthesis	Economic process: synthesis step, process time, cost of raw materials
Toxicity	REACH compliant

1.6 References

[1] W. Furter, *A Century of Chemical Engineering*, Springer New York, NY, **1982**, p.

[2] A. Mutic in *The Ghost Towns of Northern Chile*, *Vol.* **2012**.

[3] T. M. Klapötke, *Chemistry of High-Energy Materials*, De Gruyter, **2022**, p.

[4] A. Nobel in *Improved Explosive Compound*, *Vol. US78317A* United states, **1868**.

[5] S. Meyers and E. S. Shanley, *J. Hazard. Mater.* **1990**, *23*, 183–201.

[6] G. Ertl, *Angew. Chem. Int. Ed. Engl.* **1990**, *29*, 1219–1227.

[7] W. Ostwald in *Improvement in the Manufacture of Nitric Acid and Nitrogen Oxides*, *Vol.* **1902**.

[8] G. Steinhauser, J. Evers, S. Jakob, T. M. Klapötke and G. Oehlinger, *Gold Bulletin* **2008**, *41*, 305–317.

[9] a) F. Kurzer, *Annals of Science* **1999**, *56*, 113–141; b) E. Howard, *Philos. Trans. R. Soc. London* **1800**, *90*, 204–238.

[10] J. R. Payne, *Thermochim. Acta* **1994**, *242*, 13–21.

[11] R. Matyáš and J. Pachman, *Primary Explosives*, Springer, Berlin, **2013**, p.

[12] L. V. Clark, *Ind. Eng. Chem.* **1933**, *25*, 663–669.

[13] J. W. Fronabarger, M. D. Williams, W. B. Sanborn, J. G. Bragg, D. A. Parrish and M. Bichay, *Propellants Explos. Pyrotech.* **2011**, *36*, 541–550.

[14] T. M. Klapötke, *Energetic Materials Encyclopedia*, De Gruyter, **2021**, p.

[15] D. Fischer, T. M. Klapötke and J. Stierstorfer, *Angew. Chem. Int. Ed.* **2014**, *53*, 8172–8175.

[16] M. S. Gruhne, M. Lommel, M. H. H. Wurzenberger, N. Szimhardt, T. M. Klapötke and J. Stierstorfer, *Propellants Explos. Pyrotech.* **2020**, *45*, 147–153.

[17] A. T. Nielsen, A. P. Chafin, S. L. Christian, D. W. Moore, M. P. Nadler, R. A. Nissan, D. J. Vanderah, R. D. Gilardi, C. F. George and J. L. Flippen-Anderson, *Tetrahedron* **1998**, *54*, 11793–11812.

[18] N. Fischer, D. Fischer, T. M. Klapötke, D. G. Piercey and J. Stierstorfer, *J. Mater. Chem.* **2012**, *22*, 20418–20422.

[19] T. E. Dawag and J. Morris in *Nitrotriazolone Process Optimization*, *Vol. 2022* U.S.Army Research, Developtment and Engineering Command, **2012**.

[20] K. G. Shipp, *J. Org. Chem.* **1964**, *29*, 2620-2623.

[21] T. M. Klapötke, J. Stierstorfer, M. Weyrauther and T. G. Witkowski, *Chem. Eur. J.* **2016**, *22*, 8619–8626.

[22] E. C. A. (ECHA) in *Verordnung (EG) Nr. 1907/2006 des Europäischen Parlaments und des Rates vom 18. Dezember 2006 zur Registrierung, Bewertung, Zulassung und Beschränkung chemischer Stoffe (REACH), zur Schaffung einer Europäischen Agentur für chemische Stoffe, zur Änderung der Richtlinie 1999/45/EG und zur Aufhebung der Verordnung (EWG) Nr. 793/93 des Rates, der Verordnung (EG) Nr. 1488/94 der Kommission, der Richtlinie 76/769/EWG des Rates sowie der Richtlinien 91/155/EWG, 93/67/EWG, 93/105/EG und 2000/21/EG der Kommission.*, *Vol.* **2006**.

[23] R. Huisgen and I. Ugi, *Chem. Ber.* **1957**, *90*, 2914–2927.

[24] a) N. Szimhardt, M. H. H. Wurzenberger, L. Zeisel, M. S. Gruhne, M. Lommel and J. Stierstorfer, *J. Mater. Chem. A* **2018**, *6*, 16257–16272; b) M. H. H. Wurzenberger, M. S. Gruhne, M. Lommel, N. Szimhardt, T. M. Klapötke and J. Stierstorfer, *Asian J. Chem.* **2019**, *14*, 2018–2028.

[25] I. L. Dalinger, I. A. Vatsadse, T. K. Shkineva, G. P. Popova, B. I. Ugrak and S. A. Shevelev, *Russ. Chem. Bull.* **2010**, *59*, 1631–1638.

[26] A. A. Dippold and T. M. Klapötke, *J. Am. Chem. Soc.* **2013**, *135*, 9931–9938.

[27] D. Fischer, J. L. Gottfried, T. M. Klapötke, K. Karaghiosoff, J. Stierstorfer and T. G. Witkowski, *Angew. Chem. Int. Ed.* **2016**, *55*, 16132–16135.

[28] a) R. Lewczuk, M. Szala, J. Rećko, S. Cudziło, T. M. Klapötke, W. A. Trzciński and L. Szymańczyk, *Cent. Eur. J. Energ. Mater.* **2016**, *13*, 612–626; b) P.-B. Lian, J. Chen, L.-Z. Chen, C.-Y. Zhao, J.-L. Wang and F.-F. Shen, *J. Heterocycl. Chem.* **2020**, *56*, 55–59.

[29] a) V. Bhardwaj, D. Gumber, V. Abbot, S. Dhiman and P. Sharma, *RSC Advances* **2015**, *5*, 15233-15266; b) H. Nakano, S. Umio, K. Kariyone, K. Tanaka, T. Kishimoto, H. Noguchi, I.

Ueda, H. Nakamura and T. Morimoto, *Tetrahedron Lett.* **1966**, *7*, 737–740; c) N. D. Kimpe, K. A. Tehrani, C. Stevens and P. D. Cooman, *Tetrahedron* **1997**, *53*, 3693–3706; d) R. J. Holt, *J. Cutan. Pathol.* **1976**, *3*, 45–59; e) X. Zheng, Z. Ma and D. Zhang, *Pharmaceuticals* **2020**, *13*, 37.

[30] M. L. Lieberman, *Ind. Eng. Chem. Res.* **1985**, *24*, 436–440.

[31] M. B. Talawar, A. P. Agrawal and S. N. Asthana, *J. Hazard. Mater.* **2005**, *120*, 25–35.

[32] L. R. Bates, *Symposium on Explosives and Pyrotechnics* (Hilton Head Island, S.C.) **1986**.

[33] M. Joas and T. M. Klapötke, *Propellants Explos. Pyrotech.* **2015**, *40*, 246–252.

[34] M. H. H. Wurzenberger, N. Szimhardt and J. Stierstorfer, *J. Am. Chem. Soc.* **2018**, *140*, 3206–3209.

[35] M. H. H. Wurzenberger, M. Lommel, M. S. Gruhne, N. Szimhardt and J. Stierstorfer, *Angew. Chem. Int. Ed.* **2020**, *59*, 12367–12370.

[36] M. H. H. Wurzenberger, V. Braun, M. Lommel, T. M. Klapötke and J. Stierstorfer, *Inorg. Chem.* **2020**, *59*, 10938–10952.

[37] M. H. H. Wurzenberger, S. M. J. Endraß, M. Lommel, T. M. Klapötke and J. Stierstorfer, *ACS Appl. Energy Mater.* **2020**, *3*, 3798–3806.

[38] M. S. Gruhne, T. Lenz, M. Rösch, M. Lommel, M. H. H. Wurzenberger, T. M. Klapötke and J. Stierstorfer, *Dalton Trans.* **2021**, *50*, 10811–10825.

[39] a) M. S. Gruhne, M. H. H. Wurzenberger, M. Lommel and J. Stierstorfer, *Chem. Eur. J.* **2021**, *27*, 9112–9123; b) H. M. Titi, J. M. Marrett, G. Dayaker, M. Arhangelskis, C. Mottillo, A. J. Morris, G. P. Rachiero, T. Friščić and R. D. Rogers, *Science Advances* **2019**, *5*, eaav9044; c) C. Wang, Y.-J. Wang, C.-L. He, Q.-Y. Wang and S.-Q. Zang, *JACS Au* **2021**, *1*, 2202–2207; d) Q.-Y. Wang, J. Wang, S. Wang, Z.-Y. Wang, M. Cao, C.-L. He, J.-Q. Yang, S.-Q. Zang and T. C. W. Mak, *J. Am. Chem. Soc.* **2020**, *142*, 12010–12014.

2 Selective Synthesis and Characterization of the Highly Energetic Materials 1-Hydroxytetrazole (CHN_4O), its Anion 1-Oxidotetrazolate (CN_4O^-) and Bis(1-hydroxytetrazol-5-yl)triazene

Thomas M. Klapötke, Moritz Kofen, Laszlo Schmidt, Jörg Stierstorfer, and Maximilian H. H. Wurzenberger

Published in *Chemistry – An Asian Journal* **2021**, *16*, 1–13.

DOI: 10.1002/asia.202100714

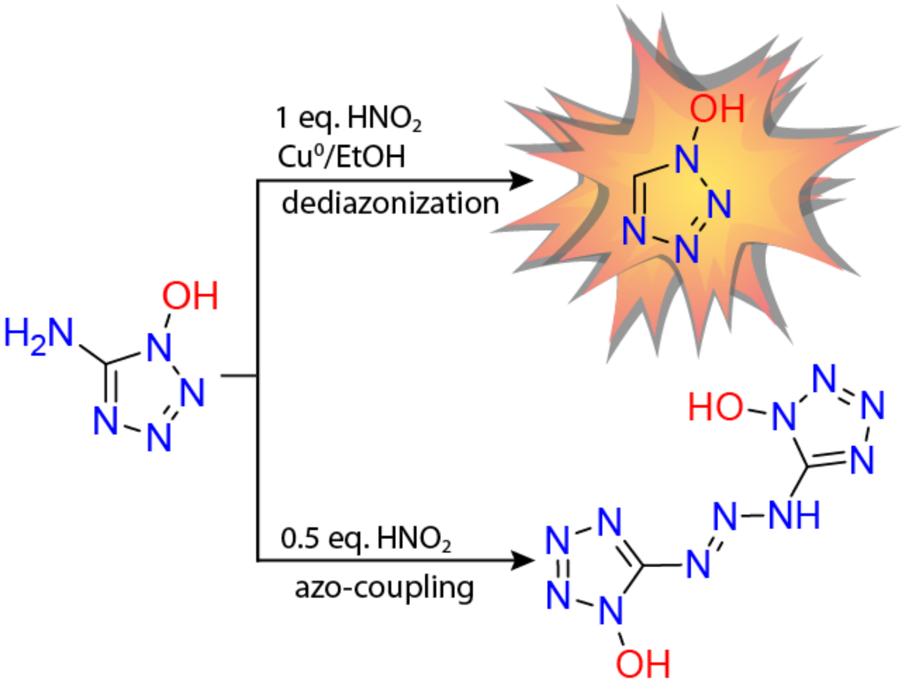

Abstract: For the first time, the selective synthesis, circumventing the formation of the 2-hydroxytetrazole, of 1-hydroxytetrazole (HTO), as well as the synthesis of bis(1-hydroxytetrazol-5-yl)triazene (H_3T) are reported. Several salts thereof were synthesized and characterized which resulted in the formation of new primary and secondary explosives containing the 1-oxidotetrazolate unit. Molecular structures are characterized by single crystal X-ray diffraction, ^1H and ^{13}C NMR, IR, and elemental analysis. Calculation of the detonation performance using the EXPLO5 code confirmed the energetic properties of 1-hydroxytetrazole. The detonation properties

can be adjusted to the requirements for those of a secondary explosive by forming the hydroxylammonium (**6**) or hydrazinium (**7**) salts, or to meet the requirements of a primary explosive by forming the silver salt **4**, which shows a fast DDT on contact with a flame. The sensitivities of all compounds towards external stimuli such as impact, friction, and electrostatic discharge were measured.

2.1 Introduction

Tetrazoles are a class of heterocycles that exhibit a wide variety of possible applications. A prominent representative is *Losartan*, which is included in the WHO's List of Essential Medicines[1] as a treatment for hypertension.[2] In addition to pharmaceutical uses, tetrazoles show great potential for application as energetic materials with high nitrogen contents like in copper(I) nitrotetrazolate (DBX-1).[3-4] The high endothermic heat of formation of tetrazoles (e.g. +236 kJ mol^{-1} for 1*H*-tetrazole) is advantageous for possible applications as energetic materials, since a large amount of energy is released upon detonation.[5] General protocols to further increase the enthalpy of formation of tetrazoles include *N*-oxidation by Oxone®,[6] HOF,[7] or H_2O_2[8], which also has the advantage of increasing the oxygen balance and crystal density.[9] In 2012, *Klapötke et al.*[10] obtained dihydroxylammonium-5,5'-bistetrazolyl-1,1'-diolat (TKX-50) through the *N*-oxidation of 5,5'-bistetrazole followed by formation of the hydroxylammonium salt. This compound possesses excellent detonation properties while being thermally stable (221 °C) and moderately sensitive towards impact (20 J) and friction (120 N), thus being stable enough to be safely used as a high-performing secondary explosive. TKX-50 surpasses properties of 1,3,5-Trinitro-1,3,5-triazinan (RDX) and 1,3,5,7-Tetranitro-1,3,5,7-tetrazocan (HMX), which have long been used as the main charge in detonation devices. Even though the 5,5'-bistetrazole has been known since 1913,[11] it took nearly 100 years until its potential for use as an explosive was discovered in the compound TKX-50. It is therefore surprising that 1*H*-tetrazole has been known since 1892,[12] but complete characterization of the corresponding *N*-oxide, namely 1-hydroxytetrazole, is missing.

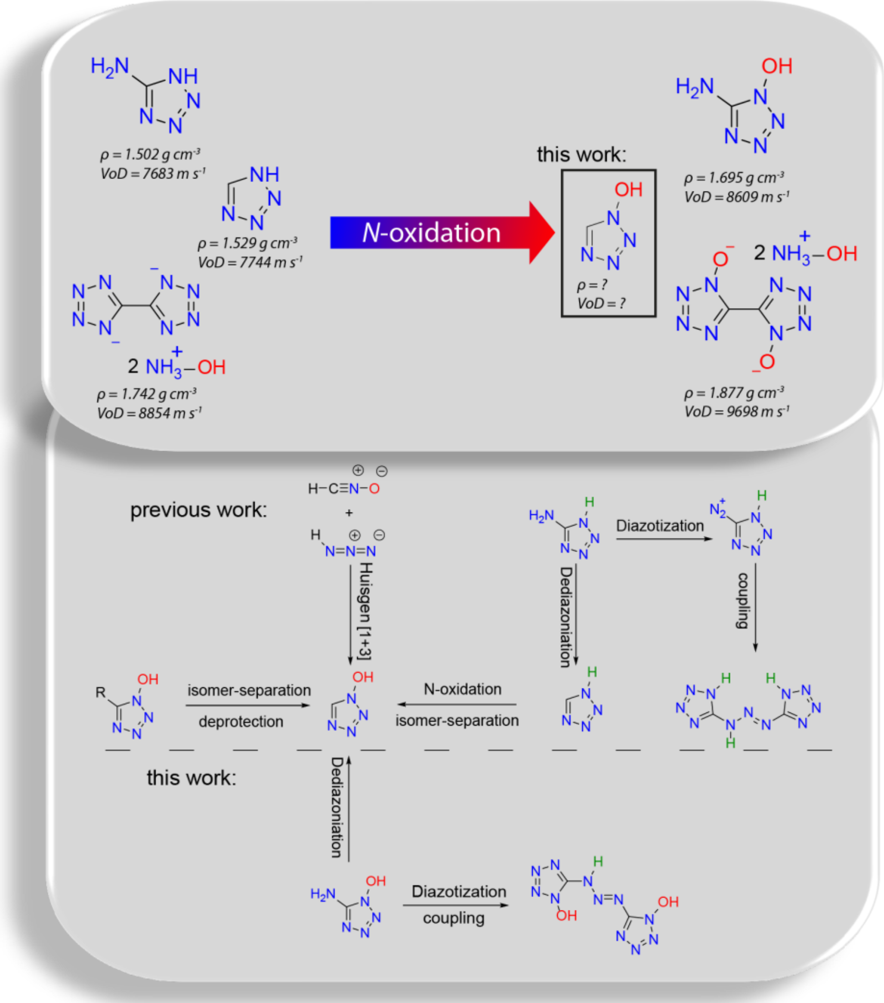

Figure 1. Top: Increasing the density and enhancing the performance of energetic compounds can be achieved by *N*-oxidation. Bottom: Previous work concerned with the synthesis of 1-hydroxytetrazole and bis(tetrazol-5-yl)triazene.

The first synthesis was reported by *Pallazzo* in 1910,[13] however, the addition of hydrazoic acid to sodium fulminate is not suitable nor desired for a synthesis on gram-scale due to the high risks involved when working with fulminates. In 1956, *Bettinetti et al.* successfully synthesized 1-hydroxytetrazole by the addition of hydrazoic acid to nitrolic acids, which too is not desired for the work on gram-scale.[14] *Bettinetti et al.* also described the silver salt of 1-hydroxytetrazole, yet an extensive characterization is missing. In 1995, *Begtrup et al.*[15] used Oxone® to oxidize 1*H*-tetrazole. This idea was then followed by *Giles et al.* [16] in 1999 for oxidizing ethyl tetrazole-5-carboxylate. Both procedures result in an isomeric mixture of the 1-hydroxy- and 2-hydroxy-tetrazole derivatives, requiring further protection (for the oxidized 1*H*-tetrazole), as well as separation of the isomers and subsequent secession of the protecting group. In a previous paper in 2013, we showed that the addition of hydroxylamine to a solution of cyanogen azide results in a cyclization forming 5-amino-1-hydroxytetrazole (5-ATO).[17] In 1954, *Henry et al.* showed that *1H*-tetrazole can be obtained by the elimination of the amino group of 5-amino-1*H*-tetrazole through diazotization followed by subsequent reduction of the diazonium cation. These so-called *hydro-dediazonizations* are performed by boiling a diazonium cation in acidic ethanol. However, this procedure usually results in *ethoxy-dediazonization*.[18] *Kornblum et al.* later replaced the step in which reduction with acidic ethanol occurs by using hypophosphorous acid as the reducing agent instead.[19] Independently from the applied reduction procedure, the *dediazonization* always starts with a diazotization of the amine, which, for several azoles, can instantly explode and therefore should never be isolated. It can also couple with other compounds and this well-known behavior is exploited to produce azo dyes, such as Methyl red (2-(*N*,*N*-dimethyl-4-aminophenyl)[20] or Tartrazine (trisodium 1-(4-sulfonatophenyl)-4-(4-sulfonatophenylazo)-5-pyrazolone-3-carboxylate).[21] Lesser known are triazenes, which result from the coupling of a diazonium cation with an amine. In 1910 *Hofmann et al.* published the first synthesis of sodium bis(tetrazol-5-yl)triazene by diazotization of amino guanidinium nitrate with sodium nitrite, intermediately producing 5-aminotetrazole which then further reacts to the triazene species.[22] When applying the systems analogously to 5-ATO, the *dediazonization* selectively produces 1-hydroxytetrazole, thus representing the first adequate selective synthesis for this long over-due compound, whereas following *Hofmann et al.* results in the formation of bis(1-hydroxytetrazol-5-yl)triazene, the twice *N*-oxidized bis(tetrazol-5-yl)triazene. Therefore, we report the first adequate procedure to obtain 1-hydroxytetrazole without the need of protection groups and elaborate workups. Additionally, the first synthesis of bis(1-hydroxytetrazol-5-yl)triazene is reported. Both acids as well as salts thereof are prepared and are characterized by single crystal X-ray diffraction experiments, complemented by NMR and IR spectrometry as well as thermal and physical analysis.

2.2 Results and Discussion

2.2.1 Synthesis

Warning! The synthetic work described in this section involves the handling of very sensitive intermediates (diazotetrazole-1N-oxide) and products (e.g., silver salt ***4****). Proper protective measurements and equipment must be used!*

The starting material 5-ATO is readily available from the reaction of cyanogen azide and hydroxylamine.[17] 1-Hydroxytetrazole (**1**) can be obtained by dissolving 5-ATO in semi-concentrated sulfuric acid (40%) and diazotizing with sodium nitrite, while keeping the temperature below 5 °C (Scheme 1). The diazotization solution is then added to a mixture of ethanol and elemental copper and stirred at 55 °C for 2 hours. Due to the intermediate formation of 5-diazonium-1-hydroxytetrazole, the ratio of 5-ATO to sulfuric acid (40%) should be quite low. A ratio of 1:10 was used for the synthesis of all herein investigated compounds, as a higher concentration of 5-diazonium-1-hydroxytetrazole leads to micro-detonations within the reaction solution. An attempt to reduce the amount of acid to a ratio of 1:2 resulted in a violent detonation of the whole reaction solution, destroying the round-bottom flask. Compound **1** was extracted into DCM, and the ammonium salt (**5**) was subsequently precipitated by passing gaseous ammonia through the organic phase. The sodium (**2**) and potassium (**3**) salts were obtained by refluxing a solution of the corresponding carbonate and **5** in water, followed by evaporating to complete dryness, extracting the residue with ethanol, and precipitating the salts by adding diethyl ether. The silver salt (**4**) can be precipitated by adding silver nitrate to a solution of **1** in water and filtering off the solid. The hydroxylammonium (**6**) and hydrazinium (**7**) salts were obtained by adding the corresponding base to a solution of **1** in ethanol and precipitating with diethyl ether. Due to coextraction of sulfuric acid after dediazonization pure **1** is obtained by dissolving **3** in 2 M hydrochloric acid, extracting with ethyl acetate, and removing the solvent in vacuo. Bis-(1-hydroxytetrazol-5-yl)triazene **8** was obtained as a monohydrate by dissolving 5-ATO in concentrated hydrochloric acid followed by diazotization with half an equivalent of sodium nitrite, adjusting to pH>10 with sodium hydroxide, and extraction into ethyl acetate. Compound **8** crystallized by slow evaporation of the solvent. Salts **9–14** were precipitated by adding the corresponding hydroxide (**9**, **10**), carbonate (**11–13**), or free base (**14**) dissolved in the minimal volume methanol to a solution of **8** in ethyl acetate. The copper ammonium salt **15** was obtained by precipitating the copper salt of **8** using copper sulfate followed by recrystallization from concentrated ammonia. When preparing compound **8**, it is important to make sure any trace amounts of the diazonium cation are removed by stirring under basic conditions (pH>10), since it is possible to co-extract it into the organic solvent. When removing the solvent in vacuo, a detonation occurred on slightly touching the solid with a plastic spatula, leading to the person performing the experiment being injured.

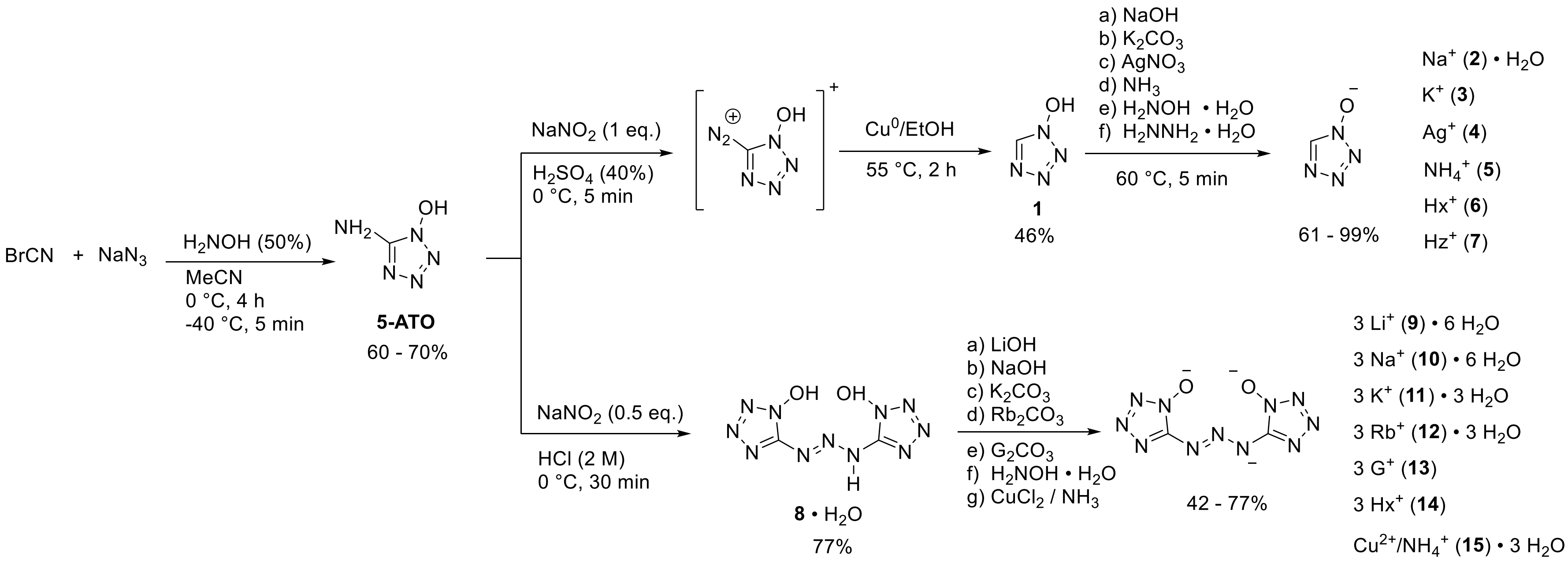

Scheme 1. Synthesis of 1-hydroxytetrazole (**1**) and its salts thereof (**2**–**7**), as well as the synthesis of bis(1-hydroxytetrazol-5-yl)-triazene (**8**) and its salts thereof (**9**–**15**). Hx$^+$: hydroxylammonium; Hz$^+$: hydrazinium; G$^+$: guanidinium.

2.2.2 Crystal Structures

The solid-state crystal structure of all of the compounds synthesized in this work, except compound **14**, were determined using low-temperature single-crystal X-ray diffraction. All of the data and parameters of the measurements, as well as of the refinements are given in the Supporting Information Table S1. All crystal densities are recalculated to their respective room temperature crystal density. Crystal datasets were deposited in the CSD database and can be obtained free of charge with the following codes: CCDC 2088975 (**1**), 2088974 (**2a**), 2088980 (**2b**), 2088977 (**3**), 2088979 (**4**), 2088985 (**5**), 2088982 (**6**), 2088986 (**7**), 2088988 (**8**), 2088983 (**9**), 2088978 (**10**), 2088976 (**11**), 2088987 (**12**), 2088981 (**13**) and 2088984 (**15**). 1-Hydroxytetrazole (**1**) crystallizes in the monoclinic space group $P2_1/n$. The density of **(1)** (1.63 g cm^{-3}) is comparable to that of the parent molecule 5-amino-1-hydroxytetrazole (1.66 g cm^{-3})[17] and is significantly higher than that of 1-aminotetrazole (1-AT, 1.48 g cm^{-3}).[23] Figure 2 shows the crystal structure of **1**, which forms wave-like layers in an ABA layering (along the b and c-axis) due to the two H atoms present per molecule participating in a total of three hydrogen bonds to two different 1-hydroxytetrazole molecules – one of which lies within the same wave-like layer (A), whereas the other is from a different layer (B) (Figure 2B).

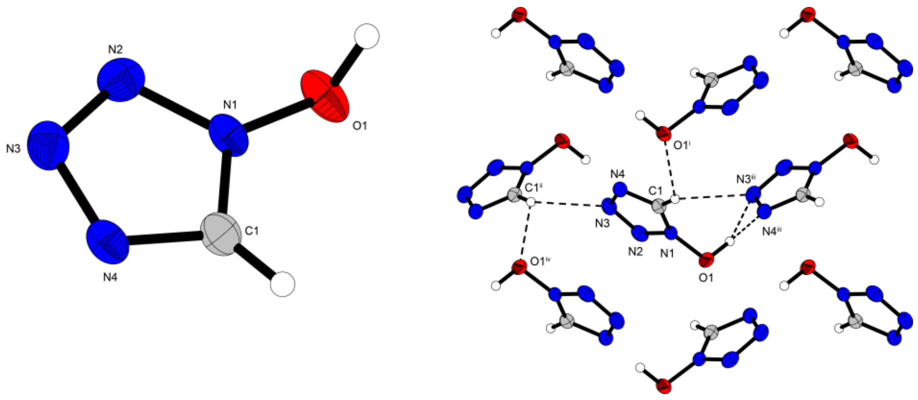

Figure 2. Crystal structure of compound **1** (**A**) as well as crystal packing (**B**) due to hydrogen bonds between four symmetrically distinct 1-hydroxytetrazole molecules; ellipsoids in all structures are shown with a probability of 50%; Selected bond lengths [Å]: O1–N1 1.354(2), N1–N2 1.337(2), N2–N3 1.299(2), N3–N4 1.353(2), N4–C1 1.316(2), C1–N1 1.324(2); Angles [°]: O1–N1–N2 121.17(11), O1–N1–C1 127.85(12), N1–N2–N3 105.07(11), N2–N3–N4 110.51(12), N3–N4–C1 106.81(12), N4–C1–N1 106.91(12). Selected hydrogen bond lengths [Å] and angles [°] (D–H···A, d(D–H), d(H···A), d(D···A), <(D–H···A)): O1–H2···N3^{iii}: 1.02(2), 1.57(2), 2.5878(16), 178(2); O1–H2···N4^{iii}: 1.02(2), 2.53(2), 3.4431(18), 150.1(17); C1–H1···O1^{i}: 0.913(16), 2.600(15), 3.2504(19), 128.8(12); C1^{ii}–H1^{ii}···N3: 0.913(16), 2.543(16), 3.325(2), 144.1(13). Symmetry codes: i) 5/2−x, ½+y, ½−z; ii) 1/2+x, ½−y, ½+z; iii) ½+x, ½−y, −1/2+z.

Interestingly, the respective C-N and N-N bond lengths within the tetrazole ring are nearly equivalent for compound **1** compared to 5-ATO and 1-AT. The bond length of between the hydroxy group and the tetrazole ring in **1** is the same as that reported for 5-ATO but is slightly shorter than the corresponding bond of the amine in 1-AT, thus explaining the higher density. All the bond lengths are in the typical range for N–N, C–N, and N–O single bonds, as well as N–N and C–N double bonds. The tetrazole ring in **1** is planar, with the oxygen atom slightly protruding from the plane (O1 – N1 – N2 – N3 = 5°). In all the salts of **1** investigated in this work, a planar arrangement of the oxygen atom with respect to the tetrazole-plane was observed for the 1-oxidotetrazolate anions.

Sodium 1-oxidotetrazolate (**2**) crystallizes as a monohydrate in two polymorphs, one in the triclinic space group *P*1 (**2a**) with a density of 1.81 g cm^{-3} and one in the orthorhombic space group $P2_12_12_1$ (**2b**) with a slightly lower density of 1.78 g cm^{-3}. The triclinic form is obtained by crystallization from water. whereas the orthorhombic polymorph from ethanol. Deprotonation of **1** results in marginal changes in the bond lengths of the tetrazole ring, with the N1–O1 bond length being generally shorter by 0.03–0.04 Å for all investigated salts in comparison with the neutral compound **1**. Potassium (**3**) and silver 1-oxidotetrazolate (**4**) both crystallize in the orthorhombic space group $Pna2_1$ with densities of 1.88 g cm^{-3} (**3**) and 3.48 g cm^{-3} (**4**), respectively. Figure 3 shows the crystal structure of **4**, where all silver cations are threefold coordinated by individual anions bridging between the cations.

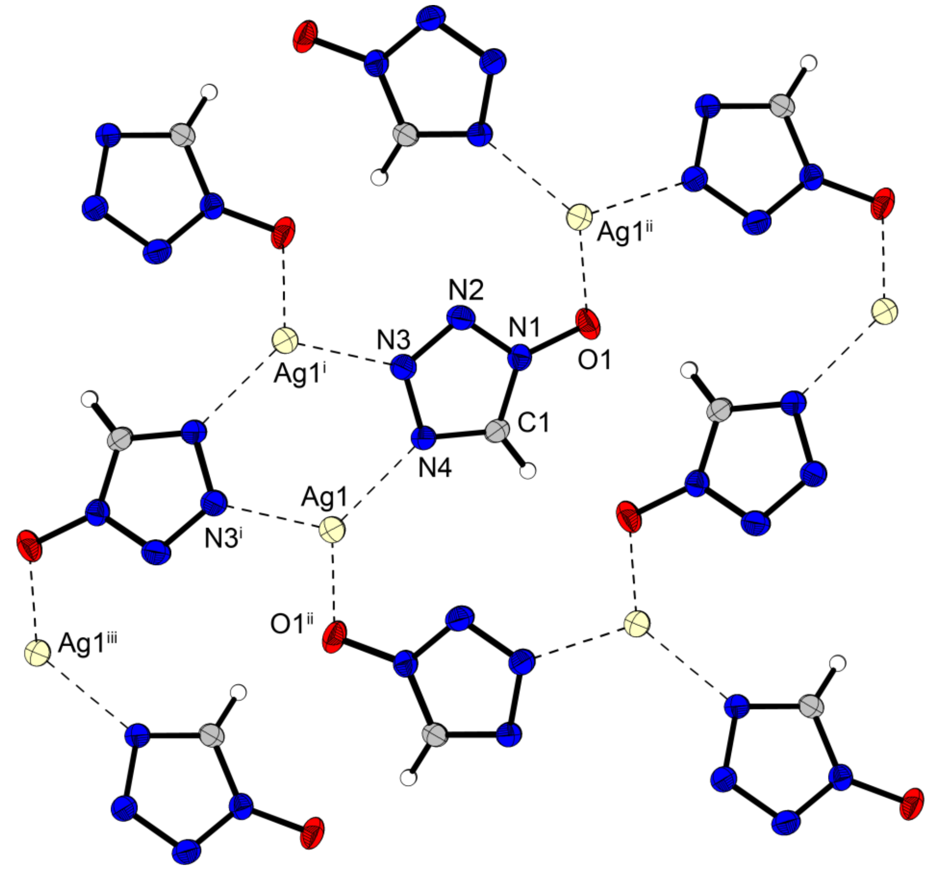

Figure 3. Crystal structure of silver 1-oxidotetrazolate (**4**) showing the coordination environment of the silver cations. Selected bond distances [Å]: N4–Ag1^{i}: 2.235(3), N3–Ag1^{ii}: 2.275(3), O1–Ag1^{iii}: 2.628(8), O1^{ii}–Ag1^{iv}: 2.406(7); angles [°]: O1^{ii}–Ag1–N4 124.97(12), N3^{i}–Ag1–N4 122.14(11), O1^{ii}–Ag1–N3^{i} 81.73(12); Symmetry codes: i) −x, 1−y, ½+z; ii) ½−x, ½+y, ½+z; iii) −1/2+x, ½−y, z.

Ammonium 1-oxidotetrazolate (**5**) also crystallizes in the orthorhombic space group $Pna2_1$ with four molecular units in the unit cell and a density of 1.40 g cm^{-3}. The crystal packing shows the presence of strong hydrogen bonds involving all the protons of the ammonium cations (Figure 4), with bonds towards three oxygen atoms and one nitrogen atom of four different 1-oxidotetrazolate anions. The observed density is the lowest of all the herein investigated compounds, and remarkably, it is even lower than that of comparable compounds such as ammonium 1-oxido-5-aminotetrazolate (1.50 g cm^{-3})[17] and ammonium 5-azidotetrazolate (1.61 g cm^{-3}).[24]

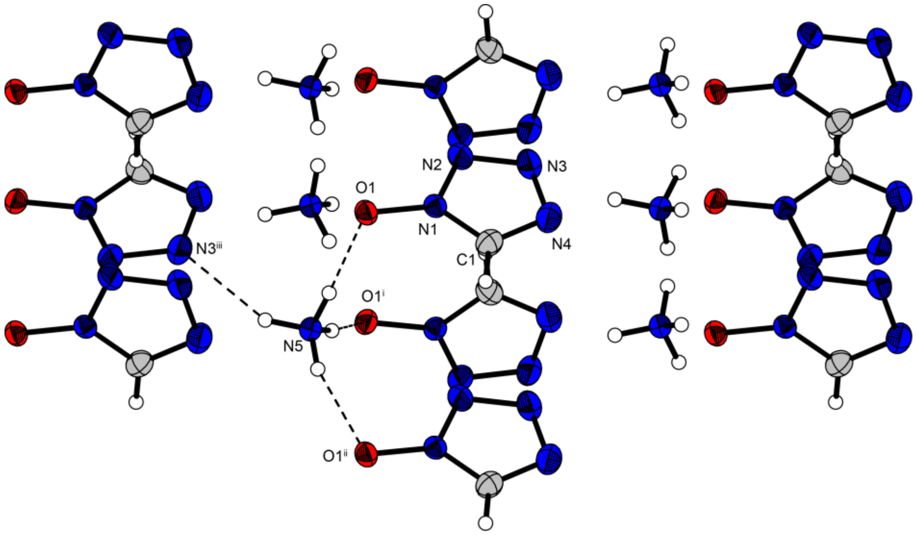

Figure 4. Packing of ammonium 1-oxidotetrazolate (**5**) showing layering due to the presence of hydrogen bonds between the hydrogen atoms of an ammonium cation with four distinct tetrazolate anions. Selected hydrogen bond lengths [Å] and angles [°] (D–H···A, d(D–H), d(H···A), d(D···A), <(D–H···A)): N5–H3···O1: 0.93(2), 1.86(2), 2.7762(18), 172(2); N5–H2···O1^{i}: 0.91(2), 1.90(2), 2.8036(19), 171(2); N5–H5···O1^{ii}: 0.90(3), 2.04(3), 2.9063(18), 162(2); N5–H4···N3^{iii}: 0.88(3), 2.18(2), 2.976(2), 151(2). Symmetry codes: i) 1/2+x,1/2−y, z; ii) x, −1+y, z; iii) 1−x, 1−y, −1/2+z.

Hydroxylammonium 1-oxidotetrazolate (**6**) crystallizes in the triclinic space group *P*1 with a density of 1.67 g cm^{-3} (@ 298 K) with one molecular unit in the unit cell as shown in Figure 5. Even although all the protons participate in hydrogen bonds, the density of **6** is significantly lower than that of comparable molecules such as dihydroxylammonium dinitro-bis-1,2,4-triazole-1,1'-diol (MAD-X1) (1.90 g cm^{-3} at 298 K)[6] or TKX-50 (1.92 g cm^{-3} at 298 K).[10]

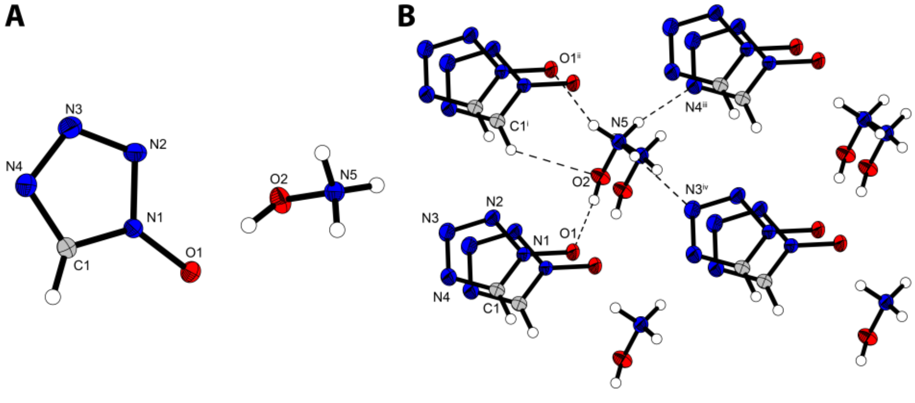

Figure 5. A) Crystal structure of hydroxylammonium 1-oxidotetrazolate (**6**). B) Packing due to the presence of strong hydrogen bonds involving of all the protons. Selected bond lengths [Å]: O1–N1 1.319(2), N1–N2 1.343(3), N2–N3 1.304(3), N3–N4 1.350(3), N4–C1 1.328(3), C1–N1 1.332(3), N5–O2 1.411(2); Angles [°] O1–N1–N2 122.13(2), N1–N2–N3 106.19(18), N2–N3–N4 110.74(18), N3–N4–C1 105.86(18), N4–C1–N1 108.36(18), C1–N1–O1 129.02(18); Selected hydrogen bond lengths [Å] and angles [°] (D–H···A, d(D–H), d(H···A), d(D···A), <(D–H···A)): O2–H2···O1: 0.82(4), 1.76(4), 2.576(2), 172(4); C1^{i}–H1^{i}···O2: 0.92(3), 2.57(3), 3.274(2), 134(2); N5–H5A···N3^{iv}: 0.81(3), 2.18(3), 2.913(3), 151(3); N5–H5B···N4^{iii}: 0.84(3), 2.05(3), 2.883(3), 170(3); N5–5C···O1^{ii}: 0.88(3), 1.93(3), 2.766(2), 160(3). Symmetry codes: i)−1+x, 1+y, z ii) x,1+y, z iii) −1+x, 1+y, −1+z iv) x, y, −1+z.

The lower density is also indicated by a lower packing coefficient[25] (Figure 6) of **6** (0.752) compared to TKX-50 (0.811) and MAD-X1 (0.797). Interestingly, the packing coefficient of **6** is comparable to the hydroxylammonium salt of 5-ATO (0.762) but is significantly higher than that for *1H*-tetrazole (0.675). This confirms the positive effect of *N*-oxidation on the density as stated by Fischer *et al.*,[17] whereas amination at the carbon position does not lead to significant changes in density. Generally, it can be assumed that the introduction of a bicycle (TKX-50, MAD-X1) is beneficial as it increases the packing coefficient, and thus increases the density.

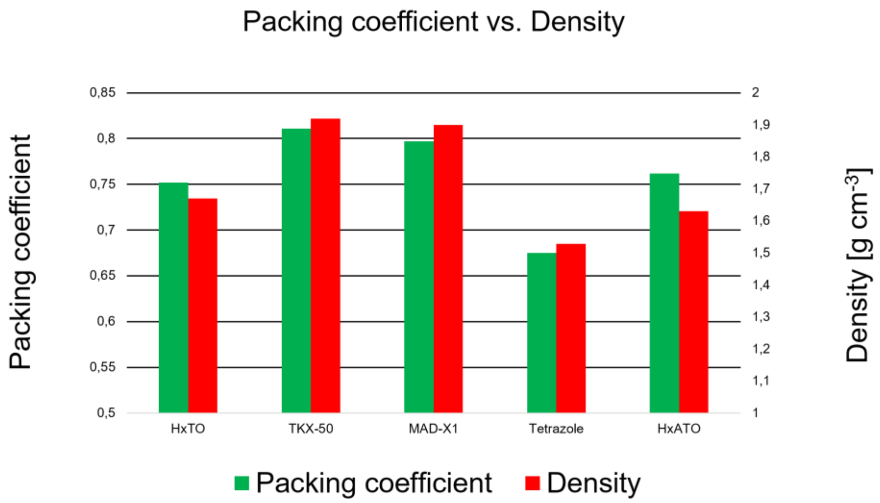

Figure 6. Packing coefficient and crystal densities of compound **6** (HxTO) and comparable compounds such as MAD-X1, TKX-50, tetrazole and hydroxylammonium 5-amino-1-oxidotetrazolate (HxATO).

Hydrazinium 1-oxidotetrazolate (**7**) crystallizes in the monoclinic space group *Pc* with two molecular units in the unit cell and a density of 1.6 g cm^{-3}, following the trend observed of hydrazinium salts having lower densities compared to the corresponding hydroxylammonium salts. The crystal structure of **7** is shown in Figure 7A, in which all hydrogen atoms are participating in hydrogen bonds resulting in one $N_2H_5^+$ cation being linked to four anions (Figure 7B).

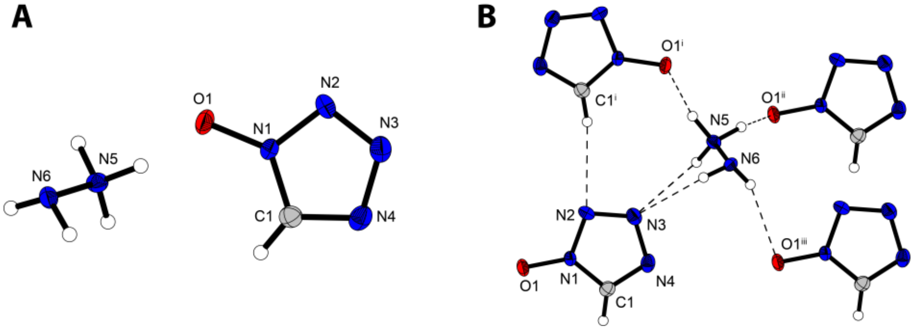

Figure 7. A) Crystal structure of hydrazinium 1-oxidotetrazolate (**7**). B) Packing due to strong hydrogen bonds of all protons, linking four distinct anions by one hydrazinium cation. Selected bond lengths [Å]: O1–N1 1.329(3), N1–N2 1.3336(3), N2–N3 1.316(4), N3–N4 1.344(4), N4–C1 1.329(4), C1–N1 1.329(4), N5–N6 1.443(4); Angles [°] O1–

N1–N2 120.8(2), N1–N2–N3 105.7(2), N2–N3–N4 111.0(3), N3–N4–C1 105.6(3), N4–C1–N1 108.6(3) , C1–N1–O1 130.1(3); Selected hydrogen bond lengths [Å] and angles [°] (D–H···A, d(D–H), d(H···A), d(D···A), <(D–H···A)): C1^{i}–H1^{i}···N2: 0.88(4), 2.59(4), 3.453(4), 165(3); N5–H5A···O1^{i}: 0.97(4), 1.80(5), 2.742(4), 165(4); N5–H5B···O1^{ii}: 0.99(4), 1.94(4), 2.826(4), 148(4), N5–H5C···N3: 0.89(4), 2.45(4), 3.047(4), 125(3); N6–H6A···N3: 0.91(3), 2.50(3), 3.147(4), 128(3), N6–H6B···O1^{iii}: 0.81(4), 2.36(4), 3.112(4), 156(3). Symmetry codes: i)−1+x, 1−y, −1/2+z ii) −1+x,−1+y, z iii) x, −1+y, z.

Bis-(1-hydroxytetrazol-5-yl)triazene (**8**) crystallizes in the monoclinic space group $P2_1/n$ as a monohydrate with a density of 1.80 g cm^{-3} and four molecular units in the unit cell (Figure 8). Due to the high acidity of the hydroxy group next to the azo-moiety, **8** crystallizes in a zwitterionic form where one tetrazole ring (N4) is protonated by its own hydroxy group (O1). While the self-protonation only leads to small differences in bond lengths between the two, changes in bond angles between the two moieties of up to 4.7° (N3–N4–C1 = 109.4(2), N10–N11–C2 = 104.7(1)) are observed. The largest difference in bond lengths and angles is observed for the triazene bridge. Within the triazene bridge, the N5–N6 bond (1.269(2) Å) is significantly shorter than the N6–N7 bond (1.327(2) Å), suggesting a higher bond order and therefore more double bond character for the N5–N6 bond. Additionally, the zwitterionic ring is more strongly bent towards the triazene bridge (N6–N5–C1 = 107.9(1)°) than its counterpart (N6–N7–C2 = 114.8(1)°). Compounds **9** and **10** both crystallize as hexahydrates in the triclinic space group P–1 with a density of 1.67 g cm^{-3} and 1.71 g cm^{-3}, respectively. Tripotassium bis(1-oxidotetrazol-5-yl)triazenide (**11**) crystallizes as a trihydrate in the orthorhombic space group $P2_12_12_1$ with a density of 1.98 g cm^{-3} (Figure 9) While complete deprotonation of **8** doesn't appear to lead to significant changes in bond lengths within the tetrazole rings, the double bond character of the N5-N6 bond in the triazene-bridge has now been more delocalized, which is indicated by the equality of the N5–N6 and N6–N7 bond lengths which are both 1.309(3) Å in **11**. The most drastic change in the structure of the anion resulting from complete deprotonation of **8** is the arrangement of the 1-oxidotetrazolate moieties with respect to the triazenide bridge. While the two moieties are not equally bent towards the triazene bridge in **8**, after complete deprotonation, the anion in **11** now shows two 1-oxidotetrazolate units which are oriented in the same way towards the triazenide bridge.

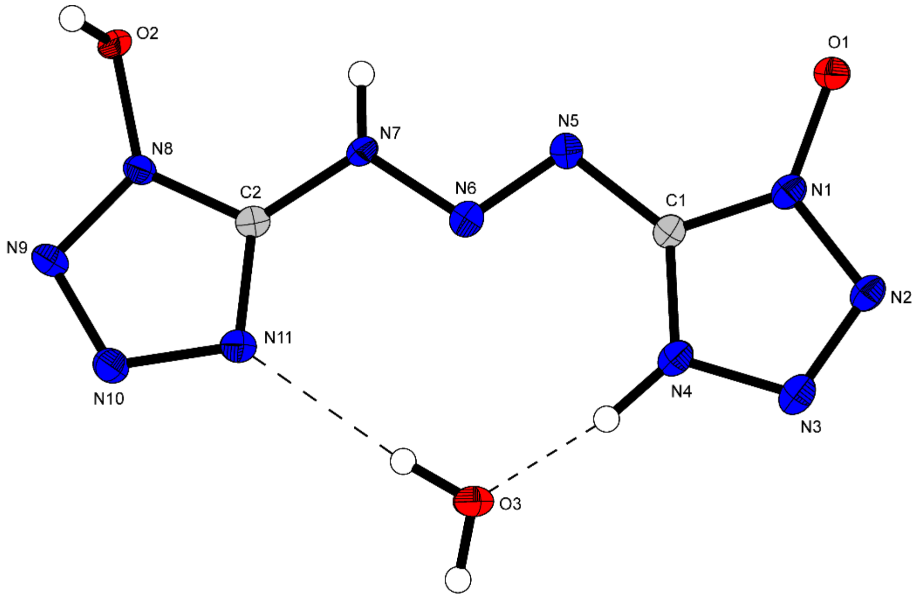

Figure 8. Crystal structure of bis(1-hydroxytetrazol-5-yl)triazene monohydrate (**8**), showing the zwitterionic form. Selected bond lengths [Å]: O1–N1 1.321(2), N8–O2 1.349(2), N3–N4 1.338(2), N4–C1 1.337(2), C1–N5 1.382(2), N5–N6 1.269(2), N6–N7 1.317(2), N7–C2 1.368(2), N11–N10 1.361(2), N11–C2 1.318(2); Angles [°] O1–N1–N2 121.8(1), O1–N1–C1 128.3(1), O2–N8–N9 123.5(1), O2–N8–C2 126.6(1), N3–N4–C1 109.4(2), N10–N11–C2 104.7(1), C1–N5–N6 107.9(1), C2–N7–N6 114.8(1).

Compounds **12** and **13** both crystallize as trihydrates. It was not possible to obtain crystals of compound **14** suitable for single crystal X-ray diffraction experiments. The crystal structures of compounds **9, 10**, **12** and **13** are shown in the Supporting Information (Figures S1-S4).

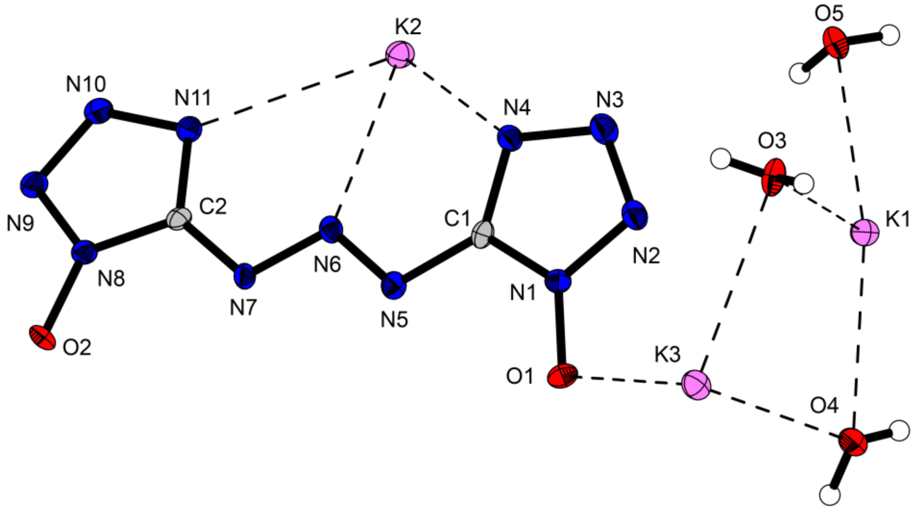

Figure 9. Crystal structure of tripotassium bis(1-oxidotetrazol-5-yl)triazenide trihydrate (**11**). Selected bond lengths of the anion [Å]: O1–N1 1.330(3), N1–N2 1.352(4), N2–N3 1.311(3), N3–N4 1.359(3), N4–C1 1.340(4), C1–N1 1.339(4), C1–N5 1.384(4), N5–N6 1.309(3), N6–N7 1.309(3), N7–C2 1.375(4), C2–N8 1.346(4), N8–O2 1.330(3), N8–N9 1.346(2), N9–N10 1.316(4), N10–N11 1.359(3), N11–C2 1.340(4); Angles [°]: O1–N1–N2 122.0(2), O1–N1–C1 129.1(3), O2–N8–N9 122.8(2), O2–N8–C2 127.7(2), C1–N4–N3 105.5(2), C2–N11–N10 105.9(3), N6–N5–C1 111.4(3), N6–N7–C2 111.1(2).

Ammonium copper bis(1-oxidotetrazol-5-yl)triazenide (**15**) crystallizes in the triclinic space group *P*–1 with two molecular units in the unit cell and a density of 1.96 g cm^{-3} (Figure 10). As was observed for compound **11**, the bond lengths and angles of the anion are not significantly influenced by deprotonation. The drastic conformational change observed in **11** is a result of the unequal coordination of the copper(II)-cation with the two 1-oxidotetrazolate moieties. Whereas the most favored conformation for compounds **8**—**14** is apparently a triazene bridge with a double (*E*-) arrangement along N5–N6 and N6–N7, threefold coordination of the copper(II) cation by the anion in **15** results in rotation along the N6–N7 bond, resulting in a *E/Z*- conformation along N5–N6 and N6–N7, respectively. Interestingly, the copper(II) cation shows a nearly perfectly square pyramidal coordination by the anion and two aqua ligands. The angles involving O3 and atoms forming the equatorial plane (O1, N8, N11, O4) range from 89.13° (O1–Cu1–O3) to 104.42° (O3–Cu1–N11).

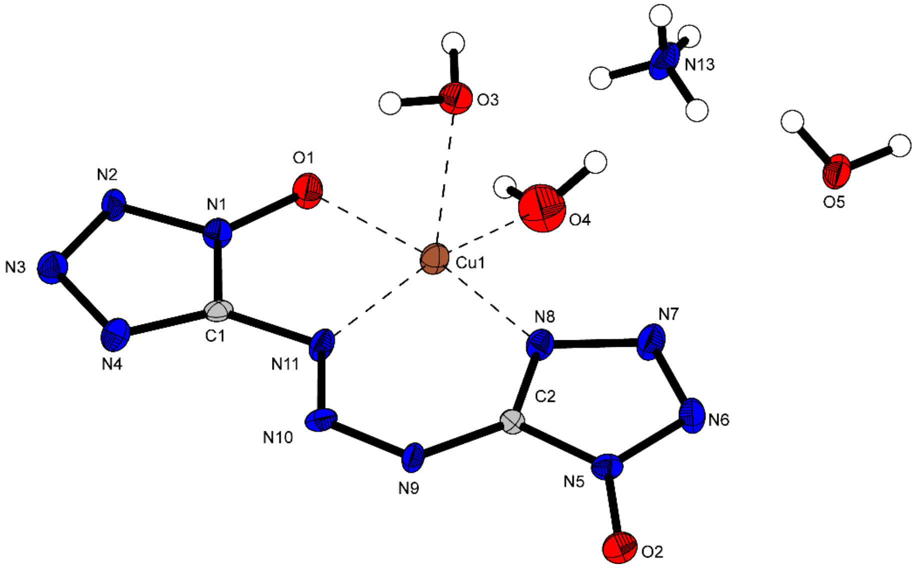

Figure 10. Crystal structure of ammonium copper bis(1-oxidotetrazol-5-yl)triazenide trihydrate (**15**). Selected bond lengths [Å]: O1–N1 1.347(6), N1–N2 1.341(6), N2–N3 1.321(6), N3–N4 1.374(6), N4–C1 1.323(7), C1–N1 1.338(7), C1–N5 1.379(6), N5–N6 1.343(6), N6–N7 1.284(6), N7–C2 1.386(6), C2–N8 1.354(7), N8–O2 1.305, N8–N9 1.352(6), N9–N10 1.304(6), N10–N11 1.351(6), N11–C2 1.336(7), Cu1–O1 1.982(4), Cu1–N11 1.993(4), Cu1–N8 1.938(4), Cu1–O3 2.332(4), Cu1–O4 1.977(5); Angles [°]: O1–N1–C1 125.1(4), O2–N8–C2 128.4(4), C1–N5–N6 113.8(4), N6–N7–C2 121.3(4), O1–Cu1–O3 89.19(14), O1–Cu1–O4 93.85(17), O1–Cu1–N8 169.87(16), O1–Cu1–N11 85.17(15), O3–Cu1–N8 95.84(16), O3–Cu1–N11 104.42(16), O3–Cu1–O4 91.82(17).

2.2.3 NMR Spectroscopy

NMR spectroscopy was performed in DMSO-d$_6$, D$_2$O or acetone-d$_6$ and spectra are depicted in the Supporting Information. The ^{1}H NMR spectrum of compound **1** in DMSO-d$_6$ shows one signal at $\delta = 9.48$ ppm for the proton attached to the carbon atom of the tetrazole ring. The ^{13}C NMR of compound **1** in DMSO-d$_6$ shows one signal at $\delta = 137.7$ ppm, which is shifted upfield compared to the starting material 5-ATO (δ = 150.5 ppm). Deprotonation of **1** leads to a shift in the signals observed in the ^{1}H as well as ^{13}C NMR spectra. For example, the ^{1}H NMR of potassium 1-oxidotetrazolate (**3**) in D_2O shows one signal at δ = 8.54 ppm, which is shifted upfield compared to the free acid **1**. Additionally, the signal in the ^{13}C NMR of **3** in D_2O is shifted downfield to δ = 164.5 ppm. The ^{13}C NMR of compound **8** in DMSO-d$_6$ shows one signal at δ = 150.0 attributing both carbon atoms (Figure 11). Compared to the parent molecule, 5-ATO (δ = 150.5 ppm), the carbon atoms of **8** are, contrary to **1**, not drastically shifted. Deprotonation of **8** results in a downfield shift of the signal. The ^{13}C NMR of the tripotassium salt (**11**) in D_2O shows one signal at δ = 153.2 ppm. The influence of deprotonation of **8** on the ^{13}C NMR signal is not as prominent as that observed for compound **1**.

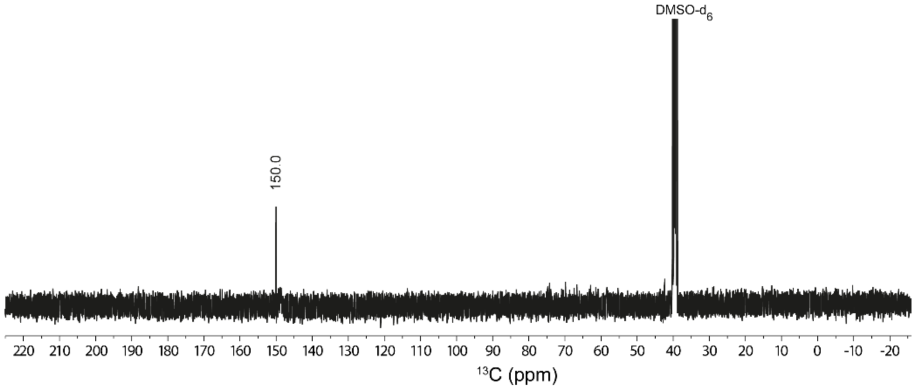

Figure 11. ^{13}C NMR spectrum of compound **8** in DMSO-d$_6$, showing only one carbon atom.

2.2.4 Physicochemical Properties

Thermal behavior. The thermal behaviors of compounds **1**–**7** are shown in Figure 12. Compound **1** shows a decomposition temperature of 186 °C (Figure 12), and two endothermic events at 80 °C and 96 °C, which TGA indicates as corresponding to a phase transition and/or melting point. Compound **1**, 1-hydroxytetrazole, exhibits a higher thermal stability compared to the similar compound 5-amino-1-hydroxytetrazole[17], and is almost identical with that of 1-aminotetrazole (182 °C).[23] Compound **2** shows loss of water at 110 °C and a decomposition temperature of 273 °C, which is the highest of all of the 1-hydroxytetrazole salts reported in this work (Figure 12). The potassium (**3**) and the silver (**4**) salts, which are both free of water, show decomposition temperatures of 236 °C and 211 °C, respectively. Both of these salts detonate violently on reaching their critical temperatures. The silver salt (**4**) also immediately detonates on contact with a flame. Compound **5** shows an endothermic event at 180 °C, which corresponds to the loss of ammonia due to evaporation, as indicated by the onset of mass loss in the TG. The endothermic event seamlessly evolves into an exothermic decomposition at 188 °C, at which temperature a significant mass loss of 85.5 wt.% occurs as shown by the TG (Figure 12).

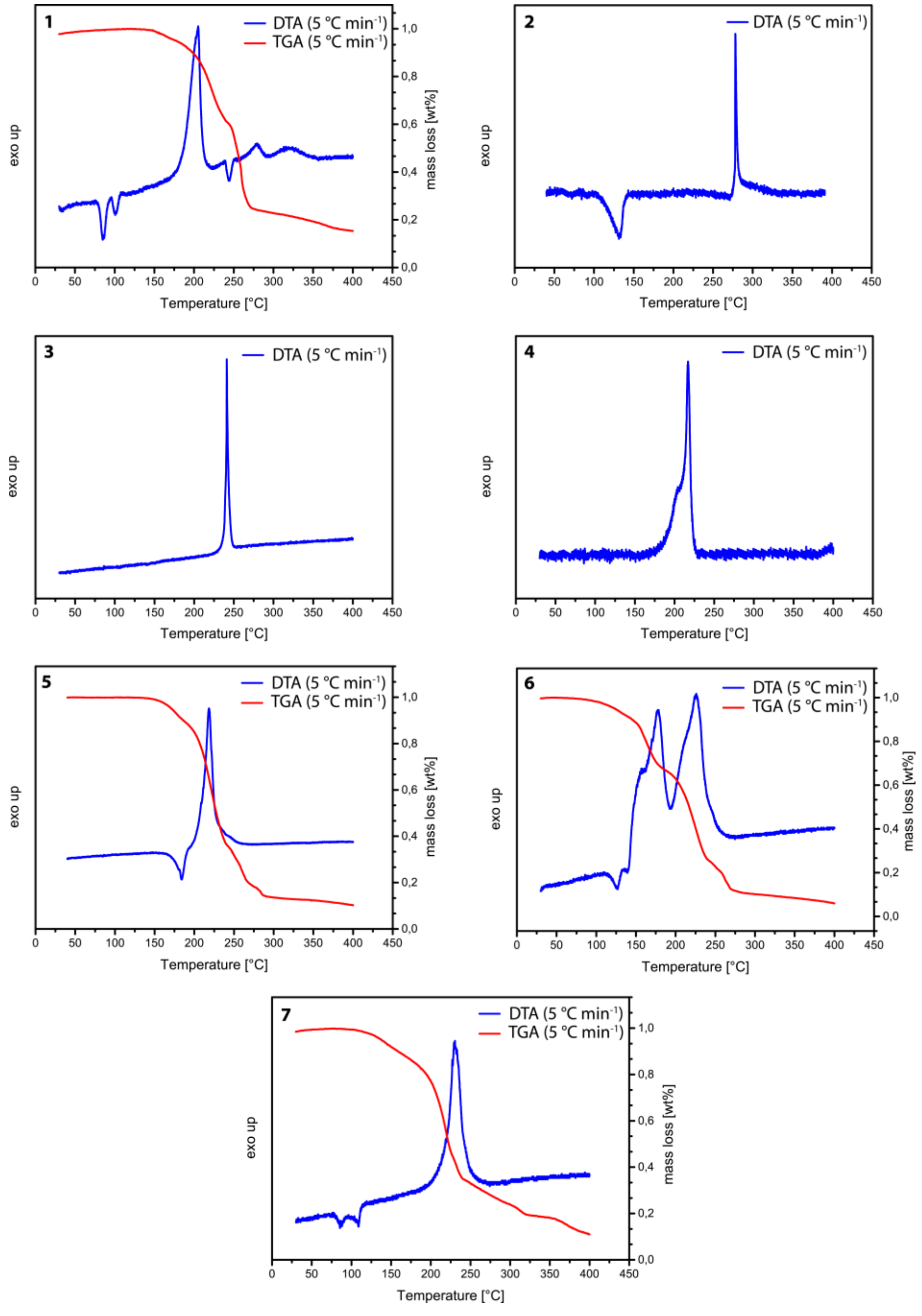

Figure 12. Thermal analytic measurements (DTA) of HTO (**1**), NaTO • H$_2$O (**2**), KTO (**3**), AgTO (**4**), NH$_4$TO (**5**), HxTO (**6**), HzTO (**7**). For compounds **1**, **5**, **6**, and **7**, additional TGA measurements were performed to analyze the endothermic events observed in the DTA.

The same behavior is observed for the hydroxylammonium salt **6**. Figure 12 shows an endothermic event at 115 °C, which evolves into the first of two exothermic decomposition events at 159 °C. TGA measurements revealed the first decomposition to correspond to the decomposition of hydroxylamine accompanied by a weight loss of 24.9 wt.%. The second exothermic event with onset at 203 °C is attributed to the decomposition of the residual 1-Hydroxytetrazole. Compound **7** shows an exothermic decomposition temperature of 213 °C, with two endothermic events in addition observed at 80 °C and 103 °C. The TG measurement of **7** shows a mass loss of 13 wt.% with onset at 103 °C, which corresponds to the evaporation of hydrazine. Therefore, it can be assumed that the exothermic event corresponds to thermal decomposition of residual neutral compound **1**, rather than the hydrazinium salt itself. Figure 13 shows that bis(1-hydroxytetrazol-5-yl)triazene monohydrate (**8**) is thermally stable up to 95 °C. Despite being a monohydrate, no endothermic event which could be attributed to a loss of water was observed in the DTA spectrum of **8**. Due to stabilization by crystal water, **8** decomposes immediately on reaching a temperature (95 °C) high enough to remove the crystal water molecule. The alkaline salts **9** – **12** all show the presence of endothermic events between 85–135 °C corresponding to the loss of water in each compound (Figure 13). In general, these compounds are very thermally stable, with decomposition temperatures of between 292 °C (**12**) and 335 °C (**10**). Interestingly, the triguanidinium salt **13** shows no endothermic event in the DTA, which confirms loss of water already occurring at room temperature. This agrees with the measured elemental analysis, which fits perfectly with the values calculated for the anhydrous salt, which shows a thermal stability of up to 222 °C. The hydroxylammonium salt **14** shows an endothermic event at 104 °C which evolves into an exothermic decomposition, in behavior like that of compound **5** (Figure 12). This can be explained by the evaporation of hydroxylamine occurring, which results in the formation of an unstable residue that immediately decomposes at 148 °C. Interestingly, compound **15** shows no loss of water until the onset of decomposition at 198 °C, indicating strong coordinative bonds of the aqua ligands to the copper(II) cation as well as a high stability of the crystal water.

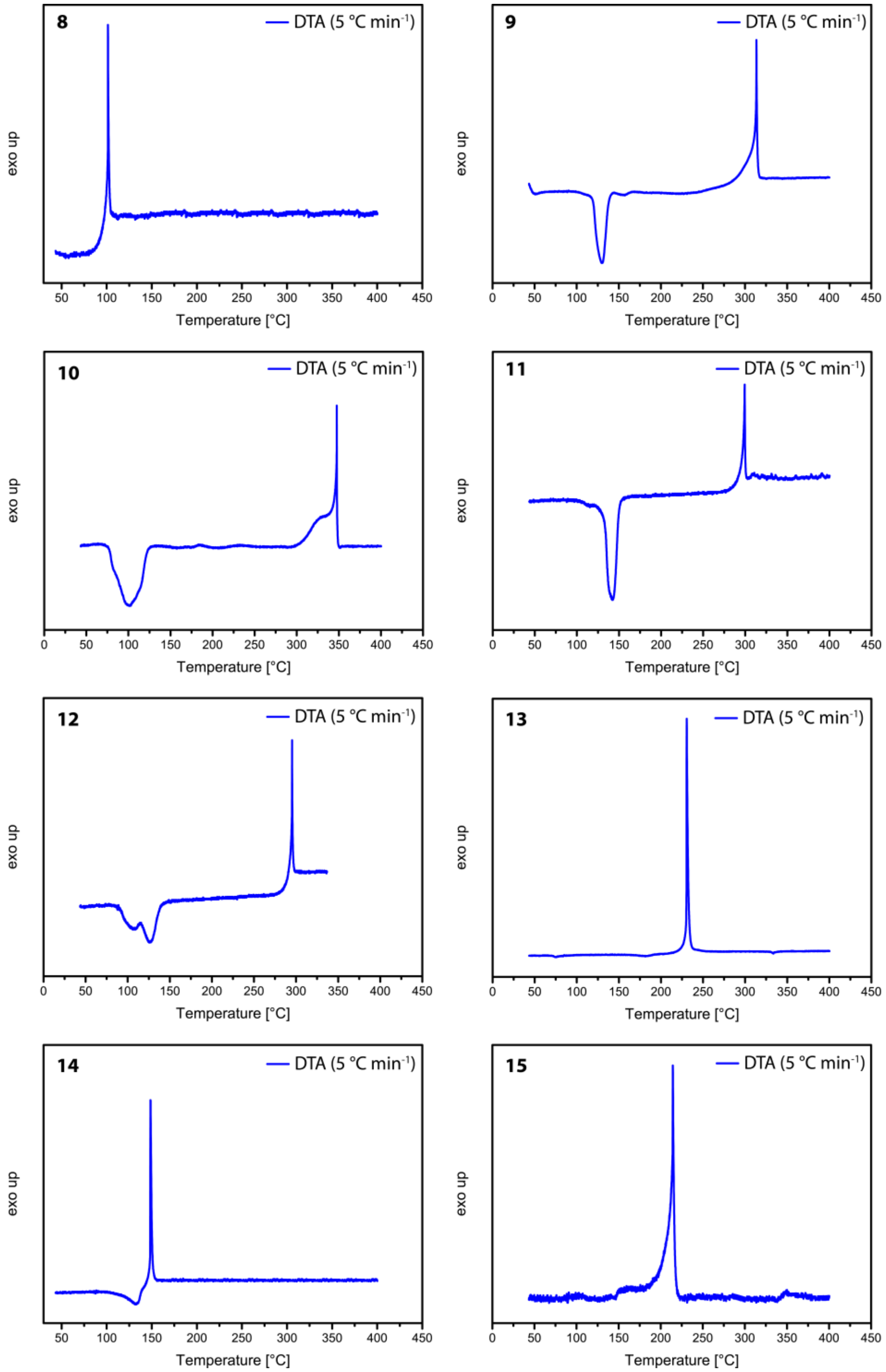

Figure 13. DTA measurements of bis-(1-hydroxytetrazol-5-yl)triazene monohydrate (**8**), Li_3T • 6 H_2O (**9**), Na_3T • 6 H_2O (**10**), K_3T • 3 H_2O (**11**), Rb_3T • 3 H_2O (**12**), Gua_3T (**13**), Hx_3T (**14**), $Cu(NH_4)T$ (**15**).

Heats of formation, sensitivity, and detonation parameters. The calculated and measured explosive properties of all compounds are listed in Tables 1 and 2. Heat of formations were calculated by applying the atomization method using room temperature CBS-4M enthalpies.[24-28] A detailed explanation of the calculation can be found in the Supporting Information. Compound **1** shows a comparable heat of formation (252 kJ mol^{-1}) to its parent molecule 5-amino-1-hydroxytetrazole (256 kJ mol^{-1}). However, **1** possesses a slightly lower density than its parent compound, which results in a minor reduction of the detonation velocity (8405 m s^{-1}) and detonation pressure (269 kbar) compared to 5-ATO (8609 m s^{-1}, 298 kbar). While the impact sensitivity of **1** (10 J) is comparable to that of 5-ATO (10 J), the friction sensitivity is higher for **1** (28 N) than for 5-ATO (108 N), meaning **1** is more sensitive towards external stimuli than 5-ATO. In contrast, the hydroxylammonium (**6**) salt of 1-hydroxytetrazole shows a higher heat of formation (259 kJ mol^{-1} (**6**)) compared to the corresponding salt of 5-ATO (Hx$^+$: 227 kJ mol^{-1}). Compound **6** shows a very high detonation velocity (9284 m s^{-1}) compared to compound **5** (8013 m s^{-1}), which is due to the higher density of **6** 1.67 g cm^{-3} (**5**: 1.40 g cm^{-3}). Although compound **7** shows a slightly lower density (1.60 g cm^{-3}) than compound **6**, the significantly higher enthalpy of formation of **7** (346 kJ mol^{-1}) results in its even higher detonation velocity of 9437 m s^{-1}. Compounds **6** and **7** both outperform even HMX in terms of detonation velocity. While compound **5** is completely insensitive (IS >40 J, FS >360 N), compounds **6** (IS = 6 J, FS 240 N) and **7** (IS = 26 J, FS >360 N) show higher impact sensitivities, but crucially, are comparable to (**6**) or less sensitive (**7**) than HMX. The monohydrate sodium salt (**2**) is completely insensitive towards external stimuli, whereas the potassium (**3**) salt is more sensitive (IS = 4 J, FS = d54 N). The silver salt (**4**) is the most sensitive out of all of the compounds, and has to be classified as extremely sensitive, with an impact sensitivity below 1 J and a friction sensitivity of 1 N. The silver salt shows the characteristics of a primary explosive, immediately detonating on contact with a flame (Figure 14).

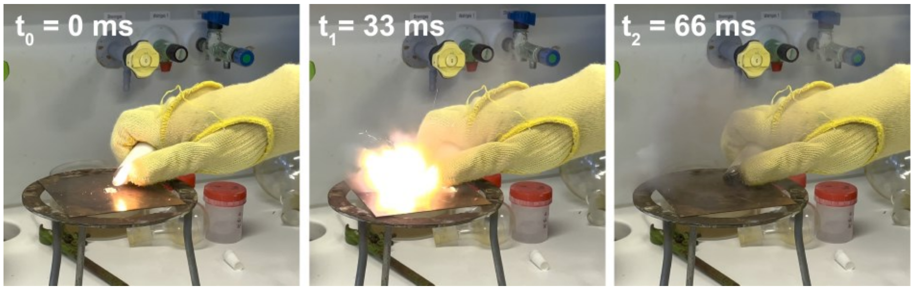

Figure 14. Initiation of silver 1-oxidotetrazolate (**4**) by a lighter. t_0) right before the flame is in contact with the compound; t_1) immediate detonation of **4** on contact with the flame; t_2) smoke residue after detonation.

Due to this behavior, the initiation capability of **4** towards Pentaerythrityltetranitrat (PETN) was tested, whereby it was found that 50 mg of **4** were able to initiate 200 mg of pressed PETN (Figure 15). Compound **2a** shows a low detonation velocity of 7555 m s^{-1}, which is attributed to its low heat of formation as well as being a monohydrate. The orthorhombic form **2b** exhibits a slightly lower detonation velocity (7428 m s^{-1}) than triclinic **2a**, due to the lower density of **2b**. Interestingly, the potassium salt **3** exhibits an even lower detonation velocity than **2a/b**, even though it has a higher density (1.88 g cm^{-3}). Due to the high heat of formation of compound **8** (734 kJ mol^{-1}), it shows an outstanding detonation velocity of 9433 m s^{-1}, as well as a very high detonation temperature (3940 K), which even outperforms HMX. However, in addition to its low thermal stability (decomposition temperature of only 100 °C), compound **8** is also very sensitive towards impact (<1 J) and friction (4 N), preventing application of **8** as a high-performance secondary explosive

Table 1. Energetic properties of 1-hydroxytetrazole (**1**) and its salts **2**–**7**.

	1	**2a**	**2b**	**3**	**4**	**5**	**6**	**7**	**HMX**[q]
Formula	CH_2N_4O	$CH_3N_4O_2Na$	$CH_3N_4O_2Na$	CHN_4OK	CHN_4OAg	CH_5N_5O	$CH_5N_5O_2$	CH_6N_6O	$C_4H_8N_8O_8$
M [g mol^{-1}]	86.05	126.05	126.05	124.14	192.91	103.09	119.08	118.10	296.16
IS [J][a]	10	>40	>40	4	<1	>40	6	26	7[31]
FS [N][b]	28	>360	>360	54	1	>360	240	>360	112[31]
ESD [mJ][c]	960	1080	1080	63	<0.28	>1500	>1500	740	200[31]
ρ [g cm^{-3}][d]	1.63	1.81	1.78	1.88	3.47	1.40	1.67	1.60	1.91
N [%][e]	65.11	44.45	44.45	45.13	29.04	67.94	58.81	71.16	37.84
Ω_{CO} [%][f]	−18.59	−12.36	−12.36	−32.22	−8.29	−38.80	−20.15	−40.64	0.0
Ω_{CO2} [%][g]	−37.19	−25.39	−25.39	−45.11	−16.59	−54.33	−33.59	−54.19	−21.61
T_{endo} [°C][h]	80, 96	110	110	–	–	180	115	80, 103	–
T_{exo} [°C][i]	186	273	273	236	211	188	159, 203	213	275
$\Delta_f H^0$ [kJ mol^{-1}][j]	252	−366	−364	47	–	207	259	346	75
$\Delta_f H^0$ [kJ kg^{-1}][k]	3042	−2803	−2780	441	–	2170	2325	3100	369
EXPLO5 V6.05.04									
$-\Delta_{Ex}U^0$ [kJ kg^{-1}][l]	5333	2792	2817	3265	–	4663	6137	5409	5699
T_{det} [K][m]	3744	2070	2088	2669	–	2978	3666	3114	3622
V_0 [L kg^{-1}][n]	469	451	456	426	–	549	461	485	401
P_{CJ} [kbar][o]	269	189	182	187	–	213	331	319	378
V_{det} [m s^{-1}][p]	8405	7555	7428	7056	–	8013	9284	9437	9192

[a] Impact sensitivity (BAM drophammer (1 of 6)). [b] Friction sensitivity (BAM friction tester (1 of 6)). [c] Electrostatic discharge device (OZM research). [d] From X-ray diffraction analysis recalculated to 298 K. [e] Nitrogen content. [f] Oxygen balance towards CO formation [g] Oxygen balance towards CO_2 formation [h] Temperature of endothermic event (DTA; β = 5 °C min^{-1}). [i] Temperature of exothermic event (DTA; β = 5 °C min^{-1}). [j] Calculated enthalpy of formation. [k] Calculated mass related enthalpy of formation. [l] Energy of explosion. [m] Detonation temperature. [n] Volume of detonation products (assuming only gaseous products). [o] Detonation pressure at Chapman-Jouguet point. [p] Detonation velocity. [q] Values based on the EXPLO5 Database.

Table 2. Energetic properties of bis-(1-hydroxytetrazol-5-yl)triazene monohydrate (**8**) and its salts **9**–**15**.

	8	**9**	**10**	**11**	**12**	**13**	**14**	**15**
Formula	$C_2H_5N_{11}O_3$	$C_2H_{12}N_{11}O_8Li_3$	$C_2H_{12}N_{11}O_8Na_3$	$C_2H_6N_{11}O_5K_3$	$C_2H_6N_{11}O_5Rb_3$	$C_5H_{18}N_{20}O_2$	$C_2H_{12}N_{14}O_5$	$C_2H_{10}N_{12}O_5Cu$
M [g mol^{-1}]	234.14	339.01	387.16	381.45	520.55	390.34	312.22	345.73
IS [J][a]	<1	>40	>40	>40	>40	>40	4	11
FS [N][b]	4	>360	>360	>360	288	>360	128	288
ρ [g cm^{-3}][c]	1.80	1.67	1.71	1.97	2.55	1.59[p]	1.79[p]	1.96
N [%][d]	66.66	45.45	39.80	40.39	29.60	71.77	62.81	48.62
Ω_{CO} [%][e]	−10.38	−7.08	−6.20	−25.17	−9.22	−49.19	−15.37	−13.88
Ω_{CO2} [%][f]	−24.23	−16.52	−14.46	−33.56	−15.37	−69.69	−25.62	−23.14
T_{endo} [°C][g]	–	122	85	135	99, 121	–	123	–
T_{exo} [°C][h]	100	311	339	294	292	222	146	205
$\Delta_f H°$ [kJ mol^{-1}][i]	734	−1505	−1480	−1475	–	158	464	−53
$\Delta_f H°$ [kJ kg^{-1}][j]	3248	−4303	−3705	−3786	–	559	1633	−38
EXPLO5 V6.05.04								
$-\Delta_{Ex}U^0$ [kJ kg^{-1}][k]	5896	3568	3003	1239	–	2106	5330	3173
T_{det} [K][l]	3940	2208	2150	1316	–	1736	3299	2654
V_0 [L kg^{-1}][m]	429	476	474	420	–	501	437	402
P_{CJ} *[kbar]*[n]	362	213	173	143	–	201	364	249
V_{det}*[m s^{-1}]*[o]	9433	7941	7352	6546	–	7870	9663	7725

[a] Impact sensitivity (BAM drophammer (1 of 6)). [b] Friction sensitivity (BAM friction tester (1 of 6)). [c] From X-ray diffraction analysis recalculated to 298 K. [d] Nitrogen content. [e] Oxygen balance towards CO formation [f] Oxygen balance towards CO_2 formation [g] Temperature of endothermic event (DTA; β = 5 °C min^{-1}). [h] Temperature of exothermic event (DTA; β = 5 °C min^{-1}). [i] Calculated enthalpy of formation. [j] Calculated mass related enthalpy of formation. [k] Energy of explosion. [l] Detonation temperature. [m] Volume of detonation products (assuming only gaseous products). [n] Detonation pressure at Chapman-Jouguet point. [o] Detonation velocity. [p] Density measured pycnometrically.

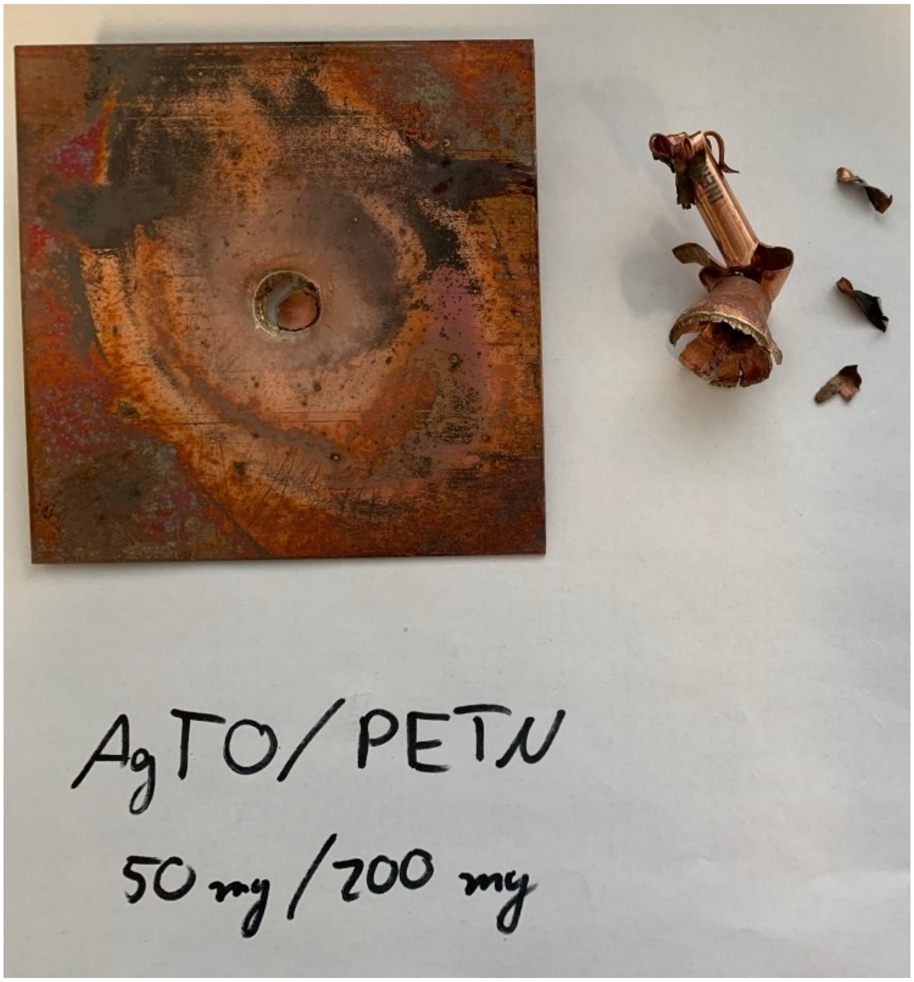

Figure 15. Positive initiation of PETN (200 mg) by **4** (50 mg) indicated by the perforated witness plate.

Complete deprotonation of **8** forming the alkali salts **9** (Li^+), **10** (Na^+), and **11** (K^+) results in a drastic decrease in energetic performance. This is due to the presence of a large amount of crystal water which results in highly exothermic enthalpy of formations (-1475 – -1505 kJ mol^{-1}). Additionally, the absence of protons, not included as crystal water, leads to a decrease in detonation velocity within the series of increasing cation weight. Compound **13** crystallizes as a trihydrate, but completely loses its crystal water by drying in air at room temperature, as confirmed by elemental analysis as well as IR spectroscopy. Therefore, the heat of formation and detonation properties were calculated for the anhydrous compound, showing an endothermic heat of formation (158 kJ mol^{-1}). The rather low density for **13** of 1.59 g cm^{-3}, detonation velocity of 7870 m s^{-1} and detonation pressure of 201 kbar means it lies in the range of the other alkali salts. Compound **14** was obtained as an amorphous solid which is thermally stable up to 146 °C. It has an endothermic heat of formation of 464 kJ mol^{-1} and density of 1.79 g cm^{-3}, with a calculated detonation velocity of 9663 m s^{-1}, which surpasses that of HMX. Compound **14** has a calculated detonation pressure of 364 kbar as well as moderate sensitivities to external sources (IS = 4 J, FS = 128 N), which are comparable to those of HMX.

2.3 Conclusion

For the first time, an adequate selective synthesis, circumventing the formation of 2-hydroxytetrazole, of 1-hydroxytetrazole is reported by the *dediazonization* of the readily available precursor, 5-amino-1-hydroxytetrazole. Diazotization was followed by reduction of the diazonium cation using either hypophosphorous acid or a mixture of ethanol/copper(0). While ethanol/copper(0) was inferior to hypophosphorous acid in terms of yields, this procedure was chosen for the synthesis of 1-hydroxytetrazole (**1**), as it is far easier to workup. Diazotization of 5-ATO with half an equivalent of sodium nitrite resulted in the formation of bis(1-hydroxytetrazol-5-yl)triazene monohydrate (**8**). Compound **1** was converted to the sodium (**2**), potassium (**3**), silver (**4**), ammonium (**5**), hydroxylammonium (**6**) and hydrazinium (**7**) salts. Compound **8** was converted to the lithium (**9**), sodium (**10**), potassium (**11**), rubidium (**12**), guanidinium (**13**), hydroxylammonium (**14**), and ammonium copper(II) (**15**) salts. All compounds, except **14**, were analyzed using single crystal X-ray diffraction, as well as NMR, IR, and EA analysis. The thermal stabilities were investigated, sensitivities towards external stimuli were determined, and the detonation performances were calculated using the EXPLO5 code. Compound **1** shows a good detonation performance (8405 m s^{-1}) which can compete with that of RDX. The detonation performance, thermal stability and sensitivities of **1** could be adjusted to meet the requirements of a primary explosive by formation of the silver salt (**4**), or to those of a highly energetic secondary explosive by formation of **6** (VoD = 9284 m s^{-1}) or **7** (VoD = 9437 m s^{-1}), which surpass the detonation velocity of even HMX (9192 m s^{-1}). Bis(1-hydroxytetrazol-5-yl)triazene monohydrate (**8**) is a highly sensitive (IS <1 J, FS = 4 N) material, with the performance of a high energetic secondary explosive (VoD = 9433 m s^{-1}). Salts of **8** are completely insensitive due to the incorporation of up to six equivalents of crystal water (for the lithium salt), which is accompanied by a drastic loss of performance. The hydroxylammonium salt (**14**) is an anhydrous compound (as proven by elemental analysis), which shows a very high detonation velocity of 9663 m s^{-1} but with impact and friction sensitivities comparable to those of PETN (IS = 4 J, FS = 80 N).

2.4 Experimental Section

1-Hydroxytetrazole (**1**): 5-Amino-1-hydroxytetrazole (1.00 g, 10 mmol) was dissolved in sulfuric acid (16 mL, 40%) and cooled below 5 °C with an ice-bath. Sodium nitrite (684 mg, 10 mmol) dissolved in water (20 mL) was slowly added keeping the temperature below 5 °C. After complete addition, the reaction solution was stirred for 5 minutes, and was then added to a flask containing a mixture of elemental copper (628 mg, 10 mmol) and ethanol (20 mL) which was warmed to 55 °C. After stirring for 2 hours, the reaction mixture was extracted by DCM/Et_2O (1:1, 200 mL), the organic phase was dried over magnesium sulfate and the solvent was removed *in vacuo*. The yellow oil which was obtained contained 1-hydroxytetrazole and residual sulfuric acid as a by-product. Pure 1-hydroxytetrazole was obtained by dissolving the potassium salt (**3**) in hydrochloric acid (2 M), followed by extraction into ethyl acetate. After drying the organic phase over $MgSO_4$, the solvent was removed by a stream of nitrogen gas, and 1-hydroxytetrazole (**1**) was obtained as a colorless crystalline solid in moderate yield (400 mg, 4.65 mmol, 46%).

^{1}H NMR (acetone-*d*$_6$, 25 °C): $\delta = 9.23$ ppm (s, 1H, C*H*); **^{13}C NMR** (acetone-*d*$_6$, 25 °C): $\delta = 137.5$ ppm (N4-*C*); **IR** (ATR, cm^{-1}): $\tilde{v} = 3001$ (w), 2952 (w), 2924 (w), 1652 (vs), 1575 (s), 1416 (s), 1351 (s), 1284 (vs), 1244 (s), 1214 (vs), 1106 (w), 1059 (s), 1004 (m), 976 (s), 952 (s), 902 (s), 841 (vs), 750 (vs), 737 (s), 695 (vs), 667 (s), 635 (s), 588 (s); **DTA** (5 °C min^{-1}): 186 °C (T_{exo}); **elemental analysis** calcd. [%] for CH_2N_4O (86.05): C 13.96, H 2.34, N 65.11; found: C 14.15, H 2.31, N 64.96; **BAM drophammer**: 10 J, **BAM friction tester**: 28 N, **ESD**: 960 mJ.

Sodium 1-oxidotetrazolate monohydrate (**2**): Compound **1** (500 mg, 5.81 mmol) was dissolved in methanol (10 mL) and sodium hydroxide (232 mg, 5.81 mmol) in methanol was added. After stirring for 5 minutes, the precipitate was filtered off and recrystallized from ethanol. Sodium 1-oxidotetrazolate monohydrate (**2**) was obtained as yellow crystals in quantitative yield (625 mg, 5.78 mmol, 99%).

^{1}H NMR (DMSO-*d*$_6$, 25 °C): $\delta = 8.07$ ppm (s, 1H, C*H*); **^{13}C NMR** (DMSO-*d*$_6$, 25 °C): $\delta = 133.1$ ppm (N4-*C*); **IR** (ATR, cm^{-1}): $\tilde{v} = 3465$ (m), 3427 (m), 3281 (w), 3150 (m), 1652 (m), 1472 (m), 1433 (vw), 1407 (m), 1384 (w), 1350 (vw), 1309 (w), 1247 (s), 1192 (m), 1158 (w), 1114 (w), 1065 (w), 982 (w), 824 (m), 738 (m), 715 (w), 670 (m), 529 (s), 481 (vs); **DTA** (5 °C min^{-1}): 273 °C (T_{exo}); **elemental analysis** calcd. [%] for $CH_3N_4NaO_2$ (126.05): C 9.53, H 2.40, N 44.45; found: C 9.71, H 2.45, N 43.54; **BAM drophammer**: >40 J, **BAM friction tester**: >360 N, **ESD**: 1080 mJ.

Potassium 1-oxidotetrazolate (**3**): Compound **5** (500 mg, 4.85 mmol) was dissolved in water (10 mL) and potassium carbonate (670 mg, 4.85 mmol) was added. The solvent was completely dried off in air, and the solid obtained was extracted with hot ethanol and filtered. After adding diethyl ether, pure potassium 1-oxidotetrazolate (**3**) was filtered off and obtained as a yellow powder in good yield (518 mg, 4.17 mmol, 86%). Crystals suitable for single crystal X-Ray measurements were obtained by recrystallization from water.

^{1}H NMR (DMSO-*d*$_6$, 25 °C): δ = 8.45 ppm (s, 1H, C*H*); **^{13}C NMR** (DMSO-*d*$_6$, 25 °C): δ = 135.1 ppm (N4-*C*); **IR** (ATR, cm^{-1}): ṽ = 1632 (m), 1622 (m), 1475 (m), 1435 (w), 1402 (m), 1386 (m), 1369 (m), 1352 (w), 1290 (s), 1234 (vs), 1187 (s), 1137 (m), 1124 (w), 1098 (m), 1067 (m), 1012 (m), 968 (m), 923 (w), 874 (w), 836 (m), 817 (s), 781 (w), 731 (m), 718 (m), 690 (s), 675 (m), 645 (m), 625 (w), 585 (w), 477 (m); **DTA** (5 °C min^{-1}): 236 °C (T_{exo}); **elemental analysis** calcd. [%] for $CHKN_4O$ (124.14): C 9.68, H 0.81, N 45.13; found: C 9.93, H 1.03, N 44.96; **BAM drophammer**: 4 J, **BAM friction tester**: 54 N, **ESD**: 63 mJ.

Silver 1-oxidotetrazolate (**4**): Compound **1** (150 mg, 1.74 mmol) was dissolved in ethanol (10 mL) and silver nitrate (296 mg, 1.74 mmol) was added. After stirring for several minutes, the precipitate was filtered off and washed with ethanol (10 mL) and diethyl ether (10 mL). Silver 1-oxidotetrazolate (**4**) was obtained as a white powder in quantitative yield (332 mg, 1.72 mmol, 99%). Crystals suitable for single crystal X-Ray measurements were obtained by a three-layer diffusion crystallization over several days.

IR (ATR, cm^{-1}): ṽ = 3100 (m), 1454 (s), 1414 (vs), 1404 (s), 1371 (w), 1340 (w), 1301 (w), 1246 (vs), 1206 (s), 1159 (m), 1108 (s), 1058 (w), 995 (w), 859 (s), 810 (vw), 732 (s), 701 (m), 667 (m), 495 (s); **DTA** (5 °C min^{-1}): 211 °C (T_{exo}); **elemental analysis** calcd [%] for $CHAgN_4O$ (192.91): C 6.23, H 0.52, N 29.04; found: C 6.11, H 0.63, N 28.38; **BAM drophammer**: <1 J, **BAM friction tester**: 1 N, **ESD**: <0.28 mJ.

Ammonium 1-oxidotetrazolate (**5**): Compound **5** was obtained by passing gaseous ammonia through a solution of **1** in DCM/Et_2O. The precipitate in the DCM/Et_2O solution was filtered off, extracted with methanol (40 mL), prior to diethyl ether being added. The precipitate was filtered off and dried in air. Ammonium 1-oxidotetrazolate (**5**) was obtained as an off-white powder in moderate yield (629 mg, 6.11 mmol, 61%). Crystals suitable for single crystal X-Ray measurements were obtained by recrystallization from water.

^{1}H NMR (DMSO-*d*$_6$, 25 °C): δ = 8.44 ppm (s, 1H, C*H*); **^{13}C NMR** (DMSO-*d*$_6$, 25 °C): δ = 135.1 ppm (N4-*C*); **IR** (ATR, cm^{-1}): ṽ = 3465 (m), 3427 (m), 3281 (w), 3150 (m), 1652 (m), 1472 (m), 1433 (vw), 1407 (m), 1384 (w), 1350 (vw), 1309 (w), 1247 (s), 1192 (m), 1158 (w), 1114 (w), 1065 (w), 982 (w), 824 (m), 738 (m), 715 (w), 670 (m), 529 (s), 481 (vs); **DTA** (5 °C min^{-1}): 188 °C (T_{exo}); **elemental analysis** calcd [%] for CH_5N_5O (103.09): C 11.65, H 4.89, N 67.94; found: C 11.26, H 4.89, N 68.58; **BAM drophammer**: >40 J, **BAM friction tester**: >360 N, **ESD**: >1500 mJ.

Hydroxylammonium 1-oxidotetrazolate (**6**): Compound **1** (500 mg, 5.81 mmol) was dissolved in ethanol (10 mL) and aqueous hydroxylamine solution (50%, 479 mg, 7.20 mmol) was added. After stirring for 5 minutes at 50 °C, the precipitate was filtered off, washed with diethyl ether and dried in air. Hydroxylammonium 1-oxidotetrazolate (**6**) was obtained as a yellowish powder in good yield (546 mg, 4.59 mmol, 79%). Crystals suitable for single crystal X-Ray measurements were obtained by recrystallization from water.

^{1}H NMR (DMSO-*d*$_6$, 25 °C): δ = 8.51 ppm (s, 1H, C*H*); **^{13}C NMR** (DMSO-*d*$_6$, 25 °C): δ = 135.0 ppm (N4-*C*); **IR** (ATR, cm^{-1}): $\tilde{\nu}$ = 3160 (m), 2889 (s), 2791 (s), 1864 (w), 1687 (w), 1643 (w), 1597 (w), 1468 (s), 1433 (s), 1399 (vs), 1379 (s), 1333 (m), 1233 (vs), 1182 (s), 1147 (m), 1098 (s), 1046 (w), 967 (s), 824 (s), 717 (vs), 666 (s), 485 (m), 421 (w); **DTA** (5 °C min^{-1}): 159 (T_{exo}), 203 (T_{exo}); **elemental analysis** calcd [%] for $CH_5N_5O_2$ (119.08): C 10.09, H 4.23, N 58.81; found: C 10.26, H 3.86, N 58.01; **BAM drophammer**: 6 J, **BAM friction tester**: 240 N, **ESD**: >1500 mJ.

Hydrazinium 1-oxidotetrazolate (**7**): Compound **1** (500 mg, 5.81 mmol) was dissolved in ethanol (10 mL) and hydrazinium hydrate (100%, 291 mg, 5.81 mmol) was added. After stirring for 5 minutes at 50 °C, the precipitate was filtered off, washed with diethyl ether and dried in air. Hydrazinium 1-oxidotetrazolate (**7**) was obtained as a white powder in quantitative yield (685 mg, 5.80 mmol, 99%). Crystals suitable for single crystal X-Ray measurements were obtained by recrystallization from water.

^{1}H NMR (DMSO-*d*$_6$, 25 °C): δ = 8.52 ppm (s, 1H, C*H*); **^{13}C NMR** (DMSO-*d*$_6$, 25 °C): δ = 135.1 ppm (N4-*C*); **IR** (ATR, cm^{-1}): $\tilde{\nu}$ = 3297 (m), 3139 (s), 2754 (s), 2628 (s), 1587 (s), 1532 (s), 1455 (m), 1400 (s), 1379 (s), 1336 (w), 1286 (w), 1267 (w), 1238 (s), 1217 (s), 1185 (m), 1134 (s), 1106 (s), 1077 (s), 1042 (m), 957 (vs), 832 (m), 779 (w), 760 (vw), 732 (s), 717 (s), 667 (m), 483 (m), 417 (m), 404 (m); **DTA** (5 °C min^{-1}): 213 °C (T_{exo}); **elemental analysis** calcd [%] for

CH_6N_6O (118.10): C 10.17, H 5.12, N 71.16; found: C 10.11, H 5.25, N 71.33; **BAM drophammer**: 26 J, **BAM friction tester**: >360 N, **ESD**: 740 mJ.

Bis(1-hydroxytetrazol-5-yl)triazene monohydrate (**8**): Aqueous sodium nitrite (85.3 mg, 1.24 mmol, 5 mL) was added to a solution of 5-amino-1-hydroxytetrazole (250 mg, 2.47 mmol) in hydrochloric acid (2 M, 5 mL) and cooled to 0–5 °C. After stirring for 30 minutes, the pH of the solution was adjusted to pH ≥ 10 by adding sodium hydroxide solution (32%) and stirred at 35 °C for another 30 minutes. The pH of the solution was then adjusted to pH ≤ 2 using hydrochloric acid (37%) and extracted into ethyl acetate (4 x 50 mL). After slowly evaporating the solvent in air, bis(1-hydroxytetrazol-5-yl)triazene monohydrate (**8**) was obtained as a brown crystalline solid. Due to the immediate onset of slow decomposition of **8**, elemental analysis and IR spectroscopic analysis were not performed. Sensitivity measurements were performed immediately after synthesis was complete without determining the purity of the sample.

^{13}C NMR (DMSO-d$_6$, 25 °C): $\delta = 150.0$ ppm; **DTA** (5 °C min^{-1}): 100 °C (T$_{exo}$); **BAM drophammer**: <1 J, **BAM friction tester**: 4 N.

General procedure for the synthesis of bis(1-oxidotetrazol-5-yl)triazenide salts:

Stoichiometric equivalents of hydroxides, carbonates or free bases (**14**), dissolved in methanol/water were added to a solution of **8** in ethyl acetate. The resulting solution was stirred for 5 minutes or until precipitation was complete. The precipitate was filtered off and recrystallized from water.

Trilithium bis(1-oxidotetrazol-5-yl)triazenide hexahydrate (**9**): Compound **9** was obtained as brown needles in good yield (324 mg, 0.96 mmol, 77%).

^{13}C NMR (D_2O, 25 °C): $\delta = 153.0$ ppm; **IR** (ATR, cm^{-1}): $\tilde{\nu}$ = 3338 (s), 3085 (s), 1650 (m), 1579 (m), 1544 (s), 1518 (s), 1455 (m), 1435 (m), 1354 (s), 1325 (s), 1251 (s), 1243 (s), 1227 (s), 1176 (s), 1152 (s), 1125 (m), 1035 (m), 1011 (m), 963 (m), 826 (s), 753 (s), 732 (s), 649 (vs), 544 (vs), 489 (vs), 481 (vs), 465 (s), 457 (vs), 419(vs), 410 (vs); **DTA** (5 °C min^{-1}): 311 °C (T$_{exo}$); **elemental analysis** calcd [%] for $C_2H_{12}Li_3N_{11}O_8$ (339.01): C 7.09, H 3.57, N 45.45; found: C 7.38, H 3.59, N 45.24; **BAM drophammer**: > 40 J; **BAM friction tester**: > 360 N; **ESD**: ≥ 1500 mJ.

Trisodium bis(1-oxidotetrazol-5-yl)triazenide hexahydrate (**10**): Compound **10** was obtained as yellow-brown needles in moderate yield (283 mg, 0.73 mmol, 59%).

^{13}C NMR (D_2O, 25 °C): δ = 153.1 ppm; **IR** (ATR, cm^{-1}): $\tilde{\nu}$ = 3334 (m), 1664 (m), 1639 (m), 1518 (m), 1497 (m), 1444 (m), 1426 (m), 1357 (s), 1302 (s), 1256 (s), 1242 (s), 1210 (s), 1168 (m), 1147 (m), 1114 (m), 955 (m), 817 (m), 753 (m), 735 (m), 653 (m), 645 (m), 582 (s), 561 (vs), 561 (vs), 512 (vs), 491 (vs), 412 (s); **DTA** (5 °C min^{-1}): 338 °C (T_{exo}); **elemental analysis** calcd. [%] for $C_2H_{12}N_{11}Na_3O_8$ (387.16): C 6.20, H 3.12, N 39.80; found: C 6.19 , H 2.83, N 39.02; **BAM drophammer**: > 40 J; **BAM friction tester**: > 360 N; **ESD**: 1060 mJ.

Tripotassium bis(1-oxidotetrazol-5-yl)triazenide trihydrate (**11**): Compound **11** was obtained as yellow needles in moderate yield (248 mg, 0.65 mmol, 53%).

^{13}C NMR (D_2O, 25 °C): δ = 153.2 ppm; **IR** (ATR, cm^{-1}): $\tilde{\nu}$ = 3489 (m), 3478 (m), 3262 (m), 3230 (m), 3084 (m), 1688 (w), 1654 (w), 1521 (m), 1505 (s), 1444 (m), 1419 (m), 1320 (vs), 1254 (s), 1238 (s), 1224 (s), 1213 (s), 1159 (m), 1134 (m), 1023 (w), 999 (w), 952 (w), 808 (s), 747 (m), 734 (s), 716 (m), 678 (m), 620 (s), 561 (s), 480 (m), 458 (s); **DTA** (5 °C min^{-1}): 292 °C (T_{exo}); **elemental analysis** calcd [%] for $C_2H_6K_3N_{11}O_5$ (381.44): C 6.30, H 1.59, N 40.39; found: C 6.32, H 1.46, N 40.43; **BAM drophammer**: >40 J; **BAM friction tester**: > 360 N; **ESD**: >1500 mJ.

Trirubidium bis(1-oxidotetrazol-5-yl)triazenide trihydrate (**12**): Compound **12** was obtained as yellow-brown needles in moderate yield (392 mg, 0.75 mmol, 61%).

^{13}C NMR (D_2O, 25 °C): δ = 153.2 ppm; **IR** (ATR, cm^{-1}): $\tilde{\nu}$ = 3486 (m), 3158 (s), 2159 (w), 1668 (w), 1562 (vw), 1516 (m), 1498 (s), 1428 (m), 1409 (m), 1309 (vs), 1249 (s), 1227 (vs), 1208 (s), 1163 (m), 1146 (s), 1027 (m), 1002 (w), 952 (w), 811 (s), 744 (s), 733 (s), 675 (m), 667 (m), 624 (s), 595 (s), 572 (s), 518 (s), 501 (s), 492 (s), 435 (m); **DTA** (5 °C min^{-1}): 292 °C (T_{exo}); **elemental analysis** calcd [%] for $C_2H_6N_{11}O_5Rb_3$ (520.55): C 4.61, H 1.16, N 29.60; found: C 4.75, H 1.04, N 29.53; **BAM drophammer**: > 40 J; **BAM friction tester**: 288 N; **ESD**: ≥ 750 mJ.

Triguanidinium bis(1-oxidotetrazol-5-yl)triazenide (**13**): Compound **13** was obtained as yellow plates in good yield (328 mg, 0.84 mmol, 68%).

^{13}C NMR (D_2O, 25 °C): δ = 157.9, 153.0 ppm; **IR** (ATR, cm^{-1}): $\tilde{\nu}$ = 3046 (vw), 3349 (vw), 3404 (w) , 2815 (w), 1644 (w), 1519 (vw), 1490 (w), 1434 (vw), 1412 (m), 1340 (vw), 1299 (w), 1242 (w), 1229 (w), 1213 (w), 1158 (w), 1140 (w), 1121 (w), 999 (vw), 954 (vw), 880 (vw), 812 (w), 771 (w), 738 (w), 721 (w), 680 (w), 654 (w), 589 (w), 554 (w), 526 (w), 504 (w), 491 (w), 430 (w), 405 (w); **DTA** (5 °C min^{-1}): 222 °C (T_{exo}); **elemental analysis** calcd [%] for $C_5H_{18}N_{20}O_2$ (390.24):

C 15.39, H 4.65, N 71.77; found: C 15.33, H 4.65, N 70.31; **BAM drophammer**: >40 J; **BAM friction tester**: >360 N; **ESD**: >1500 mJ.

Tri(hydroxylammonium) bis(1-oxidotetrazol-5-yl)triazenide (**14**): Compound **14** was obtained as a pale yellow solid in moderate yield (228 mg, 0.73 mmol, 59%).

IR (ATR, cm^{-1}): $\tilde{\nu}$ = 3597 (m), 3511 (w), 3157 (w), 3059 (m), 3048 (m), 2858 (m), 2724 (s), 2445 (s), 1606 (s), 1558 (m), 1519 (m), 1497 (m), 1472 (s), 1460 (s), 1440 (s), 1415 (s), 1338 (w), 1286 (m), 1263 (s), 1245 (s), 1234 (s), 1199 (vs), 1146 (s), 1126 (s), 1029 (m), 1016 (m), 1004 (m), 991 (m), 933 (s), 886 (m), 810 (s), 742 (m), 727 (m), 710 (m), 692 (m), 668 (m), 645 (s), 576 (m), 483 (m), 455 (m), 440 (s), 426 (m), 403 (s); **DTA** (5 °C min^{-1}): 148 °C (T_{exo}); **elemental analysis** calcd [%] for $C_2H_{12}N_{14}O_5$ (312.21): C 7.69, H 3.87, N 62.81; found: C 8.05 , H 3.64, N 61.28; **BAM drophammer**: 4 J; **BAM friction tester**: 128 N; **ESD**: ≥ 750 mJ.

Ammonium copper(II) bis(1-oxidotetrazol-5-yl)triazenide (**15**): Aqueous sodium nitrite (85.3 mg, 1.24 mmol, 5 mL) was added to a solution of 5-amino-1-hydroxytetrazole (250 mg, 2.47 mmol) in hydrochloric acid (2 M, 5 mL) and cooled to 0–5 °C. After stirring for 30 minutes, the pH of the solution was adjusted to pH ≥ 10 by adding aqueous sodium hydroxide solution (32%), and stirred at 35 °C for another 30 minutes. Copper sulfate pentahydrate (926.4 mg, 3.71 mmol) dissolved in water (5 mL) was added to the reaction solution, and after stirring for 5 minutes, the precipitate was filtered off and washed with water. Recrystallization from aqueous ammonia resulted in compound **15** as green crystalline plates in moderate yield (205 mg, 0.52 mmol, 42%).

IR (ATR, cm^{-1}): $\tilde{\nu}$ = 3323 (m), 3259 (m), 3176 (m), 1609 (m), 1536 (m), 1466 (m), 1433 (w), 1374 (vs), 1319 (s), 1298 (s), 1250 (vs), 1237 (vs), 1219 (vs), 1122 (m), 1052 (m), 1005 (m), 976 (m), 833 (m), 750 (s), 715 (s), 679 (s), 659 (s), 608 (s), 574 (s), 536 (s), 499 (s), 476 (s), 457 (s), 445 (s), 433 (s); DTA (5 °C min^{-1}): 212 °C (T_{exo}); **elemental analysis** calcd [%] for $C_2H_{10}CuN_{12}O_5$ (345.73): C 6.95, H 2.92, N 48.62; found: C 6.68, H 2.98, N 48.63; **BAM drophammer**: 11 J; **BAM friction tester**: 288 N; **ESD**: 380 mJ.

2.5 Acknowledgements

Financial support of this work by the Ludwig-Maximilian University of Munich (LMU), the Office of Naval Research (ONR) under grant no. N00014-19-1-2078 as well as the Strategic Environmental Research and Development Program (SERDP) under grant no. WP19-1287 is gratefully acknowledged.

Keywords: tetrazoles • explosives • triazenes • diazotation • dediazonization

2.6 References

[1] WHO, World Health Organization, Geneva, **2019**.

[2] O. Chung, T. Csikós, T. Unger, Journal of Human Hypertension **1999**, *13*, 11-20.

[3] T. M. Klapötke, *Energetic Materials Encyclopedia*, De Gruyter, **2021**.

[4] N. Fischer, K. Karaghiosoff, T. M. Klapötke, J. Stierstorfer, *Z. Anorg. Allg. Chem.* **2010**, *636*, 735-749.

[5] T. M. Klapötke, *Chemistry of High-Energy Materials*, De Gruyter, **2019**.

[6] A. A. Dippold, T. M. Klapötke, *J. Am. Chem. Soc.* **2013**, *135*, 9931-9938.

[7] D. E. Chavez, D. A. Parrish, L. Mitchell, G. H. Imler, *Angew. Chem. Int. Ed.* **2017**, *56*, 3575-3578.

[8] Y. Wang, Y. Liu, S. Song, Z. Yang, X. Qi, K. Wang, Y. Liu, Q. Zhang, Y. Tian, *Nat. Commun.* **2018**, *9*, 2444.

[9] Y. Cao, W. Lai, T. Yu, Y. Liu, B. Wang, *FirePhysChem* **2021**, *1*, 27-32.

[10] N. Fischer, D. Fischer, T. M. Klapötke, D. G. Piercey, J. Stierstorfer, *J. Mater. Chem.* **2012**, *22*, 20418-20422.

[11] E. Oliveri-Mandala, T. Passalacqua, *Gazz. Chim. Ital.* **1913**, *43 II*, 473.

[12] J. A. Bladin, *Chem. Ber.* **1892**, *25*, 1411-1413.

[13] J. Pallazzo, Atti della Accademia Nazionale dei Lincei, Classe di Scienze Fisiche, Matematiche e Naturali, Rendiconti **1910**, *5*, 220.

[14] S. Maffei, G. F. Bettinetti, *Ann. Chim. (Rome, Italy)* **1956**, *46*, 812-815.

[15] M. Begtrup, P. Vedsø, *J. Chem. Soc., Perkin Trans. 1* **1995**, 243-247.

[16] R. G. Giles, N. J. Lewis, P. W. Oxley, J. K. Quick, *Tetrahedron Lett*. **1999**, *40*, 6093-6094.

[17] D. Fischer, T. M. Klapötke, D. G. Piercey, J. Stierstorfer, *Chem. Eur. J.* **2013**, *19*, 4602-4613.

[18] H. Zollinger, *Diazotization of Amines and Dediazoniation of Diazonium Ions*, John Wiley & Sons, Ltd., Weinheim, **2009**.

[19] N. Kornblum, *Org. React.* pp. 262-340.

[20] T. S. Basu Baul, D. Dutta, A. Duthie, M. F. C. Guedes da Silva, *Inorg. Chim. Acta* **2017**, *455*, 627-637.

[21] J. W. Staples, J. M. Stine, E. Mäki-Lohiluoma, E. Steed, K. M. George, C. M. Thompson, E. L. Woodahl, *Food Chem. Toxicol*. **2020**, *146*, 111785.

[22] K. A. Hofmann, H. Hock, *Ber. Dtsch. Chem. Ges*. **1910**, *43*, 1866-1871.

[23] N. Szimhardt, M. H. H. Wurzenberger, L. Zeisel, M. S. Gruhne, M. Lommel, J. Stierstorfer, *J. Mater. Chem. A* **2018**, *6*, 16257-16272.

[24] T. M. Klapötke, J. Stierstorfer, *J. Am. Chem. Soc*. **2009**, *131*, 1122-1134.

[25] A. L. Spek, (Ed.: T. N. Utrecht University), **1999**.

[26] J. A. Montgomery Jr., M. J. Frisch, J. W. Ochterski, G. A. Petersson, *J. Chem. Phys*. **2000**, *112*, 6532-6542.

[27] J. W. Ochterski, G. A. Petersson, J. A. Montgomery Jr., *J. Chem. Phys*. **1996**, *104*, 2598-2619.

[28] L. A. Curtiss, K. Raghavachari, P. C. Redfern, J. A. Pople, *J. Chem. Phys*. **1997**, *106*, 1063-1079.

[29] B. M. Rice, S. V. Pai, J. Hare, *Combust. Flame* **1999**, *118*, 445-458.

[30] E. F. C. Byrd, B. M. Rice, *J. Phys. Chem. A* **2006**, *110*, 1005-1013.

[31] R. Mayer, J. Köhler, A. Homburg, *Explosives*, 5th ed., Wiley-VCH, Weinheim, **2002**.

2.7 Supporting Information

2.7.1 Overview of Compounds

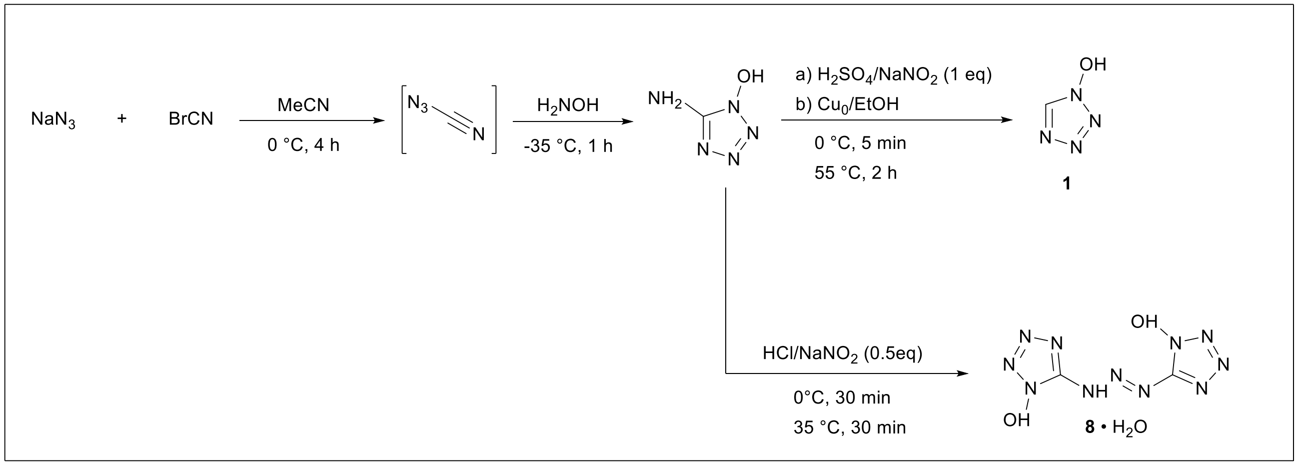

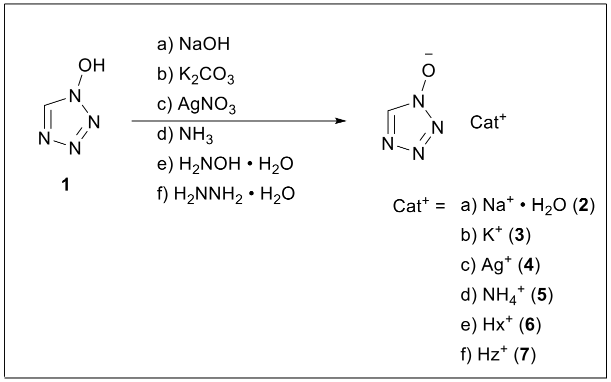

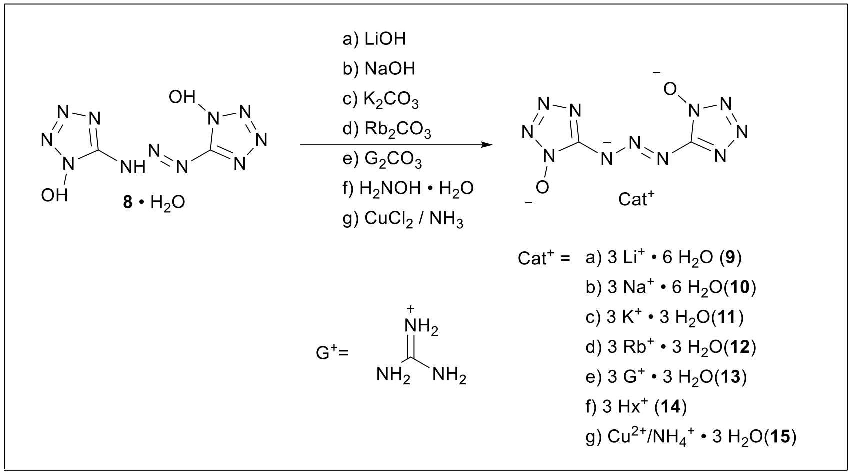

2.7.2 Single Crystal X-ray Diffraction

For all crystalline compounds, an Oxford Xcalibur3 diffractometer with a CCD area detector or Bruker D8 Venture TXS diffractometer equipped with a multilayer monochromator, a Photon 2 detector and a rotating-anode generator were employed for data collection using Mo-K_α radiation (λ = 0.7107 Å). On the Oxford device, data collection and reduction were carried out using the CrysAlisPRO software.[S1] On the Bruker diffractometer, the data were collected with the Bruker Instrument Service v3.0.21, the data reduction was performed using the SAINT V8.18C software (Bruker AXS Inc., 2011). The structures were solved by direct methods (SIR-92,[S2] SIR-97,[S3,S4] SHELXS-97[S5,S6] or SHELXT[S7]) and refined by full-matrix least-squares on $F2$ (SHELXL[S5,S6]) and finally checked using the PLATON software[S8] integrated in the WinGX[S7,S9] or Olex2[S8] software suite. The non-hydrogen atoms were refined anisotropically and the hydrogen atoms were located and freely refined. The absorptions were corrected by a SCALE3 ABSPACK or SADABS Bruker APEX3 multi-scan method.[S11,S12] All DIAMOND2 plots are shown with thermal ellipsoids at the 50% probability level and hydrogen atoms are shown as small spheres of arbitrary radius.

Table S1. Crystallographic data and structure refinement details for compounds **1** and **2a/b.**

	*HTO (**1**)*	*NaTO_P1 (**2a**)*	*NaTO_P21 (**2b**)*
Formula	CH_2N_4O	$CH_3N_4NaO_2$	$CH_3N_4NaO_2$
FW [g mol^{-1}]	86.07	126.06	126.06
Crystal system	Monoclinic	Triclinic	Orthorhombic
Space group	$P2_1/n$ (No. 14)	$P1$ (No. 1)	$P2_12_12_1$ (No. 19)
Color / Habit	White needle	Colorless block	Colorless rod
Size [mm]	0.08 x 0.21 x 0.21	0.04 x 0.04 x 0.09	0.02 x 0.02 x 0.10
a [Å]	5.1610(4)	3.5162(3)	3.5145(3)
b [Å]	7.6125(4)	4.9474(5)	8.8624(7)
c [Å]	8.7911(5)	6.8684(6)	14.6572(12)
α [°]	90	76.042(3)	90
β [°]	98.147(6)	78.148(3)	90
γ [°]	90	80.657(3)	90
V [Å^3]	341.90(4)	112.680(18)	456.53(6)
Z	4	1	4
$\rho_{calc.}$ [g cm^{-3}]	1.672	1.858	1.834
μ [mm^{-1}]	0.145	0.242	0.239
F(000)	176	64	256
$\lambda_{MoK\alpha}$ [Å]	0.71073	0.71073	0.71073
T [K]	123	108	112
θ Min-Max [°]	3.6, 26.4	3.1, 30.5	2.8, 26.4
Dataset	-6: 6 ; -9: 9 ; -10: 10	-5: 5 ; -7: 7 ; -9: 9	-4: 4 ; -11: 11 ; -18: 18
Reflections collected	2466	3134	6490
Independent refl.	696	1325	924
R_{int}	0.023	0.032	0.030
Observed reflections	585	1298	890
Parameters	63	82	82
R_1 (obs)[a]	0.0320	0.0239	0.0200
wR_2 (all data)[b]	0.0818	0.0625	0.0465
S [c]	1.06	1.07	1.15
Resd. dens [e Å^{-3}]	-0.16, 0.57	-0.19, 0.20	-0.19, 0.15
Device type	Oxford Xcalibur3	Bruker D8 Venture TXS	Bruker D8 Venture TXS
Solution	SIR-92	SIR-92	SIR-92
Refinement	SHELXL-2018	SHELXL-2018	SHELXL-2018
Absorption correction	multi-scan	multi-scan	multi-scan

[a] $R_1 = \Sigma||F_0|-|F_c||/\Sigma|F_0|$; [b] $wR_2 = [\Sigma[w(F_0^2-F_c^2)^2]/\Sigma[w(F_0)^2]]^{1/2}$; $w = [\sigma c^2(F_0^2)+(xP)^2+yP]^{-1}$ and $P=(F_0^2+2F_c^2)/3$; [c] $S = \{\Sigma[w(F_o^2-F_c^2)^2]/(n-p)\}^{1/2}$ (n = number of reflections; p = total number of parameters).

Table S2. Crystallographic data and structure refinement details for compounds **3**, **4**, and **5**.

	KTO (3)	*AgTO (4)*	*NH_4TO (5)*
Formula	$CHKN_4O$	$CHAgN_4O$	CHN_4O, H_4N
FW [g mol^{-1}]	124.16	192.93	103.10
Crystal system	Orthorhombic	Orthorhombic	Orthorhombic
Space group	$Pna2_1$ (No. 33)	$Pna2_1$ (No. 33)	$Pna2_1$ (No. 33)
Color / Habit	Colorless block	Colorless rod	Colorless block
Size [mm]	0.21 x 0.22 x 0.42	0.02 x 0.03 x 0.13	0.45 x 0.52 x 0.82
a [Å]	7.2219(4)	10.2602(5)	7.8330(7)
b [Å]	4.7357(2)	10.2774(5)	4.5703(4)
c [Å]	12.5270(6)	3.4349(2)	13.2268(14)
α [°]	90	90	90
β [°]	90	90	90
γ [°]	90	90	90
V [Å^3]	428.43(4)	362.20(3)	473.51(8)
Z	4	4	4
$\rho_{calc.}$ [g cm^{-3}]	1.925	3.538	1.446
μ [mm^{-1}]	1.095	5.393	0.123
F(000)	248	360	216
$\lambda_{MoK\alpha}$ [Å]	0.71073	0.71073	0.71073
T [K]	121	173	99
θ Min-Max [°]	4.6, 26.4	4.0, 29.6	3.1, 32.5
Dataset	-8: 9 ; -5: 5 ; -15: 15	-14: 14 ; -14: 14 ; -4: 4	-11: 11 ; -6: 6 ; -19: 15
Reflections collected	2778	8144	4905
Independent refl.	863	1004	1419
R_{int}	0.024	0.056	0.022
Observed reflections	843	972	1283
Parameters	69	65	81
R_1 (obs)[a]	0.0183	0.0203	0.0321
wR_2 (all data)[b]	0.0458	0.0478	0.0840
S [c]	1.12	1.05	1.08
Resd. dens [e Å^{-3}]	-0.19, 0.21	-0.60, 0.57	-0.13, 0.19
Device type	Oxford Xcalibur3	Oxford Xcalibur3	Oxford Xcalibur3
Solution	SIR-92	SHELXT	SHELXT
Refinement	SHELXL-2018	SHELXL-2018	SHELXL-2018
Absorption correction	multi-scan	multi-scan	multi-scan

[a]$R_1 = \Sigma||F_0|-|F_c||/\Sigma|F_0|$; [b]$wR_2 = [\Sigma[w(F_0^2-F_c^2)^2]/\Sigma[w(F_0)^2]]^{1/2}$; $w = [\sigma c^2(F_0^2)+(xP)^2+yP]^{-1}$ and $P=(F_0^2+2F_c^2)/3$; [c]$S = \{\Sigma[w(F_o^2-F_c^2)^2]/(n-p)\}^{1/2}$ (n = number of reflections; p = total number of parameters).

Table S3. Crystallographic data and structure refinement details for compounds **6**, **7**, and **8**.

	*HxTO (**6**)*	*HzTO (7)*	*H3(TO)2T (**8**)*
Formula	CHN_4O, H_4NO	CHN_4O, H_5N_2	$C_2H_3N_{11}O_2$, H_2O
FW [g mol^{-1}]	119.10	118.12	231.17
Crystal system	Triclinic	Monoclinic	Monoclinic
Space group	$P1$ (No. 1)	Pc (No. 7)	$P2_1/n$ (No. 14)
Color / Habit	Colorless platelet	Colorless rod	Orange block
Size [mm]	0.03 x 0.08 x 0.10	0.06 x 0.17 x 0.57	0.09 x 0.20 x 0.37
a [Å]	3.6986(5)	4.8164(6)	12.0542(5)
b [Å]	4.8897(8)	7.0591(10)	5.7942(2)
c [Å]	6.5638(11)	7.0853(11)	12.1983(4)
α [°]	88.745(6)	90	90
β [°]	86.322(6)	98.485(15)	103.718(4)
γ [°]	79.164(6)	90	90
V [Å^3]	116.34(3)	238.26(6)	827.68(5)
Z	1	2	4
$\rho_{calc.}$ [g cm^{-3}]	1.700	1.646	1.855
μ [mm^{-1}]	0.153	0.139	0.164
F(000)	62	124	472
$\lambda_{MoK\alpha}$ [Å]	0.71073	0.71073	0.71073
T [K]	173	102	107
θ Min-Max [°]	4.2, 27.5	2.9, 32.3	3.4, 26.4
Dataset	-4: 4 ; -6: 6 ; -8: 7	-7: 6 ; -10: 10 ; -10: 6	-15: 15 ; -7: 6 ; -13: 15
Reflections collected	1707	2003	5264
Independent refl.	871	1077	1688
R_{int}	0.035	0.037	0.027
Observed reflections	848	851	1406
Parameters	93	98	165
R_1 (obs)[a]	0.0277	0.0461	0.0340
wR_2 (all data)[b]	0.0703	0.0982	0.0874
S [c]	1.10	1.05	1.06
Resd. dens [e Å^{-3}]	-0.16, 0.20	-0.28, 0.28	-0.17, 0.26
Device type	Bruker D8 Venture TXS	Oxford Xcalibur3	Oxford Xcalibur3
Solution	SHELXT	SHELXT	SIR-92
Refinement	SHELXL-2018	SHELXL-2018	SHELXL-2018
Absorption correction	multi-scan	multi-scan	multi-scan

[a] $R_1 = \Sigma||F_0|-|F_c||/\Sigma|F_0|$; [b] $wR_2 = [\Sigma[w(F_0^2-F_c^2)^2]/\Sigma[w(F_0)^2]]^{1/2}$; $w = [\sigma c^2(F_0^2)+(xP)^2+yP]^{-1}$ and $P=(F_0^2+2F_c^2)/3$; [c] $S = \{\Sigma[w(F_o^2-F_c^2)^2]/(n-p)\}^{1/2}$ (n = number of reflections; p = total number of parameters).

Table S4. Crystallographic data and structure refinement details for compounds **9**, **10**, and **11**.

	*Li3(TO)2T (**9**)*	*Na3(TO)2T (**10**)*	*K3(TO)2T (**11**)*
Formula	$C_2H_{12}Li_3N_{11}O_8$	$C_2H_{12}N_{11}Na_3O_8$	$C_2H_6K_3N_{11}O_5$
FW [g mol^{-1}]	339.05	387.20	381.48
Crystal system	Triclinic	Triclinic	Orthorhombic
Space group	P-1 (No. 2)	P-1 (No. 2)	$P2_12_12_1$ (No. 19)
Color / Habit	Yellow block	Yellow platelet	Yellow needle
Size [mm]	0.14 x 0.29 x 0.42	0.07 x 0.16 x 0.22	0.10 x 0.13 x 0.55
a [Å]	6.9812(9)	7.1050(12)	6.6032(3)
b [Å]	8.7124(9)	8.1609(10)	11.3834(4)
c [Å]	11.2511(13)	13.507(2)	16.6430(7)
α [°]	81.165(9)	95.747(11)	90
β [°]	84.575(10)	93.543(13)	90
γ [°]	76.353(10)	109.254(14)	90
V [Å^3]	655.90(14)	731.9(2)	1251.00(9)
Z	2	2	4
$\rho_{calc.}$ [g cm^{-3}]	1.717	1.757	2.026
μ [mm^{-1}]	0.156	0.233	1.137
F(000)	348	396	768
$\lambda_{MoK\alpha}$ [Å]	0.71073	0.71073	0.71073
T [K]	124	125	122
θ Min-Max [°]	3.2, 26.4	3.3, 26.4	3.3, 26.4
Dataset	-8: 8 ; -10: 10 ; -14: 9	-5: 8 ; -10: 9 ; -14: 16	-8: 8 ; -12: 14 ; -19: 20
Reflections collected	4572	4006	9475
Independent refl.	2677	2954	2557
R_{int}	0.053	0.031	0.043
Observed reflections	1609	2100	2390
Parameters	259	265	191
R_1 (obs)[a]	0.0582	0.0538	0.0256
wR_2 (all data)[b]	0.1226	0.1128	0.0539
S [c]	0.99	1.04	1.04
Resd. dens [e Å^{-3}]	-0.33, 0.47	-0.34, 0.35	-0.22, 0.27
Device type	Oxford Xcalibur3	Oxford Xcalibur3	Oxford Xcalibur3
Solution	SIR-92	SIR-92	SIR-92
Refinement	SHELXL-2018	SHELXL-2018	SHELXL-2018
Absorption correction	multi-scan	multi-scan	multi-scan

[a]$R_1 = \Sigma||F_0|-|F_c||/\Sigma|F_0|$; [b]$wR_2 = [\Sigma[w(F_0^2-F_c^2)^2]/\Sigma[w(F_0)^2]]^{1/2}$; $w = [\sigma c^2(F_0^2)+(xP)^2+yP]^{-1}$ and $P=(F_0^2+2F_c^2)/3$; [c]$S = \{\Sigma[w(F_o^2-F_c^2)^2]/(n-p)\}^{1/2}$ (n = number of reflections; p = total number of parameters).

Table S5. Crystallographic data and structure refinement details for compounds **12**, **13**, and **15**.

	*Rb3(TO)2T (**12**)*	*Gua3(TO)2T (**13**)*	*Cu(NH$_4$)(TO)2T (**15**)*
Formula	$C_2H_6N_{11}O_5Rb_3$	$C_2N_{11}O_2$, 3(CH_6N_3), 3(H_2O)	$C_2H_4CuN_{11}O_4$, H_2O, H_4N
FW [g mol^{-1}]	520.59	444.44	345.76
Crystal system	Triclinic	Monoclinic	Triclinic
Space group	*P*-1 (No. 2)	*P*2$_1$/*c* (No. 14)	*P*-1 (No. 2)
Color / Habit	Colorless rod	Yellow block	Green plate
Size [mm]	0.02 x 0.02 x 0.10	0.05 x 0.06 x 0.07	0.06 x 0.08 x 0.35
a [Å]	6.6520(2)	6.9605(4)	7.0091(7)
b [Å]	8.5339(3)	14.0622(8)	7.1350(7)
c [Å]	13.0590(5)	19.5249(12)	12.4292(11)
α [°]	98.618(1)	90	104.065(8)
β [°]	99.173(1)	98.069(2)	105.838(8)
γ [°]	112.219(1)	90	94.746(8)
V [Å^3]	659.35(4)	1892.18(19)	572.61(10)
Z	2	4	2
$\rho_{calc.}$ [g cm^{-3}]	2.622	1.560	2.005
μ [mm^{-1}]	11.134	0.133	1.958
F(000)	492	936	350
$\lambda_{MoK\alpha}$ [Å]	0.71073	0.71073	0.71073
T [K]	106	102	133
θ Min-Max [°]	2.6, 26.4	2.9, 26.4	3.5, 27.5
Dataset	-8: 8 ; -10: 10 ; -16: 16	-8: 8 ; -17: 17 ; -24: 24	-9: 9 ; -9: 8 ; -15: 16
Reflections collected	9632	29861	4778
Independent refl.	2686	3866	2618
R_{int}	0.028	0.058	0.065
Observed reflections	2489	3353	1786
Parameters	214	367	221
R_1 (obs)[a]	0.0178	0.0337	0.0605
wR_2 (all data)[b]	0.0408	0.0861	0.1169
S [c]	1.09	1.10	1.01
Resd. dens [e Å^{-3}]	-0.35, 0.46	-0.28, 0.21	-0.80, 0.66
Device type	Bruker D8 Venture TXS	Bruker D8 Venture TXS	Oxford Xcalibur3
Solution	SIR-92	SIR-92	SIR-92
Refinement	SHELXL-2018	SHELXL-2018	SHELXL-2018
Absorption correction	multi-scan	multi-scan	multi-scan

[a] $R_1 = \Sigma||F_0|-|F_c||/\Sigma|F_0|$; [b] $wR_2 = [\Sigma[w(F_0^2-F_c^2)^2]/\Sigma[w(F_0)^2]]^{1/2}$; $w = [\sigma c^2(F_0^2)+(xP)^2+yP]^{-1}$ and $P=(F_0^2+2F_c^2)/3$; [c] $S = \{\Sigma[w(F_o^2-F_c^2)^2]/(n-p)\}^{1/2}$ (n = number of reflections; p = total number of parameters).

2.7.3 Crystal Structures of 9, 10, 12 and 13

Compound **9** crystallizes in the triclinic space group *P*−1 as a hexahydrate (Figure S1) in the form of yellow plates. The unit cell contains two formula units and **9** has a calculated density of 1.717 g cm^{-3} at 124 K. The anion is nearly planar with a torsion angle between the two 1-oxidotetrazole moieties of 0.7°.

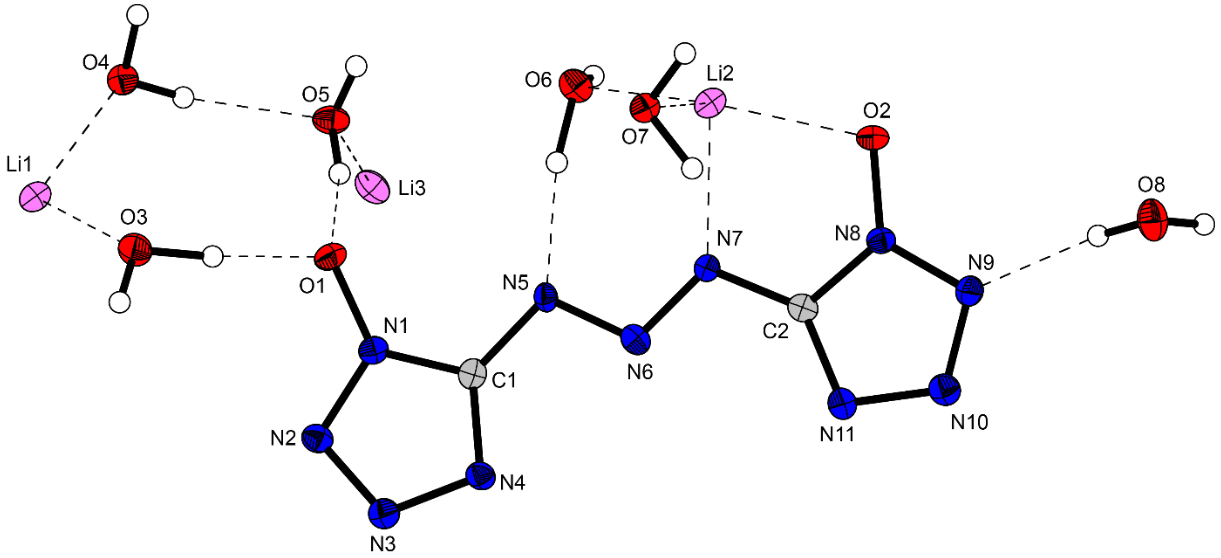

Figure S1. Crystal structure of compound **9**; Selected interatomic distances [Å]: O1–N1 1.337(4), N1–N2 1.354(4), N1–C1 1.341(5), N2–N3 1.319(5), N3–N4 1.357(4), N4–C1 1.328(4), N5–C1 1.378(4), N5–N6 1.310(4), N6–N7 1.312(4), N7–C2 1.366(4), O3–Li1 1.975(6), O4–Li1 2.111(6), O2–Li2 2.164(6), O6–Li2 2.078(6), O7–Li2 2.071(6), O5–Li3 1.958(7), O7–Li3 1.965(6); Angles [°] O1–N1–N2 122.1(3), O1–N1–C1 128.5(3), N2–N1–C1 109.3(3), N1–N2–N3 105.1(3), N2–N3–N4 111.4(3), N3–N4–C1 105.7(3), N6–N5–C1 109.3(2), N5–N6–N7 110.4(3), N6–N7–C2 112.9(2), N7–C2–N11 135.4(3).

Compound **10** crystallizes in the triclinic space group *P*−1 as a hexahydrate (Figure S2) in the form of yellow platelets. The unit cell contains two formula units and **10** has a calculated density of 1.757 g cm^{-3} at 125 K. The anion is slightly twisted with a torsion angle between the two tetrazole rings of 3° (N4–C1–C2–N11).

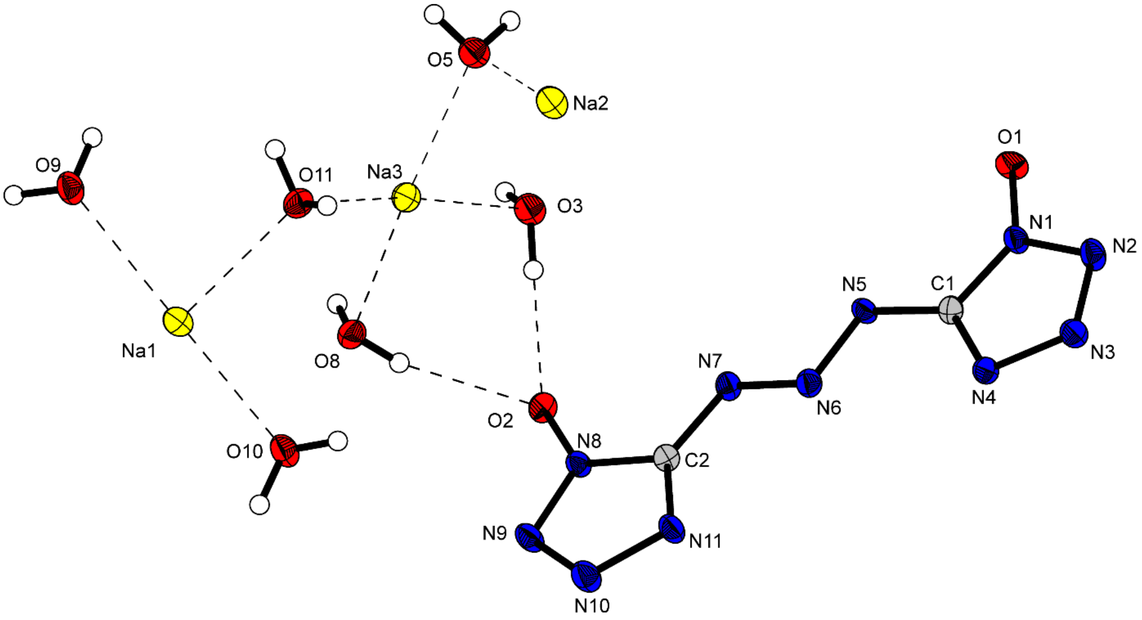

Figure S2. Crystal structure of compound **10**; Selected interatomic distances [Å]: O1–N1 1.323(3), N1–N2 1.350(3), N2–N3 1.316(3), N3–N4 1.371(4), N4–C1 1.337(4), C1–N1 1.347(4), C1–N5 1.382(4), N5–N6 1.325(3), N6–N7 1.304(3), N7–C2 1.377(4), Na1–O9 2.450(3), Na1–O10 2.404(3), Na1–O11 2.366(3), Na2–O5 2.267(3), Na3–O3 2.420(3), Na3–O5 2.407(3), Na3–O8 2.392(3), Na3–O11 2.335(3); Angles [°] O1–N1–N2 122.1(2), O1–N1–C1 128.9(2), N2–N1–C1 109.0(2), N1–N2–N3 106.2(2), N2–N3–N4 110.7(2), N3–N4–C1 105.5(2), N4–C1–N5 130.9(3), N1–C1–N4 108.5(3), N1–C1–N5 120.6(3), N6–N5–C1 110.3(2), N5–N6–N7 110.9(2), N6–N7–C2 113.4(2), N8–C2–N11 107.3(2), N7–C2–N8 118.0(3), N7–C2–N11 134.6(3).

Compound **12** crystallizes as colorless rods in the triclinic space group *P*−1, and contains two formula units in the unit cell. Like compound **11** it is a trihydrate and has a calculated density of 2.622 g cm^{-3} at 106 K (Figure S3). The anion is nearly planar with a small torsion angle between the two 1-oxidotetrazole moieties of 1.8° (O1–N1–N8–O2).

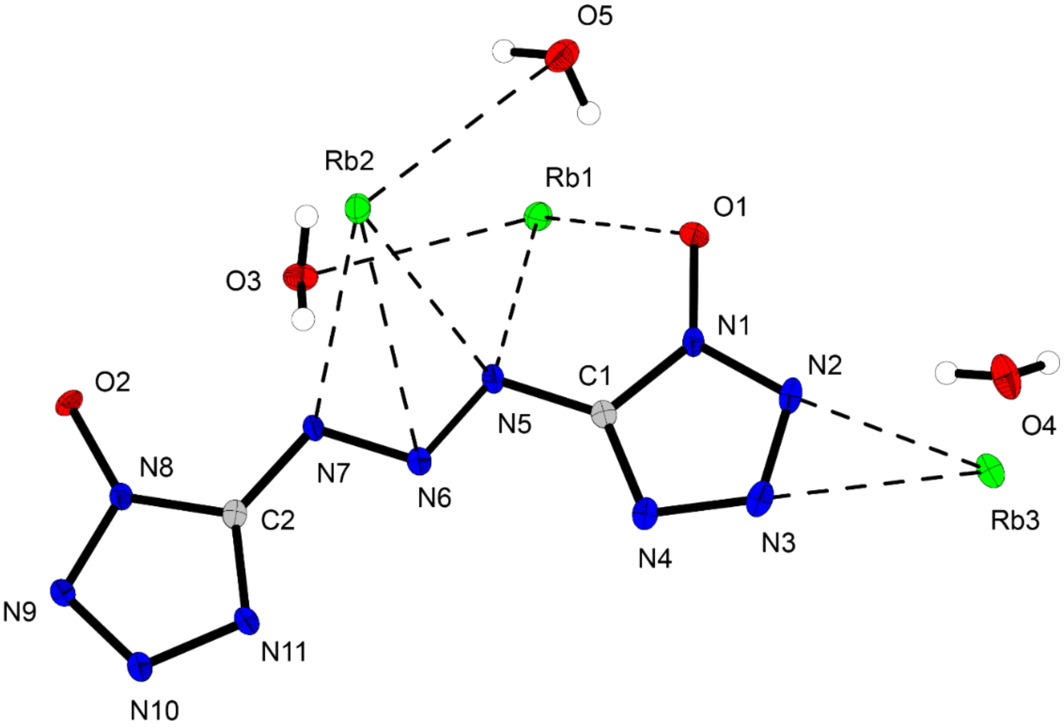

Figure S3. Crystal structure of compound **12**; Selected interatomic distances [Å]: O1–N1 1.333(2), N1–N2 1.348(3), N2–N3 1.313(3), N4–N4 1.350(3), N4–C1 1.341(3), N1–C1 1.350(3), C1–N5 1.381(3), N5–N6 1.309(3), N6–N7 1.316(3), N7–C2 1.380(3), Rb1–O1 2.9309(16), Rb1–O3 2.8886(18), Rb1–N5 3.3111(19), Rb2–N5 3.0573(19), Rb2–N6 3.1407(19), Rb2–N7 3.1339(19), Rb2–O5 3.1863(19), Rb3–N2 3.1668(19), Rb3–N3 3.595(2), Rb3–O4 2.912(2); Angles [°] O1–N1–N2 121.76(18), O1–N1–C1 129.51(19), N2–N1–C1 108.72(19), N3–N1–106.24(18), N2–N3–N4 111.16(18), C1–N4–N3 105.91(19), N6–N5–C1 110.50(19), N5–N6–N7 110.82(18), N6–N7–C2 111.66(19), N4–C1–N1 107.97(19), N4–C1–N5 131.9(2), N1–C1–N5 120.1(2), N11–C2–N7 131.8(2), N8–C2–N7 120.2(2).

Compound **13** (Figure 4) crystallizes in the monoclinic space group $P2_1/c$ as a trihydrate, with a density of 1.560 g cm^{-3} at 102 K. As was observe for compound **10**, the structure of the anion in **13** is twisted with a torsion angle of 21.8° between the 1-oxidotetrazole moieties. In contrast to **10**, in compound **13** this is caused by hydrogen bonding involving the guanidinium cations, bridging between anions in different layers, resulting in the protrusion of O2 out of the plane.

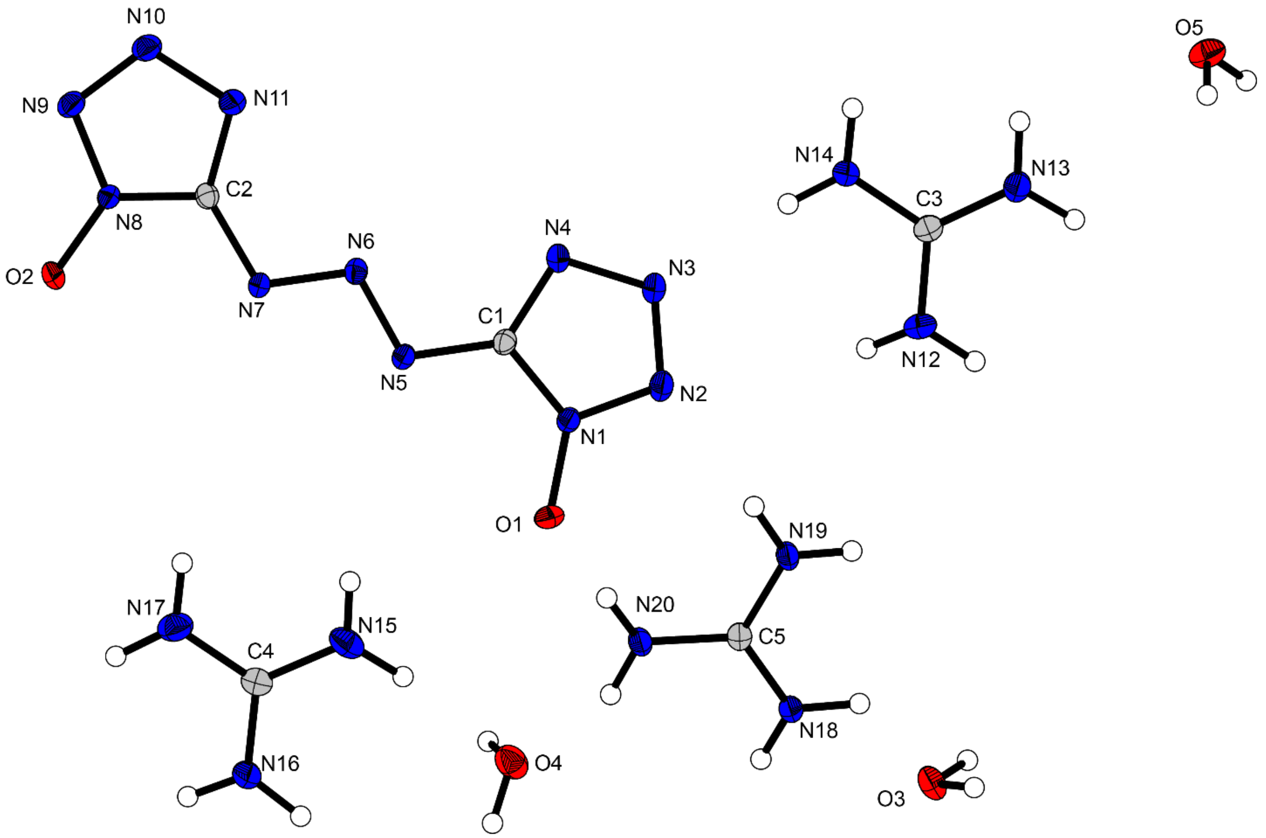

Figure S4. Crystal structure of compound **13**; Selected interatomic distances [Å]: O1–N1 1.3340(15), O2–N8 1.3365(15), N1–N2 1.3433(16), N1–C1 1.3455(17), N2–N3 1.3123(16), N3–N4 1.3545(16), N4–C1 1.3429(18), N5–N6 1.3058(16), N5–C1 1.3771(17), N6–N7 1.3098(15), N7–C2 1.3807(17), N8–N9 1.3372(16), N8–C2 1.3407(16), N9–N10 1.3105(16), N10–N11 1.3565(16), N11–C2 1.3340(18), N12–C3 1.3319(19), N13–C3 1.3203(19), N14–C3 1.3269(19), N15–C4 1.327(2), N16–C4 1.3154(19), N17–C4 1.329(2), N18–C5 1.3186(17), N19–C5 1.3377(18), N20–C5 1.3301(18); Angles [°]: O1–N1–N2 122.06(11), O1–N1–C1 128.87(11), N2–N1–C1 109.07(11), N1–N2–N3 106.39(10), N2–N3–N4 110.79(11), N3–N4–C1 105.94(11), N6–N5–C1 110.82(11), N5–N6–N7 110.96(11), N6–N7–C2 112.34(11), O2–N8–N9 122.93(10), O2–N8–C2 127.33(11), N9–N8–C2 109.74(11), N8–N9–N10 105.69(10), N9–N10–N11 111.11(11), N10–N11–C2 105.69(11), N1–C1–N4 107.81(11), N1–C1–N5 120.89(12), N4–C1–N5 131.28(12), N7–C2–N8 118.63(12), N7–C2–N11 133.56(12), N8–C2–N11 107.77(11).

2.7.4 Computations

All calculations were carried out using the Gaussian G09 program package.[S13] The enthalpies (H) and free energies (G) were calculated using the complete basis set (CBS) method of Petersson and coworkers in order to obtain very accurate energies. The CBS models use the known asymptotic convergence of pair natural orbital expressions to extrapolate from calculations using a finite basis set to the estimated complete basis set limit. CBS-4 begins with a HF/3-21G(d) geometry optimization; the zero point energy is computed at the same level. It then uses a large basis set SCF calculation as a base energy, and a MP2/6-31+G calculation with a CBS extrapolation to correct the energy through second order. A MP4(SDQ)/6-31+(d,p) calculation is used to approximate higher order contributions. In this study we applied the modified CBS-4M method (M referring to the use of minimal population localization) which is a re-parametrized version of the original CBS-4 method and also includes some additional empirical corrections. The enthalpies of the gas-phase species M were computed according to the atomization energy method (E1) (Table S6 & 7).[S13–18]

$$\Delta_f H^\circ_{(g,\ M,\ 298)} = H_{(\mathrm{Molecule},\ 298)} - \sum H^\circ_{(\mathrm{Atoms},\ 298)} + \sum \Delta_f H^\circ_{(\mathrm{Atoms},\ 298)} \qquad \text{(E1)}$$

Table S6. Literature values for atomic $\Delta H^\circ{}_f{}^{298}$ / kcal mol^{-1}

	$-H^{298}$ [a.u.]	NIST[S19]
H	0.50091	52.1
C	37.786156	171.3
N	54.522462	113.0
O	74.991202	59.6

The gas-phase heat of formations were converted to the solid/liquid state ones (i) for neutrals: by subtracting the vaporization/sublimation enthalpies (calculated using the Trouton rule)[S20,21] (ii) for ionics: using the Jenkins' equations for XY and X_2Y salts[S22,S23] based on the molecular volumes Vm (taken from X-Ray strucutres) in order to calculate the lattice energies (ΔE_L) and enthalpies (ΔH_L). At last, the molar standart enthalpies of formation ($\Delta_f H_M$) were used to calculate the molar solid state energie of formation (ΔU_m) according to equation (E2), Δn being the change of moles of gaseous components. The calculation results are summarized in Table S7.

$$\Delta U_m = \Delta H_m - \Delta n\ R\ T \qquad \text{(E2)}$$

Table S7. CBS-4M results, Gas phase enthalpies of formation, calculated sublimation/vaporization enthalpies and solid-state heat of formation.

Compound	$-H^{298}$ / a.u.	$\Delta_f H^\circ$(g) / kJ mol^{-1}	ΔE_L, ΔH_L (**2-7**, **9-15**); ΔH°_{sub} (**1**, **8**) / kJ mol^{-1}	V_m / nm^3	Δn
1	–332.996269	333.4	25.9335		3.5
1 anion	–332.478900	158.4			
8	–829.380882	775.6	12.264676		8
8 anion	–827.534674	1268.8			
Li$^+$	–7.434217	159.3			

Na^+	–161.848174	107.5			
K^+	–599.035967	487.7			
NH_4^+	–56.796608	635.3			
NH_4O^+	–131.863249	686.4			
$N_2H_5^+$	–112.030523	773.4			
Cu^{2+}	–1639.2574	337.5			
Guanidinium cation	–205.453192	409.8			
2a		265.8	630.9, 632.1	0.088	3
2b		265.8	628.0, 6293	0.090	3
3		645.8	597.8, 599.0	0.107	3
5		793.7	581.6, 586.5	0.118	5.5
6		844.8	581.0, 586.0	0.119	6
7		931.8	580.6, 585.5	0.119	6.5
9		1428.1	3252.6, 3251.4	0.181	6.5
10		1376.3	3072.8, 3071.5	0.219	6.5
11		1357.8	3012.3, 3011.0	0.239	6.5
13		713.4	2819.5, 2829.4	0.452	20
14		796.0	2862.6, 2868.8	0.425	15.5
15		532.5	3415.2, 3425.1	0.213	13.5
TNT	–	–	–	−59.346	

2.7.5 NMR Spectroscopy of 1–3 and 5–13

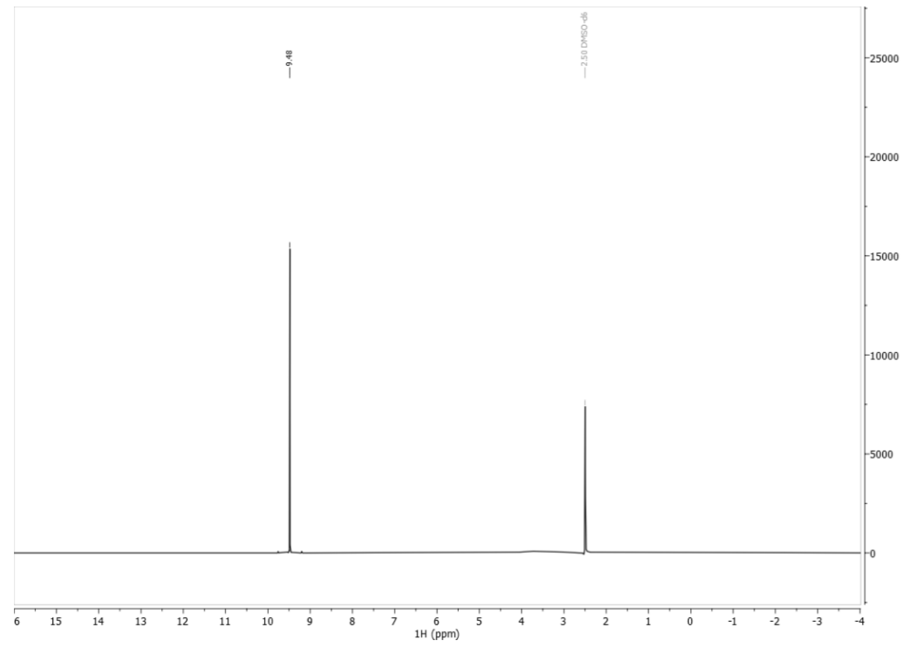

Figure S5. ^{1}H NMR spectrum of 1-hydroxytetrazole (**1**) in DMSO-d_6.

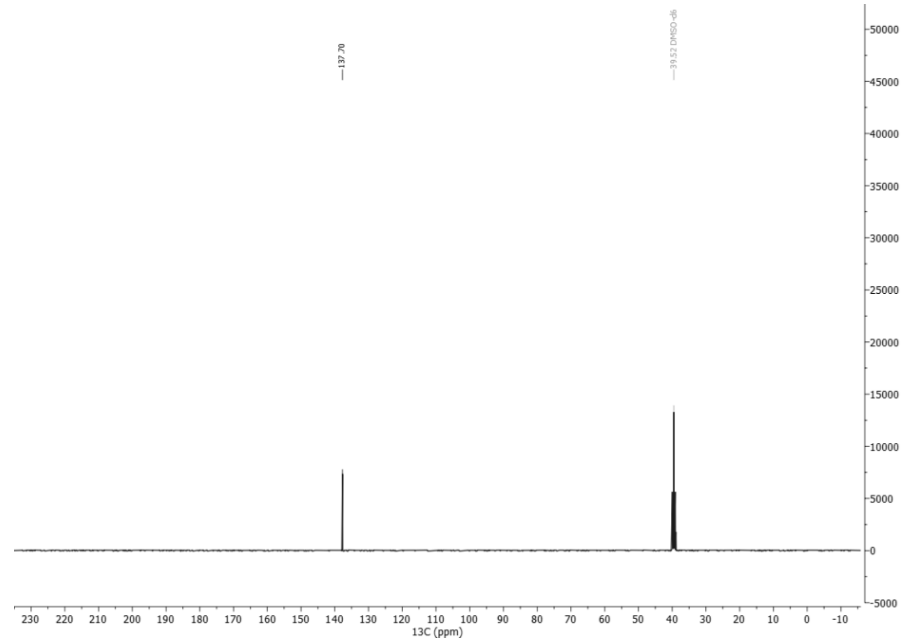

Figure S6. ^{13}C{^{1}H} NMR spectrum of 1-hydroxytetrazole (**1**) in DMSO-d_6.

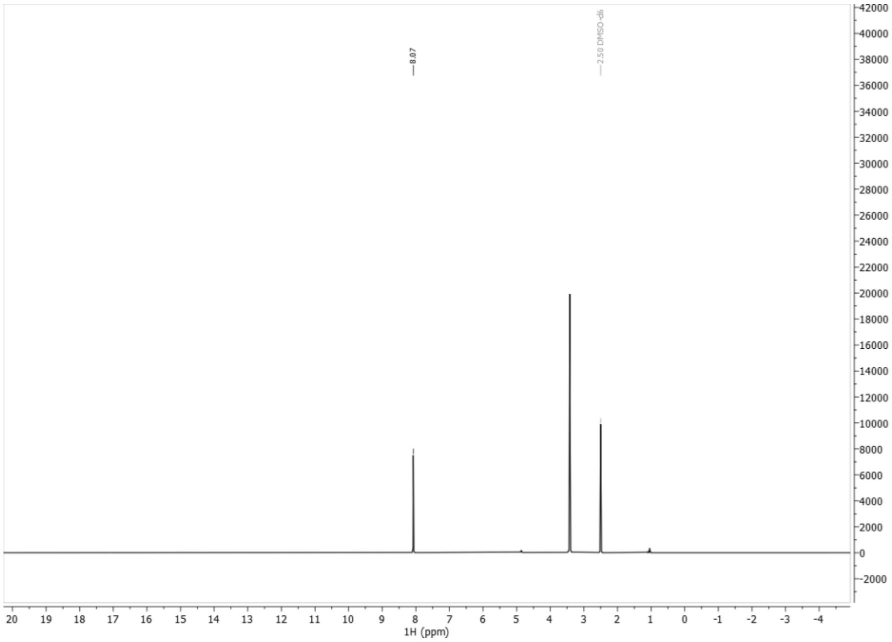

Figure S7. ^{1}H NMR spectrum of sodium 1-oxidotetrazolate (**2**) in DMSO-d$_6$.

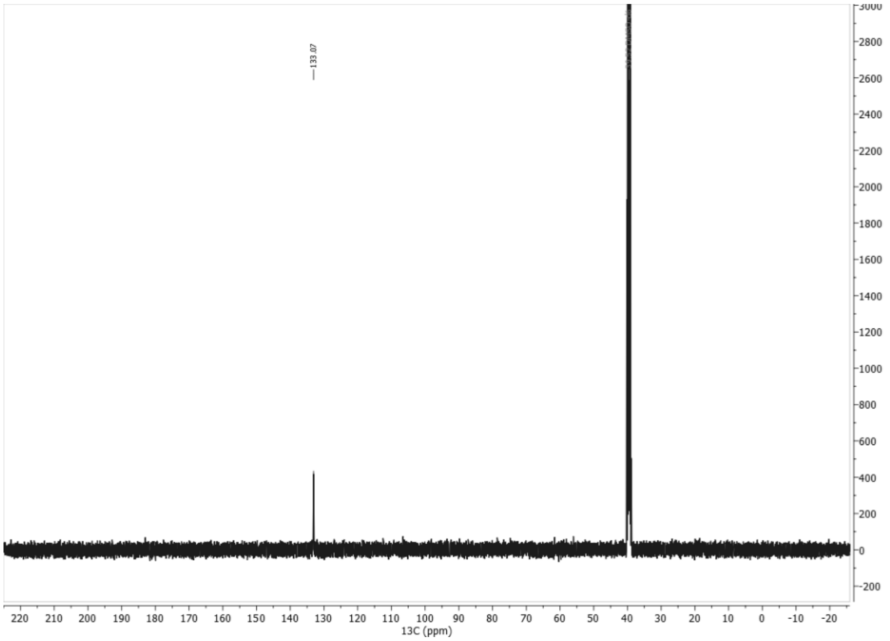

Figure S8. ^{13}C{^{1}H} NMR spectrum of sodium 1-oxidotetrazolate (**2**) in DMSO-d$_6$

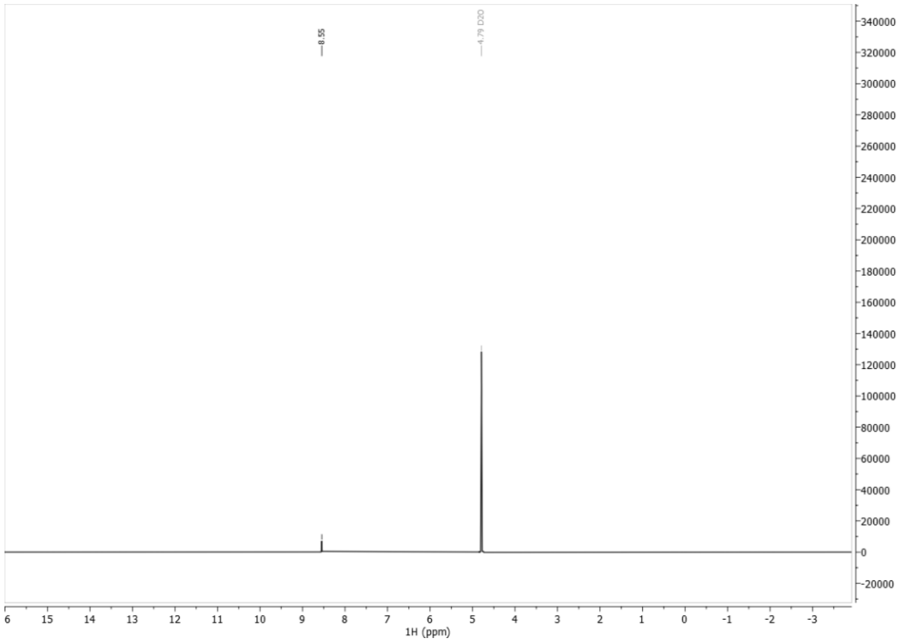

Figure S9. ^{1}H NMR spectrum of potassium 1-oxidotetrazolate (**3**) in D_2O.

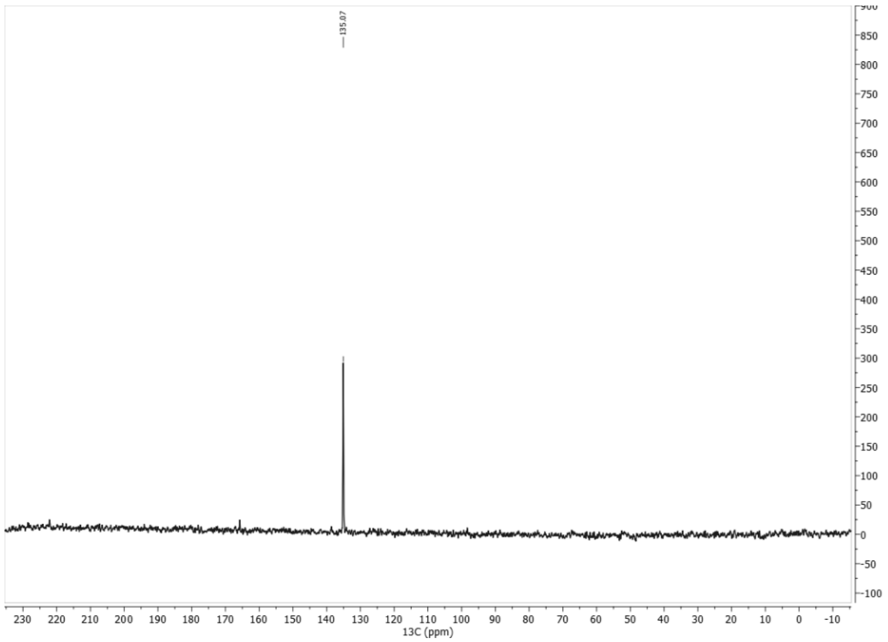

Figure S10. $^{13}C\{^1H\}$ NMR spectrum of potassium 1-oxidotetrazolate (**3**) in D_2O.

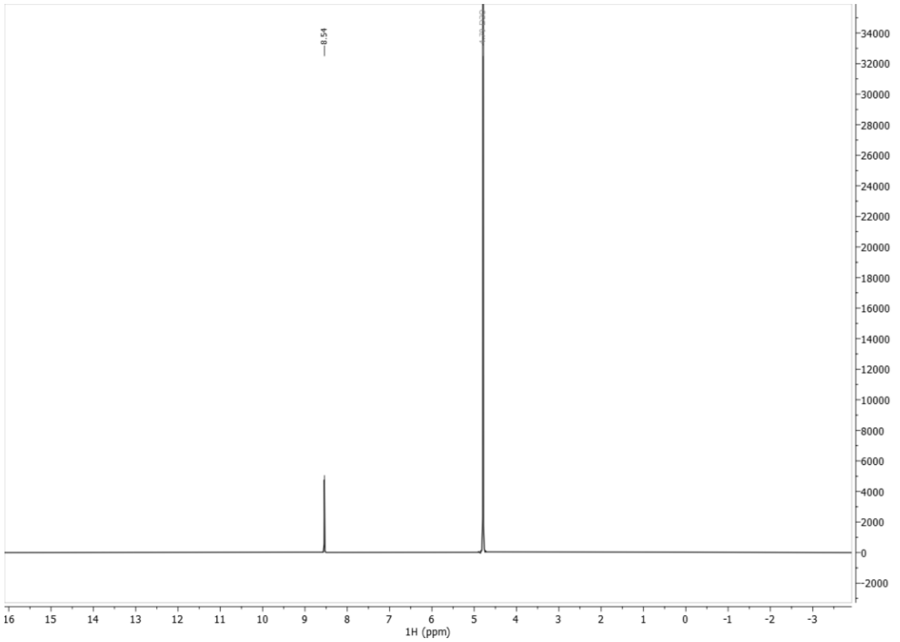

Figure S11. ^{1}H NMR spectrum of ammonium 1-oxidotetrazolate (**5**) in D_2O.

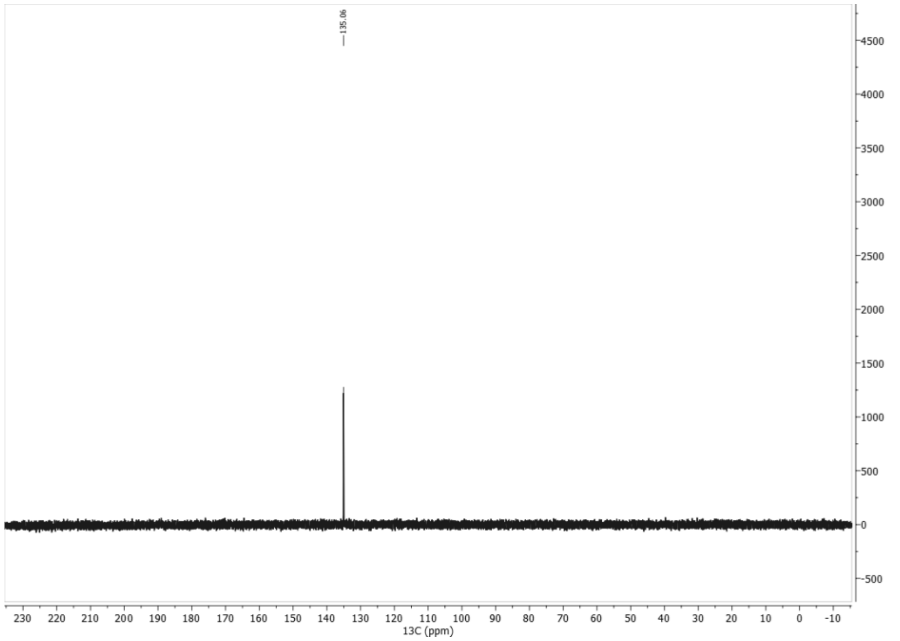

Figure S12. ^{13}C{^{1}H} NMR spectrum of ammonium 1-oxidotetrazolate (**5**) in D_2O.

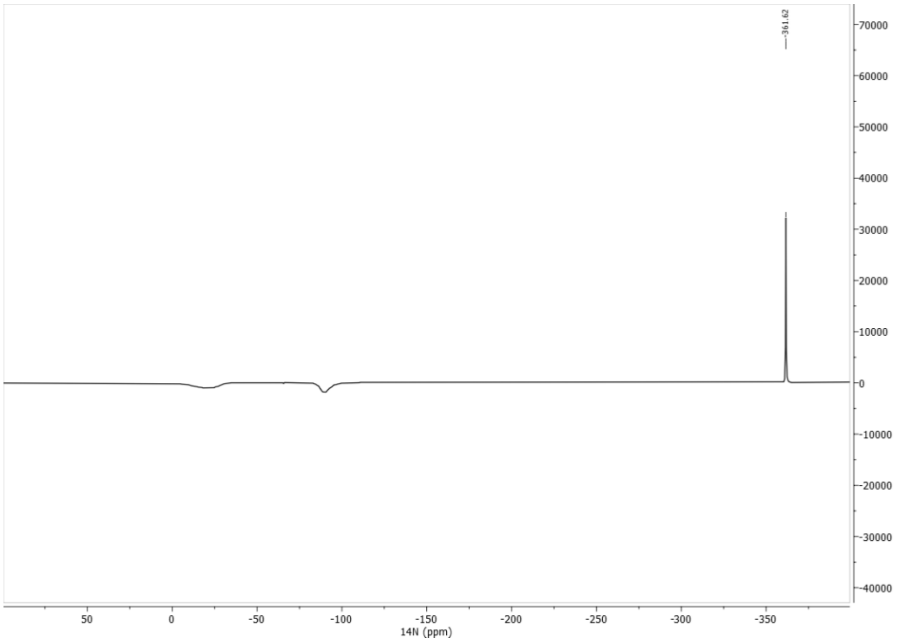

Figure S13. ^{14}N NMR spectrum of ammonium 1-oxidotetrazolate (**5**) in D_2O.

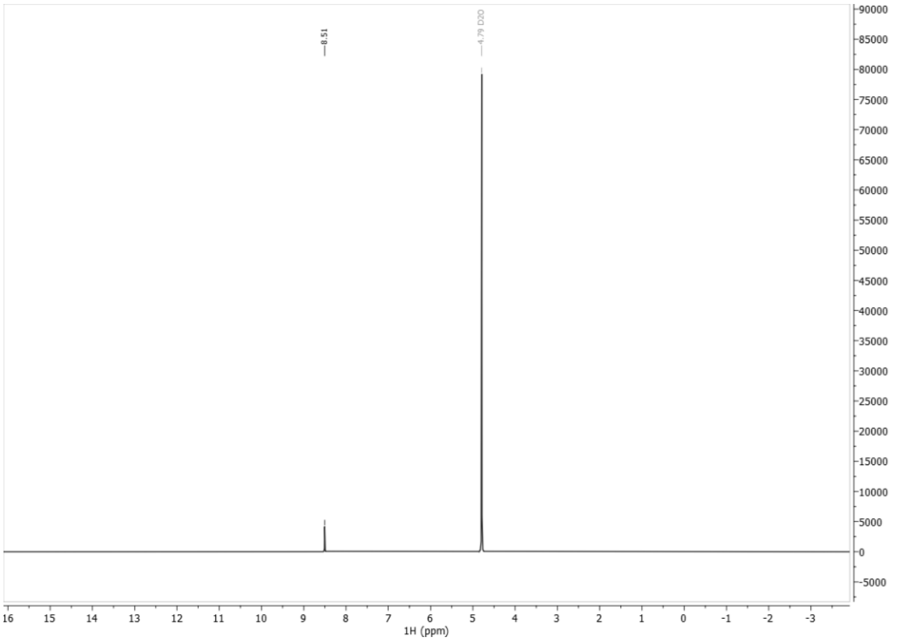

Figure S14. ^{1}H NMR spectrum of hydroxylammonium 1-oxidotetrazolate (**6**) in D_2O.

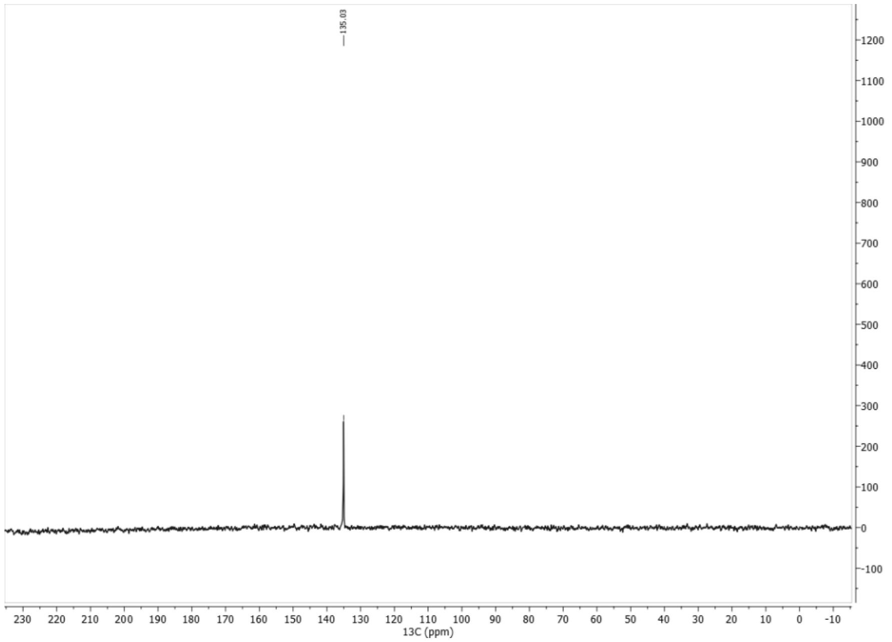

Figure S15. $^{13}C\{^1H\}$ NMR spectrum of hydroxylammonium 1-oxidotetrazolate (**6**) in D_2O.

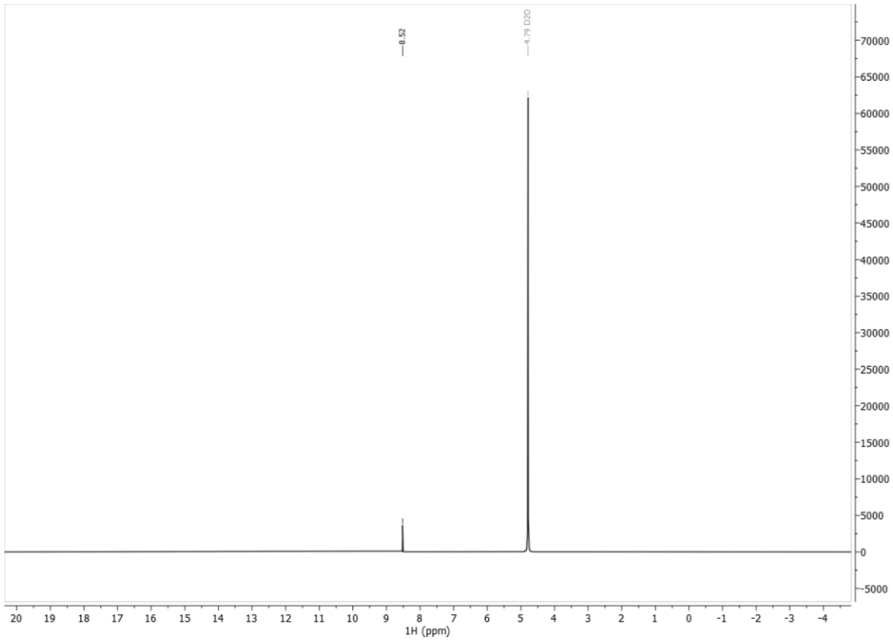

Figure S16. ^1H NMR spectrum of hydrazinium 1-oxidotetrazolate (**7**) in D_2O.

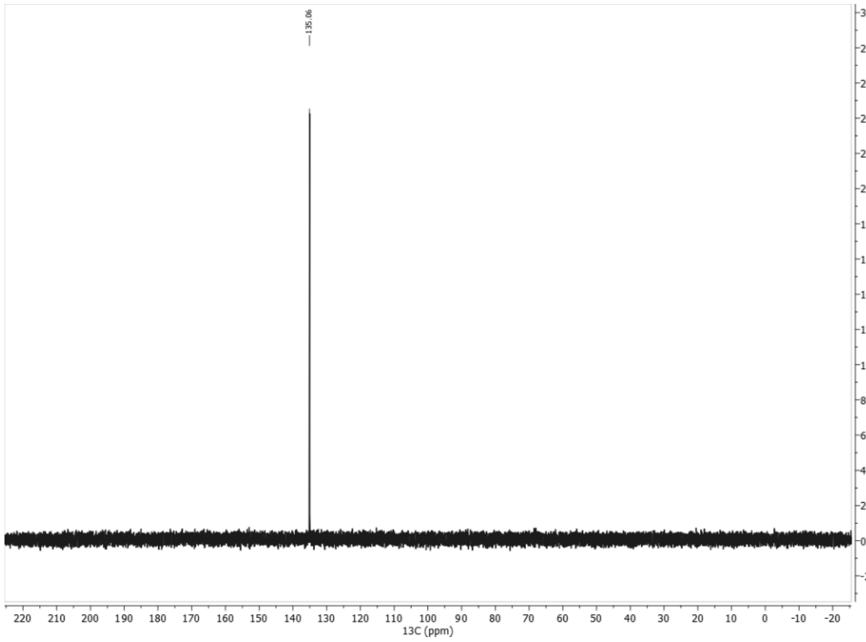

Figure S17. $^{13}C\{^1H\}$ NMR spectrum of hydrazinium 1-oxidotetrazolate (**7**) in D_2O.

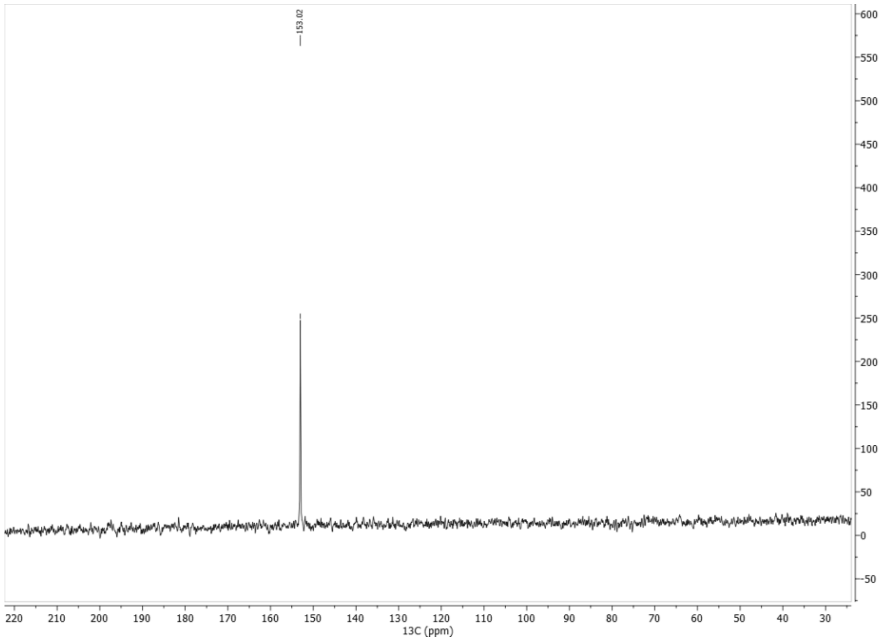

Figure S18. $^{13}C\{^1H\}$ NMR spectrum of Trilithium bis(1-oxidotetrazol-5-yl)triazenide (**9**) in D_2O.

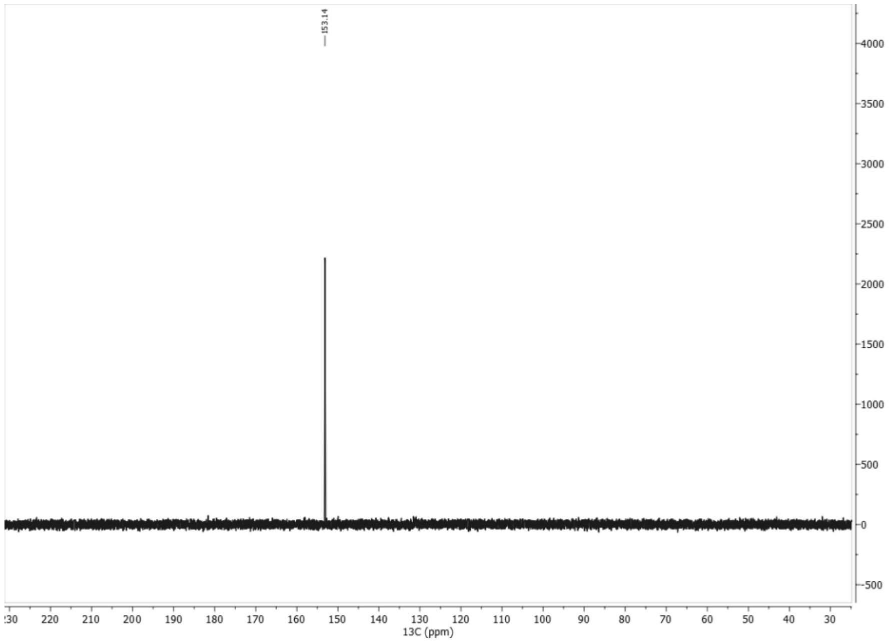

Figure S19. $^{13}C\{^{1}H\}$ NMR spectrum of Trisodium bis(1-oxidotetrazol-5-yl)triazenide (**10**) in D_2O.

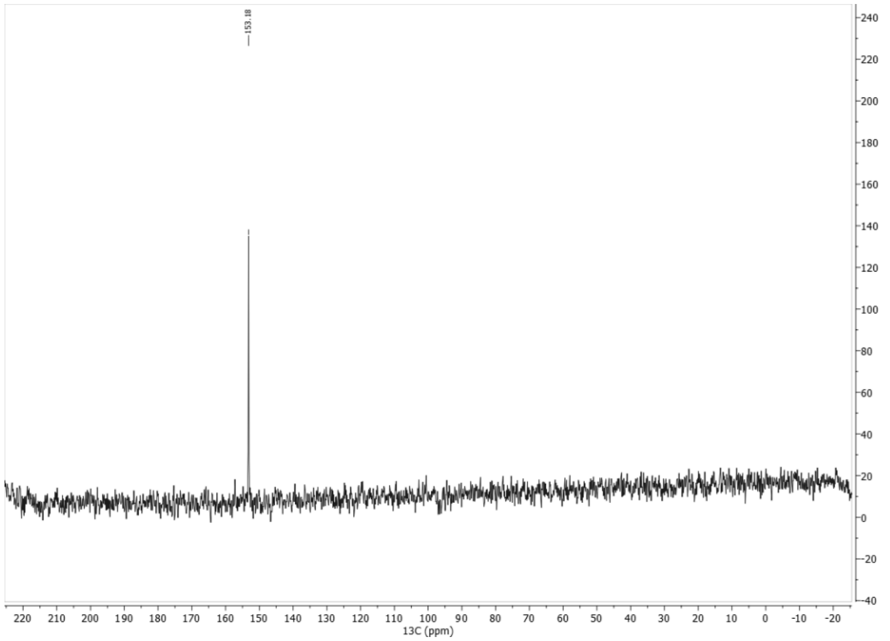

Figure S20. $^{13}C\{^{1}H\}$ NMR spectrum of Tripotassium bis(1-oxidotetrazol-5-yl)triazenide (**11**) in D_2O.

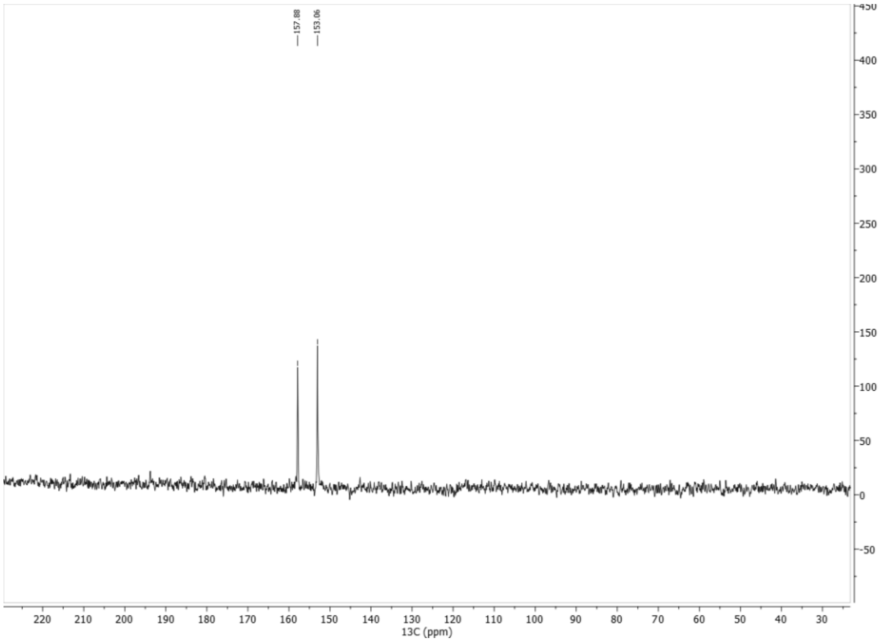

Figure S21. $^{13}C\{^1H\}$ NMR spectrum of Triguanidinium bis(1-oxidotetrazol-5-yl)triazenide (**13**) in D_2O.

2.7.6 IR Spectroscopy of 1–15

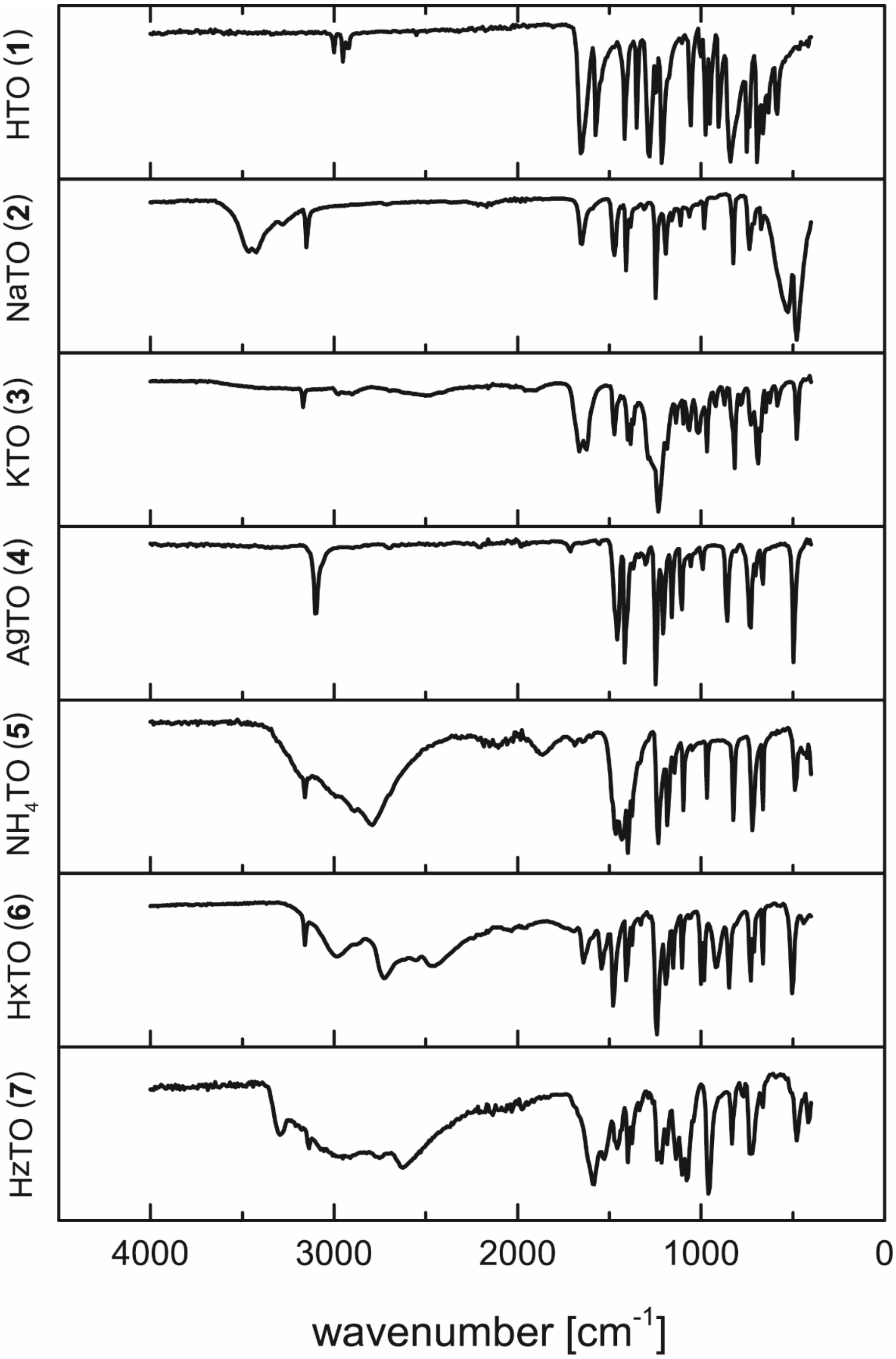

Figure S22. IR spectra of 1-hydroxytetrazole (**1**) and its salts **2**–**7.**

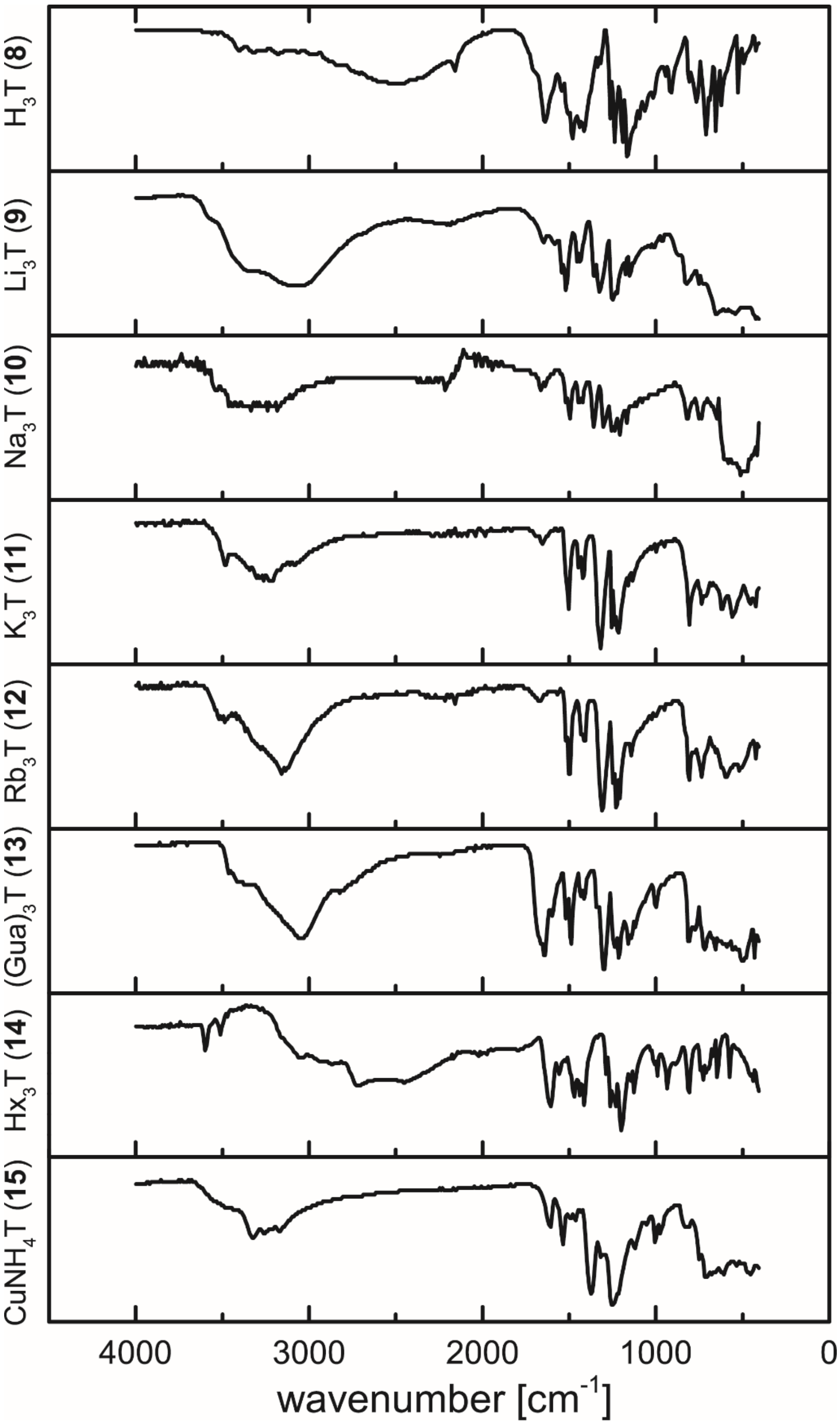

Figure S23. IR spectra of Bis(1-hydroxytetrazol-5-yl)triazene monohydrate (**8**) and its salts **9** – **15**. All salts except **14** are hexahydrates (**9**, **10**) or trihydrates (**11**-**13**, **15**)

2.7.7 General Methods

All chemicals and solvents were employed as received (Sigma-Aldrich, Fluka, Acros, ABCR). ^{1}H, ^{13}C{^{1}H}, ^{14}N, spectra were recorded at ambient temperature using a JEOL Bruker 27400, Eclipse 270, JEOL EX 400 or a JEOL Eclipse 400 instrument. The chemical shifts quoted in ppm in the text refer to typical standards such as tetramethylsilane (^{1}H, ^{13}C) nitromethane (^{14}N,^{15}N) in DMSO-*d*$_6$, D$_2$0 or acetone-*d*$_6$ as the solvent. Endothermic and exothermic events of the described compounds, which indicate melting, loss of crystal water or decomposition, are given as the extrapolated onset temperatures. The samples were measured in a range of 25–400 °C at a heating rate of 5 °C min^{-1} through differential thermal analysis (DTA) with an OZM Research DTA 552-Ex instrument and in some cases additionally by thermal gravimetric analysis (TGA) with a PerkinElmer TGA4000. Infrared spectra were measured with pure samples on a Perkin-Elmer BXII FT-IR system with a Smith DuraSampler IR II diamond ATR at a resolution of 4 cm^{-1} and 12 scans each. Spectra were analysed with the Perkin Elmer Spectrum 10 STD software suite.[S24] Determination of the carbon, hydrogen, and nitrogen contents was carried out by combustion analysis using an Elementar Vario El (nitrogen values determined are often lower than the calculated ones' due to their explosive behavior). Impact sensitivity tests were carried out according to STANAG 4489[S25] with a modified instruction[S26] using a BAM (Bundesanstalt für Materialforschung) drophammer.[S27] Friction sensitivity tests were carried out according to STANAG 4487[S30] with a modified instruction[S31] using the BAM friction tester.[S27,28] The classification of the tested compounds results from the "UN Recommendations on the Transport of Dangerous Goods".[S32,33] Additionally, all compounds were tested upon the sensitivity toward electrical discharge using the OZM Electric Spark XSpark10 device.[S28] Energetic properties have been calculated with the EXPLO5 6.05.04 computer code[S34] using the, to RT converted, X-ray density and calculated solid state heats of formation. These were computed by the atomization method as described in recently published papers. Electronic enthalpies were calculated with the Gaussian09 software[S13] suite using the CBS-4M method.

2.7.8 References

S1 CrysAlisPRO (Version 171.33.41), Oxford Diffraction Ltd., **2009**.

S2 A. Altomare, G. Cascarano, C. Giacovazzo, and A. Guagliardi, *J. Appl. Crystallogr.* **1992**, *26*, 343.

S3 A. Altomare, G. Cascarano, C. Giacovazzo, A. Guagliardi, A. G. G. Moliterni, M. C. Burla, G. Polidori, M. Camalli and R. Spagna, SIR97, **2003**.

S4 A. Altomare, M. C. Burla, M. Camalli, G. L. Cascarano, C. Giacovazzo, A. Guagliardi, A. G. G. Moliterni, G. Polidori and R. Spagna, *J. Appl. Crystallogr.* **1999**, *32*, 115.

S5 G. M. Sheldrick, SHELXL-97, University of Göttingen, Germany, **1997**.

S6 G. M. Sheldrick, *Acta Crystallogr. Sect. A* **2008**, *64*, 112.

S7 G. M. Sheldrick, *Acta Cryst. A* **2015**, *71*, 3–8.

S8 A. L. Spek, PLATON, Utrecht University, The Netherlands, **1999**.

S9 L.J. Farrugia, *J. Appl. Cryst.* **2012**, *45*, 849.

S10 O. V. Dolomanov, L. J. Bourhis, R. J. Gildea, J. A. K. Howard and H. Puschmann, *J. Appl. Cryst*. **2009**, *42*, 339–341.

S11 Empirical absorption correction using spherical harmonics, implemented in SCALE3 ABSPACK scaling algorithm (CrysAlisPro Oxford Diffraction Ltd., Version 171.33.41, **2009**).

S12 APEX3, Bruker AXS Inc., Madison, Wisconsin, USA.

S13 M. J. Frisch, G. W. Trucks, H. B. Schlegel, G. E. Scuseria, M. A. Robb, J. R. Cheeseman, G. Scalmani, V.Barone, B. Mennucci, G. A. Petersson, H. Nakatsuji, M. Caricato, X. Li, H.P. Hratchian, A. F. Izmaylov, J. Bloino, G. Zheng, J. L. Sonnenberg, M. Hada, M. Ehara, K. Toyota, R. Fukuda, J. Hasegawa, M. Ishida, T. Nakajima, Y. Honda, O. Kitao, H. Nakai, T. Vreven, J. A. Montgomery, Jr., J. E. Peralta, F. Ogliaro, M. Bearpark, J. J. Heyd, E. Brothers, K. N. Kudin, V. N. Staroverov, R. Kobayashi, J. Normand, K. Raghavachari, A. Rendell, J. C. Burant, S. S. Iyengar, J. Tomasi, M. Cossi, N. Rega, J. M. Millam, M.Klene, J. E. Knox, J. B. Cross, V. Bakken, C. Adamo, J. Jaramillo, R. Gomperts, R. E. Stratmann, O. Yazyev, A. J. Austin, R. Cammi, C. Pomelli, J. W. Ochterski, R. L. Martin, K. Morokuma, V. G. Zakrzewski, G. A. Voth, P. Salvador, J. J. Dannenberg, S. Dapprich, A. D. Daniels, O. Farkas, J.B. Foresman, J. V. Ortiz, J. Cioslowski and D. J. Fox, Gaussian 09 A.02, Gaussian, Inc., Wallingford, CT, USA, **2009**.

S14 J. W. Ochterski, G. A. Petersson and J. A. Montgomery Jr., *J. Chem. Phys.* **1996**, *104*, 2598–2619.

S15 J. A. Montgomery Jr., M. J. Frisch, J. W. Ochterski and G. A. Petersson, *J. Chem. Phys.* **2000**, *112*, 6532–6542.

S16 L. A. Curtiss, K. Raghavachari, P. C. Redfern and J. A. Pople, *J. Chem. Phys.* **1997**, ***106***, 1063–1079.

S17 E. F. C. Byrd and B. M. Rice, *J. Phys. Chem. A* **2006**, *110*, 1005–1013.

S18 B. M. Rice, S. V. Pai and J. Hare, *Comb. Flame* **1999**, *118*, 445–458.

S19 P. J. Lindstrom and W. G. Mallard, NIST Standard Reference Database Number 69, http://webbook.nist.gov/chemistry/, (accessed March **2021**).

S20 M. S. Westwell, M. S. Searle, D. J. Wales and D. H. Williams, *J. Am. Chem. Soc.* **1995**, *117*, 5013–5015.

S21 F. Trouton, *Philos. Mag.* **1884**, *18*, 54–57.

S22 H. D. B. Jenkins, H. K. Roobottom, J. Passmore, L. Glasser, *Inorg. Chem.* **1999**, *38*, 3609–3620.

S23 H. D. B. Jenkins, D. Tudela, L. Glasser, *Inorg. Chem.* **2002**, *41*, 2364–2367

S24 PerkinElmer Inc., Spectrum™ 10 STD, Waltham, USA, **2010**.

S25NATO standardization agreement (STANAG) on explosives, impact sensitivity tests, no. 4489, 1st ed., Sept. 17, **1999**.

S26 WIWEB-Standardarbeitsanweisung 4-5.1.02, Ermittlung der Explosionsgefährlichkeit, hier der Schlagempfindlichkeit mit dem Fallhammer, Nov. 8, **2002**.

S27 BAM, http://www.bam.de, (accessed March **2021**).

S28 OZM, http://www.ozm.cz, (accessed March **2021**).

S29 Military Standard 1751A (MIL-STD-1751A): safety and performance tests for qualification of explosives (high explosives, propellants and pyrotechnics), method 1016, Dec. 11, **2001**.

S30 NATO standardization agreement (STANAG) on explosive, friction sensitivity tests, no. 4487, 1st ed., Aug. 22, **2002**.

S31 WIWEB-Standardarbeitsanweisung 4-5.1.03, Ermittlung der Explosionsgefährlichkeit oder der Reibeempfindlichkeit mit dem Reibeapparat, Nov. 8, **2002**.

S32 UN Model Regulation: Recommendations on the Transport of Dangerous Goods – Manual of Tests and Criteria, section 13.4.2.3.3, **2015**.

S33 Impact: insensitive > 40 J, less sensitive ≥ 35 J, sensitive ≥ 4 J, very sensitive ≤ 3 J; Friction: insensitive > 360 N, less sensitive = 360 N, sensitive < 360 N and > 80 N, very sensitive ≤ 80 N, extremely sensitive ≤ 10 N. According to the UN Recommendations on the Transport of Dangerous Goods, 5th ed., **2009**.

S34 M. Sućeska, EXPLO5 Version 6.05 User's Guide. Zagreb, Croatia: OZM; **2018**.

3 *N*-Fluoromethylated Tetrazoles: Manipulating Thermal and Energetic Properties

Marco Reichel, Maximilian H. H. Wurzenberger, Marcus Lommel, Moritz Kofen, Burkhard Krumm, Jörg Stierstorfer and Konstantin Karaghiosoff

Dedicated to Prof. Dr. Thomas M. Klapötke on the occasion of his 60th birthday.

Reprinted (adapted) from *Z. Anorg. Allg. Chem.* **2021**, *647*, 341–349.

DOI: 10.1002/zaac.202000341

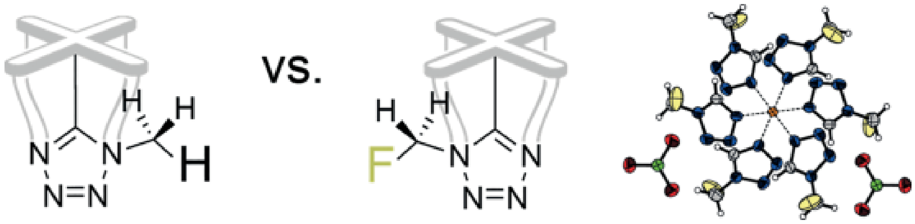

Abstract: Fluoroiodomethane was allowed to react with the sodium salts of tetrazole and 5-aminotetrazole to give in each case the two corresponding isomers 1-fluoromethyltetrazole (**1a**) and 2-fluoromethyltetrazole (**1b**), as well as 1-fluoromethyl-5-aminotetrazole (**2a**) and 2-fluoromethyl-5-aminotetrazole (**2b**). The new tetrazoles were isolated and characterized by spectroscopic methods (IR, Raman, multinuclear NMR), mass spectrometry, and in the case of fluoromethyl-5-aminotetrazole the crystal structures of both isomers were obtained and discussed. Differential thermal analysis (DTA) gave insight in how a FCH_2 moiety attached to a tetrazole effects the ther-mal behavior compared to its CH_3 analog. In addition, the detonation parameters were calculated and compared to those of the corresponding methyl tetrazoles. In addition, the preparation of energetic copper complexes of the new ligands was attempted. Complexes of copper(II) perchlorate and chlorate are crystallographically described and their energetic properties discussed.

3.1 Introduction

Tetrazoles, whose discovery dates back to the year 1885,[1] are well investigated long known substances and can be easily synthesized. There are numerous ways to obtain substituted tetrazoles. The most common and applied protocols nowadays either use a [3+2] cycloaddition of nitriles and azides in presence of a proton source or a [3+1+1] cyclization starting from an amine, triethyl orthoformate and sodium azide with acetic acid as reaction medium.[1] Another approach those of the substitution reactions of 1*H*-tetrazoles to introduce functional groups such as amines,[2] alkanes,[3] or even *N*-oxides[4] to the nitrogen atoms of the heterocycle. This synthetic pathway allows the preparation of 2*N*-substituted tetrazoles, which are often obtained as isomeric mixtures with the 1*N*-substituted compound. Since tetrazoles are bioisoster to carboxylate groups, they are mostly used as pharmaceutical agents and show central nervous system-, anti-inflammatory-, anti-allergic-, anti-microbial-, cardiovascular- and miscellaneous activity.[1,5] Furthermore, it is well known that tetrazoles can be used for the synthesis of coordination compounds with various metal ions, and there has been a growing interest over the last years.[6] The resulting complexes further expand the field of possible applications for tetrazole-based substances (e.g. metal-organic frameworks (MOFs) with unique properties,[7] spin crossover systems,[8] and energetic materials[9]). It is also well-known, that most tetrazole derivatives are melting above 150 °C and exhibit explosive properties when heated above their melting points or touched with a hot wire.[10] Furthermore, the impact sensitive behavior of tetrazole cycle linked to nitrogen atoms and the explosive nature of heavy metal salts of 5-monosubstituted tetrazoles were mentioned in literature before.[10] However, Klapötke and co-workers were the first who recognized, that tetrazoles are good starting materials for the synthesis of new highly energetic nitrogen-rich materials.[11] Because tetrazoles combine the desired endothermicity with kinetic stability, forming non-toxic reaction products, producing a high temperature and having a high burning rate during decomposition,[11] Klapötke and co-workers investigated tetrazole derivatives as green[12] high performance explosive replacements.[13] Therefore, this class of compounds was applied in primary explosives,[14] secondary explosives,[11,13] and pyrotechnics.[11,15] Fluorine containing tetrazoles are especially interesting as oxidizers in magnesium based flare compositions (decoy flares)[15] (Figure 1) or in agent defeat weapons, as fluorine containing payloads are effective in destroying biological threats like anthrax.[11] More recent investigations showed that the replacement of a CH_3 with a FCH_2 moiety can lead to a drastic change in the physical- and sensitivity properties of a compound.[16] However, until very recently this year, the first and only fluoromethyl containing tetrazole, 5-fluoromethyl-tetrazole[17] and one non-energetic complex[18] were reported. Since a large number of fluoromethylating agents for various nucleophiles are available until now[19] and only *N*-methylated but no *N*-fluoromethylated tetrazoles are known up to date, this prompted us to synthesize fluoromethylated tetrazoles und investigate their thermal-, energetic- and complexation behavior.

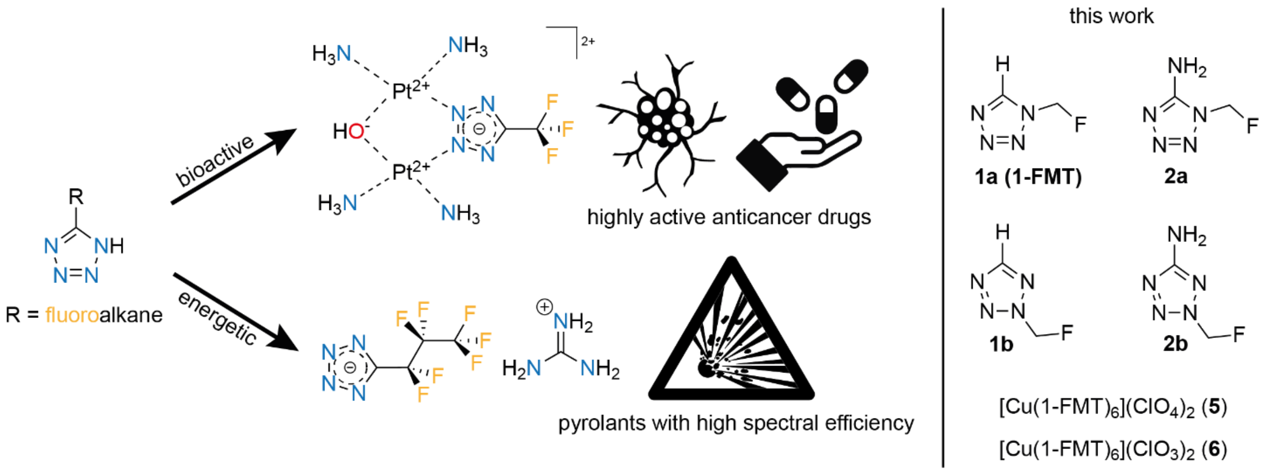

Figure 1. Selected fluorine containing tetrazoles.

3.2 Results and Discussion

N-Fluoromethylated tetrazoles were obtained in a simple, mild and high yield synthesis from the reaction of the corresponding sodium or potassium tetrazolate salts with fluoroiodomethane in acetone or acetonitrile (Scheme 1). Unlike for the reaction of sodium 5-aminotetrazolate (NaAT) with CH_3I or $(CH_3O)_2SO_2$, water[20] or ethanol[21] should be avoided as solvent for the synthesis, since such use did cause extensive decomposition during the reaction.

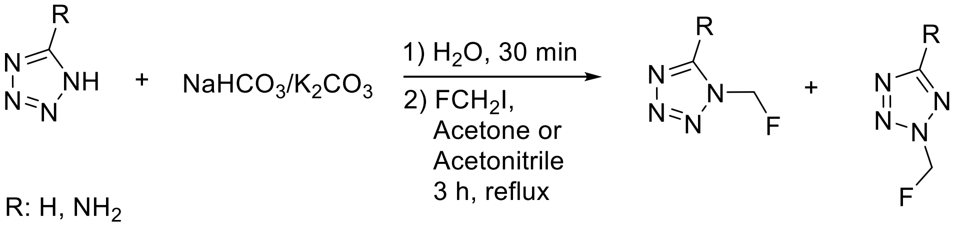

Scheme 1: Synthesis of *N*-fluoromethylated tetrazoles.

This synthetic pathway leads to the formation of two isomers which have to be specially purified. Different to their methyl analog, special synthetic routs[15] which lead exclusively to the formation of only one isomer (Scheme 2), did not work using fluoroiodomethane, as both isomers were formed. The reaction of NaAT with CH_2FI in acetone provided 83% of a 2:1 mixture of 5-amino-1-fluoromethyltetrazole **1a** and 5-amino-2-fluoromethyltetrazole **1b**. From this mixture **1a** was isolated with 51% and **1b** with 24% yield. Both isomers are colorless solids and can be easily distinguished via multinuclear NMR spectroscopy [D_6-DMSO]. In the ^1H NMR spectrum, the FCH_2 signal for **1a** is observed at $\delta = 6.25$ ppm with a coupling constant of $^2J(F,H) = 51.9$ Hz and the resonance of the amino group at $\delta = 7.32$ ppm. In comparison with **1a**, the CH_2F resonance of **1b** at $\delta = 6.46$ ppm with a coupling constant of $^2J(F,H) = 50.8$ Hz is shifted to higher frequencies and the signal of the amino group is shifted to lower frequencies ($\delta = 6.45$ ppm). The ^{13}C NMR resonances of compound **1a** appear at $\delta = 86.6$ ppm with a coupling constant of $^1J(F,C) = 202.2$ Hz (CH_2F) and at $\delta = 168.0$ ppm as singlets. Both signals are shifted to lower frequencies compared to **1b**. Here, the CH_2F signal at $\delta = 81.2$ ppm, having a coupling constant of $^1J(F,C) = 197.7$ Hz differs clearly. However, final distinction of the two isomers in the ^{13}C NMR spectra is given by the CNH_2 resonance of **1b**, which splits into a doublet $^4J(F,C) = 1.4$ Hz having a chemical shift of $\delta = 156.1$ ppm. A simple distinction of the two isomers can also be made, using ^{19}F NMR spectroscopy. The resonance of **1a** is detected at $\delta = -170.8$ ppm as triplet, and is shifted to lower frequencies, compared to **1b** with a chemical shift of $\delta = -169.7$ ppm (triplet). The ^{15}N NMR chemical shift of the NH_2 group is shifted to lower frequencies for **1b** compared to **1a**. The NCH_2F resonance in **1b** splits in a doublet with a coupling constant of $^2J(F,N) = 17.4$ Hz. However, due to the low solubility of **1a** in DMSO, this resonance is missing in the corresponding spectra. Whereby only one long range coupling at $\delta = -23.8$ ppm $^xJ(F,N) = 1.1$ Hz, forming a doublet is observed for **1a**, **1b** displays two long range couplings at $\delta = -71.6$ and -120.7 ppm forming a doublet with $^xJ(F,N) = 0.7$ and 1.2 Hz is observed. Single crystals of the two compounds were obtained by dissolving the products in water and cooling the solution to 3 °C for several days. The molecular structures of **1a** and **1b** in the crystal are shown in Figure 3.

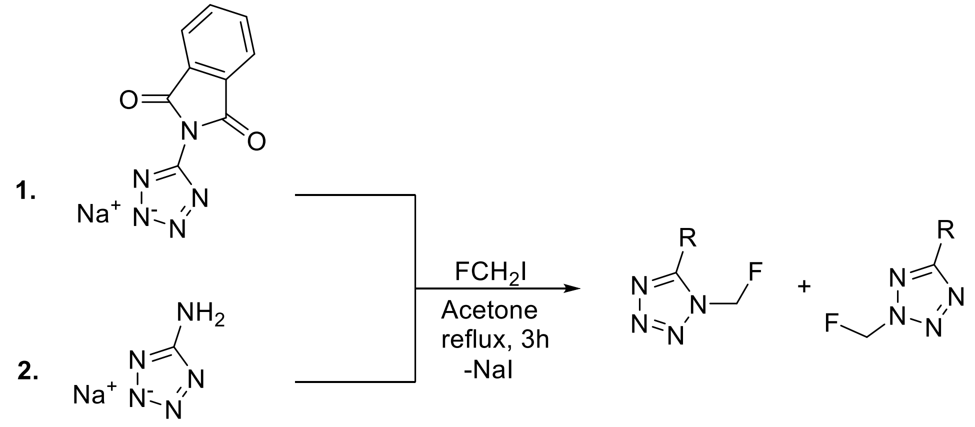

Scheme 2: Synthesis of fluoromethylated 5-amino tetrazoles.

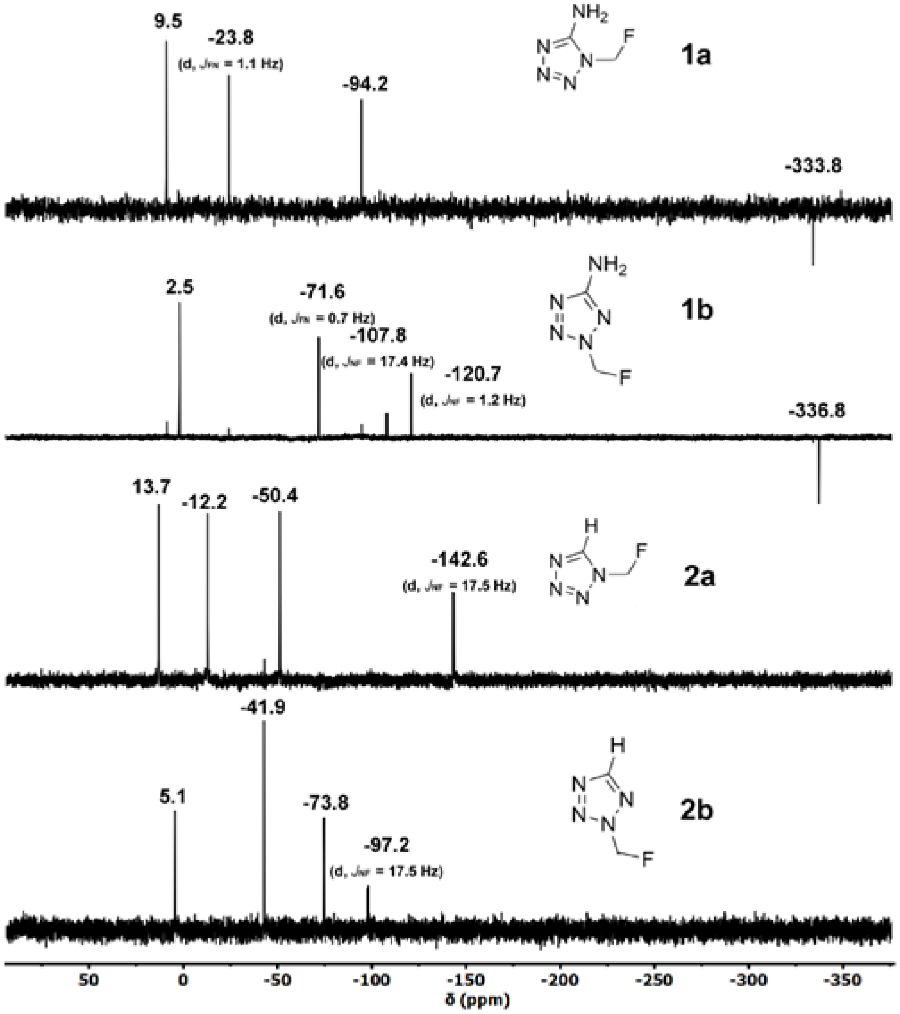

Figure 2: ^{15}N NMR spectra of **1a/b-2a/b** (DMSO-D$_6$ or CDCl$_3$, 25 °C).

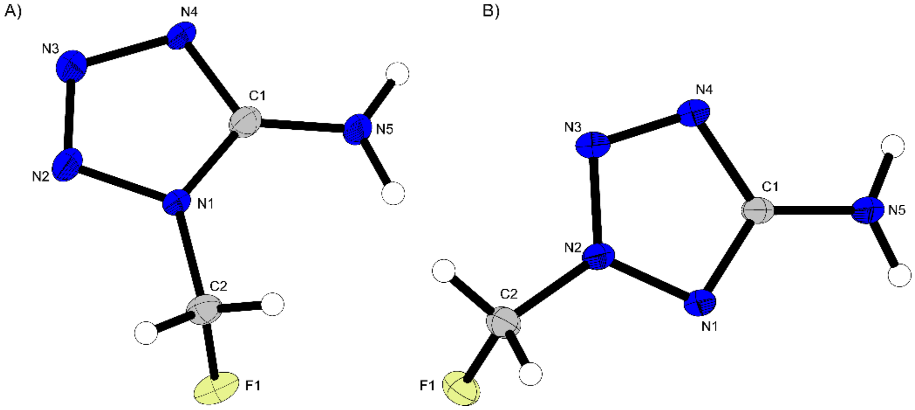

Figure 3: Molecular structure of **1a** (A) and **1b** (B) in the crystal. DIAMOND representation, thermal ellipsoids are drawn with 50% probability. Selected bond lengths and angles of **1a**: F1–C2, 1.382(3); C2–N1, 1.429(4); F1–C2–N1, 109.3(2); F1–C2–N1–C1, -82.7(4). **1b**: F1–C2, 1.380(2); C2–N2, 1.439(2); F1–C2–N2, 108.6(2); F1–C2–N2–N1, -70.0(2).

The nitrogen atom bonded to the CH_2F group in **1a** and **1b** displays a trigonal planar environment. The corresponding N1–C2 and N2–C2 bond lengths of 1.429(4) and 1.439(2) Å, respectively, compare well to each other and are shortened compared to the know $[Me_3NCH_2F]^+$ moiety. The C2–F1 distance of 1.382(3) Å (**1a**) and 1.380(2) Å (**1b**) compare well with those reported for PCH_2F (1.379(5) Å)[12c] CH_2FI (1.380(17) Å)[16] and CH_2FBr (1.377(4 Å).[16] Noteworthy is the different thermal behavior observed for **1a** and **1b**. The melting points of these two compounds differ by almost 60 °C. Analogous properties are reported for the methyl derivatives.[17]

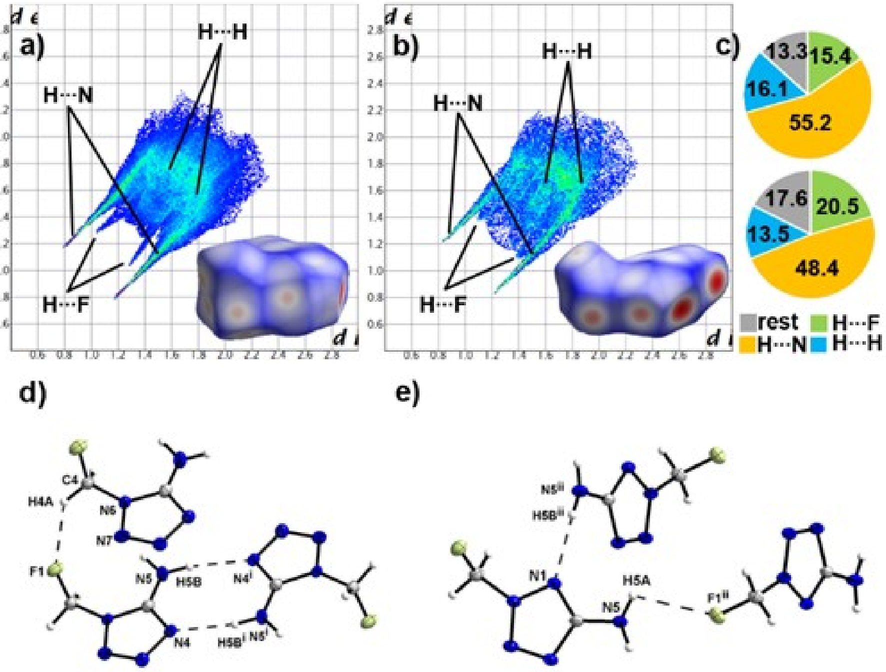

Figure 4: Two-dimensional fingerprint plot as well as the corresponding Hirshfeld surface (bottom right in 2D plot) of **1a** (a) and **1b** (b). Color coding: white, distance d equals VDW distance; blue, d exceeds VDW distance, red, d, smaller than VDW distance). Population of close contacts of **1a** (c) top and **1b** (c) bottom in crystal stacking. Strongest hydrogen bonds in **1a** (d) and **1b** (e). DIAMOND representation. Thermal ellipsoids are drawn at 50% probability level. Symmetry codes: *i*) 2−x, 1−y, −z; *ii*) 0.5+x, 0.5−y, 0.5+z; *iii*) 0.5−x, 0.5+y, 0.5−z.

In order to understand this behavior, intermolecular interactions in the crystal have to be investigated and a Hirshfeld analysis was performed on the crystal structures of **1a** and **1b** (Figure 4). The sum $d_i + d_e$ (d_i: distance from the Hirshfeld surface to the nearest atom interior; d_e: distance from the Hirshfeld surface to the nearest atom exterior) in the 2D plot of **1a** and **1b** reveals, that the spikes for N···H contacts are similarly wide for both compounds and only slightly longer for **1a**. Thus, for both compounds, the N···H contacts in this range are similarly strong and the strong interactions occur with a similar frequency. However, there are clear differences regarding the F···H contacts. These are clearly stronger for **1a** (distinct long spikes) than for **1b**, as indicated also by the shorter hydrogen bridges in the crystal structure. With H···F contact distances of 2.37(3) Å (**1a**) vs. 2.60(3) Å (**1b**) the attractive forces in the crystal of 1-fluoromethyl-5-aminotetrazole (**1a**) are clearly stronger than for **1b**. The sum of the attractive interactions for **1a** (70.6%) and for **1b** (68.9%) is almost the same. As consequence, the sum of all intermolecular interactions in the crystal of **1a** are stronger than in **1b**. This results in dramatic differences in the thermal behavior of the two isomers **1a** and **1b**. Compound **1a** decomposes while melting at 131 °C, whereas the isomer **1b** melts at 75 °C and decomposes at 166 °C. It is interesting to compare these thermal properties with those of the corresponding methyl derivatives. The 5-amino-1-methyltetrazole (m.p. 226 °C[17a]) and 5-amino-2-methyltetrazole (m.p. 105 °C[17b]) show in both cases a higher melting point than their fluorine containing derivative (Figure 5). The reaction of potassium tetrazolate with CH_2FI gave 85% of a mixture of 1-fluoromethyltetrazole (**2a**) and 2-fluoromethyltetrazol (**2b**). From this mixture the isomers were separated as colorless oils via distillation with 10% (**2a**) and 40% (**2b**) yield. Both substances can easily be differentiated by multinuclear NMR spectroscopy [$CDCl_3$].

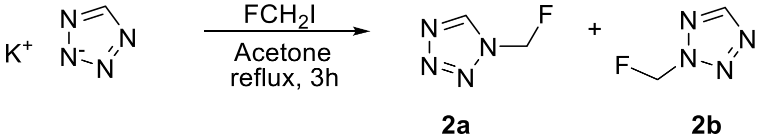

Scheme 3: Synthesis of *N*-fluoromethylated tetrazoles.

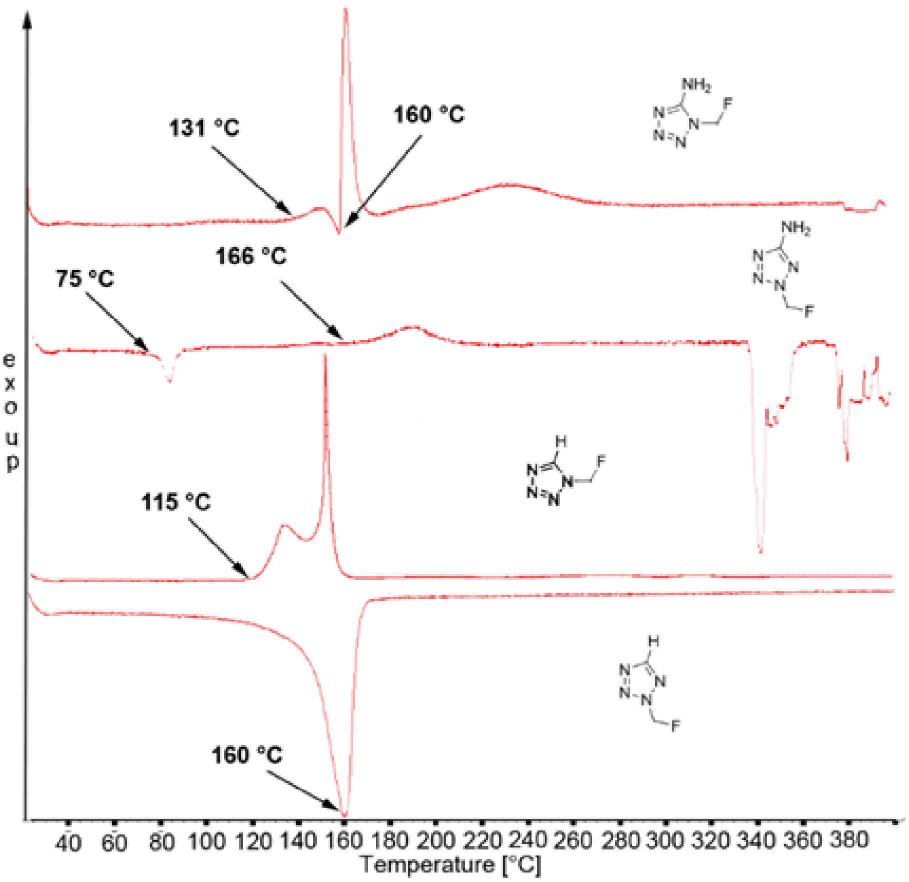

Figure 5: DTA of compounds **1a**/**b**-**2a**/**b**.

In the ^{1}H NMR spectrum, the FCH2 signal for **2a** is observed at δ = 6.40 ppm with a coupling constant of ^2J(F,H) = 50.0 Hz and the resonance of C*H* protone at δ = 8.90 ppm. In comparison with **2a**, the CH2F resonance of **2b** at δ = 6.55 ppm with a coupling constant of ^2J(F,H) = 49.7 and ^5J(H,H) = 0.4 Hz is shifted to higher frequencies and the signal of the C*H* proton is shifted to lower frequencies (δ = 8.65 ppm). This trend is similar to fluoromethylated aminotetrazole as mentioned above. The ^{13}C NMR resonances of compound **2a** appear at δ = 82.8 ppm with a coupling constant of ^1J(F,C) = 209.5 Hz (CH2F) and at δ = 143.7 ppm as singlet. Both signals are shifted to lower frequencies compared to **2b**. Here, the CH2F signal appears at δ = 86.1 ppm, having a coupling constant of ^1J(F,C) = 211.7 Hz and the *C*H signal is detected at δ = 154.1 ppm. A simple distinction of the two isomers can also be made, using ^{19}F NMR spectroscopy. The resonance of **2a** is detected at δ = –169.4 ppm as triplet, and is shifted to higher frequencies, compared to **2b** with a chemical shift of δ = –171.4 ppm (triplet). Different to compounds **1a** and **1b** no long-range couplings in the ^{15}N NMR could be observed for **2a** and **2b**. The *N*CH2F group shows in **2a** a drastic shift to lower frequencies (δ = –142.6 ppm (**2a**) vs δ = –97.2 ppm (**2b**)). However, the coupling constant of the doublet with ^{2}J(F,N) = 17.5 Hz remains the same. Like for compound **1**, the fluorine effects the thermal properties of compound **2** – compared to its methyl analog – in a similar manner. Compound **2a** has a melting point of 19 °C. Compared to its methyl derivate (extrapolated boiling point 259 °C/110 °C, 5 Torr; melting point 39 °C)[18] the thermal properties are shifted to lower values. This is also the case for **2b**.

3.2.1 Energetic Properties

The sensitivities towards friction and impact of **1** and **2** were determined experimentally according to standards of the German Federal Institute for Material Research and Testing (BAM). According to the UN recommendations on transport of dangerous goods, **1** and **2** have to be classified as insensitive towards impact and friction (Table 1). *Ab initio* calculations were carried out to compute the heat of formation for **1**, **2** and the corresponding methyl derivatives. Using the optimized geometry of the molecules starting from the X-ray diffraction experiment. In general, the methyl derivatives show a higher heat of formation than their fluoromethyl derivatives. Further, compound **1a** and **2a** show a higher heat of formation than for the isomers (**1b**, **2b**) thereof. That's also the case for the methyl derivatives. Based on the heats of formation and the corresponding densities determined from the X-ray experiment or calculations, the detonation parameters were calculated using the EXPLO5 V6.03 code. The detonation parameters were calculated at the Chapman-Jouguet (C-J) point with the help of a stationary detonation model using a modified Becker-Kistiakowski-Wilson state equation for the system. The C-J point was located using the first derivative of the Hugoniot curve of the system. With an extrapolated boiling point of 160 °C and a melting point of 0 °C it boils and melts lower as the corresponding methyl derivative, which has an extrapolated boiling point of 213 °C (145 °C, 118 Torr) and a melting point of 10 °C.[18, 22] Interestingly the heat of detonation of the methyl derivatives exceed – except for **1MATz** – those of the fluoromethylmethyl compounds. However, the detonation temperature and pressure show better performance parameters for the fluoromethyl compounds than for their methyl derivatives. Whereby, the detonation velocity is always higher for the fluoromethyl compounds (except for **2a**), the volume of detonation gases varies. In summary, the conversion of a CH_3 to a CH_2F group seem to increase the performance parameters like in the most cases. Further regarding the fluoromethyl compounds, as a general trend, the 1-isomers exhibit better performance parameters, than the 2-isomers.

Table 1: Energetic Parameters of **1-2**.

	1a	**1b**	**2a**	**2b**	**1MATz**	**2MATz**	**1MHTz**	**2MHTz**
formula	$C_2H_4FN_5$	$C_2H_4FN_5$	$C_2H_3FN_4$	$C_2H_3FN_4$	$C_2H_5N_5$	$C_2H_5N_5$	$C_2H_4N_4$	$C_2H_4N_4$
M [g mol^{-1}]	117.04	117.04	102.03	102.03	99.10	99.10	84.08	84.08
IS[a] [J]	>40	>40	>40	>40	>40[7a]	>40[7a]	>40[7a]	>40[7a]
FS[b] [N]	>360	>360	>360	>360	>360[7a]	>360[7a]	>360[7a]	>360[7a]
N[c] [%]	59.81	59.81	54.89	54.89	70.67	70.67	66.63	66.63
Ω_{CO}[d] [%]	−47.8	−47.8	−47.0	−47.0	−72.6	−72.6	−76.1	−76.1
Ω_{CO2}[d] [%]	−75.2	−75.2	−78.4	−78.4	−104.9	−104.9	−114.2	−114.2
T_{melt}[e] [°C]	131	75	19	0	225[7a]	104[7a]	39[7a]	9[18]
ρ_{293K}[f] [g cm^{-3}]	1.648	1.638	1.593	1.581	1.42[19]	1.341[20]	1.432[21]	1.31[19]
ΔH_f^0 [g] [kJ mol^{-1}]	44.5	34.4	71.0	56.3	210.2	206.3	244.1	227.9
EXPLO5 V 6.03								
ΔU_f^0 [h] [kJ kg^{-1}]	−2773	−2691	−3235	−3096	−2725	−2713	−3316	−3210
T_{C-J}[i] [K]	2220	2184	2533	2465	1967	1974	2225	2227
P_{C-J}[j] [GPa]	20.4	19.8	17.8	17.1	16.5	14.0	16.7	13.8
V_{det}[k] [ms^{-1}]	7677	7589	7221	7105	7313	6897	7321	6876
V_o[l] [dm^3 kg^{-1}]	858	859	826	826	864	872	817	825

[a] Impact sensitivity (BAM drop-hammer, method 1 of 6); [b] friction sensitivity (BAM friction tester, method 1 of 6); [c] nitrogen content; [d] absolute oxygen balance assuming the formation of CO or CO2 and HF; [e] melting point; [f] density at 293 K; [g] heat of formation calculated at the CBS-4M level of theory [h] detonation energy; [i] detonation temperature; [j] detonation pressure; [k] detonation velocity; [l] volume of detonation gases at standard temperature and pressure conditions.

3.2.2 *N*-Fluoromethylated Tetrazoles as Ligands

For investigating the complexation behavior of the nitrogen-rich molecules and comparing it with their fluorine-free analogs, it was attempted to synthesize complexes according to literature procedures.[8] Various combinations of the ligands **1a**–**2b** with different central metals (Ag^+, Mn^{2+}, Fe^{2+}, Fe^{3+}, Cu^{2+}, and Zn^{2+}) and anions (Cl^-, NO_3^-, ClO_3^-, ClO_4^-) were investigated. In the cases of **1b** and **2b** solely starting material was isolated regardless of the used solvent systems (water, methanol, ethanol, acetonitrile, and mixtures of them). Most of the silver salt solutions showed decompositions and arise of elemental silver within hours or days, which also occurred when stored in the dark. Combining 1-fluormethyl-5-aminotetrazole with silver(I), iron(II), or copper(II) salts lead to the immediate formation of viscid brownish precipitates. It was possible to pick one single crystal out of the batch consisting of copper(II) chlorate and **1a**. The single-crystal diffraction experiment revealed a copper(I) chlorate complex (**3**), indicating the occurrence of a redox reaction between the transition metal salts and **1a**. To the best of our knowledge, **3** is the first copper(I) chlorate complex described in literature, but unfortunately it was impossible to synthesize the compound selectively, due to the absence of a known copper(I) chlorate source. Following this, tetrakis(acetonitrile)copper(I) perchlorate was synthesized, starting from Cu_2O and perchloric acid in acetonitrile and further reacted with **1a**. This synthetic approach led to the analog perchlorate complex **4**, showing almost the same built up as coordination compound **3**. Both compounds **3** and **4** are highly instable under ambient conditions. When applying **2a** for the synthesis of complexes, it is possible to achieve an analogous hexa-coordination to copper(II) central metals as with 1-methyltetrazole.[8c] In contrast to **3** and **4**, the resulting complexes **5** and **6** when using copper(II) (per)chlorate as starting material are stable in air.

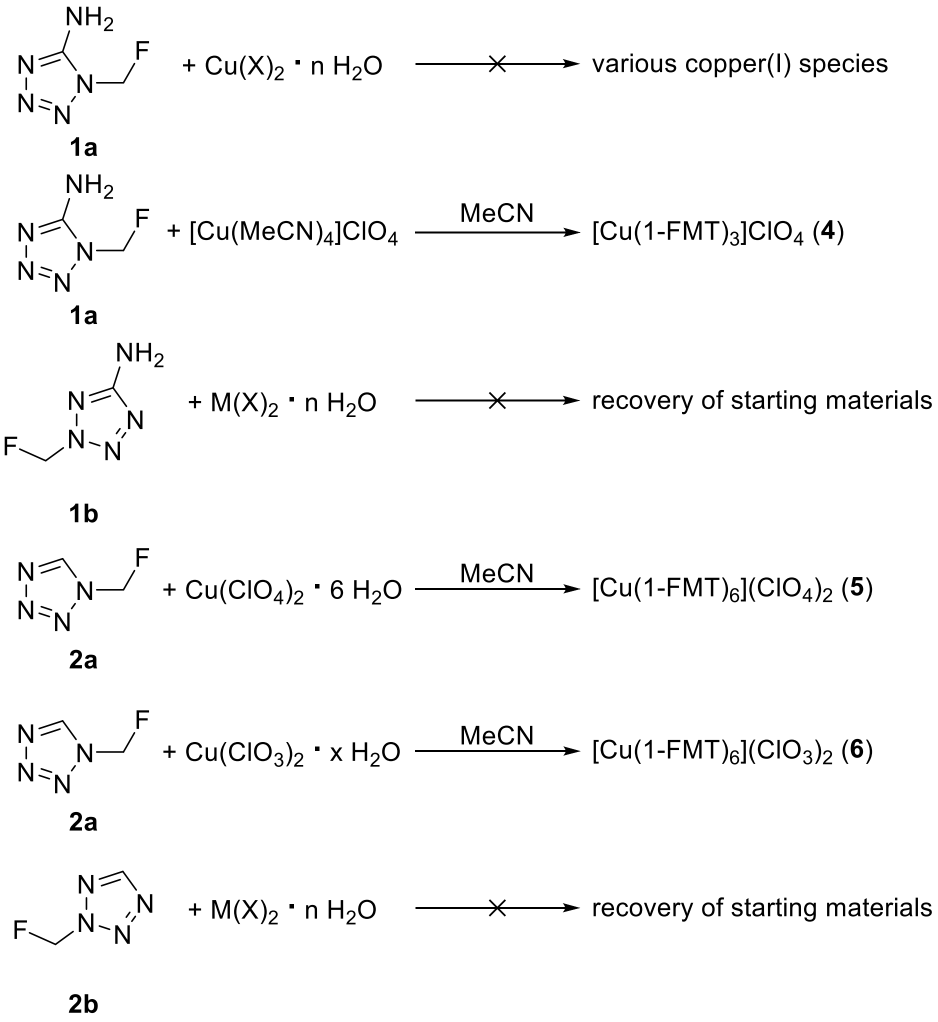

Scheme 4: Results of using **1a**–**2b** as ligands in complexation reactions.

The bond lengths and angles of the tetrazole ligands are in all complexes similar to the ones of **1a** and **2a**. Coordination compound **3** crystallizes in the hexagonal space group *P*6_3 with two formula units per unit cell and a calculated density of 1.895 g cm^{-3} (133 K). The molecular unit consists of one copper(I) cation trigonal-planarly coordinated by three tetrazole ligands and one non-coordinating chlorate anion. The Cu–N bond lengths are in the typical range of trigonal-planar copper(I) complexes.[9]

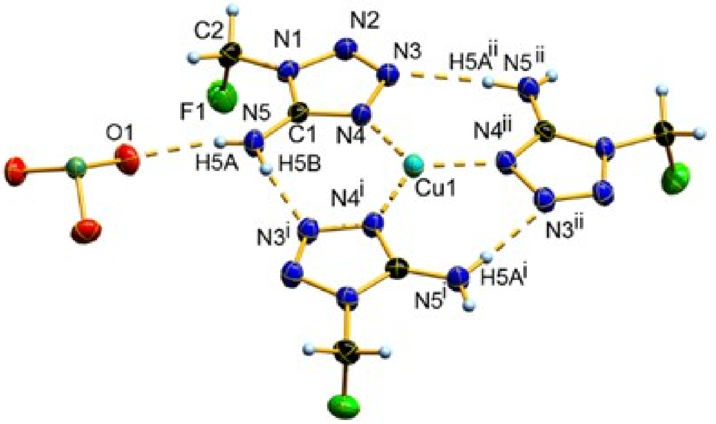

Figure 6: Molecular unit of **3**. DIAMOND representation, thermal ellipsoids are drawn with 50% probability. Selected bond length and angle of **3**: Cu1–N4 1.952(3), N4–Cu1–N4^{i} 119.95(12). Symmetry codes: *i*) 2−y, 1+x−y, z; *ii*) 1−x+y, 2−x, z.

Complex **5** with a hexacoordination around the copper(II) center, crystallizes in the monoclinic space group $P2_1/c$ with two formula units per unit cell and a calculated density of 1.911 g cm^{-3} (107 K). The molecular unit consists of one copper(I) cation trigonal-planarly coordinated by three tetrazole ligands and one non-coordinating chlorate anion. The Cu–N bond lengths are in the typical range of trigonal-planar copper(I) complexes.

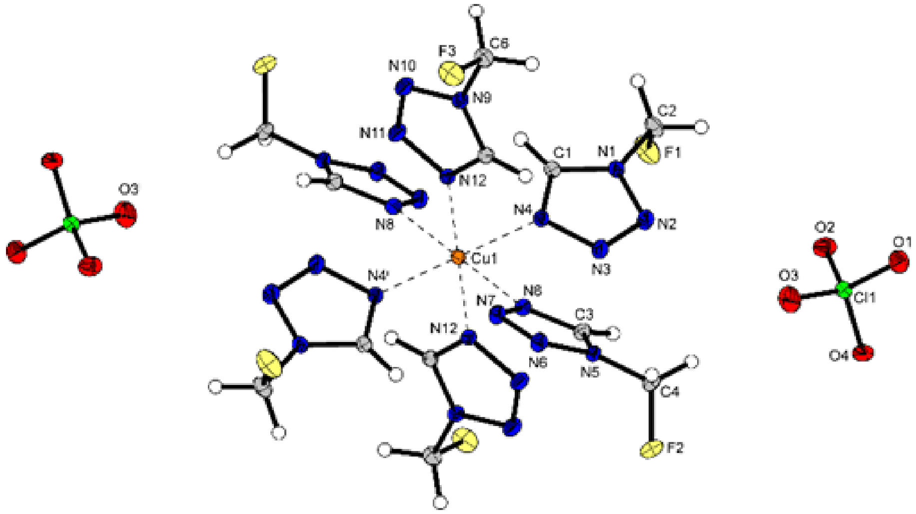

Figure 7: Molecular unit of **5**. DIAMOND representation, thermal ellipsoids are drawn with 50% probability. Selected bond lengths and angles of **5**: Cu1–N4 2.0489(12), Cu1–N8 2.4377(13), Cu1–N12 2.0133(12), N4–Cu1–N8 90.94(5), N4–Cu1–N8 90.71(5), N4–Cu1–N4^{i} 180.00. Symmetry code: *i*) −x, 1−y,1−z.

Compound	$T_{\mathrm{endo.}}$ [°C][a]	$T_{\mathrm{exo.}}$ [°C][b]	*IS* [J][c]	*FS* [N][d]	*ESD* [mJ][e]
$[Cu(1\text{-}FMT)_6](ClO_4)_2$ (**5**)	-	184	≤ 1	24	181
$[Cu(1\text{-}FMT)_6](ClO_3)_2$ (**6**)	96	138	2	168	181
$[Cu(1\text{-}MTZ)_6](ClO_4)_2$[7i]	178	211	2.5	54	80
$[Cu(ClO_3)_2(1\text{-}MTZ)_4]$[7f]	-	159	3	7	100

[a] Endothermic peak, which indicates melting, dehydration, or loss of aqua ligands. Onset temperature at a heating rate of 5 °C min^{-1} measured by DTA; [b] Exothermic peak, which indicates decomposition. Onset temperature at a heating rate of 5 °C min^{-1} measured by DTA; [c] Impact sensitivity according to the BAM drop hammer (method 1 of 6); [d] Friction sensitivity according to the BAM friction tester (method 1 of 6); [e] Electrostatic discharge sensitivity (OZM Electric Spark XSpark10).

3.3 Conclusion

In summary we have synthesized new fluoromethylated tetrazoles, which can act as versatile interesting ligands, especially in energetic complexes. Single X-ray diffraction reveals structural information of a nitrogen bonded to a CH_2F moiety in heterocycles, the first of its kind. The NCH_2F moiety has a shortened N-C and C-F bond length compared to the know $[Me_3NCH_2F]^+$ moiety. Only weak fluorine hydrogen interactions were observed. Using Hirshfeld analysis, it could be demonstrated that in 2-fluoromethyl-5-aminotetrazole the reduced number of stronger N···H contacts – replaced by weaker F···H contacts is the main reason for the drastically changed thermal behavior between the isomers. As a general trend, thermal properties are influenced in that mannor, that a CH_2F group lowers the boiling and melting point compared to a CH_3 group. Whereby the fluoromethyl derivatives lead to a lower heat of formation, the detonation parameters exhibit in most cases better performance.

3.4 Experimental Section

Fluoroiodomethane was distilled prior use. All other chemicals were commercially available from ABCR. For NMR spectroscopy the solvents were dried using 3 Å molecular sieve. Spectra were recorded on a Bruker Avance III spectrometer operating at 400.1 MHz (^1H), 100.6 MHz (^{13}C), 376.4 MHz (^{19}F), and 40.6 MHz (^{15}N). Chemical shifts are referred to TMS (^1H, ^{13}C), $CFCl_3$ (^{19}F) and $MeNO_2$ (^{15}N). The ^{19}F NMR spectra were also recorded in the ^1H decoupled mode. Raman spectra were recorded with a Bruker MultiRam FT Raman spectrometer using a neodymium doped yttrium aluminum garnet (Nd:YAG) laser ($\lambda = 1064$ nm) with 1074 mW. The samples for Infrared Spectroscopy were placed under ambivalent conditions onto an ATR unit using a Perkin–Elmer Spectrum BX II FT-IR System spectrometer. Melting and / or decomposition points were detected with an OZM DTA 552-Ex. The scanning temperature range was set from 293 K to 673 K at a scanning rate of 5 K min^{-1}. Elemental analysis was done with a Vario EL instrument and a Metrohm 888 Titrando device. The mass spectrum was recorded on a Thermos Fischer GC/ MS instrument. Crystallographic Data collection was performed with an Oxford Xcalibur 3 diffractometer equipped with a Spellman generator (50 kV, 40 mA) and a Kappa CCD detector, operating with Mo–Kα radiation ($\lambda = 0.71073$ Å). Data collection and data reduction were performed with the CrysAlisPro software[32] Absorption correction using the multiscan method[33] was applied. The structures were solved with SHELXS-97[34] refined with SHELXL-97[34] and finally checked using PLATON[35] All thermal ellipsoids are shown at 50% probability level.

Crystallographic data (excluding structure factors) for the structures in this paper have been deposited with the Cambridge Crystallographic Data Centre, CCDC, 12 Union Road, Cambridge CB21EZ, UK. Copies of the data can be obtained free of charge on quoting the depository numbers CCDC-2020838, CCDC-2020839, CCDC-2020905, CCDC-2020906, CCDC-2020907, and CCDC-2020908. (Fax: +44-1223-336-033; E-Mail: deposit@ccdc.cam.ac.uk, http://www.ccdc.cam.ac.uk). Details for data collection and structure refinement are summarized in the Supporting Information.

2-Fluoromethyltetrazole (1b): Tetrazole (0.83 mg, 11.8 mmol) was solved in acetone (35 mL) and potassium carbonate (0.82 g, 5.70 mmol) was added in one portion. After 30 min, fluoroiodomethane (0.8 mL, 11.8 mmol) was added dropwise and refluxed overnight. After the precipitate was filtered, the solvent was removed by distillation. The residue was dissolved in water and extracted with ethyl acetate (3 x 50 mL). The combined organic phases were washed with brine, dried with anhydrous magnesium sulfate, and the solvent was removed at reduced pressure. The crude liquid product was distilled in high vacuum to obtain tetrazole **1b** as a colorless liquid (0.48 g, 40%). 0 °C (m.p.), 160 °C (b.p.). **^{1}H NMR** (400 MHz, $CDCl_3$): $\delta = 8.65$ (s, 1 H), 6.55 (dd, J = 49.7, J = 0.4 Hz, 2 H) ppm. **^{19}F NMR** (376 MHz, $CDCl_3$): $\delta = -171.4$ (t, J = 50.0 Hz) ppm. **^{13}C{^{1}H} NMR** (101 MHz, $CDCl_3$): $\delta = 151.1$, 86.1 (d, J = 211.7 Hz) ppm. **^{15}N{^{1}H} NMR** (40.6 MHz, $CDCl_3$): $\delta = 5.1$ (s), –41.9 (s), –73.8 (s), –97.2 (d, J = 17.5 Hz) ppm. **IR** (ATR): $\tilde{\nu} = 3150$ (w), 3058 (w), 3000 (w), 2404 (w), 2361 (w), 2129 (w), 1704 (w), 1545 (w), 1461 (w), 1403 (m), 1367 (s), 1323 (w), 1283 (s), 1224 (m), 1184 (s), 1118 (m), 1046 (s), 1019 (s), 995 (s), 890 (m), 768 (s), 707 (s), 680 (s) cm^{-1}. **Raman** (1074 mW): $\tilde{\nu} = 3153$ (m), 3056 (w), 3001 (s), 2921 (w), 1461 (m), 1403 (m), 1370 (m), 1320 (m), 1285 (s), 1226 (m), 1186 (m), 1120 (w), 1053 (w), 1023 (m), 998 (s), 772 (m), 683 (m), 440 (m), 156 (s) cm^{-1}. **HRMS** (GC/EI) *m/z*: $[M]^+$ Calcd for $C_2H_4FN_4$ 102.0342; Found: 102.0336.

1-Fluoromethyltetrazole (1a): The 1-fluoromethyltetrazole **1a** remained in the distillation flask after **1b** was separated by distillation. Therefore, the remaining residue was dissolved in acetone (50 mL) and filtered through a silica plug. After removing the solvent at reduced pressure, tetrazole **1a** was obtained as colorless liquid (0.42 g, 35%). 115 °C (dec). **^{1}H NMR** (400 MHz, $CDCl_3$): $\delta = 8.90$ (s, 1 H), 6.40 (d, $J = 50.0$ Hz, 2 H) ppm. **^{19}F NMR** (376 MHz, $CDCl_3$): $\delta = -169.4$ (t, $J = 50.0$ Hz) ppm. **^{13}C{^{1}H} NMR** (101 MHz, $CDCl_3$): $\delta = 143.7$, 82.8 (d, $J = 209.5$ Hz) ppm. **^{15}N{^{1}H} NMR** (40.6 MHz, $CDCl_3$): $\delta = 13.7$ (s), –12.2 (s), –50.4 (s), –142.6 (d, $J = 17.5$ Hz) ppm.

IR (ATR): $\tilde{\nu}$ =3139 (w), 1487 (m), 1460 (w), 1431 (w), 1403 (w), 1370 (w), 1312 (w), 1274 (w), 1205 (w), 1170 (s), 1102 (m), 1025 (s), 993 (m), 947 (w), 881 (w), 754 (s), 716 (w), 656 (m), 440 (w) cm^{-1}. **Raman** (1074 mW): $\tilde{\nu}$ = 3142 (m), 3053 (m), 3003 (s), 2966 (w), 2916 (w), 2794 (w), 1488 (w), 1482 (m), 1433 (m), 1404 (w), 1315 (s), 1276 (m), 1204 (w), 1173 (m), 1104 (w), 1036 (m), 998 (m), 948 (w), 759 (m), 717 (w), 660 (w), 440 (w), 336 (w), 211 (w), 159 (s), 93 (s) cm^{-1}. **HRMS** (GC/EI) *m*/*z*: $[M]^+$ Calcd for $C_2H_4FN_4$ 102.0342; Found: 102.0337.

1-Fluoromethyl-5-aminotetrazole (2a): 5-Aminotetrazole (10.2 g, 120 mmol) was dissolved in water (50 mL) and sodium hydrogen carbonate (10.8 g, 120 mmol) was added slowly in small portions. After the solution was stirred for 30 min, the solvent was removed. The obtained sodium 5-aminotetrazolate (12.6 g, 117 mmol), was slurried in acetone (50 mL) and fluoroiodomethane (7.94 mL, 117 mmol) was added dropwise. After the reaction mixture was refluxed for 3 h, the solvent was removed *in vacuo*. The beige crude product slurried in water (70 mL), was filtered and washed with diethyl ether (200 mL), and pure aminotetrazole **2a** was obtained (7.05 g, 51%). 131 °C (m.p.), 160 °C (dec). **^{1}H NMR** (400 MHz, DMSO-D$_6$): $\delta = 7.32$ (s, 2 H), 6.25 (d, $J = 51.9$ Hz, 2 H) ppm. **^{19}F NMR** (376 MHz, DMSO-D$_6$): $\delta = -170.8$ (t, $J = 51.8$ Hz) ppm. **^{13}C{^{1}H} NMR** (101 MHz, DMSO-D$_6$): $\delta = 168.0$ (d, $J = 1.1$ Hz), 86.6 (d, $J = 202.2$ Hz) ppm. **^{15}N{^{1}H} NMR** (40.6 MHz, DMSO-D$_6$): $\delta = 9.5$ (s), –23.8 (d, $J = 1.1$ Hz), –94.2 (s), –333.8 (s) ppm. **IR** (ATR): $\tilde{\nu}$ =3319 (w), 3137 (w), 2798 (w), 2750 (w), 1652 (m), 1591 (m), 1485 (w), 1459 (w), 1400 (w), 1342 (w), 1305 (w), 1284 (w), 1183 (w), 1104 (w), 1007 (m), 960 (m), 805 (m), 752 (w), 720 (m), 472 (m) cm^{-1}. **Raman** (1074 mW): $\tilde{\nu}$ =3057 (w), 2996 (w), 1593 (w), 1464 (w), 1403 (w), 1342 (w), 1309 (w), 1141 (w), 1100 (w), 1011 (w), 964 (w), 807 (s), 753 (w), 722 (w), 480 (w), 443 (w), 299 (w), 164 (w), 143 (m), 102 (s) cm^{-1}. $C_2H_4FN_5$: C, 20.52; H, 3.44. Found: C, 20.30; H, 3.45. **HRMS** (DEI) *m*/*z*: [M] Calcd for $C_2H_4FN_5$ 117.0451; Found: 117.0446.

2-Fluoromethyl-5-aminotetrazole (2b): The solvent of the received filtrate from the synthesis of **2a**, was removed *in vacuo*. The obtained solid was dissolved in water (100 mL) and extracted with diethyl ether (100 mL). The aminotetrazole **2b** was obtained as a white solid (3.32 g, 24%). 75 °C (m.p.), 166 °C (dec). **^{1}H NMR** (400 MHz, (DMSO-D$_6$): $\delta = 6.46$ (d, $J = 50.8$ Hz, 2 H), 6.45 (s, 2 H) ppm. **^{19}F NMR** (376 MHz, DMSO-D$_6$): $\delta = -169.7$ (t, $J = 50.9$ Hz) ppm. **^{13}C{^{1}H} NMR** (101 MHz, DMSO-D$_6$): $\delta = 156.1$ (d, $J = 1.4$ Hz), 81.2 (d, $J = 197.7$ Hz) ppm. **^{15}N{^{1}H} NMR** (40.6 MHz, DMSO-D$_6$): $\delta = 2.5$ (s), –71.6 (d, $J = 0.7$ Hz), –107.8 (d, $J = 17.4$ Hz), –120.7 (d, $J = 1.2$), –336.8 (s) ppm. **IR** (ATR): $\tilde{\nu}$ = 3387 (w), 3310 (w), 3237 (w), 3177 (w), 3049 (w), 2996 (w), 2005 (w), 1633 (w), 1565 (w), 1442 (w), 1409 (w), 1369 (w), 1213 (w), 1027 (w), 983 (w), 820 (w), 759 (w), 711 (w), 533 (w) 464 (w) cm^{-1}. **Raman** (1074 mW): $\tilde{\nu}$ = 3310 (w), 3047 (w), 2994 (m), 1544 (w), 1463 (w), 1410 (w), 1234 (w), 1212 (w), 1105 (w), 1088 (w), 1022 (w), 986 (s), 713 (w), 661 (w), 467 (m), 339 (w), 294 (w), 142 (s), 115 (m) 102 (s) cm^{-1}. $C_2H_4FN_5$: calcd. C, 20.52; H, 3.44%; found: C, 20.21; H, 3.34%. **HRMS** (DEI) *m*/*z*: [M] Calcd for $C_2H_4FN_5$ 117.0451; found: 117.0443.

[Hexakis(1-fluoromethyl-tetrazole) copper(II)] perchlorate (3): 1a (0.273 g, 2.7 mmol) was added dropwise to a stirring solution of copper(II) perchlorate hexahydrate (0.17 g, 0.45 mmol) in water (10 mL). The reaction mixture was heated to 100 °C for 10 min and filtered while hot. After solvent evaporation, the complex **3** was obtained in the form of dark blue crystals (0.27 g, 70%). 184 °C (dec). **IR** (ATR): $\tilde{\nu}$ =3152 (w), 3114 (w), 3014 (vw), 2022 (vw), 1503 (m), 1490 (w), 1462 (w), 1450 (w), 1406 (m), 1395 (w), 1329 (w), 1290 (w), 1205 (w), 1177 (s), 1107 (s), 1082 (s), 1042 (vs), 1032 (vs), 998 (s), 983 (s), 960 (m), 938 (w), 921 (w), 905 (m), 882 (m), 756 (vs), 714 (m), 656 (s), 624 (vs) cm^{-1}. $C_{12}H_{18}Cl_2CuF_6N_{24}O_8$: calcd. C, 16.47; H, 2.07; N, 38.42%; found: C, 16.60; H, 1.87; N, 38.32%. **BAM drophammer**: <1 J; **BAM friction tester**: 24 N; **ESD**: 181 mJ (grain size 100– 500 µm).

[Hexakis(1-fluoromethyl-tetrazole) copper(II)] chlorate (4): Copper(II) chlorate (0.11 g, 0.45 mmol) was prepared via metathesis reaction of copper sulfate pentahydrate and barium chlorate monohydrate. **1a** (279 mg, 2.7 mmol) was added dropwise to the stirring solution of copper chlorate in water (5 mL). The reaction mixture was heated to 100 °C for 10 min and filtered while hot. After solvent evaporation, the complex **4** was obtained as greenish turquoise crystals (0.26 g, 67%). 87 °C (dec). **IR** (ATR): $\tilde{\nu}$ =3106 (m), 3061 (w), 2997 (vw), 1504 (m), 1469 (w), 1447 (w), 1408 (m), 1334 (w), 1209 (m), 1183 (s), 1108 (m), 1039 (s), 993 (m), 960 (vs), 934 (s), 909 (s), 758 (vs), 714 (s), 657 (s), 604 (m), 479 (s) cm^{-1}. $C_{12}H_{18}Cl_2CuF_6N_{24}O_6$: calcd. C, 17.10; H, 2.15; N, 39.88%, found: C, 17.37; H, 2.02; N, 39.64%. **BAM drophammer**: <1 J; **BAM friction tester**: 24 N; **ESD**: 226 mJ (grain size <100 µm).

[Tris(1-fluoromethyl-5-aminotetrazole) copper(I)] perchlorate (6): Tetra(acetonitrile)copper(I) perchlorate (0.33 g, 1.0 mmol) was prepared according to the literature and dissolved in dry acetonitrile (10 mL) under nitrogen atmosphere.[36] Amino tetrazole **2a** (0.35 g, 3.0 mmol) was dissolved in acetonitrile (10 mL) separately and dropwise added to the acetonitrile complex solution at 80 °C. A color change to yellow indicated product formation and the opaque solution was filtered. The solvent was removed *in vacuo*, yielding a yellow microcrystalline solid **6** (0.32 g, 62%). At ambient conditions the complex decomposed rapidly, accompanied with a color change to dark brown.

3.5 Acknowledgements

Financial support by the Ludwig-Maximilian University is grateful acknowledged. We are also thankful to F-Select GmbH for a generous donation of fluoroiodomethane.

Keywords: Fluoromethylation; Energetic materials; Tetrazoles; Spectroscopy; Fluorine effect.

3.6 References

[1] S. Wittenberger, *Org. Prep. Proced. Int.* **1994**, *26*, 499–531.

[2] R. Raap, *Can. J. Chem.* **1969**, *47*, 3677–3681.

[3] P. L. Franke, J. G. Haasnoot, A. Zuur, *Inorg. Chim. Acta* **1982**,*59*, 5–9.

[4] M. A. C. Härtel, T. M. Klapötke, D. G. Piercey, J. Stierstorfer, *Z.Anorg. Allg. Chem.* **2012**, *638*, 2008–2014.

[5] a) A. Warrilow, C. M. Hull, J. E. Parker, E. P. Garvey, W. J. Hoekstra, W. R. Moore, R. J. Schotzinger, D. E. Kelly, S. L. Kelly, *Antimicrob. Agents Chemother.* **2014**, *58*, 7121–7127; b) S. R. Lockhart, A. W. Fothergill, N. Iqbal, C. B. Bolden, N. T. Grossman, E. P. Garvey, S. R. Brand, W. J. Hoekstra, R. J. Schotzinger, E. Ottinger, T. F. Patterson, N. P. Wiederhold, *Antimicrob. Agents Chemother.* **2016**, *60*, 2528–2531.

[6] V. A. Ostrovskii, E. A. Popova, R. E. Trifonov, *Adv. Heterocycl. Chem.* **2017**, *123*, 1–62.

[7] J.-S. Qin, S.-J. Bao, P. Li, W. Xie, D.-Y. Du, L. Zhao, Y.-Q. Lan, Z.-M. Su, *Chem. Asian J.* **2014**, *9*, 749–753.

[8] A. Rudavskyi, R. W. A. Havenith, R. Broer, C. de Graaf, C. Sousa, *Dalton Trans.* **2013**, *42*, 14702–14709.

[9] S. Li, Y. Wang, C. Qi, X. Zhao, J. Zhang, S. Zhang, S. Pang, *Angew. Chem.* **2013**, *125*, 14281–14285; *Angew. Chem. Int. Ed.* **2013**, *52*, 14031–14035.

[10] F. R. Benson, *Chem. Rev.* **1947**, *41*, 1–61.

[11] T. M. Klapötke, *Chemie der hochenergetischen Materialien*, DeGruyter, **2009**.

[12] T. M. Klapötke, J. Stierstorfer, *Green Energetic Materials*, John Wiley & Sons Ltd., **2014**, pp. 133–177.

[13] N. Fischer, K. Karaghiosoff, T. M. Klapötke, J. Stierstorfer, *Z. Anorg. Allg. Chem.* **2010**, *636*, 735–749.

[14] a) L. Zeisel, N. Szimhardt, M. H. H. Wurzenberger, T. M. Klapötke, J. Stierstorfer, *New J. Chem.* **2019**, *43*, 609–616; b) M. H. H. Wurzenberger, M. S. Gruhne, M. Lommel, N. Szimhardt, T. M. Klapötke, J. Stierstorfer, *Chem. Asian J.* **2019**, *14*, 2018–2028; c) M. H. H. Wurzenberger, B. R. G. Bissinger, M. Lommel, M. S. Gruhne, N. Szimhardt, J. Stierstorfer, *New J. Chem.* **2019**, *43*, 18193–18202; d) N. Szimhardt, M. H. H. Wurzenberger, P. Spiess, T. M. Klapötke, J. Stierstorfer, *Propellants Explos. Pyrotech.* **2018**, *43*, 1203–1209; e) M. H. H. Wurzenberger, N. Szimhardt, J. Stierstorfer, *Inorg. Chem.* **2018**, *57*, 7940–7949; f) M. H. H. Wurzenberger, N. Szimhardt, J. Stierstorfer, *J. Am. Chem. Soc.* **2018**, *140*, 3206–3209; g) N. Szimhardt, M. H. H. Wurzenberger, T. M. Klapötke, J. T. Lechner, H. Reichherzer, C. C. Unger, J. Stierstorfer, *J. Mater. Chem. A* **2018**, *6*, 6565–6577; h) N. Szimhardt, M. H. H. Wurzenberger, L. Zeisel, M. S. Gruhne, M. Lommel, J. Stierstorfer, *J. Mater. Chem. A* **2018**, *6*, 16257–16272; i) N. Szimhardt, M. H. H. Wurzenberger, A. Beringer, L. J. Daumann, J. Stierstorfer, *J. Mater. Chem. A* **2017**, *5*, 23753–23765.

[15] E.-C. Koch, A. Hahma, T. M. Klapötke, H. Radies, *Propellants Explos. Pyrotech.* **2010**, *35*, 248–253.

[16] a) M. Reichel, B. Krumm, Y. V. Vishnevskiy, S. Blomeyer, J. Schwabedissen, H.-G. Stammler, K. Karaghiosoff, N. W. Mitzel, *Angew. Chem.* **2019**, *131*, 18730–18734; *Angew. Chem. Int. Ed.* **2019**, *58*, 18557–18561; b) M. Reichel, B. Krumm, K. Karaghiosoff, *J. Fluorine Chem.* **2019**, *226*, 109351–109355.

[17] H. Yoneyama, N. Oka, Y. Usami, S. Harusawa, *Tetrahedron Lett.* **2020**, *61*, 151517–151520.

[18] S. Komeda, H. Yoneyama, M. Uemura, T. Tsuchiya, M. Hoshiyama, T. Sakazaki, K. Hiramoto, S. Harusawa, *J. Inorg. Biochem.* **2019**, *192*, 82–86.

[19] a) M. Reichel, K. Karaghiosoff, *Angew. Chem.* **2020**, *132*, 12364–12377; *Angew. Chem. Int. Ed.* **2020**, *59*, 12268–12281; b) M. Reichel, M. Egenhöfer, B. Krumm, K. Karaghiosoff, *Z. Anorg. Allg. Chem.* **2020**, *646*, 328–331; c) M. Reichel, J. Martens, E. Woellner, L. Huber, A. Kornath, K. Karaghiosoff, *Eur. J. Inorg. Chem.* **2019**, 2530–2534; d) M. Reichel, J. Martens, C. C. Unger, K. Karaghiosoff, *Phosphorus Sulfur Silion Relat. Elem.* **2019**, *194*, 467–468.

[20] C. Stadler, J. Daub, J. Koehler, R. W. Saalfrank, V. Coropceanu, V. Schuenemann, C. Ober, A. X. Trautwein, S. F. Parker, M. Poyraz, T. Inomata, R. D. Cannon, *J. Chem. Soc., Dalton Trans.* **2001**, 3373–3383.

[21] E. Vieira, J. Huwyler, S. Jolidon, F. Knoflach, V. Mutel, J. Wichmann, *Bioorg. Med. Chem. Lett.* **2005**, *15*, 4628–4631.

[22] T. M. Klapötke, C. M. Sabate, A. Penger, M. Rusan, J. M. Welch, *Eur. J. Inorg. Chem.* **2009**, 880–896.

[23] a) X. Hua, W. Liao, Y. Tang, P. Li, P. Shi, D. Zhao, R. Xiong, *J. Am. Chem. Soc.* **2018**, *140*, 12296–12302; b) M. Feller, K. Lux, A. Kornath, *Eur. J. Inorg. Chem.* **2015**, 5357–5362.

[24] a) K. Karaghiosoff, T. M. Klapötke, P. Mayer, C. M. Sabate, A. Penger, J. M. Welch, *Inorg. Chem.* **2008**, *47*, 1007–1019; b) R. A. Henry, W. G. Finnegan, *J. Am. Chem. Soc.* **1954**, *76*, 923–926; c) T. M. Klapötke, N. K. Minar, J. Stierstorfer, *Polyhedron* **2009**, *28*, 13–26.

[25] O. Gryszkiewicz-Trochimowski, *Compt. Rend.* **1958**, *246*, 2627–2629.

[26] M. Jafari, K. Ghani, M. H. Keshavarz, F. Derikvandy, *Propellants Explos. Pyrotech.* **2018**, *43*, 1236–1244.

[27] J. H. Bryden, *Acta Crystallogr.* **1956**, *9*, 874–878.

[28] M. H. Palmer, S. Parsons, *Acta Crystallogr., Sect. C: Cryst. Struct. Commun.* **1996**, *52*, 2818–2822.

[29] E. Oliveri-Mandala, T. Passalacqua, *Gazz. Chim. Ital.* **1914**, *44*, 465–475.

[30] a) L. Zeisel, N. Szimhardt, M. H. H. Wurzenberger, T. M. Klapötke, J. Stierstorfer, *New J. Chem.* **2019**, *43*, 609–616; b) P. N. Gaponik, M. M. Degtyarik, A. S. Lyakhov, V. E. Matulis, O. A. Ivashkevich, M. Quesada, J. Reedijk, *Inorg. Chim. Acta* **2005**, *358*, 3949–3957; c) N. Szimhardt, M. H. H. Wurzenberger, A. Beringer, L. J. Daumann, J. Stierstorfer, *J. Mater. Chem. A* **2017**, *5*, 23753–23765; d) M. H. H. Wurzenberger, M. Lommel, M. S. Gruhne, N. Szimhardt, J. Stierstorfer, *Angew. Chem.* **2020**, *132*, 12466–12469; *Angew. Chem. Int. Ed.* **2020**, *59*, 12367–12370; e) M. H. H. Wurzenberger, N. Szimhardt, J. Stierstorfer, *J. Am. Chem. Soc.* **2018**, *140*, 3206–3209.

[31] a) V. A. K. Adiraju, J. A. Flores, M. Yousufuddin, H. V. R. Dias, *Organometallics* **2012**, *31*, 7926–7932; b) T. Chavez-Gil, J. Lugo, D. L. Cedeño, C. G. Hamaker, *J. Chem. Crystallogr.* **2015**, *45*, 189–192.

[32] Program package CrysAlisPro 1.171.38.46 Rigaku OD, **2015**. [33] G. M. Sheldrick, SHELXS-97, Program for Crystal Structure Solution, University of Göttingen, Germany, **1997**.

[34] G. M. Sheldrick, SHELXL-97, Program for the Refinement of Crystal Structures, University of Göttingen, Germany, **1997**.

[35] A. L. Spek, PLATON: A Multipurpose Crystallographic Tool, Utrecht University, Utrecht, Netherlands, **1999**.

[36] P. Hemmerich, C. Sigwart, *Experientia* **1963**, *19*, 488–489.

3.7 Supporting Information

3.7.1 NMR Spectroscopy

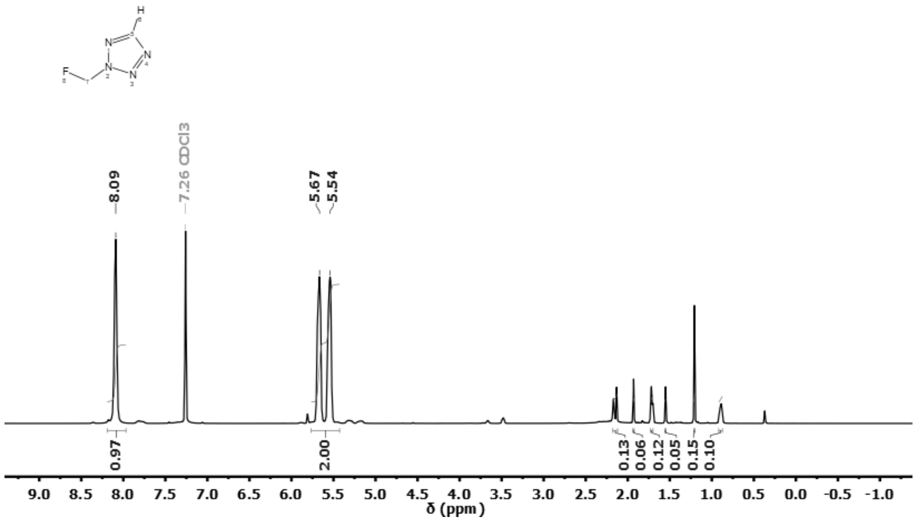

Figure S1. ^{1}H NMR of compound **1b**.

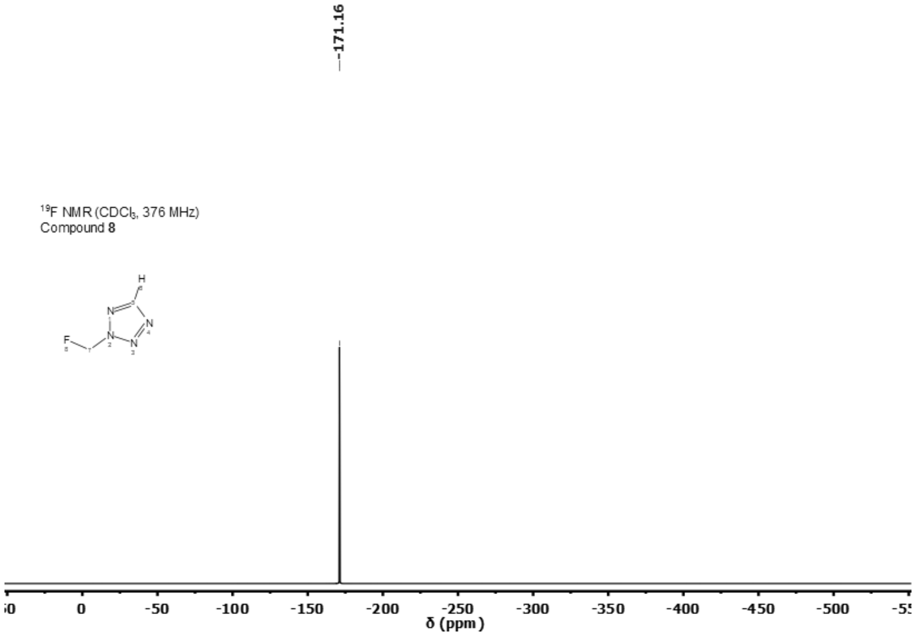

Figure S2. ^{19}F{^{1}H} NMR of compound **1b**.

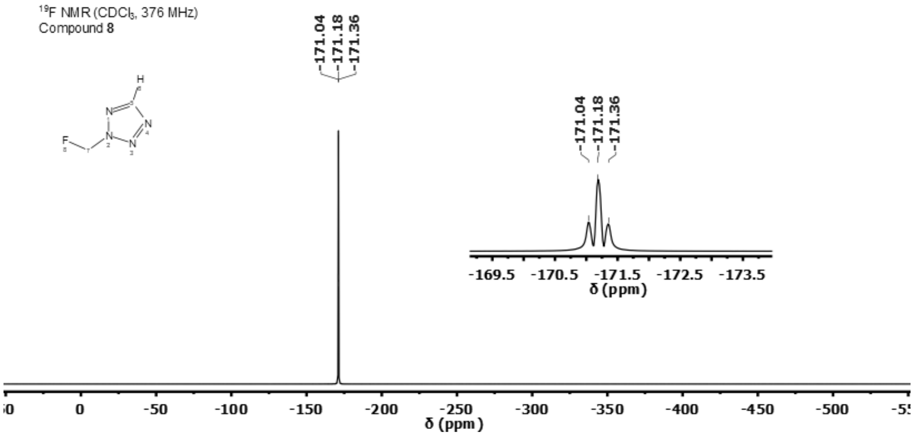

Figure S3. ^{19}F NMR of compound **1b**.

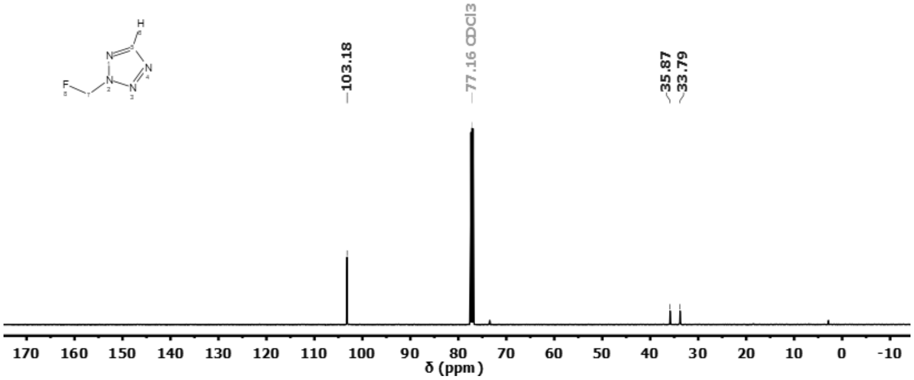

Figure S4. ^{13}C{^{1}H} NMR of compound **1b**.

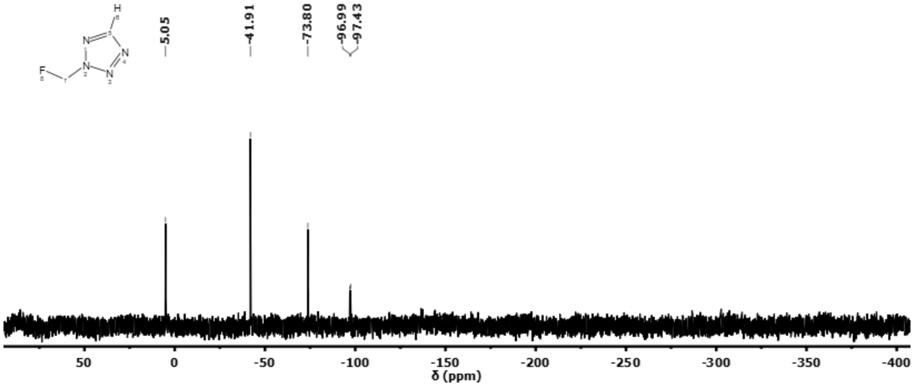

Figure S5. ^{15}N NMR of compound **1b**.

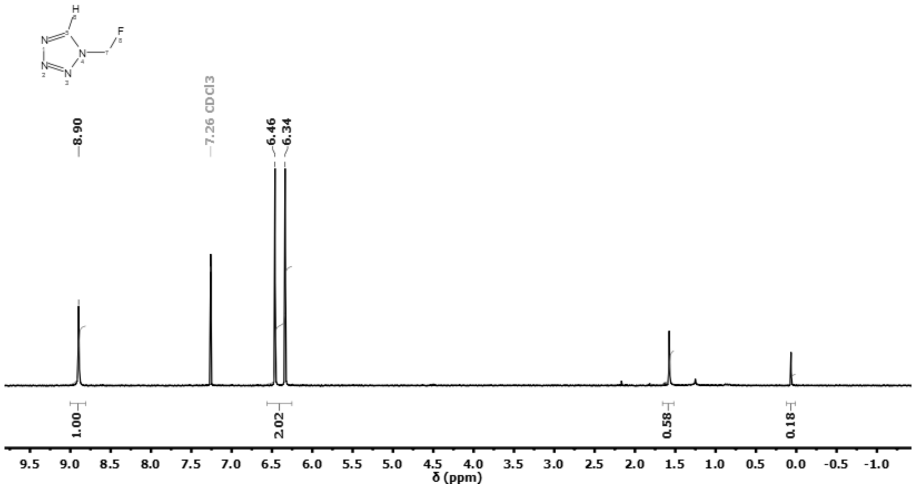

Figure S6. ^{1}H NMR of compound **1a**.

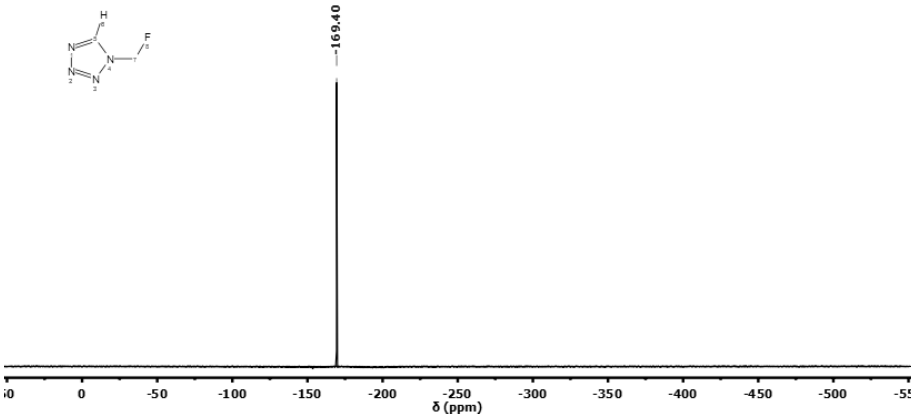

Figure S7. $^{19}F\{^{1}H\}$ NMR of compound **1a**.

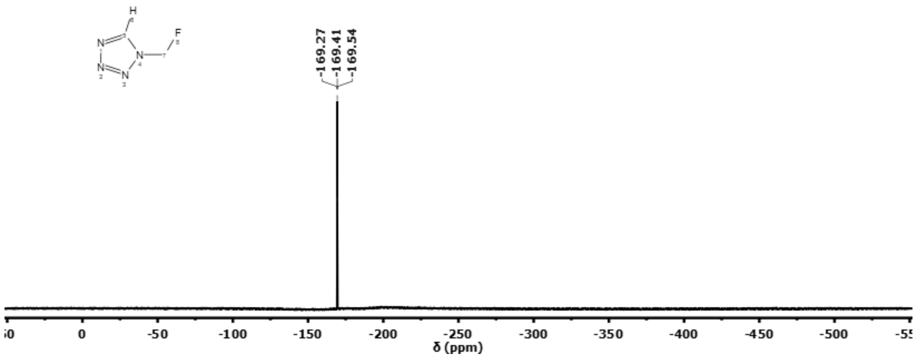

Figure S8. ^{19}F NMR of compound **1a**.

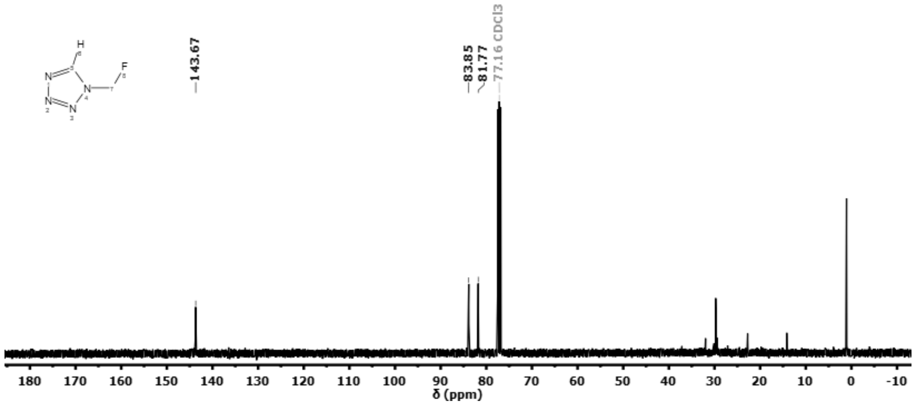

Figure S9. $^{13}C\{^{1}H\}$ NMR of compound **1a**.

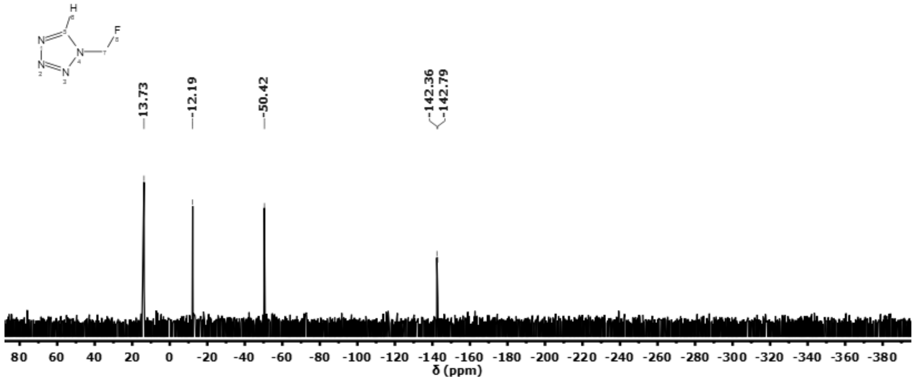

Figure S10. $^{15}N\{^{1}H\}$ NMR of compound **1a**.

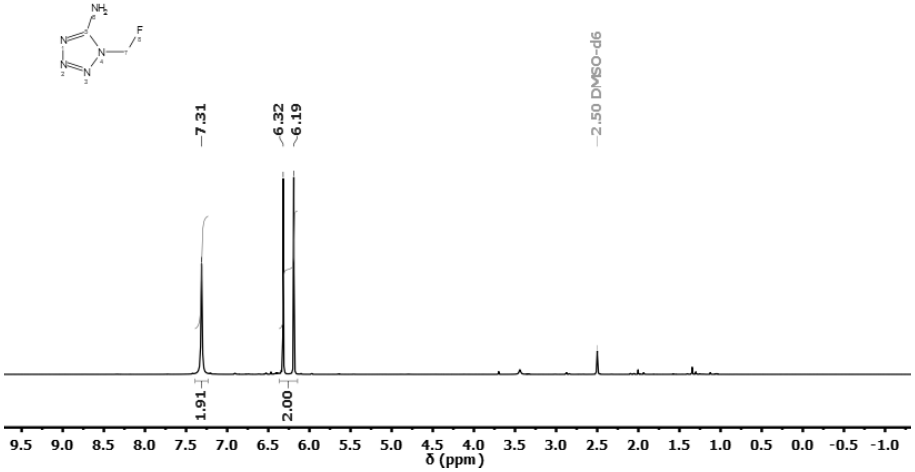

Figure S11. ^{1}H NMR of compound **2a**.

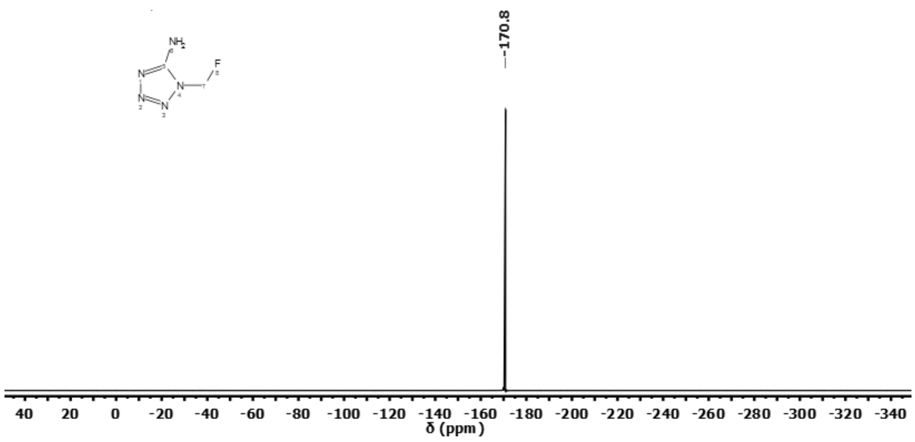

Figure S12. $^{19}F\{^{1}H\}$ NMR of compound **2a**.

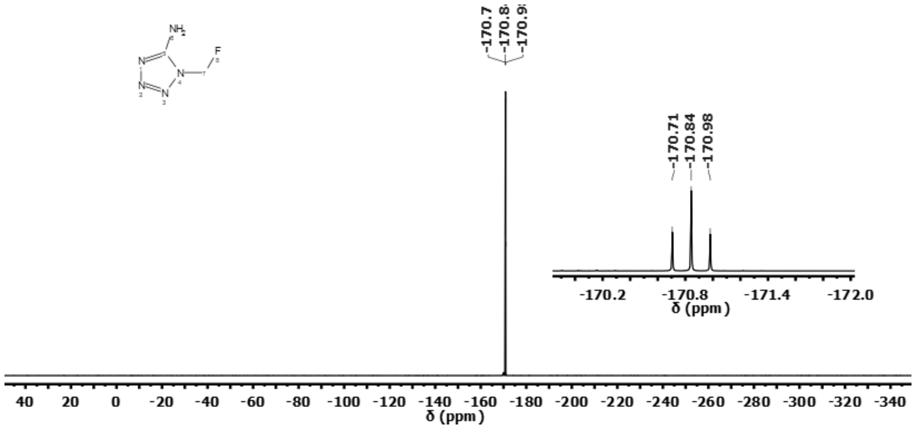

Figure S13. ^{19}F NMR of compound **2a**.

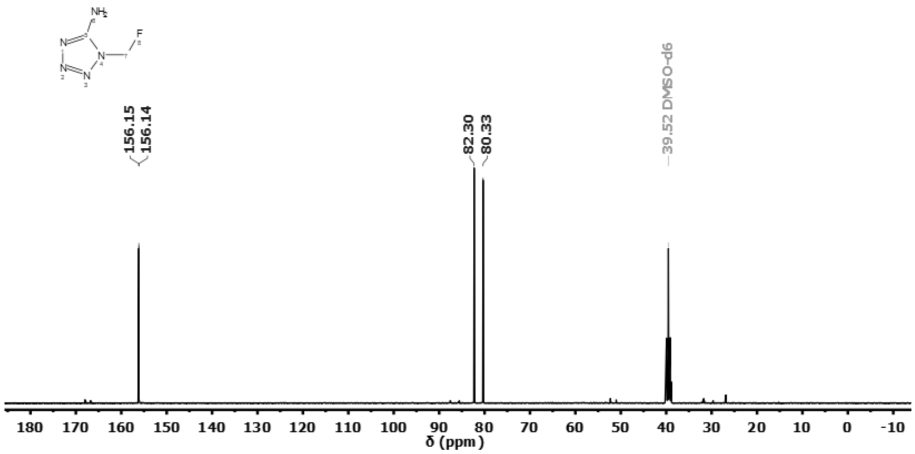

Figure S14. $^{13}C\{^{1}H\}$ NMR of compound **1a**.

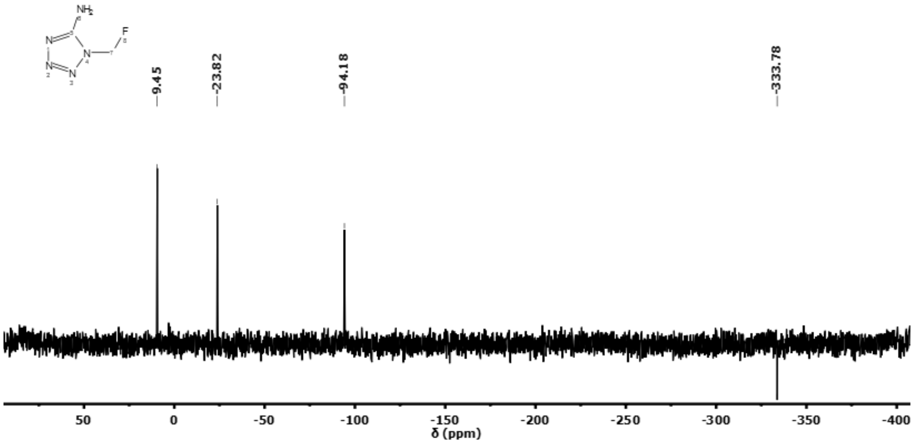

Figure S15. $^{15}N\{^{1}H\}$ NMR of compound **1a**.

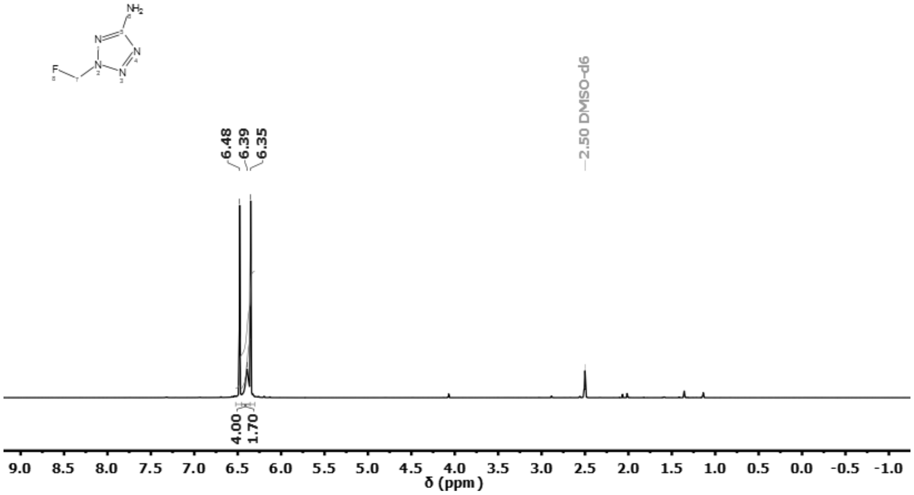

Figure S16. ^{1}H NMR of compound **2b**.

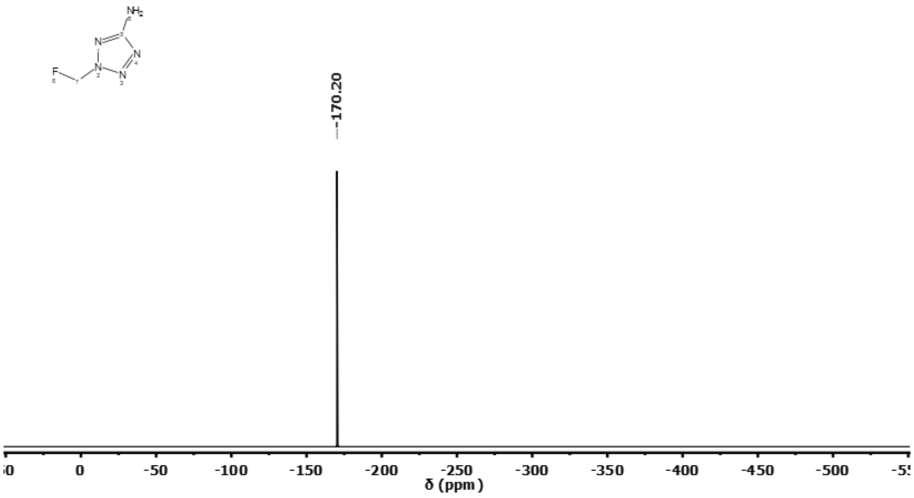

Figure S17. $^{19}F\{^{1}H\}$ NMR of compound **2b**.

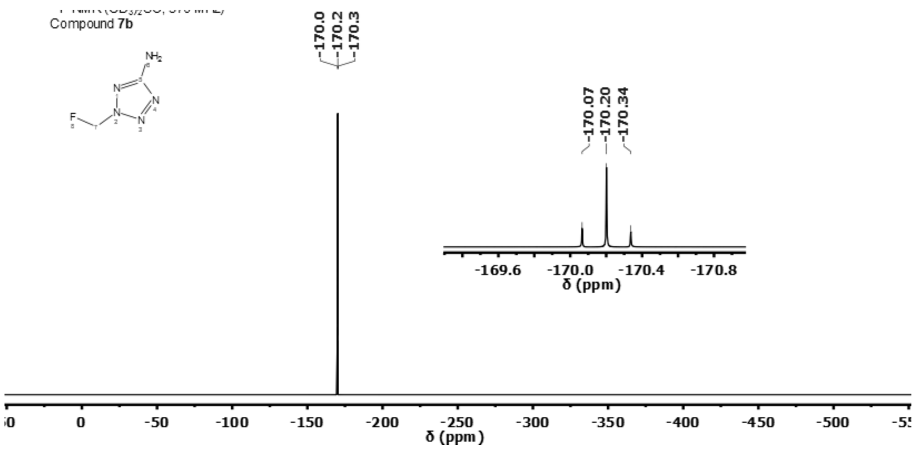

Figure S18. ^{19}F NMR of compound **2b**.

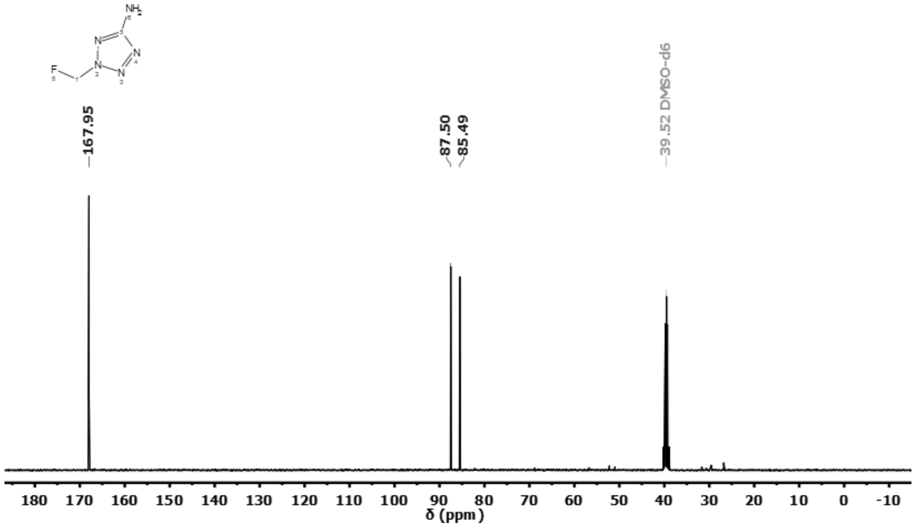

Figure S19. ^{13}C NMR of compound **2b**.

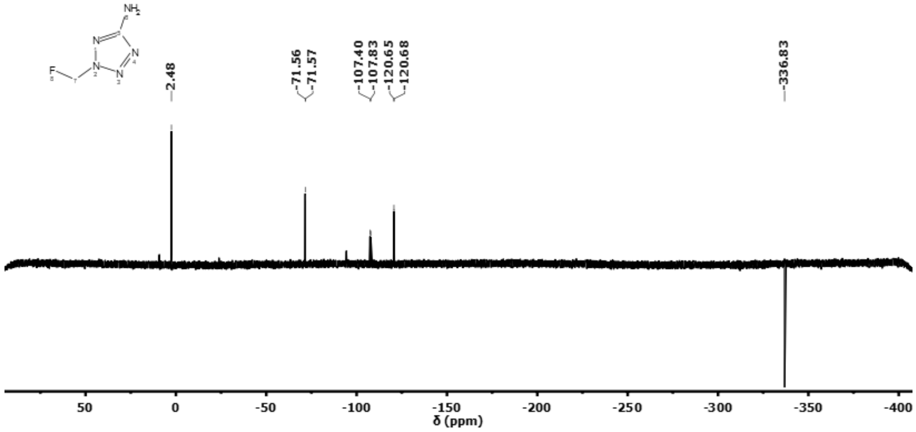

Figure S20. ^{15}N{^{1}H} NMR of compound **2b**.

3.7.2 Hirshfeld Fingerprint Plots

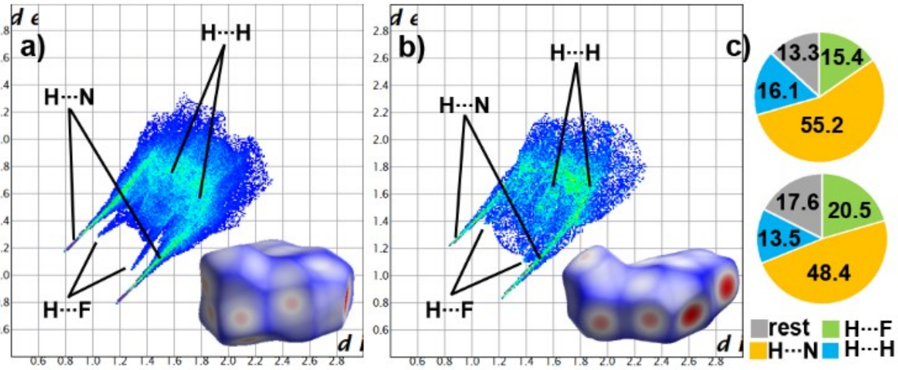

Figure S21. Two-dimensional fingerprint plot as well as the corresponding Hirschfeld surface (bottom right in 2D plot) of **2a** (a) and **2b** (b). Color coding: white, distance d equals VDW distance; blue, d exceeds VDW distance, red, d, smaller than VDW distance). Population of close contacts of **2a** ((c) top) and **2b** ((c) bottom) in crystal stacking.

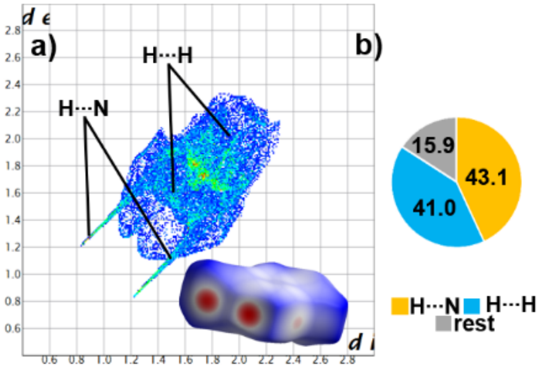

Figure 22. Two-dimensional fingerprint plot as well as the corresponding Hirschfeld surface (bottom right in 2D plot) of 2-Methyltetrazole. Color coding: white, distance d equals VDW distance; blue, d exceeds VDW distance, red, d, smaller than VDW distance). Population of close contacts in crystal stacking (b).

3.7.3 EXPLO5 Calculation Results

2-Fluoromethyltetrazol (1b)

C(2,000) H(3,000) N(4,000) F(1,000)

Molecular weight = 102,08

Density of explosive = 1,581 g/cm3

Oxygen balance = -78,36808 %

Enthalpy of formation = 551,55 kJ/kg

Internal energy of formation = 648,68 kJ/kg

Detonation parameters (at the C-J point) :

```
-----------------------

    Heat of detonation                       = -3096,925   kJ/kg
    Detonation temperature            = 2465,767   K
    Detonation pressure                      = 17,11472  GPa
    Detonation velocity                      = 7105,664   m/s
    Particle velocity                        = 1523,468   m/s
    Sound velocity                           = 5582,196   m/s
    Density of  products                     = 2,012479   g/cm3
    Volume of  products                      = 0,4968995  cm3/g
    Exponent 'Gamma'                         = 3,664138
    Moles of gaseous products                = 3,449334   mol/mol explosive
    Moles of condensed products              = 1,749259   mol/mol explosive
    Volume of gas at STP                     = 826,4128  dm3/kg
    Mean molecular mass of gas. prod.        = 23,5001  g/mol
    Mean molecular mass of cond.prod.        = 12,011  g/mol
    Mean molecular mass of all prod.         = 19,63417  g/mol
    Entropy of products                      = 6,088365  kJ/kg K
    Internal energy of products              = 4257,409   kJ/kg,  i.e.  6,730963  kJ/cm3
    Compression energy                       = 1160,484   kJ/kg,  i.e.  1,834725  kJ/cm3
    Total heat energy                        = -3096,925  kJ/kg, i.e.  -4,896238  kJ/cm3


Composition of detonation products:
   Products         mol/mol             mol/kg              Mol %
--------------------------------------------------------------------
   N2 = 1,845793            18,0825435,50564
   C(d) =           1,749259             17,1368333,6487
   HF =             0,9996492                     9,79318619,22923
   NH3 =            0,3059407                     2,9971855,885067
   CH4 =            0,1572127                     1,5401533,024139
   H2 = 0,09266659                      0,9078196            1,782532
   C2H6 =           0,04179493                    0,4094491            0,8039661
   C2H4 =           0,003713249                   0,0363773            0,07142796
   HCN =            0,002384885                   0,02336382           0,04587559
   CH2F2 =          7,927873E-05                  0,0007766638         0,001525004
```

```
    CF4 =         4,804902E-05             0,000470718     0,0009242697
    N2H4 =        4,024095E-05             0,0003942254    0,0007740739
    NH2 =         7,005771E-06             6,863289E-05    0,0001347628
    H =           3,778774E-06             3,701922E-05    7,26884E-05
    C(gr) =       9,807811E-10             9,608343E-09    1,886628E-08
    N =           7,578168E-10             7,424044E-09    1,457734E-08
    CFN =         1,694119E-10             1,659664E-09    3,258803E-09
    F2 =          1,02627E-11              1,005398E-10    1,974129E-10
    NF =          3,63629E-12              3,562336E-11    6,994758E-11
    CF2 =         1,730354E-12             1,695162E-11    3,328504E-11
    CF = 7,131345E-14              6,986309E-13     1,371784E-12

Running parameters:
-----------------------
  - Equation of state:  BKW EOS
  - 'BKWN' set of constants
  - Covolumes set 1
    (Alpha=0,5, Beta=0,38, Kappa=9,32, Theta=4120)
  - Activity: Model 1: Condensed products form pure phase (Default)
```

1-Fluoromethyltetrazol (1a)

```
    C(2,000) H(3,000) N(4,000) F(1,000)


     Molecular weight                    = 102,08
     Density of explosive                = 1,593   g/cm3
     Oxygen balance                      = -78,36808  %
     Enthalpy of formation               = 695,56  kJ/kg
     Internal energy of formation        = 792,69  kJ/kg



Detonation parameters (at the C-J point) :
-----------------------


     Heat of detonation                  = -3235,073   kJ/kg
     Detonation temperature        = 2533,108   K
```

```
Detonation pressure                 = 17,82487  GPa
Detonation velocity                 = 7221,131   m/s
Particle velocity                   = 1549,549   m/s
Sound velocity                      = 5671,582   m/s
Density of  products                = 2,028228   g/cm3
Volume of  products                 = 0,4930412  cm3/g
Exponent 'Gamma'                    = 3,66015
Moles of gaseous products           = 3,448214   mol/mol explosive
Moles of condensed products         = 1,759722   mol/mol explosive
Volume of gas at STP                = 826,1443  dm3/kg
Mean molecular mass of gas. prod.   = 23,4713  g/mol
Mean molecular mass of cond.prod.   = 12,011  g/mol
Mean molecular mass of all prod.    = 19,59895  g/mol
Entropy of products                 = 6,135625  kJ/kg K
Internal energy of products         = 4435,631   kJ/kg,  i.e.  7,06596  kJ/cm3
Compression energy                  = 1200,558   kJ/kg,  i.e.  1,912488  kJ/cm3
Total heat energy                   = -3235,073  kJ/kg, i.e.  -5,153472  kJ/cm3


Composition of detonation products:
  Products        mol/mol           mol/kg            Mol %
--------------------------------------------------------------------
    N2 = 1,839541          18,0212835,32188
    C(d) =        1,759722          17,2393333,78924
    HF =          0,9995835                 9,79254219,19347
    NH3 =         0,3180839                 3,1161486,107678
    CH4 =         0,1484461                 1,45427          2,850382
    H2 = 0,09514176                 0,9320679        1,826861
    C2H6 =        0,04051623                0,3969222        0,777971
    C2H4 =        0,003965512               0,03884863       0,07614366
    HCN =         0,002719156               0,02663854       0,05221178
    CH2F2 =       9,079252E-05              0,00088946       0,00174335
    CF4 =         5,873582E-05              0,0005754126     0,001127814
    N2H4 =        5,33112E-05               0,0005222697     0,001023653
    NH2 =         9,200113E-06              9,013003E-05     0,0001766557
    H =           4,984084E-06              4,882719E-05     9,570172E-05
```

```
   N =          1,382537E-09           1,354419E-08     2,654673E-08
   C(gr) =      8,956583E-10           8,774426E-09     1,719795E-08
   CFN =        2,23883E-10            2,193297E-09     4,298881E-09
   F2 =         2,045242E-11           2,003646E-10     3,927165E-10
   NF =         6,891152E-12           6,751001E-11     1,323202E-10
   CF2 =        2,364777E-12           2,316682E-11     4,540718E-11
   CF = 1,208718E-13           1,184136E-12     2,320917E-12

Running parameters:
-----------------------
  - Equation of state:  BKW EOS
  - 'BKWN' set of constants
  - Covolumes set 1
   (Alpha=0,5, Beta=0,38, Kappa=9,32, Theta=4120)
  - Activity: Model 1: Condensed products form pure phase (Default)
```

1-Fluoromethyl-5-aminotetrazol (2a)

```
   C(2,000) H(4,000) N(5,000) F(1,000)

    Molecular weight               = 117,09
    Density of explosive           = 1,648   g/cm3
    Oxygen balance                 = -75,14988  %
    Enthalpy of formation          = 380,04  kJ/kg
    Internal energy of formation   = 485,89  kJ/kg


Detonation parameters (at the C-J point) :
-----------------------

    Heat of detonation                    = -2773,24   kJ/kg
    Detonation temperature         = 2220,644   K
    Detonation pressure                   = 20,43652  GPa
    Detonation velocity                   = 7677,034   m/s
    Particle velocity                     = 1615,311   m/s
    Sound velocity                        = 6061,723   m/s
```

```
    Density of  products                  = 2,087154   g/cm3
    Volume of  products                   = 0,4791212  cm3/g
    Exponent 'Gamma'                      = 3,752666
    Moles of gaseous products             = 4,111014   mol/mol explosive
    Moles of condensed products           = 1,664585   mol/mol explosive
    Volume of gas at STP                  = 858,6321  dm3/kg
    Mean molecular mass of gas. prod.     = 23,61736  g/mol
    Mean molecular mass of cond.prod.     = 12,011  g/mol
    Mean molecular mass of all prod.      = 20,27229  g/mol
    Entropy of products                   = 5,899384  kJ/kg K
    Internal energy of products           = 4077,861   kJ/kg,  i.e.  6,720315  kJ/cm3
    Compression energy                    = 1304,621   kJ/kg,  i.e.  2,150016  kJ/cm3
    Total heat energy                     = -2773,24  kJ/kg, i.e.  -4,5703  kJ/cm3


Composition of detonation products:
   Products         mol/mol            mol/kg              Mol %
--------------------------------------------------------------------
    N2 = 2,221792             18,9747538,46859
    C(d) =          1,664585            14,2160528,821
    HF =            0,9996918                   8,53766117,30888
    NH3 =           0,5557111                   4,7459359,621704
    CH4 =           0,1984353                   1,6946953,435752
    H2 = 0,06649277                     0,5678678           1,151271
    C2H6 =          0,0664919                   0,5678603           1,151255
    C2H4 =          0,001652073                 0,01410919          0,02860436
    HCN =           0,0005959799                0,005089842         0,01031893
    CF4 =           5,869497E-05                0,0005012722        0,001016258
    N2H4 =          5,380852E-05                0,0004595405        0,0009316525
    CH2F2 =         3,671409E-05                0,0003135491        0,0006356759
    NH2 =           1,719467E-06                1,468476E-05        2,977124E-05
    H =             5,16133E-07                 4,407927E-06        8,93644E-06
    C(gr) =         2,727509E-10                2,329372E-09        4,722469E-09
    N =             5,334089E-11                4,555469E-10        9,23556E-10
    CFN =           2,717836E-12                2,321111E-11        4,705721E-11
    F2 =            6,600214E-13                5,636776E-12        1,142776E-11
```

```
   NF =           9,780267E-14              8,352634E-13     1,693377E-12

   CF2 =          1,093631E-14              9,33993E-14      1,893537E-13

   CF = 2,327707E-16                1,98793E-15       4,030244E-15


Running parameters:

-----------------------

  - Equation of state:  BKW EOS

  - 'BKWN' set of constants

  - Covolumes set 1

   (Alpha=0,5, Beta=0,38, Kappa=9,32, Theta=4120)

  - Activity: Model 1: Condensed products form pure phase (Default)
```

2-Fluoromethyl-5-aminotetrazol (2b)

```
   C(2,000) H(4,000) N(5,000) F(1,000)


    Molecular weight                      = 117,09

    Density of explosive                  = 1,638   g/cm3

    Oxygen balance                         = -75,14988  %

    Enthalpy of formation                 = 293,79  kJ/kg

    Internal energy of formation          = 399,63  kJ/kg



Detonation parameters (at the C-J point) :

-----------------------


    Heat of detonation                    = -2691,981   kJ/kg

    Detonation temperature        = 2184,589   K

    Detonation pressure                   = 19,87498  GPa

    Detonation velocity                   = 7589,758   m/s

    Particle velocity                     = 1598,693   m/s

    Sound velocity                        = 5991,066   m/s

    Density of  products                  = 2,075094   g/cm3

    Volume of  products                   = 0,4819059  cm3/g

    Exponent 'Gamma'                      = 3,747479

    Moles of gaseous products             = 4,113533   mol/mol explosive
```

```
    Moles of condensed products          = 1,651087   mol/mol explosive
    Volume of gas at STP                 = 859,1584  dm3/kg
    Mean molecular mass of gas. prod.    = 23,6423  g/mol
    Mean molecular mass of cond.prod.    = 12,011  g/mol
    Mean molecular mass of all prod.     = 20,3109  g/mol
    Entropy of products                  = 5,873193  kJ/kg K
    Internal energy of products          = 3969,896   kJ/kg,  i.e.  6,50269  kJ/cm3
    Compression energy                   = 1277,915   kJ/kg,  i.e.  2,093225  kJ/cm3
    Total heat energy                    = -2691,981  kJ/kg, i.e.  -4,409465  kJ/cm3


Composition of detonation products:
  Products       mol/mol          mol/kg           Mol %
-----------------------------------------------------------------------
   N2 = 2,229872          19,0437538,68201
   C(d) =        1,651087         14,1007728,64174
   HF =          0,9997297               8,53798417,3425
   NH3 =         0,539615         4,60847          9,360807
   CH4 =         0,2078902               1,7754433,606311
   C2H6 =        0,06859396              0,5858124        1,189913
   H2 = 0,06555182                0,5598317        1,13714
   C2H4 =        0,001599487             0,01366009       0,02774662
   HCN =         0,0005511101            0,004706642      0,009560214
   CF4 =         5,070569E-05            0,0004330414     0,0008796014
   N2H4 =        4,435502E-05            0,0003788048     0,0007694351
   CH2F2 =       3,374966E-05            0,000288232      0,0005854619
   NH2 =         1,438145E-06            1,228218E-05     2,494778E-05
   H =           4,305783E-07            3,677265E-06     7,469325E-06
   C(gr) =       2,862551E-10            2,444702E-09     4,965722E-09
   N =           3,526133E-11            3,011421E-10     6,116852E-10
   CFN =         2,334233E-12            1,993503E-11     4,049239E-11
   F2 =          4,090586E-13            3,49348E-12      7,096019E-12
   NF =          6,378983E-14            5,447838E-13     1,106575E-12
   CF2 =         9,248372E-15            7,898381E-14     1,604333E-13
   CF = 1,684529E-16              1,438637E-15     2,922186E-15
```

```
Running parameters:
-----------------------
  - Equation of state:  BKW EOS
  - 'BKWN' set of constants
  - Covolumes set 1
    (Alpha=0,5, Beta=0,38, Kappa=9,32, Theta=4120)
  - Activity: Model 1: Condensed products form pure phase (Default)
```

1MATz

```
   C(2,000) H(5,000) N(5,000)


    Molecular weight                    = 99,1
    Density of reactant                 = 1,42   g/cm3
    Initial pressure                    = 0,1  MPa
    Oxygen balance                      = -104,9379  %
    Enthalpy of formation               = 2121,09  kJ/kg
    Internal energy of formation        = 2277,42  kJ/kg



Detonation parameters (at the C-J point) :
------------------------------------------


    Heat of detonation                  = -2725,019   kJ/kg
    Detonation temperature        = 1967,995   K
    Detonation pressure                 = 16,46349  GPa
    Detonation velocity                 = 7313,191   m/s
    Particle velocity                   = 1585,346   m/s
    Sound velocity                      = 5727,845   m/s
    Density of  products                = 1,813026   g/cm3
    Volume of  products                 = 0,5515641  cm3/g
    Exponent 'Gamma'                    = 3,612972
    Moles of gaseous products           = 3,501066   mol/mol explosive
    Moles of condensed products         = 1,089372   mol/mol explosive
    Volume of gas at STP                = 863,9967  dm3/kg
    Mean molecular mass of gas. prod.   = 24,56676  g/mol
```

```
   Mean molecular mass of cond.prod.      = 12,011  g/mol
   Mean molecular mass of all prod.       = 21,58711  g/mol
   Entropy of products                    = 6,2045  kJ/kg K
   Internal energy of products            = 3981,695   kJ/kg,  i.e.  5,654007  kJ/cm3
   Compression energy                     = 1256,677   kJ/kg,  i.e.  1,784481  kJ/cm3
   Total heat energy                      = -2725,019  kJ/kg, i.e.  -3,869526  kJ/cm3


Composition of detonation products  (13):
-----------------------------------------------------------------------------
    Products        mol/mol EM                 mol/kg EM        Mol %    Mass %
-----------------------------------------------------------------------------
     N2 = 2,204283E+00                2,224301E+01       48,0190  62,3094
     C(d) =         1,089372E+00                1,099266E+01     23,7313  13,2033
     NH3 =          5,910033E-01                5,963706E+00     12,8747  10,1568
     CH4 =          4,151943E-01                4,189650E+00     9,0448   6,7215
     C2H6 =         2,451414E-01                2,473677E+00     5,3403   7,4379
     H2 = 4,265299E-02                4,304035E-01       0,9292   0,0868
     C2H4 =         2,390858E-03                2,412571E-02     0,0521   0,0677
     HCN =          3,687629E-04                3,721119E-03     0,0080   0,0101
     N2H4 =         3,128359E-05                3,156770E-04     0,0007   0,0010
     NH2 =          5,188361E-07                5,235481E-06     0,0000   0,0000
     H =            7,595624E-08                7,664605E-07     0,0000   0,0000
     N =            1,756743E-12                1,772697E-11     0,0000   0,0000
     C(gr) =        1,070430E-18                1,080151E-17     0,0000   0,0000


Running parameters:
------------------------
  Equation of state:  BKW EOS
  'BKWN' set of constants; Covolumes set 1
   (Alpha=0,5, Beta=0,38, Kappa=9,41, Theta=4250)
```

1MHTz

```
     C(2,000) H(4,000) N(4,000)


   Molecular weight                       = 84,08
```

```
      Density of reactant                  = 1,432   g/cm3
      Initial pressure                     = 0,1  MPa
      Oxygen balance                       = -114,1644  %
      Enthalpy of formation                = 2903,05  kJ/kg
      Internal energy of formation         = 3050,45  kJ/kg


Detonation parameters (at the C-J point) :
-----------------------------------------


      Heat of detonation                   = -3316,189   kJ/kg
      Detonation temperature         = 2225,121   K
      Detonation pressure                  = 16,68146  GPa
      Detonation velocity                  = 7321,235   m/s
      Particle velocity                    = 1591,124   m/s
      Sound velocity                       = 5730,11   m/s
      Density of  products                 = 1,829635   g/cm3
      Volume of  products                  = 0,5465572  cm3/g
      Exponent 'Gamma'                     = 3,601275
      Moles of gaseous products            = 2,810217   mol/mol explosive
      Moles of condensed products          = 1,295082   mol/mol explosive
      Volume of gas at STP                 = 817,3572  dm3/kg
      Mean molecular mass of gas. prod.    = 24,38411  g/mol
      Mean molecular mass of cond.prod.    = 12,011  g/mol
      Mean molecular mass of all prod.     = 20,48081  g/mol
      Entropy of products                  = 6,4341  kJ/kg K
      Internal energy of products          = 4582,043   kJ/kg,  i.e.  6,561486  kJ/cm3
      Compression energy                   = 1265,854   kJ/kg,  i.e.  1,812702  kJ/cm3
      Total heat energy                    = -3316,189  kJ/kg, i.e.  -4,748783  kJ/cm3


Composition of detonation products  (13):
---------------------------------------------------------------------------
    Products          mol/mol EM                 mol/kg EM          Mol %    Mass %
---------------------------------------------------------------------------
     N2 = 1,754146E+00                 2,086183E+01       42,7288  58,4402
```

```
    C(d) =        1,295082E+00           1,540224E+01    31,5466  18,4996
    NH3 =         4,904887E-01           5,833318E+00    11,9477  9,9347
    CH4 =         3,164911E-01           3,763987E+00    7,7093   6,0386
    C2H6 =        1,889986E-01           2,247736E+00    4,6038   6,7585
    H2 = 5,426616E-02               6,453804E-01     1,3219   0,1301
    C2H4 =        4,672509E-03           5,556954E-02    0,1138   0,1559
    HCN =         1,084299E-03           1,289543E-02    0,0264   0,0349
    N2H4 =        6,639904E-05           7,896750E-04    0,0016   0,0025
    NH2 =         2,539866E-06           3,020629E-05    0,0001   0,0000
    H =           5,005858E-07           5,953401E-06    0,0000   0,0000
    N =           4,537777E-11           5,396719E-10    0,0000   0,0000
    C(gr) =       2,875742E-13           3,420082E-12    0,0000   0,0000

Running parameters:
------------------------
  Equation of state:  BKW EOS
 'BKWN' set of constants; Covolumes set 1
  (Alpha=0,5, Beta=0,38, Kappa=9,41, Theta=4250)
  Activity : Model 1:  Condensed products form pure phase (Default)
```

2MATz

```
    C(2,000) H(5,000) N(5,000)

     Molecular weight                    = 99,1
     Density of reactant                 = 1,341   g/cm3
     Initial pressure                    = 0,1  MPa
     Oxygen balance                      = -104,9379  %
     Enthalpy of formation               = 2081,74  kJ/kg
     Internal energy of formation        = 2238,06  kJ/kg



Detonation parameters (at the C-J point) :
-------------------------------------------

     Heat of detonation                  = -2713,442   kJ/kg
```

```
    Detonation temperature              = 1974,349   K
    Detonation pressure                         = 13,98272  GPa
    Detonation velocity                         = 6897,544   m/s
    Particle velocity                           = 1511,699   m/s
    Sound velocity                              = 5385,845   m/s
    Density of  products                        = 1,717392   g/cm3
    Volume of  products                         = 0,5822783  cm3/g
    Exponent 'Gamma'                            = 3,56275
    Moles of gaseous products                   = 3,533406   mol/mol explosive
    Moles of condensed products                 = 1,007579   mol/mol explosive
    Volume of gas at STP                        = 871,9775  dm3/kg
    Mean molecular mass of gas. prod.           = 24,61993  g/mol
    Mean molecular mass of cond.prod.           = 12,011  g/mol
    Mean molecular mass of all prod.            = 21,82219  g/mol
    Entropy of products                         = 6,3632  kJ/kg K
    Internal energy of products                 = 3856,076   kJ/kg,  i.e.  5,170998  kJ/cm3
    Compression energy                          = 1142,634   kJ/kg,  i.e.  1,532272  kJ/cm3
    Total heat energy                           = -2713,442  kJ/kg, i.e.  -3,638726  kJ/cm3


Composition of detonation products  (13):
------------------------------------------------------------------------------
   Products          mol/mol EM                    mol/kg EM          Mol %    Mass %
------------------------------------------------------------------------------
    N2 = 2,260405E+00               2,280933E+01        49,7779  63,8958
    C(d) =          1,007574E+00                 1,016724E+01       22,1884  12,2119
    CH4 =           4,858335E-01                 4,902457E+00       10,6989  7,8650
    NH3 =           4,785036E-01                 4,828493E+00       10,5374  8,2234
    C2H6 =          2,492504E-01                 2,515140E+00       5,4889    7,5625
    H2 = 5,502617E-02               5,552590E-01        1,2118   0,1119
    C2H4 =          3,719114E-03                 3,752890E-02       0,0819   0,1053
    HCN =           6,485322E-04                 6,544220E-03       0,0143   0,0177
    N2H4 =          1,846056E-05                 1,862822E-04       0,0004   0,0006
    C(gr) =         5,234513E-06                 5,282051E-05       0,0001   0,0001
    NH2 =           7,078879E-07                 7,143168E-06       0,0000   0,0000
    H =             1,369764E-07                 1,382204E-06       0,0000   0,0000
```

```
    N =              2,330931E-12               2,352100E-11      0,0000    0,0000
Running parameters:
-----------------------
  Equation of state:  BKW EOS
  'BKWN' set of constants; Covolumes set 1
   (Alpha=0,5, Beta=0,38, Kappa=9,41, Theta=4250)
  Activity : Model 1:  Condensed products form pure phase (Default)
```

2MHTz

```
      C(2,000) H(4,000) N(4,000)


     Molecular weight                         = 84,08
     Density of explosive                     = 1,31   g/cm3
     Oxygen balance                           = -114,1644  %
     Enthalpy of formation                    = 2710,39  kJ/kg
     Internal energy of formation             = 2828,30  kJ/kg



Detonation parameters (at the C-J point) :
-----------------------


     Heat of detonation                       = -3210,51   kJ/kg
     Detonation temperature             = 2227,507   K
     Detonation pressure                      = 13,87424  GPa
     Detonation velocity                      = 6876,944   m/s
     Particle velocity                        = 1540,077   m/s
     Sound velocity                           = 5336,867   m/s
     Density of  products                     = 1,688031   g/cm3
     Volume of  products                      = 0,5924062  cm3/g
     Exponent 'Gamma'                         = 3,465324
     Moles of gaseous products                = 2,839265   mol/mol explosive
     Moles of condensed products              = 1,18648   mol/mol explosive
     Volume of gas at STP                     = 825,8058  dm3/kg
     Mean molecular mass of gas. prod.        = 24,59402  g/mol
     Mean molecular mass of cond.prod.        = 12,011  g/mol
```

```
    Mean molecular mass of all prod.        = 20,88551  g/mol
    Entropy of products                     = 6,624269  kJ/kg K
    Internal energy of products             = 4396,438   kJ/kg,  i.e.  5,759334  kJ/cm3
    Compression energy                      = 1185,927   kJ/kg,  i.e.  1,553565  kJ/cm3
    Total heat energy                       = -3210,51  kJ/kg, i.e.  -4,205769  kJ/cm3

Composition of detonation products:
  Products        mol/mol            mol/kg             Mol %
--------------------------------------------------------------------
   N2 = 1,820159           21,6469145,21296
   C(gr) =        0,9605564                    11,4237723,86034
   CH4 =          0,3762853                    4,4751129,346973
   NH3 =          0,3575318                    4,2520798,881133
   C(d) =         0,2259239                    2,6868835,611976
   C2H6 =         0,2092719                    2,4888435,198339
   H2 = 0,06559397                  0,7801005            1,629362
   C2H4 =         0,008305328                  0,09877418           0,2063054
   HCN =          0,002080003                  0,02473721           0,05166754
   N2H4 =         3,391831E-05                 0,000403386          0,0008425351
   NH2 =          3,176361E-06                 3,777605E-05         7,89012E-05
   H =            8,488321E-07                 1,009505E-05         2,108509E-05
   N =            4,303401E-11                 5,117978E-10         1,06897E-09

Running parameters:
-----------------------
  - Equation of state:  BKW EOS
  - 'BKWN' set of constants
  - Covolumes set 1
   (Alpha=0,5, Beta=0,38, Kappa=9,32, Theta=4120)
  - Activity: Model 1: Condensed products form pure phase (Default)
```

3.7.4 Crystal Data Refinement Parameter

Table S1. Crystallographic data of **1a**, **1b**, and **5**.

	1a	**1b**	**5**
Formula	$C_2H_4FN_5$	$C_2H_4FN_5$	$C_6H_{12}ClCuF_3N_{15}O_3$
FW [g mol^{-1}]	117.10	117.10	498.31
Crystal system	triclinic	monoclinic	hexagonal
Space Group	$P{-}1$	$P2_1/n$	$P6_3$
Color / Habit	colorless plate	colorless rod	colorless rod
Size [mm]	0.20 x 0.10 x 0.10	0.20 x 0.10 x 0.10	0.01 x 0.02 x 0.10
a [Å]	5.9640(8)	4.0877(3)	12.3154(5)
b [Å]	11.3520(11)	14.1054(8)	12.3154(5)
c [Å]	13.9347(11)	8.0338(4)	6.6489(9)
α [°]	100.396(7)	90	90
β [°]	91.285(9)	92.394(5)	90
γ [°]	96.475(9)	90	120
V [Å^3]	921.14(17)	462.81(5)	873.33(16)
Z	8	4	2
$\rho_{calc.}$ [g cm^{-3}]	1.689	1.681	1.895
μ [mm^{-1}]	0.152	0.151	1.484
F(000)	480	240	500
$\lambda_{MoK\alpha}$ [Å]	0.71073	0.71073	0.71073
T [K]	143	133	133
θ Min–Max [°]	3.4, 28.9	3.8, 30.5	3.3, 26.4
Dataset	−7: 7; −14: 15; −17: 17	−5: 5; −20: 20; −11: 11	−15: 15; −15: 15; −8: 8
Reflections collected	6967	8680	13355
Independent refl.	4138	1407	1202
R_{int}	0.036	0.051	0.046
Observed reflections	2358	1167	1145
Parameters	353	89	88
R_1 (obs)[a]	0.0562	0.0410	0.0255
wR_2 (all data)[b]	0.1247	0.1087	0.0685
GooF[c]	1.01	1.07	1.15
Resd. Dens. [e Å^{-3}]	−0.30, 0.27	−0.24, 0.26	−0.19, 0.77
Absorption correction	multi-scan	multi-scan	multi-scan
CCDC	2020838	2020839	2020906

a) $R_1 = \Sigma||F_0| - |F_c||/\Sigma|F_0|$; b) $wR_2 = [\Sigma[w(F_0^2-F_c^2)^2]/\Sigma[w(F_0)^2]]^{1/2}$; $w = [\sigma c^2(F_0^2)+(xP)^2+yP]^{-1}$ and $P=(F_0^2+2F_c^2)/3$; c) GooF = $\{\Sigma[w(F_o^2-F_c^2)^2]/(n-p)\}^{1/2}$ (n = number of reflections; p = total number of parameters).

Table S2. Crystallographic data of **3**, **4**, and **6**.

	3	**4**	**6**
Formula	$C_6H_{12}ClCuF_3N_{15}O_4$	$C_{12}H_{18}Cl_2CuF_6N_{24}O_8$	$C_{12}H_{18}Cl_2CuF_6N_{24}O_6$
FW [g mol^{-1}]	514.30	874.94	842.94
Crystal system	hexagonal	monoclinic	trigonal
Space Group	$P6_3$	$P2_1/c$	$R{-}3$
Color / Habit	yellow block	blue block	blue platelet
Size [mm]	0.14 x 0.21 x 0.54	0.20 x 0.28 x 0.54	0.03 x 0.09 x 0.10
a [Å]	12.4025(9)	10.0103(5)	10.6246(2)
b [Å]	12.4025(9)	14.4362(6)	10.6246(2)
c [Å]	6.5639(6)	10.5506(5)	24.5252(9)
α [°]	90	90	90
β [°]	90	94.372(5)	90
γ [°]	120	90	120
V [Å^3]	874.40(17)	1520.24(12)	2397.55(15)
Z	2	2	3
$\rho_{\text{calc.}}$ [g cm^{-3}]	1.953	1.911	1.752
μ [mm^{-1}]	1.490	1.016	0.958
F(000)	516	878	1269
$\lambda_{\text{MoK}\alpha}$ [Å]	0.71073	0.71073	0.71073
T [K]	112	107	298
θ Min–Max [°]	3.6, 26.4	2.4, 26.4	2.4, 26.4
Dataset	−9: 15; −15: 14; −8: 8	−12: 12; −18: 18; −13: 13	−13: 13; −13: 13; −30: 30
Reflections collected	2863	20268	15488
Independent refl.	1202	3102	1097
R_{int}	0.029	0.022	0.024
Observed reflections	1057	2884	1027
Parameters	100	241	90
R_1 (obs)[a]	0.0309	0.0225	0.0356
wR_2 (all data)[b]	0.0678	0.0605	0.1267
GooF[c]	1.06	1.04	1.20
Resd. Dens. [e Å^{-3}]	−0.21, 0.47	−0.41, 0.31	−0.41, 0.49
Absorption correction	multi-scan	multi-scan	multi-scan
CCDC	2020905	2020908	2020907

a) $R_1 = \Sigma||F_0|- |F_c||/ \Sigma|F_0|$; b) $wR_2 = [\Sigma[w(F_0^2-F_c^2)^2]/\Sigma[w(F_0)^2]]^{1/2}$; $w = [\sigma c^2(F_0^2)+(xP)^2+yP]^{-1}$ and $P=(F_0^2+2F_c^2)/3$; c) GooF = $\{\Sigma[w(F_o^2-F_c^2)^2]/(n-p)\}^{1/2}$ (n = number of reflections; p = total number of parameters).

4 1-(Azidomethyl)tetrazole – a Powerful New Ligand for Highly Energetic Coordination Compounds

Moritz Kofen, Marcus Lommel, Maximilian H. H. Wurzenberger, Thomas M. Klapötke, Jörg Stierstorfer

Dedicated to Professor Dr. Wolfgang Beck on the occasion of his 90th birthday

Reprinted (adapted) from *Chemistry – A European Journal* **2022**, *28*, 38, e202200492.

DOI: 10.1002/chem.202200492

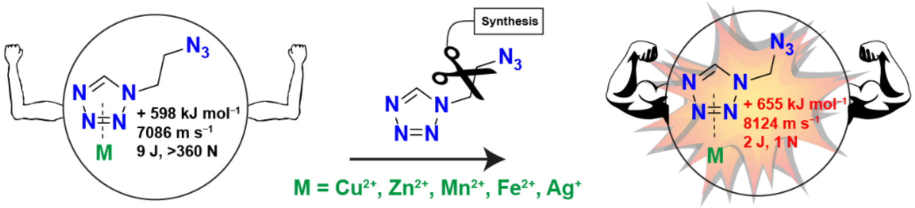

Abstract: Highly energetic 1-(azidomethyl)tetrazole (**AzMT**, **3**) is synthesized and characterized. This completes the series of 1-(azidoalkyl)tetrazoles represented by 1-(azidoethyl)tetrazole (AET) and 1-(azidopropyl)tetrazole (APT). AzMT is thoroughly analyzed by single crystal X-ray diffraction experiments, elemental analysis, IR spectroscopy and multinuclear (^{1}H, ^{13}C, ^{14}N, ^{15}N) NMR measurements. Several ECCs of 3d metals (Mn, Fe, Cu, Zn) and silver in combination with anions such as (per)chlorate, mono- and di-hydroxy-trinitrophenolate are prepared, giving insight on the coordination behavior of **AzMT** as ligand. The synthesized ECCs are also analyzed by X-ray diffraction experiments, elemental analysis, and IR spectroscopy. Differential thermal analysis for all compounds is conducted and the sensitivity towards external stimuli (impact, friction, and ESD) are measured. Due to the high enthalpy of formation of AzMT (+654.5 kJ mol^{-1}), some of the resulting coordination compounds are extremely sensitive, yet are able to undergo deflagration-to-detonation transition (DDT) and initiate pentaerythritol tetranitrate (PETN). Therefore, they are to be ranked as primary explosives.

4.1 Introduction

The design of novel energetic materials is mostly subjected to a pure synthetical approach, generally delimited by the same synthetical strategies. While some of those strategies are known and applied since the early 19th century, such as the introduction of several nitro groups to a molecular framework[1-5], the concept of using energetic materials as ligands for energetic coordination compounds (ECCs) is relatively new[6-7]. By combining a variety of metal cations (Cu^{2+}, Fe^{2+}, Zn^{2+}, Mn^{2+}, Ag^{+}) with energetic anions (e.g., NO_3^-, ClO_3^-, ClO_4^-, N_3^-, and nitrophenolates) as well as a practically unlimited number of energetic ligands, ECCs offer a great adjustability and tuning of the energetic properties. It therefore expands the traditional approaches of synthesizing energetic materials, now used as ligands, by the possibility to further tuning the properties by the formation of coordination compounds. While the tetrazole moiety, with its high nitrogen content, is introduced in several recent high performing energetic materials[8-14] as well as potential pharmaceuticals[15-17], several 1*N*-functionalised tetrazoles[18] such as 1-methyltetrazole[19] (1-MTZ) and 1-aminotetrazole[20] (1-AT) promoted the range of adjustability of energetic properties of ECCs. 1-MTZ is able to stabilize sensitive materials (e.g., AgCNO), thus performs well when desensitizing an energetic coordination compound, whereas 1-AT drastically increases the sensitivity. Due to the exceptional high enthalpy of formation (5535 kJ kg^{-1})[21] and low oxidative resistance of the 1-AT molecule, the corresponding ECCs are among the most sensitive compounds, some being on par with pure copper(II) azide in terms of sensitivity. Efforts to find the perfect balance between performance and sensitivity has led to the formation of ECCs with 1-(azidopropyl)tetrazole[22] and 1-(azidoethyl)tetrazole[23] as ligands.

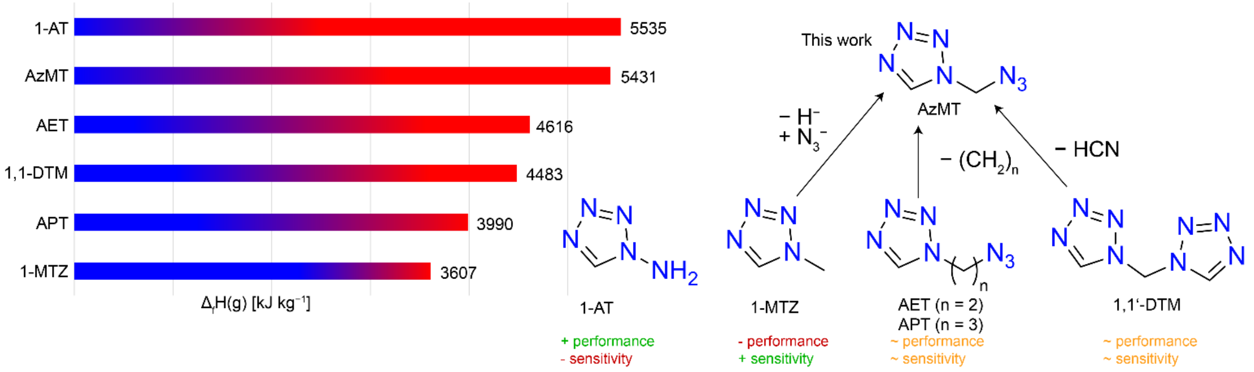

Figure 1. Molecular structure of 1-methyltetrazole (1-MTZ), di(tetrazol-1-yl)-methan (1,1'-DTM), 1-(azidopropyl)tetrazole (APT), 1-(azidoethyl)tetrazole (AET), 1-aminotetrazole (1-AT) and 1-(azidomethyl)tetrazole (AzMT). The structural relationship between 1-MTZ, 1,1-DTM and AET/APT is indicated (right), and a comparison of the calculated gas phase enthalpies of formation of all six ligands is shown (left).

Both compounds exhibit lower gas phase enthalpies of formation (APT: 3990 kJ kg^{-1}, AET: 4616 kJ kg^{-1}) and lower sensitivities (APT: >40 J, >360 N; AET: 9 J, >360 N) towards impact and friction than pure 1-AT (<1 J, 64 N). By comparing ECCs of copper(II) and iron(II) perchlorate of 1-AT, AET, and APT, a clear success in lowering the sensitivities can be demonstrated. The high sensitivities of both metal perchlorate complexes with 1-AT (<1 J, <0.1 N), can be decreased by applying AET (1–3 J, 4–15 N) or APT (3 J, 24–28 N) as ligand. Another promising ligand is di-(tetrazol-1,1'-yl)-methane (1,1'-DTM), being structurally similar to 1-MTZ, having one proton substituted by another tetrazole moiety (Figure 1). 1,1'-DTM validated the concept of adjustability of energetic coordination compounds by selecting appropriate metal cations and energetic anions, as can be seen from the different sensitivities of the copper(II) perchlorate (<1 J, <1 N) and the copper(II) picrate (6 J, >360 N) coordination compounds. Considering the molecular structures of 1-MTZ, AET, and 1,1'-DTM, a structurally similar, yet missing compound is 1-(azidomethyl)tetrazole. It is formally obtained by substitution of one hydrogen atom of 1-MTZ by an azide functionality, as well as formally removing hydrogen cyanide from 1,1'-DTM (Figure 1). More obvious, it is obtainable by formally further decreasing the alkyl chain from AET to a methylene moiety. Independent from the synthesis, the resulting 1-(azidomethyl)tetrazol represents the smallest tetrazole with an *N*-azidoalkyl functionality, having a drastically increased gas phase enthalpy of formation (5431 kJ kg^{-1}), compared to its three parent compounds (Figure 1), only surpassed by 1-AT. While methylene bridged functional groups on the tetrazole moiety can be found in literature[24-26], especially 5-(azidomethyl)-1*H*-tetrazole[27], they always show 5-substitution of the tetrazole ring[28-29]. Sadly, all 5-substituted derivatives still exhibit acidic protons, making them not suitable to be used as ligands in energetic coordination compounds. Independent to the synthesis, the resulting 1-(azidomethyl)tetrazol represents the smallest tetrazole with an *N*-azidoalkyl functionality, having a drastically increased gas phase enthalpy of formation (5431 kJ kg^{-1}), compared to its three parent compounds (Figure 1), only surpassed by 1-AT. Therefore, we opted to synthesize the highly energetic and hardly accessible 1-(azidomethyl)tetrazole (**3**) for the first time. In this paper, next to the synthesis and characterization of highly energetic 1-(azidomethyl)tetrazole, several energetic coordination compounds of the new ligand are synthesized. Single crystal X-ray diffraction experiments were conducted, and all compounds were analyzed by elemental analysis and IR spectroscopy. The ligand was characterized by multinuclear NMR (^{1}H, ^{13}C, ^{14}N, and ^{15}N) spectroscopy and the thermal and physicochemical properties of all compounds were determined.

4.2 Results and Discussion

4.2.1 Synthesis

*Warning! The synthetic work described in this section involves the handling of very sensitive intermediates such as 1-(azidomethyl)tetrazole (**3**) and ECCs **5–14**. Proper protective measurements and equipment must be used!*

The synthesis of 1-(azidomethyl)tetrazol (**3**) is shown in Scheme 1. The literature[30] known hydroxy methylation of *1H*-tetrazole with formaldehyde (37%) in aqueous solution was optimized towards a 66% shorter reaction time with an improved yield of 80% (over 65%). Isomeric mixture of 1- and 2-(hydroxymethyl)tetrazole (**1a**, **1b**) is obtained as a colorless oil. Due to the polarity of the alcohol functionality, a separation of the isomers by column chromatography is not possible at this stage. The isomeric mixture **1** is mesylated by methanesulfonyl chloride in DCM at room temperature with a good overall yield of 64%. After quenching the reaction solution in water, pure 1-(methanesulfonyl-methyl)tetrazole (**2a**) precipitates and is filtered off. **2a** is obtained as a colorless solid in moderate yield (48%). The organic layer is separated, washed with hydrochloric acid (2M) and water and the solvent removed *in vacuo* to obtain crude 2-(methanesulfonyl-methyl)tetrazole (**2b**) in poor yield (18%). After refluxing **2a** with an excess of sodium azide in a water/acetone mixture (1:1) overnight, the reaction solution is extracted with DCM and the organic phase is washed with water and dried over magnesium sulfate. By removing the solvent in vacuo, 1-(azidomethyl)tetrazole (**3**) is obtained as colorless solid in quantitative yield. Crystals suitable for single crystal X-ray diffraction experiments are obtained by recrystallization from acetone.

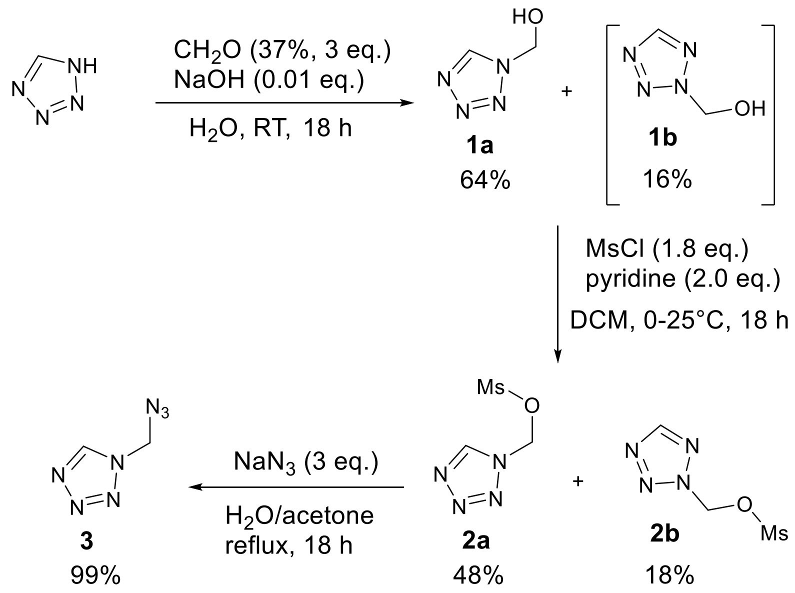

Scheme 1. Synthesis of 1-(azidomethyl)tetrazole (AzMT, **3**), starting from *1H*-tetrazole.

4.2.2 NMR Spectroscopy

The ^{1}H NMR of the crude isomeric mixture **1** in DMSO-d_6 shows two signals at $\delta = 9.31$ and 8.77 ppm attributing the tetrazole protons of **1a** and **1b** isomers, respectively. Integration of the signals reveals a distribution of 4/1 favoring **1a** over **1b**. The two signals at $\delta = 6.11$ and 6.03 ppm attribute the respective CH_2 group of **1a** and **1b**. The ^{1}H NMR of **2a** in acetone-d_6 shows three signals at $\delta = 9.43$, 6.67, and 3.27 ppm attributing the CH, the CH_2 and the CH_3 group, respectively. The ^{1}H NMR of compound **3** in DMSO-d_6 shows two signals at $\delta = 9.60$ and 6.02 ppm attributing to the CH and CH_2 group. Compared to **1a**, the tetrazole CH is downfield shifted by 0.29 ppm whereas the upfield shift of the CH_2 unit (0.01 ppm) is negligible. The ^{13}C NMR spectrum also shows two signals at $\delta = 144.2$ and 60.5 ppm, marking the tetrazole- and the methylene carbon atoms, respectively. ^{14}N NMR measurement of **3** in DMSO-d_6 shows two broadened signals at $\delta = -135.6$ and -160.4 ppm corresponding to the N_β atom of the azide moiety and to the N1 atom of the tetrazole. Due to the invisibility of the missing nitrogen atoms, proton coupled ^{15}N NMR measurement (Figure 2) was performed. The resonance for the azide at $\delta = -302.1$ (N_α), -158.9 (N_γ), and -136.3 (N_β) are in the same range as comparable azido-methyl compounds. The signal at $\delta = -158.9$ splits into a triplet due to ^{3}J-coupling to the methylene protons. The signals for the tetrazole at $\delta = 14.4$ (N_3), -14.0(N_2), -50.4 (N_4), and -141.9 ppm (N_1) are also in the typical range of 1*N*-subsituted tetrazoles[22]. While the signal at $\delta = -14.0$(N_2) appears as a singlet, the remaining resonances appear as doublets with coupling constants of 3.3 Hz (14.4 ppm), 12.7 Hz (-50.4 ppm), and 9.5 Hz (-50.4 ppm) due to ^{3}J and ^{2}J coupling with the tetrazole proton.

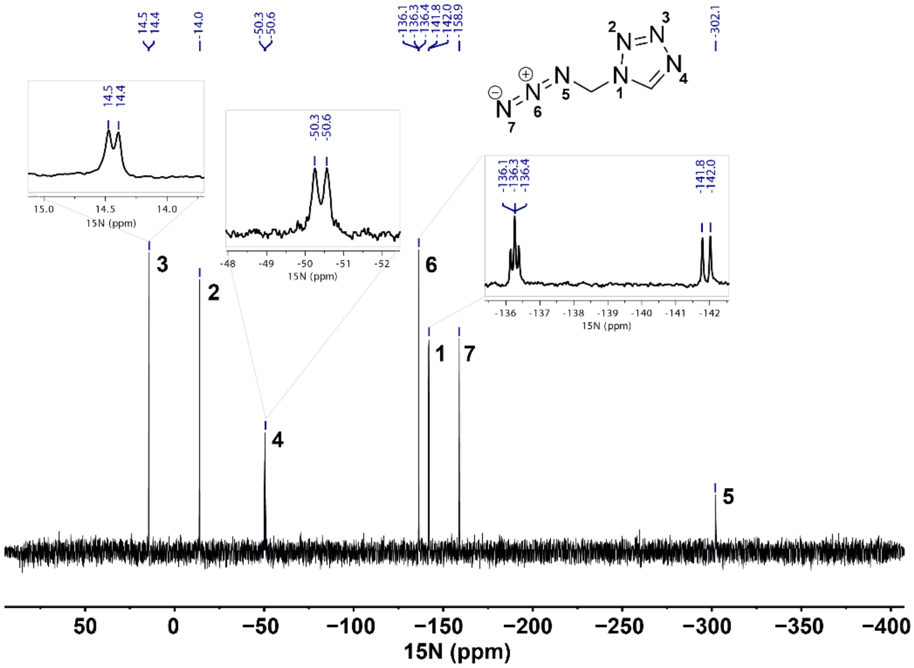

Figure 2. ^{15}N NMR spectrum of 1-(azidomethyl)tetrazole (**3**) in acetone-d$_6$.

4.2.3 Detonation Properties

The detonation performance parameters of **3** are calculated with the EXPLO5 program code[31], for which the enthalpy of formation was determined by applying the atomization method using room temperature CBS-4M enthalpy. Since the performance properties for AET and APT are not reported in literature, their enthalpies of formation are also calculated to further obtain their detonation performances. Table 1 compares all calculated values for **3**, AET and APT. A small increase in density of 0.06 g cm^{-3} (Table 1) is observed by decreasing the alkyl-chain by one CH$_2$-group from APT to AET, whereas further shortening the alkyl chain by a second CH$_2$-group to AzMT causes a more drastic increase in density by 0.24 g cm^{-3}. The higher increase in density can be explained due to the liquid state of APT and AET at room temperature, whereas AzMT is already a solid at room temperature. Additionally, the enthalpy of formation from **3** (654.5 kJ mol^{-1}) to APT (568.4 kJ mol^{-1}) is also drastically decreasing. As the performance of energetic compounds depends on their enthalpy of formation and their densities, combining both into an enthalpy density offers an appropriate value to quickly elucidate the differences. Here, AzMT shows a very high enthalpy density of 8110 J cm^{-3}, followed by AET (5630 J cm^{-3}) and APT (4639 J cm^{-3}). Therefore, the calculated detonation performances show a drastic increase in performance from APT (6757 m s^{-1}) to AzMT (8124 m s^{-1}), hence also a significantly higher performance of the corresponding ECCs can be estimated.

Table 1. Energetic properties of AzMT (**3**), compared to AET[23] and APT[22].

	AzMT (**3**)	AET[23]	APT[22]
Formula	$C_2H_3N_7$	$C_3H_5N_7$	$C_4H_7N_7$
M [g mol^{-1}]	125.1	139.1	153.2
ρ [g cm^{-3}]	1.545[a]	1.31[b]	1.25[b]
N [%][c]	78.38	70.48	64.02
Ω_{CO} [%][d]	−70.34	−97.75	−120.13
$\Delta_f H°$ [kJ mol^{-1}][e]	655	598	568
$\Delta_f H°$ [kJ kg^{-1}][f]	5232	4427	3853
$\Delta_f H°$ [J cm^{-3}] [g]	8110	5630	4639
EXPLO5 V6.05.04			
$-\Delta_{ex}U^0$ [kJ kg^{-1}][h]	5127	4449	4121
T_{det} [K][i]	3473	3169	2609
V_0 [L kg^{-1}][j]	502	540	620
P_{CJ} [kbar][k]	229	192	130
V_{det} [m s^{-1}][l]	8124	7086	6757

[a] From single crystal X-ray diffraction analysis recalculated to room temperature. [b] Measured with a gas pycnometer. [c] Nitrogen content. [d] oxygen balance towards the formation of CO. [e] Calculated enthalpy of formation. [f] Calculated mass related enthalpy of formation. [g] calculated volume related enthalpy of formation. [h] Energy of explosion. [i] Detonation temperature. [j] Volume of detonation products (assuming only gaseous products). [k] Detonation pressure at Chapman-Jouguet point. [l] Detonation velocity.

4.2.4 Energetic Coordination Compounds

Due to the absence of acidic protons in compound **3**, it can be used as a well-suited neutral ligand for ECCs. The application of several oxidizing anions such as nitrate, chlorate, perchlorate, fulminate, picrate, styphnate, and trinitro phloroglucinol, and reducing anions such as azide, enables the tuning of the energetic properties of the resulting coordination compound. Energetic coordination compounds **4**–**9** are obtained by dissolving the corresponding metal(II) salts in water at elevated temperatures (60–80 °C) and adding **3** in stoichiometric amounts (Scheme 2). Due to the commercial unavailability of copper(II) chlorate, it was synthesized according to a previously published procedure[23].

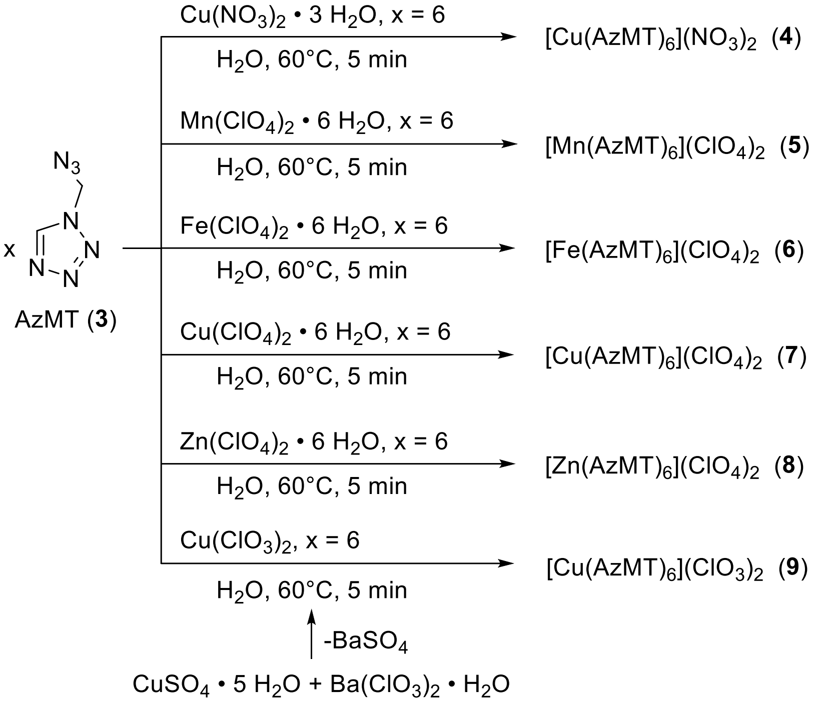

Scheme 2. Synthesis of energetic coordination compounds of copper(II) nitrate (**4**), 3d-metal perchlorates (**5**–**8**) and copper(II) chlorate (**9**) with 1-(azidomethyl)tetrazole.

The copper(II) nitroaromatic salts for compounds **10**–**12** were synthesized by dissolving basic copper(II) carbonate in water and adding stoichiometric amounts of the free acids of the corresponding nitroaromatic anion (Scheme 3). Compound **13** was synthesized by dissolving copper(II) chloride dihydrate in water, adding one equivalent of **3**, followed by adding two equivalents of sodium azide dissolved in water. Immediately after the addition of the azide, a brown precipitate of **13** is formed, filtered off, and washed with little hot water. Compound **14a/b** is obtained by dissolving silver(I) fulminate in acetonitrile at 30 °C and adding one equivalent of ligand. Crystals of compound **14a** are starting to form in the mother liquor after one day. By filtering off the platelets, crystals suitable for single crystal X-ray diffraction are obtained. When leaving the mother liquor for several days, white needles, suitable for X-ray diffraction, of compound **14b** start to crystallize on top of the crystals of **14a**, ultimately completely turning **14a** into **14b**. Crystallization of the coordination compounds **4**–**12** was achieved by slowly evaporating the mother liquor for 1–2 days, and collecting the formed solids by filtration with subsequent drying in air. Single crystals suitable for X-ray diffraction experiments were also obtained from the mother liquor for compounds **4**, **9**, and **10.** Single crystals of compound **13** were obtained by a three-layered crystallization approach. Sodium azide together with **3** was dissolved in water and added to a test tube. A second layer consisting of a 1:1 mixture of water and ethanol was layered on top, and the third layer of copper(II) chloride dissolved in ethanol was slowly added. The test tube was carefully stoppered as not to mix the three layers and was set aside. After several days, crystals of compound **13** had formed and were collected by filtration and washed with little hot water. It was not possible to obtain crystals suitable for single-crystal X-ray diffraction of compounds **5**–**8**, **11**, and **12**, their composition was analyzed and proven by elemental analysis. Generally, all energetic coordination compounds were fully characterized by elemental analysis, infrared spectroscopy, differential thermal analysis, as well as their sensitivity towards impact (IS), friction (FS), and electrostatic discharge (ESD) were tested. Hot needle (HN) and hot plate (HP) tests were performed to obtain insight into their initiation capabilities, which were then tested for several chosen compounds.

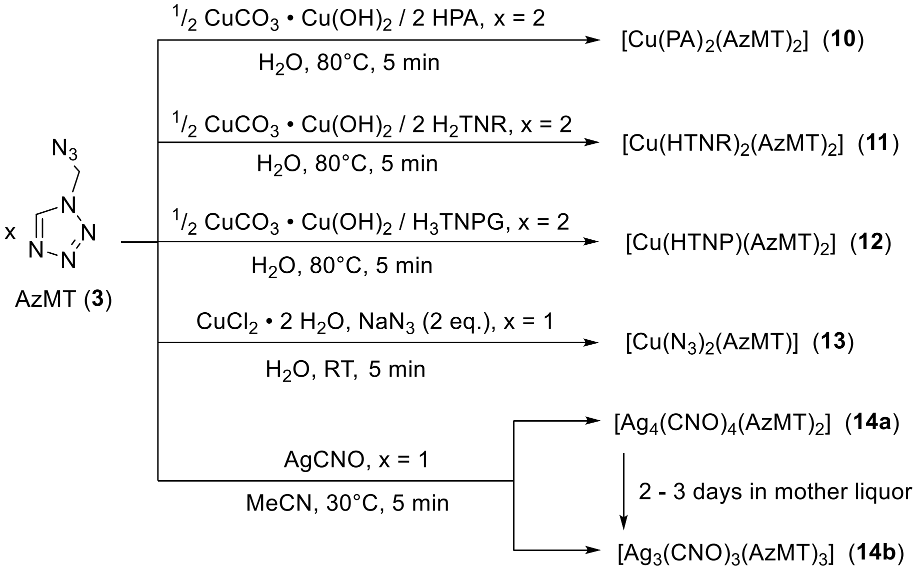

Scheme 3. Synthesis of nitroaromatic coordination compounds **10**–**12**, as well as the coordination compound of copper(II) azide (**13**) and silver(I) fulminate (**14a/b**) with AzMT.

4.2.5 Crystal Structures

Solid-state crystal structures of compounds **3**, **4**, **9**, **10**, and **14a/b** were determined using low-temperature single-crystal X-ray diffraction. All of the data and parameters of the measurements as well as of the refinements are given in the Supporting Information Table S1. All crystal densities are recalculated to their respective room temperature crystal density. Deposition Numbers 2124092 (for **3**), 2124093 (for **10**), 2124094 (for **9**), 2124095 (for **13**), 2124096 (for **14b**), 2124097 (for **4**), 2144883 (for **14a**) contain the supplementary crystallographic data for this paper. These data are provided free of charge by the joint Cambridge Crystallographic Data Centre and Fachinformationszentrum Karlsruhe Access Structures service.

Compound **3** crystallizes in the orthorhombic space group *Pbca* with eight formula units in the unit cell and a density of 1.55 g cm^{-3} (Figure 3). All bond lengths are in the typical range for C–N, N–N single and double bonds. The tetrazole moiety forms a nearly perfectly level plane (C1–N1–N2–N3 = 0.3°) from which the methylene group is slightly protruding by an angle of C1–N1–N2–N3 = 1.4°. Typical for covalently bound azides, the $-N_3$ unit protrudes from the tetrazole plane with an angle of N1–C2–N5 = 111° as shown in Figure 3.

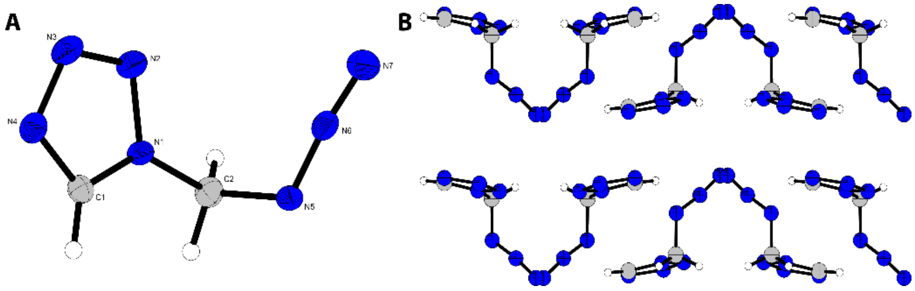

Figure 3. A) Crystal structure of 1-(azidomethyl)tetrazole (**3**); B) crystal packing along the *a* axis; ellipsoids in all structures are shown with a probability of 50%; Selected bond lengths [Å]: N1-N2 1.35(2), N1-C1 1.33(3), N1-C2 1.46(3), N2-N3 1.29(3), N3-N4 1.37(3), N4-C1 1.31(3), N5-C2 1.47(4), N5-N6 1.25(3), N6-N7 1.12(3); Angles [°]: N2-N1-C1 108.0(15), N1-C2-N5 111.6(2), N2-N1-C2 120.8(18), N1-C1-H1 125.3(13), C1-N1-C2 131.2(18), N4-C1-H1 124.8(13), N1-N2-N3 106.1(17), N1-C2-H2A 107.9(12), N2-N3-N4 111.0(18), N1-C2-H2B 106.1(13), N3-N4-C1 105.0(19), N5-C2-H2A 112.4(13), N6-N5-C2 113.9(19), N5 -C2-H2B 107.3(13), N5-N6-N7 172.6(3), H2A-C2-H2B 111.4(18), N1-C1-N4 109.9(19).

Compound **4** crystallizes in the monoclinic space group *Cc* with four formula units in the unit cell and a density of 1.66 g cm^{-3} (Figure 4). The copper(II) cation is sixfold coordinated by 1-(azidomethyl)tetrazole ligands whereas the two nitrate anions are non-coordinating. While the bond lengths within the six ligands are equivalent as for pure compound **3**, the bond lengths towards the copper(II) center range between 2.02 – 2.33 Å with angles of nearly perfect 180° between opposing ligands. Two of them (N4 and N25) show a longer bond distance towards the copper(II) cation than the four other ligands. Hence, the copper(II) cation is coordinated in a square bipyramidal conformation, caused by a typical *Jahn-Teller*-like distortion, due to the electron configuration of [Ar]3d^9 of the copper(II) cation.

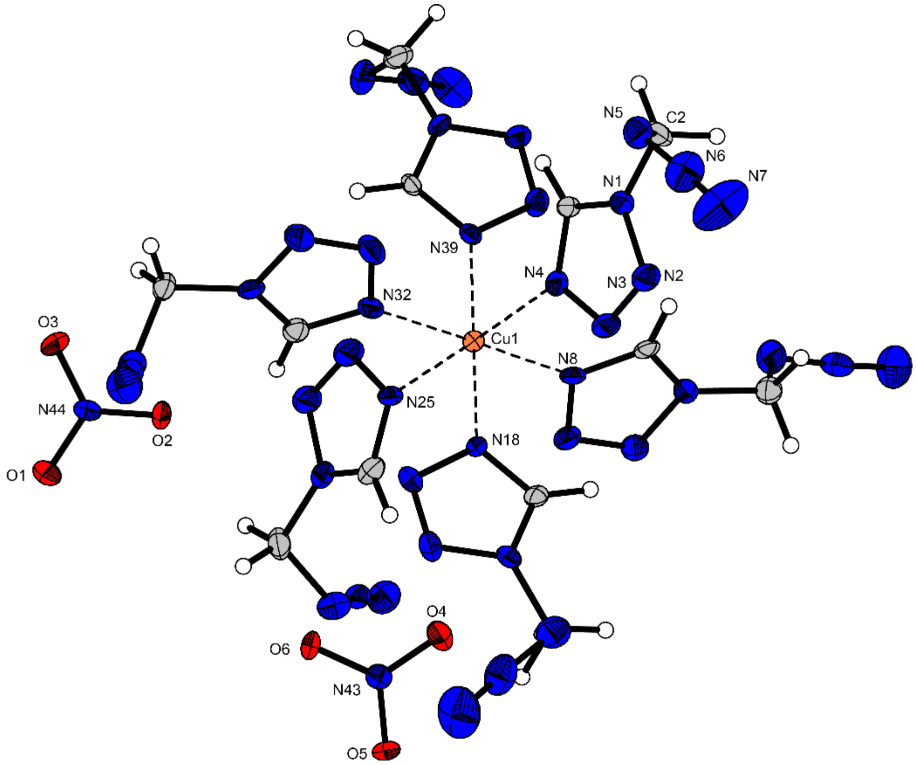

Figure 4. Molecular unit of $[Cu(AzMT)_6](NO_3)_2$ (**4**); Selected bond lengths [Å]: Cu1-N4 2.30(6), Cu1-N8 2.07(6), Cu1-N18 2.02(6), Cu1-N25 2.33(6), Cu1-N32 2.07(6), Cu1-N39 2.03(6); Angles [°]: N4-Cu1-N8 89.5(2), N4-Cu1-N18 91.6(2), N4-Cu1-N25 178.3(2), N4-Cu1-N32 93.5(2), N4-Cu1-N39 87.9(2).

The chlorate complex **9** crystallizes in the triclinic space group *P*−1 with two formula units in the unit cell and a density of 1.71 g cm^{-3} (Figure 5). The copper(II) cation is sixfold coordinated by AzMT ligands, all binding via their respective N4-nitrogen atom. Like in **4**, the coordination sphere is a square bipyramid due to *Jahn-Teller*-like distortion along the N1-Cu1-$N1^i$ axis. The change of anion from nitrate (**4**) to chlorate (**9**) does not induce a change of bond lengths within the ligands. The bond lengths between the ligands and the copper(II) center are in the same range as in **4** (2.02–2.36 Å). The two chlorate anions are also non-coordinating.

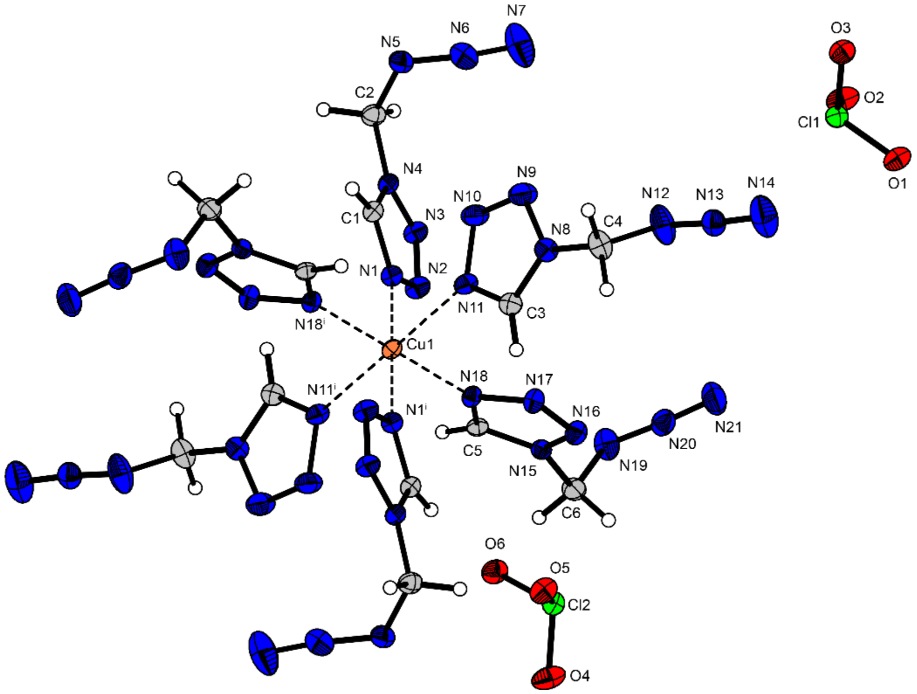

Figure 5. Molecular unit of $[Cu(AzMT)_6](ClO_3)_2$ (**9**); Selected bond lengths [Å]: Cu1-N1 2.05(2), Cu1-N11 2.36(2), Cu1-N18 2.02(2); Angles [°]: N1-Cu1-N11 91.2(9), N1-Cu1-N18 91.6(8), N11-Cu1-N11^{i} 180.0.

Copper(II) picrate **10** (Figure 6) crystallizes in the monoclinic space group $P2_1/c$ with two formula units in the unit cell and a density of 1.83 g cm^{-3}. The copper(II) cation is coordinated by two equatorial AzMT ligands and two coordinating picrate anions, acting as bidentate ligands. The two picrates are coordinating via their deprotonated hydroxyl group as well as a second oxygen atom of one of the *ortho*- nitro groups. The bond lengths between the copper(II) and the AzMT ligands (2.01 Å) are in the same range as for the copper(II) nitrate (**4**) and chlorate (**9**). The deprotonated hydroxy groups also coordinate in the equatorial plane, whereas the nitro groups oxygen atoms are axial standing with a bond length of 2.35 Å, resulting in a typical *Jahn-Teller*-like distortion along the O2-Cu1-O2^{i} axis.

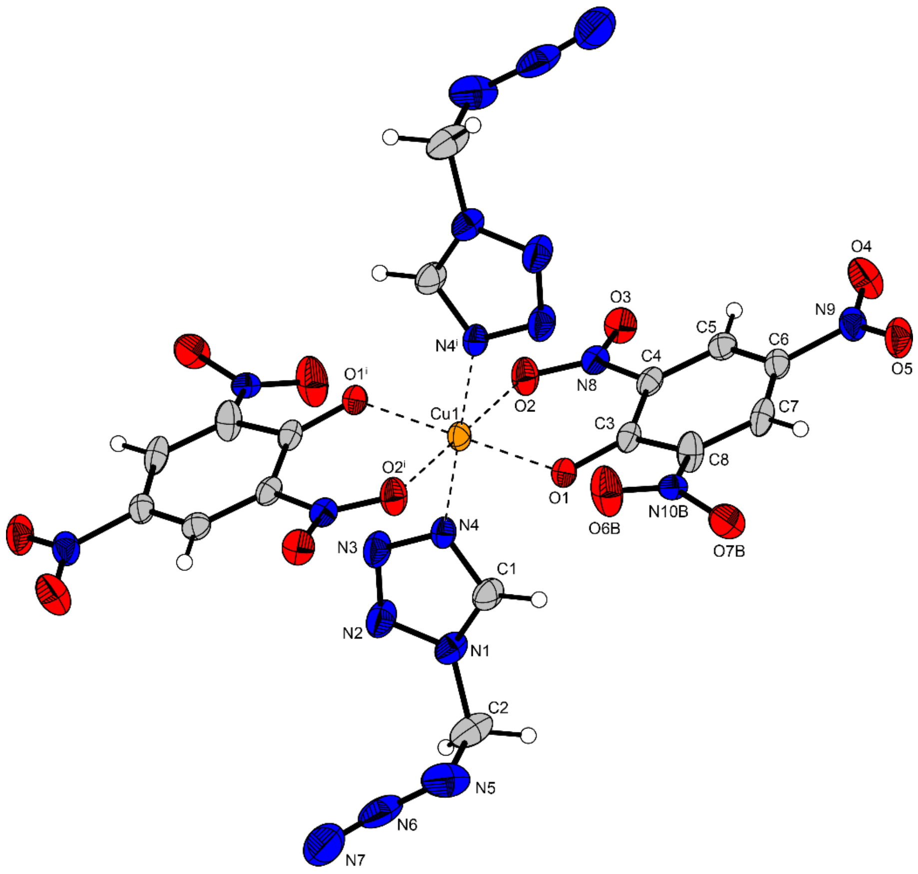

Figure 6. Molecular unit of $[Cu(PA)_2(AzMT)_2]$ (**10**); Selected bond lengths [Å]: Cu1-O1 1.92(2), Cu1-O2 2.35(2), Cu1-N4 2.01(2); Angles [°]: O1-Cu1-O2 78.9(7), O1-Cu1-N4 86.8(7), O2-Cu1-N4 90.13(7).

The copper(II) azide complex **13** crystallizes in the monoclinic space group $P2_1/c$ with four formula units in the unit cell and a density of 1.93 g cm^{-3}. The copper(II) cation is coordinated by five azide anions as well as one AzMT (**3**) ligand (Figure 7) forming a strongly distorted octahedron due to high deviations from the 90° coordination angles, observed in compounds **4**, **9**, and **10**. The deviation of up to 13.5° (N1-Cu1-N11^{ii}) from a linear arrangement of two opposing coordinating compounds is caused by two different bridging modes of the azide anions. Two of the coordinating azide anions are bridging between two copper cations, thereby forming strands, which are interconnected by the other three anions which are bridging between three copper cations. Interestingly, the coordination of the copper(II) cation, as well as the two different bridging modes of the azide anions, are nearly identical to those of the 1-MTZ analogous, proving the structural similarity of the 1-MTZ and AzMT ligand.[32] For the silver(I) fulminate complexes crystallization in two different space groups was observed. The initially formed platelets (**14a**) crystallized in the monoclinic space group $I2/a$ with eight formula units in the unit cell and a density of 2.71 g cm^{-3}, the highest of all herein investigated compounds (Figure 8). The molecular unit consists of a tetrameric cluster of silver fulminate (SF), with the silver cations forming a nearly planar rhombus with angles of 75.72° (Ag2^{i}-Ag1-Ag2) and 104.28° (Ag1-Ag2-Ag1^{i}), and a torsion angle of 3.32°.

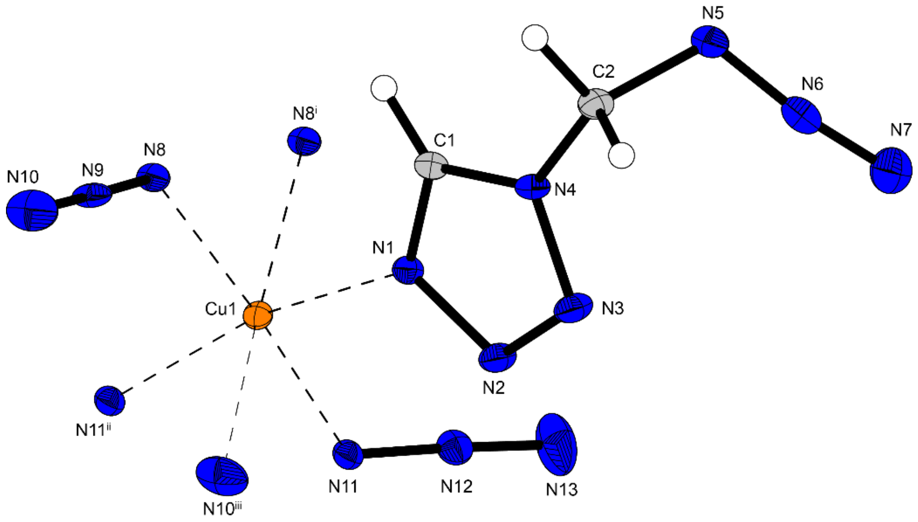

Figure 7. Molecular unit of [Cu(N$_3$)$_2$(AzMT)] (**13**); Selected bond lengths [Å]: Cu1-N1 2.01(2), Cu1-N8 1.97(2), Cu1-N11 2.00(2), Cu1-N10^{iii} 2.65(3), Cu1-N11^{ii} 2.02(2), Cu1-N8^{i} 2.43(2); Angles [°]: N1-Cu1-N11^{ii} 166.5(9), N8-Cu1-N11 172.8(9), N8^{i}-Cu1-N10^{iii} 169.4(8), N1-Cu1-N8 91.7(9), N1-Cu1-N11 95.2(9).

The fulminate anions are bridging between the silver cations with their terminal carbon and oxygen atoms, having shorter Ag-C (2.17 – 2.27 Å) interactions than Ag-O interactions (2.50 – 2.73 Å). Like in previously reported silver fulminate complexes[33], the carbon atoms of the fulminate anions are bridging between two silver cations of a tetramer. While the same bridging between two silver cations of the tetramer is observed for the oxygen atoms, a third interaction with a silver cation of a second tetrameric unit causes the formation of an extended three-dimensional structure. Due to the bridging character of the fulminate anions, Ag–Ag interactions (Figure 8) are observed within the tetrameric unit. Comparable to previously reported coordination compounds of SF with monodentate ligands[33], the bond lengths of these argentophilic interactions (2.91–2.77 Å) are in the range to be classified as sub-van der Waals contacts (<3.44 Å).[34] Additionally, the shortest argentophilic interaction observed has a distance of 2.7675(7) Å, being close to the shortest reported distance of 2.746(1) Å[34]. Standing in the mother liquor for several days, white crystalline needles started to form on top of the platelets. These crystalline needles were also suitable for single crystal X-ray diffraction experiments, showing compound **14b** crystallizing in the triclinic space group *P*−1 with two formula units in the unit cell and a density of 2.30 g cm^{-3}. In contrast to **14a**, the molecular unit consists of a trimeric cluster of silver fulminate coordinated by three AzMT ligands (Figure 9). Here, the fulminate anions are also bridging between silver cations, but in contrast to **14a**, only by their terminal carbon atom, forming monomers with argentophilic interactions between the silver cations, slightly longer (2.81–2.87 Å) than those in the tetrameric structure.

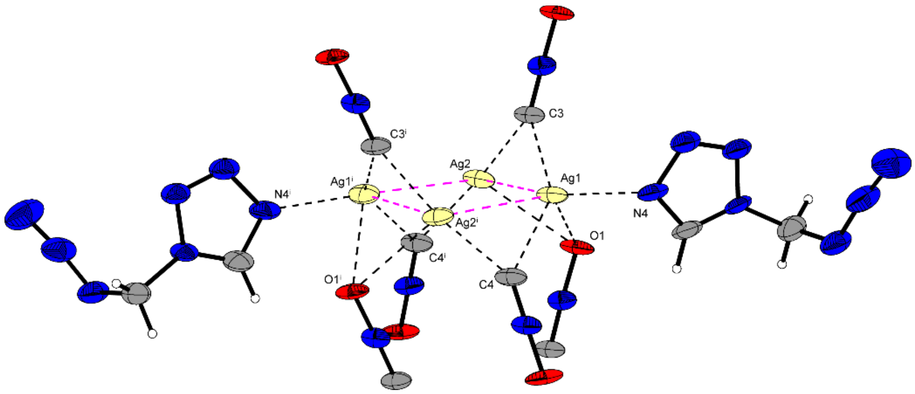

Figure 8. Molecular unit of [Ag$_4$(CNO)$_4$(AzMT)$_2$] (**14a**); Selected bond lengths [Å]: Ag1-Ag2 2.91(8), Ag1-Ag2^{i} 2.77(7), Ag1-N4 2.29(5), Ag1-C3 2.27(5), Ag1-O2 2.66(3), Ag2-C3 2.17(5); Angles [°]: Ag2-Ag1-N4 121.92(12), N4-Ag1-C3 100.34(18), Ag2-C3-Ag1 81.94(20), Ag2-Ag1-O2 129.02(11), Ag2^{i}-Ag1-O2 66.85(10), Ag1-Ag2^{i}-C3^{i} 93.11(13), Ag2^{i}-Ag1-C3 74.66(11); Torsion angles [°] Ag2^{i}-Ag1-Ag2-Ag1^{i} 3.32(2).

Like in the tetrameric structure, the silver fulminate cluster is built nearly planar with a torsion angle of 7.8° (C6-Ag2-Ag1-C9). Interestingly, a different protrusion for every AzMT ligand from the plane, formed by the SF trimer, is observed. While the first AzMT (via N4) is nearly perpendicular with the plane, the AzMT ligands (coordinated via N12 and N20) are protruding from the plane by 8.0° and 46.5°, respectively.

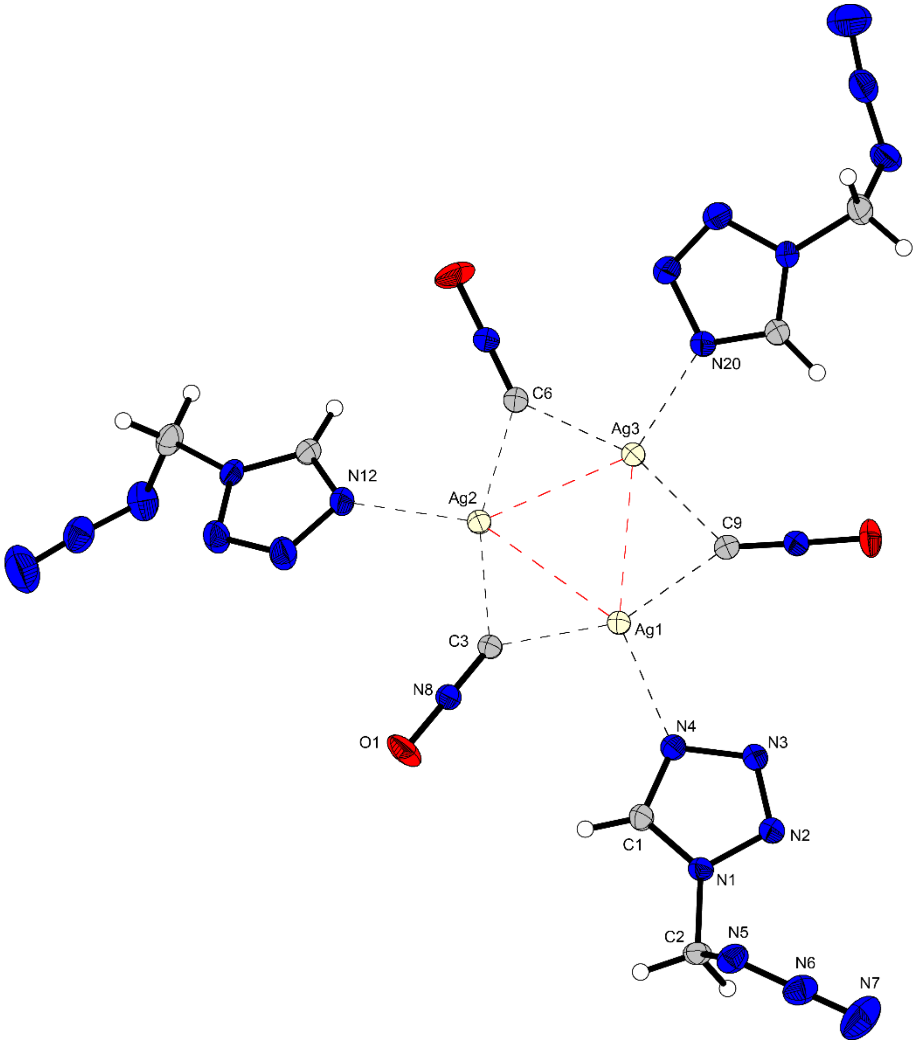

Figure 9. Molecular unit of [$Ag_3(CNO)_3(AzMT)_3$] (**14b**); Selected bond lengths [Å]: Ag1-Ag2 2.87(7), Ag1-Ag3 2.84(7), Ag2-Ag3 2.81(7), Ag1-N4 2.31(2), Ag2-N12 2.31(2), Ag3-N20 2.31(2), Ag1-C3 2.22(3), Ag1-C9 2.20(2), Ag2-C3 2.17(2), Ag2-C6 2.19(2), Ag3-C6 2.18(3), Ag3-C9 2.20(3); Angles [°]: Ag1-Ag2-Ag3 59.9(1), Ag2-Ag1-Ag3 58.9(1), Ag1-Ag3-Ag2 61.2(1), Ag1-C3-Ag2 81.7(8), Ag2-C6-Ag3 79.7(9), Ag1-C9-Ag3 80.4(9), C3-Ag1-C9 155.2(9), C3-Ag2-C6 159.1(10), C6-Ag3-C9 159.3(9).

4.2.6 Physicochemical Properties

Thermal behavior. Differential thermal analyses of compounds **3**–**14** are shown in Figures 10 and 11. DTA plots for compounds **4**, **9** and **12** are shown in the Supporting Information. Compound **3** shows an endothermic event at 54 °C, due to a melting of the compound, and an exothermic decomposition temperature of 167 °C, lower than the comparable 1-(azidoethyl)tetrazole (AET) derivative (193 °C)[23]. All energetic coordination compounds show lower thermal stability, which is also observed for ECCs of AET. Compound **4** shows a small endothermic event at 60 °C, attributing a melting of the compound, with a first exothermic event happening already at 123 °C contributing to explosive decomposition. The same behavior is observed for compound **9**, showing an endothermic event at 112 °C, immediately evolving into an exothermic event at 123 °C. The metal perchlorate compounds **5**–**8** exhibit exothermic decompositions between 127 °C (**6**) and 137 °C (**5**) where all four compounds violently detonate. The nitroaromatic compounds **10** (165 °C), **11** (154 °C), and **12** (151 °C) exhibit slightly higher thermal stabilities, yet they are less stable than pure **3**. The coordination compounds of copper(II) azide (**13**) and silver(I) fulminate (**14b**) are thermally stable up to 147 °C and 109 °C, respectively. Here the formation of complexes with 1-(azidomethyl)tetrazole (**3**) leads to a more drastic drop in thermal stability compared to their parent salts copper(II) azide (205 °C) and silver(I) fulminate (196 °C).

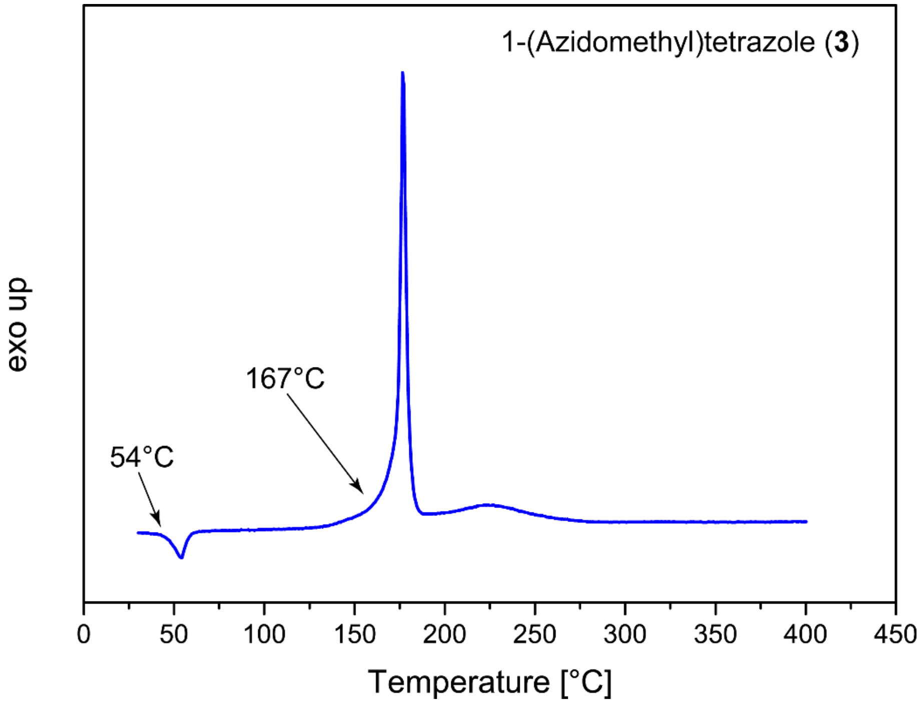

Figure 10. Differential thermal analysis of compound **3** with a heating rate of 5 °C min^{-1}.

Sensitivities. 1-(Azidomethyl)tetrazole (**3**) is a very sensitive compound with an impact and friction sensitivity of 2 J and 1 N (Table 2). (Both values are considered as very sensitive.) While it is not sensitive (540 mJ) towards electrostatic discharge (ESD) due to its mechanical sensitivities it has to be ranked as a primary explosive. By applying **3** as ligand in ECCs of copper(II) nitrate (**4**), picrate, (**10**), styphnate (**11**), and trinitrophloroglycinolate (**12**), it is possible to stabilize the friction sensitivity of **3**. While **4** is only slightly less sensitive (15 N) than pure **3**, compound **10** is completely insensitive (360 N). With an increasing amount of hydroxy groups, **11** shows a higher sensitivity (192 N) and **12** the highest friction sensitivity of 45 N. Yet all nitroaromatic compounds are by far less sensitive than the copper(II) nitrate complex **4**. When changing from copper(II) nitrate to perchlorate (**7**) or chlorate (**9**) the resulting coordination compounds exhibits drastically increased sensitivities (<1 J, <0.1 N) compared to pure **3**. Changing to manganese(II) (**5**), iron(II) (**6**), or zink(II) perchlorate (**8**) the same increase in sensitivities is observed. While all compounds show very high sensitivities towards impact (<1 J), compound **5** is neglectable lower sensitive towards friction (0.5 N) than **6**, **7**, and **8** (<0.1 N). Compound **13** also shows a very high mechanical sensitivity of <1 J and <0.1 N. Yet it seems to be more stable than pure copper(II) azide, derived from the fact that we had no problems handling compound **13**, while several minor explosions happened when handling pure copper(II) azide. The coordination compound of silver(I) fulminate with **3** leads to an increase in impact sensitivity (<1 J) compared to pure silver fulminate (5 J), while the friction sensitivity is approximately equal to pure SF (<0.1 N). The same trends of stabilization or destabilization as for the mechanical sensitivities of the ligand (**3**) is observed comparing the ESD sensitivities. Compounds **4**, **10**, and **11** are completely insensitive towards ESD (>1500 mJ), while compound **12** (1220 mJ) is nearly insensitive. Changing to metal perchlorates or chlorates the ESD sensitivity of the resulting complex (**6**: 380 mJ; **7**: 480 mJ; **8**: 380 mJ; **9**: 380 mJ) is increased compared to the pure ligand (540 mJ). Here, only compound **5**, the manganese perchlorate complex shows a slightly lower sensitivity (740 mJ) than **3**. The highest sensitivity towards ESD is observed for the silver(I) fulminate complex **14b** (10 mJ), followed by the copper(II) azide complex **13** (38 mJ). Here, the addition of **3** to the corresponding salt results in a stabilization of the otherwise sensitive parent compound. Due to the high sensitivities of the metal (per)-chlorates, as well as **14b** towards impact (<1J), ball drop impact measurements were performed, allowing a more detailed differentiation of the compounds. For compounds **5** and **7** (Table 1) a ball drop impact sensitivity (BDIS) of 25 mJ was observed, while compounds **8**, and **14b** are slightly more sensitive (20 mJ) and iron(II) perchlorate (**6)**, as well as the copper(II) chlorate (**9**) showed the highest sensitivity (16 mJ).

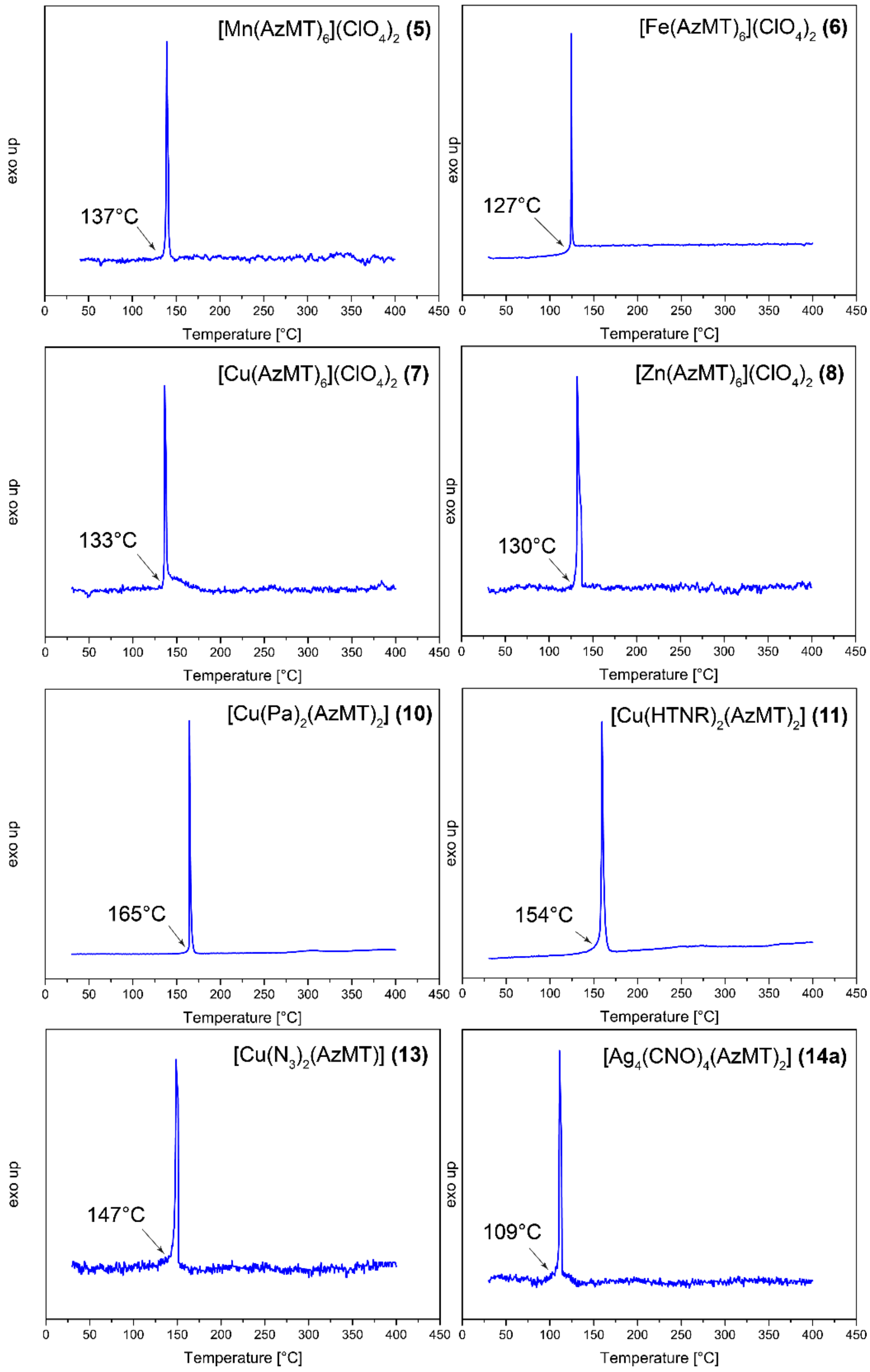

Figure 11. Differential thermal analysis of compounds **5**–**8**, **10**–**11**, and **13**–**14a**, with a heating rate of 5 °C min^{-1}.

Initiation capabilities. To get a further insight on the behavior upon fast heating with and without confinement, hot plate (HP) and hot needle (HN) tests were carried out. This also allows for a first evaluation of the applicability of the tested compounds as primary explosives. The detailed experimental procedure is given in the Supporting Information, the results are summarized in Table

1. Pure compound **3** showed a detonation in the HP test and a deflagration in the HN test. While the copper(II) nitrate (**4**) and the nitroaromatic compounds **10**, **11**, and **12** show deflagration or decomposition (**10**, **11**), the (per)chlorate metal complexes show a violent detonation (**6**, **7**, and **9**) or sharp deflagration (**5** and **8**) in the HP test (Figure 13).

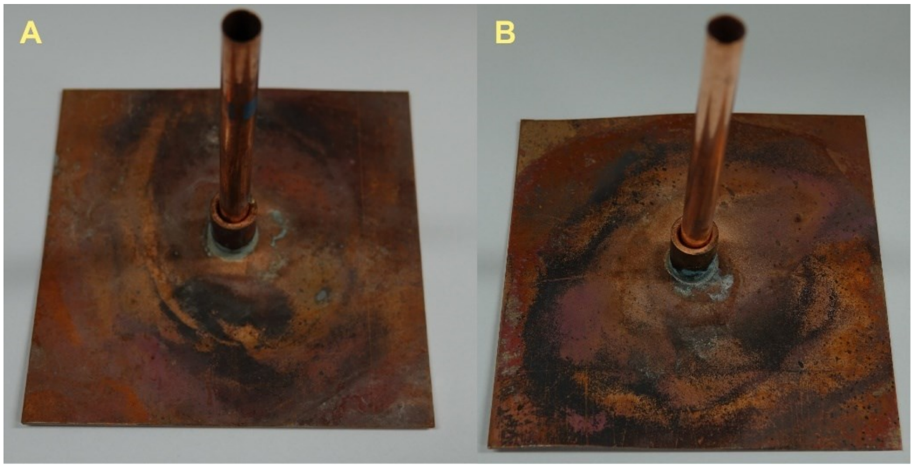

Figure 12. Intact witness plates and copper tubes after the initiation testing of compounds **3** and **12**.

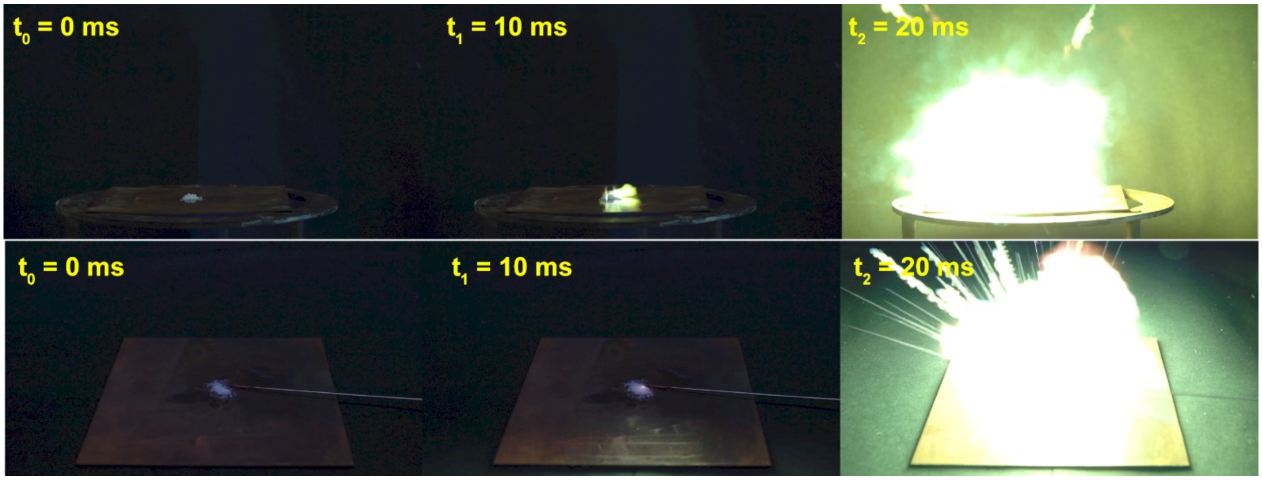

Figure 13. Top row: Hot plate test of $[Mn(AzMT)_6](ClO_4)_2$ (**5**); Bottom row: Hot needle test of **5**; The time between each frame is 10 ms and shows the moment before (t_0), at the onset (t_1) and during (t_2) the decomposition

The complexes of copper(II) azide (**13**) and silver(I) fulminate (**14**) detonate both in the HP and HN test. For compounds **3**, **5**, **7**, **8**, and **12** initiation tests were performed. The detailed testing setup and procedure is given in the Supporting Information. Compounds **3** and **12** showed no positive initiation of PETN, which is indicated by the still intact witness plate (Figure 12). Therefore, both compounds were not able to undergo deflagration to detonation transition (DDT) in this setup, which is a necessary characteristic for a compound to be used as a primary explosive.

Nonetheless, the perchlorates **5**, **7**, and **8** were able to undergo DDT and initiate the PETN sample, indicated by a perforation of the copper witness plate (Figure 14).

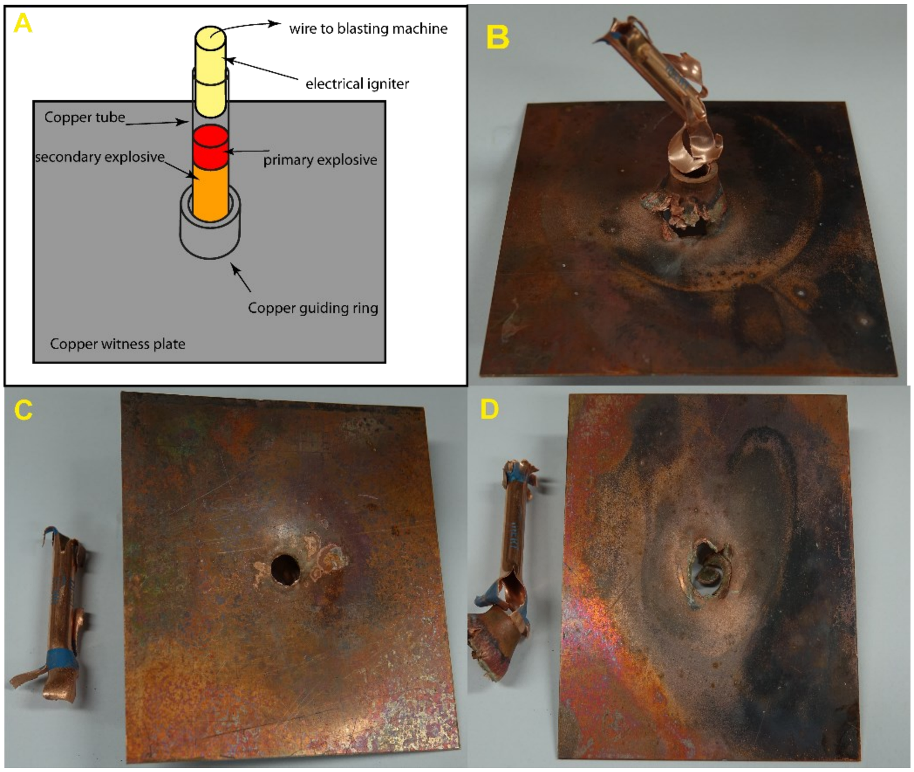

Figure 14. A) Schematic test setup for initiation testing. B) Positive initiation of PETN by [Mn(AzMT)$_6$](ClO$_4$)$_2$ (**5**), C) by [Cu(AzMT)$_6$](ClO$_4$)$_2$ (**7**), and D) by [Zn(AzMT)$_6$](ClO$_4$)$_2$ (**8**), indicating a DDT for all three compounds. The positive initiation of PETN is indicated by the perforation of the copper witness plate.

Table 2. Thermal Stability[a] as well as sensitivities to mechanical and electrical stimuli of compounds **3**–**14**, compared to copper azide and silver fulminate.

Compound	T_{endo}[b] (°C)	T_{exo}[c] (°C)	IS[d] (J)	FS[e] (N)	ESD[f] (mJ)	BDIS[g] (mJ)	HP	HN
AzMT (**3**)	54	167	2	1	540		Det	Def
$[Cu(AzMT)_6](NO_3)_2$ (**4**)	60	123	2	15	>1500		Def	Def
$[Mn(AzMT)_6](ClO_4)_2$ (**5**)		137	<1	0.5	740	25	Def	Det
$[Fe(AzMT)_6](ClO_4)_2$ (**6**)		127	<1	<0.1	380	16	Det	Det
$[Cu(AzMT)_6](ClO_4)_2$ (**7**)		133	<1	<0.1	480	25	Det	Det
$[Zn(AzMT)_6](ClO_4)_2$ (**8**)		130	<1	<0.1	380	20	Def	Def
$[Cu(AzMT)_6](ClO_3)_2$ (**9**)	112	123	<1	<0.1	380	16	Det	Def
$[Cu(Pa)_2(AzMT)_2]$ (**10**)		165	<1	360	>1500		Def	Dec
$[Cu(HTNR)_2(AzMT)_2]$ (**11**)		154	<1	192	>1500		Dec	Dec
$[Cu(HTNPG)(AzMT)_2]$ (**12**)		151	<1	45	1220		Def	Def
$[Cu(N_3)_2(AzMT)]$ (**13**)		147	<1	<0.1	38		Det	Det
$[Ag_4(CNO)_4(AzMT)_2]$ (**14a**)		109	<1	<0.1	10	20	Det	Det
$Cu(N_3)_2$		205	$\ll 1$	$\ll 0.1$	≤0.28			
AgCNO[33]		196	5	≤0.1	≤0.28			

[a] DTA onset temperatures at a heating rate of 5 °C min^{-1}. [b] Oset temperature of endothermic event in the DTA, indicating a melting of the compound. [c] Onset temperature of exothermic event in the DTA. [d] Impact sensitivity (BAM drophammer (1 of 6)). [e] Friction sensitivity (BAM friction tester (1 of 6)). [f] Electrostatic discharge device (OZM XSpark10). [g] Ball drop impact sensitivity (OZM BIT-132) determined with the 1of 6 method in accordance with the MIL-STD 1751A (method 1016).

4.3 Conclusion

Successful hydroxymethylation of *1H*-tetrazole with aqueous formalin solution can only be achieved by the addition of catalytic amounts (3-5 wt%) of sodium hydroxide to the reaction solution. Subsequent protection of the alcohol by methanesulfonyl chloride provided the precursor compound needed to successfully synthesize the highly energetic 1-(azidomethyl)tetrazole (**3**) for the first time. While its structural isomer 5-(azidomethyl)-1*H*-tetrazole is already reported, **3** represents the smallest tetrazole derivate with the shortest *N*-alkyl-azide functionality reported showing a very high positive heat of formation. Single-crystal X-ray analysis of **3** is supplemented by elemental analysis, infrared spectroscopy as well as multinuclear NMR (^{1}H, ^{13}C, ^{14}N, and ^{15}N) spectroscopy. The thermal behavior is determined by DTA measurement, and the sensitivities towards external stimuli are determined. Like other azido alkyl-tetrazoles, it performs well as a ligand in the formation of energetic coordination compounds. Here, the ECCs of copper(II) nitrate (**4**), chlorate (**9**), perchlorate (**7**), azide (**13**), manganese(II) (**5**), iron(II) (**6**), and zinc(II) perchlorate (**8**) were synthesized. The ECCs of copper(II) nitroaromatic salts (**10–12**), as well as that of silver(I) fulminate (**14a/b**) were prepared. Suitable crystals were analyzed by single-crystal X-ray diffraction experiments, giving insight into the molecular structure of the ligand itself, as well as its coordination behavior towards 3d- and 4d- metals. The successful syntheses of the ECCs are supported by elemental analysis as well as infrared spectroscopy. Analysis of the sensitivities towards external stimuli showed the high sensitivity (impact: 2 J, friction: 1 N) of the ligand, which is generally increased by the formation of ECCs. While the impact sensitivity of the ligand is increased by the formation of ECCs (<1 J (**5–14**)), the friction sensitivity can be decreased by forming the copper(II) picrate (360 N), styphnate (192 N), and trinitrophloroglycinolate (45 N) complex. The same trend is observed for the thermal stability of **3** (177 °C). Analyzing the thermal stabilities of the ECCs by DTA, showed decreasing thermal stabilities of the ECCs compared to the ligand itself. Initiation testing of the ligand itself and the ECC of copper(II) trinitrophloroglycinolate (**12**) showed no DDT, thus no initiation of the PETN sample. Testing the perchlorate salts of manganese, copper, and zinc showed a DDT with a positive initiation of PETN.

4.4 Experimental Section

WARNING: This paper contains a large amount of extremely sensitive compounds. Full body protection containing Kevlar® gloves, Kevlar® sleeves, face shield, leather coat and ear protection must be worn when manipulating those compounds! The equipment used must be earthed!

1- and 2-(Hydroxymethyl)tetrazole[30] (**1**)

1H-tetrazole (20 g, 285 mmol), synthesized according to literature[35-36], and sodium hydroxide (0.5 g, 12.5 mmol) were dissolved in water (200 mL) and formalin solution (37%, 66 mL, 917 mmol) was added. The reaction mixture was stirred over night at room temperature and was extracted into ethyl acetate (3x400 mL). The organic phase was dried over $MgSO_4$ and the solvent was removed *in vacuo*, resulting in crude isomeric mixture **1** as a colourless oil in good yield (22.1 g, 221 mmol, 80%).

^{1}H NMR (DMSO-d6, 25 °C): **1a** δ = 9.45 (s, C*H*), 5.77 (s, CH_2); **1b** δ = 8.97 (s, C*H*), 5.92 (s, CH_2).

(Tetrazol-1-yl)methyl methane sulfonate (**2a**)

Crude isomeric mixture **1** (5.0 g, 50 mmol) is suspended in DCM (100 mL), cooled to 0 °C. Methanesulfonyl chloride (6.87 g, 60 mmol, 1.2 eq.) is added, the reaction mixture is stirred for 1 h while cooling, and pyridine (5.93 g, 75 mmol, 1.5 eq.) is added, keeping the temperature below 5 °C. The reaction mixture is allowed to slowly warm and is stirred for 18 h at room temperature. The reaction mixture is then transferred to a separatory funnel, and is washed with water (100 mL), hydrochloric acid (2 M, 50 mL), and water (50 mL). Colourless crystals of compound **2a** slowly start to crystallize from the aqueous phase in moderate yield (3.12 g, 17.5 mmol, 35%). The organic phase in dried over $MgSO_4$ and the solvent is removed *in vacuo*, leaving a colourless oil consisting of compounds **2a** and **2b**, separated by flash column chromatography over silica with n-hexane/ethyl acetate (50/50) as the eluting solvent. After removing the solvent *in vacuo*, additional compound **2a** is obtained in a yield of 13%, whereas still crude compound **2b** is obtained.

^{1}H NMR (acetone-d$_6$, 25 °C): **2a** δ = 9.43 (s, C*H*), 6.66 (s, CH_2), 3.27 ppm (s, CH_3); **2b** δ = 8.95 (s, C*H*), 6.77 (s, CH_2), 3.24 ppm (s, CH_3). **^{13}C NMR** (acetone-d$_6$, 25 °C): **2a** δ = 145.5 (s, C*H*), 72.7 (s, CH_2), 39.0 ppm (s, CH_3);

1-(Azidomethyl)tetrazole (AzMT, 3)

Compound **2a** (350 mg, 1.96 mmol) and sodium azide (383 g, 5.89 mmol) are dissolved in a mixture of water (10 mL) and acetone (10 mL) and the mixture is refluxed for 18 h at 75 °C. After cooling to room temperature, water (40 mL) is added and the mixture is extracted into DCM (3x50 mL). The organic phase is dried over $MgSO_4$, the solvent is removed *in vacuo*, and 1-(azidomethyl)tetrazole (**3**) is obtained as an off-white solid in quantitative yield (243 mg, 1.94 mmol, 99%).

^{1}H NMR (DMSO-d_6, 25 °C): $\delta = 9.60$ (s, C*H*), 6.02 ppm (s, CH_2); **^{13}C NMR** (DMSO-d_6, 25 °C): $\delta = 144.2$ (s, *C*H), 60.5 ppm (s, *C*H_2); **^{14}N NMR** (DMSO-d_6, 25 °C): $\delta = -135.6.2$ (br, s, N_β), −160.4 ppm (br, s, N_γ); **^{15}N NMR** (DMSO-d_6, 25 °C): $\delta = 14.4$ (d, $N_{(3)}$), −14.0 (s, $N_{(2)}$), −50.4 (d, $N_{(4)}$), −136.3 (t, $N_{(\alpha)}$), −141.9 (d, $N_{(1)}$), −158.9 (s, $N_{(\gamma)}$), −302.1 ppm (s, $N_{(\beta)}$); **Elemental Analysis** calcd. [%] for $C_2H_3N_7$ (125.10): C 19.20, H 2.42, N 78.38; found C 19.02, H 2.32, N 76.00; **DTA** (5 °C min^{-1}): 54 °C (T_{endo}), 177 °C (T_{exo}); **BAM Drophammer**: 2 J; **BAM friction tester**: 1 N; **ESD**: 540 mJ; **IR** (ATR, cm^{-1}): 3154 (m), 3048 (w), 2979 (w), 2460 (w), 2236 (w), 2153 (s), 2106 (vs), 1819 (vw), 1762 (w), 1478 (s), 1443 (m), 1428 (m), 1370 (w), 1317 (w), 1294 (s), 1263 (m), 1230 (vs), 1161 (vs), 1100 (vs), 1026 (w), 1000 (w), 951 (m), 911 (s), 881 (s), 754 (s), 716 (s), 655 (vs), 562 (s), 416 (w).

Synthesis of energetic coordination compounds

General procedure: Compound **3** (125 mg, 1 mmol) was dissolved in water at 60–80 °C. In a second container, the corresponding equivalents of metal salt (**4**–**9**: 0.16 mmol, **10**–**12**: 0.5 mmol, **13**–**14**: 1 mmol) was dissolved in water (**4**–**13**) or acetonitrile (**14**) at 60–80 °C. After all solids dissolved, the solution containing compound **3** was added to the metal salt solution with stirring. After stirring for 5 minutes at 60 °C, any undissolved solids were filtered off, and the solution was left to crystallize for compounds **4**–**12**, and **14a**/**b**. After the solvent was evaporated, the remaining solids were dried under high vacuum for 1 hour. Compound **13** is obtained by combining the two solutions, stirring for 5 minutes at 60 °C, filtering off the precipitate and washing with cold water.

$[Cu(AzMT)_6](NO_3)_2$ (4)

Obtained as blue platelets in good yield (124.6 mg, 0.133 mmol, 83%). **Elemental Analysis** calcd. [%] for $C_{12}H_{18}CuN_{44}O_6$ (938.12): C 15.36, H 1.93, N 65.70; found C 15.46, H 1.94, N 62.97; **DTA**

(5 °C min^{-1}): 60 °C (T_{endo}), 123 °C (T_{exo}); **BAM Drophammer**: 2 J; **BAM friction tester**: 15 N; **ESD**: >1500 mJ. **IR** (ATR, cm^{-1}): 3086 (m), 3043 (m), 2984 (m), 2454 (w), 2394 (w), 2352 (w), 2315 (w), 2156 (s), 2106 (s), 1588 (m), 1501 (m), 1447 (m), 1342 (vs), 1290 (s), 1277 (s), 1230 (s), 1169 (s), 1162 (s), 1100 (vs), 1043 (m), 997 (m), 913 (s), 829 (m), 781 (m), 748 (s), 716 (m), 648 (s), 561 (m), 421 (w), 413 (w).

[Mn(AzMT)$_6$](ClO$_4$)$_2$ (5)

Obtained as white platelets in quantitive yield (160.5 mg, 0.16 mmol, 100%). **Elemental Analysis** calcd. [%] for $C_{12}H_{18}Cl_2MnN_{42}O_8$ (1004.40): C 14.35, H 1.81, N 58.87; found C 14.79, H 1.91, N 58.01; **DTA** (5 °C min^{-1}): 137 °C (T_{exo}); **BAM Drophammer**: <1 J; **Ball Drop Impact**: 25 mJ; **BAM friction tester**: 0.5 N; **ESD**: 740 mJ; **IR** (ATR, cm^{-1}): 3128 (m), 3096 (m), 3038 (m), 2982 (m), 2157 (s), 2105 (s), 1586 (m), 1497 (s), 1448 (m), 1373 (m), 1311 (m), 1283 (m), 1232 (s), 1174 (s), 1100 (vs), 1041 (m), 978 (s), 935 (s), 913 (s), 747 (s), 713 (m), 647 (s), 622 (s), 604 (m), 561 (m), 479 (m), 425 (w), 420 (w).

[Fe(AzMT)$_6$](ClO$_4$)$_2$ (6)

Obtained as orange-brown solid in very good yield (149.6 mg, 0.149 mmol, 99%). **Elemental Analysis** calcd. [%] for $C_{12}H_{18}Cl_2FeN_{42}O_8$ (1005.31): C 14.34, H 1.80, N 58.52; found C 15.10, H 2.02, N 58.86; **DTA** (5 °C min^{-1}): 127 °C (T_{exo}); **BAM Drophammer**: <1 J; **Ball Drop Impact**: 16 mJ; **BAM friction tester**: <0.1 N; **ESD**: 380 mJ; **IR** (ATR, cm^{-1}): 3135 (w), 3043 (vw), 2986 (vw), 2163 (m), 2106 (s), 1497 (m), 1440 (w), 1375 (w), 1314 (m), 1285 (m), 1237 (s), 1172 (m), 1075 (vs), 1039 (m), 983 (m), 914 (s), 896 (m), 746 (m), 712 (m), 655 (s), 651 (s), 622 (s), 560 (m), 425 (vw), 413 (w), 407 (vw).

[Cu(AzMT)$_6$](ClO$_4$)$_2$ (7)

Obtained as blue platelets in quantitative yield (162 mg, 0.16 mmol, 100%). **Elemental Analysis** calcd. [%] for $C_{12}H_{18}Cl_2CuN_{42}O_8$ (1013.01): C 14.23, H 1.79, N 58.07; found C 14.33, H 1.97, N 57.50; **DTA** (5 °C min^{-1}): 133 °C (T_{exo}); **BAM Drophammer**:<1 J; **Ball Drop Impact**: 25 mJ; **BAM friction tester**: <0.1 N; **ESD**: 480 mJ; **IR** (ATR, cm^{-1}): 3136 (m), 3045 (w), 2992 (w), 2155 (m), 2106 (s), 1591 (vw), 1556 (vw), 1503 (m), 1447 (w), 1375 (w), 1284 (m), 1236 (m), 1175 (m), 1100 (s), 1074 (vs), 992 (m), 909 (m), 747 (m), 711 (m), 655 (s), 647 (s), 622 (vs), 560(m).

[Zn(AzMT)$_6$](ClO$_4$)$_2$ (8)

Obtained as white solid in good yield (141.3 mg, 0.139 mmol, 87%). **Elemental Analysis** calcd. [%] for $C_{12}H_{18}Cl_2N_{42}O_8Zn$ (1014.84): C 14.20, H 1.79, N 57.97; found C 14.60, H 1.86, N 57.37; **DTA** (5 °C min^{-1}): 130 °C (T_{exo}); **BAM Drophammer**: <1 J; **Ball Drop Impact**: 20 mJ; **BAM friction tester**: <0.1 N; ESD: 380 mJ; **IR** (ATR, cm^{-1}): 3136 (w), 3048 (vw), 2986 (vw), 2163 (m), 2108 (s), 1793 (vw), 1498 (m), 1442 (w), 1375 (w), 1315 (w), 1284 (m), 1238 (m), 1175 (m), 1074 (vs), 1040 (m), 985 (m), 915 (m), 897 (m), 746 (m), 711 (m), 656 (m), 647 (m), 622 (s), 560 (m), 416 (w).

$[Cu(AzMT)_6](ClO_3)_2$ (9)

Obtained as light-blue blocks in good yield (146 mg, 0.149 mmol, 93%). **Elemental Analysis** calcd. [%] for $C_{12}H_{18}Cl_2CuN_{42}O_6$ (981.01): C 14.69, H 1.85, N 59.97; found C 14.94, H 2.04, N 58.84; **DTA** (5 °C min^{-1}): 112 °C (T_{endo}), 123 °C (T_{exo}); **BAM Drophammer**: <1 J; **BAM friction tester**: <0.1 N; **ESD**: 380 mJ; **IR** (ATR, cm^{-1}): 3098 (s), 3039 (m), 2985 (m), 2458 (w), 2227 (w), 2155 (s), 2104 (s), 1588 (w), 1499 (m), 1448 (m), 1373 (m), 1310 (m), 1292 (m), 1281 (m), 1230 (s), 1176 (s), 1163 (s), 1100 (vs), 1042 (m), 958 (vs), 935 (s), 912 (vs), 775 (m), 747 (m), 715 (m), 646 (s), 603 (s), 562 (m), 479 (s), 426 (w), 411 (w).

$[Cu(PA)_2(AzMT)_2]$ (10)

Obtained as green platelets in good yield (338.8 mg, 0.44 mmol, 88%). **Elemental Analysis** calcd. [%] for $C_{16}H_{10}CuN_{20}O_{14}$ (769.93): C 24.96, H 1.31, N 36.39; found C 24.84, H 1.29, N 35.97; **DTA** (5 °C min^{-1}): 165 °C (T_{exo}); **BAM Drophammer**: <1 J; **BAM friction tester**: >360 N; **ESD**: >1500 mJ. **IR** (ATR, cm^{-1}): 3147 (w), 3094 (w), 3060 (w), 2158 (m), 2106 (s), 1608 (s), 1574 (s), 1542 (s), 1517 (s), 1493 (s), 1420 (m), 1349 (s), 1321 (s), 1276 (s), 1239 (s), 1163 (vs), 1092 (s), 1037 (m), 1012 (m), 988 (m), 941 (m), 933 (m), 910 (s), 899 (s), 847 (m), 825 (m), 788 (s), 741 (s), 707 (vs), 659 (s), 542 (s), 515 (m), 460 (m), 427 (m), 418 (m).

$[Cu(HTNR)_2(AzMT)_2]$ (11)

Obtained as dark green blocks in moderate yield (312.8 mg, 0.39 mmol, 78%). **Elemental Analysis** calcd. [%] for $C_{16}H_{10}CuN_{20}O_{16}$ (801.93): C 23.96, N 1.26, N 34.93,; found C 24.01, H 1.60, N 34.78; **DTA** (5 °C min^{-1}): 154 °C (T_{exo}); **BAM Drophammer**: <1 J; **BAM friction tester**: 192 N; **ESD**: >1500 mJ. **IR** (ATR, cm^{-1}): 3135 (w), 3052 (w), 2149 (m), 2098 (m), 1627 (m), 1561 (s), 1520 (s), 1490 (m), 1477 (m), 1456 (s), 1443 (m), 1368 (s), 1334 (s), 1321 (m), 1307 (s), 1274 (vs), 1247 (s), 1222 (s), 1204 (s), 1173 (s), 1160 (s), 1094 (vs), 1037 (m), 987 (s), 948 (m), 931 (m), 915 (s), 891 (s), 829 (w), 783 (m), 775 (m), 763 (m), 747 (m), 734 (s), 705 (s), 697 (vs), 646 (vs), 578 (m), 562 (m), 527 (m), 464 (m), 456 (m), 421 (m).

[Cu(HTNPG)(AzMT)$_2$] (12)

Obtained as dark brown blocks in moderate yield (203.4 mg, 0.36 mmol, 71%). **Elemental Analysis** calcd. [%] for $C_{10}H_7CuN_{17}O_9$ (572.82): C 20.97, H 1.23, N 41.57; found C 21.00, H 1.66, N 39.33; **DTA** (5 °C min^{-1}): 151 °C (T$_{exo}$); **BAM Drophammer**: <1 J; **BAM friction tester**: 45 N; **ESD**: 1220 mJ. **IR** (ATR, cm^{-1}): 3142 (m), 3043 (w), 2984 (w), 2163 (m), 2112 (s), 2105 (s), 1645 (m), 1589 (m), 1569 (s), 1521 (s), 1515 (s), 1503 (s), 1494 (s), 1447 (m), 1436 (m), 1404 (m), 1375 (m), 1337 (s), 1318 (s), 1288 (s), 1237 (s), 1164 (vs), 1092 (vs), 1032 (m), 1008 (m), 1001 (m), 984 (m), 916 (s), 905 (m), 872 (w), 833 (m), 820(m), 805 (m), 786 (m), 760 (m), 740 (m), 710 (s), 694 (s), 645 (s), 559 (m), 503 (m), 493 (m), 457 (w), 418 (w).

[Cu(N$_3$)$_2$(AzMT)] (13)

Obtained as brown powder in moderate yield (171.8 mg, 0.63 mmol, 63%). **Elemental Analysis** calcd. [%] for $C_2H_3CuN_{13}$ (272.68): C 8.81, H 1.11, N 66.78; found C 8.92, H 1.46, N 63.60; **DTA** (5 °C min^{-1}): 147 °C (T$_{exo}$); **BAM Drophammer**: <1 J; **BAM friction tester**: <0.1 N; **ESD**: 38 mJ. **IR** (ATR, cm^{-1}): 3104 (m), 3047 (w), 2463 (w), 2158 (m), 2080 (vs), 2047 (vs), 1501 (s), 1447 (m), 1377 (m), 1340 (m), 1309 (m), 1286 (s), 1239 (s), 1171 (vs), 1101 (s), 1039 (m), 1024 (m), 993 (m), 909 (s), 895 (s), 759 (s), 713 (m), 689 (m), 654 (vs), 597 (m), 587 (s), 562 (m), 403 (s).

[Ag$_4$(CNO)$_4$(AzMT)$_2$] (14a)

Obtained as colourless platelets in moderate yield (280.4 mg, 0.66 mmol, 66%). **Elemental Analysis** calcd. [%] for $C_4H_3Ag_2N_9O_2$ (424.87): C 11.31, H 0.71, N 29.67; found C 11.37, H 0.86, N 29.90; **DTA** (5 °C min^{-1}): 109 °C (T$_{exo}$); **BAM Drophammer**: <1 J; **BAM friction tester**: <0.1 N; **ESD**: 10 mJ; **IR** (ATR, cm^{-1}): 3220 (w), 3134 (m), 3032 (w), 2960 (w), 2458 (w), 2303 (w), 2292 (w), 2246 (w), 2154 (m), 2104 (vs), 2090 (vs), 1818 (w), 1487 (m), 1449 (m), 1439 (w), 1376 (w), 1301 (m), 1276 (m), 1235 (s), 1152 (vs), 1130 (vs), 1099 (s), 1035 (m), 1008 (m), 976 (m), 909 (s), 885 (s), 767 (w), 746 (m), 710 (m), 654 (s), 563 (m), 498 (w), 481 (m), 462 (m), 418 (w), 405 (w).

4.5 Acknowledgements

Financial support of this work by the Ludwig-Maximilian University of Munich (LMU), the Office of Naval Research (ONR) under grant no. N00014-19-1-2078 as well as the Strategic Environmental Research and Development Program (SERDP) under grant no. WP19-1287 is gratefully acknowledged.

Keywords: tetrazole • alkylazides • energetic coordination compounds • primary explosives • initiation

4.6 References

[1] J. Wilbrand, *Justus Liebigs Annalen der Chemie* **1863**, *128*, 178-179.

[2] *Justus Liebigs Annalen der Chemie* **1848**, *64*, 396-398.

[3] D. Kumar, Y. Tang, C. He, G. H. Imler, D. A. Parrish, J. n. M. Shreeve, *Chem. Eur. J.* **2018**, *24*, 17220-17224.

[4] E. C. Johnson, T. A. Reid, C. W. Miller, J. J. Sabatini, R. C. Sausa, E. F. C. Byrd, J. A. Orlicki, *ChemPlusChem* **2021**, *86*, 875-878.

[5] E. C. Johnson, J. J. Sabatini, D. E. Chavez, L. A. Wells, J. E. Banning, R. C. Sausa, E. F. C. Byrd, J. A. Orlicki, *ChemPlusChem* **2020**, *85*, 237-239.

[6] J. Fronabarger, A. Schuman, R. Chapman, W. Fleming, W. Sanborn, T. Massis, in 31st Joint Propulsion Conference and Exhibit.

[7] T. W. Myers, K. E. Brown, D. E. Chavez, R. J. Scharff, J. M. Veauthier, *Inorg. Chem*. **2017**, *56*, 2297-2303.

[8] M. L. Gettings, M. T. Thoenen, E. F. C. Byrd, J. J. Sabatini, M. Zeller, D. G. Piercey, *Chem. Eur. J.* **2020**, *26*, 14530-14535.

[9] S. Manzoor, Q.-u.-n. Tariq, X. Yin, J.-G. Zhang, *Def. Tech.* **2021**, *17*, 1995-2010.

[10] A. A. Larin, L. L. Fershtat, *Energetic Materials Frontiers* **2021**, *2*, 3-13.

[11] A. A. Larin, N. V. Muravyev, A. N. Pivkina, K. Y. Suponitsky, I. V. Ananyev, D. V. Khakimov, L. L. Fershtat, N. N. Makhova, *Chem. Eur. J.* **2019**, *25*, 4225-4233.

[12] Q. Wu, Q. Li, K. Li, H. Li, B. Kou, Z. Hang, W. Zhu, *Can. J. Chem.* **2018**, *96*, 459-465.

[13] S. R. Yocca, M. Zeller, E. F. C. Byrd, D. G. Piercey, *J. Mater. Chem. A* **2022**, *10*, 1876-1884.

[14] P. He, J.-G. Zhang, X. Yin, J.-T. Wu, L. Wu, Z.-N. Zhou, T.-L. Zhang, *Chem. Eur. J.* **2016**, *22*, 7670-7685.

[15] K. Y. Titenkova, A. V. Shaferov, A. A. Larin, M. A. Epishina, A. S. Kulikov, I. V. Ananyev, L. L. Fershtat, *Tetrahedron* **2022**, *103*, 132563.

[16] T. Liu, Y.-G. Ji, L. Wu, *Org. Biomol. Chem*. **2019**, *17*, 2619-2623.

[17] A. Qian, Y. Zheng, R. Wang, J. Wei, Y. Cui, X. Cao, Y. Yang, *Bioorg. Med. Chem. Lett*. **2018**, *28*, 344-350.

[18] T. M. Klapötke, M. Kofen, L. Schmidt, J. Stierstorfer, M. H. H. Wurzenberger, *Chem. Asian J.* **2021**, *16*, 3001-3012.

[19] N. Szimhardt, M. H. H. Wurzenberger, A. Beringer, L. J. Daumann, J. Stierstorfer, J. *Mater. Chem. A* **2017**, *5*, 23753-23765.

[20] N. Szimhardt, M. H. H. Wurzenberger, L. Zeisel, M. S. Gruhne, M. Lommel, J. Stierstorfer, *J. Mater. Chem. A* **2018**, *6*, 16257-16272.

[21] M. H. H. Wurzenberger, B. R. G. Bissinger, M. Lommel, M. S. Gruhne, N. Szimhardt, J. Stierstorfer, *New J. Chem*. **2019**, *43*, 18193-18202.

[22] M. H. H. Wurzenberger, S. M. J. Endraß, M. Lommel, T. M. Klapötke, J. Stierstorfer, *ACS Appl. Energy Mater.* **2020**, *3*, 3798-3806.

[23] M. H. H. Wurzenberger, M. S. Gruhne, M. Lommel, N. Szimhardt, T. M. Klapötke, J. Stierstorfer, *Chem. Asian J.* **2019**, *14*, 2018-2028.

[24] G. Bélanger-Chabot, S. M. Kaplan, P. Deokar, N. Szimhardt, R. Haiges, K. O. Christe, *Chem. Eur. J.* **2017**, *23*, 13087-13099.

[25] R. Haiges, K. O. Christe, *Dalton Trans*. **2015**, *44*, 10166-10176.

[26] A. R. Katritzky, C. N. Fali, I. V. Shcherbakova, S. V. Verin, *J. Heterocycl. Chem*. **1996**, *33*, 335-339.

[27] O. N. Verkhozina, V. N. Kizhnyaev, L. I. Vereshchagin, A. V. Rokhin, A. I. Smirnov, *Russ. J. Org. Chem*. **2003**, *39*, 1792-1796.

[28] D. A. Chaplygin, A. A. Larin, N. V. Muravyev, D. B. Meerov, E. K. Kosareva, V. G. Kiselev, A. N. Pivkina, I. V. Ananyev, L. L. Fershtat, *Dalton Trans*. **2021**, *50*, 13778-13785.

[29] L. Y. Peng Lei, Yang Yuzhang, Liu Wei, Zhang Xuejiao, Pang Siping, *Chin. J. Org. Chem*. **2012**, *32*, 667-676.

[30] I. V. Tselinskii, A. A. Mel'nikov, L. G. Varyagina, I. G. Zhigadlova, *Chem. Heterocycl. Compd*. **1983**, *19*, 341-343.

[31] M. Sućeska, EXPLO5 Version 6.05 User’s Guide, Zagreb (Croatia), **2018**.

[32] M. H. H. Wurzenberger, M. Lommel, M. S. Gruhne, N. Szimhardt, J. Stierstorfer, *Angew. Chem. Int. Ed.* **2020**, *59*, 12367-12370.

[33] M. H. H. Wurzenberger, M. S. Gruhne, M. Lommel, V. Braun, N. Szimhardt, J. Stierstorfer, *Inorg. Chem.* **2020**, *59*, 17875-17879.

[34] H. Schmidbaur, A. Schier, *Angew. Chem. Int. Ed.* **2015**, *54*, 746-784.

[35] R. Bronisz, *Inorg. Chim. Acta* **2002**, 215-220.

[36] T. M. Klapötke, M. Stein, J. Stierstorfer, *Z. Anorg. Allg. Chem.* **2008**, *634*, 1711-1723.

4.7 Supporting Information

4.7.1 Overview of Compounds

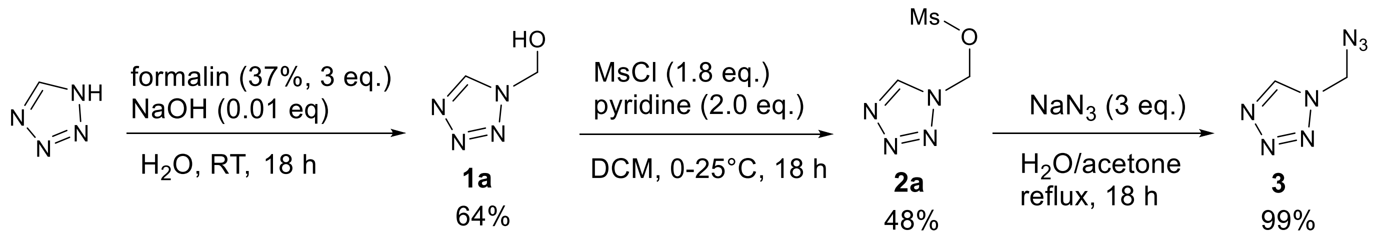

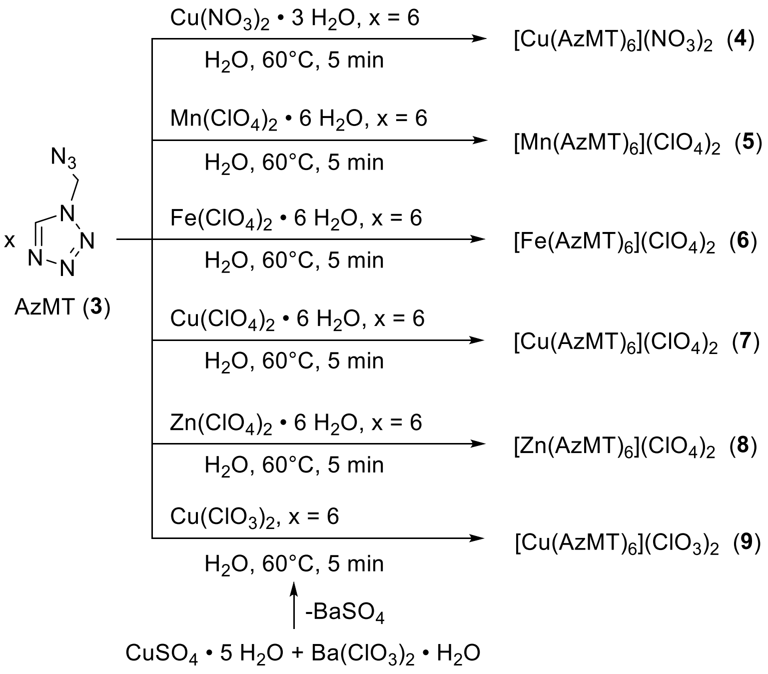

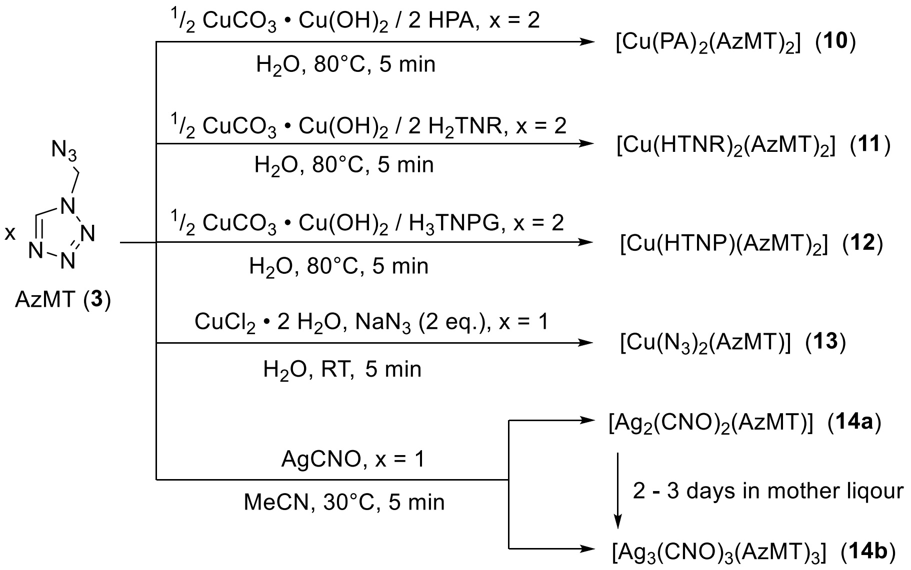

4.7.2 Single Crystal X-Ray Diffraction

For all crystalline compounds, an Oxford Xcalibur3 diffractometer with a CCD area detector or Bruker D8 Venture TXS diffractometer equipped with a multilayer monochromator, a Photon 2 detector, and a rotating-anode generator were employed for data collection using Mo-K_α radiation (λ = 0.7107 Å). On the Oxford device, data collection and reduction were carried out using the CrysAlisPRO software.[S1] On the Bruker diffractometer, the data were collected with the Bruker Instrument Service v3.0.21, the data reduction was performed using the SAINT V8.18C software (Bruker AXS Inc., 2011). The structures were solved by direct methods (SIR-92,[S2] SIR-97,[S3,S4] SHELXS-97[S5,S6] or SHELXT[S7]), refined by full-matrix least-squares on $F2$ (SHELXL[S5,S6]) and finally checked using the PLATON software[S8] integrated in the WinGX[S7,S9] or Olex2[S8] software suite. The non-hydrogen atoms were refined anisotropically and the hydrogen atoms were located and freely refined. The absorptions were corrected by a SCALE3 ABSPACK or SADABS Bruker APEX3 multi-scan method.[S11,S12] All DIAMOND2 plots are shown with thermal ellipsoids at the 50% probability level and hydrogen atoms are shown as small spheres of arbitrary radius.

Table S1. Crystallographic data and structure refinement details for compounds **3**, **4**, and **9.**

	AzMT (3)	**4**	**9**
Formula	$C_2H_3N_7$	$C_{12}H_{18}CuN_{44}O_6$	$C_{12}H_{18}CuN_{42}Cl_2O_6$
FW [g mol^{-1}]	125.11	938.24	981.12
Crystal system	orthorhombic	monoclinic	triclinic
Space group	*Pbca* (No. 61)	*Cc* (No. 9)	*P*-1 (No. 2)
Color / Habit	colorless block	blue platelet	blue block
Size [mm]	0.07 x 0.10 x 0.36	0.07 x 0.17 x 0.30	0.27 x 0.42 x 0.43
a [Å]	6.7828(7)	10.0179(7)	10.1101(6)
b [Å]	11.3306(19)	17.9322(9)	10.2068(5)
c [Å]	13.6136(17)	20.4520(14)	20.841(1)
α [°]	90	90	86.942(4)
β [°]	90	95.777(6)	80.881(5)
γ [°]	90	90	60.690(6)
V [Å^3]	1046.3(2)	3655.4(4)	1850.9(2)
Z	8	4	2
$\rho_{calc.}$ [g cm^{-3}]	1.589	1.705	1.760
μ [mm^{-1}]	0.124	0.699	0.832
F(000)	512	1900	990
$\lambda_{MoK\alpha}$ [Å]	0.71073	0.71073	0.71073
T [K]	110	103	114
θ Min-Max [°]	3.0, 26.0	2.0, 26.4	2.3, 26.4
Dataset	-7: 8; -9: 13; -16: 16	-12: 12; -22: 22; -25: 25	-12: 12; -7: 12; -22: 26
Reflections collected	6247	24281	10869
Independent refl.	1031	7447	7485
R_{int}	0.077	0.082	0.024
Observed reflections	682	5490	6207
Parameters	94	569	571
R_1 (obs)[a]	0.0488	0.0554	0.0404
wR_2 (all data)[b]	0.0984	0.0879	0.1331
S [c]	1.07	1.02	0.92
Resd. dens [e Å^{-3}]	-0.19, 0.21	-0.49, 0.96	-0.45, 0.62
Device type	Oxford Xcalibur3	Oxford Xcalibur3	Oxford Xcalibur3
Solution	SHELXT	SHELXT	SHELXT
Refinement	SHELXL-2018	SHELXL-2018	SHELXL-2018
Absorption correction	multi-scan	multi-scan	multi-scan

---

[a] $R_1 = \Sigma||F_0|-|F_c||/\Sigma|F_0|$; [b] $wR_2 = [\Sigma[w(F_0^2-F_c^2)^2]/\Sigma[w(F_0)^2]]^{1/2}$; $w = [\sigma c^2(F_0^2)+(xP)^2+yP]^{-1}$ and $P=(F_0^2+2F_c^2)/3$; [c] $S = \{\Sigma[w(F_o^2-F_c^2)^2]/(n-p)\}^{1/2}$ (n = number of reflections; p = total number of parameters).

Table S2. Crystallographic data and structure refinement details for compounds **10**, **13**, and **14a**

	10	**13**	**14a**
Formula	$C_{16}H_{10}CuN_{20}O_{14}$	$C_2H_3CuN_{13}$	$C_4H_3Ag_2N_9O_2$
FW [g mol^{-1}]	769.98	272.71	424.89
Crystal system	monoclinic	monoclinic	monoclinic
Space group	$P2_1/c$ (No. 14)	$P2_1/c$ (No. 14)	$I2/a$ (No. 15)
Color / Habit	green block	brown plate	colorless platelet
Size [mm]	0.24 x 0.38 x 0.66	0.02 x 0.24 x 0.63	0.02 x 0.10 x 0.40
a [Å]	9.7058(11)	12.1752(9)	12.8907(7)
b [Å]	18.0227(17)	5.7388(4)	5.5319(2)
c [Å]	7.7834(8)	13.0612(9)	29.175(2)
α [°]	90	90	90
β [°]	90.975(10)	93.975(7)	91.266(5)
γ [°]	90	90	90
V [Å^3]	1361.3(2)	910.40(11)	2080.0(2)
Z	2	4	8
$\rho_{calc.}$ [g cm^{-3}]	1.878	1.990	2.714
μ [mm^{-1}]	0.913	2.399	3.773
F(000)	774	540	1600
$\lambda_{MoK\alpha}$ [Å]	0.71073	0.71073	0.71073
T [K]	103	102	105
θ Min-Max [°]	2.3, 26.4	3.1, 29.1	2.8, 26.4
Dataset	-12: 12 ; -22: 22 ; -7: 9	-16: 15 ; -7: 4 ; -16: 17	-16: 13 ; -6: 6 ; -36: 34
Reflections collected	11796	4057	6587
Independent refl.	2786	2079	2118
R_{int}	0.046	0.029	0.036
Observed reflections	2130	1681	1632
Parameters	261	145	154
R_1 (obs)[a]	0.0388	0.0364	0.0368
wR_2 (all data)[b]	0.1007	0.0903	0.0694
S [c]	1.02	1.04	1.06
Resd. dens [e Å^{-3}]	-0.26, 0.43	-0.44, 0.65	-0.55, 0.64
Device type	Oxford Xcalibur3	Oxford Xcalibur3	Oxford Xcalibur3
Solution	SHELXT	SHELXT	SHELXT
Refinement	SHELXL-2018	SHELXL-2018	SHELXL-2018
Absorption correction	multi-scan	multi-scan	multi-scan

---

[a]$R_1 = \Sigma||F_0|-|F_c||/\Sigma|F_0|$; [b]$wR_2 = [\Sigma[w(F_0^2-F_c^2)^2]/\Sigma[w(F_0)^2]]^{1/2}$; $w = [\sigma c^2(F_0^2)+(xP)^2+yP]^{-1}$ and $P=(F_0^2+2F_c^2)/3$; [c]$S = \{\Sigma[w(F_o^2-F_c^2)^2]/(n-p)\}^{1/2}$ (n = number of reflections; p = total number of parameters).

Table S3. Crystallographic data and structure refinement details for compound **14b**.

	14b
Formula	$C_9H_9Ag_3N_{24}O_3$
FW [g mol^{-1}]	825.01
Crystal system	triclinic
Space group	*P*-1 (No. 2)
Color / Habit	colorless rod
Size [mm]	0.02 x 0.03 x 0.12
a [Å]	3.8316(7)
b [Å]	18.221(3)
c [Å]	19.080(3)
α [°]	117.720(4)
β [°]	94.189(5)
γ [°]	93.814(6)
V [Å^3]	1168.4(3)
Z	2
$\rho_{calc.}$ [g cm^{-3}]	2.345
μ [mm^{-1}]	2.560
F(000)	792
$\lambda_{MoK\alpha}$ [Å]	0.71073
T [K]	173
θ Min-Max [°]	3.2, 26.4
Dataset	-4: 4; -22: 22; -23: 23
Reflections collected	19270
Independent refl.	4760
R_{int}	0.038
Observed reflections	4384
Parameters	352
R_1 (obs)[a]	0.0214
wR_2 (all data)[b]	0.0464
S [c]	1.07
Resd. dens [e Å^{-3}]	-0.34, 0.56
Device type	Bruker D8 Venture TXS
Solution	SHELXT
Refinement	SHELXL-2018
Absorption correction	multi-scan

---

[a] $R_1 = \Sigma||F_0|-|F_c||/\Sigma|F_0|$; [b] $wR_2 = [\Sigma[w(F_0^2-F_c^2)^2]/\Sigma[w(F_0)^2]]^{1/2}$; $w = [\sigma c^2(F_0^2)+(xP)^2+yP]^{-1}$ and $P=(F_0^2+2F_c^2)/3$; [c] $S = \{\Sigma[w(F_o^2-F_c^2)^2]/(n-p)\}^{1/2}$ (n = number of reflections; p = total number of parameters).

4.7.3 Computations

All calculations were carried out using the Gaussian G09 program package.[S13] The enthalpies (H) and free energies (G) were calculated using the complete basis set (CBS) method of Petersson and coworkers in order to obtain very accurate energies. The CBS models use the known asymptotic convergence of pair natural orbital expressions to extrapolate from calculations using a finite basis set to the estimated complete basis set limit. CBS-4 begins with a HF/3-21G(d) geometry optimization; the zero-point energy is computed at the same level. It then uses a large basis set SCF calculation as a base energy, and a MP2/6-31+G calculation with a CBS extrapolation to correct the energy through second order. A MP4(SDQ)/6-31+(d,p) calculation is used to approximate higher order contributions. In this study we applied the modified CBS-4M method (M referring to the use of minimal population localization) which is a re-parametrized version of the original CBS-4 method and also includes some additional empirical corrections. The enthalpies of the gas-phase species M were computed according to the atomization energy method (E1) (Table S6 & 7).[S13–18]

$$\Delta_f H^\circ_{(g,\,M,\,298)} = H_{(\text{Molecule},\,298)} - \sum H^\circ_{(\text{Atoms},\,298)} + \sum \Delta_f H^\circ_{(\text{Atoms},\,298)} \qquad \text{(E1)}$$

Table S6. Literature values for atomic $\Delta H^\circ{}_f{}^{298}$ / kcal mol^{-1}

	$-H^{298}$ [a.u.]	NIST[S19]
H	0.50091	52.1
C	37.786156	171.3
N	54.522462	113.0
O	74.991202	59.6

The gas-phase heat of formations were converted to the solid/liquid state ones for neutrals: by subtracting the vaporization/sublimation enthalpies (calculated using the Trouton rule)[S20,21] The calculation results are summarized in Table S7.

$$\Delta U_m = \Delta H_m - \Delta n\, R\, T \qquad \text{(E2)}$$

Table S7. CBS-4M results, Gas phase enthalpies of formation, calculated sublimation/vaporization enthalpies and solid-state heat of formation.

Compound	$-H^{298}$ / a.u.	$\Delta_f H°(g)$ / kJ mol^{-1}	$\Delta_{s/v}H°$/ kJ mol^{-}	V_m / nm^3	Δn
3	–460.528989	679.5	39.1635		–3.5
AET	–499.771217	639.9	41.9535		–6
APT	–539.009606	775.6	42.1335		–8

4.7.4 NMR Spectroscopy of 1, 2 and 3

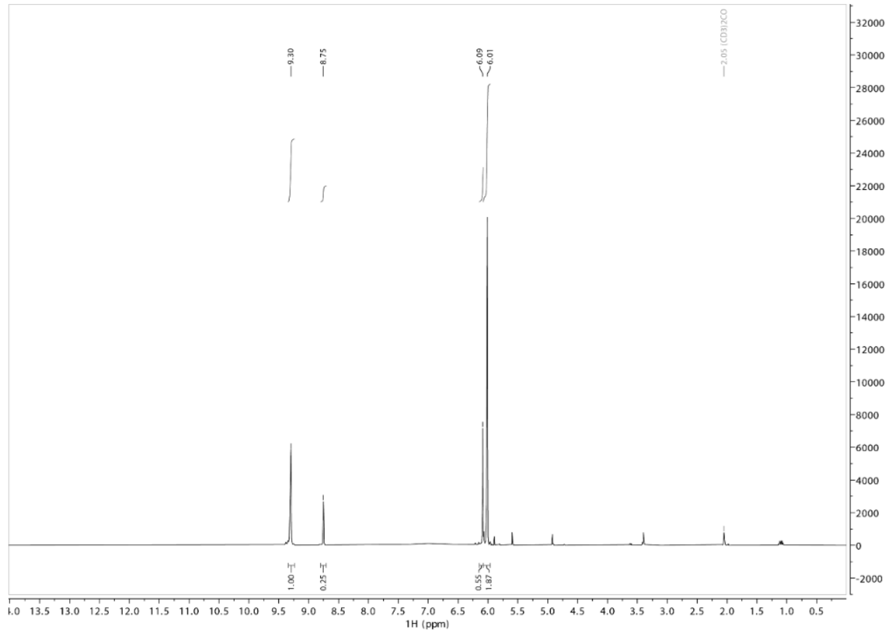

Figure S1. ^{1}H NMR of crude isomeric mixture **1** in acetone-d$_6$.

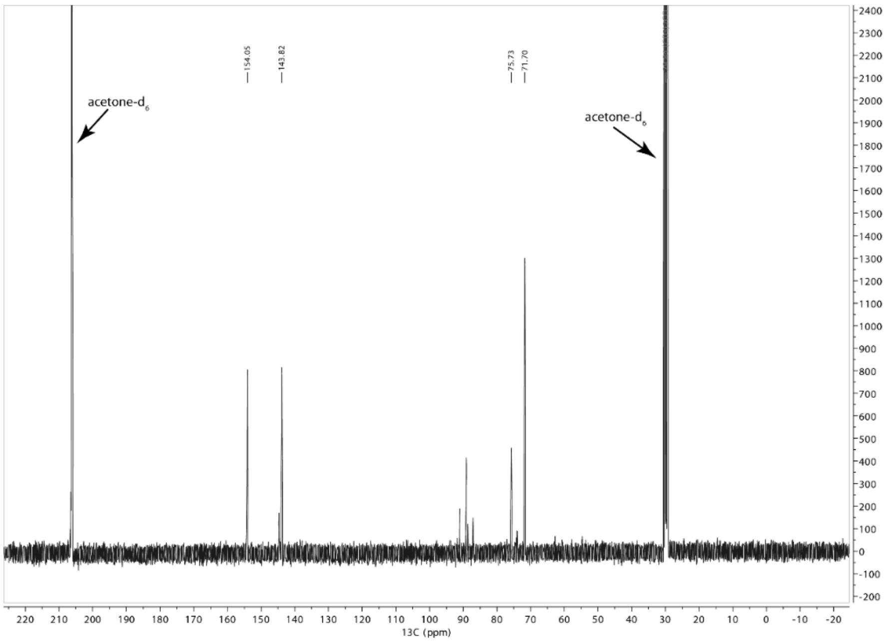

Figure S2. ^{13}C NMR of crude isomeric mixture **1** in acetone-d$_6$.

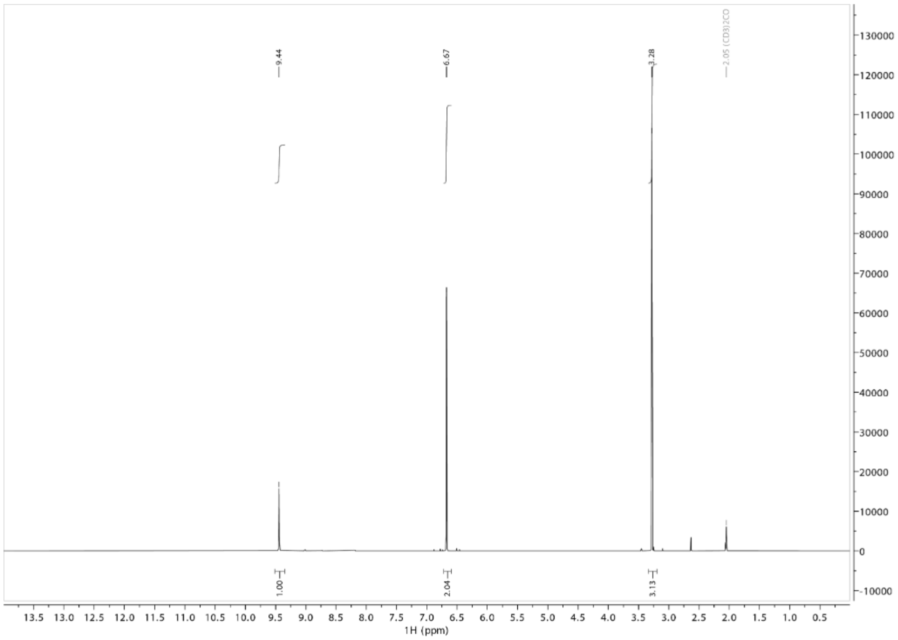

Figure S3. ^{1}H NMR of compound **2a** in acetone-d$_6$.

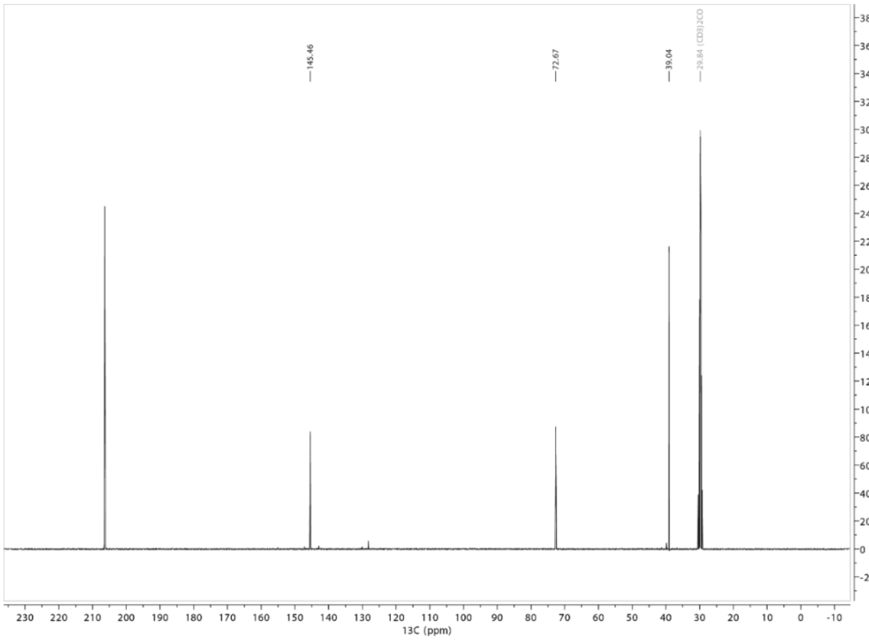

Figure S4. ^{13}C NMR of compound **2a** in acetone-d$_6$.

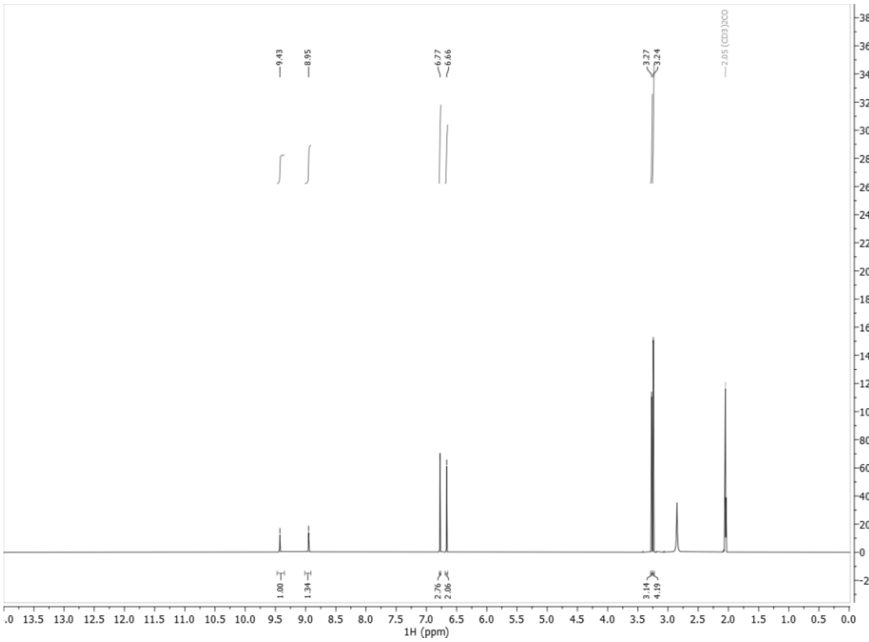

Figure S5. ^{1}H NMR of compound **3** in DMSO-d$_6$.

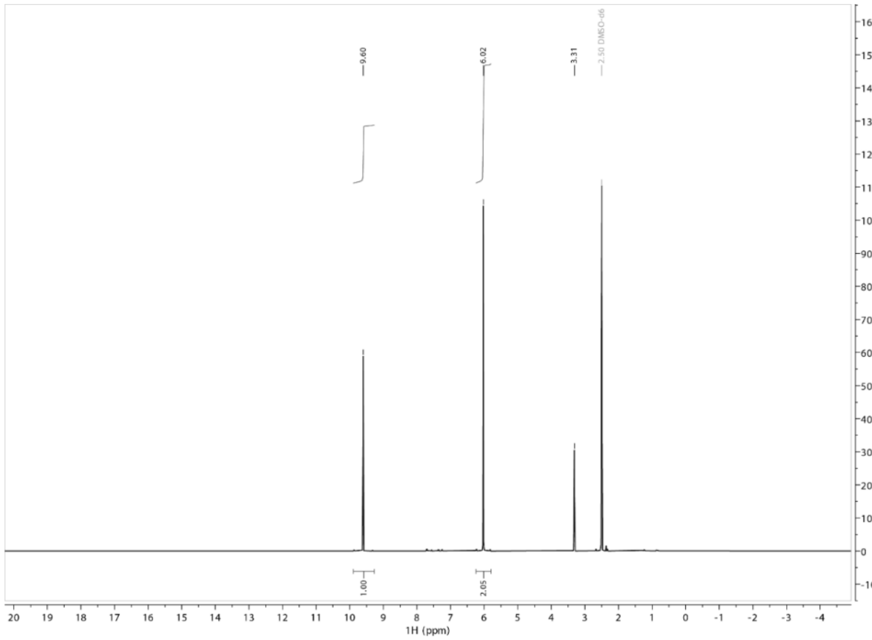

Figure S6 ^{1}H NMR of compound **3** in DMSO-d$_6$.

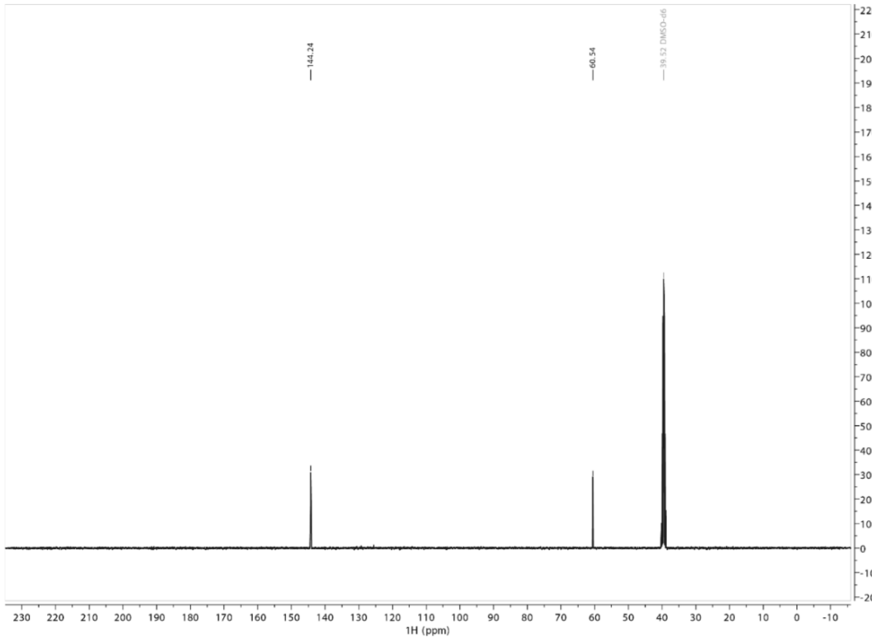

Figure S7. ^{13}C NMR of compound **3** in DMSO-d$_6$.

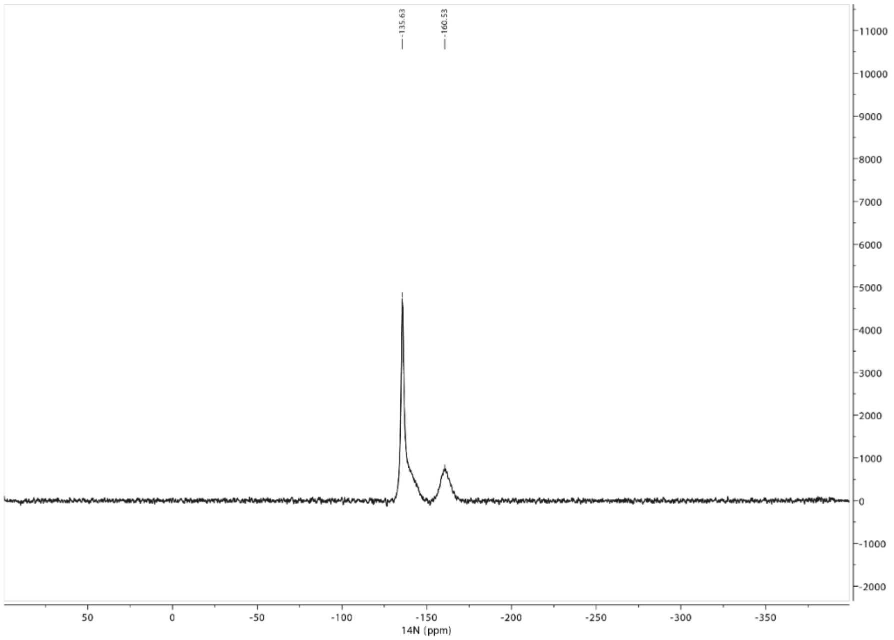

Figure S8. ^{14}N NMR of compound **3** in DMSO-d$_6$.

4.7.5 IR Spectroscopy of 1–15

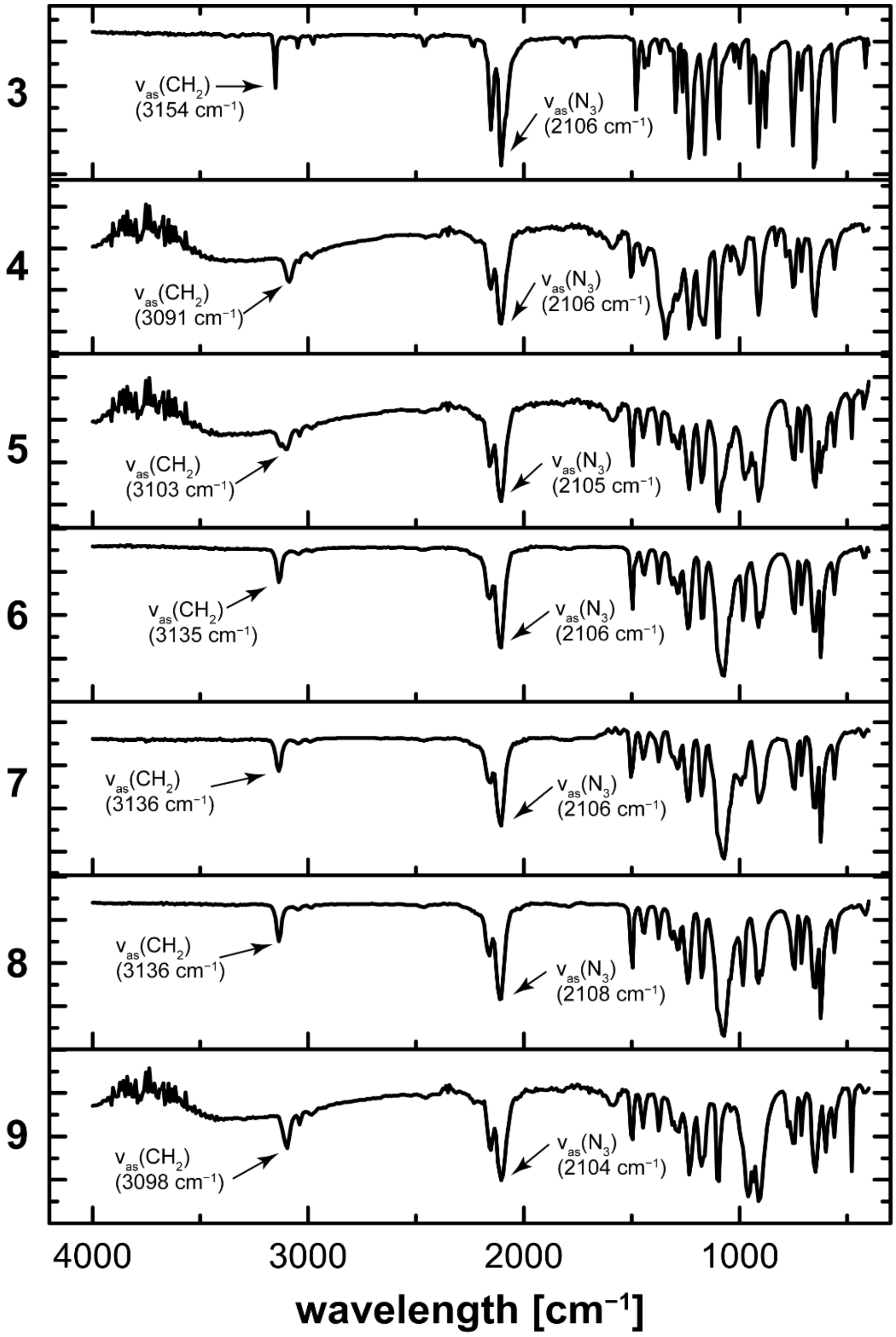

Figure S9. IR spectra of compounds **3** – **9**.

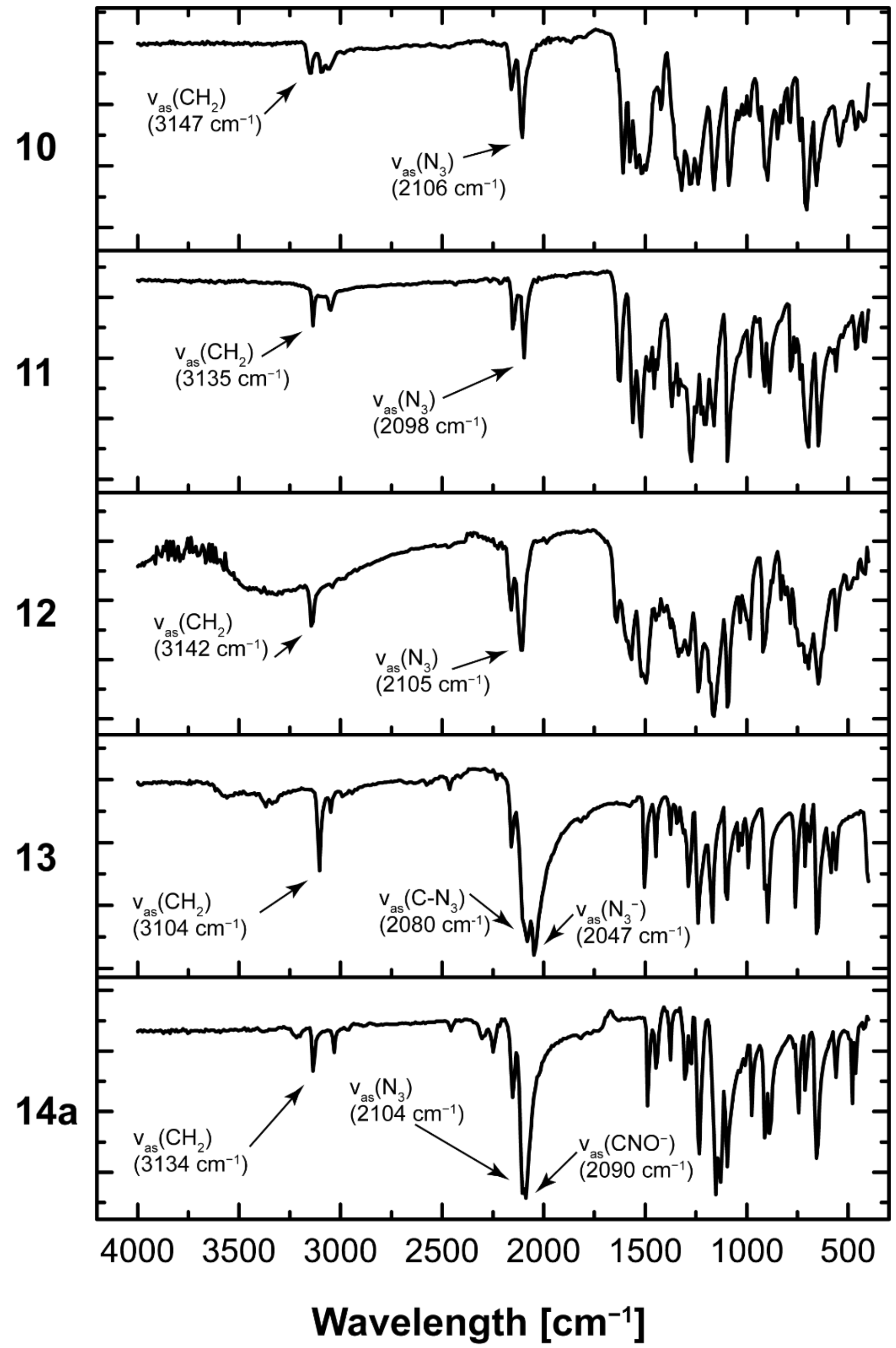

Figure S10. IR spectra of compounds **10** – **14a**.

4.7.6 Hot Plate and Hot Needle Test of Compounds 3–14

Figure S11. Hot plate (left) and hot needle (right) test of compound **3**.

Figure S12. Hot plate (left) and hot needle (right) test of compound **4**.

Figure S13. Hot plate (left) and hot needle (right) test of compound **6**.

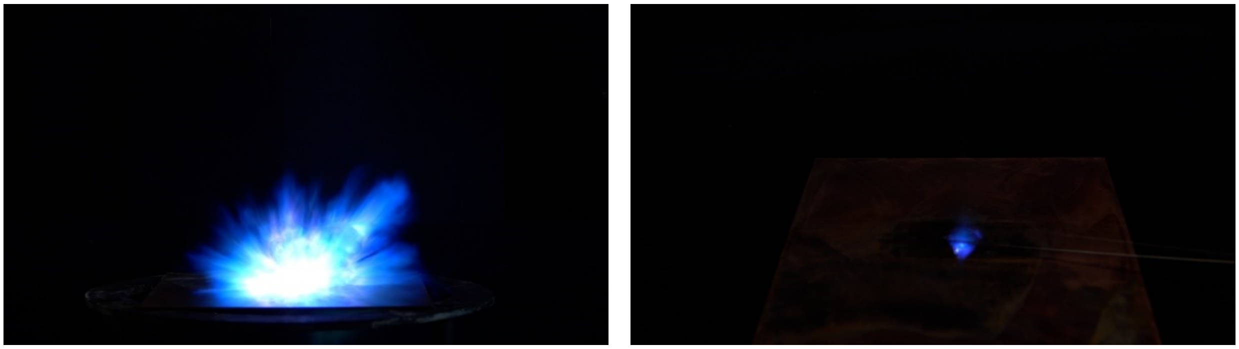

Figure S14. Hot plate (left) and hot needle (right) test of compound **7**.

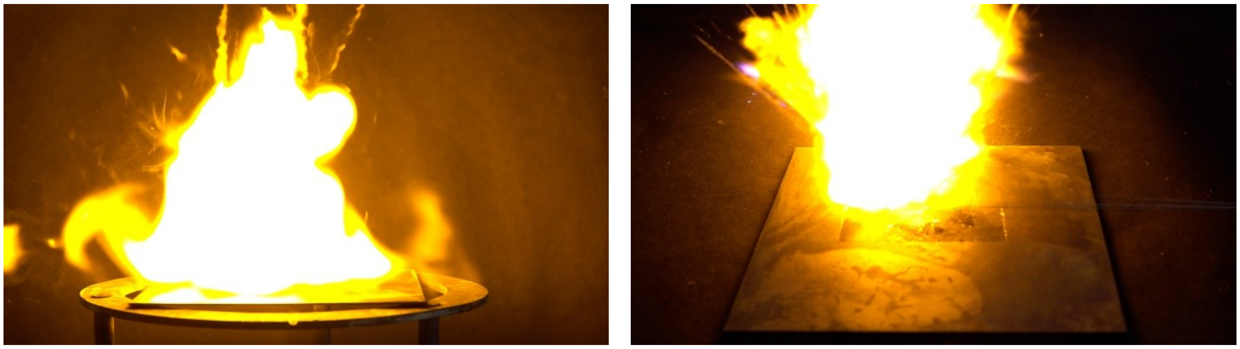

Figure S15. Hot plate (left) and hot needle (right) test of compound **8**.

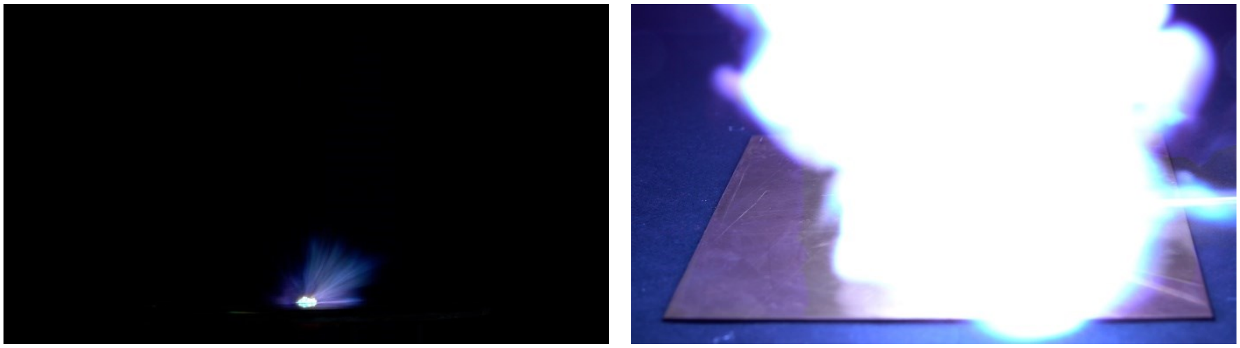

Figure S16. Hot plate (left) and hot needle (right) test of compound **9**.

Figure S17. Hot plate (left) and hot needle (right) test of compound **10**.

Figure S18. Hot plate (left) and hot needle (right) test of compound **11**.

Figure S19. Hot plate (left) and hot needle (right) test of compound **12**.

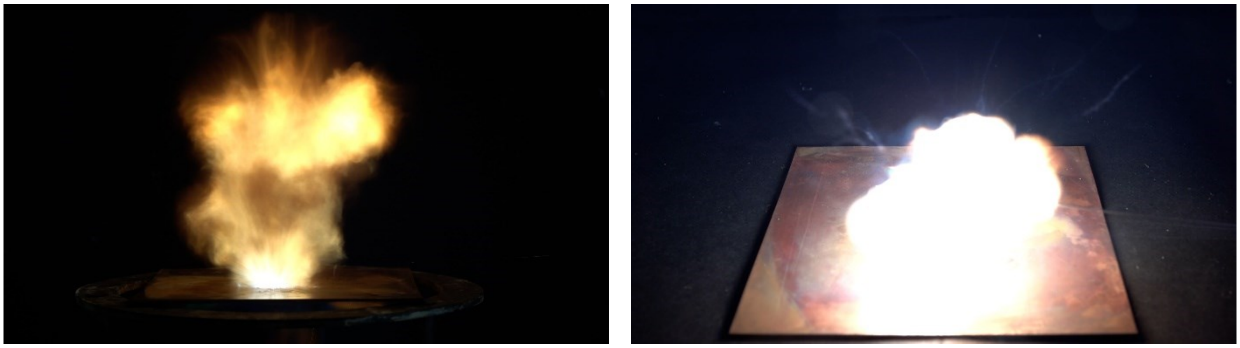

Figure S20. Hot plate (left) and hot needle (right) test of compound **13**.

Figure S21. Hot plate (left) and hot needle (right) test of compound **14a**.

4.7.7 General Methods

All chemicals and solvents were employed as received (Sigma-Aldrich, Fluka, Acros, ABCR). ^{1}H, $^{13}C\{^{1}H\}$, ^{14}N, $^{15}N\{^{1}H\}$ spectra were recorded at ambient temperature using a JEOL Bruker 27400, Eclipse 270, JEOL EX 400 or a JEOL Eclipse 400 instrument. The chemical shifts quoted in ppm in the text refer to typical standards such as tetramethylsilane (^{1}H, ^{13}C) nitromethane (^{14}N,^{15}N) in DMSO-d_6, D_2O or acetone-d_6 as the solvent. Endothermic and exothermic events of the described compounds, which indicate melting, loss of crystal water or decomposition, are given as the extrapolated onset temperatures. The samples were measured in a range of 25–400 °C at a heating rate of 5 °C min^{-1} through differential thermal analysis (DTA) with an OZM Research DTA 552-Ex instrument. Infrared spectra were measured with pure samples on a Perkin-Elmer BXII FT-IR system with a Smith DuraSampler IR II diamond ATR. Determination of the carbon, hydrogen, and nitrogen contents was carried out by combustion analysis using an Elementar Vario El (nitrogen values determined are often lower than the calculated ones' due to their explosive behavior). Impact sensitivity tests were carried out according to STANAG 4489[S22] with a modified instruction[S23] using a BAM (Bundesanstalt für Materialforschung) drophammer.[S24] Friction sensitivity tests were carried out according to STANAG 4487[S28] with a modified instruction[S29] using the BAM friction tester.[S24,25] The classification of the tested compounds results from the "UN Recommendations on the Transport of Dangerous Goods".[S30,31] Additionally, all compounds were tested upon the sensitivity toward electrical discharge using the OZM Electric Spark XSpark10 device.[S29] Energetic properties have been calculated with the EXPLO5 6.05.04 computer code[S32] using the, to RT converted, X-ray density and calculated solid state heats of formation. These were computed by the atomization method as described in recently published papers. Electronic enthalpies were calculated with the Gaussian09 software[S13] suite using the CBS-4M method.

4.7.8 References

S1 CrysAlisPRO (Version 171.33.41), Oxford Diffraction Ltd. **2009**.

S2 A. Altomare, G. Cascarano, C. Giacovazzo, and A. Guagliardi, *J. Appl. Crystallogr.* **1992**, *26*, 343.

S3 A. Altomare, G. Cascarano, C. Giacovazzo, A. Guagliardi, A. G. G. Moliterni, M. C. Burla, G. Polidori, M. Camalli and R. Spagna, SIR97 **2003**.

S4 A. Altomare, M. C. Burla, M. Camalli, G. L. Cascarano, C. Giacovazzo, A. Guagliardi, A. G. G. Moliterni, G. Polidori and R. Spagna, *J. Appl. Crystallogr.* **1999**, *32*, 115.

S5 G. M. Sheldrick, SHELXL-97, University of Göttingen, Germany **1997**.

S6 G. M. Sheldrick, *Acta Crystallogr. Sect. A* **2008**, *64*, 112.

S7 G. M. Sheldrick, *Acta Cryst. A* **2015**, *71*, 3–8.

S8 A. L. Spek, PLATON, Utrecht University, The Netherlands, **1999**.

S9 L.J. Farrugia, *J. Appl. Cryst.* **2012**, *45*, 849.

S10 O. V. Dolomanov, L. J. Bourhis, R. J. Gildea, J. A. K. Howard and H. Puschmann, *J. Appl. Cryst*. **2009**, *42*, 339–341.

S11 Empirical absorption correction using spherical harmonics, implemented in SCALE3 ABSPACK scaling algorithm (CrysAlisPro Oxford Diffraction Ltd., Version 171.33.41, **2009**).

S12 APEX3, Bruker AXS Inc., Madison, Wisconsin, USA.

S13 M. J. Frisch, G. W. Trucks, H. B. Schlegel, G. E. Scuseria, M. A. Robb, J. R. Cheeseman, G. Scalmani, V.Barone, B. Mennucci, G. A. Petersson, H. Nakatsuji, M. Caricato, X. Li, H.P. Hratchian, A. F. Izmaylov, J. Bloino, G. Zheng, J. L. Sonnenberg, M. Hada, M. Ehara, K. Toyota, R. Fukuda, J. Hasegawa, M. Ishida, T. Nakajima, Y. Honda, O. Kitao, H. Nakai, T. Vreven, J. A. Montgomery, Jr., J. E. Peralta, F. Ogliaro, M. Bearpark, J. J. Heyd, E. Brothers, K. N. Kudin, V. N. Staroverov, R. Kobayashi, J. Normand, K. Raghavachari, A. Rendell, J. C. Burant, S. S. Iyengar, J. Tomasi, M. Cossi, N. Rega, J. M. Millam, M.Klene, J. E. Knox, J. B. Cross, V. Bakken, C. Adamo, J. Jaramillo, R. Gomperts, R. E. Stratmann, O. Yazyev, A. J. Austin, R. Cammi, C. Pomelli, J. W. Ochterski, R. L. Martin, K. Morokuma, V. G. Zakrzewski, G. A. Voth, P. Salvador, J. J. Dannenberg, S. Dapprich, A. D. Daniels, O. Farkas, J.B. Foresman, J. V. Ortiz, J. Cioslowski and D. J. Fox, Gaussian 09 A.02, Gaussian, Inc., Wallingford, CT, USA, **2009**.

S14 J. W. Ochterski, G. A. Petersson and J. A. Montgomery Jr., *J. Chem. Phys.* **1996**, *104*, 2598–2619.

S15 J. A. Montgomery Jr., M. J. Frisch, J. W. Ochterski and G. A. Petersson, *J. Chem. Phys.* **2000**, *112*, 6532–6542.

S16 L. A. Curtiss, K. Raghavachari, P. C. Redfern and J. A. Pople, *J. Chem. Phys.* **1997**, *106*, 1063–1079.

S17 E. F. C. Byrd and B. M. Rice, *J. Phys. Chem. A* **2006**, *110*, 1005–1013.

S18 B. M. Rice, S. V. Pai and J. Hare, *Comb. Flame* **1999**, *118*, 445–458.

S19 P. J. Lindstrom and W. G. Mallard, NIST Standard Reference Database Number 69, http://webbook.nist.gov/chemistry/, (accessed March **2021**).

S20 M. S. Westwell, M. S. Searle, D. J. Wales and D. H. Williams, *J. Am. Chem. Soc*. **1995**, *117*, 5013–5015.

S21 F. Trouton, *Philos. Mag.* **1884**, *18*, 54–57.

S22NATO standardization agreement (STANAG) on explosives, impact sensitivity tests, no. 4489, 1st ed., Sept. 17, **1999**.

S23 WIWEB-Standardarbeitsanweisung 4-5.1.02, Ermittlung der Explosionsgefährlichkeit, hier der Schlagempfindlichkeit mit dem Fallhammer, Nov. 8, **2002**.

S24 BAM, http://www.bam.de, (accessed March **2021**).

S25 OZM, http://www.ozm.cz, (accessed March **2021**).

S26 Military Standard 1751A (MIL-STD-1751A): safety and performance tests for qualification of explosives (high explosives, propellants and pyrotechnics), method 1016, Dec. 11, **2001**.

S27 M. S. Gruhne, M. Lommel, M. H. H. Wurzenberger, N. Szimhradt, T. M. Klapötke and J. Stierstorfer, *Propellants Explos. Pyrotech.* **2020**, *45*, 147–153.

S28 NATO standardization agreement (STANAG) on explosive, friction sensitivity tests, no. 4487, 1st ed., Aug. 22, **2002**.

S29 WIWEB-Standardarbeitsanweisung 4-5.1.03, Ermittlung der Explosionsgefährlichkeit oder der Reibeempfindlichkeit mit dem Reibeapparat, Nov. 8, **2002**.

S30 UN Model Regulation: Recommendations on the Transport of Dangerous Goods – Manual of Tests and Criteria, section 13.4.2.3.3, **2015**.

S31 Impact: insensitive > 40 J, less sensitive ≥ 35 J, sensitive ≥ 4 J, very sensitive ≤ 3 J; Friction: insensitive > 360 N, less sensitive = 360 N, sensitive < 360 N and > 80 N, very sensitive ≤ 80 N, extremely sensitive ≤ 10 N. According to the UN Recommendations on the Transport of Dangerous Goods, 5th ed., **2009**.

S32 M. Sućeska, EXPLO5 Version 6.05 User's Guide. Zagreb, Croatia: OZM; **2018**.

5 1-(Nitratomethyl)tetrazole: A Highly Sensitive Ligand with an Improved Oxygen Balance for Laser Ignitable Coordination Compounds

Moritz Kofen, Vanessa Braun, Simon M. J. Endraß, Thomas M. Klapötke, and Jörg Stierstorfer

Published in *Inorganic Chemistry*, **2022**

DOI: 10.1021/acs.inorgchem.2c02805

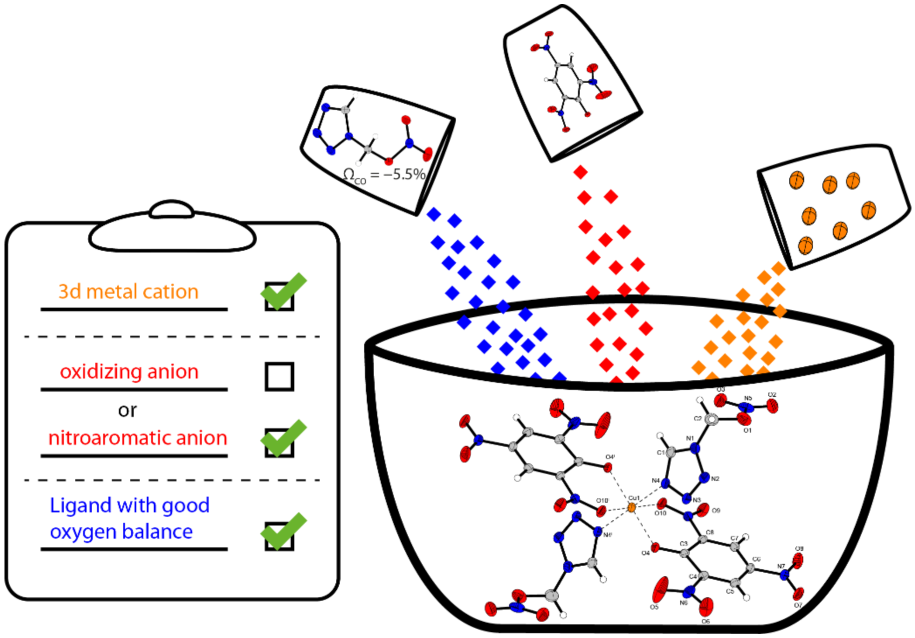

Abstract: For the first time the highly sensitive 1-(Nitratomethyl)tetrazole (1-NAMT) was synthesized, representing the shortest possible 1-(Nitratoalkyl)tetrazole with a combined nitrogen and oxygen content of 81.4 %. Compared to its related ethyl-derivative (1-NET) it exhibits an improved oxygen balance, resulting in higher detonation parameters. 1-NAMT was thoroughly analyzed by single-crystal diffraction experiments accompanied by elemental analysis, IR spectroscopy, and multinuclear (^{1}H, ^{13}C, ^{14}N) NMR measurements. The thermal behavior of 1-NAMT was analyzed by Differential Thermal Analysis supported by Thermogravimetric Analysis. Furthermore, energetic coordination compounds of Cu with different inorganic (e.g. nitrate, chlorate, and perchlorate) and nitroaromatic anions (e.g. picrate and styphnate) were synthesized and thoroughly analyzed. It is shown that the formation of energetic coordination compounds with

nitroaromatic anions (T_{dec} ~ 180 °C) is a suitable strategy to improve the rather low thermal stability of 1-NAMT (125 °C).

5.1 Introduction

Since the structure elucidation of the DNA by Crick & Watson[1], the importance of N-heterocyclic compounds cannot be questioned. The four nucleobases adenine, guanine, cytosine and thymine (Figure 1) that were found to build up the double helical DNA strands are key examples of N-heterocyclic compounds. Other representatives of important heterocyclic compounds are based on the porphyrin scaffold, which are known for building hemes, the most prominent being heme B, the oxygen transporting iron coordination compound of blood.[2] The application of heterocycles as ligands in coordination compounds offers a nearly infinite amount of possible compounds which chemical and physical properties can be tuned towards their intended use. Prominent examples of heterocycles applied as ligands are found in the Grubbs I[3] and Grubbs II[4] catalysts as well as in the B vitamins with their most prominent representative being vitamin B_{12}[5]. A recently emerged, closely related, field of research is that of energetic coordination compounds (ECCs) used in pyrotechnic mixtures[6], burn rate modifiers[7] and primary explosives[8]. Here, energetic and nitrogen-rich heterocycles are combined with transition metal salts of oxidizing (e.g., nitrate, chlorate and perchlorate) or reducing (e.g. azide) anions. Promising ligands for ECCs should exhibit several characteristics.

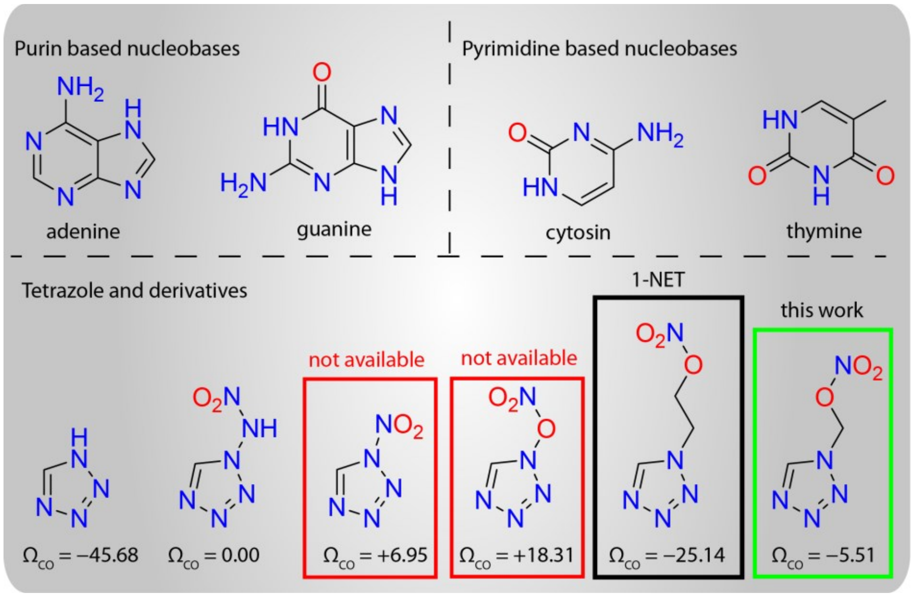

Figure 1. Comparison of oxygen balances between *1H*-tetrazole and derivatives with different substitution patterns.

Like for any energetic material, a high endothermic enthalpy of formation is favorable. Furthermore, the sensitivities of the pure ligand should be approximately in the range that is desired for the intended use of the resulting ECC. As the formation of ECCs most often leads to an increase in sensitivity[9], it is easily possible to overstate the sensitivities of the resulting ECCs as seen in the work on 1-Aminotetrazole[10] (1-AT) or 1-(Azidomethyl)tetrazole[11] (AzMT). Among the nitrogen-rich heterocyclic compounds, those based on the *1H*-tetrazole (Figure 1) motive are promising substances to be applied as ligands. Due to a wide variety of possible substitutions of the tetrazole scaffold, a huge amount of (highly) energetic neutral compounds are feasible.[12] This enables a broad spectrum of potential applications as antitumor-drugs, as low toxic antifungal drugs but also in green energetic coordination compounds, dependent on the size and type of substituents.[13-15] Additionally, the tetrazole scaffold offers a highly endothermic enthalpy of formation (*1H*-tetrazole: 4732 kJ kg^{-1}) due to a very high nitrogen content of the underlying tetrazole moiety (N = 79.98%). Besides the drawback an acidic proton of *1H*-tetrazole, the absence of oxygen atoms in the molecular structure leads to an incomplete decomposition into gaseous products as elemental carbon may be produced upon exothermic decomposition. Therefore, increasing the amount of oxygen within the molecular structures improves the overall oxygen balance[1], which also generally increases the performance of an energetic material. This can be achieved by the functionalization with explosophores such as nitro-, nitramino-, and nitrate ester moieties that all introduce oxygen to the molecular structure (Figure 1). While the direct functionalization of tetrazoles at the 1*N* position is generally easy, the substitution by a nitro group or a nitrate ester is not reported yet. Here, only the nitramino derivative is known to literature[16]. Due to the inaccessibility of a direct substitution at the 1*N*-position of tetrazole by a nitrate ester, the introduction of alkyl bridges between the azole and nitrate ester is necessary. Recently, *Klapötke et al.* published the derivative containing a bridging ethyl chain namely 1-(Nitratoethyl)tetrazole[17] (1-NET). This compound exhibits a decreased nitrogen content of 44.0% compared to pure tetrazole, but an oxygen content of 30.2%, 1-NET therefore possess an oxygen balance towards the formation of CO of $\Omega_{CO} = -25.1\%$. This drastically increased the oxygen balance compared to *1H*-tetrazole ($\Omega_{CO} = -45.7\%$). Additionally, the introduction of oxygen atoms in 1-NET (1.55 g cm^{-3}) also increases the density of pure *1H*-tetrazole (1.41 g cm^{-3}), even though a more sterically demanding substituent is introduced. This increase in density would noticeably

---

[1] $OB_{CO} = \frac{\left[d-a-\frac{b}{2}\right]*1600}{M}$; M = molar mass; formula for $C_aH_bN_cO_d$.

be more drastic when comparing *1H*-tetrazole to the methyl-bridged derivative, which is not published yet. Interestingly, there are only a few examples of methylene-bridged explosophores published[18-20], and even less when focusing solely on 1*N*-subtitution[21]. While the introduction of an ethylene moiety is synthetically rather easy, the challenge to introduce a methylene moiety is to find a suitable starting material that is chemically inert enough to be further functionalized. We recently published a procedure for the synthesis of 1-(Hydroxymethyl)tetrazole (1-HMT), which is at least stable enough to be smoothly converted to the mesylated derivative. Since 1-HMT also represents a suitable precursor for 1-(Nitratomethyl)tetrazole (1-NAMT), we opted to synthesize it for the first time and apply it as ligand for new ECCs. In this work we present the synthesis of 1-(Nitratomethyl)tetrazole (1-NAMT), as well as several new energetic coordination compounds of 1-NAMT. The ligand was analyzed by multinuclear NMR spectroscopy, and all compounds were analyzed by single crystal X-ray diffraction experiments. Additionally, the physico-chemical properties of all compounds were determined.

5.2 Results and Discussion

5.2.1 Synthesis of 1-(Nitratomethyl)tetrazole

*Warning! The synthetic work described includes the handling of very sensitive compounds such as 1-NAMT (**1**) and ECCs (**2–8**). Appropriate protective equipment (leather coat, face shield, Kevlar® wrist protectors, and hearing protection) must be worn at all times when handling these materials!*

The synthesis of 1-(nitratomethyl)tetrazole (**1**) is shown in Scheme 1. The crude isomeric mixture of 1- and 2-(hydroxymethyl)tetrazole was synthesized according to literature [11]. The isomeric mixture was added to a stirring mixture of acetic anhydride and fuming nitric acid cooled to 5 °C. A previous separation of the isomers is not necessary, due to a complete decomposition of the 2*N* isomer after nitration. The target molecule 1-(Nitratomethyl)tetrazole (**1**) was obtained as a colorless solid by stirring at 5 °C for 1.5h, quenching on ice, adjusting to pH = 6, and extracting into ethyl acetate. To remove trace amounts of spent acid, **1** was purified via column chromatography with a mixture of iso-hexane/ethyl acetate (1/1) as eluting solvent. After removing the solvent *in vacuo,* the resulting oil (**1**) started to solidify after standing undisturbed for 1–2 hours. **1** was obtained as colorless solid in moderate yield of 21%.

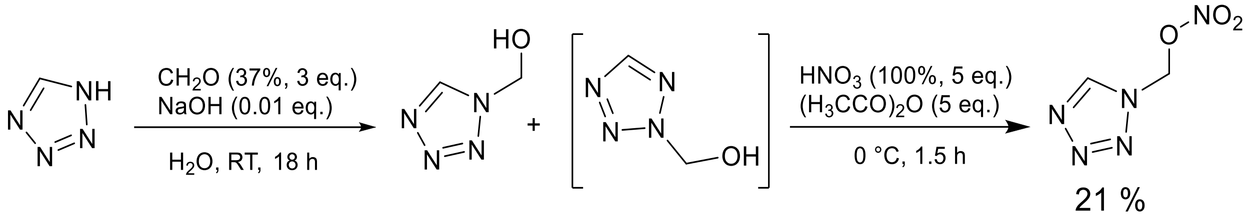

1

Scheme 1. Synthesis of 1-(Nitratomethyl)tetrazole (**1**), with the hydroxy methylation of *1H*-tetrazole.

5.2.2 Synthesis of the ECCs

Several energetic coordination compounds with 1-NAMT as a ligand were synthesized according to Schemes 2 and 3. Due to the commercial unavailability of copper(II) chlorate, it was freshly produced according to literature[22]. Generally, compounds **2**–**4** (Scheme 2) were produced by adding the corresponding copper(II) salt to a solution of **1** in ethanol at elevated temperatures. After stirring for several minutes, the solutions were left to crystallize for up to 3 days. Before complete evaporation of the solvent, the compounds were filtered off and washed with little ice-cold ethanol. The compounds thus obtained were suitable for single crystal X-Ray diffraction experiments without any further recrystallisation necessary.

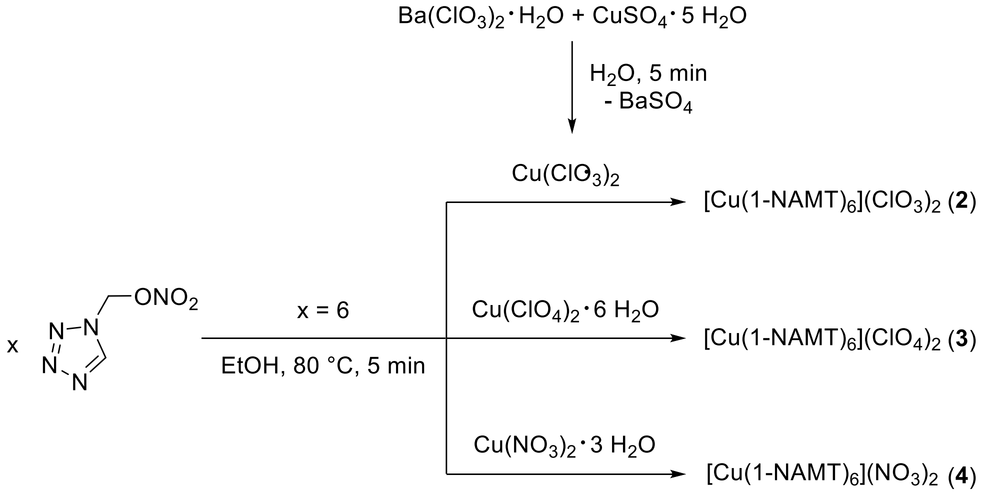

Scheme 2. Preparation of [Cu(1-NAMT)$_6$](ClO$_3$)$_2$ (**2**), [Cu(1-NAMT)$_6$](ClO$_4$)$_2$ (**3**) and [Cu(1-NAMT)$_6$](NO$_3$)$_2$ (**4**).

Compounds **5**–**8** were synthesized by adding the corresponding free nitroaromatic acid to a suspension of basic copper carbonate in water and stirring at 80 °C until a clear solution is obtained (Scheme 3). The solutions are left for crystallization for several days.

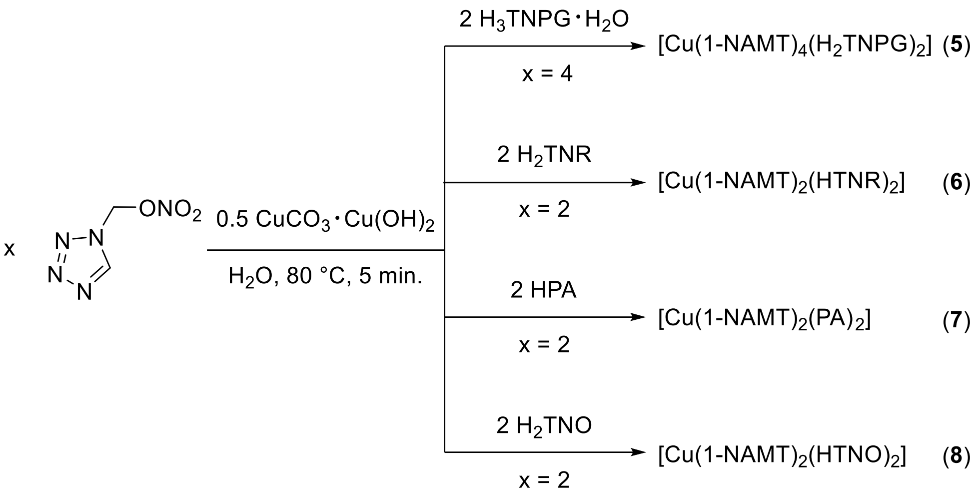

Scheme 3. Preparation of several copper trinitrophenolate complexes of **1**.

5.2.3 Crystal Structures

The obtained compounds were further analyzed by low-temperature single crystal X-Ray diffraction analysis. The low-temperature densities of all compounds are recalculated[2] to their respective density at room temperature. The data and parameters of the measurements as well as the refinements are given in the supporting information Table S1. The crystal datasets are uploaded to the CSD database and can be obtained free of charge with CCDC 2176031 (**1**), 2176030 (**2**), 2176033 (**3**), 2176032 (**4**), 2176035 (**5**), 2176029 (**6**), 2176036 (**7**), 2176034 (**8**).

Compound **1** crystallizes as colorless platelets in the orthorhombic space group $P2_12_12_1$, with a density of 1.68 g cm^{-3} and four formula units in the unit cell (Figure 2A). The bond lengths within the tetrazole moiety are in the expected range for 1*N*-substituted tetrazoles. [17, 23] The tetrazole unit forms a nearly perfect level plane together with the methylene moiety, which is marginally protruding by 0.3 °. A second plane is also constructed by the methylene carbon atom with the planar nitrate group. Both planes are intersecting at an angle of 111 °, which derives from the sp^3-hybridization of the methylene carbon atom. The bond lengths within the nitrate group are similar to comparable nitrate esters [19, 24] with an elongated bond of 1.42 Å between O1–N5, and two nearly equivalent bonds of 1.20 Å between O2–N5 and O3–N5. Figure 2B shows the crystal packing of **1** along the *c* axis. This highlights the screw axis along *c*, which leads to a slight offset of the methylene groups of two stacked molecules of **1**. This results in a clear distinction of areas

---

[2] $d_{298\,K} = \frac{dT}{1+\,\alpha_V(298-T_0)}$; $\alpha_V = 1.5 * 10^{-4}K^{-1}$

of stacked but twisted nitrate units (red blocks) and tetrazole moieties (blue pentagons). Interestingly, there are only non-classical hydrogen bond between two tetrazole rings without any participation in hydrogen bonding of the nitrate moieties. For all ECCs, octahedral coordination of the copper(II) centers are observed. All three ECCs crystallize isotypically in the trigonal space group $\bar{R}3$ with calculated densities of 1.77 g cm^{-3} (**2**) 1.80 g cm^{-3} (**3**), 1.76 g cm^{-3} (**4**) as well as three units per unit cell. In the molecular structures, **2**–**4** (Figures 3–5) show almost perfect octahedral coordination of the copper(II) cation with only slightly tilted axes but Cu–N distances of 2.12 Å. Due to the symmetry the expected Jahn-Teller distortion (always present for Cu^{2+} d^9 systems) cannot be allocated.

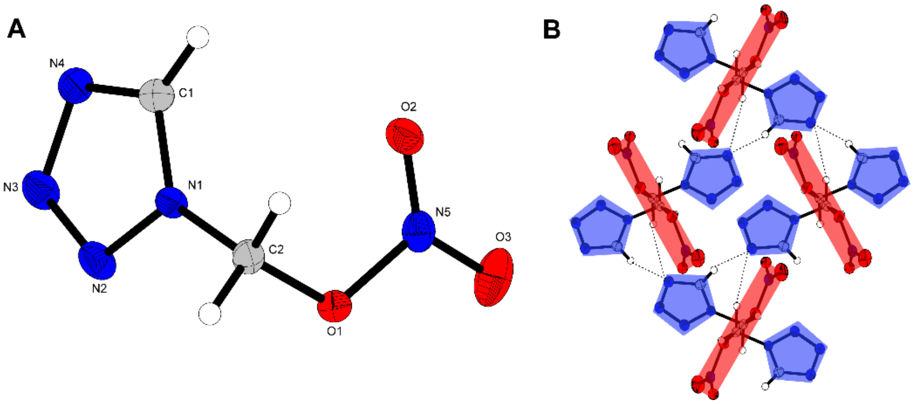

Figure 2. A) Molecular structure of 1-(Nitratomethyl)tetrazole (**1**); B) crystal packing of **1** along the *c* axis highlighting areas of stacked nitro groups (red) and tetrazole moieties (blue); all ellipsoids are shown with a probability of 50%; selected bond lengths [Å]: N1–C2 1.44(2), O1–C2 1.43(2), O1–N5 1.42(2), O2–N5 1.20(2), O3–N5 1.20(2); Angles [°]: O1–C2–N1 111.00(15), N5–O1–C2 113.46(14), O1–N5–O2 117.83(16), O1–N5–O3 111.50(16); torsion angles [°]: N1–N2–N3–N4 −0.3(2), C2–O1–N5–O2 −6.0(2).

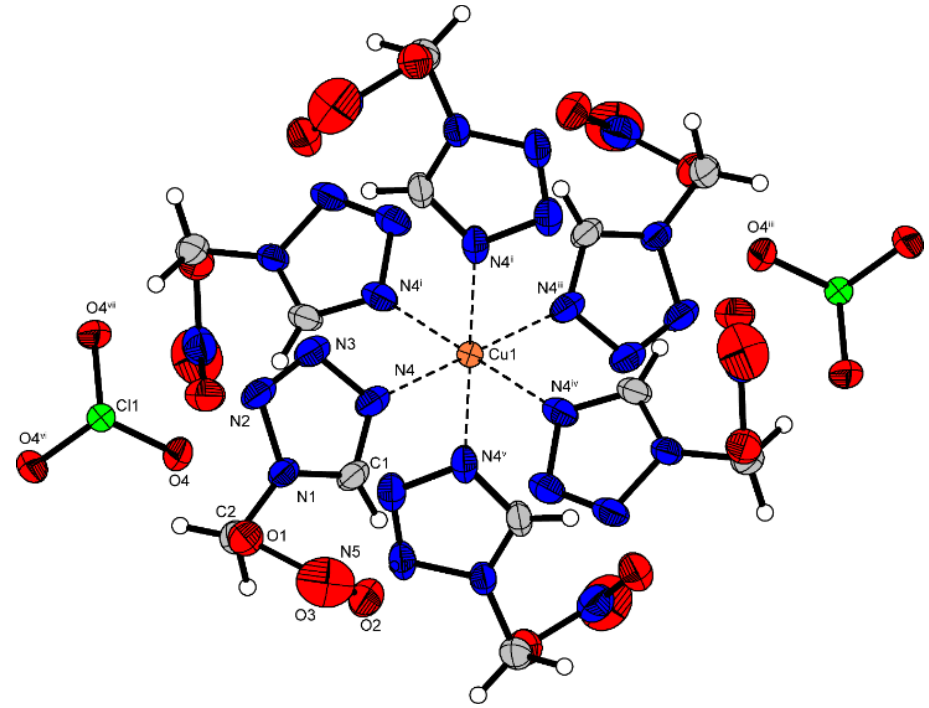

Figure 3. Molecular structure of $[Cu(1\text{-}NAMT)_6](ClO_3)_2$. Selected bond lengths [Å]: Cu1–N1 2.13(2); selected bond angles [°]: N1–Cu1–N1^{iii} 92.49(9), N1–Cu1–N1^{v} 180.00, N1–Cu1–N1^{vi} 87.51(9).

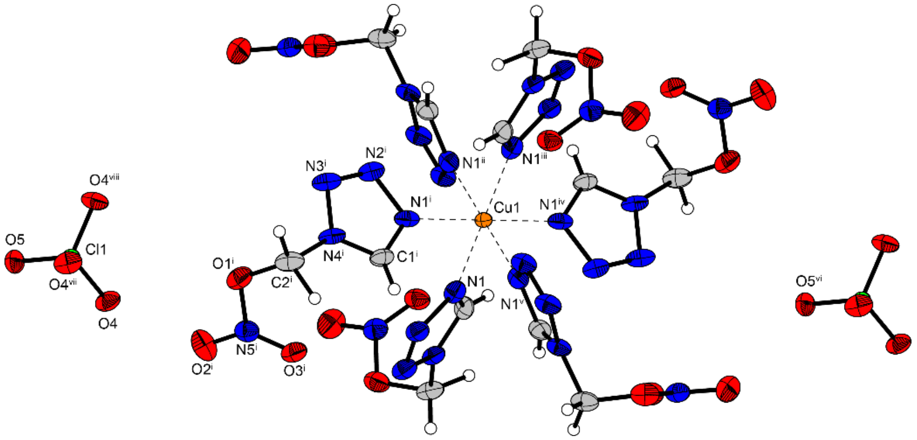

Figure 4. Molecular structure of $[Cu(1\text{-}NAMT)_6](ClO_4)_2$. Selected bond lengths [Å]: Cu1–N1 2.12(5); selected bond angles [°]: N1–Cu1–N1^{iv} 91.83(17), N1–Cu1–N1^{vii} 88.16(17), N1–Cu1–N1^{v} 180.00.

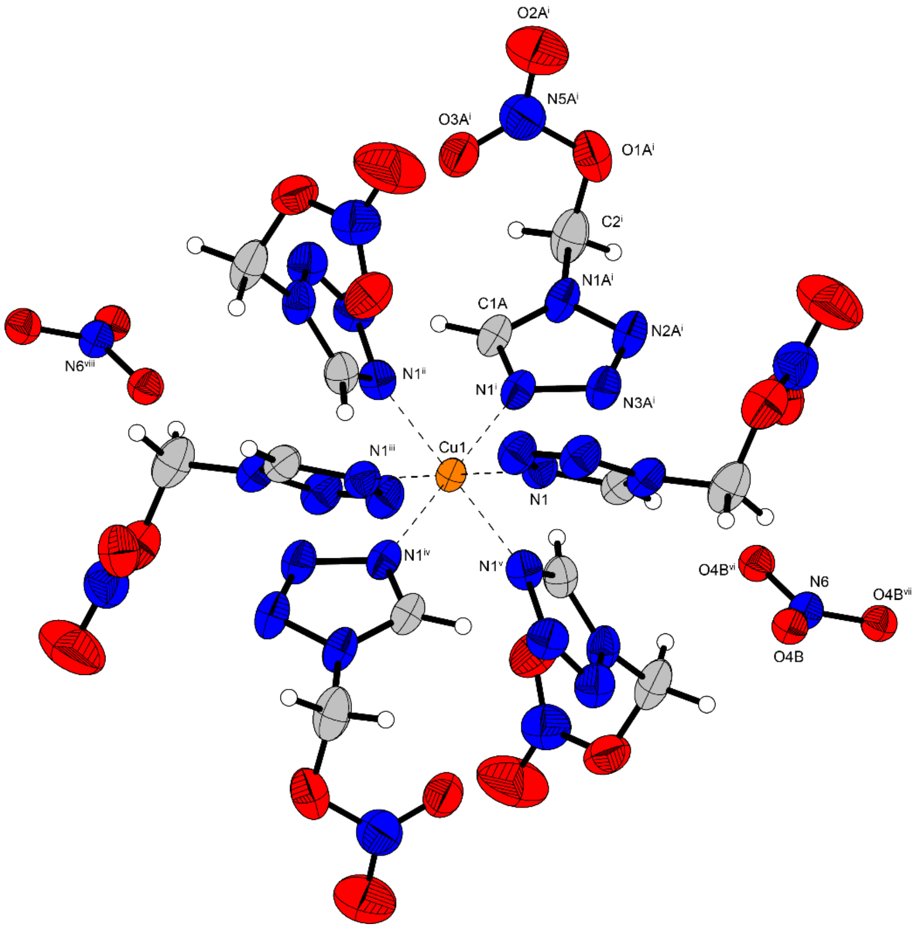

Figure 5. Molecular structure of compound **4**. Selected bond length (Å): Cu1–N1 2.12(3). Selected bond angles (°): N1–Cu1–N1^{i}, N1–Cu1–N1^{ii}, N1–Cu1–N1^{iii}, N1–Cu1–N1^{iv}, N1–Cu1–N1^{v}.

Compound **5** crystallizes in the triclinic space group $P{-}1$ with a density of 1.88 g cm^{-3} and one molecular formula in the unit cell (Figure 6). The copper(II) cation is sixfold coordinated by two single deprotonated trinitro phloroglucinate anions as well as four molecules of **1** forming a distorted octahedron. The four ligands of **1** are positioned in the equatorial plane with bond lengths of 2.00 Å (Cu1–N4) and 2.03 Å (Cu1–N9), with minor deviations of 1.4 ° (N4–Cu1–N9) from the ideal 90 °. The anions are positioned in the axial position with bond lengths of 2.32 Å. This distortion is caused by a high steric demand of the anions together with copper(II) being a d^{9} cation with an electronic configuration of $t_{2g}{}^{6}e_{g}{}^{3}$, ultimately leading to a degradation of the z^{2}-orbital. This causes a *Jahn-Teller*-like distortion. As displayed in Figure 6, the trinitro phloroglucinate anions form intermolecular hydrogen bonds between the two hydroxy groups and the *para*-positioned nitro group, which is hence nearly perfectly planar with the aromatic ring. This ultimately leads to a rotation of the two remaining nitro groups out of plane, positioning them in an orientation disfavoring a coordination of the metal center by the nitro groups, as is observed in comparable compounds[11].

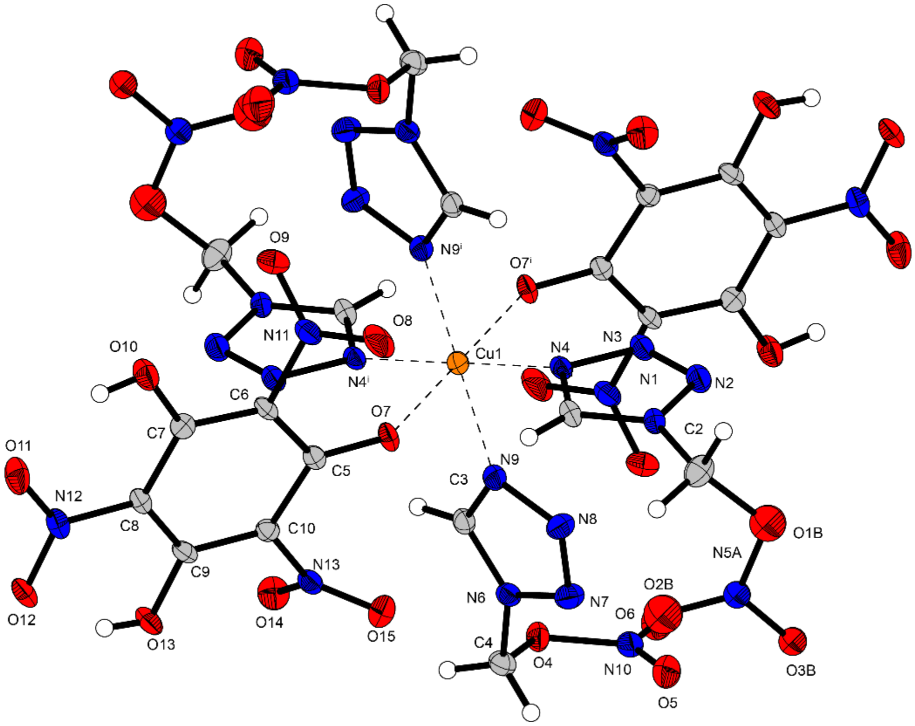

Figure 6. Octahedral coordination in [Cu(1-NAMT)$_4$(H$_2$TNPG)$_2$] (**5**). Selected bond lengths [Å]: Cu1–O7 2.32(19), Cu1–N4 2.00(3), Cu1–N9 2.03(2); selected bond angles [°]: O7–Cu1–N4 85.05(8), O7–Cu1–N9 89.14(8), N4–Cu1–N9 88.60(10).

Compound **6** (Figure 7) crystallizes in the triclinic space group *P*−1 with a density of 1.88 g cm^{-3} and one formula unit in the unit cell. The copper(II) cation is sixfold coordinated by two single deprotonated anions as well as two molecules of **1** in the form of a *Jahn-Teller*-like distorted octahedron, like in compound **5**. The equatorial plane is built by the two ligands of **1** with bond lengths of 2.00 Å and the two deprotonated hydroxy groups of the anions with bond lengths of 1.93 Å. The absence of a third hydroxy group, like in the anions of **5**, leads to only one nitro group being rotated out of the aromatic ring plane, which now enables the remaining level nitro group (N6) to additionally coordinate to the metal cation. This results in the occupation of four coordination sites of the copper(II) cation by the anions, thus only two sites remain to be coordinated by molecules of **1**.

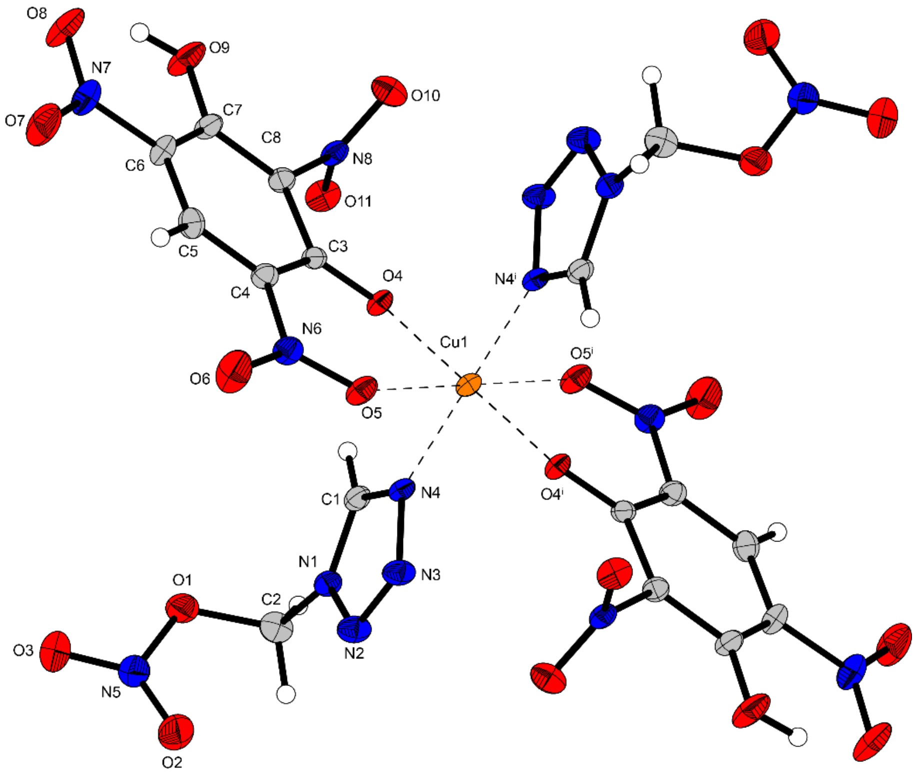

Figure 7. Molecular structure of [Cu(1-NAMT)$_2$(HTNR)$_2$] showing a *Jahn-Teller*-like distorted coordination sphere (**6**). Selected bond lengths [Å]: Cu1–O4 1.93(16), Cu1–O5 2.33(2), Cu1–N4 2.00(2); selected bond angles [°]: O4–Cu1–O5 81.77(7), O4–Cu1–N4 89.48(7), O5–Cu1–N4 86.14(7).

Compound **7** (Figure 8) crystallizes in the monoclinic space group *P*2$_1$/*c* with two formula units in the unit cell and a density of 1.91 g cm^{-3}, the highest of all herein investigated compounds. Like in **6**, the copper(II) cation is coordinated in a *Jahn-Teller*-like distorted octahedron, with an equatorial plane build by two ligands of **1** and the two deprotonated hydroxy groups of the picrate anions. Here, the bond lengths are similar to those previously observed with a length of 1.90 Å and 2.01 Å, respectively for the deprotonated hydroxy groups and the tetrazole ligands. Like for the styphnate anions, the absence of hydroxy groups leads to a nearly perfectly planar anion, again enabling the additional coordination of the copper(II) cation by the nitro groups.

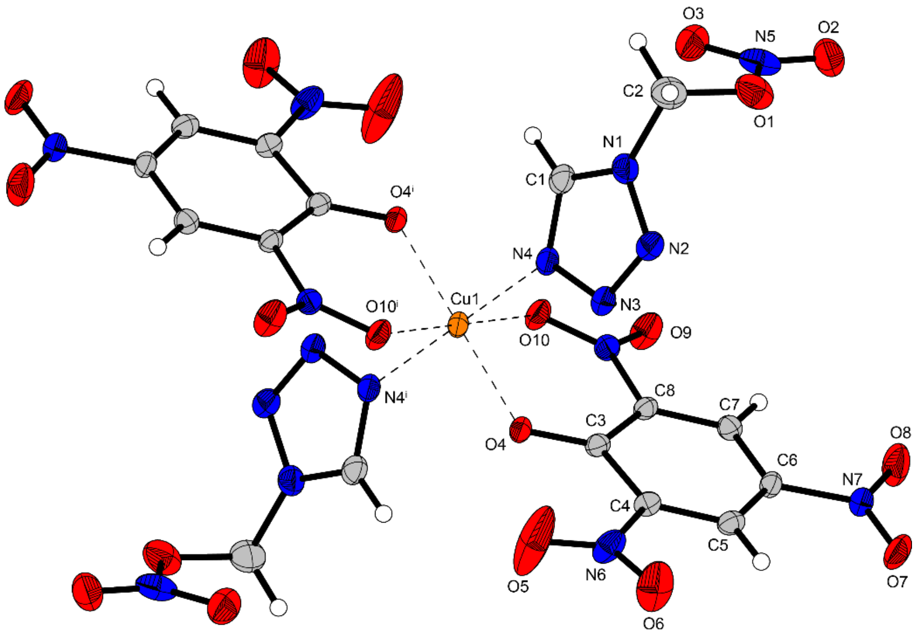

Figure 8. Coordination center of [Cu(1-NAMT)$_2$(PA)$_2$] (**7**). Selected bond lengths [Å]: Cu1–O4 1.93(2), Cu1–O10 2.30(3), Cu1–N4 2.01(3); selected bond angles [°]: O4–Cu1–O10 80.27(11), O4–Cu1–N4 92.29(11), O10–Cu1–N4 90.92(12).

Compound **8** crystallizes in the triclinic space group *P*−1 with a density of 1.87 g cm^{-3} and one formula unit in the unit cell. Like in the previously discusses nitroaromatic ECCs, the copper(II) cation is sixfold coordinated in the form of a distorted octahedron. The equatorial plane is again built by two molecules of **1** as well as the deprotonated hydroxy groups, whereas the coordinating nitro groups are positioned in axial position. Here, the bond lengths towards all coordinating atoms are in the same range as previously observed (Figure 9). Interestingly, the introduction of one methyl group to the styphnate anion leads to a slight rotation (14.6 °) of the nitro group (N1), which is normally planar to the aromatic ring due to stabilization by the hydroxy group. A more drastic change is observed for the coordinating nitro group (N2) which is now clearly twisted out of the plane (36.4 °) compared to the coordinating nitro group of the styphnate anions of **6**. Nevertheless, this rotation lead to a slightly decreased Cu(II)–NO$_2$ (κO) bond length of 2.28 Å compared to that of compounds **6** (2.32 Å) and **7** (2.30 Å).

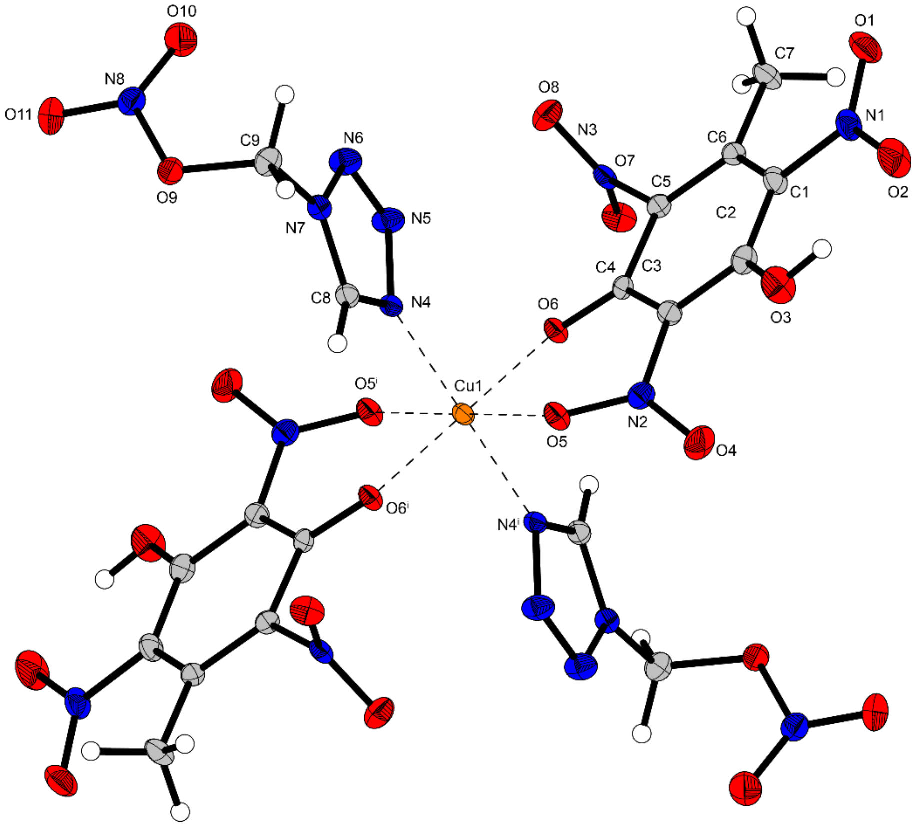

Figure 9. Molecular structure of [Cu(1-NAMT)$_2$(HTNO)$_2$] (**8**). Selected bond lengths [Å]: Cu1–O5 2.28 (14), Cu1–O6 1.92(14), Cu1–N4 2.02(18); selected bond angles [°]: O5–Cu1–O6 83.60(5), O5–Cu1–N4 90.72(6), O6–Cu1–N4 90.37(7).

5.2.4 Physicochemical Properties

Characterization of 1-NAMT. Table 1 compares the physical and energetic properties of compound **1** with its structural related compounds 1-(Azidomethyl)tetrazole (AzMT), 1-(Nitratoethyl)tetrazole (1-NET). Here, an increase in density of +0.13 g cm^{-3} is observed when changing from the explosophoric azide (AzMT) functionalization to a nitrate ester. A more drastic change is observed when comparing the enthalpies of formation, where **1** (187 kJ mol^{-1}) is a significantly less endothermic compound than AzMT (655 kJ mol^{-1}), which directly derives from the lack of two N-N double bonds found in the azide functionality. Comparing the energetic properties of all three compounds, calculated with the EXPLO5[25, 26] program code, a clear increase in performance is observed for the methyl-containing (**1** and AzMT) compounds over the ethyl-containing 1-NET. Compound **1** exhibits a detonation velocity of 8294 m s^{-1}, slightly outperforming AzMT with a detonation velocity of 8124 m s^{-1}, whereas 1-NET does not reach a detonation velocity of over 8000 m s^{-1}. Overall, the nitrate ester **1** outperforms its structural analogous azides (AzMT), expressing the high importance of a high theoretical maximum density

(TMD), which is even able to compensate the lack of enthalpy of formation. Interestingly, 1-NET is completely insensitive towards friction (>360 N) and moderately sensitive towards impact (10 J). By shortening the alkyl-chain the sensitivities are drastically increased, as compound **1** (<1 J, 9 N) exhibits sensitivities in the range of a primary explosive. Even higher sensitivities were reported for AzMT (<1 J, 2 N).

Table 1. Energetic properties of 1-NAMT (1), compared to AzMT, and 1-NET.

	1-NAMT (**1**)	AzMT	1-NET
Formula	$C_2H_3N_5O_3$	$C_2H_3N_7$	$C_3H_5N_5O_3$
M [g mol^{-1}]	145.08	125.1	159.1
ρ [g cm^{-3}]	1.68[a]	1.55[a]	1.55
N / N+O [%][c]	48.27 / 81.35	78.38 / 78.38	44.02 / 74.19
Ω_{CO} [%][d]	−5.51	−70.34	−25.14
IS [J][e]	<1	<1	10
FS [N][f]	9	2	>360
ESD [mJ][g]	150	540	n.d.
T_{exo} [°C][h]	119	167	168
$\Delta_f H°$ [kJ mol^{-1}][i]	187	655	174
$\Delta_f H°$ [kJ kg^{-1}][j]	1398	5232	1094
EXPLO5 V6.05.04			
$-\Delta_{ex} U°$ [kJ kg^{-1}][k]	5301	5127	4861
T_{det} [K][l]	3789	3473	3336
V_0 [L kg^{-1}][m]	451	502	815
P_{CJ} [kbar][n]	280	229	215
V_{det} [m s^{-1}][o]	8294	8124	7583

[a] From single crystal X-ray diffraction analysis recalculated to room temperature. [b] Measured with a gas pycnometer. [c] Nitrogen and combined nitrogen +oxygen content. [d] Oxygen balance towards the formation of CO. [e] Impact sensitivity (BAM drop hammer test). [f] friction sensitivity (BAM friction tester). [g] Electrostatic discharge sensitivity (OZM XSpark10). [h] DTA onset temperature of exothermic decomposition at a heating rate of 5 °C min−1. [i] Calculated enthalpy of formation (CBS-4M + atomization method). [j] Calculated mass related enthalpy of formation. [k] Energy of explosion. [l] Detonation temperature. [m] Volume of detonation products (assuming only gaseous products). [n] Detonation pressure at Chapman-Jouguet point. [o] Detonation velocity.

Hirshfeld surface analysis of compound **1** and AzMT (Figure 10), shows the intermolecular contacts for each type of atoms within the molecules. Here, generally destabilizing N···N, N···O, and O···O contacts are observed for compound **1**, contributing to the surface by 40 %. Contrary, stabilizing contacts such as O···H, and N···H make up 50 % of the Hirshfeld surface, showing a nearly equal distribution of destabilizing to stabilizing contacts for compound **1**. Additionally, all repulsive interactions exhibit very long distances of over 2.9 Å, while for the stabilizing interactions distances of 2.2 Å are observed. For AzMT the Hirshfeld surface consists of 29 %

destabilizing contacts, whereas attractive N···H contacts alone build up 63 % of the surface. Here, also long contact distances of over 3.0 Å are observed for the destabilizing contacts, with distances of 2.4 Å for the destabilizing contacts. Therefore, the stabilizing interactions in **1** seem to be a little stronger than in AzMT, which is correlating with the measured friction sensitivities, showing a more sensitive AzMT (2 N) than 1-NAMT (9 N). The same correlation is not observed for the impact sensitivity, which is mostly due to both compounds exhibiting sensitivities below the limit of measurement of 1 J. Therefore, no distinction between both compounds can be concluded based on their impact sensitivity. Differential thermal analysis (DTA) of compound **1** observed an endothermic event at 57 °C (Figure 11), which was confirmed as a melting point by a conducted thermal gravimetric analysis (TGA). The exothermic event happening in the DTA at 119 °C correlates to the decomposition temperature, confirmed by the TGA measurement, showing a major mass loss of 58.6% between 123–174 °C. Therefore, 1-NAMT is significantly less thermally stable compared to its azide analogous (167 °C) as well as compared to 1-NET (168 C).

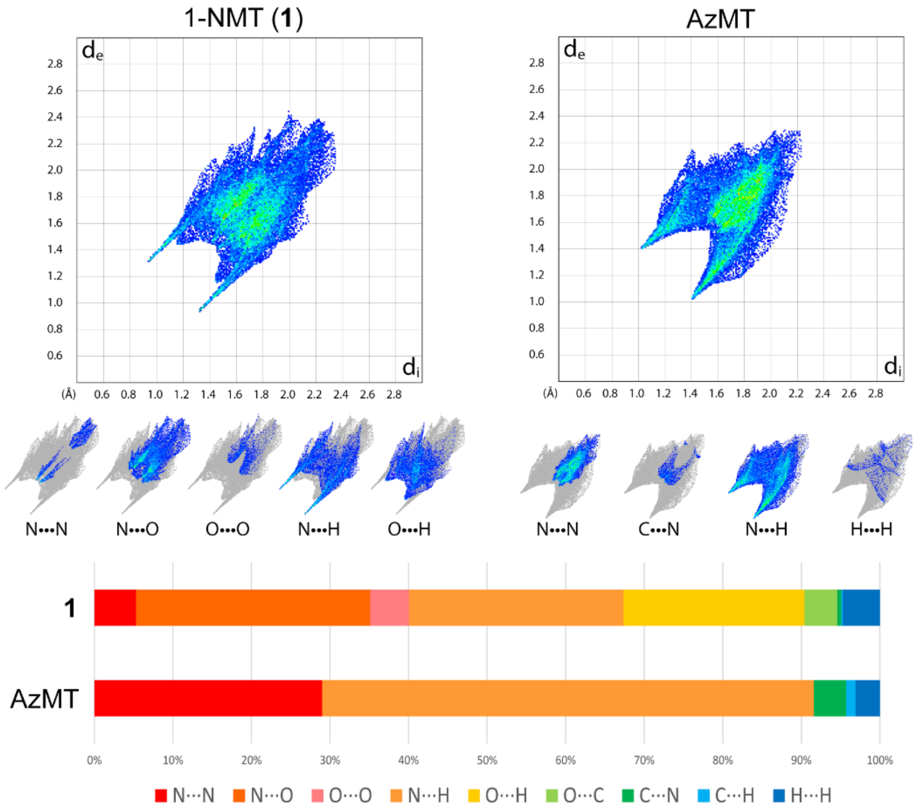

Figure 10. Hirshfeld analysis of compound **1** compared to AzMT. Stabilizing interactions observed in **1** are a shorter, hence stronger than in AzMT.

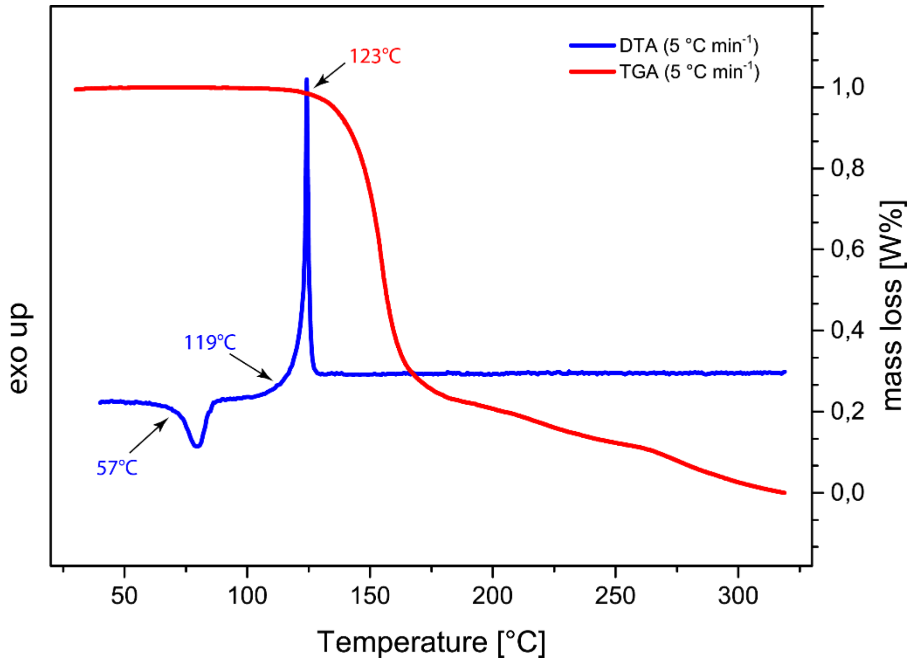

Figure 11. Combined DTA and TGA measurement of compound **1** with heating rates of 5 °C min^{-1}, exhibiting a melting of **1** at 57 °C and an exothermic decomposition at 119 °C.

Characterization of ECC. The thermal stabilities of all ECCs were analyzed by DTA measurements with a heating rate of $\beta = 5$ °C min^{-1}. Additionally, the sensitivities towards impact, friction and electrostatic discharge were measured according to BAM[27] standards (Table 2). Compound **2** exhibits an exothermic decomposition at 145 °C, while **3** and **4** exhibit exothermic decomposition temperatures of about 120 °C, which is equivalent to that of pure ligand **1**. Additionally, the DTA of **4** shows an endothermic event happening at 102 °C, which derives from a melting of the compound shortly before decomposition, which is confirmed by *Büchi* melting point analysis. For all nitroaromatic ECCs (**5**–**8**), exothermic decomposition, without any endothermic events happening before, was observed. Generally, a significant increase in stability of the ECCs compared to the pure ligand is observed for compounds **6**, **7**, and **8**. Compound **5** exhibits a thermal stability of 135 °C, which is rather low compared to those of **6** (176 °C), **7** (181 °C) and **8** (161 °C). This can be explained by the higher ligand to metal salt ratio of **5** (4:1) compared to the other nitroaromatic compounds (2:1). Therefore, the overall low thermal stability of 1 is inherited to the resulting ECC. On the other hand, the more balanced (2:1) ratio of ligand to metal salt of compounds **6**–**8**, leads to a stabilization of the low thermal stability of **1** by the nitroaromatic anions, which is contrary to previous findings[11, 23, 28]. While a stabilizing effect was previously observed for some cases[28], it was never as significant as in this study. The drastic increase in thermal stability is most likely owing to the low thermal stability of **1**, resulting in high relative differences between the pure ligand and the resulting ECCs.

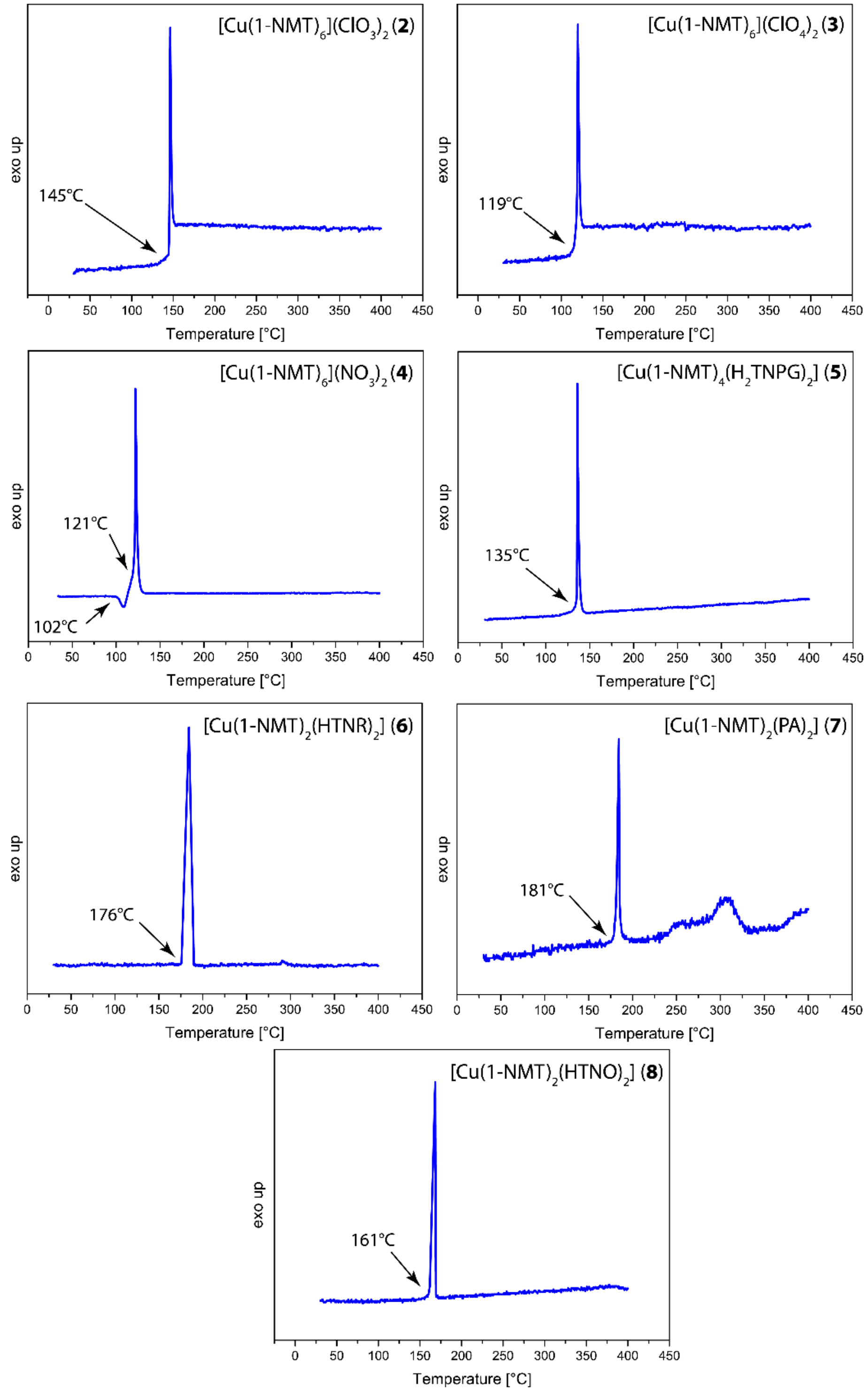

Figure 12. Differential thermal analysis of ECCs **2**–**8** with heating rate of 5 °C min^{-1}.

Following an increment method by Ilyushin[29], it was possible to estimate the detonation velocities of all ECCs, except for **2**, due to the unavailability of data for chlorate anions (Table 2). Detailed information can be found in the Supporting Information. Overall, a slight decrease in detonation velocity compared to the pure ligand is observed. Compounds **3** and **4** exhibit velocities between 7800–7900 m s^{-1}, which is about 300 m s^{-1} slower than pure **1**. Generally, for the nitroaromatic ECCs **5** – **8** a more distinct decrease is observed. Compounds **6** and **7** have estimated detonation velocities of below 7800 m s^{-1}, while for **8** a velocity of 7500 m s^{-1} was calculated. Interestingly, **5** shows the highest estimated detonation velocity (7918 m s^{-1}) by far surpassing the other nitroaromatic ECCs. Due to the incremental method, a higher contribution of ligand **1** to the detonation velocity is introduced, since the ligand to metal salt ratio differs between **5** (4:1) and **6**–**8** (2:1). Overall, all herein synthesized compounds outperform lead azide (6187 m s^{-1}) as well as lead styphnate (6137 m s^{-1}) by at least 21%.

Sensitivities. According to the UN Recommendation on the Transport of Dangerous Goods[30] compound **1** has to be classified as extremely sensitive with an impact sensitivity of <1 J and a friction sensitivity of 9 N. It is significantly more sensitive towards an electrostatic discharge (150 mJ) compared to AzMT (540 mJ) but less sensitive than typical primaries such as lead azide (Table 2). Compound **2**–**8** are also extremely sensitive towards impact, all exhibiting a sensitivity <1 J, except compound **3**, having an impact sensitivity of 2 J. Therefore, all ECCs exhibit a higher impact sensitivity than lead azide (LA) or lead styphnate (LS). While no clear trend in stability is deriving from the impact sensitivities, the formation of ECCs **2**–**4** results in compounds distinctively more sensitive towards friction than pure compound **1**. While all three compounds are classified as extremely sensitive towards friction, the nitrate compound **4** (5 N), is less sensitive than the chlorate (**2**, 0.4 N) and perchlorate (**3**, 0.75 N) compound, which are on par with LA and LS. The ECCs containing nitroaromatic anions, on the other hand, show a stabilization of **1**, as their friction sensitivities are lowered compared to pure **1**. Interestingly, compound **5** (72 N) is less sensitive than compound **6** (40 N), which is contrary to the higher amount of 1-NAMT in compound **5** than in **6**. While compound **8** exhibits a friction sensitivity (84 N) comparable to that of **5**, compound **7** (120 N) exhibits the lowest friction sensitivity of all herein analyzed compounds, highlighting the high stability of the picrate anion. All ECC exhibit an ESD sensitivity (90–160 mJ) comparable to pure **1** (150 mJ), the only exception being compound **4** exhibiting a sensitivity of 13 mJ. Nonetheless, all compounds are less sensitive than LA (5–8 mJ) or LS (0.04–1 mJ).[31, 32]

Table 2. Overview of the thermal stability and sensitivity toward external stimuli.

Compound		$T_{\text{endo.}}$ [°C][a]	$T_{\text{exo.}}$ [°C][b]	*IS* [J][c]	*FS* [N][d]	*ESD* [mJ][e]	V_{det} [m s^{-1}][f]
1-NAMT	1	57	119	<1	9	150	8294
[Cu(1-NAMT)$_6$](ClO$_3$)$_2$	2	–	145	<1	0.4	139	–[h]
[Cu(1-NAMT)$_6$](ClO$_4$)$_2$	3	–	119	2	0.75	13	7910[h]
[Cu(1-NAMT)$_6$](NO$_3$)$_2$	4	102	121	<1	5	90	7865[h]
[Cu(1-NAMT)$_4$(H$_2$TNPG)$_2$]	5	–	135	<1	72	160	7918[h]
[Cu(1-NAMT)$_2$(HTNR)$_2$]	6	–	176	<1	40	140	7715[h]
[Cu(1-NAMT)$_2$(PA)$_2$]	7	–	181	<1	120	90	7767[h]
[Cu(1-NAMT)$_2$(HTNO)$_2$]	8	–	161	<1	84	90	7507[h]
LA[33, 34]		–	320–350	4	≤0.1	5–8	6187[g]
LS[33, 34]		–	260–310	8	0.45	0.04–1	6138[g]

[a] endothermic peak, which indicates melting of the substance; [b] exothermic peak, which indicates decomposition; [c] impact sensitivity (BAM drop hammer test); [d] friction sensitivity (BAM friction tester); [e] electrostatic discharge sensitivity (OZM XSpark10); [f] Details can be found in the ESI. [g] calculated with Explo5_V6.05.04.

Initiation capabilities. To get an insight into the behavior of the sample towards fast heating with and without confinement, hot plate (HP) and hot needle (HN) tests were performed. These tests allow for a first evaluation of their capability to be applied as primary explosives. Detailed procedures for HP and HN tests are given in the Supporting Information. While the HP reflects on the behavior towards fast heating without confinement, the HN test allows for an assessment of the compound's behavior upon fast heating with confinement. Table 3 summarizes the results from HN and HP tests of all compounds. Here, all compounds showed deflagration, except compound **2** showing detonation. Thus only **2** exhibits detonation behavior which is crucial to be applied as detonating primary explosives.

Table 3. Results from HN, HP, and initiation tests.

Compound	HP	HN
2	def.	det.
3	def.	def.
4	def.	def.
5	def.	def.
6	def.	def.
7	def.	def.
8	def.	def.

def. = deflagration; det. = detonation

While HP and HN tests asses the susceptibility towards initiation by heat and flame, the possibility of ignition by laser impulse cannot be concluded and was additionally tested (Table 4). All ECCs were directly irradiated by a single-pulsed 45 W InGaAs laser diode. About 25 mg of each compound was pressed into a transparent polycarbonate percussion cap and sealed with UV curing adhesive. The sample was placed in the focused beam path and irradiated with a single laser pulse with a wavelength of 915 nm, a voltage of 4 V, a current of 6–7 A, and a pulse length of 0.1, 1.0, 15, or 30 ms. The results of these experiments are listed in Table 4.

Table 4. Results of laser initiation of compounds 2–8.

Compound	6 A	7 A		
2	τ = 0.1 ms x	τ = 0.1 ms det.	τ = 1 ms det.	–
3	–	τ = 0.1 ms det.	–	–
4	τ = 0.1 ms x	τ = 0.1 ms det.	–	–
5	τ = 0.1 ms x	τ = 1 ms def.	τ = 15 ms def.	τ = 30 ms def.
6	–	τ = 1 ms def.	τ = 15 ms def.	τ = 30 ms def.
7	–	τ = 1 ms x	τ = 15 ms x	τ = 30 ms x
8	–	τ = 1 ms dec.	τ = 15 ms dec.	τ = 30 ms dec.

Operating parameters: current I = 6 and 7 A; voltage U = 4 V; theoretical maximum output power P_{max} = 45 W; theoretical energy E_{max} = 0.1–17 mJ; wavelength λ = 915 nm; pulse length τ = 0.1–1 ms. (– = not tested; x = no ignition; dec. = decomposition; def. = deflagration; det. = detonation).

While compounds **2**–**4** exhibited no ignition at the lowest tested energy of 0.1 mJ, strong detonations were observed for all compounds already at 1.7 mJ, strong enough to destroy parts of the laser setup. The moment of detonation of compound **2** is shown in Figure 13A. Compound **5** showed no ignition at the lowest tested energy, and therefore this energy was not tested for all other nitroaromatic compounds. Nevertheless, **5** and **6** showed deflagrations already at 17 mJ (Figure 13B/C), as well as at 255 and 510 mJ. Compound **7** shows no ignition at any of the tested energies (17, 255, and 510 mJ) which derives from the lower energetic character of the picrate anions compared to the styphnate and trinitrophloroglucinate anions. Compound **8** shows a slow burning of the material at all tested energies (Figure 13D). Due to the substitution of one hydroxy group of each trinitrophloroglucinate anion by methylene groups, the resulting ECC is lacking energetic performance, thus a self-sustained deflagration is not observed, which is additionally accompanied by the formation of soot.

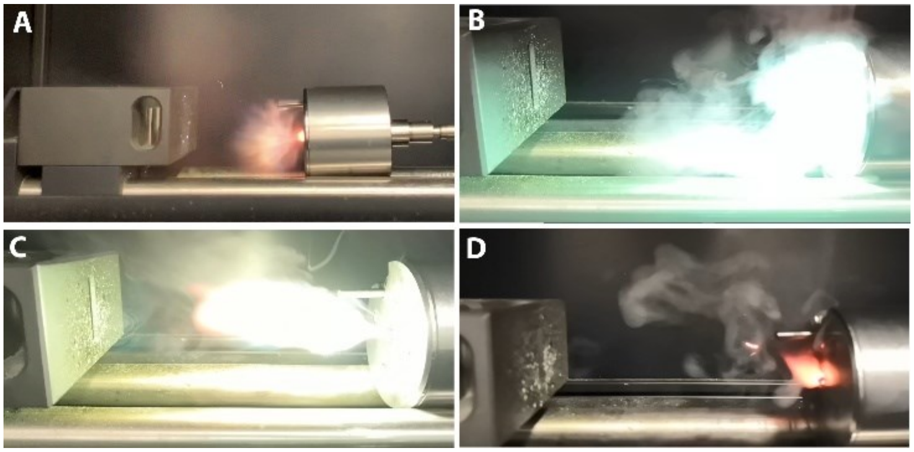

Figure 13. A: Moment of detonation of compound **2** at 1.7 mJ; B/C: moments of deflagration of compounds **5** and **6**; D: burning of compound **8**.

5.3 Conclusion

The synthesis of 1-(Nitratomethyl)tetrazole (1-NAMT, **1**) was possible by the nitration of the literature known isomeric mixture of 1- and 2-(Hydroxymethyl)tetrazole with acetyl nitrate in moderate yield (21 %). 1-NAMT was investigated by low temperature single crystal X-ray diffraction experiments, multinuclear ^{1}H, ^{13}C, ^{14}N NMR spectroscopy as well as elemental analysis and infrared spectroscopy. Differential thermal analysis observed a rather low thermal stability of **1** (119 °C) while BAM sensitivity measurements revealed a high impact (<1 J) and friction (9 N) sensitivity, both in the range of typical primary explosives. Comparing the molecular interactions of **1** with its structural analogous azide (AzMT) on the basis of Hirshfeld analysis, showed stronger stabilizing interactions for **1**, ultimately explaining the differences in friction sensitivities. **1** was further used as ligand for the formation of seven energetic coordination compounds of copper(II) chlorate (**2**), perchlorate (**3**), nitrate (**4**), trinitro phloroglucinolate (**5**), styphnate (**6**), picrate (**7**) and trinitro-orcinolate (**8**). All ECCs were obtained pure according to elemental analysis and were further analyzed by low temperature single crystal X-ray diffraction experiments, accompanied by differential thermal analysis, infrared spectroscopy and their sensitivities towards external stimuli (IS, FS, and ESD) were measured according to BAM standards. For all ECCs an extremely high impact sensitivity of <1–2 J was observed, while compounds **2**–**4** exhibited increased friction sensitivities (0.4–5 N) compared to pure **1**. The nitroaromatic containing ECCs **5**–**8** exhibited friction sensitivities (40–120 N) in the range of a booster explosive. The thermal stabilities of **2**–**5** are in the same range (119–145 C) as the thermal stability of **1**. Interestingly, the formation of ECCs **6**–**8** led to a drastic increase of the thermal stability of **1**. Hot plate and needle tests revealed deflagration of all compounds, except for **2** showing a violent detonation in the hot needle test. Thus only **2** exhibits a fast DDT, which is necessary to be discussed as primary explosive. Further assessment of laser initiability was positive for compounds **2**–**4** already at low energies (1.7 mJ), while the nitroaromatic compounds showed deflagration or burning at all tested energies. Lastly, detonation velocity predictions suggested velocities of up to 7900 m s^{-1} for all ECCs investigated in this study.

5.4 Acknowledgement

Financial support of this work by the Ludwig Maximilian University of Munich (LMU), the Office of Naval Research (ONR) under grant no. N00014-19-1-2078 is gratefully acknowledged. The authors want to further thank Stefan Huber for sensitivity measurements.

Keywords: Tetrazoles, Nitrate esters, Energetic Coordination Compounds, Laser Initiation, N-Ligands

5.5 References

[1] J. D. Watson, F. H. C. Crick, *Nature* **1953,** *171*, 737-738.

[2] G. Thews, Atemgastransport und Säure-Basen-Status des Blutes. In *Physiologie des Menschen*, Eds. Springer Berlin Heidelberg: Berlin, Heidelberg, **1993**.

[3] P. Schwab, R. H. Grubbs, J. W. Ziller, *J. Am. Chem. Soc.* **1996,** *118*, 100-110.

[4] M. Scholl, S. Ding, C. W. Lee, R. H. Grubbs, *Org. Lett.* **1999,** *1*, 953-956.

[5] D. C. Hodgkin, J. Kamper, M. Mackay, J. Pickworth, K. N. Trueblood, J. G. White, *Nature* **1956,** *178*, 64-66.

[6] T. M. Klapötke, *Chemistry of High-Energy Materials*. De Gruyter: **2019**.

[7] M. A. Ilyushin, I. V. Tselinsky, I. V. Bachurina, L. O. Novoselova, E. N. Konyushenko, A. S. Kozlov, Y. A. Gruzdev, *AIP Conference Proceedings* **2006,** *849*, 213-217.

[8] T. M. Klapötke, M. Kofen, L. Schmidt, J. Stierstorfer, M. H. H. Wurzenberger, *Chem. Asian J.* **2021,** *16*, 3001-3012.

[9] M. Kofen, M. Lommel, J. Stierstorfer, T. M. Klapötke, *New Trends in Research of Energetic Materials*, Pardubice, Czech Republic, **2022**; pp 114 - 118.

[10] N. Szimhardt, M. H. H. Wurzenberger, L. Zeisel, M. S. Gruhne, M. Lommel, J. Stierstorfer, *J. Mater. Chem. A* **2018,** *6*, 16257-16272.

[11] M. Kofen, M. Lommel, M. H. H. Wurzenberger, T. M. Klapötke, J. Stierstorfer, *Chem. Eur. J.* **2022,** *28*, e202200492.

[12] V. A. Ostrovskii, R. E. Trifonov, E. A. Popova, *Russ. Chem. Bull., Int. Ed.* **2012,** *61*, 768–780.

[13] A. E. Popova, V. A. Protas, E. R. Trifonov, *Anti-Cancer Agents Med. Chem.* **2017,** *17*, 1856–1868.

[14] S.-Q. Wang, Y.-F. Wang, Z. Xu, *Eur. J. Med. Chem.* **2019,** *170*, 225–234.

[15] N. Szimhardt, M. H. H. Wurzenberger, A. Beringer, L. J. Daumann, J. Stierstorfer, *J. Mater. Chem. A* **2017**, *5*, 23753–23765.

[16] M. A. Ilyushin, A. N. Terpigorev. I. V. Tselinskii, *Russ. J. Gen. Chem.* **1999,** *69*, 1645-1657.

[17] M. S. Gruhne, T. Lenz, M. Rösch, M. Lommel, M. H. H Wurzenberger, T. M. Klapötke, J. Stierstorfer, *Dalton Transactions* **2021,** *50*, 10811-10825.

[18] O. N. Verkhozina, V. N. Kizhnyaev, L. I. Vereshchagin, A. V. Rokhin, A. I. Smirnov, *Russ. J. Org. Chem.* **2003,** *39*, 1792-1796.

[19] T. M. Klapötke, M. Kofen, J. Stierstorfer, *Dalton Trans.* **2021,** *50*, 13656-13660.

[20] Y. Li, W. Liu, S. Pang, *Molecules* **2012,** *17*, 5040-5049.

[21] A. R. Katritzky, C. N. Fali, I. V. Shcherbakova, S. V. Verin, *J. Heterocycl. Chem.* **1996,** *33*, 335-339.

[22] M. H. H Wurzenberger, N. Szimhardt, J. Stierstorfer, *J. Am. Chem. Soc.* **2018,** *140*, 3206-3209.

[23] M. H. H. Wurzenberger, M. S. Gruhne, M. Lommel, N. Szimhardt, T. M. Klapötke, J. Stierstorfer, *Chem. Asian J.* **2019,** *14*, 2018-2028.

[24] E. C. Johnson, J. J. Sabatini, D. E. Chavez, R. C. Sausa, E. F. C Byrd, L. A. Wingard, P. E. Guzmàn, *Org. Process Res. Dev.* **2018,** *22*, 736-740.

[25] M. Sućeska, *Propellants Explos. Pyrotech.* **1991,** *16*, 197–202.

[26] M. Sućeska, *Explo5 V6.05.02*, Zagreb (Croatia), **2018**.

[27] BAM www.bam.de (accessed March 2022).

[28] M. H. H. Wurzenberger, B. R. G. Bissinger, M. Lommel, M. S. Gruhne, N. Szimhardt, J. Stierstorfer, *New J. Chem.* **2019,** *43*, 18193-18202.

[29] M. A. Ilyushin, A. V. Smirnov, A. A. Kotomin, I. V. Tselinskii, *J. Energ. Mater.* **1994,** *2*, 16-20.

[30] W. Beck, J. Evers, M. Göbel, G. Oehlinger, T. M. Klapötke, *Z. Anorg. Allg. Chem.* **2007,** *633*, 1417–1422.

[31] M. B. Talawar, A. P. Agrawal, M. Anniyappan, D. S. Wani, M. K. Bansode, G. M. Gore, *J. Hazard. Mat.* **2006,** *137*, 1074–1078.

[32] K. Raha, J. S. Chhabra, *J. Hazard. Mat.* **1993,** *34* (3), 385–391.

[33] T. M. Klapötke, *Energetic Materials Encyclopedia*. 2nd ed.; DeGruyter: Berlin/Boston, **2021**; Vol. 1–3.

[34] M. S. Gruhne, M. Lommel, M. H. H Wurzenberger, N. Szimhardt, T. M. Klapötke, J. Stierstorfer, *Propellants Explos. Pyrotech.* **2020,** *45* (1), 147–153.

5.6 Supporting Information

5.6.1 Overview of Compounds

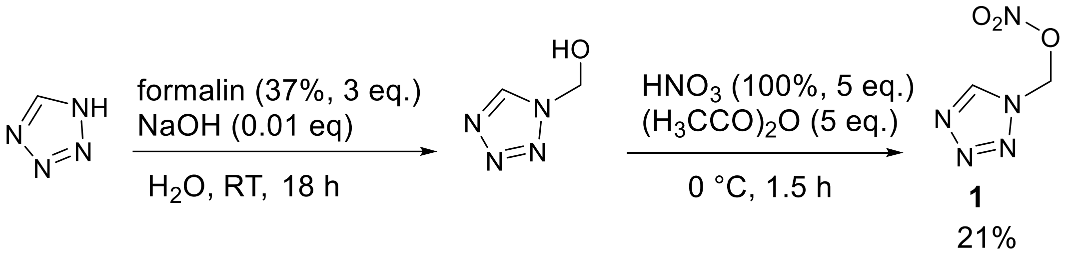

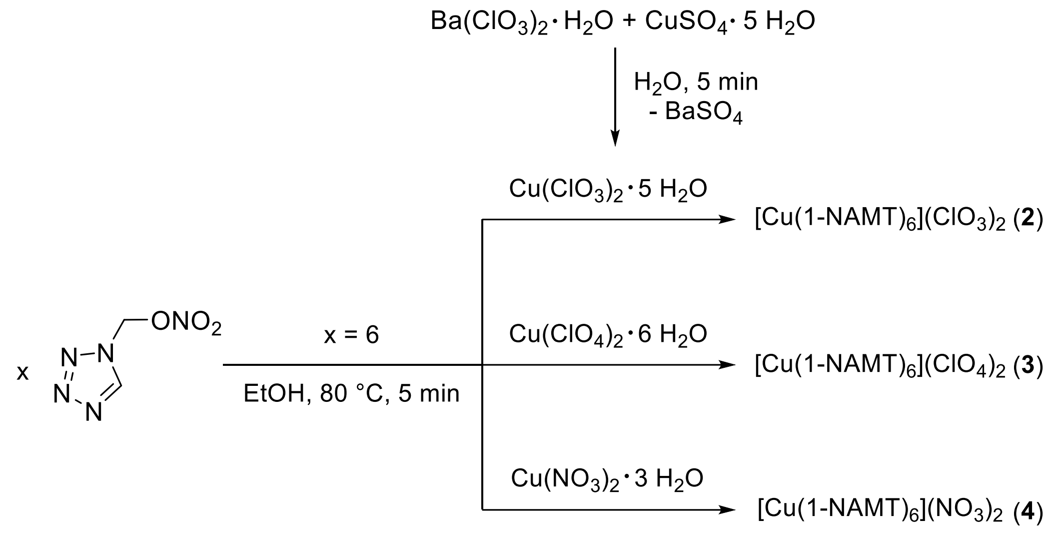

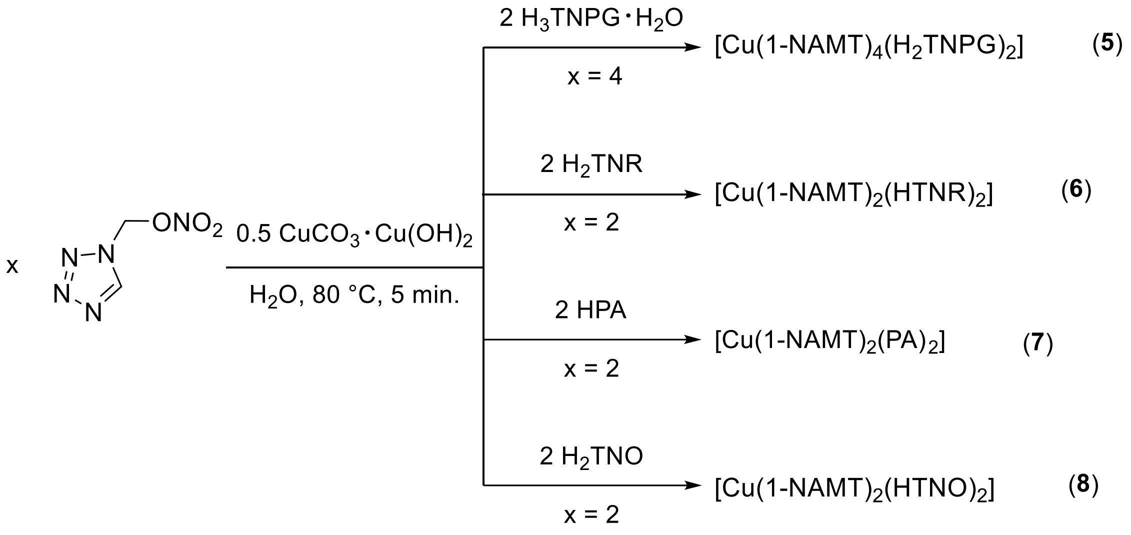

5.6.2 Single Crystal X-Ray Diffraction

For all crystalline compounds an Oxford Xcalibur3 diffractometer with a CCD area detector or Bruker D8 Venture TXS diffractometer equipped with a multilayer monochromator, a Photon 2 detector, and a rotating-anode generator were employed for data collection using Mo-K_α radiation (λ = 0.7107 Å). On the Oxford device, data collection and reduction were carried out using the CrysAlisPRO software.[S1] On the Bruker diffractometer, the data were collected with the Bruker Instrument Service v3.0.21, the data reduction was performed using the SAINT V8.18C software (Bruker AXS Inc., 2011). The structures were solved by direct methods (SIR-92,[S2] SIR-97,[S3,S4] SHELXS-97[S5,S6] or SHELXT[S7]), refined by full-matrix least-squares on $F2$ (SHELXL[S5,S6]) and finally checked using the PLATON software[S8] integrated in the WinGX[S7,S9] or Olex2[S8] software suite. The non-hydrogen atoms were refined anisotropically and the hydrogen atoms were located and freely refined. The absorptions were corrected by a SCALE3 ABSPACK or SADABS Bruker APEX3 multi-scan method.[S11,S12] All DIAMOND2 plots are shown with thermal ellipsoids at the 50% probability level and hydrogen atoms are shown as small spheres of arbitrary radius.

Table S1. Crystallographic data and structure refinement details for compounds **1 – 3.**

	1	**2**	**3**
Formula	$C_2H_3N_5O_3$	$C_{12}H_{18}CuN_{30}O_{24}Cl_2$	$C_{12}H_{18}CuN_{30}O_{26}Cl_2$
FW [g mol^{-1}]	145.09	1101.00	1133.00
Crystal system	orthorhombic	trigonal	trigonal
Space group	$P2_12_12_1$ (No. 19)	*R*-3 (No.148)	R-3 (No.148)
Color / Habit	colorless platelet	blue platelet	colorless block
Size [mm]	0.02 x 0.09 x 0.10	0.05 x 0.30 x 0.35	0.02 x 0.03 x 0.04
a [Å]	6.8187(3)	10.5825(7)	10.5929(5)
b [Å]	8.4487(4)	10.5825(7)	10.5929(5)
c [Å]	9.6666(4)	31.031(4)	31.436(3)
α [°]	90	90	90
β [°]	90	90	90
γ [°]	90	120	120
V [Å^3]	556.89(4)	3009.6(6)	3054.8(5)
Z	4	3	3
$\rho_{calc.}$ [g cm^{-3}]	1.731	1.822	1.848
μ [mm^{-1}]	0.158	0.803	0.797
F(000)	296	1665	1713
$\lambda_{MoK\alpha}$ [Å]	0.71073	0.71073	0.71073
T [K]	102	111	107
θ Min-Max [°]	3.2, 26.4	2.3, 26.3	2.6, 25.4
Dataset	-8:8; -10:10; -12:12	-13:13; -10:13; -38:36	-12:12; -12:12; -37:37
Reflections collected	8145	8370	16560
Independent refl.	1138	1359	1253
R_{int}	0.030	0.041	0.064
Observed reflections	1090	1101	1032
Parameters	91	117	120
R_1 (obs)[a]	0.0257	0.0318	0.0529
wR_2 (all data)[b]	0.0637	0.0838	0.1352
S [c]	1.14	1.06	1.13
Resd. dens [e Å^{-3}]	-0.17, 0.20	-0.21, 0.37	-0.38, 1.41
Device type	Bruker D8 Venture TXS	Oxford Xcalibur3	Bruker D8 Venture TXS
Solution	SHELXT	SHELXT	SHELXT
Refinement	SHELXL-2018	SHELXL-2018	SHELXL-2018
Absorption correction	multi-scan	multi-scan	multi-scan

---

[a]R1 = Σ||F0|−|Fc||/Σ|F0|; [b]wR2 = [Σ[w(F02−Fc2)2]/Σ[w(F0)2]]1/2; w = [σc2(F02)+(xP)2+yP]−1 and P=(F02+2Fc2)/3; [c]S = {Σ[w(Fo2−Fc2)2]/(n−p)}1/2 (n = number of reflections; p = total number of parameters).

Table S2. Crystallographic data and structure refinement details for compounds **4 – 6.**

	4	**5**	**6**
Formula	$C_{12}H_{18}CuN_{32}O_{24}$	$C_{20}H_{16}CuN_{26}O_{30}$	$C_{16}H_{10}CuN_{16}O_{22}$
FW [g mol^{-1}]	1058.12	1164.13	841.94
Crystal system	Trigonal	triclinic	triclinic
Space group	*R*-3 (No.148)	*P*-1 (No. 2)	*P*-1 (No. 2)
Color / Habit	blue block	green block	green block
Size [mm]	0.04 x 0.06 x 0.07	0.10 x 0.25 x 0.50	0.30 x 0.62 x 0.76
a [Å]	10.5666(3)	8.9582(5)	6.2404(6)
b [Å]	10.5666(3)	10.8979(6)	10.9239(10)
c [Å]	30.1912(19)	11.4623(6)	11.0430(11)
α [°]	90	88.678(4)	87.784(8)
β [°]	90	73.117(5)	73.859(9)
γ [°]	120	69.752(5)	86.409(8)
V [Å^3]	2919.3(3)	1000.87(11)	721.52(12)
Z	3	1	1
$\rho_{calc.}$ [g cm^{-3}]	1.806	1.931	1.938
μ [mm^{-1}]	0.692	0.690	0.887
F(000)	1605	587	423
$\lambda_{MoK\alpha}$ [Å]	0.71073	0.71073	0.71073
T [K]	106	101	103
θ Min-Max [°]	3.5, 28.3	2.5, 26.4	2.7, 26.4
Dataset	-14:14; -14:14; -40:40	-11:11; -13:13; -14:14	-6:7; -13:13; -13:13
Reflections collected	23575	11632	4860
Independent refl.	1623	4103	2935
R_{int}	0.039	0.040	0.024
Observed reflections	1463	3204	2573
Parameters	204	370	251
R_1 (obs)[a]	0.0465	0.0431	0.0359
wR_2 (all data)[b]	0.1163	0.1059	0.0942
S [c]	1.06	1.03	1.05
Resd. dens [e Å^{-3}]	-0.46, 0.44	-0.58, 0.40	-0.39, 0.70
Device type	Bruker D8 Venture TXS	Oxford Xcalibur3	Oxford Xcalibur3
Solution	SHELXT	SHELXT	SHELXT
Refinement	SHELXL-2018	SHELXL-2018	SHELXL-2018
Absorption correction	multi-scan	multi-scan	multi-scan

---

[a]$R_1 = \Sigma||F_0|-|F_c||/\Sigma|F_0|$; [b]$wR_2 = [\Sigma[w(F_0^2-F_c^2)^2]/\Sigma[w(F_0)^2]]^{1/2}$; $w = [\sigma c^2(F_0^2)+(xP)^2+yP]^{-1}$ and $P=(F_0^2+2F_c^2)/3$; [c]$S = \{\Sigma[w(F_o^2-F_c^2)^2]/(n-p)\}^{1/2}$ (n = number of reflections; p = total number of parameters).

Table S3. Crystallographic data and structure refinement details for compound **7 – 8**.

	7	**8**
Formula	$C_{16}H_{10}CuN_{16}O_{20}$	$C_{18}H_{14}CuN_{16}O_{22}$
FW [g mol^{-1}]	809.94	869.99
Crystal system	monoclinic	triclinic
Space group	$P2_1/c$ (No. 14)	P-1 (No. 2)
Color / Habit	green plate	green plate
Size [mm]	0.11 x 0.44 x 0.86	0.10 x 0.50 x 0.50
a [Å]	10.0938(5)	6.2429(4)
b [Å]	16.9067(8)	11.0903(6)
c [Å]	8.0880(4)	11.2709(7)
α [°]	90	87.832(5)
β [°]	94.911(5)	74.073(6)
γ [°]	90	87.494(5)
V [Å^3]	1375.17(12)	749.40(8)
Z	2	1
$\rho_{calc.}$ [g cm^{-3}]	1.956	1.928
μ [mm^{-1}]	0.921	0.857
F(000)	814	439
$\lambda_{MoK\alpha}$ [Å]	0.71073	0.71073
T [K]	123	101
θ Min-Max [°]	2.0, 26.4	2.6, 26.4
Dataset	-12:12; -21:21; -10:10	-7:7; -12:13; -14:12
Reflections collected	20148	5684
Independent refl.	2803	3055
R_{int}	0.055	0.019
Observed reflections	2311	2715
Parameters	241	261
R_1 (obs)[a]	0.0569	0.0339
wR_2 (all data)[b]	0.1293	0.0830
S [c]	1.09	1.04
Resd. dens [e Å^{-3}]	-0.51, 1.51	-0.28, 0.43
Device type	Oxford Xcalibur3	Oxford Xcalibur3
Solution	SHELXT	SHELXT
Refinement	SHELXL-2018	SHELXL-2018
Absorption correction	multi-scan	multi-scan

---

[a] $R_1 = \Sigma||F_0|-|F_c||/\Sigma|F_0|$; [b] $wR_2 = [\Sigma[w(F_0^2-F_c^2)^2]/\Sigma[w(F_0)^2]]^{1/2}$; $w = [\sigma c^2(F_0^2)+(xP)^2+yP]^{-1}$ and $P=(F_0^2+2F_c^2)/3$; [c] $S = \{\Sigma[w(F_o^2-F_c^2)^2]/(n-p)\}^{1/2}$ (n = number of reflections; p = total number of parameters).

5.6.3 Computations

All calculations were carried out using the Gaussian G09 program package.[S13] The enthalpies (H) and free energies (G) were calculated using the complete basis set (CBS) method of Petersson and coworkers in order to obtain very accurate energies. The CBS models use the known asymptotic convergence of pair natural orbital expressions to extrapolate from calculations using a finite basis set to the estimated complete basis set limit. CBS-4 begins with a HF/3-21G(d) geometry optimization; the zero point energy is computed at the same level. It then uses a large basis set SCF calculation as a base energy, and a MP2/6-31+G calculation with a CBS extrapolation to correct the energy through second order. A MP4(SDQ)/6-31+(d,p) calculation is used to approximate higher order contributions. In this study we applied the modified CBS-4M method (M referring to the use of minimal population localization) which is a re-parametrized version of the original CBS-4 method and also includes some additional empirical corrections. The enthalpies of the gas-phase species M were computed according to the atomization energy method (E1) (Table S4 & 5).[S13–18]

$$\Delta_f H°_{(g,\ M,\ 298)} = H_{(\mathrm{Molecule},\ 298)} - \sum H°_{(\mathrm{Atoms},\ 298)} + \sum \Delta_f H°_{(\mathrm{Atoms},\ 298)} \qquad \text{(E1)}$$

Table S4. Literature values for atomic $\Delta H°_f{}^{298}$ / kcal mol^{-1}

	$-H^{298}$ [a.u.]	NIST[S19]
H	0.50091	52.1
C	37.786156	171.3
N	54.522462	113.0
O	74.991202	59.6

The gas-phase heat of formations were converted to the solid/liquid state ones for neutrals: by subtracting the vaporization/sublimation enthalpies (calculated using the Trouton rule)[S20,21] The calculation results are summarized in Table S7.

$$\Delta U_m = \Delta H_m - \Delta n\ R\ T \qquad \text{(E2)}$$

Table S5. CBS-4M results, Gas phase enthalpies of formation, calculated sublimation/vaporization enthalpies and solid-state heat of formation.

Compound	$-H^{298}$ / a.u.	$\Delta_f H°$(g) / kJ mol^{-1}	$\Delta_{s/v}H°$/ kJ mol^{-}	V_m / nm^3	Δn
1	–576.542850	258.0	70.7162		*–5.5*

5.6.4 NMR Spectroscopy

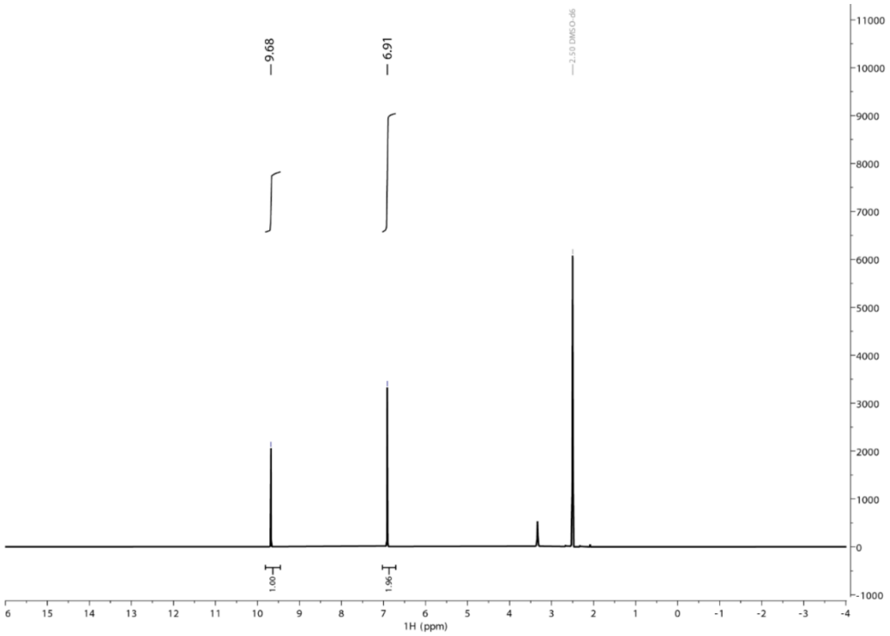

Figure S1. ^{1}H NMR of **1** in DMSO-d$_6$.

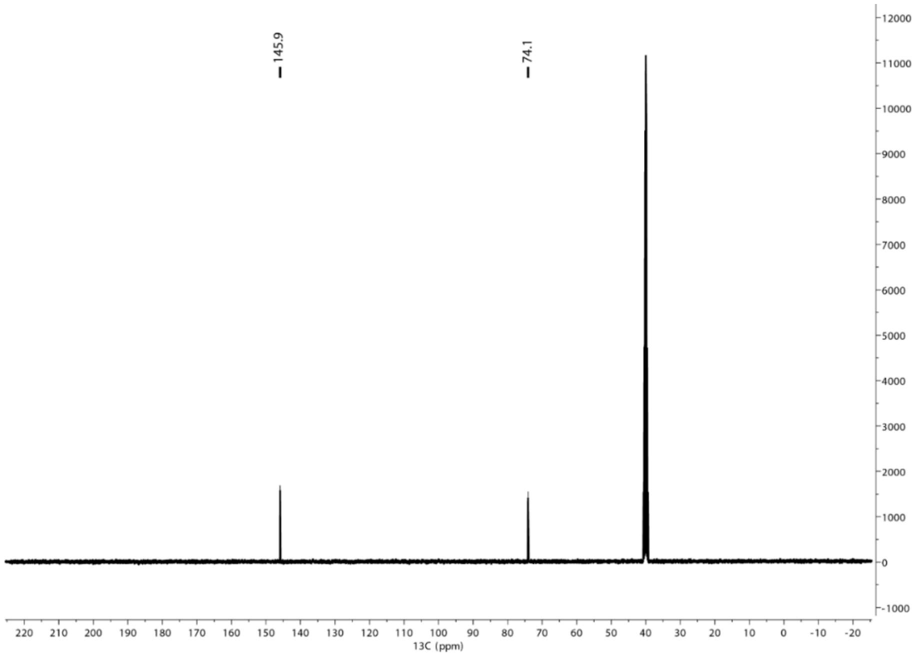

Figure S2. ^{13}C NMR of **1** in DMSO-d$_6$.

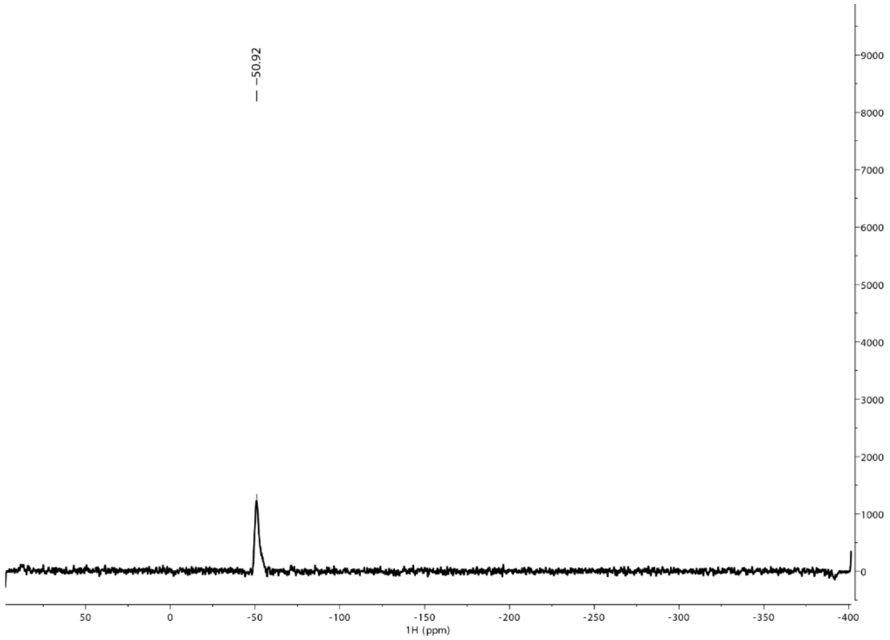

Figure S3. ^{14}N NMR of **1** in DMSO-d$_6$.

5.6.5 IR Spectroscopy

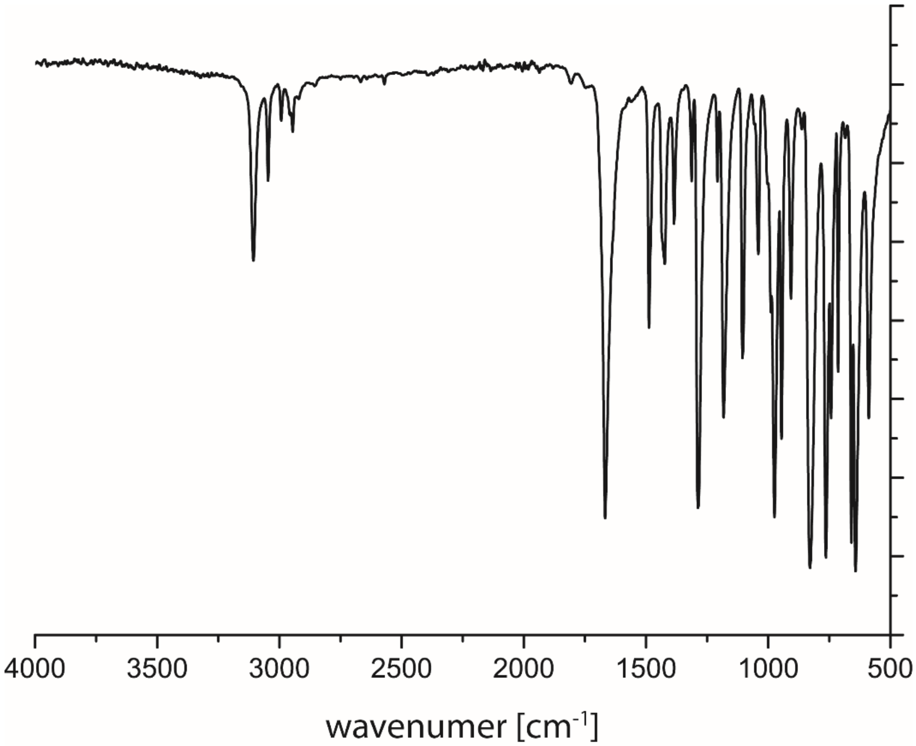

Figure S4. IR spectrum of compound **2**.

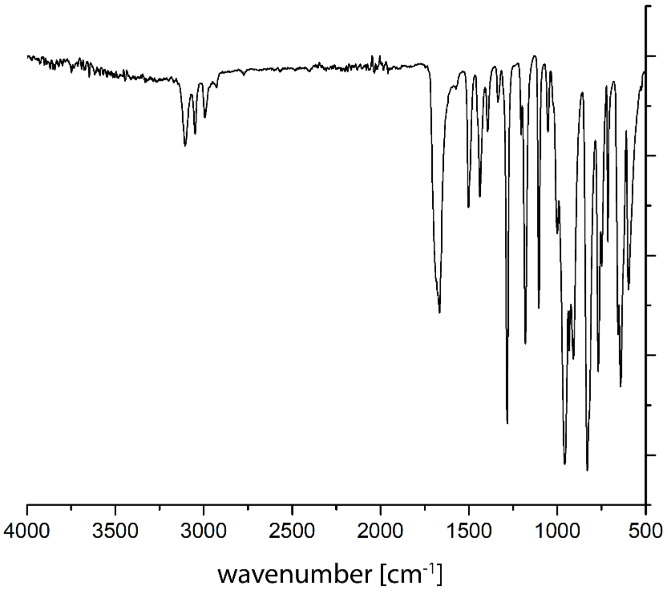

Figure S5. IR spectrum of compound **2**.

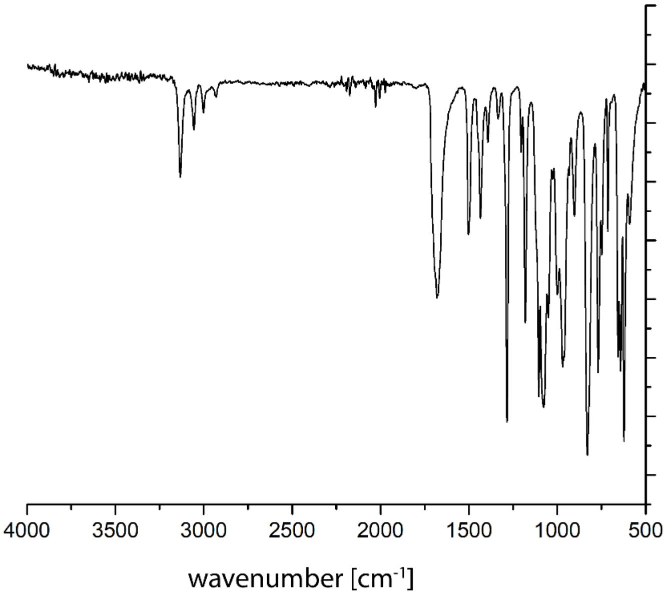

Figure S6. IR spectrum of compound **3**.

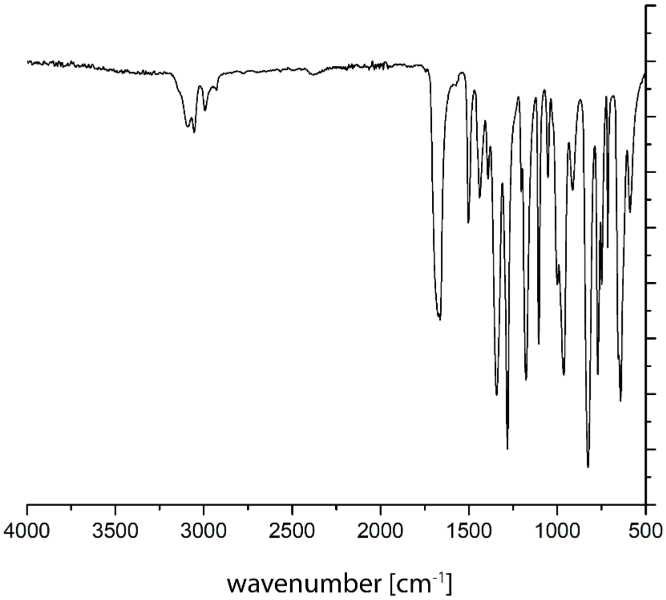

Figure S7. IR spectrum of compound **4**.

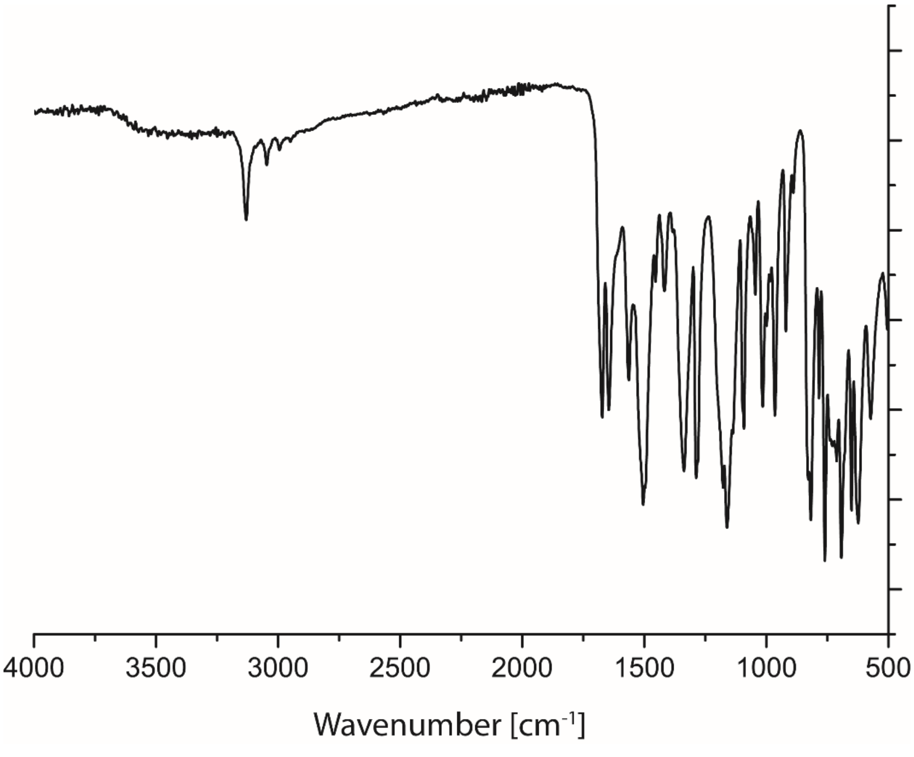

Figure S8. IR spectrum of compound **5**.

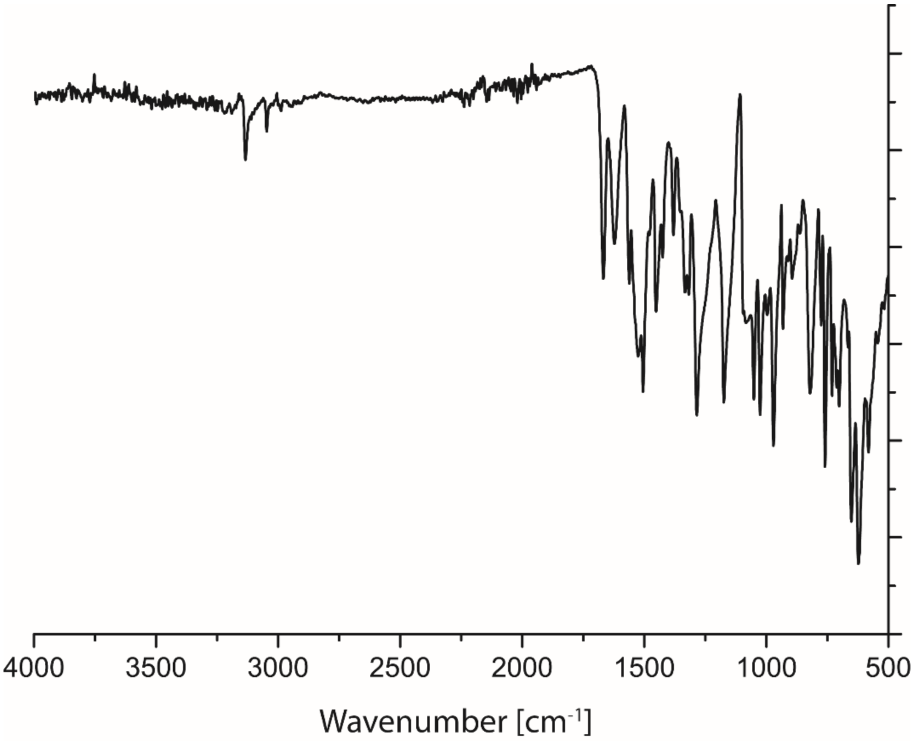

Figure S9. IR spectrum of compound **6**.

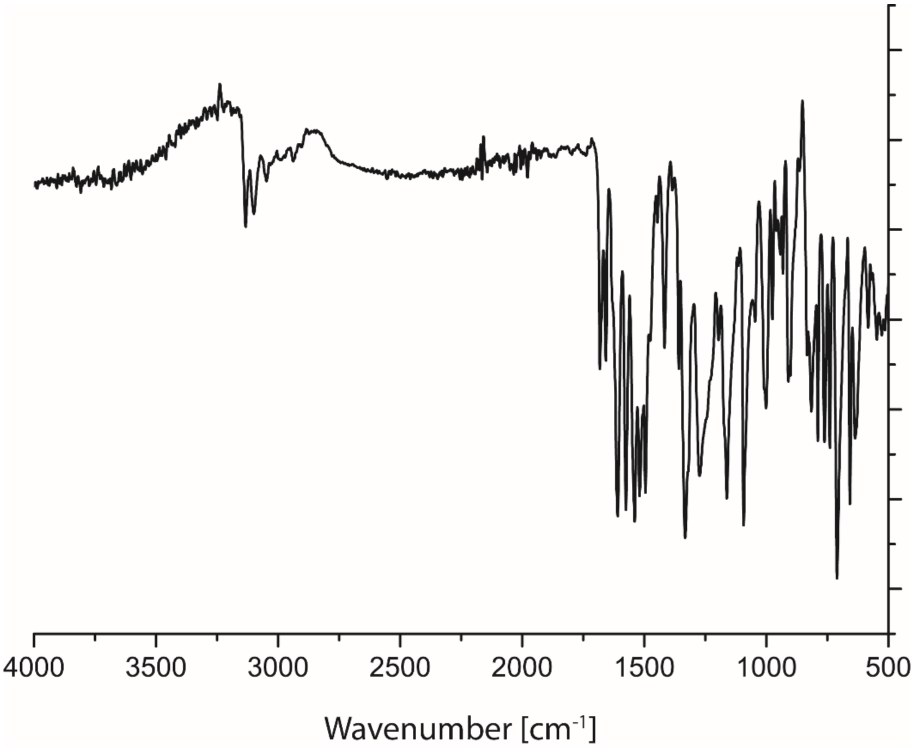

Figure S10. IR spectrum of compound **7**.

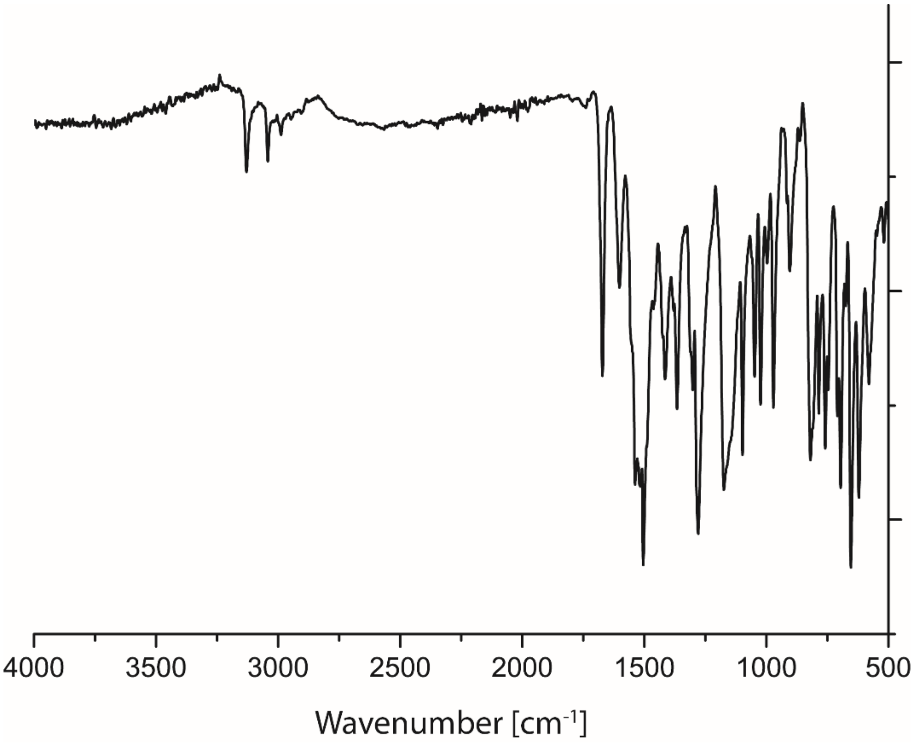

Figure S11. IR spectrum of compound **8**.

5.6.6 Hot Plate and Hot Needle Test

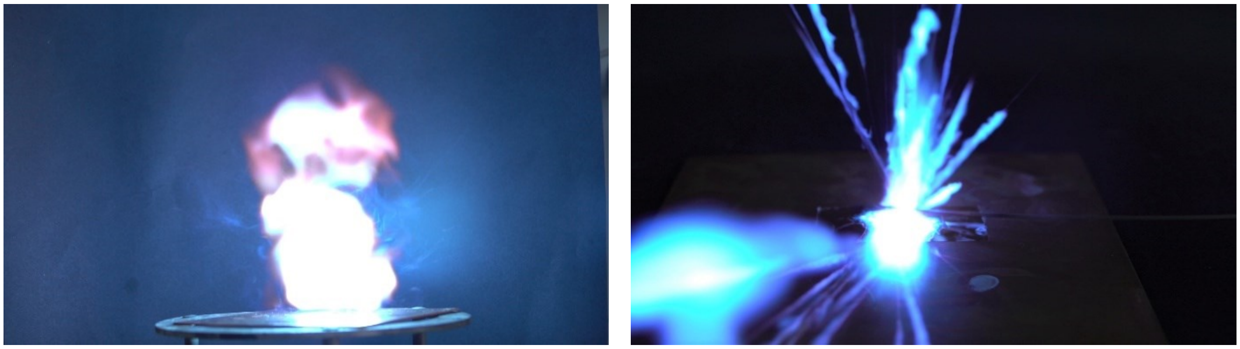

Figure S12. Hot plate (left) and hot needle (right) test of compound **2**.

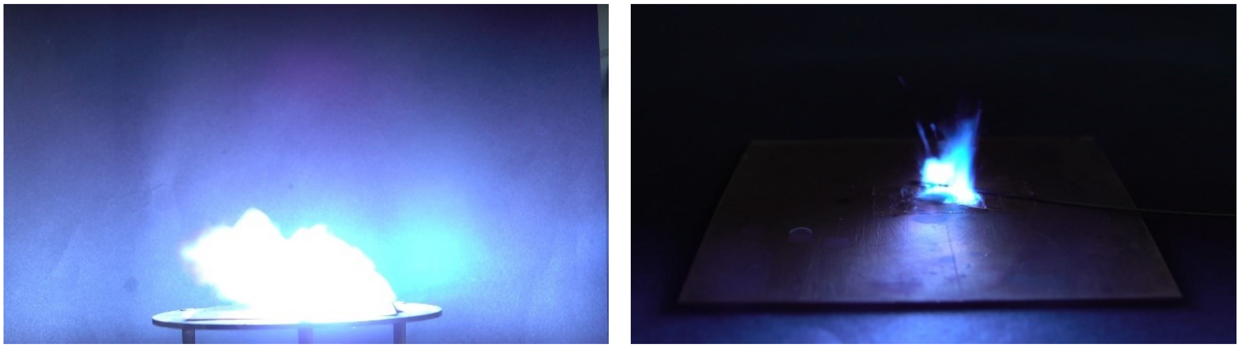

Figure S13. Hot plate (left) and hot needle (right) test of compound **3**.

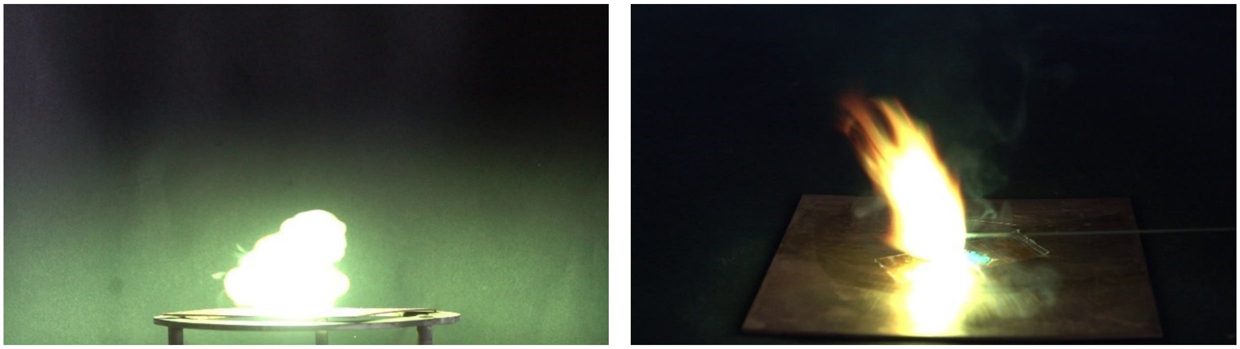

Figure S14. Hot plate (left) and hot needle (right) test of compound **4**.

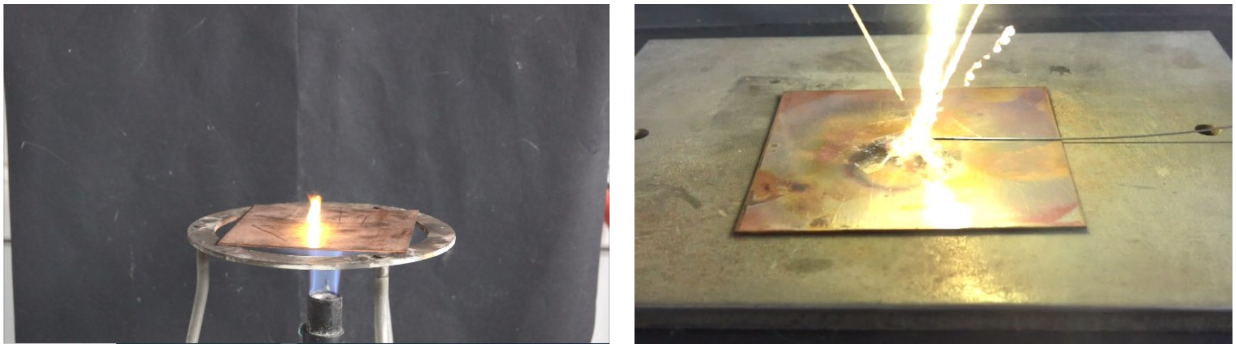

Figure S15. Hot plate (left) and hot needle (right) test of compound **5**.

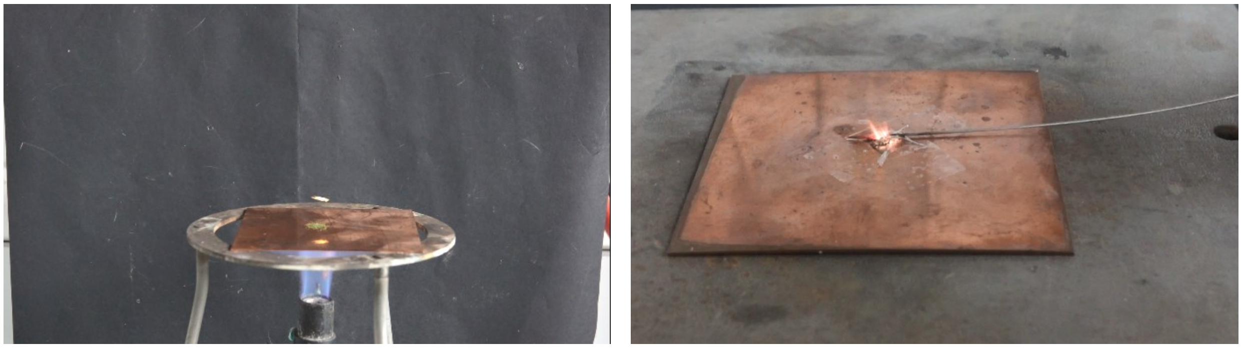

Figure S16. Hot plate (left) and hot needle (right) test of compound **6**.

Figure S17. Hot plate (left) and hot needle (right) test of compound **7**.

Figure S18. Hot plate (left) and hot needle (right) test of compound **8**.

5.6.7 General Methods

All chemicals and solvents were employed as received (Sigma-Aldrich, Fluka, Acros, ABCR). ^{1}H, $^{13}C\{^{1}H\}$, ^{14}N, $^{15}N\{^{1}H\}$ spectra were recorded at ambient temperature using a JEOL Bruker 27400, Eclipse 270, JEOL EX 400 or a JEOL Eclipse 400 instrument. The chemical shifts quoted in ppm in the text refer to typical standards such as tetramethylsilane (^{1}H, ^{13}C) nitromethane (^{14}N,^{15}N) in DMSO-d_6, D_2O or acetone-d_6 as the solvent. Endothermic and exothermic events of the described compounds, which indicate melting, loss of crystal water or decomposition, are given as the extrapolated onset temperatures. The samples were measured in a range of 25–400 °C at a heating rate of 5 °C min^{-1} through differential thermal analysis (DTA) with an OZM Research DTA 552-Ex instrument. Infrared spectra were measured with pure samples on a Perkin-Elmer BXII FT-IR system with a Smith DuraSampler IR II diamond ATR. Determination of the carbon, hydrogen, and nitrogen contents was carried out by combustion analysis using an Elementar Vario El (nitrogen values determined are often lower than the calculated ones' due to their explosive behavior). Impact sensitivity tests were carried out according to STANAG 4489[S22] with a modified instruction[S23] using a BAM (Bundesanstalt für Materialforschung) drophammer.[S24] Friction sensitivity tests were carried out according to STANAG 4487[S28] with a modified instruction[S29] using the BAM friction tester.[S24,25] The classification of the tested compounds results from the "UN Recommendations on the Transport of Dangerous Goods".[S30,31] Energetic properties have been calculated with the EXPLO5 6.05.04 computer code[S32] using the, to RT converted, X-ray density and calculated solid state heats of formation. These were computed by the atomization method as described in recently published papers. Electronic enthalpies were calculated with the Gaussian09 software[S13] suite using the CBS-4M method.

5.6.8 Detonation Velocity Estimations

The room temperature densities used for calculation of the detonation velocity were obtained by recalculation of the the low temperature densities, obtained by X-ray diffraction experiments. Detonation velocities were calculated according to an increment method, adapted for ECC by Ilyushin.[S33] Analogue to pyrotechnical mixtures, the respective ECCs were divided into an explosive part (anion, ligand) and an inactive ultratispersed metal additive (copper). The active part was further divided into chemical bonds and structural fragments. Corresponding increment values can be found in the literature.[S34] Some of the values are dependent on the hydrogen and oxygen content of the coordination compound, the summarized values for each fragment are listed in Table S6.

Table S6. Values of increments used for fragments.

Fragment	F_i
1-NAMT	453.0
H_2TNPG	716.3
HTNR	666.2
PA	616.1
HTNO	663.1

5.6.9 Experimental Part

All investigated compounds are potentially explosive energetic materials (the compounds lie in the range of primary explosives), which show partly increased sensitivities towards various stimuli (e.g. elevated temperatures, impact, friction or electrostatic discharge). Therefore, proper security precautions (safety glasses, face shield, earthed equipment and shoes, leather jacket, Kevlar gloves, Kevlar sleeves and ear plugs) have to be worn while synthesizing and handling the described compounds. These very sensitive compounds must be handled with great care!

1-(Nitratomethyl)tetrazole (1)

Fuming nitric acid (3.13 mL, 75 mmol) is slowly added to acetic anhydride (8.5 mL, 90 mmol) cooled with an ice-water bath. After complete addition, the mixture is stirred for 30 minutes at 0–5 °C. An isomeric mixture of 1- and 2-(hydroxymethyl)tetrazole (1.5 g, 15 mmol), synthesized according to literature[S35], is added while keeping the temperature below 10 °C. The reaction solution is stirred at 0 °C for 1.5 h, quenched on ice water and the solution was adjusted to pH = 6 with sodium hydroxide. The solution is then extracted into ethyl acetate (3 x 100 mL) and the organic phase in washed with little cold water and dried over magnesium sulfate. After slow evaporation of the solvent by a stream of nitrogen gas, compound **1** is obtained as white solid in moderate yield (455 mg, 3.2 mmol, 21%).

DTA (5 °C min^{-1}): 57 °C (T_{endo}), 123 °C (T_{exo}); **IR** (ATR, cm^{-1}): ῦ = 3106 (m), 3046 (w), 2993 (w), 2946 (w), 1667 (s), 1488 (m), 1423 (m), 1385 (m), 1313 (w), 1287 (s), 1208 (w), 1182 (s), 1105 (m), 1040 (m), 989 (m), 975 (s), 946 (s), 907 (m), 862 (w), 829 (vs), 764 (vs), 743 (s), 714 (s), 660 (vs), 643 (vs), 589 (s), 414 (s); **^{1}H NMR** (DMSO-d$_6$, 25 °C, ppm) δ = 9.67 (s, 1H), 6.91 (s, 2H); **^{13}C NMR** (DMSO-d$_6$, 25 °C, ppm) δ = 145.9, 74.1; **^{14}N NMR** (DMSO-d$_6$, 25 °C, ppm) δ = −50.9; **EA** ($C_2H_3N_5O_3$, 145.08) calcd.: C 16.56, H 2.08, N 48.27%, found: C 16.84, H 1.95, N 48.10%; BAM drophammer: <1 J; **BAM friction tester**: 9 N; **ESD**: >1500 mJ (grain size 100–500 µm).

General procedure for ECC **2–4**

Barium chlorate monohydrate (145 mg, 0.45 mmol, 1.0 equiv.) and copper(II) sulphate pentahydrate (112 mg, 0.45 mmol, 1.0 equiv.) were dissolved in water (5 mL), combined and stirred for 5 min. The mixture was cooled to 0 °C and the precipitated barium sulphate, filtered off. The solvent was evaporated under reduced pressure and pure copper(II) chlorate was dissolved in ethanol (2 mL).

The respective amounts of copper(II) salt (**2**: $Cu(ClO_3)_2$ 57.6 mg, **3**: $Cu(ClO_4)_2$ 6 H_2O 92.6 mg, **4**: $Cu(NO_3)_2$ 3 H_2O 60.4 mg, 0.25 mmol, 1.0 equiv.) was dissolved in ethanol (2 mL) and added dropwise to the in ethanol dissolved **1** (218 mg, 1.50 mmol, 6.0 equiv.) while stirring at room temperature. The reaction mixture was stirred for 5 min at 80 °C before it was allowed to crystallize at room temperature. Crystallization process took up 1–3 days. The crystalline compounds were filtered off before complete evaporation of the solvent and were washed with cold ethanol. It is also possible to precipitate the compounds by adding a large excess of *n*-hexane to the ethanolic solution. In this case, the powdered compounds were filtered off, washed with n-hexane and dried in air. The powdered compounds were checked for purity with elemental analysis.

[Cu(1-NAMT)$_6$](ClO$_3$)$_2$ (2)

Compound **2** was obtained as blue crystals within 2 h. Yield: 200 mg (0.18 mmol, 73%).

DTA (5 °C min^{-1}): 145 °C (T_{exo}); **IR** (ATR, cm^{-1}): ῦ = 3106 (w), 3049 (w), 2994 (w), 1666 (s), 1502 (m), 1438 (m), 1394 (w), 1336 (w), 1284 (s), 1205 (w), 1181 (s), 1105 (s), 1053 (w), 1000 (m), 958 (vs), 933 (s), 909 (s), 831 (vs), 768 (s), 749 (m), 714 (m), 657 (s), 657 (s), 642 (s), 597 (m), 477 (m), 410 (w); **EA** ($C_{12}H_{18}Cl_2CuN_{30}O_{24}$, 1100.91): calc.: C 13.09, H 1.65, N 38.17%, found: C 12.91, H 1.65, N 38.50%; **BAM drophammer**: <1 J, **BAM friction tester**: 0.4 N; **ESD**: 139 mJ (at grain size >1000 µm).

[Cu(1-NAMT)$_6$](ClO$_4$)$_2$ (3)

Compound **3** was obtained as blue crystals within 2 h. Yield: 150 mg (0.13 mmol, 53%).

DTA (5 °C min^{-1}): 119 °C (T_{exo}); **IR** (ATR, cm^{-1}): $\tilde{\upsilon}$ = 3133 (w), 3056 (w), 3002 (w), 2028 (w), 1682 (m), 1675 (m), 1503 (m), 1435 (m), 1393 (w), 1336 (w), 1285 (vs), 1204 (w), 1181(s), 1105 (s), 1077 (s), 1051 (s), 1026 (w), 1000 (m), 970 (s), 961 (s), 934 (w), 904 (m), 830 (vs), 769 (s), 748 (m), 714 (m), 657 (s), 642 (s), 623 (vs); **EA** ($C_{12}H_{18}Cl_2CuN_{30}O_{26}$, 1132.91): calc.: C 12.72, H 1.60, N 37.09%, found: C 12.67, H 1.63, N 37.35%; **BAM drophammer**: 2 J, **BAM friction tester**: 0.75 N; **ESD**: 13 mJ (at grain size >1000 µm).

[Cu(1-NAMT)$_6$](NO$_3$)$_2$ (4)

Compound **4** was obtained as blue crystals after 3 days. Yield: 160 mg (0.15 mmol, 61%).

DTA (5 °C min^{-1}): 102 °C (endothermic), 121 °C (exothermic.); **IR** (ATR, cm^{-1}): $\tilde{\upsilon}$ = 3091 (w), 3055 (w), 2993 (w), 2928 (vw), 1673 (s), 1663 (s), 1504 (m), 1439 (m), 1392 (w), 1343 (s), 1282 (vs), 1204 (m), 1177 (s), 1105 (s), 1053 (w), 1000 (m), 963 (s), 914 (m), 826 (vs), 771 (s), 748 (m), 715 (m), 655 (s), 642 (s), 589 (m), 411 (w); **EA** ($C_{12}H_{18}CuN_{32}O_{24}$, 1058.02): calc.: C 13.62, H 1.71, N 42.36%, found: C 13.53, H 1.76, N 43.17%; **BAM drophammer**: <1 J, **BAM friction tester**: 5 N; **ESD**: 90 mJ (at grain size >1000 µm).

General procedure for ECCs **5** – **8**

A suspension of $CuCO_3 \times Cu(OH)_2$ (27.6 mg, 0.125 mmol, 0.5 eq.) and the corresponding free nitroaromatic acid (0.50 mmol, 2.0 eq.) in 5 mL of water was heated to 80 °C until a clear solution was obtained. To this solution, compound **1** (**5**: 1.0 mmol, 4.0 eq., **6**–**8**: 0.50 mmol, 2.0 eq.) was added. The solution was kept at 80 °C for 5 min. and then left at room temperature to crystallize for 3 weeks. The resulting suspension was filtered off and washed with cold water, ethanol and diethyl ether. Here, a precipitation of the compounds like for **2** – **4** was not possible.

[Cu(1-NAMT)$_4$(H$_2$TNPG)$_2$] (**5**)

Compound **5** was obtained as a green solid. Yield: 140 mg (0.12 mmol, 48%).

DTA (5 °C min^{-1}): 135 °C (T$_{exo}$); **IR** (ATR, cm^{-1}): υ $\tilde{\nu}$ = 3130(w), 3046(w), 2995(w), 1672(s), 1645(s), 1563(s), 1505(s), 1496(s), 1454(m), 1418(m), 1384(m), 1338(s), 1287(s), 1280(s), 1177(s), 1161(vs), 1137(s), 1092(s), 1045(m), 1015(s), 999(m), 985(m), 965(s), 920(m), 890(w), 829(s), 818(vs), 784(s), 760(vs), 739(s), 730(s), 719(s), 712(s), 693(vs), 651(s), 624(vs), 573(s), 505(m), 481(m), 470(m), 463(m), 458(m), 417(m). **EA** ($C_{20}H_{16}CuN_{26}O_{30}$, 1164.05) calc.: C 20.64 H 1.39 N 31.29%, found C 20.62 H 1.46 N 31.18%; **BAM drop hammer**: <1 J; **BAM friction tester**: 72 N; **ESD**: 160 mJ (at grain size: 100–500 µm).

[Cu(1-NAMT)$_2$(HTNR)$_2$] (**6**)

Compound **6** was obtained as a greenish black solid. Yield: 167.9 mg (0.20 mmol, 80%).

DTA (5 °C min^{-1}): 176 °C (T$_{exo}$); **IR** (ATR, cm^{-1}): $\tilde{\nu}$ = 3134(w), 3047(w), 1668(m), 1622(m), 1561(m), 1525(m), 1505(s), 1479(m), 1452(m), 1425(m), 1381(m), 1352(w), 1333(m), 1318(m), 1285(s), 1174(s), 1084(m), 1051(s), 1026(s), 997(m), 971(s), 932(m), 911(m), 895(m), 863(m), 822(s), 775(m), 760(s), 731(s), 713(s); **EA** ($C_{16}H_{10}CuN_{16}O_{22}$, 841.89) calc.: C 22.83 H 1.20 N 26.62%, found C 22.79 H 1.21 N 26.52%; **BAM drop hammer**: <1 J; **BAM friction tester**: 40 N; **ESD**: 140 mJ (at grain size: 100–500 µm).

[Cu(1-NAMT)$_2$(PA)$_2$] (**7**)

Compound **7** was obtained as a green solid. Yield: 147.5 mg (0.18 mmol, 73%).

DTA (5 °C min^{-1}): 181 °C (T$_{exo}$); **IR** (ATR, cm^{-1}): υ $\tilde{\nu}$ = 3133(w), 3100(w), 3047(w), 2939(w), 1682(m), 1657(m), 1609(s), 1575(s), 1539(s), 1520(s), 1506(s), 1496(s), 1476(m), 1446(w), 1417(m), 1385(w), 1359(m), 1333(vs), 1274(s), 1196(m), 1162(s), 1093(s), 1046(m), 1009(s), 1001(s), 975(m), 959(w), 943(m), 932(m), 910(s), 902(m), 865(w), 834(m), 816(s), 789(s), 762(s), 740(s), 711(vs), 658(s), 637(s), 583(m), 547(m), 527(m), 789(s), 762(s), 740(s), 711(vs), 658(s), 637(s), 583(m), 547(m), 527(m), 514(m), 503(m), 463(m), 458(m), 435(m), 407(s); **EA** ($C_{16}H_{10}CuN_{16}O_{20}$, 809.89) calc.: C 23.73 H 1.24 N 27.67%, found C 23.68 H 1.26 N 27.80%; **BAM drop hammer**: <1 J. **BAM friction tester**: 120 N; **ESD**: 90 mJ (at grain size: 100–500 µm).

[Cu(1-NAMT)$_2$(HTNO)$_2$] (8)

Compound **8** was obtained as a green solid. Yield: 159.7 mg (0.19 mmol, 73%). **DTA** (5 °C min^{-1}): 161 °C (T$_{exo}$); **IR** (ATR, cm^{-1}): $\tilde{\upsilon}$ = 3130(w), 3042(w), 2988(w), 2948(vw), 2905(vw), 1671(s), 1602(m), 1538(s), 1520(s), 1516(s), 1505(vs), 1463(m), 1424(m), 1415(s), 1380(m), 1366(s), 1330(m), 1301(s), 1279(vs), 1174(s), 1098(s), 1048(s), 1024(s), 997(m), 971(s), 916(w), 904(m), 864(w), 820(s), 785(s), 759(s), 747(s), 709(s), 696(s), 675(m), 654(vs), 621(s), 580(s), 547(m), 518(m), 497(w), 475(w), 468(w), 675(m), 654(vs), 621(s), 580(s), 547(m), 518(m), 497(w), 475(w), 468(w), 457(w), 448(w), 417(s), 406(m); **EA** ($C_{18}H_{14}CuN_{16}O_{22}$, 869.95) calc.: C 24.85 H 1.62 N 25.76%, found C 24.73 H 1.54 N 25.93%; **BAM drop hammer**: <1 J. **BAM friction tester**: 84 N; **ESD**: 90 mJ (at grain size: 100–500 µm).

5.6.10 References

S1 CrysAlisPRO (Version 171.33.41), Oxford Diffraction Ltd., **2009**.

S2 A. Altomare, G. Cascarano, C. Giacovazzo, and A. Guagliardi, *J. Appl. Crystallogr.* **1992**, *26*, 343.

S3 A. Altomare, G. Cascarano, C. Giacovazzo, A. Guagliardi, A. G. G. Moliterni, M. C. Burla, G. Polidori, M. Camalli and R. Spagna, SIR97, **2003**.

S4 A. Altomare, M. C. Burla, M. Camalli, G. L. Cascarano, C. Giacovazzo, A. Guagliardi, A. G. G. Moliterni, G. Polidori and R. Spagna, *J. Appl. Crystallogr.* **1999**, *32*, 115.

S5 G. M. Sheldrick, SHELXL-97, University of Göttingen, Germany, **1997**.

S6 G. M. Sheldrick, *Acta Crystallogr. Sect. A* **2008**, *64*, 112.

S7 G. M. Sheldrick, *Acta Cryst. A* **2015**, *71*, 3–8.

S8 A. L. Spek, PLATON, Utrecht University, The Netherlands, **1999**.

S9 L.J. Farrugia, *J. Appl. Cryst.* **2012**, *45*, 849.

S10 O. V. Dolomanov, L. J. Bourhis, R. J. Gildea, J. A. K. Howard and H. Puschmann, *J. Appl. Cryst*. **2009**, *42*, 339–341.

S11 Empirical absorption correction using spherical harmonics, implemented in SCALE3 ABSPACK scaling algorithm (CrysAlisPro Oxford Diffraction Ltd., Version 171.33.41, **2009**).

S12 APEX3, Bruker AXS Inc., Madison, Wisconsin, USA.

S13 M. J. Frisch, G. W. Trucks, H. B. Schlegel, G. E. Scuseria, M. A. Robb, J. R. Cheeseman, G. Scalmani, V.Barone, B. Mennucci, G. A. Petersson, H. Nakatsuji, M. Caricato, X. Li, H.P. Hratchian, A. F. Izmaylov, J. Bloino, G. Zheng, J. L. Sonnenberg, M. Hada, M. Ehara, K.

Toyota, R. Fukuda, J. Hasegawa, M. Ishida, T. Nakajima, Y. Honda, O. Kitao, H. Nakai, T. Vreven, J. A. Montgomery, Jr., J. E. Peralta, F. Ogliaro, M. Bearpark, J. J. Heyd, E. Brothers, K. N. Kudin, V. N. Staroverov, R. Kobayashi, J. Normand, K. Raghavachari, A. Rendell, J. C. Burant, S. S. Iyengar, J. Tomasi, M. Cossi, N. Rega, J. M. Millam, M.Klene, J. E. Knox, J. B. Cross, V. Bakken, C. Adamo, J. Jaramillo, R. Gomperts, R. E. Stratmann, O. Yazyev, A. J. Austin, R. Cammi, C. Pomelli, J. W. Ochterski, R. L. Martin, K. Morokuma, V. G. Zakrzewski, G. A. Voth, P. Salvador, J. J. Dannenberg, S. Dapprich, A. D. Daniels, O. Farkas, J.B. Foresman, J. V. Ortiz, J. Cioslowski and D. J. Fox, Gaussian 09 A.02, Gaussian, Inc., Wallingford, CT, USA, **2009**.

S14 J. W. Ochterski, G. A. Petersson and J. A. Montgomery Jr., *J. Chem. Phys.* **1996**, *104*, 2598–2619.

S15 J. A. Montgomery Jr., M. J. Frisch, J. W. Ochterski and G. A. Petersson, *J. Chem. Phys.* **2000**, *112*, 6532–6542.

S16 L. A. Curtiss, K. Raghavachari, P. C. Redfern and J. A. Pople, *J. Chem. Phys.* **1997**, *106*, 1063–1079.

S17 E. F. C. Byrd and B. M. Rice, *J. Phys. Chem. A* **2006**, *110*, 1005–1013.

S18 B. M. Rice, S. V. Pai and J. Hare, *Comb. Flame* **1999**, *118*, 445–458.

S19 P. J. Lindstrom and W. G. Mallard, NIST Standard Reference Database Number 69, http://webbook.nist.gov/chemistry/, (accessed March **2021**).

S20 M. S. Westwell, M. S. Searle, D. J. Wales and D. H. Williams, *J. Am. Chem. Soc*. **1995**, *117*, 5013–5015.

S21 F. Trouton, *Philos. Mag.* **1884**, *18,* 54–57.

S22NATO standardization agreement (STANAG) on explosives, impact sensitivity tests, no. 4489, 1st ed., Sept. 17, **1999**.

S23 WIWEB-Standardarbeitsanweisung 4-5.1.02, Ermittlung der Explosionsgefährlichkeit, hier der Schlagempfindlichkeit mit dem Fallhammer, Nov. 8, **2002**.

S24 BAM, http://www.bam.de, (accessed March **2021**).

S25 OZM, http://www.ozm.cz, (accessed March **2021**).

S26 Military Standard 1751A (MIL-STD-1751A): safety and performance tests for qualification of explosives (high explosives, propellants and pyrotechnics), method 1016, Dec. 11, **2001**.

S27 M. S. Gruhne, M. Lommel, M. H. H. Wurzenberger, N. Szimhradt, T. M. Klapötke and J. Stierstorfer, *Propellants Explos. Pyrotech.* **2020**, *45*, 147–153.

S28 NATO standardization agreement (STANAG) on explosive, friction sensitivity tests, no. 4487, 1st ed., Aug. 22, **2002**.

S29 WIWEB-Standardarbeitsanweisung 4-5.1.03, Ermittlung der Explosionsgefährlichkeit oder der Reibeempfindlichkeit mit dem Reibeapparat, Nov. 8, **2002**.

S30 UN Model Regulation: Recommendations on the Transport of Dangerous Goods – Manual of Tests and Criteria, section 13.4.2.3.3, **2015**.

S31 Impact: insensitive > 40 J, less sensitive ≥ 35 J, sensitive ≥ 4 J, very sensitive ≤ 3 J; Friction: insensitive > 360 N, less sensitive = 360 N, sensitive < 360 N and > 80 N, very sensitive ≤ 80 N, extremely sensitive ≤ 10 N. According to the UN Recommendations on the Transport of Dangerous Goods, 5th ed., **2009**.

S32 M. Sućeska, EXPLO5 Version 6.05 User's Guide. Zagreb, Croatia: OZM; **2018**.

S33 M. A. Ilyushin, A. V. Smirnov, A. A. Kotomin, I. V. Tselinskii, *Energ. Mater*. **1994**, *2*, 16–20.

S34 Н.Ю. Сугак, С.В. Мочалов, РАСЧЕТ ВЗРЫВЧАТЫХ ХАРАКТЕРИСТИК ВВ, БТИ АлтГТУ, Бийск, **2013**.

S35 M. Kofen, M. Lommel, M. H. H. Wurzenberger, T. M. Klapötke, J. Stierstorfer, *Chem. Eur. J.* **2022**, *28*, e202200492.

6 Energetic Coordination Compounds of late 3d Metals with 1*N*-(Nitromethyl)tetrazole, a Ligand with Astonishing Properties from the Rare Class of *N*-Nitromethyl azoles

Moritz Kofen, Thomas M. Klapötke and Jörg Stierstorfer

Published in *Chemical Engineering Journal*, **2022**, *452*, 139375

DOI: 10.1016/j.cej.2022.139375

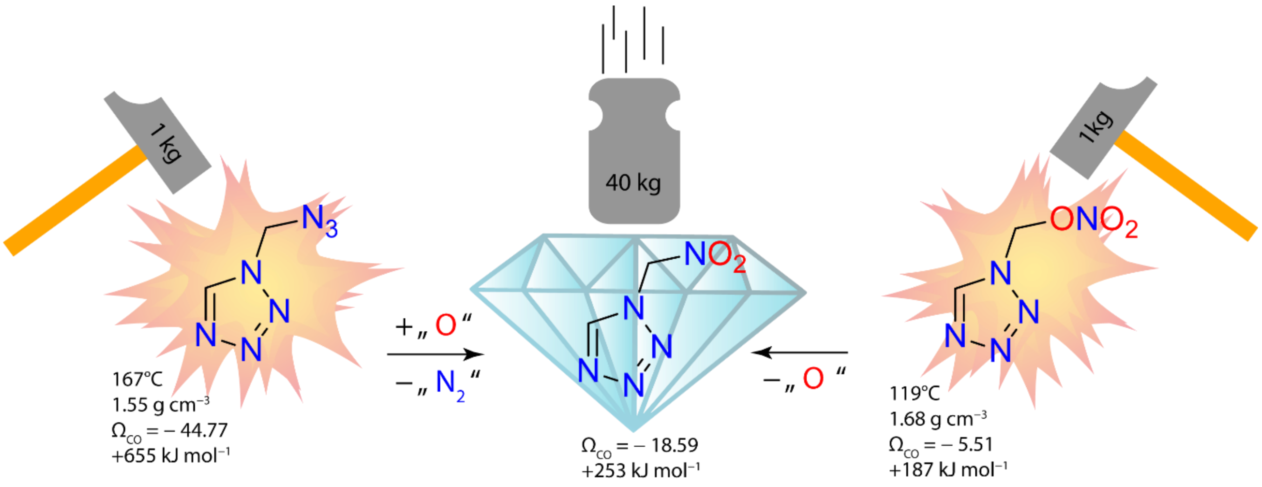

Abstract: The hardly accessible *N*-nitromethyl moiety is introduced onto the *1H*-tetrazole scaffold, representing the fourth and fifth ever synthesized *N*-nitromethyl azoles. Both compounds 1-(Nitromethyl)tetrazole (**2a**) and 2-(Nitromethyl)tetrazole (**2b**) are thoroughly analyzed by low-temperature single-crystal X-ray diffraction experiments, complemented by elemental analysis, multinuclear (^{1}H, ^{13}C, ^{14}N, ^{15}N) NMR as well as IR spectroscopy. Sensitivity measurements towards external stimuli revealed two highly insensitive compounds. Additionally, **2a** was applied as ligand for energetic coordination compounds of 3d transition metals (e.g. Cu, Fe, Ni, and Zn) in combination with oxidizing nitrate, chlorate and perchlorate anions. The synthesized ECCs were analyzed by low-temperature single-crystal X-ray diffraction experiments, elemental analysis and IR spectroscopy. The thermal behavior of all compounds was investigated by differential thermal analysis and the sensitivities towards impact and friction was measured. Due to the lack of information about the properties of *N*-nitromethyl azoles, the complete insensitivity towards external stimuli of **2a** and **2b** supports first hints of a sensitivity decreasing influence of the *N*-

nitromethyl moiety, which is highly desired when designing new high explosives. Additionally, the functional group is able to introduce meltability into molecular scaffolds.

6.1 Introduction

Some of the first compounds potentially applicable as primary explosives date back to the 17th century with the introduction of silver(I) fulminate[1] or mercury(II) fulminate[2]. Owing to the high sensitivities and toxicities of the fulminate compounds, more efficient and safer to handle primary explosives such as lead azide[3] and lead styphnate[3] were introduced. While highly efficient and extensively studied, both compounds still contain toxic[4] and environmentally harmful[5] heavy metals. Therefore, in 2011 lead azide and styphnate were added to the REACH candidate list of authorization[6]. While research had already investigated potential replacements for lead-containing primary explosives before 2011, the urgency and demand for new compounds increased the research interest. A promising concept was soon realized by the formation of energetic coordination compounds (ECCs), which gained much interest during the last decade (Figure 1A), and one of the first representatives, BNCP (Figure 1B), was applied as a primary explosive.

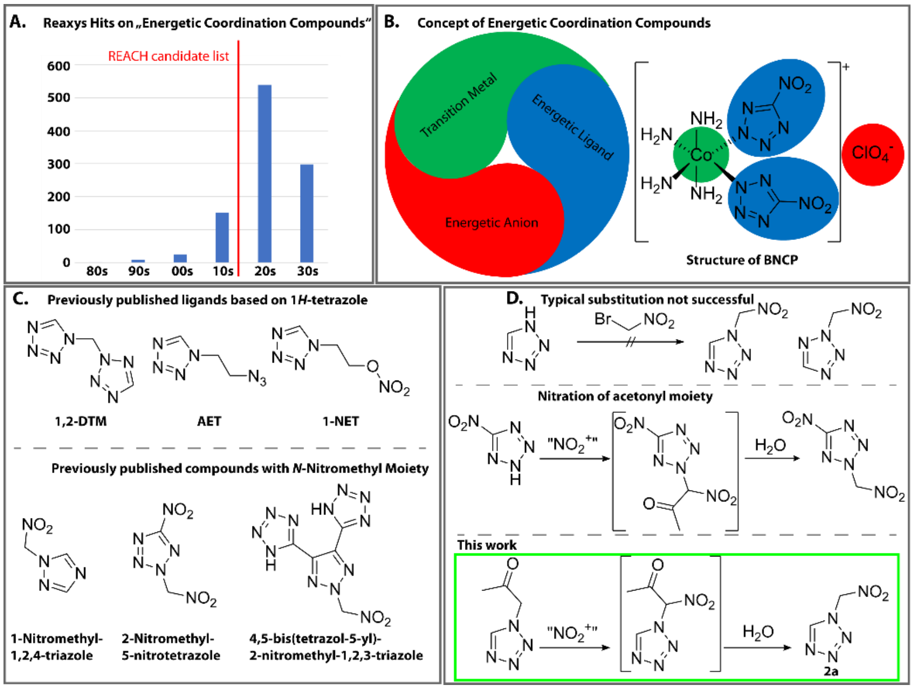

Figure 1. A) Increasing number of publications on ECCs. B) Basic concept of ECCs. C) Previously applied ligands as well as *N*-nitromethyl containing compounds. D) Failed and successful synthesis attempt towards 1- (**2a**) and 2-Nitromethyltetrazole (**2b**).

The basic approach toward ECCs combines transition metals (e.g., Cu, Zn, Ni, and Ag) with energetic ligands and oxidizing (e.g., ClO_4^-, ClO_3^-, and NO_3^-), reducing (N_3^-) or nitroaromatic (e.g., picrate, and styphnate) anions. The vast amount of possible combinations enables fine-tuning of the resulting energetic properties, especially selecting ligands (Figure 1C) with unique properties such as a bridging effect between metal centers (1,2-DTM[7]), high enthalpies of formation (AET[8]), or a high oxygen balance (1-NET[9]). Especially the latter often present the challenge of balancing their good overall performance, high density, and oxygen balance with their overall low thermal stability. Generally, the low thermal stability and heat of formation of nitro esters can be overcome by substituting the nitro ester with an azide moiety. However, a drawback of decreasing density, and oxygen balance, while most often increasing the sensitivity, has to be kept in mind. The scale of changes can be observed by comparing 1*N*-(nitratomethyl)tetrazole[10] (1-NAMT) and 1*N*-(azidomethyl)tetrazole[11] (Figure 2), which our working group has recently published.

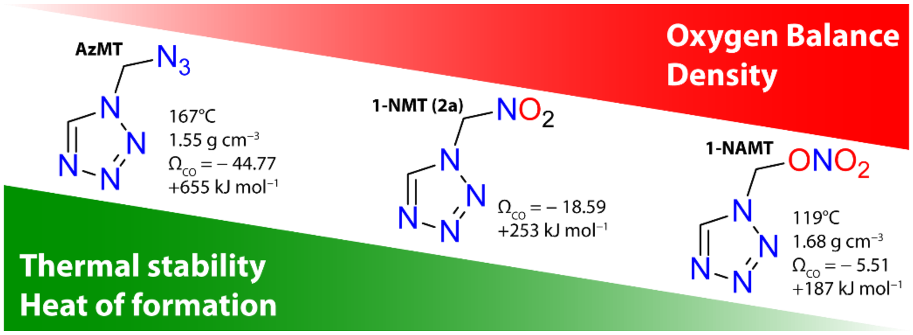

Figure 2. 1-NMT balancing the oxygen balance and enthalpy of formation of AzMT and 1-NAMT.

A good equalization of properties between the azido and nitro ester can be expected by introducing an *N*-nitromethyl group onto the *1H*-tetrazole scaffold(Figure 2). It is, therefore, surprising that there are only three azoles (Figure 1C) containing the *N*-nitromethyl group[12-14] ever reported. Therefore, we opted to synthesize 1*N*- and 2*N*-(nitromethyl)tetrazole (1-NMT, 2-NMT) to better understand the properties introduced by the *N*-nitromethyl moiety as well as apply the new compound as a ligand for ECCs. Following the procedure of typical substitution reactions with Bromo(nitro)methane was not successful (Figure 1D), and we solely obtained decomposition products. Interestingly, the synthesis of 2-nitromethyl-5-nitrotetrazole uses a different approach to convert an *N*-acetonyl function into the *N*-nitromethyl group[14]. By significantly altering this procedure, we were able to synthesize 1- (**2a**) and 2-nitromethyltetrazole (**2b**) for the first time, starting from *N*-acetonyltetrazoles (**1a**, **1b**). Ultimately, in this work, we present the synthesis of the fourth and fifth ever known *N*-nitromethyl containing azoles (**2a**, **2b**), together with a complete characterization including low-temperature single-crystal X-ray diffraction and multinuclear NMR (^{1}H, ^{13}C, and ^{15}N). Additionally, several energetic coordination compounds of **2a** as ligand are presented. All compounds were characterized by single-crystal low-temperature X-ray diffraction complemented by elemental analysis and IR spectroscopy (Figures S9–16). Additionally, the thermal behavior of all compounds and their sensitivities towards external stimuli were determined. Lastly, the obtained ECCs were tested as possible primary explosives.

6.2 Results and Discussion

6.2.1 Synthesis of Nitromethyltetrazoles

Warning! The synthetic work described includes the handling of very impact sensitive compounds such ECCs (3-8). Appropriate protective equipment (leather coat, face shield, Kevlar® wrist protectors, and hearing protection) must be worn at all times when handling these materials!

The synthesis of 1-(Nitromethyl)tetrazole (**2a**) and 2-(Nitromethyl)tetrazole (**2b**) is shown in Scheme 1. The precursor compounds *1H*-tetrazole and bromoacetone, synthesized according to literature[15, 16], are refluxed in a suspension of potassium carbonate in acetone which is a procedure adopted from literature[17]. After filtering off all solids and removing the solvent in vacuo, an isomeric mixture of **1a** and **1b** is obtained, which can be separated by column chromatography over silica with a mixture of ethyl acetate/iso-hexane (50/50) as the eluting solvent. Both compounds are obtained as off-white crystalline solids in an acceptable combined yield of 57%. The nitration of both is then performed by suspending the solid material in an ice-cold mixture of sulfuric acid (96%) and water in a ratio of 12/5. Fuming nitric acid is added while keeping temperatures below 5 °C, and by removing the ice bath after complete addition, the solution is allowed to warm up to 30 °C while stirring not longer than 55 min (**2a**) and 58 min (**2b**). The reaction solution is then quickly poured into a suspension of sodium bicarbonate in water, and after the evolution of gases is finished, the solution is extracted into ethyl acetate. The organic phase is washed with water, dried over magnesium sulfate, and concentrated *in vacuo*. The obtained solids consist of a mixture of **2a** or **2b** and their respective starting materials, which can be separated by column chromatography over silica gel with ethyl acetate/n-hexane (60:40 to 100:0) as the eluting agent. Compounds **2a** and **2b** are obtained as slightly off-white crystalline solids in moderate yields of 27% and 12%, respectively. Additionally, 56% (**1a**) and 60% (**1b**) of the respective starting material can be recovered and added to a second nitration batch. The moderate to poor yields of the nitration are due to a rather short reaction time needed to achieve the mono nitration of the *N*-acetonyl precursor compounds. We found that at reaction times higher than 1 h, the desired product (**2a** or **2b**) is slowly consumed over the formation of the double nitrated Dinitromethyltetrazole species. By further increasing reaction times over 2 h, the sole nitration products are the double nitrated species. Hence the nitration has to be quenched preliminary to inhibit the double nitration. Since it was proven that the nitration mechanism is an electrophilic addition of a nitronium cation to the C-C double bond of the enol form of the precursor compound[14], it might be possible to increase the yield by changing to a precursor compound that favors its enol form.

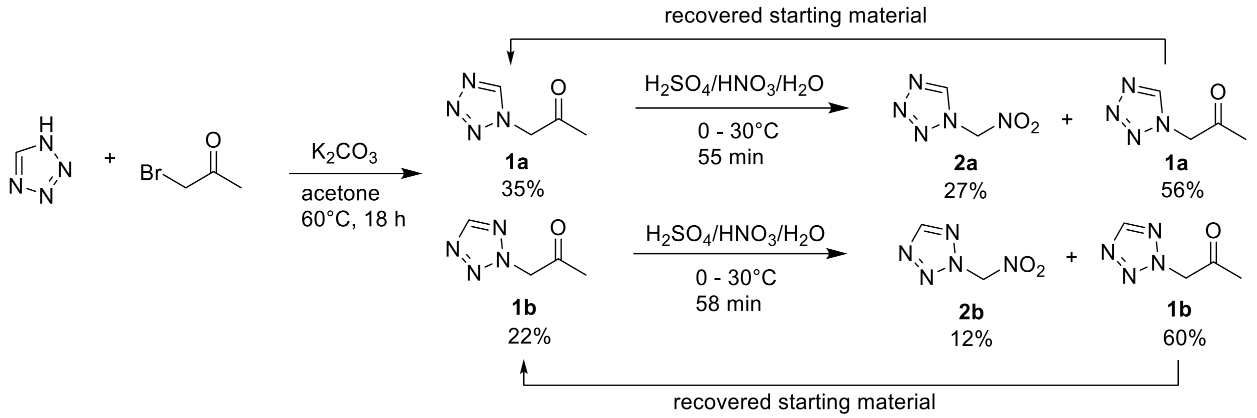

Scheme 1. Synthesis of 1- and 2-(Nitromethyl)tetrazole (**2a**, **2b**) starting from *1H*-tetrazole and bromoacetone.

6.2.2 Crystal Structures of 2a and 2b

The solid-state crystal structures of compounds **2a** and **2b** were obtained by low-temperature single crystal X-ray diffraction experiments. The data and parameters of the measurements, as well as of the refinements, are given in Table S1 in the Supporting Information. All herein included low-temperature X-Ray densities were recalculated to their respective density at room temperature $\left(d_{298\,K} = \frac{dT}{1+\alpha_V(298-T_0)};\ \alpha_V = 1.5 * 10^{-4} K^{-1}\right)$. All ellipsoids are shown with a probability of 50%. The crystal datasets are uploaded to the CSD database and can be obtained free of charge with CCDC 2194762 (**2a**), 2194763 (**2b**), 2194757 (**3**), 2194756 (**4**), 2194758 (**5**), 2194760 (**6**@173 K), 2194759 (**6**@133 K), 2195850 (**8**).

Compounds **2a** (Figure 3A), and **2b** (Figure 3B) crystallize in the orthorhombic space group $P2_12_12_1$ and the monoclinic space group $P2_1/c$, with densities of 1.62 g cm^{-3} and 1.65 g cm^{-3}, respectively. Both compounds contain four formula units in the unit cell, and the bond lengths of the tetrazole rings are in the typical range of 1*N* substituted tetrazoles, while the bond lengths toward the methylene moieties are comparable to similar compounds.[11] Additionally, the carbon nitro bond lengths of 1.52 Å (**2a**) and 1.51 Å (**2b**) are only minorly elongated compared to pure nitromethane[18] (1.49 Å). Both methylene carbon atoms lie nearly perfectly in the plane built by the tetrazole rings with small torsion angles between 0.5–1.3 °. Due to the sp^3 hybridization of the C2 atoms, the nitro groups are protruding from these planes by angles of 110.3 °.

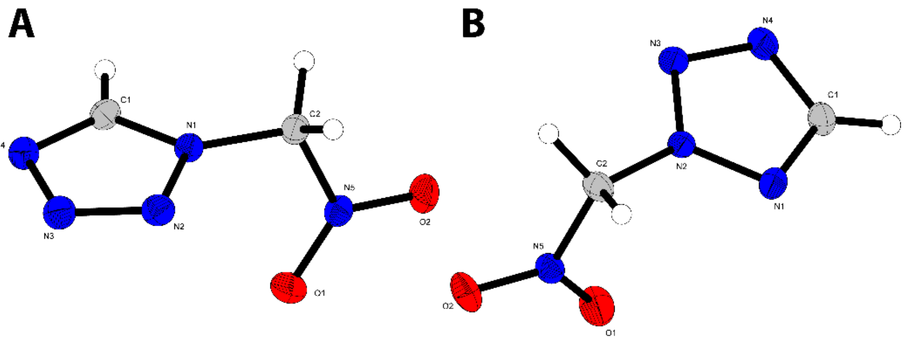

Figure 3. A) Crystal structure of 1-(Nitromethyl)tetrazole (**2a**); B) Crystal structure of 2-(Nnitromethyl)tetrazole (**2b**).

Figure 4 shows the crystal packing of compounds **2a** and **2b** along their respective *a* axis. Compound **2a** shows areas of stacked nitro groups of individual molecules, whereas **2b** exhibits more isolated nitro groups in the crystal. Nonetheless, the shortest distances between oxygen atoms of two individual molecules observed in **2a** (3.15 Å) are equal to those observed in **2b** (3.14 Å).

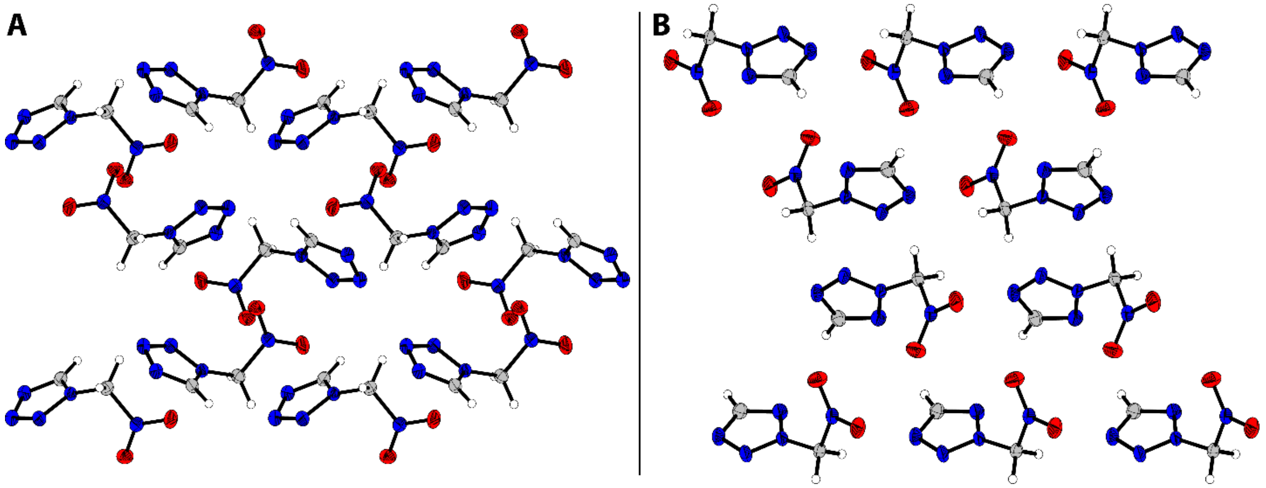

Figure 4. Crystal packing of compound **2a** (A) and **2b** (B) viewed along the *a* axis.

6.2.3 NMR Spectroscopy

The ^{1}H NMR spectra (Figure S1 (**2a**) and S3 (**2b**)) of compounds **2a**/**2b** both show two signals at δ = 9.50/9.05 and 7.20/7.39 ppm attributing to the tetrazole CH protons and the methylene protons, respectively. The pattern of a downfield shifted tetrazole proton and upfield shifted methylene protons of the 1*N*-isomer (**2a**) compared to the 2*N*-isomer (**2b**) is typical for *N*-substituted tetrazoles[11, 19]. The ^{13}C NMR spectra of both compounds (Figure S2 and S4) show two signals at (**2a**/**2b**) δ = 146.6/155.3 and 77.9/81.6 ppm attributing to the tetrazole and methylene carbon atoms, respectively. Here, both signals of **2b** appear downfield shifted to those of **2a**, owing to a stronger magnetic de-shielding, which is typically for 2*N* substituted tetrazoles.[19] The ^{15}N NMR spectrum (Figure 5) of **2a** shows five signals at δ = 15.6, −9.1, −11.3, −49.7, and −154.5 ppm, together with a spike from the instrument during the measurement. The signal at δ = 15.6 ppm (N3) is split into a doublet due to proton ^{3}J coupling with the tetrazole proton.

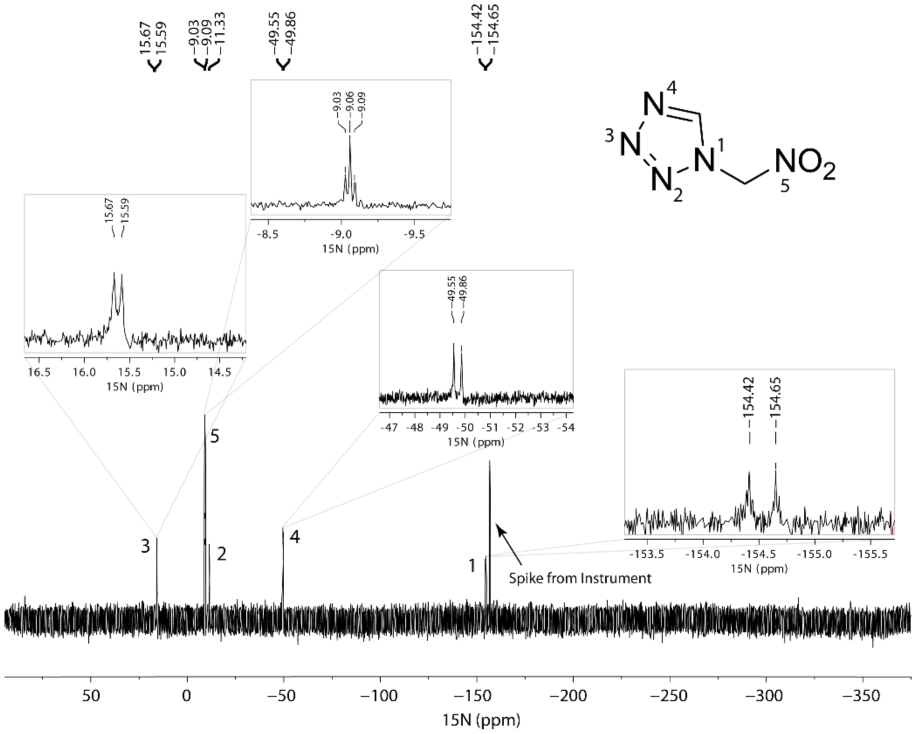

Figure 5. ^{15}N NMR spectrum of **2a** in acetone-d$_6$.

The signal at δ = −11.3 ppm, attributing to the N2 nitrogen atom, is not split as the ^{3}J coupling with the tetrazole proton is not observed. The signal at δ = −9.1 ppm allocates the nitro group, which is in the typical range of alkyl nitro groups.[20] The signal at δ = −49.6 ppm (N4) is also split into a doublet caused by a ^{2}J coupling with the tetrazole proton, whereas the doublet at δ = −154.4 ppm is attributed to the N1 atom of the tetrazole. Here, the splitting into a doublet due to ^{2}J proton coupling with the aromatic tetrazole proton is prominent, whereas a remote coupling with the methylene protons is hardly recognized. Due to the poor overall yield of **2b** (2.6%), no ^{15}N spectrum was recorded. Nonetheless, the ^{14}N spectrum (Figure S5) shows one signal at δ = −10 ppm attributing to the nitro group, which is in the typical range of alkyl-nitro groups.[20]

6.2.4 Physicochemical Properties

The detonation properties of compounds **2a** and **2b** were calculated with the EXPLO5 program code[21]. Therefore, the room temperature densities, together with the enthalpy of formation, were utilized as inputs. The enthalpies of formation for both compounds were obtained by applying the atomization method starting from room temperature CBS-4M enthalpies. Table 1 compares the physicochemical properties of both compounds to their structurally relative 1*N*-Azidomethyl[11] and 1*N*-Nitratomethyl analogous. The 2*N* azide and nitrate derivatives are not yet reported, and thus a comparison is not possible.

Detonation performance and sensitivities. Both compounds exhibit an endothermic enthalpy of formation of 253 kJ mol^{-1} (**2a**) and 235 kJ mol^{-1} (**2b**) and are therefore in between the enthalpies of AzMT (655 kJ mol^{-1}) and 1-NAMT (187 kJ mol^{-1}). Nonetheless, **2a** (7952 m s^{-1}) and **2b** (8009 m s^{-1}) do not exceed the detonation velocities of AzMT or 1-NAMT, owing to an exceptional high enthalpy of formation of AzMT as well as a slightly higher density of 1-NAMT. The most interesting differences are the sensitivities towards external stimuli. **2a** is completely insensitive towards impact and friction, while **2b** is only slightly more sensitive towards friction (288 N) at grain sizes between 100–500 µm. This is especially remarkable as their structural azido (AzMT) and nitrate (1-NAMT) derivatives are extremely sensitive in the range of primary explosives according to the “UN Recommendations on the Transport of Dangerous Goods”[22]. Up to our knowledge, **2a** and **2b** are, therefore the first examples of completely insensitive tetrazole derivatives containing methylene-bridged explosophores. Additionally, this supports the initial assumption of a desensitizing effect of the *N*-nitromethyl moiety. To better understand the sensitivities, Hirshfeld surface (HS) analyses were performed for compounds **2a** and **2b** (Figure 6) and is compared to analyses of AzMT and 1-NAMT[10]. On a basic level, the HS can be divided into stabilizing (OH, and NH) and destabilizing (OO, ON, and NN) intermolecular interactions. Here, the surface of **2a** consists of 66.3 % stabilizing interactions with a distance of at least 2.6 Å, being significantly shorter than the destabilizing interactions (3.0 Å), which contribute to the HS of 22.9%. In contrast, the HS of **2b** consists of 61.1% stabilizing and 19.6% of destabilizing interactions with minimum distances of 2.3 Å and 3.1 Å, respectively

Table 1. Physicochemical and detonation properties of **2a** and **2b**, compared to AzMT and 1-NAMT.

	1-NMT (**2a**)	2-NMT (**2b**)	AzMT	1-NAMT
Structure	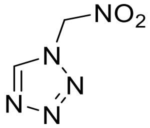	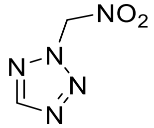	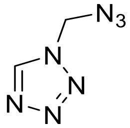	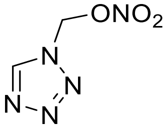
Formula	$C_2H_3N_5O_2$	$C_2H_3N_5O_2$	$C_2H_3N_7$	$C_2H_3N_5O_3$
M [g mol^{-1}]	129.08	129.08	125.1	145.1
IS [J][a]	>40	>360	2	<1
FS [N][b]	>40	288	1	9
T_{endo} [°C][c]	78	49	54	57
T_{exo} [°C][d]	145	161	167	123
ρ [g cm^{-3}][e]	1.62	1.65	1.55	1.68
N [%][f]	54.26	54.26	78.38	48.27
Ω_{CO} [%][g]	−18.59	−18.59	−70.34	−5.51
$\Delta_f H°$ [kJ mol^{-1}][h]	253	235	655	187
$\Delta_f H°$ [kJ kg^{-1}][i]	1958	1817	5232	1398
EXPLO5 V6.05.04				
$-\Delta_{ex}U^0$ [kJ kg^{-1}][k]	4988	4869	5127	5301
V_0 [L kg^{-1}][l]	470	465	502	451
P_{CJ} [kbar][m]	242	246	229	280
V_{det} [m s^{-1}][n]	7952	8009	8124	8294

[a] impact sensitivity (BAM drophammer (1 of 6)). [b] friction sensitivity (BAM friction tester (1 of 6)). [c] Onset temperature of endothermic event in the DTA. [d] Onset temperature of exothermic event in the DTA. [e] Density from X-Ray diffraction recalculated to RT. [f] Nitrogen content. [g] Oxygen balance towards the formation of CO. [h] Calculated (CBS-4M & atomization method) enthalpy of formation [i] Mass related enthalpy of formation. [k] Energy of explosion. [l] Volume of detonation products (assuming gaseous products only). [m] Detonation pressure at the Chapman-Jouguet point. [n] Detonation velocity.

Figure 6 also shows the contribution of each interaction to its respective HS, illustrating a noticeably higher portion of short-range (<3.0 Å) OH and NH interactions for **2a** compared to **2b**. Therefore, the few interactions that result in an overall lower minimum distance for **2b** are compensated by a greater overall quantity of short-range interactions. Nonetheless, these are only minor differences, explaining the overall minor differences in sensitivities observed for **2a** and **2b**. Major differences are noticed when comparing these two with their structural analogous. AzMT (62%) shows an equal, 1-NAMT (50%) a lower contribution of stabilizing interactions to their respective HS, while drastically more destabilizing interactions are observed for both AzMT (29%) and 1-NAMT (40%). This is accompanied by a simultaneous weakening of stabilizing interactions together with a strengthening of destabilizing effects for both, AzMT and 1-NAMT. These drastic differences in HS contribution distribution and strength of interactions explain the differences in sensitivities.

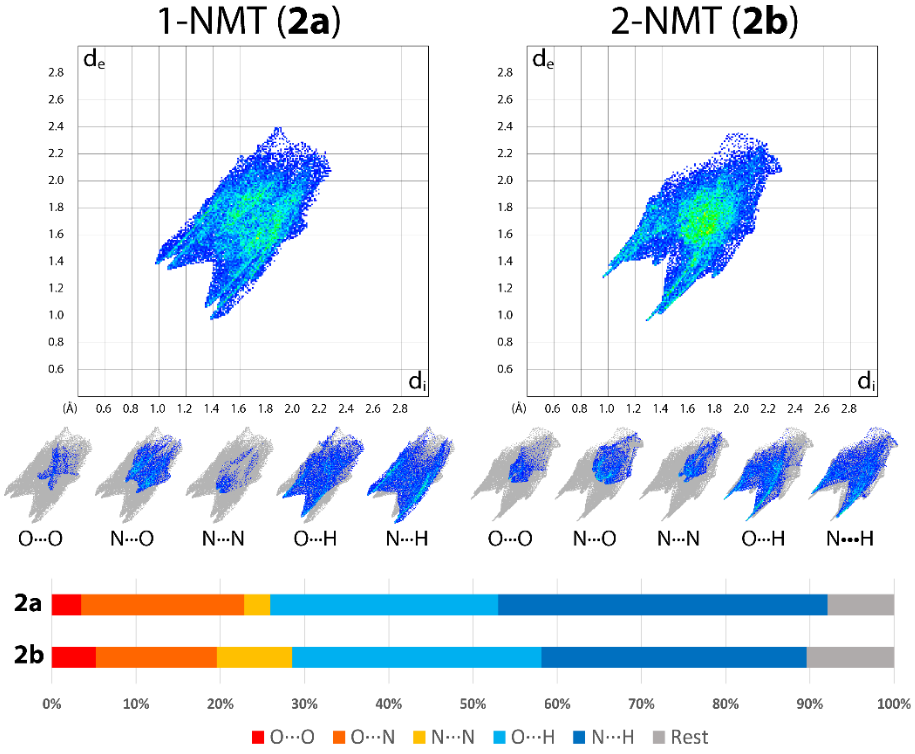

Figure 6. Hirshfeld analysis of compounds **2a** and **2b** with contribution of destabilizing (O···O, N···O, and N···N) and stabilizing (O···H, and N···H) interactions.

Thermal behavior. Additionally, the thermal behavior of **2a** and **2b** was analyzed by differential thermal analysis (Figure 7). Compound **2a** exhibits an endothermic event at an onset temperature of 78 °C, which is about 30 °C higher than the endothermic event happening in the DTA measurement of **2b**. For both compounds, these events derive from the melting of the individual compound, which was proven by *Büchi* melting point analyses. This shows the capability of the *N*-nitromethyl moiety to introduce or lower the melting point *NH* acidic compounds. Further, **2a** shows an exothermic event in the DTA at an onset temperature of 145 °C, correlating to an exothermic decomposition. The same is observed for compound **2b**, but at a higher temperature of 161 °C. Ultimately, the thermal behavior of **2b** is comparable to that of AzMT, whereas **2a** is slightly lower thermally stable besides having a higher melting point. Interestingly, the melting point of **2b** is nearly equivalent to that of 1-NAMT (57 °C), while the thermal stability is increased by 38 °C.

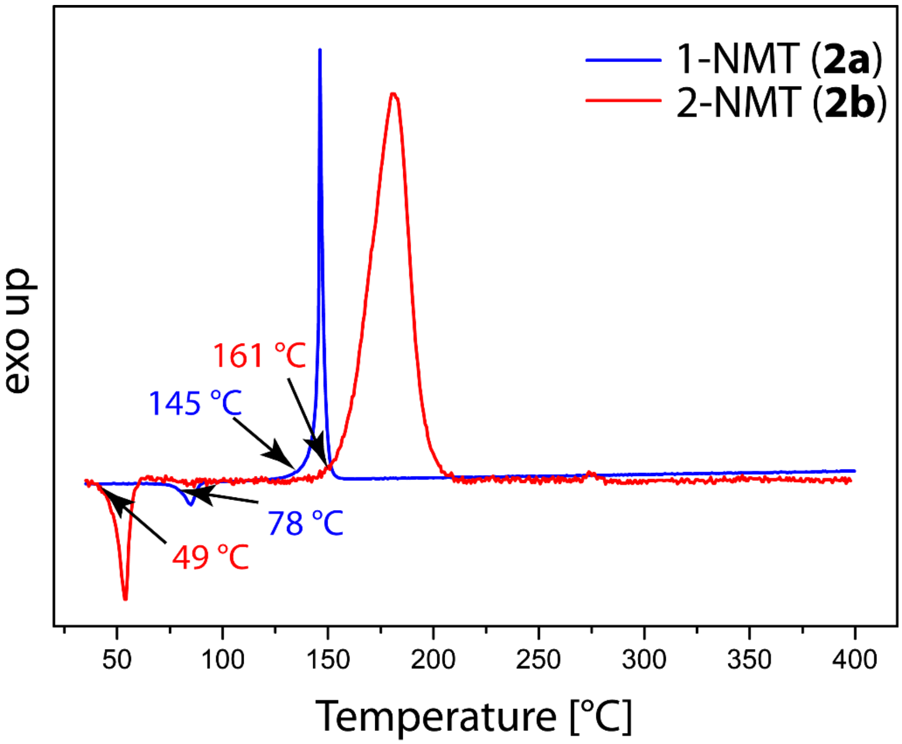

Figure 7. Differential thermal analysis of **2a** and **2b** with a heating rate of 5 °C min^{-1}.

6.2.5 Synthesis of ECCs

As the initial goal to expand the series of *N*-methylene functionalized tetrazoles as ligands for energetic coordination compounds, we applied **2a** as a ligand for ECCs of Cu(II) chlorate and nitrate as well as of the perchlorates of Cu(II), Fe(II), Ni(II), and Fe(II). We decided to focus on **2a** as a ligand for ECCs, as it was shown that the 1*N*-isomers most often exhibit advantageous properties over those of the 2*N*-isomers. Further, until a substantial improvement of the overall low yield of **2b** is found, the application of 2**b** as a ligand is rendered highly uneconomic and unecological.

The synthesis of ECCs **3**–**8** is shown in Scheme 2. Compounds **3**–**8** were obtained by dissolving the corresponding metal salt in ethanol heated to 80 °C and adding stoichiometric amounts of compound **2a**. After stirring at 80 °C for 5 minutes, the resulting clear solutions were left to crystallize. After 1–2 days, or when nearly all solvent had evaporated, the formed crystals were filtered off. It is also possible to add a large excess of n-hexane as an anti-solvent and thus precipitate the respective ECCs as a fine powder. Due to the unavailability of pure copper(II) chlorate, it had to be freshly produced by a metathesis reaction of copper(II) sulfate pentahydrate and barium(II) chlorate monohydrate, following a previously published procedure[8]. Several attempts to obtain the ECC of silver(I) perchlorate resulted in the sole formation of decomposition products. Experimental procedures can be found in the Supporting Information.

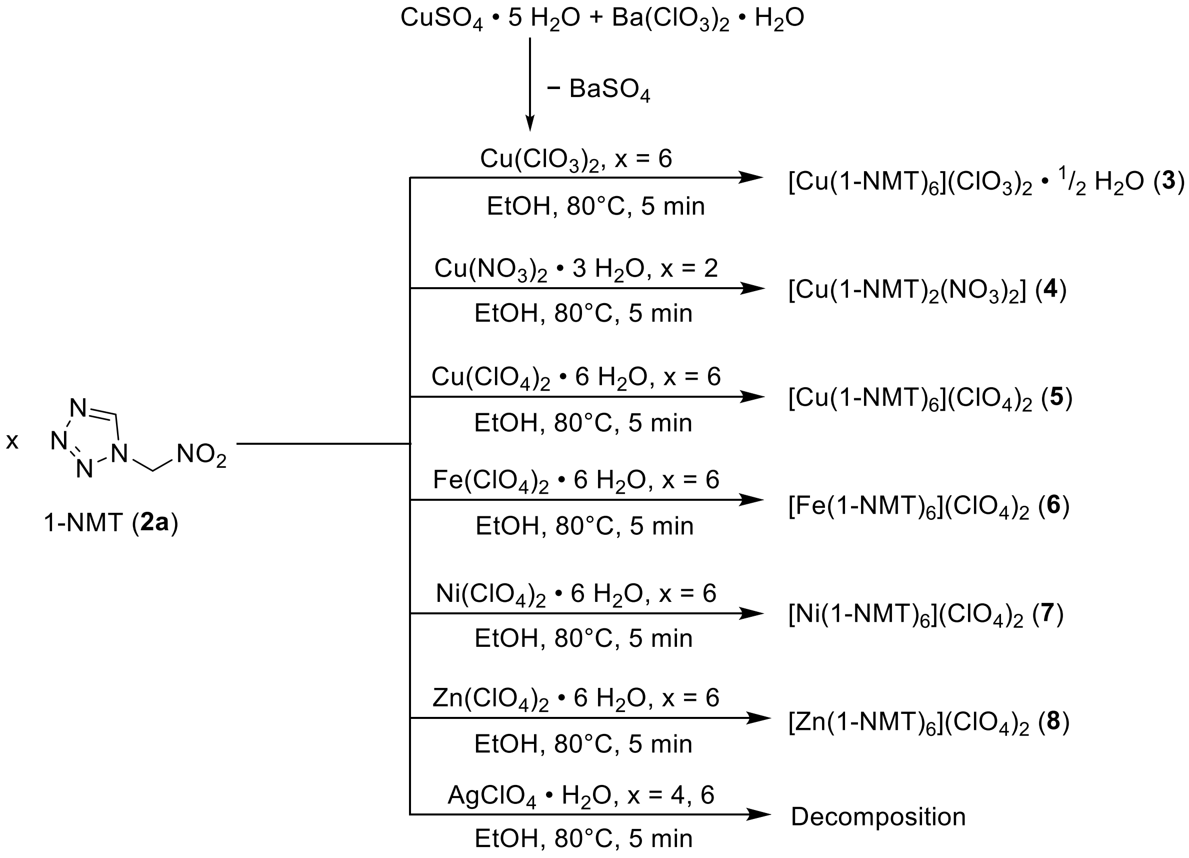

Scheme 2. Synthesis of ECCs of copper(II) chlorate (**3**), copper(II) nitrate (**4**), 3d-metal perchlorates (**5**–**8**) with 1-(Nitromethyl)tetrazole (**2a**).

6.2.6 Crystal Structures of ECCs

The crystal structures of all ECCs, except for compound **7**, were recorded by low-temperature single crystal X-ray diffraction experiments. All attempts to crystallize **7** from different solvents resulted in the formation of amorphous material, which was not suitable for X-Ray diffraction experiments. Compound **3** (Figure 8) crystallizes in the monoclinic space group *C*2/*c* with a density of 1.77 g cm^{-3} and two formula units in the unit cell. The copper(II) cation is sixfold coordinated by ligands of **2a**, forming a slightly *Jahn-Teller* distorted octahedron. Owing to the electron configuration [Ar]3d^9 of copper(II), a degradation of the dz^2 orbital leads to a stretching of the *z* axis, thus explaining the longer bond length of Cu1–N9 2.41 Å compared to Cu1–N4 (2.02 Å) and Cu1–N9 (2.03 Å). Additionally, slight deviations from the perfect 90° bond angles are observed with deviations of up to 2.63 ° (N9–Cu1–N14). Additionally, the coordination of the copper(II) cation does not result in a change in bond lengths and angles within the tetrazole ligands.

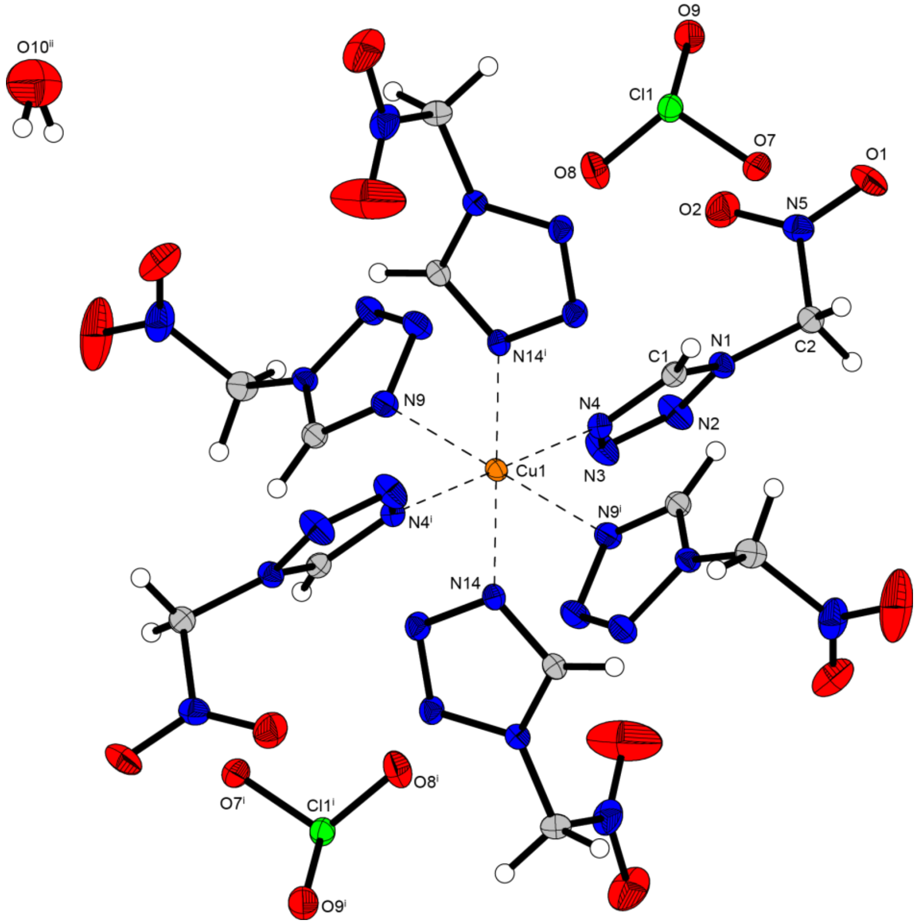

Figure 8. Crystal structure of $[Cu(1\text{-}NMT)_6](ClO_3)_2 \bullet 0.5\ H_2O$ (**3**); Selected bond lengths [Å]: Cu1–N4 2.02(16), Cu1–N9 2.41(17), Cu1–N14 2.03(17); Angles [°]: N4–Cu1–N9 88.27(6), N4–Cu1–N14 90.82(7), N9–Cu1–N14 92.63(6).

Compound **4** (Figure 9) crystallizes in the monoclinic space group *C*2/*c* with a density of 1.97 g cm^{-3}, the highest of all herein investigated compounds, and eight formula units in the unit cell. The copper(II) cation is fourfold coordinated by two ligands of **2a**, as well as the two nitrate anions with bond lengths of around 1.99 Å for all four ligands. Both tetrazole ligands and the nitrate anions are positioned opposite to each other, forming a nearly perfect square with minor angle deviations of 0.83 ° off the perfect 90 °. Due to a bending of the ligands in opposite directions by 171.02 (N4–Cu1–N9) and 171.20 (O5–Cu1–O9), the formed square is significantly twisted instead of being planar.

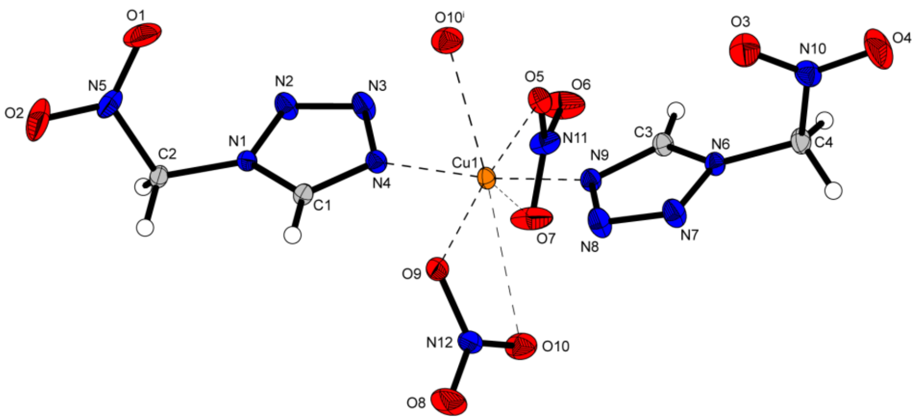

Figure 9. Crystal structure of $[Cu(1\text{-}NMT)_2(NO_3)_2]$ (**4**); Selected bond lengths [Å]: Cu1–O5 1.99(11), Cu1–O9 1.98(11), Cu1–N4 1.99(13), Cu1–N9 1.97(13); Angles [°]: O5–Cu1–O9 171.20(4), N4–Cu1–N9 171.02(4), O9–Cu1–N4 89.17(5), O5–Cu1–N9 89.69(4).

Compounds **5**, **6**, and **8** (Figures 10, S7, and S8) all crystallize in the monoclinic space group C2/c with densities of 1.75 g cm^{-3}, 1.80 g cm^{-3}, and 1.76 g cm^{-3}, respectively. All compounds contain four formula units in the unit cell. Like in compound **3**, the metal(II) cations are coordinated by six molecules of **2a**. Due to the electron configuration of $[Ar]3d^9$, a degradation of the dz^2 orbital in **5** is accompanied by longer bond distances along the *z* axis, and thus the typical *Jahn-Teller* distorted octahedron is observed. This explains the longer bond lengths of two ligands (2.30 Å) compared to their four counterparts (2.02 Å). Contrary, the metal cations of **6** and **8** exhibit electron configurations of $[Ar]d^6$ (**6**) and $[Ar]d^{10}$ (**8**), rendering a degradation of one of the e_g orbitals not beneficial, thus explaining the nearly perfect octahedrons observed for both compounds. Nonetheless, major differences in metal to ligand bond distances are observed. The bond distances in **6** are nearly all 2.00 Å long, whereas those of **8** exhibit lengths between 2.15–2.18 Å. The minor differences in bond lengths in **8** are caused by steric repulsion due to an ion radius of 0.740 Å for a sixfold coordinated zinc(II) cation, representing the smallest cation of first-row transition metals starting from manganese[23]. Interestingly, the clear crystals of **6** showed a change to a deep purple color when being cooled down (133 K) for single crystal X-ray diffraction experiments (Figure 11). This is an implication of a thermochromic effect of the coordination compound, and hence a second X-ray diffraction experiment of the same crystal at a higher temperature (173 K) was performed. At this temperature, the original orange color was still maintained. Figure S6 depicts the thus obtained second crystal structure of compound **6**. While no change in the coordination polyhedron is observed, thus equal bond angles are observed, the bond lengths between the iron(II) cation and the six ligands are significantly longer, between 2.16–2.18 Å, compared to those at low temperatures (<2.00 Å). This change in bond lengths is caused by a spin-crossover from a high spin iron(II) above 173 K to a low spin iron(II) at temperatures below 173 K. This thermochromic effect was already observed for other iron(II) perchlorate coordination compounds[24]. Additionally, the bond lengths of 2.16–2.18 Å are equal to those of **8**, which only occurs as a high-spin coordination compound.

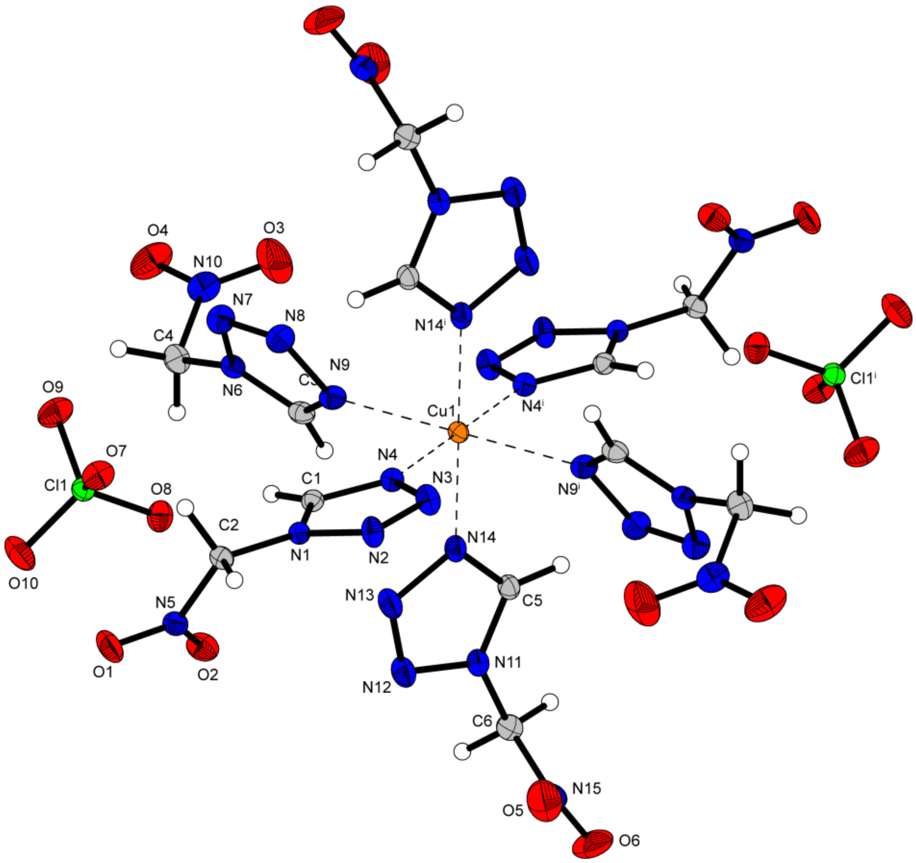

Figure 10. Crystal structure of $[Cu(1\text{-}NMT)_6](ClO_4)_2$ (**5**); Selected bond lengths [Å]: Cu1–N4 2.02(18), Cu1–N9 2.30(18), Cu1–N14 2.08(18); Angles [°]: N4–Cu1–N9 88.47(7), N4–Cu1–N14 90.14(7), N4–Cu1–N4^{i} 180.0.

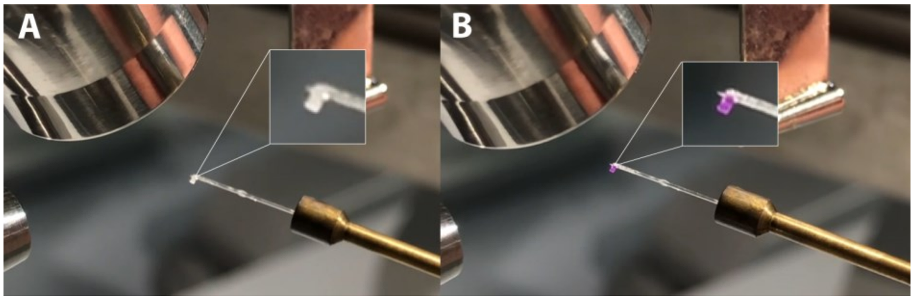

Figure 11. Thermochromic effect of **6**. A) clear crystal at RT; B) purple colored crystal at <133 K.

6.2.7 Physicochemical Properties

Table 2 compares the measured and calculated physicochemical properties of ECCs **3**–**8**. Additionally, the copper(II) perchlorate ECCs with AzMT and 1-NAMT as ligands are included for comparison. Compound **3** exhibits an exothermic signal at 102 °C (Figure S17), correlating to the exothermic decomposition, therefore being the only compound within this work that expresses lower thermal stability than the pure **2a**. This rather low thermal stability can be explained by the hygroscopicity of the compound. The inclusion of crystal water is necessary to stabilize the coordination compound. When heated to 102 °C, it is most likely that the crystal water starts to evaporate, thus leaving an anhydrous compound **3**, which is highly unstable and immediately starts to decompose. For ECCs **4**–**8** (Figure S17), sharp exothermic decompositions were observed between 155 °C (**4**) and 217 C (**7**), being significantly more stable than the ECCs based on AzMT (133 °C) and 1-NAMT (119 °C). Especially the nickel(II) complex (**7**) was able to improve the lack of thermal stability of **2a** by an impressive 72 °C. While the formation of ECCs causes a drastic increase in sensitivities overall, all compounds still exhibit lower friction sensitivities than their AzMT and 1-NAMT derivatives. The chlorate (**3**) and perchlorate (**5** – **8**) compounds exhibit friction sensitivities between 14 N (**6**) and 42 N (**3**), thereby expressing very high stabilities compared to their AzMT derivatives (<0.1 N). Compound **4** is the most stable ECC within this work, with a friction sensitivity of 80 N, which is in the range of typical booster explosives such as PETN.[25] This is particularly interesting, as any stabilizing effect of the completely insensitive ligand (**2a**) would be expected to be prominent in ECCs **3**, **5**–**8**, having a high ligand to metal salt ratio (6:1), whereas a lower stabilizing effect would be expected for **4** with a ratio of 2:1. Ultimately, the increase in sensitivity of the pure ligand **2a** is in good agreement with previous findings.[8, 26, 27]

Table 2. Thermal stability as well as sensitivities towards impact and friction and estimated detonation velocities.

Compound	T_{exo}[a] [°C]	IS[b] [J]	FS[c] [N]	V_{det}[d] [m s^{-1}]
1-NMT (**2a**)	145	>40	>360	7952
[Cu(1-NiMT)$_6$](ClO$_3$)$_2$ • 0.5 H$_2$O (**3**)	102	4	42	
[Cu(NO$_3$)$_2$(1-NiMT)$_2$] (**4**)	155	<1	80	8082
[Cu(1-NiMT)$_6$](ClO$_4$)$_2$ (**5**)	160	<1	30	7793
[Fe(1-NiMT)$_6$](ClO$_4$)$_2$ (**6**)	176	<1	14	8033
[Ni(1-NiMT)$_6$](ClO$_4$)$_2$ (**7**)	217	<1	32	
[Zn(1-NiMT)$_6$](ClO$_4$)$_2$ (**8**)	187	<1	28	7824
[Cu(AzMT)$_6$](ClO$_4$)$_2$	133	<1	<0.1	7222
[Cu(1-NAMT)$_6$](ClO$_4$)$_2$	119	2	0.75	7910

[a] Onset temperature of exothermic event in the DTA. [b] Impact sensitivity (BAM drop hammer (1 of6)). [c] Friction sensitivity (BAM friction tester (1 of 6)). [d] Calculated detonation velocity; Detailed information can be found in the SI.

By applying an increment method developed by Ilyushin[28] it was possible to estimate the detonation velocities of ECCs **4**, **5**, **6**, and **8**. Due to the unavailability of incremental data or a crystallographic density, it was not possible to estimate the detonation velocities of **3** and **7**. Compound **5** (7793 m s^{-1}) is able to outperform the corresponding complex of AzMT (7222 m s^{-1}), though the pure ligand lacks behind the detonation velocity of pure AzMT, ultimately highlighting the importance of a good oxygen balance. This is supported by an even higher detonation velocity of the corresponding ECC based on 1-NAMT (7910 m s^{-1}), which exhibits an even higher oxygen balance than 1-NMT. Ultimately, the remaining ECCs are estimated to exhibit even higher detonation velocities than **5**. Especially **4** is estimated to have the highest detonation velocity of 8082 m s^{-1}, even surpassing pure **2a** (7952 m s^{-1}) and included ECC of 1-NAMT, once again proving the big influence of a high theoretical maximum density (1.97 g cm^{-3}).

Initiation capabilities. To get a better insight into the behavior of the compounds towards fast heating with and without confinement, hot plate (HP) and hot needle (HN) tests were performed. The results from HP and HN tests are summarized in Table 3, and detailed procedures for the HP and HN test are included in the SI. As the HP test assesses the behavior upon fast heating without confinement, all tested compounds (**3**–**8**) showed deflagration (Figures S18–23) and were not able to undergo a deflagration to detonation transition (DDT).

Table 3. Behavior in HP and HN tests of compounds **3**–**8** as well as laser initiation results.

Compound	HP[a]	HN[a]	7A[b]			8A[b]
3	Def.	Def.	–	–	–	
4	Def.	Det.	τ = 1 ms dec.	τ = 15 ms dec.	τ = 30 ms dec.	τ = 30 ms dec.
5	Def.	Det.	–	τ = 15 ms dec.	τ = 30 ms dec.	τ = 30 ms det.
6	Def.	Def.	–	τ = 15 ms dec.	τ = 30 ms dec.	τ = 30 ms det.
7	Def.	Def.	–	–	–	–
8	Def.	Def.	–	–	–	–

[a] Results from HP and HN testing: Def. = deflagration; Det. = detonation. [b] Operating parameters: current I = 7 and 8 A; voltage U = 4 V; theoretical maximum output power P_{max} = 45 W; theoretical energy E_{max} = 0.8–51 mJ; wavelength λ = 915 nm; pulse length τ = 1–30 ms. (– = not tested; dec. = decomposition; det. = detonation).

Further, the HN test allows for a first analysis of the behavior towards fast heating with confinement, where compounds **4** (Figure 12) and **5** (Figure S20) showed detonation, whereas all other compounds showed deflagration (Figures 13 and S18, S21–23). Therefore, compounds **4** and **5** are able to undergo DDT, which is a crucial characteristic for the application as a primary explosive. Complementary to HP and HN tests, the capability to be initiated by a single laser pulse was checked. Here, the most promising ECCs (**4**, **5**, **6**) were irradiated by a single-pulsed 45 W InGaAs laser diode. 25 mg of the compound was filled into a transparent polycarbonate percussion cap, pressed with 1 kN, and sealed with UV curing adhesive. The sample was placed in the focused beam path and irradiated with a single laser pulse with a wavelength of 915 nm, a voltage of 4 V, a current of 7–8 A, and a pulse length of 1.0, 15, or 30 ms. The results of these experiments are listed in Table 3. Compound **4** showed deflagration (Figure S24) at all tested energies (0.8–51 mJ) and was, therefore, not successfully initiated. The same behavior was observed for compounds **5** and **6** when irradiated with energies of 12 and 24 mJ, whereas both compounds showed detonation when irradiated with the highest tested energy of 51 mJ (Figure 14). Hence, **5** and **6** were able to undergo DDT and thus are applicable as laser initiable primary explosives.

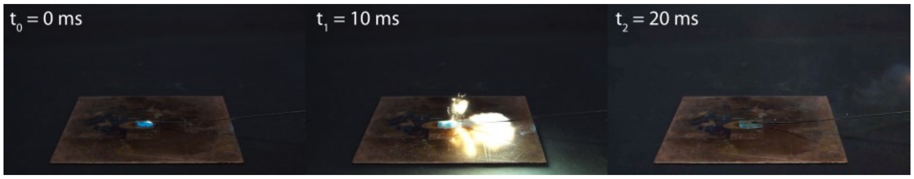

Figure 12. Moment of detonation of compound **4** in the Hot Needle test.

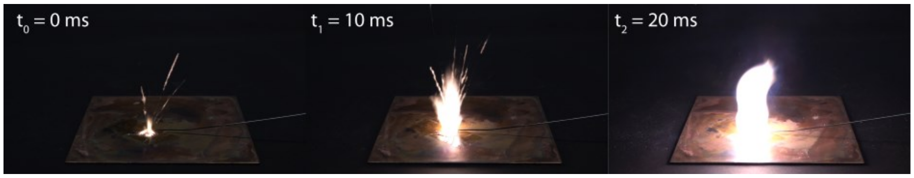

Figure 13. Moments of deflagration of compound **7** in the Hot Needle test.

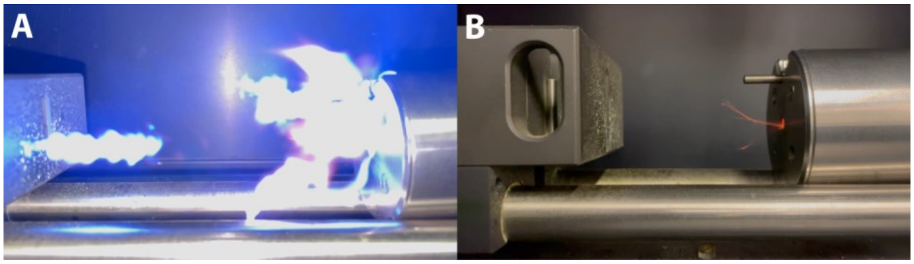

Figure 14. Moments of detonation of compound **5** and **6** during laser initiation testing at 51 mJ.

To further test the applicability as a primary explosive, typical PETN initiation tests were performed. The setup of the initiation tests can be found in the Supporting Information. Owing to the initiation of the supposed primary explosive by an electrical igniter, only compounds that had a positive HN result (**4** and **5**) were tested, as they were proven to undergo DDT upon thermal stimulation. Owing to the deflagration in the HP tests, both compounds were tested once loosely on top of the pressed PETN as well as also pressed on top of the PETN. However, all four tests involving 20 mg of the complexes were negative, as both compounds were unable to initiate PETN. This can be deducted from the still intact witness plates depicted in Figure 15.

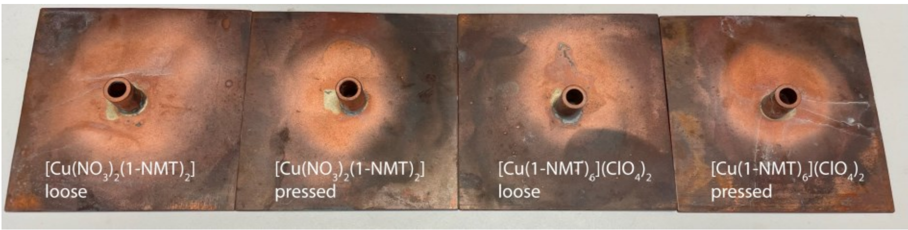

Figure 14. Intact copper witness plates after unsuccessful PETN initiation tests.

6.3 Conclusion

The nitrogen-rich 1-(Nitromethyl)tetrazole (1-NMT, **2a**) and 2-(Nitromethyl)tetrazole (2-NMT, **2b**) were synthesized for the first time, representing the fourth and fifth ever synthesized *N*-nitrometyl azoles. Although they are obtained by nitration in moderate yields, it is possible to recover the starting material. Both compounds are extensively analyzed by low-temperature X-ray diffraction experiments as well as elemental analysis, IR spectroscopy, DTA, and multinuclear (^{1}H, ^{13}C, ^{14}N (**2b**), and ^{15}N (**2a**)) NMR spectroscopy. Additionally, their sensitivities towards external stimuli were analyzed, where both compounds were unexpectedly completely (**2a**) or nearly (**2b**) insensitive towards impact and friction. This supports the first hints of drastically decreased sensitivities for *N*-nitromethyl-containing azoles, which is favorable when designing new insensitive or melt-castable high explosives. Future research should focus on the introduction of this functionality into different azole scaffolds. Further, **2a** was applied as a ligand for energetic coordination compounds of copper(II) chlorate (**3**), nitrate (**4**), and perchlorate (**5**), as well as perchlorates of iron(II) (**6**), nickel(II) (**7**) and zinc(II) (**8**). All ECCs, except **7**, were analyzed by low-temperature single crystal X-ray diffraction. Like **2a**, the sensitivities towards impact and friction were measured, revealing a drastic increase in sensitivity compared to the pure ligand but still being significantly more stable than the ECCs based on 1-(Azidomethyl)tetrazole and 1-(Nitratomethyl)tetrazole, structural relatives of **2a**. The applicability as a primary explosive of the ECCs was tested, where compounds **4** and **5** showed a DDT upon thermal ignition with confinement. Despite showing a DDT, compounds **4** and **5** were not able to initiate pressed PETN in preliminary experiments. However, compounds **5** and **6** were able to be initiated by a single laser pulse at an energy of 51 mJ which enables their further investigation and uses as laser ignitable high-energy materials.

6.4 Experimental Part

Although compounds **2a** *and* **2b** *are completely insensitive towards external stimuli, they are still to be classified as explosives. Therefore, proper security precautions (safety glasses, face shield, earthed equipment and shoes, leather jacket, Kevlar gloves, Kevlar sleeves and ear plugs) have to be worn while synthesizing and handling these compounds.*

Precursor compounds such as 1-(tetrazol-1-yl)propan-2-on (**1a**), 1-(tetrazol-2-yl)propan-2-on (**1b**) and bromoacetone were synthesized according to literature.[16, 17]

1-(Nitromethyl)tetrazol (2a)

Inspired by the procedure described by *V. V. Semenov et al.*[14], a solution of conc. H_2SO_4 (96%, 12. mL) in H_2O (4.5 mL) was prepared and cooled to 5 °C, before **1a** (2.00 g, 15.5 mmol, 1.0 eq.) was added in one portion. HNO_3 (100%, 5.0 mL) was then added dropwise to the mixture, while keeping the temperature below 5 °C. After completion of the addition, the reaction mixture was stirred for 55 min while being allowed to warm to r.t., before being quenched by pouring the solution in an aq. $NaHCO_3$ solution (57.5 g, in 100 mL H_2O). The quenched mixture was then extracted into EtOAc (800 mL), the combined organic phases were dried over $MgSO_4$ and concentrated *in vacuo*. The remaining solvent was allowed to evaporate in an open container. The residue was purified via column chromatography (silica gel, EtOAc:*n*-hexane = 60:40 to 100:0). 1-NiMT (**2a**) (0.54 g, 4.21 mmol, 27%, Rf = 0.5) was obtained as colorless crystals.

DTA (5 °C min^{-1}):78 °C (T_{endo}), 145 °C (T_{exo}); **^{1}H NMR** (400 MHz, acetone-d$_6$, 25 °C): δ = 9.49 (s, 1H), 7.20 ppm (s, 2H); **^{13}C NMR** (400 MHz, acetone-d$_6$, 25 °C): δ = 146.6 (N(CH)N), 77.9 ppm ($N(CH_2)NO_2$); **^{15}N NMR** (400 MHz, acetone-d$_6$, 25 °C): δ = 15.63 (d, J = 3.4 Hz, N3), –9.06 (t, J = 1.3 Hz, N5), –11.33 (s, N2), –49.7 (d, J = 12.6 Hz, N4), –154.54 (d, J = 9.4 Hz, N1). **IR** (ATR, cm^{-1}): $\tilde{\nu}$ = 3151 (m), 3046 (m), 2973 (m), 2944 (w), 2843 (w), 1776 (w), 1718 (w), 1567 (vs), 1500 (w), 1477 (s), 1457 (w), 1436 (m), 1375 (s), 1327 (s), 1307 (m), 1271 (m), 1179 (s), 1093 (s), 1020 (m), 1014 (w), 976 (w), 942 (m), 889 (s), 806 (vs), 719 (w), 709 (m), 683 (vs), 648 (m), 571 (m), 41 1(m); **EA** ($C_2H_3N_5O_2$, 129.08) calc.: C 18.61 H 2.34 N 54.26%, found C 19.01 H 2.48 N 53.07%; **BAM drop hammer**: >40 J. **BAM friction tester**: >360 N.

2-(Nitromethyl)tetrazol (2b)

Inspired by the procedure described by *V. V. Semenov et al.*[14], a solution of conc. H_2SO_4 (96%, 12. mL) in H_2O (6 mL) was prepared and cooled to 5 °C, before **1b** (2.00 g, 15.5 mmol, 1.0 eq.) was added in one portion. HNO_3 (100%, 5.0 mL) was then added dropwise to the mixture, while keeping the temperature below 5 °C. After completion of the addition, the reaction mixture was stirred for 58 min while being allowed to warm to r.t., before being quenched by pouring the solution in an aq. $NaHCO_3$ solution (57.5 g, in 100 mL H_2O). The quenched mixture was then extracted into EtOAc (500 mL), the combined organic phases were dried over $MgSO_4$ and concentrated *in vacuo*. The remaining solvent was allowed to evaporate in an open container. The residue was purified via column chromatography (silica gel, EtOAc:*n*-hexane = 50:50 to 100:0). 2-NiMT (**2b**) (0.24 g, 1.86 mmol, 12%, Rf = 0.5) was obtained as yellowish crystals.

DTA (5 °C min^{-1}):49 °C (T_{endo}), 161 °C (T_{exo}); **^{1}H NMR** (400 MHz, acetone-d_6, 25 °C): $\delta = 9.05$ (s, 1H), 7.39 ppm (s, 2H); **^{13}C NMR** (400 MHz, acetone-d_6, 25 °C): $\delta = 155.3$ (N(CH)N), 81.6 ppm ($N(CH_2)NO_2$); **^{14}N NMR** (400 MHz, acetone-d_6, 25 °C): $\delta = -9.92$ ppm (NO_2); **IR** (ATR, cm^{-1}): $\tilde{\upsilon}$ = 3158 (m), 3051 (m), 2977 (m), 2940 (w), 1812 (w), 1728 (w), 1580 (vs), 1458 (w), 1417 (m), 1397 (s), 1364 (s), 1336 (m), 1313 (m), 1287 (s), 1213 (s), 1166 (m), 1118 (s), 1024 (s), 1002 (s), 978 (m), 909 (s), 829 (vs), 708 (s), 698 (s), 669 (vs), 641 (m), 608 (w), 571 (m), 409 (w); **EA** ($C_2H_3N_5O_2$, 129.08) calc.: C 18.61 H 2.34 N 54.26%, found C 19.11 H 2.43 N 53.27%; **BAM drop hammer**: >40 J. **BAM friction tester**: >288 N.

6.5 Acknowledgment

Financial support of this work by the Ludwig Maximilian University of Munich (LMU), the Office of Naval Research (ONR) under grant no. N00014-19-1-2078 gratefully acknowledged.

6.6 References

[1] F. Kurzer, *J. Chem. Educ.* **2000**, *77*, 851.

[2] E. Howard, XI. *Philos. Trans. R. Soc.* **1800**, *90*, 204-238.

[3] T. M. Klapötke, *Energetic Materials Encyclopedia*, DeGruyter **2021**.

[4] P. B. Tchounwou, C. G. Yedjou, A. K. Patlolla, D. J. Sutton, *Molecular, Clinical and Environmental Toxicology* **2012**, *3*, 133–164.

[5] M. L. Sall, A. K. D. Diaw, D. Gningue-Sall, S. E. Aaron, J.-J. Aaron, *Environ. Sci. Pollut. Res.* **2020**, *27*, 29927-29942.

[6] J. Malm, Candidate List of substances of very high concern for Authorisation. https://echa.europa.eu/candidate-list-table. (Accessed 02.08.**2022**).

[7] M. H. H. Wurzenberger, V. Braun, M. Lommel, T. M. Klapötke, J. Stierstorfer, *Inorg. Chem*. **2020**, *59*, 10938-10952.

[8] M. H. H. Wurzenberger, M. S. Gruhne, M. Lommel, N. Szimhardt, T. M. Klapötke, J. Stierstorfer, *Asian J. Chem*. **2019**, *14*, 2018-2028.

[9] M. S. Gruhne, T. Lenz, M. Rösch, M. Lommel, M. H. H. Wurzenberger, T. M. Klapötke, J. Stierstorfer, *Dalton Trans*. **2021**, *50*, 10811-10825.

[10] V. Braun, M. Kofen, S. M. J. Endraß, T. M. Klapötke, and J. Stierstorfer, **2022**.

[11] M. Kofen, M. Lommel, M. H. H. Wurzenberger, T. M. Klapötke, J. Stierstorfer, *Chem. Eur. J.* **2022**, *28*, e202200492.

[12] G. Zhao, C. He, H. Gao, G. H. Imler, D. A. Parrish, J. n. M. Shreeve, *New J. Chem.* **2018**, *42*, 16162-16166.

[13] O. P. Shitov, V. L. Korolev, V. A. Tartakovsky, *Russ. Chem. Bull*. **2002**, *51*, 499-502.

[14] V. V. Semenov, M. I. Kanischev, S. A. Shevelev, A. S. Kiselyov, *Tetrahedron* **2009**, *65*, 3441-3445.

[15] T. M. Klapötke, M. Stein, J. Stierstorfer, *Z. Anorg. Allg. Chem*. **2008**, *634*, 1711-1723.

[16] P. A. Levene, *Bromoacetone*, Organic Syntheses **1930**, *10*.

[17] V. V. Semenov, V. S. Bogdanov, B. S. Él'yanov, L. G. Mel'nikova, S. A. Shevelev, V. M. Zhulin, A. A. Fainzil'berg, *J. Heterocycl. Chem*. **1982**, *18*, 859-864.

[18] S. F. Trevino, E. Prince, C. R. Hubbard, *Chem. Phys*. **1980**, *73*, 2996-3000.

[19] T. M. Klapötke, M. Kofen, J. Stierstorfer, *Dalton Trans*. **2021**, *50*, 13656-13660.

[20] Y. A. Strelenko, A. B. Sheremetev, L. I. Khmel'nitskii, Monosubstituted furazanes, *J. Heterocycl. Chem*. **1992**, *28*, 927-930.

[21] M. Sućeska, Explo5 V6.05.02, Zagreb (Croatia), **2018**.

[22] UN, "Dangerous goods list, special provisions and excepstions", Recommendations on the Transport of Dangerous Goods: Model Regulations (Nineteenth Revised Edition), New York, **2015**.

[23] R. Shannon, *Acta Crystallogr. A* **1976**, *32*, 751-767.

[24] V. Braun, M. H. H. Wurzenberger, V. Weippert, J. Stierstorfer, *New J. Chem*. **2021**, *45*, 11042-11050.

[25] T. M. Klapötke, *Chemistry of High-Energy Materials*, 6th edition ed., DeGruyter **2022**.

[26] M. H. H. Wurzenberger, N. Szimhardt, J. Stierstorfer, *J. Am. Chem. Soc*. **2018**, *140*, 3206-3209.

[27] M. Kofen, M. Lommel, J. Stierstorfer, T. M. Klapötke, *New Trends in Research of Energetic Materials*, University of Pardubice, Pardubice, Czech Republic, 2022, pp. 114 - 118.

[28] M. A. Ilyushin, A. N. Terpigorev, I. V. Tselinskii, *Russ. J. Gen. Chem*. **1999**, *69*, 1645-1657.

6.7 Supporting Information

6.7.1 Overview of Compounds

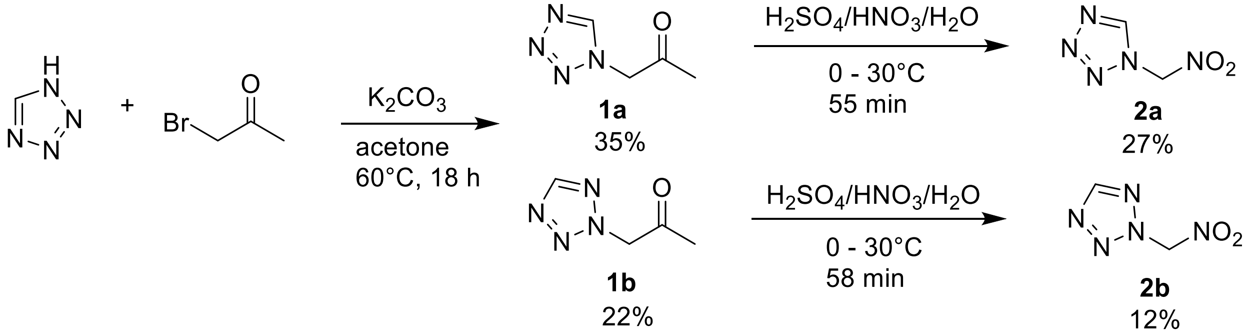

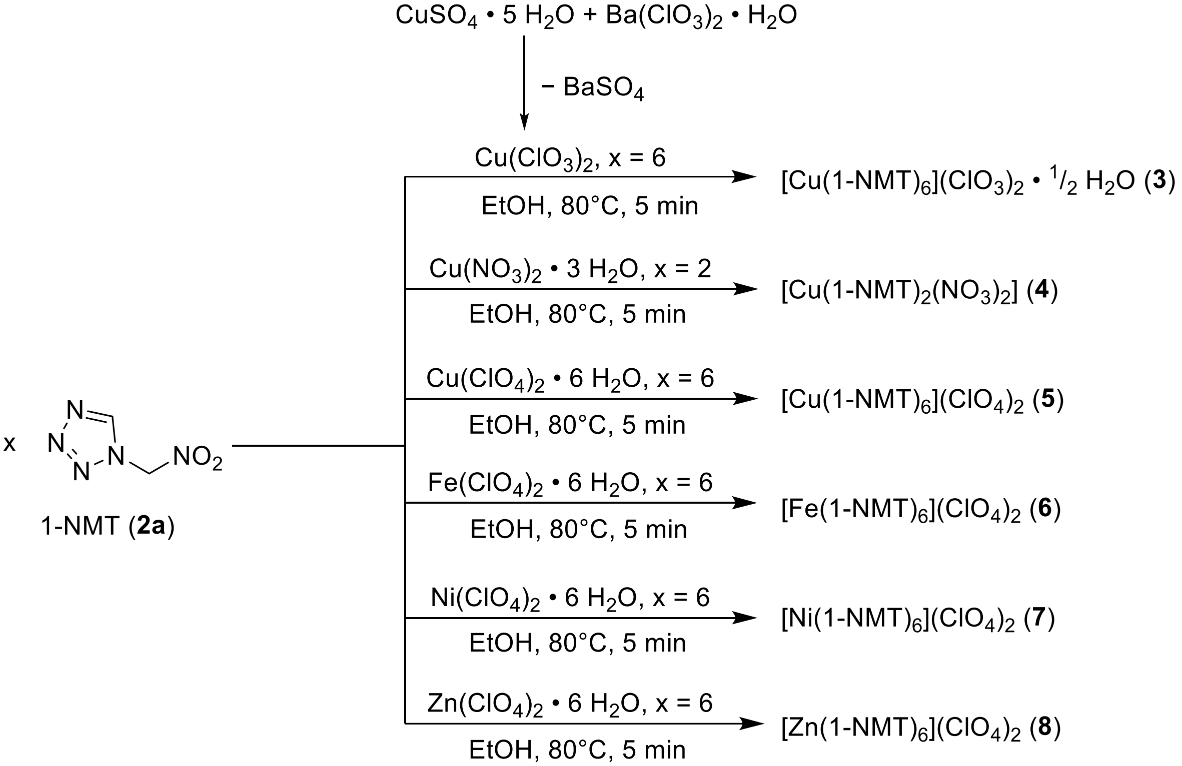

6.7.2 Single Crystal X-ray Diffration

For all crystalline compounds an Oxford Xcalibur3 diffractometer with a CCD area detector or Bruker D8 Venture TXS diffractometer equipped with a multilayer monochromator, a Photon 2 detector, and a rotating-anode generator were employed for data collection using Mo-K_α radiation (λ = 0.7107 Å). On the Oxford device, data collection and reduction were carried out using the CrysAlisPRO software.[S1] On the Bruker diffractometer, the data were collected with the Bruker Instrument Service v3.0.21, the data reduction was performed using the SAINT V8.18C software

(Bruker AXS Inc., 2011). The structures were solved by direct methods (SIR-92,[S2] SIR-97,[S3,S4] SHELXS-97[S5,S6] or SHELXT[S7]), refined by full-matrix least-squares on *F*2 (SHELXL[S5,S6]) and finally checked using the PLATON software[S8] integrated in the WinGX[S7,S9] or Olex2[S8] software suite. The non-hydrogen atoms were refined anisotropically and the hydrogen atoms were located and freely refined. The absorptions were corrected by a SCALE3 ABSPACK or SADABS Bruker APEX3 multi-scan method.[S11,S12] All DIAMOND2 plots are shown with thermal ellipsoids at the 50% probability level and hydrogen atoms are shown as small spheres of arbitrary radius.

Table S1. Crystallographic data and structure refinement details for compounds **2a/b** and **3.**

	2a	**2b**	**3**
Formula	$C_2H_3N_5O_2$	$C_2H_3N_5O_2$	$C_{24}Cl_4H_{38}CuN_{60}O_{37}$
FW [g mol^{-1}]	129.09	129.09	2028.04
Crystal system	orthorhombic	monoclinic	monoclinic
Space group	$P2_12_12_1$ (No. 19)	$P2_1/c$ (No. 14)	$C2/c$ (No. 15)
Color / Habit	colorless block	colorless block	blue lock
Size [mm]	0.22 x 0.47 x 0.73	0.06 x 0.07 x 0.13	0.10 x 0.25 x 0.50
a [Å]	6.9773(8)	5.4080(2)	18.3591(8)
b [Å]	8.5124(9)	14.7319(5)	10.1277(4)
c [Å]	8.6375(9)	6.4014(2)	20.5743(9)
α [°]	90	90	90
β [°]	90	91.790(1)	104.721(5)
γ [°]	90	90	90
V [Å^3]	513.01(10)	509.75(3)	3699.9(3)
Z	4	4	2
$\rho_{calc.}$ [g cm^{-3}]	1.671	1.682	1.820
μ [mm^{-1}]	0.146	0.147	0.851
F(000)	264	264	2048
$\lambda_{MoK\alpha}$ [Å]	0.71073	0.71073	0.71073
T [K]	102	173	95
θ Min-Max [°]	3.4, 32.6	2.8, 27.5	2.0, 29.2
Dataset	-6:9; -12:11; -12:12	-6:7; -19:18; -8:8	-24:23; -13:13; -28:18
Reflections collected	2958	9528	13151
Independent refl.	1678	1141	4394
R_{int}	0.025	0.027	0.023
Observed reflections	1360	1049	3699
Parameters	83	82	295
R_1 (obs)[a]	0.0475	0.0303	0.0367
wR_2 (all data)[b]	0.0977	0.0768	0.0930
S [c]	1.03	1.09	1.05
Resd. dens [e Å^{-3}]	-0.24, 0.26	-0.17, 0.25	-0.43, 0.63
Device type	Oxford Xcalibur3	Oxford Xcalibur3	Oxford Xcalibur3
Solution	SHELXT	SHELXT	SHELXT
Refinement	SHELXL-2018	SHELXL-2018	SHELXL-2018
Absorption correction	multi-scan	multi-scan	multi-scan

---

[a]$R_1 = \Sigma||F_0|-|F_c||/\Sigma|F_0|$; [b]$wR_2 = [\Sigma[w(F_0^2-F_c^2)^2]/\Sigma[w(F_0)^2]]^{1/2}$; $w = [\sigma c^2(F_0^2)+(xP)^2+yP]^{-1}$ and $P=(F_0^2+2F_c^2)/3$; [c]$S = \{\Sigma[w(F_o^2-F_c^2)^2]/(n-p)\}^{1/2}$ (n = number of reflections; p = total number of parameters).

Table S2. Crystallographic data and structure refinement details for compounds **4 – 6.**

	4	**5**	**6@133K**
Formula	$C_4H_6CuN_{12}O_{10}$	$C_{12}Cl_2H_{18}CuN_{30}O_{20}$	$C_{12}Cl_2H_{18}FeN_{30}O_{20}$
FW [g mol^{-1}]	445.75	1037.00	1029.31
Crystal system	monoclinic	monoclinic	monoclinic
Space group	*C*2/*c* (No. 15)	*C*2/*c* (No. 15)	*C*2/*c* (No. 15)
Color / Habit	blue block	blue platelet	purple plate
Size [mm]	0.06 x 0.14 x 0.16	0.07 x 0.21 x 0.48	0.02 x 0.10 x 0.20
a [Å]	23.4408(6)	18.1971(9)	18.1204(15)
b [Å]	5.1875(1)	10.2246(4)	10.1850(8)
c [Å]	25.6919(7)	21.1062(9)	20.6419(15)
α [°]	90	90	90
β [°]	109.477(1)	103.353(4)	103.388(3)
γ [°]	90	90	90
V [Å^3]	2945.34(13)	3820.8(3)	3706.1(5)
Z	8	4	4
$\rho_{calc.}$ [g cm^{-3}]	2.010	1.803	1.845
μ [mm^{-1}]	1.573	0.829	0.673
F(000)	1784	2092	2080
$\lambda_{MoK\alpha}$ [Å]	0.71073	0.71073	0.71073
T [K]	173	100	133
θ Min-Max [°]	2.0, 33.2	2.3, 26.4	2.3, 26.4
Dataset	-36:36; -7:7; -39:39	-22:21; -12:12; -22:26	-22:22; -12:12; -25:25
Reflections collected	39653	17257	30267
Independent refl.	5602	3913	3772
R_{int}	0.030	0.034	0.055
Observed reflections	4915	3186	3396
Parameters	244	295	295
R_1 (obs)[a]	0.0278	0.0340	0.0327
wR_2 (all data)[b]	0.0691	0.0878	0.0828
S [c]	1.05	1.03	1.06
Resd. dens [e Å^{-3}]	-0.42, 0.73	-0.36, 0.44	-0.44, 0.50
Device type	Bruker D8 Venture TXS	Bruker D8 Venture TXS	Bruker D8 Venture TXS
Solution	SHELXT	SHELXT	SHELXT
Refinement	SHELXL-2018	SHELXL-2018	SHELXL-2018
Absorption correction	multi-scan	multi-scan	multi-scan

---

[a] $R_1 = \Sigma||F_0|-|F_c||/\Sigma|F_0|$; [b] $wR_2 = [\Sigma[w(F_0^2-F_c^2)^2]/\Sigma[w(F_0)^2]]^{1/2}$; $w = [\sigma c^2(F_0^2)+(xP)^2+yP]^{-1}$ and $P=(F_0^2+2F_c^2)/3$; [c] $S = \{\Sigma[w(F_o^2-F_c^2)^2]/(n-p)\}^{1/2}$ (n = number of reflections; p = total number of parameters).

Table S3. Crystallographic data and structure refinement details for compound **6** and **8**.

	6@173K	**8**
Formula	$C_{12}Cl_2H_{18}FeN_{30}O_{20}$	$C_{12}Cl_2H_{18}N_{30}O_{20}Zn$
FW [g mol^{-1}]	1029.31	1038.83
Crystal system	monoclinic	monoclinic
Space group	*C*2/*c* (No. 15)	*C*2/*c* (No. 15)
Color / Habit	colorless plate	colorless block
Size [mm]	0.02 x 0.10 x 0.20	0.04 x 0.06 x 0.10
a [Å]	18.3493(6)	18.3161(13)
b [Å]	10.2124(3)	10.2342(7)
c [Å]	21.1693(8)	21.1225(14)
α [°]	90	90
β [°]	103.067(1)	103.215(2)
γ [°]	90	90
V [Å^3]	3864.2(2)	3854.6(5)
Z	4	4
$\rho_{calc.}$ [g cm^{-3}]	1.769	1.790
μ [mm^{-1}]	0.645	0.893
F(000)	2080	2096
$\lambda_{MoK\alpha}$ [Å]	0.71073	0.71073
T [K]	173	173
θ Min-Max [°]	2.3, 26.4	2.3, 26.4
Dataset	-22:22; -12:12; -26:26	-22:22; -12:12; -26:26
Reflections collected	31803	30764
Independent refl.	3947	3943
R_{int}	0.039	0.055
Observed reflections	3455	3131
Parameters	295	295
R_1 (obs)[a]	0.0340	0.0387
wR_2 (all data)[b]	0.0863	0.0891
S [c]	1.05	1.03
Resd. dens [e Å^{-3}]	-0.44, 0.55	-0.43, 0.45
Device type	Bruker D8 Venture TXS	Bruker D8 Venture TXS
Solution	SHELXT	SHELXT
Refinement	SHELXL-2018	SHELXL-2018
Absorption correction	multi-scan	multi-scan

---

[a]$R_1 = \Sigma||F_0|-|F_c||/\Sigma|F_0|$; [b]$wR_2 = [\Sigma[w(F_0^2-F_c^2)^2]/\Sigma[w(F_0)^2]]^{1/2}$; $w = [\sigma c^2(F_0^2)+(xP)^2+yP]^{-1}$ and $P=(F_0^2+2F_c^2)/3$; [c]$S = \{\Sigma[w(F_o^2-F_c^2)^2]/(n-p)\}^{1/2}$ (n = number of reflections; p = total number of parameters).

6.7.3 Computations

All calculations were carried out using the Gaussian G09 program package.[S13] The enthalpies (H) and free energies (G) were calculated using the complete basis set (CBS) method of Petersson and coworkers in order to obtain very accurate energies. The CBS models use the known asymptotic convergence of pair natural orbital expressions to extrapolate from calculations using a finite basis set to the estimated complete basis set limit. CBS-4 begins with a HF/3-21G(d) geometry optimization; the zero point energy is computed at the same level. It then uses a large basis set SCF calculation as a base energy, and a MP2/6-31+G calculation with a CBS extrapolation to correct the energy through second order. A MP4(SDQ)/6-31+(d,p) calculation is used to approximate higher order contributions. In this study we applied the modified CBS-4M method (M referring to the use of minimal population localization) which is a re-parametrized version of the original CBS-4 method and also includes some additional empirical corrections. The enthalpies of the gas-phase species M were computed according to the atomization energy method (E1) (Table S4 & 5).[S13–18]

$$\Delta_f H^\circ_{(g,\ M,\ 298)} = H_{(\text{Molecule},\ 298)} - \sum H^\circ_{(\text{Atoms},\ 298)} + \sum \Delta_f H^\circ_{(\text{Atoms},\ 298)} \qquad \text{(E1)}$$

Table S4. Literature values for atomic $\Delta H^\circ{}_f{}^{298}$ / kcal mol^{-1}

	$-H^{298}$ [a.u.]	NIST[S19]
H	0.50091	52.1
C	37.786156	171.3
N	54.522462	113.0
O	74.991202	59.6

The gas-phase heat of formations were converted to the solid/liquid state ones for neutrals: by subtracting the vaporization/sublimation enthalpies (calculated using the Trouton rule)[S20,21] The calculation results are summarized in Table S7.

$$\Delta U_m = \Delta H_m - \Delta n\ R\ T \qquad \text{(E2)}$$

Table S5. CBS-4M results, Gas phase enthalpies of formation, calculated sublimation/vaporization enthalpies and solid-state heat of formation.

Compound	$-H^{298}$ / a.u.	$\Delta_f H°(g)$ / kJ mol^{-1}	$\Delta_{s/v}H°$/ kJ mol^{-}	V_m / nm^3	Δn
2a	–501.433588	318.8	66.0162		–5.0
2b	–501.442607	295.1	60.5642		–5.0

6.7.4 NMR Spectroscopy

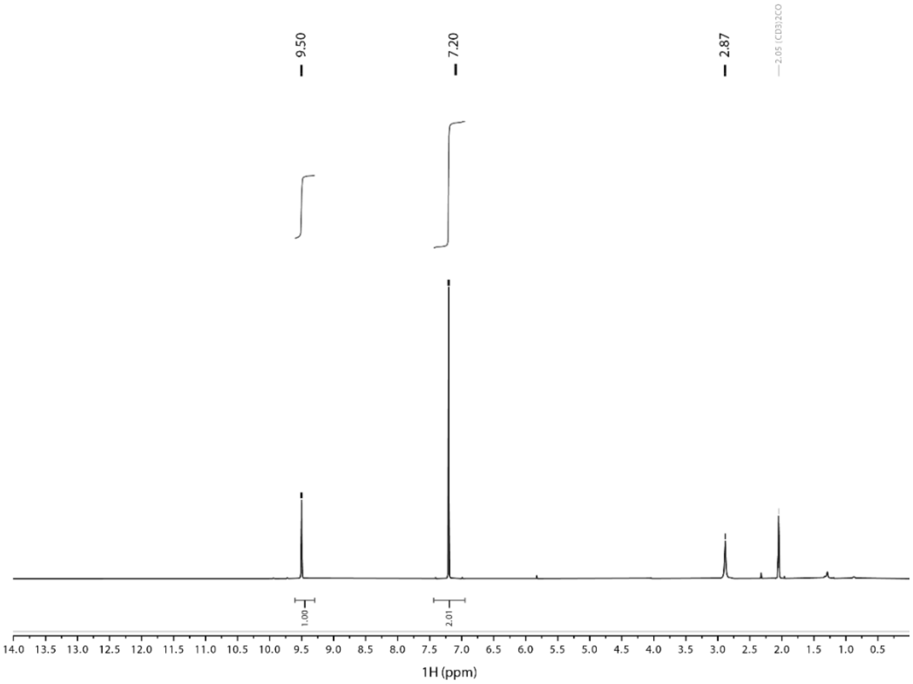

Figure S1. ^{1}H NMR of **2a** in acetone-d$_6$.

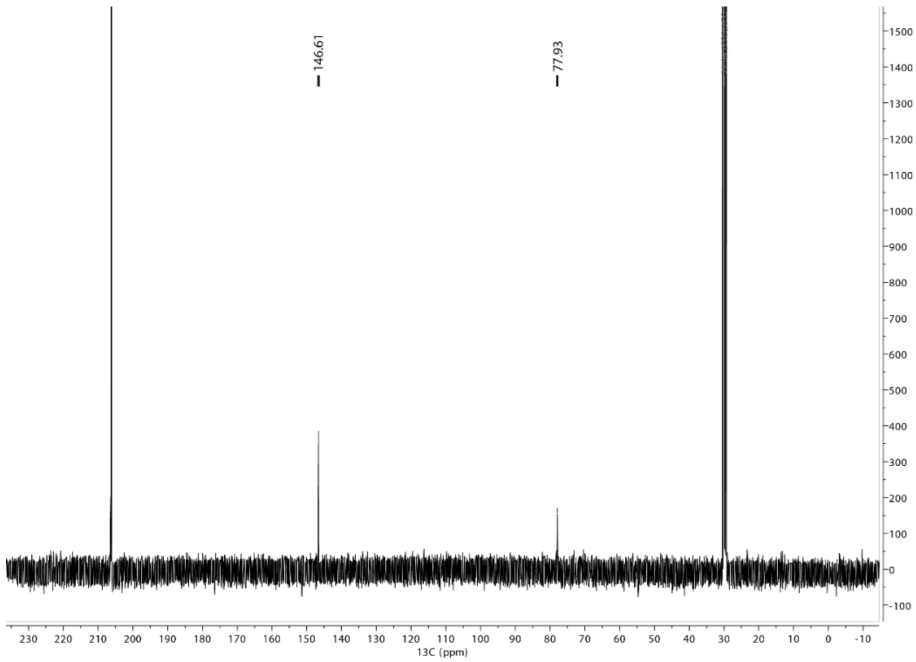

Figure S2. ^{13}C NMR of **2a** in acetone-d$_6$.

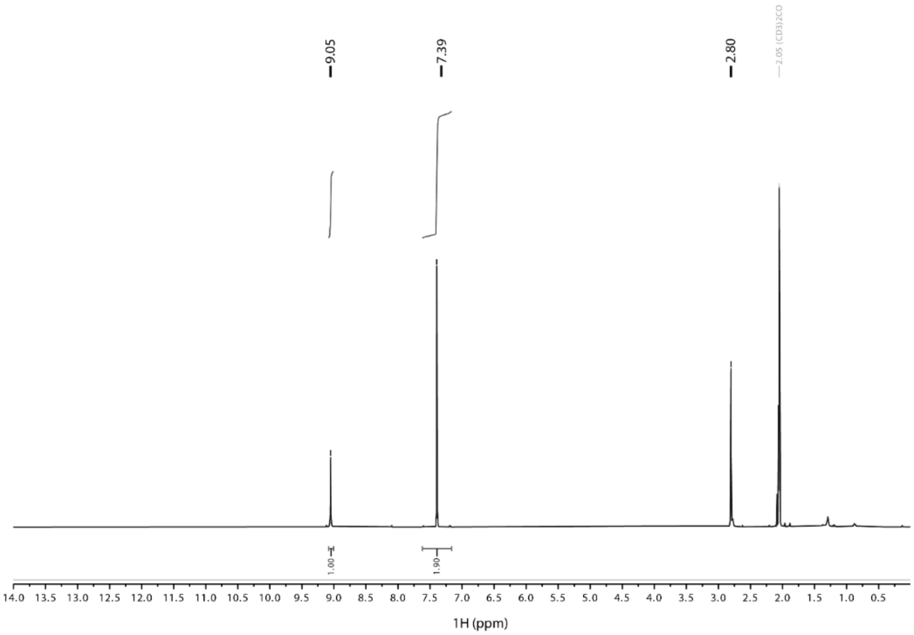

Figure S3. ^{1}H NMR of **2b** in acetone-d$_6$.

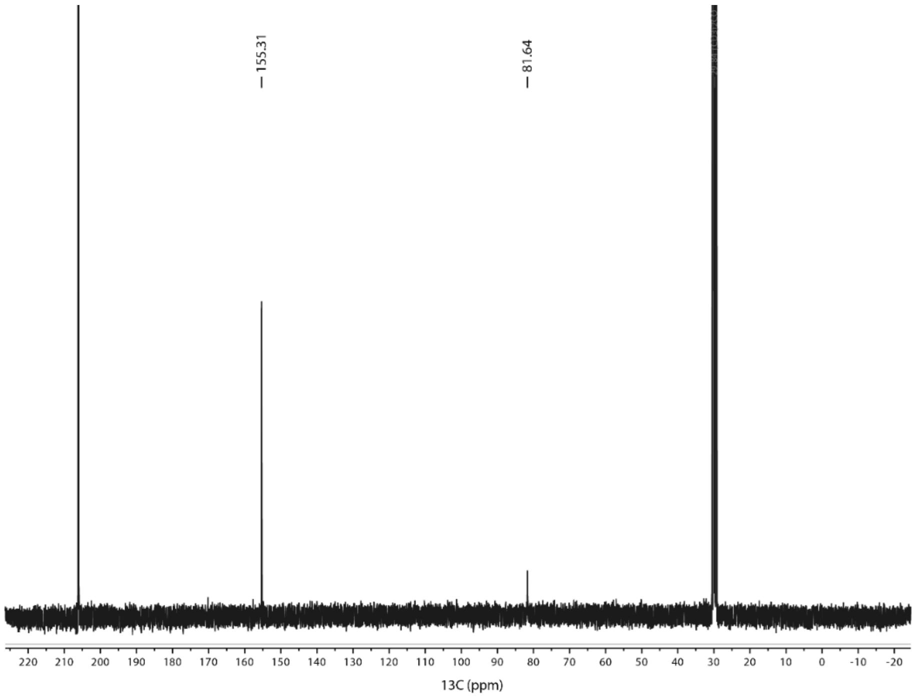

Figure S4. ^{13}C NMR of **2b** in acetone-d$_6$.

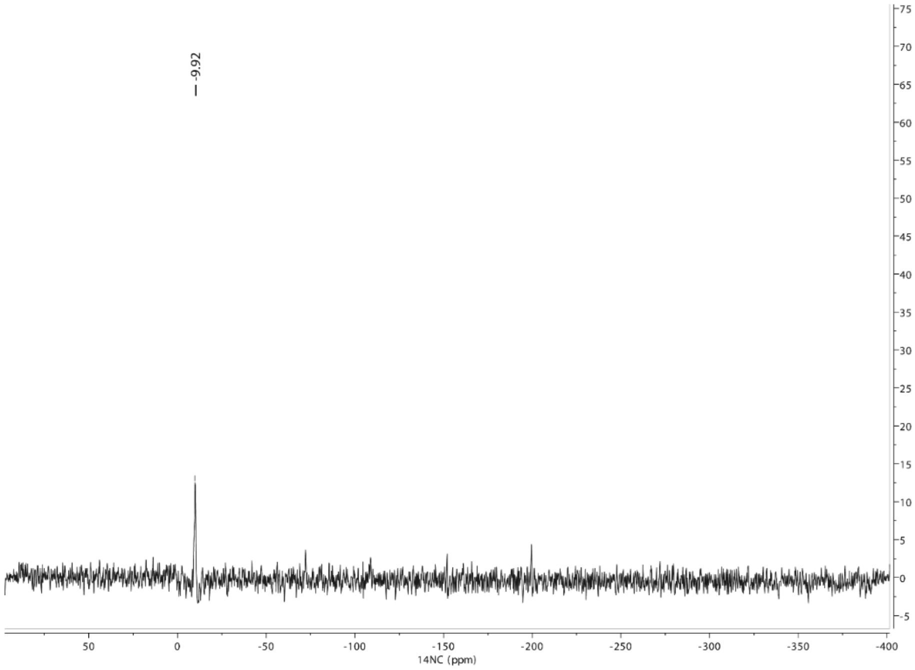

Figure S5. ^{14}N NMR of **2b** in acetone-d$_6$.

6.7.5 Crystal Structures

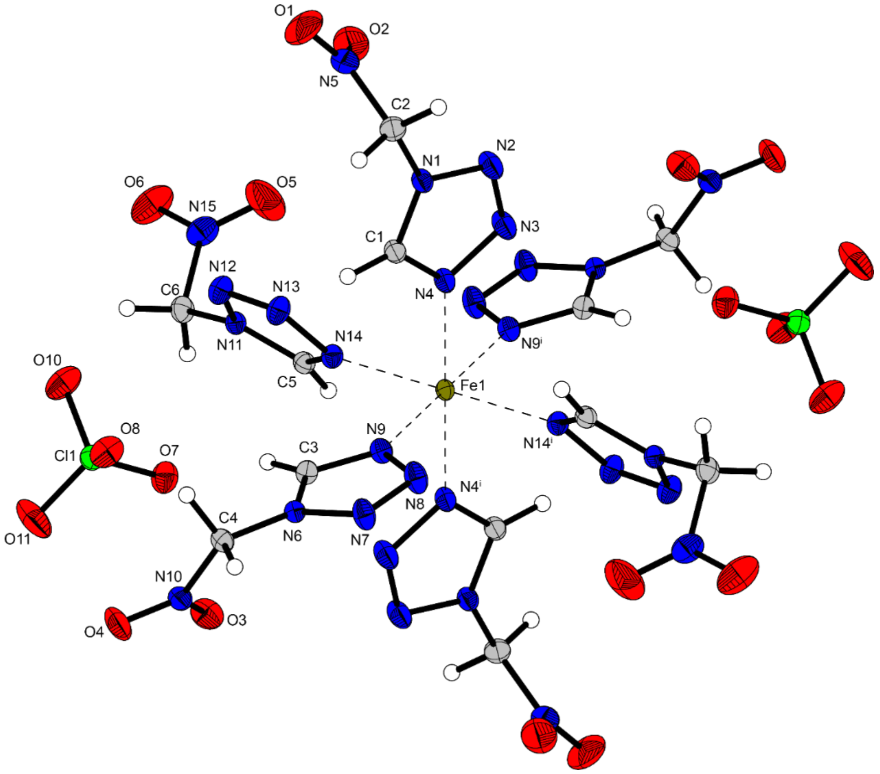

Figure S6. Crystal structure of [Fe(1-NMT)$_6$](ClO$_4$)$_2$ (**6**) at 173 K; Selected bond lengths [Å]: Fe1–N4 2.18(16), Fe1–N9 2.16(16), Fe1–N14 2.18(17); Angles [°]: N4–Fe1–N9 89.65(6), N4–Fe1–N14 89.86(7), N4–Fe1–N4i 180.00.

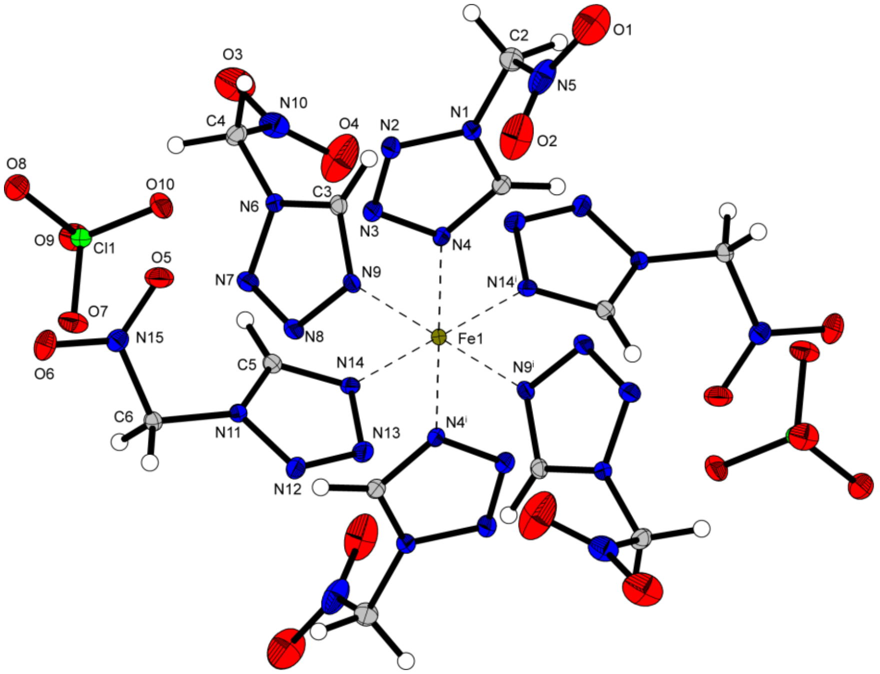

Figure S7. Crystal structure of [Fe(1-NMT)$_6$](ClO$_4$)$_2$ (**6**) at 133 K; Selected bond lengths [Å]: Fe1–N4 2.00(16), Fe1–N9 2.00(16), Fe1–N14 2.00(17); Angles [°]: N4–Fe1–N9 89.60(6), N4–Fe1–N14 90.08(7), N4–Fe1–N4i 180.00.

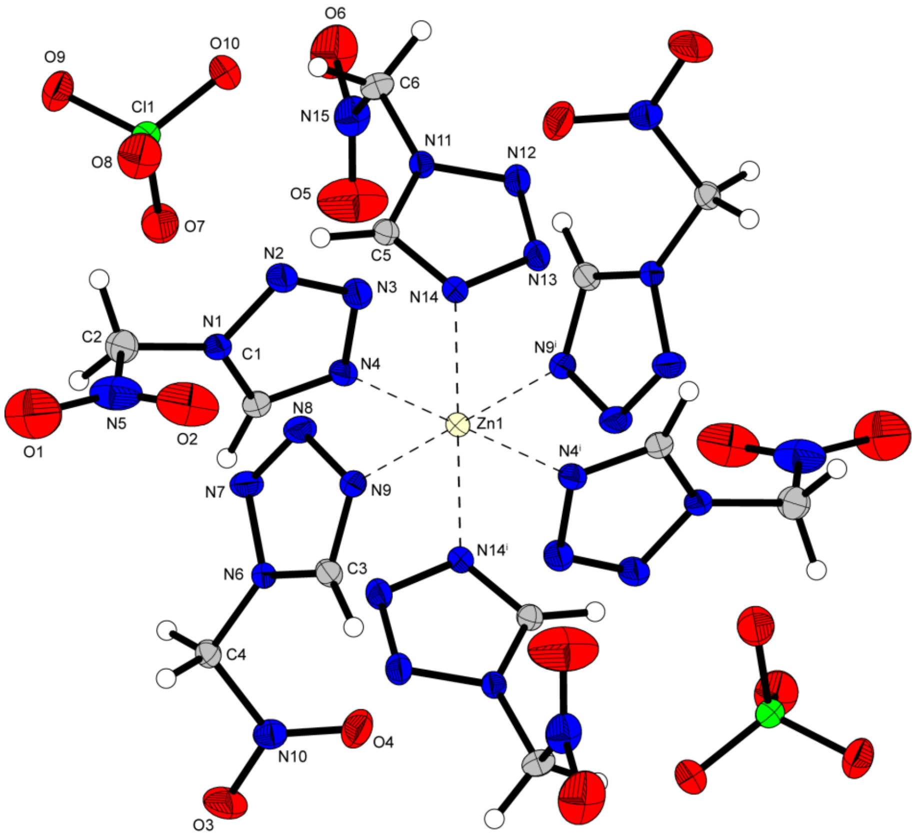

Figure S8. Crystal structure of $[Zn(1\text{-}NMT)_6](ClO_4)_2$ (**8**); Selected bond lengths [Å]: Zn1–N4 2.18(2), Zn1–N9 2.15(2), Zn1–N14 2.17(2); Angles [°]: N4–Zn1–N9 89.78(8), N4–Zn1–N14 89.47(8), N4–Zn1–N4i 180.00.

6.7.6 IR Spectroscopy

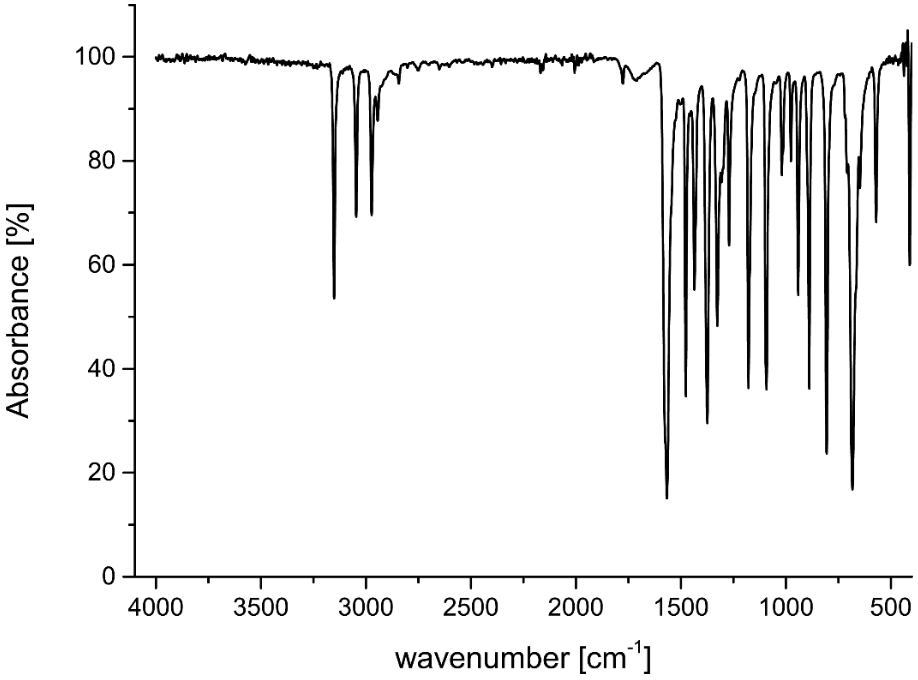

Figure S9. IR spectrum of compound **2a**.

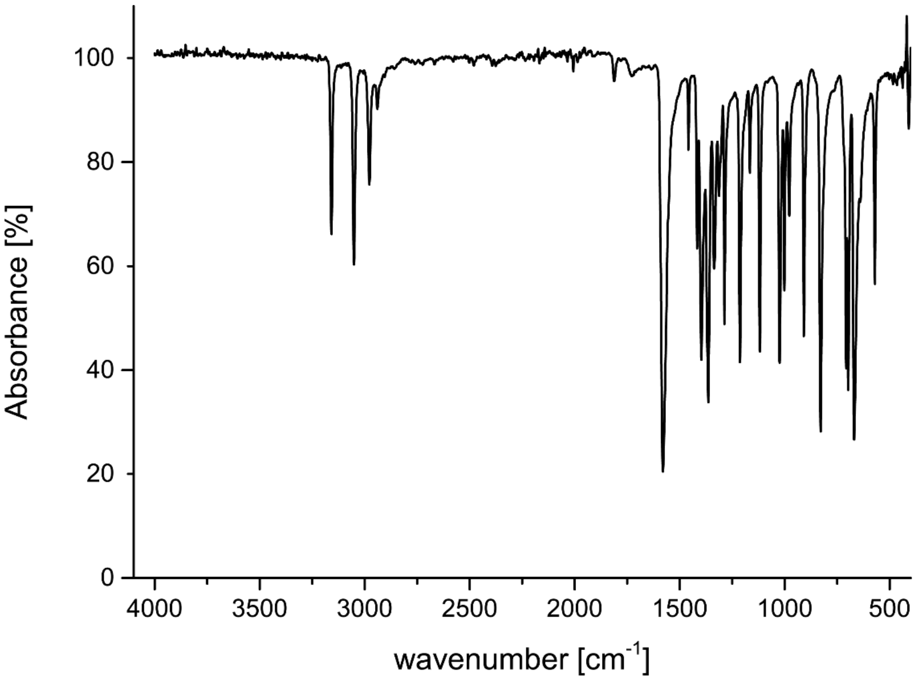

Figure S10. IR spectrum of compound **2b**.

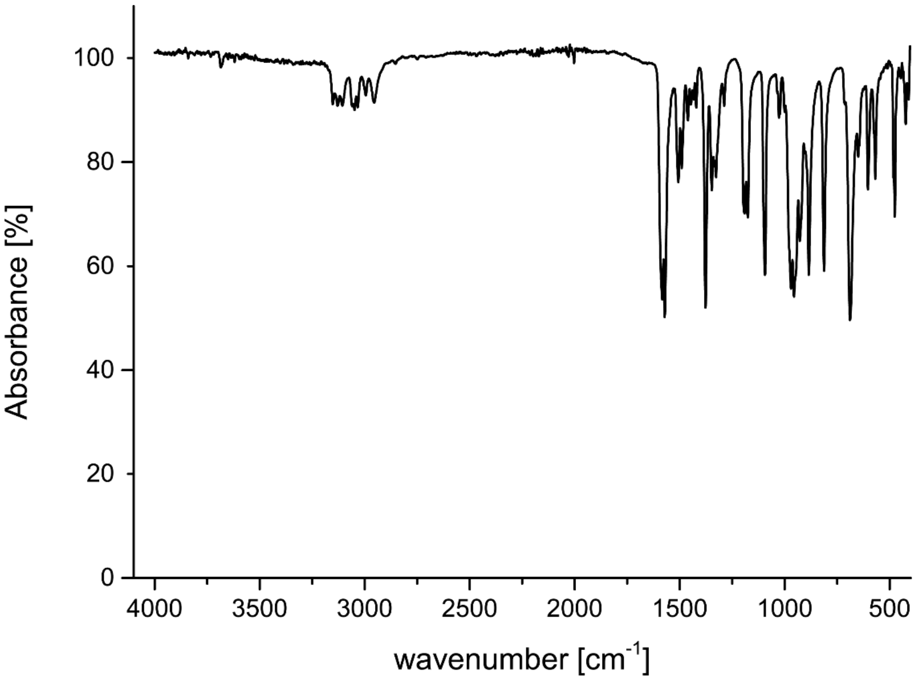

Figure S11. IR spectrum of compound **3**.

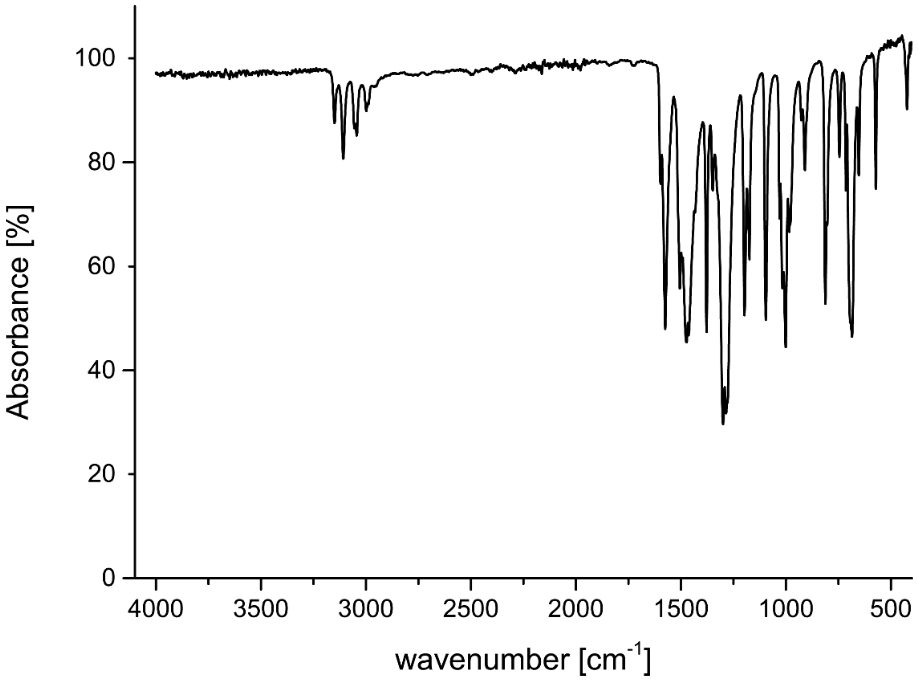

Figure S12. IR spectrum of compound **4**.

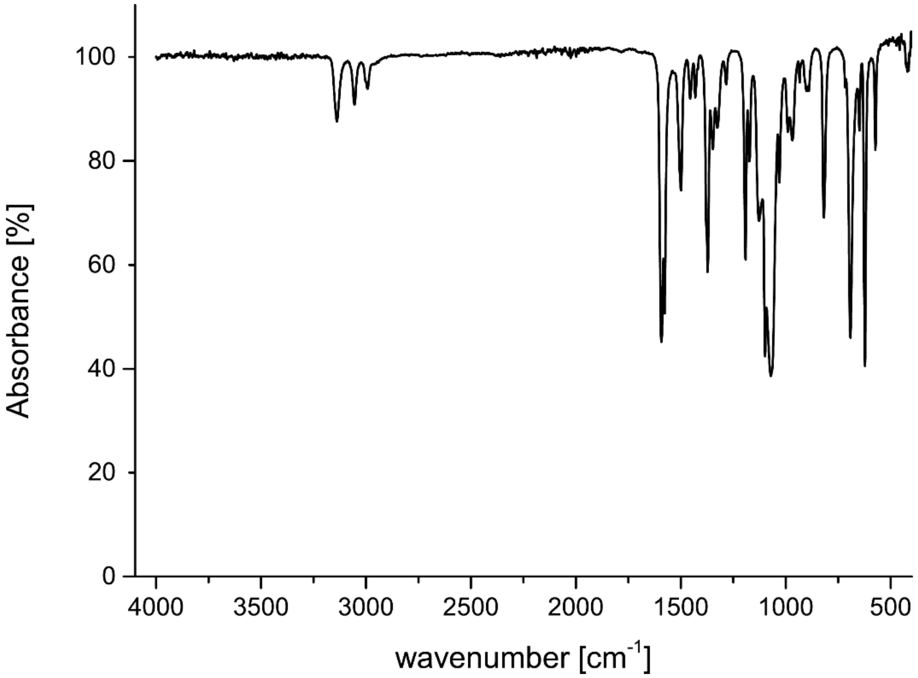

Figure S13. IR spectrum of compound **5**.

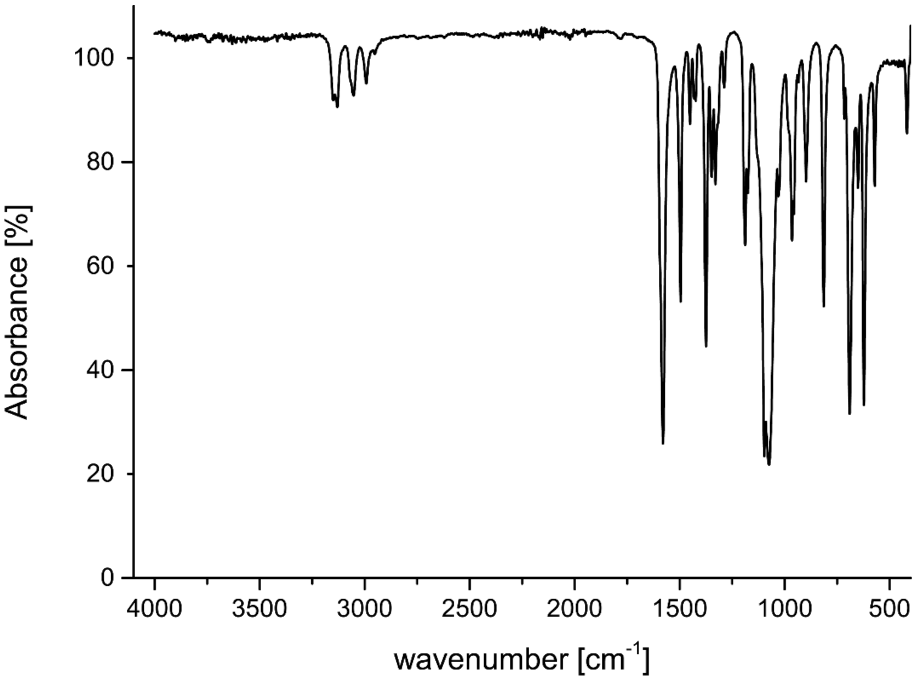

Figure S14. IR spectrum of compound **6**.

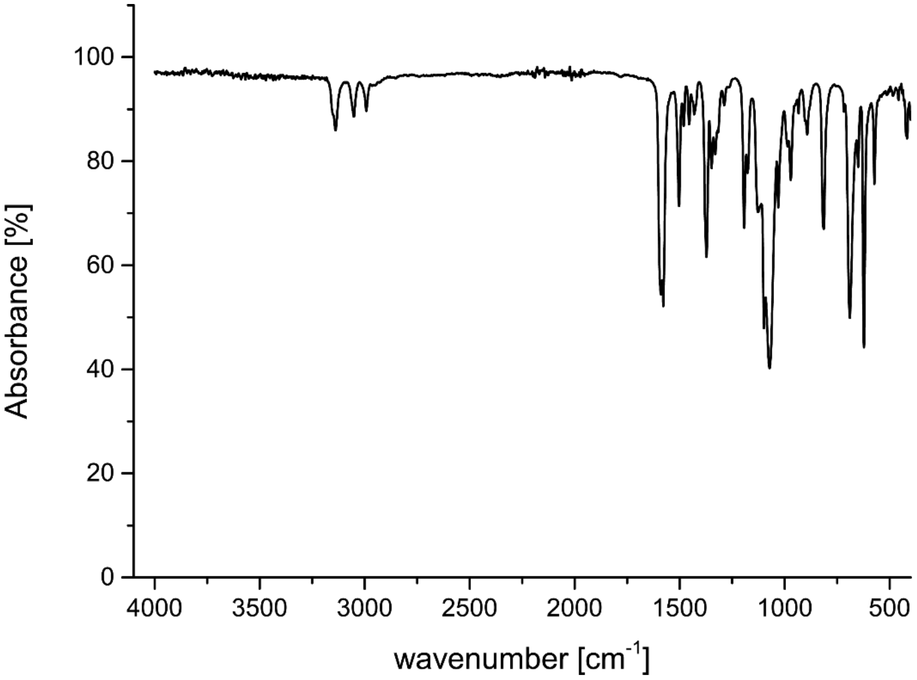

Figure S15. IR spectrum of compound **7**.

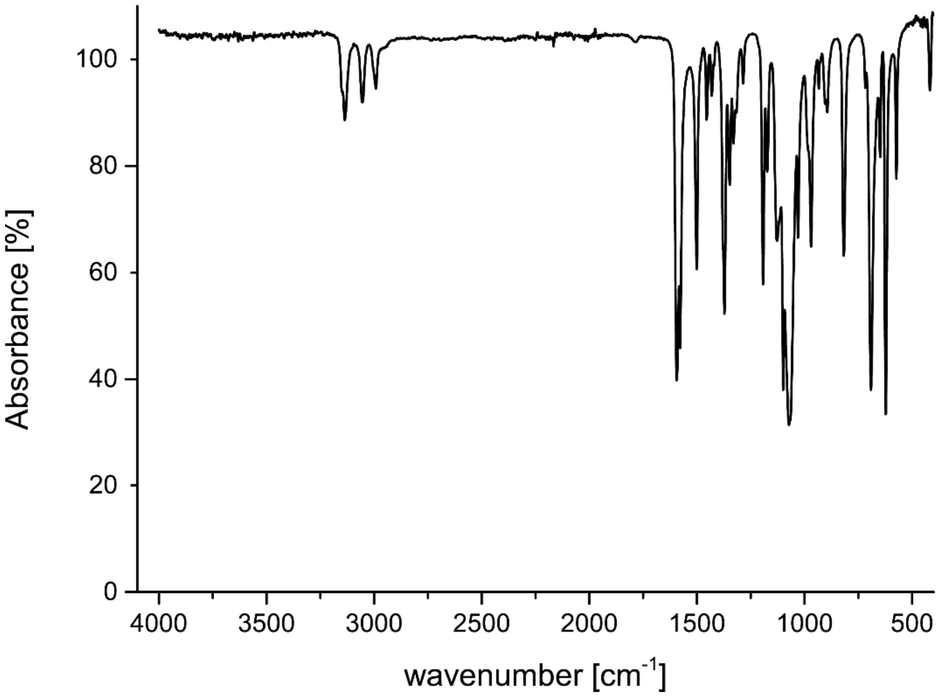

Figure S16. IR spectrum of compound **8**.

6.7.7 Differential Thermal Analysis of ECCs

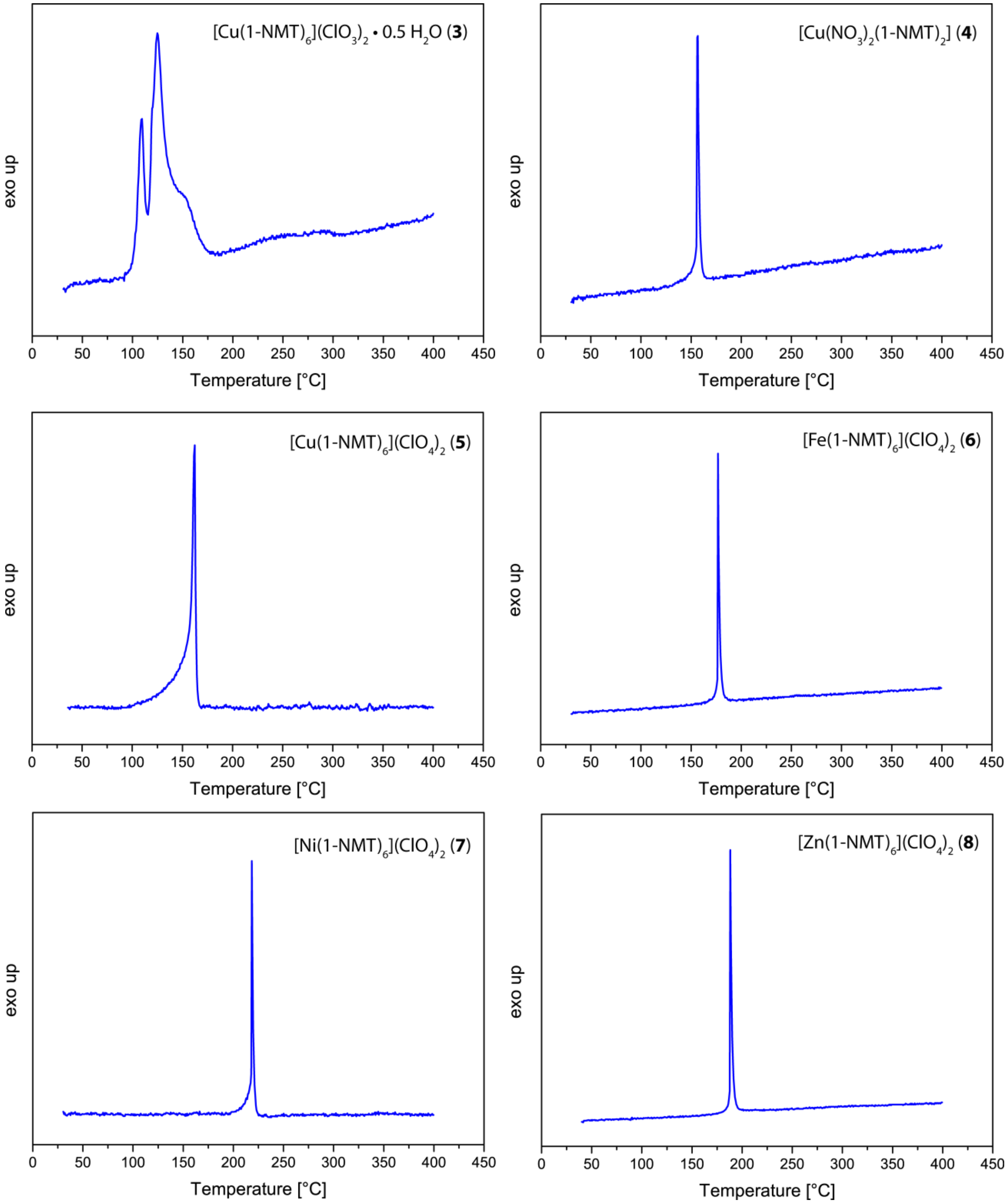

Figure S17. Differential thermal analysis of ECCs 3–8 with a heating rate of 5 °C min^{-1}.

6.7.8 Initiation Testing

Figure S18. Hot plate (left) and hot needle (right) test of compound **3**.

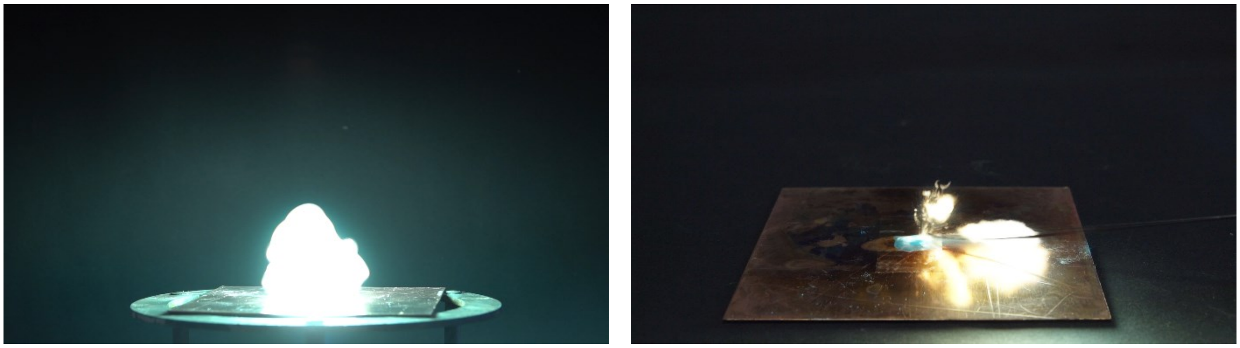

Figure S19. Hot plate (left) and hot needle (right) test of compound **4**.

Figure S20. Hot plate (left) and hot needle (right) test of compound **5**.

Figure S21. Hot plate (left) and hot needle (right) test of compound **6**.

Figure S22. Hot plate (left) and hot needle (right) test of compound **7**.

Figure S23. Hot plate (left) and hot needle (right) test of compound **8**.

Figure S24. Deflagration with formation of smoke of compound **4** at 51 mJ.

6.7.9 General Methods

All chemicals and solvents were employed as received (Sigma-Aldrich, Fluka, Acros, ABCR). ^{1}H, ^{13}C{^{1}H}, ^{14}N, ^{15}N{^{1}H} spectra were recorded at ambient temperature using a JEOL Bruker 27400, Eclipse 270, JEOL EX 400 or a JEOL Eclipse 400 instrument. The chemical shifts quoted in ppm in the text refer to typical standards such as tetramethylsilane (^{1}H, ^{13}C) nitromethane (^{14}N,^{15}N) acetone-d_6 as the solvent. Endothermic and exothermic events of the described compounds, which indicate melting, loss of crystal water or decomposition, are given as the extrapolated onset temperatures. The samples were measured in a range of 25–400 °C at a heating rate of 5 °C min^{-1} through differential thermal analysis (DTA) with an OZM Research DTA 552-Ex instrument. Infrared spectra were measured with pure samples on a Perkin-Elmer BXII FT-IR system with a Smith DuraSampler IR II diamond ATR. Determination of the carbon, hydrogen, and nitrogen contents was carried out by combustion analysis using an Elementar Vario El (nitrogen values determined are often lower than the calculated ones' due to their explosive behavior). Impact sensitivity tests were carried out according to STANAG 4489[S22] with a modified instruction[S23] using a BAM (Bundesanstalt für Materialforschung) drophammer.[S24] Friction sensitivity tests were carried out according to STANAG 4487[S28] with a modified instruction[S29] using the BAM friction tester.[S24,25] The classification of the tested compounds results from the "UN Recommendations on the Transport of Dangerous Goods".[S30,31] Energetic properties have been calculated with the EXPLO5 6.05.04 computer code[S32] using the, to RT converted, X-ray density and calculated solid state heats of formation. These were computed by the atomization method as described in recently published papers. Electronic enthalpies were calculated with the Gaussian09 software[S13] suite using the CBS-4M method. The initiation capability of compounds **4** and **5** towards PETN were performed in a copper shell with a diameter of 7 mm and a height of 88 mm. PETN is sieved to a grain size <100 μm and is pressed into the copper tube with a weight of 8 kg. The tested compound is loosely filled on top and is either directly tested or tested when also pressed with 8 kg. The copper tube is placed onto a copper witness plate with a thickness of 1 mm and is ignited with a type A electrical igniter. A perforation of the copper witness plate indicates an initiation of the PETN, thus a positive initiation test. The laser initiation experiments were performed with a 45 W InGaAs laser diode operating in the single-pulsed mode. An optical fiber with a core diameter of 400 μm and a cladding diameter of 480 μm is attached to the laser diode. The optical fiber is connected via a SMA type connecter directly to the laser and to a collimator. Ultimately, the collimator includes an optical lens, which was positioned in its focal distance (f = 29.9 mm) to the sample. A sapphire lens then protects the lens from the explosion. Approximately 15 mg of the finely powdere compound to be investigated was filled into a transparent plastic cap (PC), pressed with a pressure of 1 kN and sealed by an UV-curing adhesive. The confined samples were irradiated at a wavelength of 915 nm, a voltage of 4 V, a current of 7–8 A and pulse lengths of 1, 15 and 30 ms. The combined currents and pulse lengths result in an energy output of 0.8–51 mJ.

6.7.10 Detonation Velocity Estimations

The room temperature densities used for calculation of the detonation velocity were obtained by recalculation of the the low temperature densities, obtained by X-ray diffraction experiments. Detonation velocities were calculated according to an increment method, adapted for ECC by Ilyushin.[S33] Analogue to pyrotechnical mixtures, the respective ECCs were divided into an explosive part (anion, ligand) and an inactive ultratispersed metal additive (copper). The active part was further divided into chemical bonds and structural fragments. Corresponding increment values can be found in the literature.[S34] Some of the values are dependent on the hydrogen and oxygen content of the coordination compound, the summarized values for each fragment are listed in Table S6

Table S7. Values of increments used for fragments.

Fragment	F_i
1-NMT	413.4
1-NAMT	453.0
AzMT	358.7
ClO_4^-	278.7
NO_3^-	209.2

6.7.11 Experimental Part

All investigated compounds are potentially explosive energetic materials (some compounds lie in the range of primary explosives), which show partly increased sensitivities towards various stimuli (e.g. elevated temperatures, impact, friction or electrostatic discharge). Therefore, proper security precautions (safety glasses, face shield, earthed equipment and shoes, leather jacket, Kevlar gloves, Kevlar sleeves and ear plugs) have to be worn while synthesizing and handling the described compounds. These very sensitive compounds must be handled with great care!

General procedure for ECC **3–8**

Barium chlorate monohydrate (145 mg, 0.45 mmol, 1.0 equiv.) and copper(II) sulphate pentahydrate (112 mg, 0.45 mmol, 1.0 equiv.) were dissolved in water (5 mL), combined and stirred for 5 min. The mixture was cooled to 0 °C and the precipitated barium sulphate, filtered off. The solvent was evaporated under reduced pressure and pure copper(II) chlorate was dissolved in ethanol (2 mL).

The respective amounts of copper(II) salt (**3**: $Cu(ClO_3)_2$, 57.6 mg, 0.25 mmol; **4**: $Cu(NO_3)_2 \cdot 3\ H_2O$, 181.2 mg, 0.75 mmol; **5**: $Cu(ClO_4)_2 \cdot 6\ H_2O$, 92.6 mg, 0.25 mmol) was dissolved in ethanol (2 mL) and added dropwise to the in ethanol dissolved **2a** (218 mg, 1.50 mmol, 6.0 equiv.) while stirring at room temperature. The reaction mixture was stirred for 5 min at 80 °C before it was allowed to crystallize at room temperature. Crystallization process took up 1–2 days. The crystalline compounds were filtered off before complete evaporation of the solvent and were washed with cold *n*-hexane. It is also possible to precipitate the compounds by adding a large excess of *n*-hexane to the ethanolic solution. In this case, the powdered compounds were filtered off, washed with *n*-hexane and dried in air. The powdered compounds were checked for purity with elemental analysis.

$[Cu(1\text{-}NMT)_6](ClO_3)_2 \cdot \frac{1}{2}\ H_2O$ (3)

Compound **3** was obtained as a blue solid. Yield: 205.3 mg (0.10 mmol, 81%). **DTA** (5 °C min^{-1}): 102 °C (T_{exo}); **IR** (ATR, cm^{-1}): $\tilde{\nu}$ = 3685 (vw), 3152 (w), 3129 (w), 3106 (w), 3060 (w), 3048 (w), 3033 (w), 2994 (w), 2954 (w), 1583 (vs), 1571 (vs), 1507 (m), 1490 (m), 1461 (w), 1447 (w), 1434 (w), 1421 (w), 1377 (vs), 1347 (m), 1336 (m), 1327 (m), 1288 (w), 1192 (s), 1176 (s), 1094 (s), 1028 (w), 1000 (w), 970 (s), 956 (vs), 928 (s), 885 (s), 812 (s), 689 (vs), 650 (m), 604 (m), 569 (m), 476 (s), 447 (w), 424 (w), 410 (w); **EA** ($C_{24}H_{38}Cl_4Cu_2N_{60}O_{37}$, 2027.84) calc.: C 14.22 H 1.89 N 41.44%, found C 14.11 H 2.05 N 40.36%; **BAM drop hammer**: 4 J. **BAM friction tester**: 42 N.

$[Cu(NO_3)_2(1\text{-}NMT)_2]$ (4)

Compound **4** was obtained as a green solid. Yield: 230.6 mg (0.52 mmol, 69%). **DTA** (5 °C min^{-1}): 155 °C (T_{exo}); **IR** (ATR, cm^{-1}): $\tilde{\nu}$ = 3149 (w), 3108 (m), 3055 (w), 3044 (w), 2998 (w), 2988 (w), 1597 (m), 1575 (s), 1505 (s), 1473 (s), 1463 (s), 1433 (m), 1378 (s), 1349 (m), 1300 (vs), 1285 (vs), 1197 (s), 1174 (m), 1096 (s), 1030 (m), 1017 (s), 1002 (s), 985 (m), 927 (w), 910 (m), 812 (s), 745 (m), 715 (m), 686 (s), 653 (m), 572 (m), 424 (w); **EA** ($C_4H_6CuN_{12}O_{10}$, 445.71) calc.: C 10.78 H 1.36 N 37.71%, found C 10.02 H 1.43 N 36.39%; **BAM drop hammer**: <1 J. **BAM friction tester**: 80 N.

[Cu(1-NMT)$_6$](ClO$_4$)$_2$ (5)

Compound **5** was obtained as a green solid. Yield: 187 mg (0.18 mmol, 72%). **DTA** (5 °C min^{-1}): 160 °C (T_{exo}); **IR** (ATR, cm^{-1}): $\tilde{\upsilon}$ = 3138 (w), 3055 (w), 2993 (w), 1592 (vs), 1578 (s), 1499 (m), 1456 (w), 1431 (w), 1372 (s), 1348 (m), 1326 (w), 1284 (w), 1192 (s), 1173 (m), 1128 (m), 1099 (vs), 1071 (vs), 1031 (m), 990 (w), 969 (m), 934 (w), 900 (w), 890 (w), 819 (m), 692 (s), 649 (w), 623 (vs), 573 (m), 421 (w); **EA** ($C_{12}H_{18}Cl_2CuN_{30}O_{20}$, 1036.91) calc.: C 13.90 H 1.75 N 40.53%, found C 14.14 H 2.03 N 39.59%; **BAM drop hammer**: <1 J. **BAM friction tester**: 30 N.

[Fe(1-NMT)$_6$](ClO$_4$)$_2$ (6)

Compound **6** was obtained as a green solid. Yield: 149.2 mg (0.15 mmol, 58%). **DTA** (5 °C min^{-1}): 176 °C (T_{exo}); **IR** (ATR, cm^{-1}): $\tilde{\upsilon}$ = 3150 (w), 3130 (w), 3053 (w), 2992 (w), 1579 (vs), 1496 (s), 1451 (w), 1432 (w), 1424 (w), 1375 (s), 1348 (m), 1330 (m), 1288 (w), 1188 (m), 1177 (m), 1097 (vs), 1075 (vs), 1030 (m), 965 (m), 956 (m), 935 (w), 898 (m), 814 (s), 717 (w), 691 (s), 651 (m), 623 (s), 571 (m), 418 (w); **EA** ($C_{12}H_{18}Cl_2FeN_{30}O_{20}$, 1029.21) calc.: C 14.00 H 1.76 N 40.83%, found C 14.24 H 1.96 N 39.46%; **BAM drop hammer**: <1 J. **BAM friction tester**: 14 N.

[Ni(1-NMT)$_6$](ClO$_4$)$_2$ (7)

Compound **7** was obtained as a green solid. Yield: 157.4 mg (0.15 mmol, 61%). **DTA** (5 °C min^{-1}): 217 °C (T_{exo}); **IR** (ATR, cm^{-1}): $\tilde{\upsilon}$ = 3139 (w), 3052 (w), 2992 (w), 1590 (s), 1578 (s), 1503 (m), 1481 (w), 1455 (w), 143 1(w), 1372 (s), 1348 (m), 1331 (w), 1318 (w), 1193 (m), 1177 (m), 1127 (m), 1099 (s), 1072 (vs), 1031 (m), 986 (w), 971 (m), 934 (w), 903 (w), 893 (w), 814 (m), 718 (w), 690 (s), 650 (m), 623 (vs), 573 (m), 422 (w), 417 (w); **EA** ($C_{12}H_{18}Cl_2NiN_{30}O_{20}$, 1032.06) calc.: C 13.97 H 1.76 N 40.72%, found C 14.37 H 2.09 N 39.99%; **BAM drop hammer**: <1 J. **BAM friction tester**: 32 N.

[Zn(1-NMT)$_6$](ClO$_4$)$_2$ (8)

Compound **8** was obtained as a green solid. Yield: 200.0mg (0.19 mmol, 77%). **DTA** (5 °C min^{-1}): 187 °C (T_{exo}); **IR** (ATR, cm^{-1}): $\tilde{\upsilon}$ = 3148 (w), 3136 (w), 3055 (w), 2992 (w), 1594 (s), 1578 (s), 1501 (s), 1455 (w), 1431 (w), 1372 (s), 1348 (m), 1330 (m), 1317 (w), 1285 (w), 1193 (s), 1173 (m), 1128 (m), 1099 (vs), 1073 (vs), 1030 (m), 970 (m), 934 (w), 905 (w), 894 (w), 818 (m), 718 (w), 691 (vs), 649 (m), 623 (vs), 573 (m), 418 (w); **EA** ($C_{12}H_{18}Cl_2ZnN_{30}O_{20}$, 1038.75) calc.: C 14.09 H 1.78 N 40.33%, found C 14.09 H 1.78 N 40.33%; **BAM drop hammer**: <1 J. **BAM friction tester**: 28 N.

6.7.12 References

S1 CrysAlisPRO (Version 171.33.41), Oxford Diffraction Ltd. **2009**.

S2 A. Altomare, G. Cascarano, C. Giacovazzo, and A. Guagliardi, *J. Appl. Crystallogr.* **1992**, *26*, 343.

S3 A. Altomare, G. Cascarano, C. Giacovazzo, A. Guagliardi, A. G. G. Moliterni, M. C. Burla, G. Polidori, M. Camalli and R. Spagna, SIR97, **2003**.

S4 A. Altomare, M. C. Burla, M. Camalli, G. L. Cascarano, C. Giacovazzo, A. Guagliardi, A. G. G. Moliterni, G. Polidori and R. Spagna, *J. Appl. Crystallogr.* **1999**, *32*, 115.

S5 G. M. Sheldrick, SHELXL-97, University of Göttingen, Germany, **1997**.

S6 G. M. Sheldrick, *Acta Crystallogr. Sect. A* **2008**, *64*, 112.

S7 G. M. Sheldrick, *Acta Cryst. A* **2015**, *71*, 3–8.

S8 A. L. Spek, PLATON, Utrecht University, The Netherlands, **1999**.

S9 L.J. Farrugia, *J. Appl. Cryst.* **2012**, *45*, 849.

S10 O. V. Dolomanov, L. J. Bourhis, R. J. Gildea, J. A. K. Howard and H. Puschmann, *J. Appl. Cryst*. **2009**, *42*, 339–341.

S11 Empirical absorption correction using spherical harmonics, implemented in SCALE3 ABSPACK scaling algorithm (CrysAlisPro Oxford Diffraction Ltd., Version 171.33.41, **2009**).

S12 APEX3, Bruker AXS Inc., Madison, Wisconsin, USA.

S13 M. J. Frisch, G. W. Trucks, H. B. Schlegel, G. E. Scuseria, M. A. Robb, J. R. Cheeseman, G. Scalmani, V.Barone, B. Mennucci, G. A. Petersson, H. Nakatsuji, M. Caricato, X. Li, H.P. Hratchian, A. F. Izmaylov, J. Bloino, G. Zheng, J. L. Sonnenberg, M. Hada, M. Ehara, K. Toyota, R. Fukuda, J. Hasegawa, M. Ishida, T. Nakajima, Y. Honda, O. Kitao, H. Nakai, T. Vreven, J. A. Montgomery, Jr., J. E. Peralta, F. Ogliaro, M. Bearpark, J. J. Heyd, E. Brothers, K. N. Kudin, V. N. Staroverov, R. Kobayashi, J. Normand, K. Raghavachari, A. Rendell, J. C. Burant, S. S. Iyengar, J. Tomasi, M. Cossi, N. Rega, J. M. Millam, M.Klene, J. E. Knox, J. B. Cross, V. Bakken, C. Adamo, J. Jaramillo, R. Gomperts, R. E. Stratmann, O. Yazyev, A. J. Austin, R. Cammi, C. Pomelli, J. W. Ochterski, R. L. Martin, K. Morokuma, V. G. Zakrzewski,

G. A. Voth, P. Salvador, J. J. Dannenberg, S. Dapprich, A. D. Daniels, O. Farkas, J.B. Foresman, J. V. Ortiz, J. Cioslowski and D. J. Fox, Gaussian 09 A.02, Gaussian, Inc., Wallingford, CT, USA, **2009**.

S14 J. W. Ochterski, G. A. Petersson and J. A. Montgomery Jr., *J. Chem. Phys.* **1996**, *104*, 2598–2619.

S15 J. A. Montgomery Jr., M. J. Frisch, J. W. Ochterski and G. A. Petersson, *J. Chem. Phys.* **2000**, *112*, 6532–6542.

S16 L. A. Curtiss, K. Raghavachari, P. C. Redfern and J. A. Pople, *J. Chem. Phys.* **1997**, *106*, 1063–1079.

S17 E. F. C. Byrd and B. M. Rice, *J. Phys. Chem. A* **2006**, *110*, 1005–1013.

S18 B. M. Rice, S. V. Pai and J. Hare, *Comb. Flame* **1999**, *118*, 445–458.

S19 P. J. Lindstrom and W. G. Mallard, NIST Standard Reference Database Number 69, http://webbook.nist.gov/chemistry/, (accessed March **2021**).

S20 M. S. Westwell, M. S. Searle, D. J. Wales and D. H. Williams, *J. Am. Chem. Soc*. **1995**, *117*, 5013–5015.

S21 F. Trouton, *Philos. Mag.* **1884**, *18*, 54–57.

S22NATO standardization agreement (STANAG) on explosives, impact sensitivity tests, no. 4489, 1st ed., Sept. 17, **1999**.

S23 WIWEB-Standardarbeitsanweisung 4-5.1.02, Ermittlung der Explosionsgefährlichkeit, hier der Schlagempfindlichkeit mit dem Fallhammer, Nov. 8, **2002**.

S24 BAM, http://www.bam.de, (accessed March **2021**).

S25 OZM, http://www.ozm.cz, (accessed March **2021**).

S26 Military Standard 1751A (MIL-STD-1751A): safety and performance tests for qualification of explosives (high explosives, propellants and pyrotechnics), method 1016, Dec. 11, **2001**.

S27 M. S. Gruhne, M. Lommel, M. H. H. Wurzenberger, N. Szimhradt, T. M. Klapötke and J. Stierstorfer, *Propellants Explos. Pyrotech.* **2020**, *45*, 147–153.

S28 NATO standardization agreement (STANAG) on explosive, friction sensitivity tests, no. 4487, 1st ed., Aug. 22, **2002**.

S29 WIWEB-Standardarbeitsanweisung 4-5.1.03, Ermittlung der Explosionsgefährlichkeit oder der Reibeempfindlichkeit mit dem Reibeapparat, Nov. 8, **2002**.

S30 UN Model Regulation: Recommendations on the Transport of Dangerous Goods – Manual of Tests and Criteria, section 13.4.2.3.3, **2015**.

S31 Impact: insensitive > 40 J, less sensitive ≥ 35 J, sensitive ≥ 4 J, very sensitive ≤ 3 J; Friction: insensitive > 360 N, less sensitive = 360 N, sensitive < 360 N and > 80 N, very sensitive ≤ 80 N, extremely sensitive ≤ 10 N. According to the UN Recommendations on the Transport of Dangerous Goods, 5th ed., **2009**.

S32 M. Sućeska, EXPLO5 Version 6.05 User's Guide. Zagreb, Croatia: OZM; **2018**.

S33 M. A. Ilyushin, A. V. Smirnov, A. A. Kotomin, I. V. Tselinskii, *Energ. Mater.* **1994**, *2*, 16–20.

S34 Н.Ю. Сугак, С.В. Мочалов, РАСЧЕТ ВЗРЫВЧАТЫХ ХАРАКТЕРИСТИК ВВ, БТИ АлтГТУ, Бийск, **2013**.

S35 V. V. Semenov, V. S. Bogdanov, B. S. Él'yanov, L. G. Mel'nikova, S. A. Shevelev, V. M. Zhulin, A. A. Fainzil'berg, *Chem. Heterocycl*. **1982**, *18*, 859.

S36 P. A. Levene, *Org. Synth.* **1930**, *10*, 12.

7 *N*-Functionalisation of 5,5’-bistetrazole providing 2,2’-di(azidomethyl)bistetrazole: A Melt-Castable Metal-Free Green Primary Explosive

Thomas M. Klapötke, Moritz Kofen and Jörg Stierstorfer

Reprinted (adapted) from *Dalton Transactions* **2021**, *50*, 13656–13660.

DOI: 10.1039/d1dt02731j

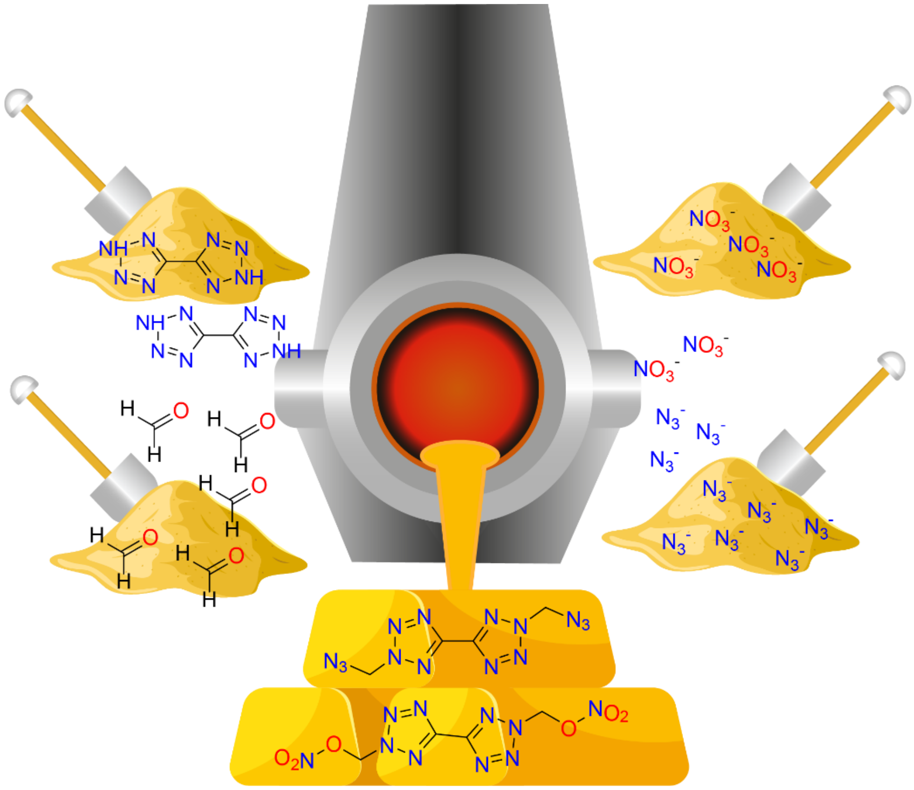

Abstract: *N*-Hydroxymethylation of heterocyclic compounds offers a promising starting procedure to ultimetly introduce nitratomethyl- as well as azidomethyl- moieties. Applied to 5,5’-bistetrazole, the resulting 2,2’-di(azidomethyl)bistetrazole (**3**) and 2,2’-di(nitratomethyl)bistetrazole (**4**) are high-performing melt-castable energetic materials. Sensitivities were predicted by Hirshfeld analysis and explored in detail by experimental analysis. Because of their increased values towards mechanical stimuli and a short deflagration to detonation transition (DDT), especially the diazidomethyl derivative shows promising as new melt-castable primary explosive.

7.1 Introduction

For a long time, research on energetic materials focused on replacing RDX and HMX with even higher performing compounds to increase the performance of an explosive device. With respective detonation velocities of 9778 m s^{-1} and 9698 m s^{-1}, CL-20[1] and TKX-50[2] are two of the best performing compounds resulting from extensive synthetic research. Especially ε-CL-20, having a theoretical maximum density of 2.04 g cm^{-3} at 298 K, reached the somewhat established threshold in crystal density of 2.0 g cm^{-3} for a compound consisting purely of carbon (C), hydrogen (H), nitrogen (N), and oxygen (O).[3] As high explosives are generally used within formulations such as Composition B, consisting of RDX (60%) and TNT (40%), the effect on the performance of an explosive device by solely replacing RDX is limited. Together with the challenge of surpassing the performance of RDX/HMX, one of the most promising strategies is the replacement of toxic melt-castable trinitrotoluene (TNT) which shows a rather low detonation velocity of 6800 m s^{-1}. Recently *Sabatini et al.*[4] published bis(1,2,4-oxadiazole)bis(methylene) dinitrate (BODN), a very promising compound to replace TNT based on the bisoxadiazole scaffold. In a previous paper, we showed that the replacement of the nitratomethyl moieties in BODN by azidomethyl moieties results in 3,3′-bis(azidomethyl)-5,5′-bis(1,2,4-oxadiazole) (DAMBO), which also shows a melting point around 80 °C.[5] Both compounds, BODN and DAMBO, possess methylene bridged azides or nitrates, a motive also found in 5-nitro-2-nitratomethyltetrazole (NNMT)[6]. While the -CH_2-N_3 (DAMBO) and -CH_2-ONO_2 (BODN) substituents are C-bond, the CH_2-ONO_2 group in NNMT is *N*-bond. The introduction of a *N*-bonded methylene moiety is achieved by *N*-hydroxymethylation of the heterocycle with formaldehyde, but extensive adjustments of the reaction conditions are required.[7] The goal of this work was to develop adequate reaction conditions as well as to apply this procedure to 5,5′-bistetrazole as it is the basic framework of several high-performing energetic materials such as TKX-50[2] and potassium 1,1′-dinitramino-5,5′-bistetrazole (K_2DNABT)[8]. Due to the high endothermic heat of formation of 5,5′-bistetrazole (+560.8 kJ mol^{-1}) a good performance of the synthesized compounds can be assumed.

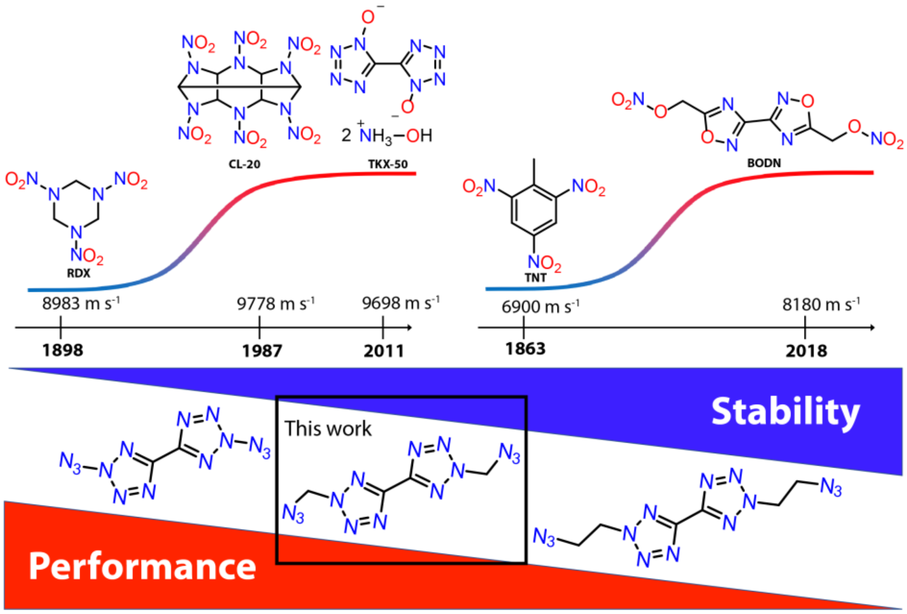

Figure 1. Evolution of high explosives as well as melt-castable explosives. N-methylene moiety balancing between stability. As such its performance and stability perfectly balances between unstable 2,2′-diazido-5,5′-bistetrazole (not described yet) and more stable 2,2′-bis(azidoethyl)-5,5′-bistetrazole (also not described yet).

7.2 Results and Discussion

7.2.1 Synthesis

*Warning! The synthetic work described in this section involves the handling of highly sensitive products (***3***, and* **4***). Proper protective measurements and equipment must be used!*

Diammonium 5,5’-bistetrazolate, synthesized according to literature[9], is dissolved in water, and formalin (37 %) together with hydrochloric acid (37 %) is added in excess. After stirring at 60 °C overnight, the isomeric mixture of 1,1’- (**1a**), 1,2’- (**1b**), and 2,2’-di(hydroxymethyl)bistetrazole (**1c**) is extracted into DCM (Scheme 1). After drying the organic phase over $MgSO_4$ and removing the solvent in vacuo, isomeric mixture **1** is obtained as a white solid in moderate yield. The ^{1}H NMR of **1** in acetone-d_6 shows four signals at $\delta = 6.34$, 6.25, 6.21, and 6.19 ppm (Figure 2). The signal at $\delta = 6.34$ ppm attributes to the two equivalent CH_2-groups of the 1,1’-isomer (**1a**), while the signals at $\delta = 6.25$ and 6.21 ppm derive from the two CH_2-groups of the 1,2’-isomer (**1b**). The signal at $\delta = 6.19$ ppm derives from the two equivalent CH_2-groups of the 2,2’-isomer (**1c**), also being the main product. Integration of the signals reveals a ratio of 1/2/5 between the three isomers. Mixture **1** is then dissolved in DCM and thionyl chloride and pyridine are added while keeping the temperature below 5 °C. The reaction solution is allowed to warm to room temperature over 2.5 h. When all solids are dissolved, the reaction solution is washed with water, hydrochloric acid (2 M), and water to remove excess thionyl chloride as well as pyridine. After removing the solvent, crude 2,2’-di(chloromethyl)bistetrazole (**2**) is obtained as an off-white solid in good yield (78 %), free of other isomers.

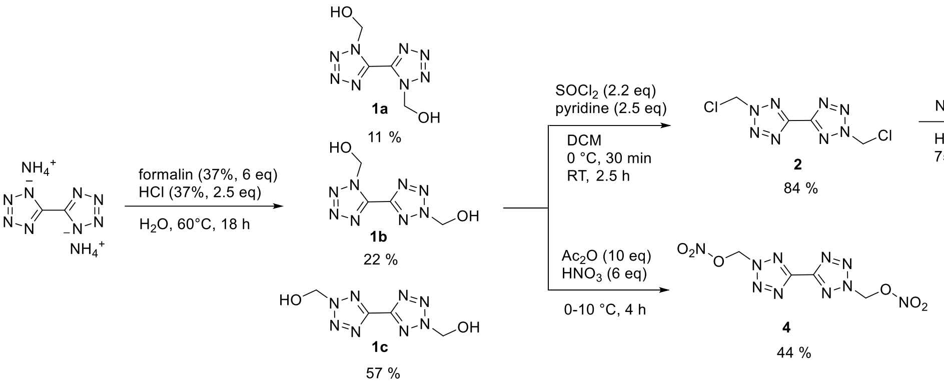

Scheme 1. Synthesis of 2,2’-di(hydroxymethyl)bistetrazole (**1c**) as well as further functionalisation towards 2,2’-di(azidomethyl)bistetrazole (**3**) and 2,2’-di(nitratomethyl)bistetrazole (**4**).

Crude compound **2** is then added to a solution of sodium azide in water/acetone (1:4) and stirred at 75 °C overnight. The reaction solution is extracted into DCM, dried over $MgSO_4$ and the solvent is removed *in vacuo,* thus obtaining a colourless oil of 2,2’ -di(azidomethyl)bistetrazole (**3**) in very good yield. The oil starts to solidify immediately after removing the flask from the water bath of the rotary evaporator, leaving **3** as a colourless, extremely sensitive (!) solid. Isomeric mixture **1** is also added to a large excess of acetic anhydride to which nitric acid (100%) was added at 0 °C. After the reaction is complete, it is quenched on ice and the precipitate is filtered off, and purified by column chromatography on silica gel with pure DCM as eluting solvent. By removing the solvent *in vacuo*, 2,2’-di(nitratomethyl)bistetrazole (**4**) is obtained as an off-white solid in moderate yield (44%), free of other isomers.

7.2.2 NMR Spectroscopy

The ^{1}H NMR of compound **3** in acetone-d_6 shows one signal at $\delta = 6.39$ ppm for the two CH_2-groups, while the ^{13}C NMR of **3** shows two signals at $\delta = 155.6$ and 65.7 ppm for the carbon atoms of the bistetrazole and the CH_2-groups, respectively. The ^{15}N NMR of compound **3** (Figure 3) shows seven distinct signals. Due to the symmetry of the molecule, all nitrogen atoms appear in pairs. The resonances for the two azides at $\delta = -302.1$ (N_α), -159.6 (N_γ), and -136.0 (N_β) ppm are in the same range as for comparable azido-methyl compounds.[5] The resonances for the bistetrazole at $\delta = -90.6$ (N2/2’), -76.9 (N1/1’), -46.9 (N4/4’), and 3.0 (N3/3’) are in the typical range for 2*N*-substituted tetrazoles[10]. The signals attributing N1/N1’ as well as the signal for both

N$_\beta$, split into triplets due to J^3-coupling with the hydrogen atoms of the CH$_2$-groups. Crystals of compound **1c–4** suitable for single crystal X-Ray diffraction were obtained by recrystallization from ethyl acetate.

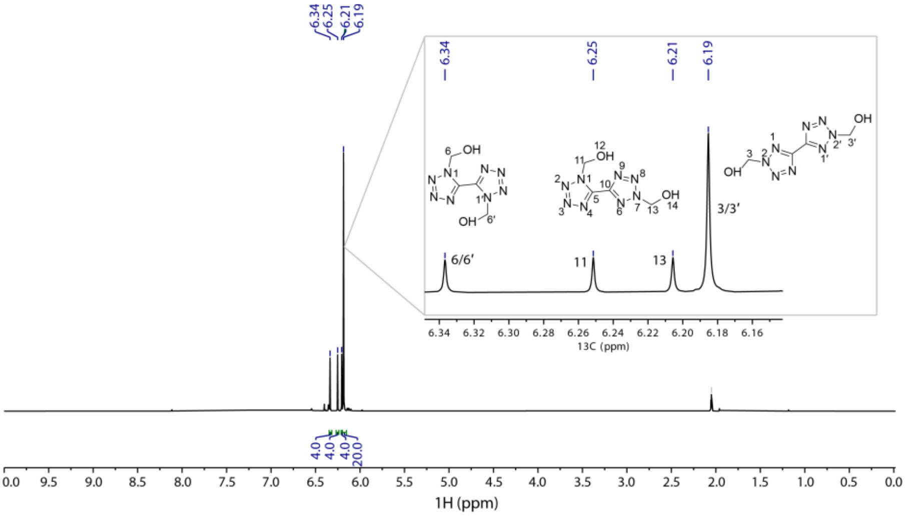

Figure 2. ^{1}H NMR spectrum and assignment of signals of isomeric mixture **1** in acetone-d$_6$.

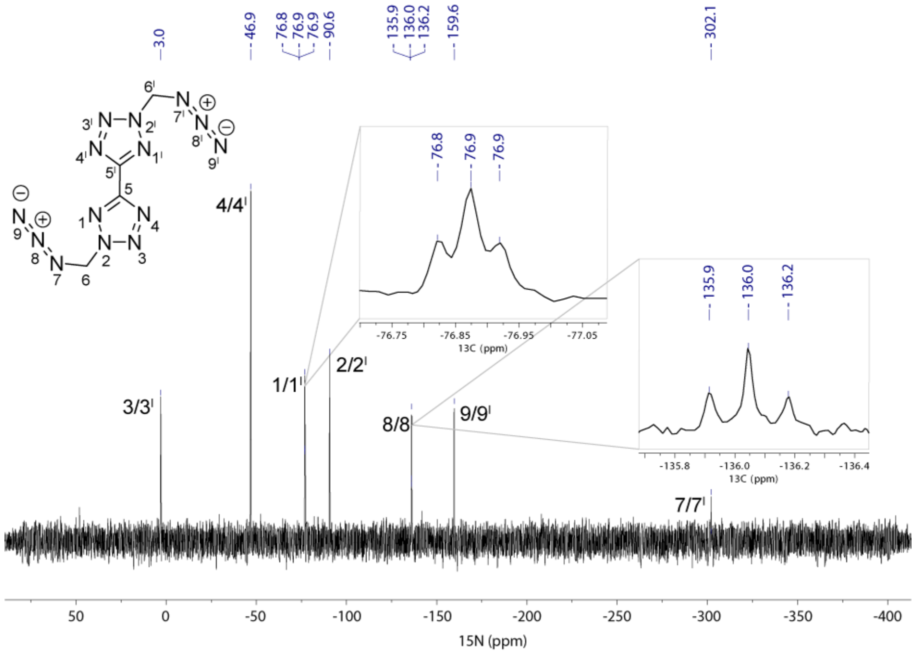

Figure 3. ^{15}N NMR spectrum and assignment of signals of **3** in acetone-d$_6$.

7.2.3 Crystal Structures

The solid-state crystal structures of all of the compounds synthesized in this work were determined using low-temperature single-crystal X-ray diffraction. Obtained crystal densities are recalculated to their respective room temperature density (calculation method is given in the Supporting

Information). All of the data and parameters of the measurements, as well as of the refinements and crystal structures of **1c** and **2** are given in the Supporting Information Table S1. The crystal datasets are uploaded to the CSD database and can be obtained free of charge with CCDC 2094642 (**1c**), 2094645 (**2**), 2094644 (**3**), and 2094643 (**4**). Compound **3** crystallizes in the tetragonal space group $I4_1/a$ with a calculated density of 1.62 g cm^{-3} (298 K) and eight molecules in the unit cell (Figure 4). The bistetrazole moiety is perfectly planar with a torsion angle of 180 ° between N1-C1-C1'-N1'. Due to the sp^3-hybridization of the methylene groups, both azides are protruding from the bistetrazole plane in opposite directions. Compound **4** (Figure 5) crystallizes in the tetragonal space group $P{-}42_1c$ with four molecules in the unit cell and a calculated density of 1.69 g cm^{-3} (298 K). Other than in compound **3**, the bistetrazole is not planar with a torsion angle of −10.7 ° between N1-C1-C1'-N4'. The torsion is induced by the arrangement of both nitratomethyl-groups in the same direction.

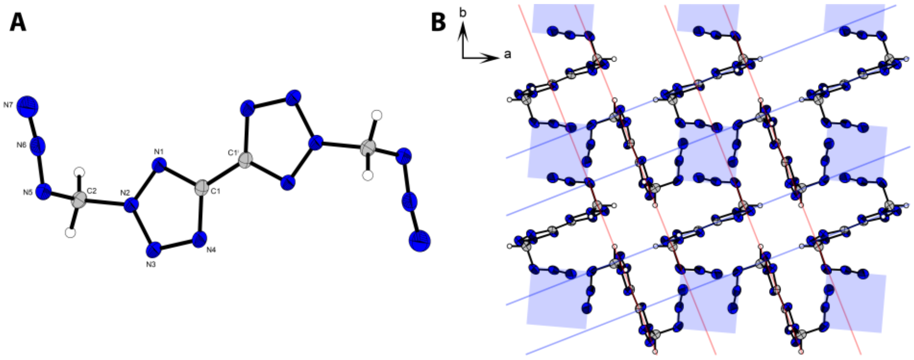

Figure 4. A) Molecular structure of compound **3**, ellipsoids are shown with a probability of 50%. B) view along the *c* axis.

This protrusion in the same direction causes the formation of dimers where two molecules are stacked with the nitrates facing towards the bistetrazole of the second molecule as can be seen in Figure 5B. The two bistetrazole scaffolds, forming the dimer, are oriented perfectly perpendicular on top of each other as highlighted in Figure 5C. Hirshfeld analysis of **3** (Figure 6) reveals a very large amount of N···N contacts (54.5 %), inducing strong repulsive interactions upon crystal lattice deformation. Those interactions are caused by four azide groups forming squares as depicted by the blue squares in Figure 4B. Even though stabilizing N···H (28.5%), C···N (7.7%) and C···H (9.4%) interactions are found, they are weak due to their large distance (>2.4 Å) and therefore, are not able to compensate the repulsive interactions[11, 12]. For compound **4**, strong repulsive N···N (9.8%) and O···O (15.6%) interactions together with a large amount of stabilizing N···O (25.9%), N···H (22.8%), O···H (19.5%), and C···O (2.7%) populations are observed. The stabilizing interactions sum up to 70.9%, hence far outnumbering the percentage of destabilizing interactions (25.4%), but due to their large distance (>2.4 Å), these interactions are weak and cannot balance the repulsive interactions. Nonetheless, the high amount of stabilizing interactions in **4** cause a slight decrease in friction sensitivity of **4** (0.3 N) compared to **3**. Still, both compounds **3** and **4** are to be classified as primary explosives according to the UN Recommendations on the Transport of Dangerous Goods.[13]

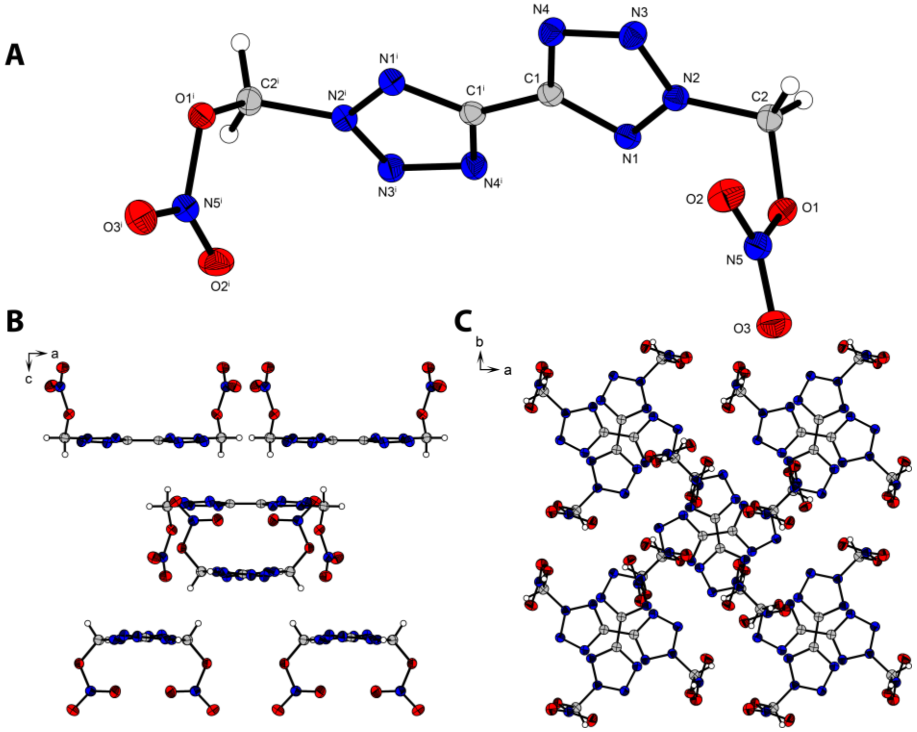

Figure 5. A) Molecular structure of compound **4**, ellipsoids are shown with a probability of 50%. B) view along the *b* axis. C) view along the *c* axis.

As such, both compounds are comparable with K_2DNABT[8] as well as lead azide (LA). While the sensitivities of **3** and **4** are comparable to those of K_2DNABT[8] (1 J, ≤1 N), they are slightly more sensitive than LA (4 J, 1 N)[14]. DTA analysis (Figure S12) exhibits endothermic events at 102 °C (**3**) and 100 °C (**4**), revealing melting points for both compounds. **3** is then thermally stable up to 177 °C, while **4** deflagrates exothermically already at a temperature of 150 °C.

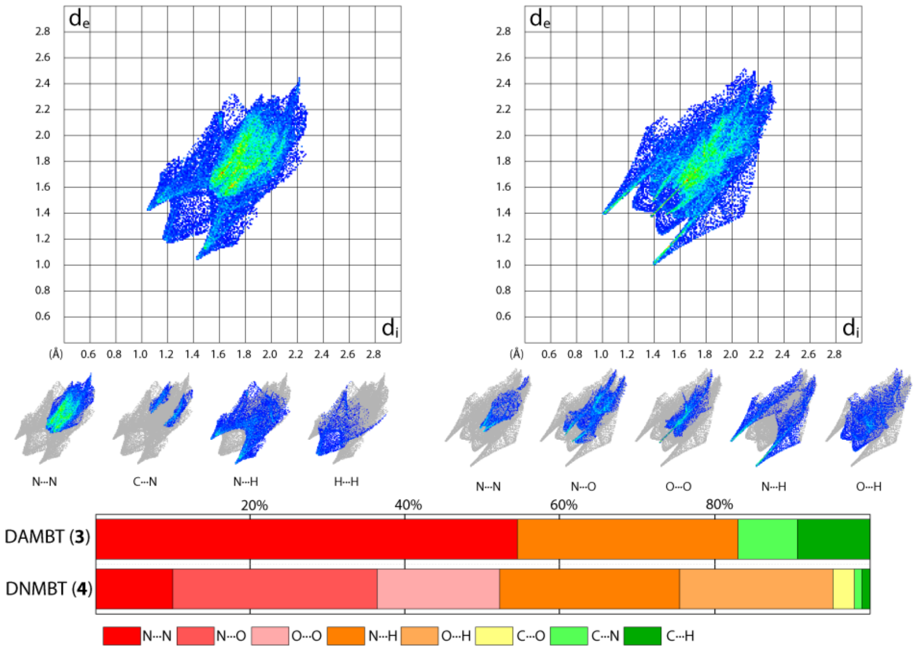

Figure 6. Two-dimensional fingerprint plot of DAMBT (left) and DNMBT (right) together with the individual atomic contribution. The atom contact percentages can be obtained from the bar chart.

For compound **3**, hot plate and hot needle tests (Figure 7) were performed, showing a very fast DDT (deflagration to detonation transition), thus promising properties for the application as a primary explosive. Experimental procedures are given in the Supporting Information. Compound **3** exhibits an exceptionally high heat of formation (1258 kJ mol^{-1}) by far exceeding that of **4** (441 kJ mol^{-1}) as well as that of K_2DNABT (326 kJ mol^{-1}) and LA (450 kJ mol^{-1}). Even though **4** has a lower heat of formation, it exhibits a higher detonation velocity and pressure than **3**, comparable to K_2DNABT (8459 m s^{-1}, 310 kbar). Initiation tests showed a positive initiation of PETN (200 mg) by 50 mg of loosely added **3** (Figure 7) while preliminary initiation testing with compound **4** was negative. We strongly want to point out the possibility of dripping molten **3** on a possible secondary charge, which to the best of our knowledge has not been described so far. Hence, compound **3** offers the possibility to replace the metal-containing lead azide with an all *CHN*-containing metal-free melt-castable green primary explosive in initiation devices.

Table 1. Physicochemical properties of 2,2'-di(azidomethyl)bistetrazole (**3**) and 2,2'-di(nitratomethyl)bistetrazole (**4**), compared with the primary explosives K_2DNABT and lead azide

	3	**4**	**K_2DNABT[8]**	**LA[14]**
Formula	$C_4H_4N_{14}$	$C_4H_4N_{10}O_6$	$C_2K_2N_{12}O_4$	N_6Pb
M [g mol^{-1}]	248.17	288.14	334.30	291.3
IS [J][a]	2	<1	1	2.5-4
FS [N][b]	< 0.1	0.3	≤1	≤1
ρ [g cm^{-3}][c]	1.62	1.69	2.11	4.8
N / O [%][d]	79.0, 0.0	48.6, 33.3	50.3, 19.1	50.3 / 0
Ω_{CO} [%][e]	−38.7	0.0	−4.8	−11.0
T_{endo}/T_{exo}[f] [°C]	102 / 177	100 / 150	− / 200	− / 315
$\Delta_f H°$ [kJ mol^{-1}][g]	1257.9	440.5	326.4	450.1
Explo5 V6.05.04				
$-\Delta_{Ex}U°$ [kJ kg^{-1}][h]	4928	5385	4948	1560
$P_{C\text{-}J}$ [kbar][i]	237	286	310	356
V_{det} [m s^{-1}][j]	8155	8377	8459	6187

[a] Impact sensitivity (BAM drophammer (1 of 6)). [b] Friction sensitivity (BAM friction tester (1 of 6)). [c] From X-ray diffraction analysis recalculated to 298 K. [d] Nitrogen and oxygen content. [e] Oxygen balance towards CO formation. [f] Temperature of endothermic (melting) and exothermic event (DTA; β = 5 °C min^{-1}). [g] Calculated enthalpy of formation. [h] Energy of explosion. [i] Detonation pressure at Chapman-Jouguet point. [j] Detonation velocity.

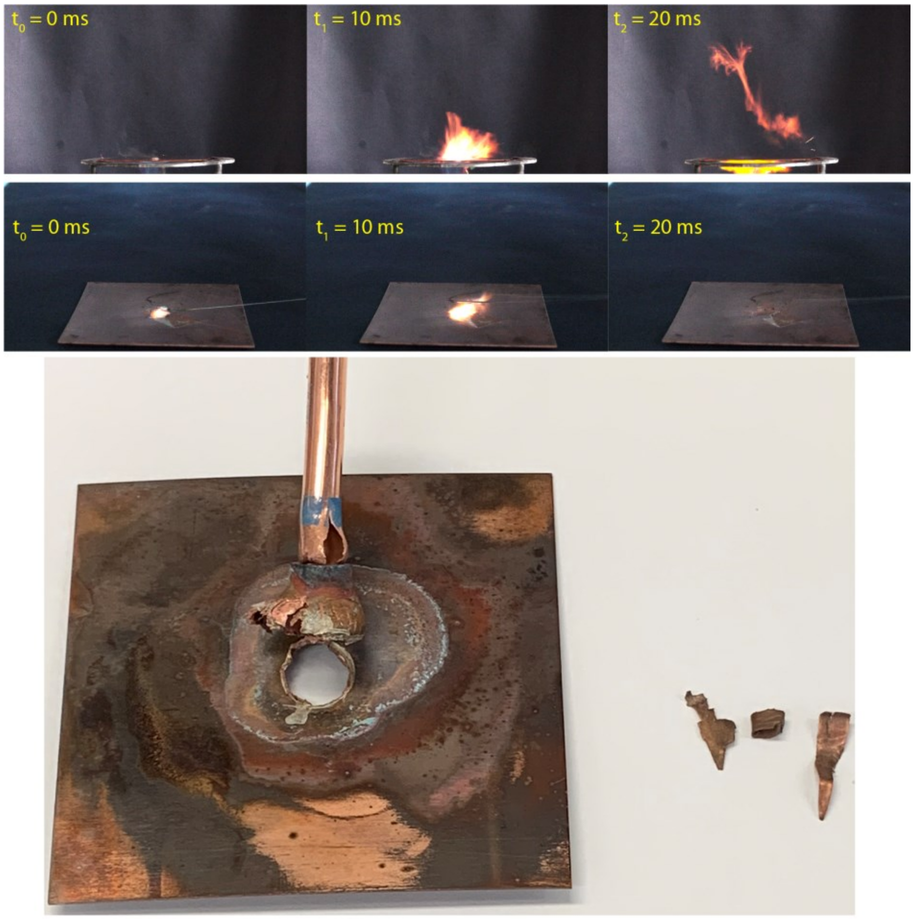

Figure 7. Top) Showing individual frames of detonation in the hot plate test. Middle) Showing individual frames of detonation upon touching with red-hot needle. Bottom) Positive initiation of PETN (200 mg) pressed into the copper tube, and loosely covered with **3**. The hole in the witness-plate confirms the positive initiation of the main charge.

7.3 Conclusion

Hydroxy methylation with further nitration or chlorination with subsequent chloride azide exchange proved to be a reliable procedure for the design of high energetic melt-castable explosives. The application of this procedure to the 5,5' -bistetrazole scaffold resulted in two high-performing but also highly sensitive compounds with melting points around 100 °C. Starting from diammonium bistetrazolate, 2,2'-di(azidomethyl)- (**3**) and 2,2'-di(nitratomethyl)bistetrazole (**4**) were synthesized by a straight forward synthesis. Both compounds were analysed by multinuclear NMR spectroscopy, accompanied by elemental analysis confirming their purity. Hirshfeld analysis of their crystal structure indicated a very high mechanical sensitivity, which was confirmed by experimental measurement of friction and impact sensitivities. Both compounds are extremely sensitive (<1–2 J, <1 N), while showing explosive properties of a secondary high explosive (>8000 m s^{-1}). The fast DDT of compound **3** together with a melting point of 100 °C and thermal stability of up to 177 °C makes it an outstanding melt-castable, metal-free green primary explosive for initiation devices.

7.4 Acknlowedgement

Financial support of this work by the Ludwig-Maximilian University of Munich (LMU), the Office of Naval Research (ONR) under grant no. N00014-19-1-2078 as well as the Strategic Environmental Research and Development Program (SERDP) under grant no. WP19-1287 is gratefully acknowledged. The authors thank Prof. K. Karaghiosoff for ^{15}N NMR measurement.

7.5 References

[1] R. L. Simpson, P. A. Urtiew, D. L. Ornellas, G. L. Moody, K. J. Scribner and D. M. Hoffman, *Propellants Explos. Pyrotech.* **1997**, *22*, 249-255.

[2] N. Fischer, D. Fischer, T. M. Klapötke, D. G. Piercey and J. Stierstorfer, *J. Mater. Chem.* **2012**, *22*, 20418-20422.

[3] W. Zhang, J. Zhang, M. Deng, X. Qi, F. Nie and Q. Zhang, *Nat. Commun.* **2017**, *8*, 181.

[4] E. C. Johnson, J. J. Sabatini, D. E. Chavez, R. C. Sausa, E. F. C. Byrd, L. A. Wingard and P. E. Guzmàn, *Org. Process Res. Dev.* **2018**, *22*, 736-740.

[5] L. Bauer, M. Benz, T. M. Klapötke, T. Lenz and J. Stierstorfer, *J. Org. Chem.* **2021**, *86*, 6371-6380.

[6] G. I. Koldobskii, D. S. Soldatenko, E. S. Gerasimova, N. R. Khokhryakova, M. B. Shcherbinin and V. P. O. Lebedev, V. A., *Russ. J. Org. Chem.* **1997**, *33*, 1771-1783.

[7] P. C. Bansal, I. H. Pitman, J. N. S. Tam, M. Mertes and J. J. Kaminski, *J. Pharm. Sci.* **1981**, *70*, 850-854.

[8] D. Fischer, T. M. Klapötke and J. Stierstorfer, *Angew. Chem. Int. Ed.* **2014**, *53*, 8172-8175.

[9] N. Fischer, D. Izsák, T. M. Klapötke, S. Rappenglück and J. Stierstorfer, *Chem. Eur. J.* **2012**, *18*, 4051-4062.

[10] G. Aridoss, C. Zhao, G. L. Borosky and K. K. Laali, *J. Org. Chem.* **2012**, *77*, 4152-4155.

[11] M. A. Spackman and D. Jayatilaka, *CrystEngComm* **2009**, *11*, 19-32.

[12] Y. Ma, A. Zhang, X. Xue, D. Jiang, Y. Zhu and C. Zhang, *Cryst. Growth Des.* **2014**, *14*, 6101-6114.

[13] UN recommendations on the Transport of Dangerous Goods: Model Regulations (21st Revised Edition), **2019**.

[14] T. M. Klapötke, *Chemistry of High-Energy Materials*, DeGruyter, **2019**.

7.6 Supporting Information

7.6.1 Experimental Part and General Methods

All chemicals and solvents were employed as received (Sigma-Aldrich, Fluka, Acros, ABCR). ^{1}H, ^{13}C{^{1}H}, ^{14}N, and ^{15}N{^{1}H} spectra were recorded at ambient temperature using a JEOL Bruker 27400, Eclipse 270, JEOL EX 400 or a JEOL Eclipse 400 instrument. The chemical shifts quoted in ppm in the text refer to typical standards such as tetramethylsilane (^{1}H, ^{13}C) nitromethane (^{14}N,^{15}N) in DMSO-d_6, D_20 or acetone-d_6 as the solvent. Endothermic and exothermic events of the described compounds, which indicate melting, loss of crystal water or decomposition, are given as the extrapolated onset temperatures. The samples were measured in a range of 25–400 °C at a heating rate of 5 °C min^{-1} through differential thermal analysis (DTA) with an OZM Research DTA 552-Ex instrument and in some cases additionally by thermal gravimetric analysis (TGA) with a PerkinElmer TGA4000. Infrared spectra were measured with pure samples on a PerkinElmer BXII FT-IR system with a Smith DuraSampler IR II diamond ATR. Determination of the carbon, hydrogen, and nitrogen contents was carried out by combustion analysis using an Elementar Vario El (nitrogen values determined are often lower than the calculated ones' due to their explosive behavior). Impact sensitivity tests were carried out according to STANAG 4489[S1] with a modified instruction[S2] using a BAM (Bundesanstalt für Materialforschung) drophammer.[S3] Friction sensitivity tests were carried out according to STANAG 4487[S4] with a modified instruction[S5] using the BAM friction tester.[S6,7] The classification of the tested compounds results from the "UN Recommendations on the Transport of Dangerous Goods".[S8, 9] Additionally, all compounds were tested upon the sensitivity toward electrical discharge using the OZM Electric Spark XSpark10 device.[S7] Energetic properties have been calculated with the EXPLO5 6.05.04 computer code[S10] using the, X-ray densities, recalculated to room temperature by applying the equation for volumetric expansion[S31] and calculated solid state heats of formation. These were computed by the atomization method as described in recently published papers. Electronic enthalpies were calculated with the Gaussian09 software[S11] suite using the CBS-4M method. Hot plate and hot needle tests were performed in order to classify the initiation capability of compound **3**. **3** was fixed on a copper plate underneath adhesive tape and initiated by a red-hot needle. Strong deflagration or detonation of the compound usually indicates a valuable primary explosive. The safe and straightforward hot plate test only shows the behavior of the unconfined sample toward fast heating on a copper plate. It does not necessarily allow any conclusions on a compound´s capability as a suitable primary explosive. Initiation capability tests of the newly synthesized compound **3** towards pentaerythritol tetranitrate (PETN) was carried out in a cooper shell with a diameter of 7 mm and a length of 88 mm filled with 200 mg of sieved PETN (grain size < 100 μm). First, nitropenta was pressed with a weight of 8 kg, then the primary explosive **3** was subsequently filled on top of the main charge. The shell was sealed by an insulator, placed in a retaining ring, which was soldered to a copper witness plate with a thickness of 1 mm and finally initiated by a type A electric igniter. A positive test is indicated by a hole in the copper plate and fragmentation of the shell caused by a deflagration-to-detonation transition (DDT) of PETN.

1,1'-, 1,2-, 2,2'-di(hydroxymethyl)bistetrazole (1a, b, c)

Ammonium bistetrazolate (15 g, 87 mmol) was dissolved in water (92.4 mL), formaldehyde (37%, 36 mL, 484 mmol, 5.6 eq.) and HCl (37%, 19.5 mL, 235.5 mmol, 2.7 eq.) was added, and the mixture was heated overnight at 60 °C. After cooling down, the solution was extracted into ethyl acetate (500 mL), cleared from water with $MgSO_4$ and dried *in vacuo*, resulting in a mixture of 1,1'- (**1a**), 1,2- (**1b**), and 2,2'-di(hydroxymethyl)bistetrazole (**2c**) as a white solid (15.66 g, 79 mmol, 90%).

^{1}H NMR (acetone-d_6, ppm) δ = 6.34 (s, 4 H, 2 CH_2), 6.25 (s, 2 H, CH_2), 6.21 (s, 2 H, CH_2), 6.19 (s, 4 H, 2 CH_2); **^{13}C NMR** (DMSO-d_6, ppm) δ = 155.4 (2 N_4C), 75.9 (2 CH_2).

2,2'-di(chloromethyl)bistetrazole (2)

The isomeric mixture of **1a**, **b** and **c** (2.5 g, 13 mmol) was suspended in dichloromethane (50 mL). $SOCl_2$ (2 mL, 28 mmol, 2.2 eq.), followed by pyridine (3 mL, 39 mmol, 3.0 eq.) was added and the reaction stirred for 30 min at temperatures below 10 °C and was then allowed to warm to room temperature over 2.5 h. The DCM-phase was then washed with water, HCl (2 M) and again water. The solvent was dried with $MgSO_4$ and removed *in vacuo*, resulting in 2,2'-di(chloromethyl)-bistetrazole (**2**) as an off-white powder in good yield (2.49 g, 11 mmol, 84%).

^{1}H NMR (acetone-d_6, ppm) δ = 6.78 (s, 4 H, 2 CH_2); **^{13}C NMR** (acetone-d_6, ppm) δ = 157.2 (2 N_4C), 57.6 (2 CH_2).

2,2'-di(azidomethyl)bistetrazole (3)

Crude 2,2'-di(chloromethyl)-bistetrazole (**2**) (200 mg, 0.85 mmol) and NaN_3 (331 mg, 5.11 mmol, 6 eq.) were added to a mixture of water and acetone (12 mL, 1:3) and refluxed at 75 °C overnight.

The product was extracted into dichloromethane (3x20 mL), washed with BRINE and dried over $MgSO_4$. After removing the solvent *in vacuo*, 2,2'-di(azidomethyl)bistetrazole (**3**) is obtained as colorless solid in good yield (196 mg, 0.79 mmol, 93%)

^{1}H NMR (DMSO-d$_6$, ppm) $\delta = 6.39$ (s, 4 H, 2 C*H*$_2$); **^{13}C NMR** (DMSO-d$_6$, ppm) $\delta = 155.6$ (2 N$_4$*C*), 65.7 (2 *C*H$_2$); **^{15}N{^{1}H}** NMR (DMSO-d$_6$, ppm) $\delta = 3.0$ (s, N3/3'), −46.9 (s, N4/4'), −76.8 - −76.9 (t, N1/1') , −90.6 (s, N2/2') , −135.9 - −136.2 (t, N8/8') , −159.6 (s, N9/9'), −302.1 (s, N7/7'). **Elemental analysis** calcd. [%] for $C_4H_4N_{14}$ (248.17): C 19.36, H 1.62, N 79.02; found C 20.28, H 1.99, N 79.25; **IR:** (ATR, cm^{-1}): $\tilde{v} = 3047$ (w), 2991 (w), 2167 (m), 2148 (m), 2126 (s), 2102 (vs), 1450 (w), 1440 (w), 1398 (m), 1364 (vw), 1338 (m), 1325 (m), 1253 (vs), 1237 (vs), 1201 (vs), 1165 (m), 1054 (s), 1010 (s), 917 (vs), 755 (vs), 728 (s), 684 (s), 655 (s), 558 (m), 413 (s); **DTA** (5 °C min^{-1}): 102 °C (T_{endo}), 177 °C (T_{exo}); **BAM drophammer**: 2 J, **BAM friction tester**: <0.1 N.

2,2'-di(nitratomethyl)bistetrazole (**4**)

Crude mixture of 2,2'-di(hydroxymethyl)bistetrazole (2 g, 10 mmol) was added to a fresh mixture of HNO_3 (2 mL, 48 mmol, 4.8 eq.) and acetic anhydride (6 mL, 63 mmol, 6.3 eq.) at temperatures below 10 °C. The mixture was then stirred for 4 h at temperatures between 0–10 °C, quenched on ice-water (50 mL) and stirred for 2 h. The precipitate is filtered off and purified by column chromatography with DCM, to obtain 2,2'-di(nitratomethyl)bistetrazole (**4**) as a white solid in moderate yield (44%).

^{1}H NMR (acetone-d$_6$, ppm) $\delta = 7.29$ (s, 4 H, 2 C*H*$_2$); **^{13}C NMR** (acetone-d$_6$, ppm) $\delta = 157.1$ (2 N$_4$*C*), 78.4 (2 *C*H$_2$); **Elemental analysis** calcd. [%] for $C_4H_4N_{10}O_6$ (288.14): C 16.67, H 1.40, N 48.61; found: C 17.02, H 1.89, N 49.16; **IR**: (ATR, cm^{-1}): $\tilde{v} = 3051$ (w), 2994 (vw), 2958 (vw), 2923 (vw), 2853 (vw), 1711 (m), 1671 (vs), 1421 (m), 1404 (m), 1391 (m), 1349 (m), 1323 (w), 1284 (vs), 1253 (m), 1218 (m), 1178 (m), 1051 (m), 1030 (s), 1002 (m), 969 (s), 826 (vs), 772 (vs), 742 (s), 731 (s), 696 (w), 680 (s), 632 (vs), 573 (s), 409 (s); **DTA** (5 °C min^{-1}): 100 °C (T_{endo}), 152 °C (T_{exo}); **BAM drophammer**: <1 J, **BAM friction tester**: 0.3 N.

7.6.2 Crystallographic Data

For all crystalline compounds, an Oxford Xcalibur3 diffractometer with a CCD area detector or Bruker D8 Venture TXS diffractometer equipped with a multilayer monochromator, a Photon 2 detector and a rotating-anode generator were employed for data collection using Mo-K_α radiation (λ = 0.7107 Å). On the Oxford device, data collection and reduction were carried out using the CrysAlisPRO software.[S13] On the Bruker diffractometer, the data were collected with the Bruker Instrument Service v3.0.21, the data reduction was performed using the SAINT V8.18C software (Bruker AXS Inc., 2011). The structures were solved by direct methods (SIR-92,[S14] SIR-97,[S15,16] SHELXS-97[S17,18] or SHELXT[S19]) and refined by full-matrix least-squares on $F2$ (SHELXL[S17,18]) and finally checked using the PLATON software[S20] integrated in the WinGX[S19,21] or Olex2[S20] software suite. The non-hydrogen atoms were refined anisotropically and the hydrogen atoms were located and freely refined. The absorptions were corrected by a SCALE3 ABSPACK or SADABS Bruker APEX3 multi-scan method.[S22,23] All DIAMOND2 plots are shown with thermal ellipsoids at the 50% probability level and hydrogen atoms are shown as small spheres of arbitrary radius.

Table S1. Crystallographic data and structure refinement details for compounds **1c** and **2**

	1c	**2**
Formula	$C_4H_6N_8O_2$	$C_4H_4Cl_2N_8$
FW [g mol^{-1}]	198.17	235.05
Crystal system	monoclinic	monoclinic
Space group	$P2_1/n$ (No. 14)	$P2_1/c$ (No. 14)
Color / Habit	colorless block	colorless platelet
Size [mm]	0.14 x 0.17 x 0.39	0.02 x 0.06 x 0.10
a [Å]	4.5207(5)	8.3693(4)
b [Å]	7.9263(9)	8.2279(4)
c [Å]	11.5245(12)	6.7862(3)
α [°]	90	90
β [°]	98.503(10)	108.194(2)
γ [°]	90	90
V [Å^3]	408.41(8)	443.95(4)
Z	2	2
$\rho_{calc.}$ [g cm^{-3}]	1.612	1.758
μ [mm^{-1}]	0.133	0.703
F(000)	204	236
$\lambda_{MoK\alpha}$ [Å]	0.71073	0.71073
T [K]	107	105
θ Min-Max [°]	3.1, 26.4	3.6, 30.5
Dataset	−5: 5; −9: 9; −14: 14	−11: 11; −11: 11; −9: 9
Reflections collected	3697	11605
Independent refl.	834	1355
R_{int}	0.024	0.033
Observed reflections	727	1190
Parameters	76	72
R_1 (obs)[a]	0.0313	0.0273
wR_2 (all data)[b]	0.0811	0.0683
S[c]	1.05	1.11
Resd. Dens [e Å^{-3}]	−0.17, 0.24	−0.30, 0.41
Device type	Oxford Xcalibur3	Oxford Xcalibur3
Solution	SIR−92	SIR-92
Refinement	SHELXL-2018	SHELXL-2018
Absorption correction	multi-scan	multi-scan

[a]$R_1 = \Sigma||F_0|-|F_c||/\Sigma|F_0|$; [b]$wR_2 = [\Sigma[w(F_0^2-F_c^2)^2]/\Sigma[w(F_0)^2]]^{1/2}$; $w = [\sigma c^2(F_0^2)+(xP)^2+yP]^{-1}$ and $P=(F_0^2+2F_c^2)/3$; [c]$S = \{\Sigma[w(F_o^2-F_c^2)^2]/(n-p)\}^{1/2}$ (n = number of reflections; p = total number of parameters).

Table S2. Crystallographic data and structure refinement details for compounds **3** and **4**

	3	**4**
Formula	$C_4H_4N_{14}$	$C_4H_4N_{10}O_6$
FW [g mol^{-1}]	248.21	288.17
Crystal system	tetragonal	tetragonal
Space group	$I4_1/a$ (No. 88)	$P{-}42_1c$ (No.114)
Color / Habit	colorless platelet	colorless block
Size [mm]	0.06 x 0.15 x 0.38	0.32 x 0.46 x 0.51
a [Å]	17.1656(10)	9.4429(1)
b [Å]	17.1656(10)	9.4429(1)
c [Å]	6.7040(7)	12.3008(3)
α [°]	90	90
β [°]	90	90
γ [°]	90	90
V [Å^3]	1975.4(3)	1096.84(4)
Z	8	4
$\rho_{calc.}$ [g cm^{-3}]	1.669	1.745
μ [mm^{-1}]	0.131	0.160
F(000)	1008	584
$\lambda_{MoK\alpha}$ [Å]	0.71073	0.71073
T [K]	113	108
θ Min-Max [°]	2.4, 26.4	2.7, 32.8
Dataset	−21: 20 ; −20: 21 ; −8: 8	−14: 14 ; −13: 13 ; −18: 18
Reflections collected	6544	22865
Independent refl.	1009	1950
R_{int}	0.073	0.040
Observed reflections	698	1764
Parameters	90	99
R_1 (obs)[a]	0.0441	0.0304
wR_2 (all data)[b]	0.0976	0.0810
S [c]	1.03	1.07
Resd. dens [e Å^{-3}]	−0.20, 0.18	−0.14, 0.29
Device type	Oxford Xcalibur3	Oxford Xcalibur3
Solution	SIR-92	SIR-92
Refinement	SHELXL-2018	SHELXL-2018
Absorption correction	multi-scan	multi-scan

[a] $R_1 = \Sigma||F_0|-|F_c||/\Sigma|F_0|$; [b] $wR_2 = [\Sigma[w(F_0^2-F_c^2)^2]/\Sigma[w(F_0)^2]]^{1/2}$; $w = [\sigma c^2(F_0^2)+(xP)^2+yP]^{-1}$ and $P=(F_0^2+2F_c^2)/3$; [c] $S = \{\Sigma[w(F_o^2-F_c^2)^2]/(n-p)\}^{1/2}$ (n = number of reflections; p = total number of parameters).

7.6.3 Crystal Structures of 1c and 2

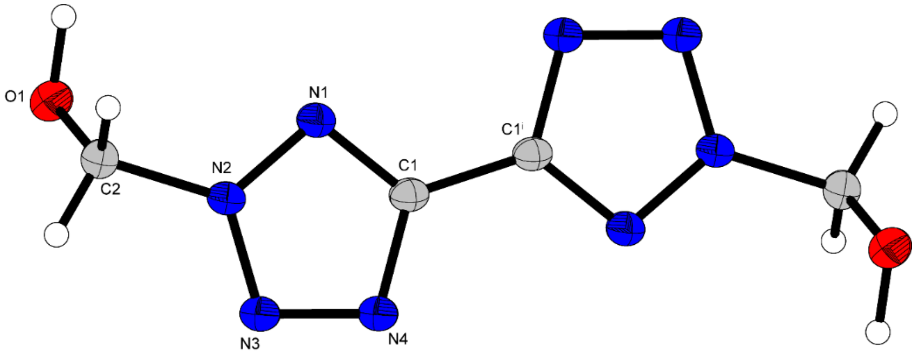

Figure S1. Crystal structure of compound **1c**; Selected interatomic distances [Å]: O1-C2 1.3854(17), N3-N4 1.3263(17), N1-N2 1.3309(15), N4-C1 1.3520(18), N1-C1 1.3228(17), C1-C1_a 1.4580(18), O1-H1 0.95(2), C2-H2A 0.969(16), N2-N3 1.3207(16), C2-H2B 0.978(15), N2-C2 1.4855(18); Angles [°]: N2-N1-C1 101.35(10), N4-C1-C1ⁱ 123.41(11), C2-O1-H1 104.4(14), N1-C1-C1ⁱ 123.58(12), N1-N2-N3 114.11(11), O1-C2-N2 110.01(11), N1-N2-C2 122.83(11), N3-N2-C2 123.06(11), N2-N3-N4 105.99(11), N3-N4-C1 105.55(11), N1-C1-N4 113.00(11).

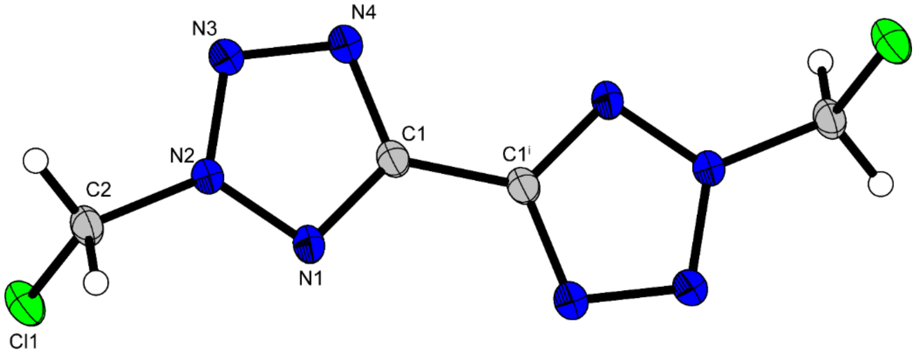

Figure S2. Crystal structure of compound **2**; Selected interatomic distances [Å]: C1-C1ⁱ 1.4568(19), N1-C1 1.3288(17), N1-N2 1.3285(17), N2-N3 1.3279(15), N2-C2 1.4480(17), N3-N4 1.3158(17), N4-C1 1.3549(17), Cl1-C2 1.7737(14); Angles [°]: N2-N1-C1 100.81(10), N4-C1-C1ⁱ 123.51(11), N1-N2-N3 114.35(11), Cl1-C2-N2 111.41(9), N1-N2-C2 123.43(11) , N3-N2-C2 122.20(11) , N2-N3-N4 106.06(11), N3-N4-C1 105.59(11), N1-C1-N4 113.19(12), N1-C1-C1ⁱ 123.30(12).

The bond angles and distances in compound **1c**-**4** are in the typical range for N–N, C–N, and N–O single bonds, as well as N–N and C–N double bonds. Compounds **1c** and **2** both show perfectly planar bistetrazole scaffolds with torsion angles between N1-C1-C1ⁱ-N1ⁱ of 180 ° (**1c**) and 179.98 (**2**). Also, the methylene groups are protruding from the bistetrazole plane in opposite directions for both compounds, too

7.6.4 Computations

All calculations were carried out using the Gaussian G09 program package.[S11] The enthalpies (H) and free energies (G) were calculated using the complete basis set (CBS) method of Petersson and coworkers in order to obtain very accurate energies.[S12] The CBS models use the known asymptotic convergence of pair natural orbital expressions to extrapolate from calculations using a finite basis set to the estimated complete basis set limit. CBS-4 begins with a HF/3-21G(d) geometry optimization; the zero point energy is computed at the same level. It then uses a large basis set SCF calculation as a base energy, and a MP2/6-31+G calculation with a CBS extrapolation to correct the energy through second order. A MP4(SDQ)/6-31+(d,p) calculation is used to approximate higher order contributions. In this study we applied the modified CBS-4M method (M referring to the use of minimal population localization) which is a re-parametrized version of the original CBS-4 method and also includes some additional empirical corrections. The enthalpies of the gas-phase species M were computed according to the atomization energy method (E1) (Table S3 & 4).[S11,13,24-27]

$$\Delta_f H^\circ_{(g,\ M,\ 298)} = H_{(Molecule,\ 298)} - \sum H^\circ_{(Atoms,\ 298)} + \sum \Delta_f H^\circ_{(Atoms,\ 298)} \qquad \text{(E1)}$$

Table S3. Literature values for atomic $\Delta H^\circ{}_f{}^{298}$ / kcal mol^{-1}

	$-H^{298}$ [a.u.]	NIST[S28]
H	0.50091	52.1
C	37.786156	171.3
N	54.522462	113.0
O	74.991202	59.6

The gas-phase heat of formations were converted to the solid/liquid state ones for neutrals: by subtracting the vaporization/sublimation enthalpies (calculated using the Trouton rule)[S29,30] At last, the molar standart enthalpies of formation ($\Delta_f H_M$) were used to calculate the molar solid state energie of formation (ΔU_m) according to equation (E2), Δn being the change of moles of gaseous components. The calculation results are summarized in Table S4.

$$\Delta U_m = \Delta H_m - \Delta n\, R\, T \qquad \text{(E2)}$$

Table S4. CBS-4M results, Gas phase enthalpies of formation, calculated sublimation/vaporization enthalpies and solid-state heat of formation.

Compound	$-H^{298}$ / a.u.	$\Delta_f H°(g)$ / kJ mol^{-1}	$\Delta H°_{sub}$ / kJ mol^{-1}	Δn
3	–919.901609	1328.3	1258.0	–9
4	–1151.921856	505.0	440.5	–10

7.6.5 NMR Spectroscopy

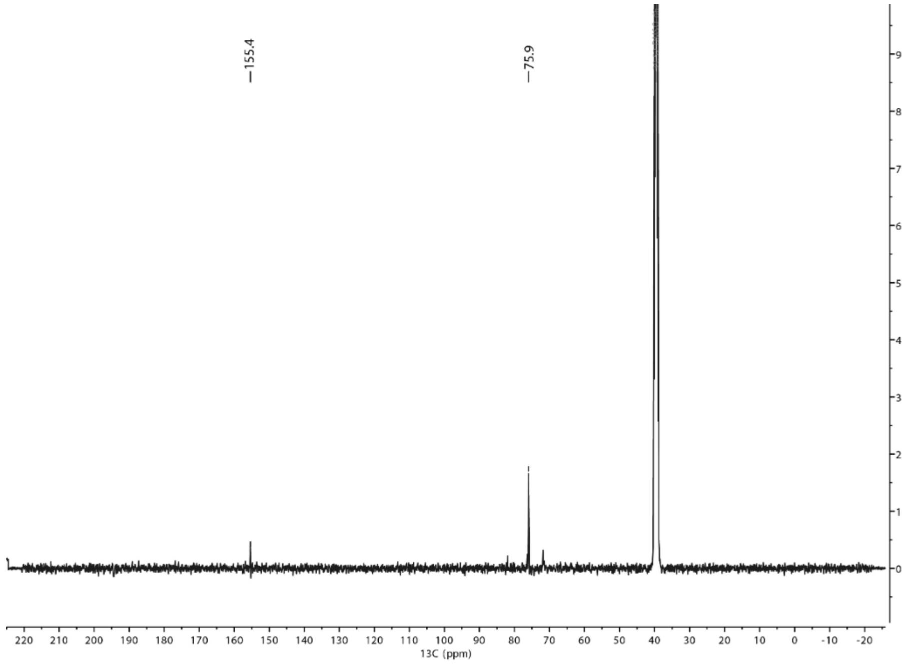

Figure S3. $^{13}C\{^1H\}$ NMR of **1c** in DMSO-d$_6$.

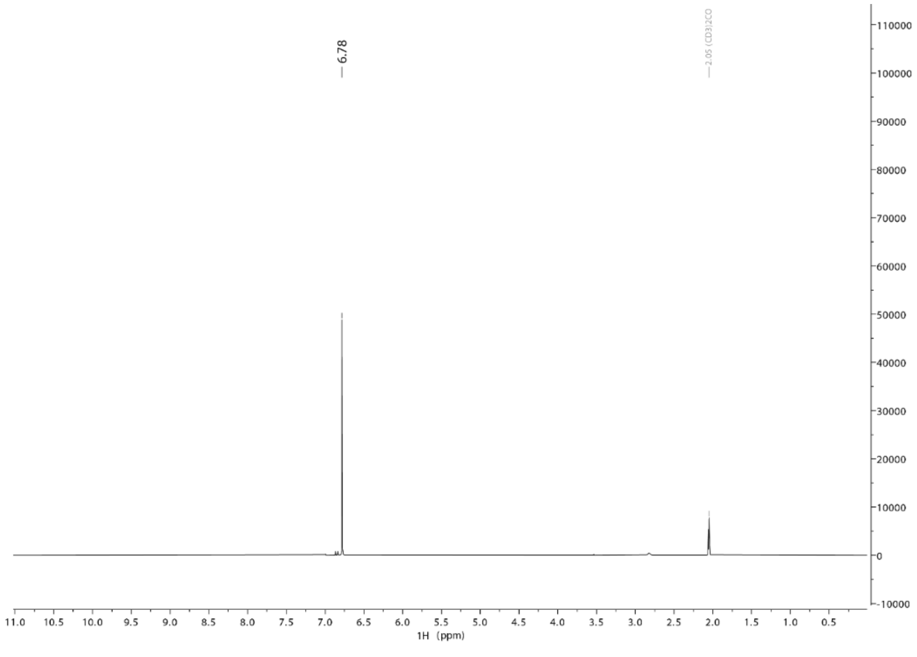

Figure S4. ^{1}H NMR of **2** in acetone-d$_6$.

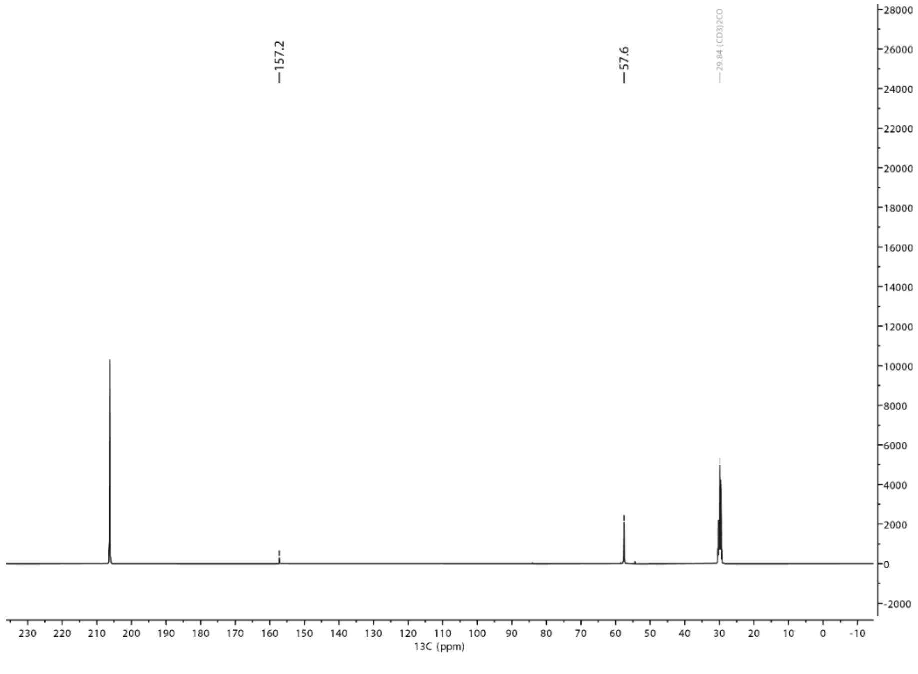

Figure S5. ^{13}C{^{1}H} NMR of **2** in acetone-d$_6$.

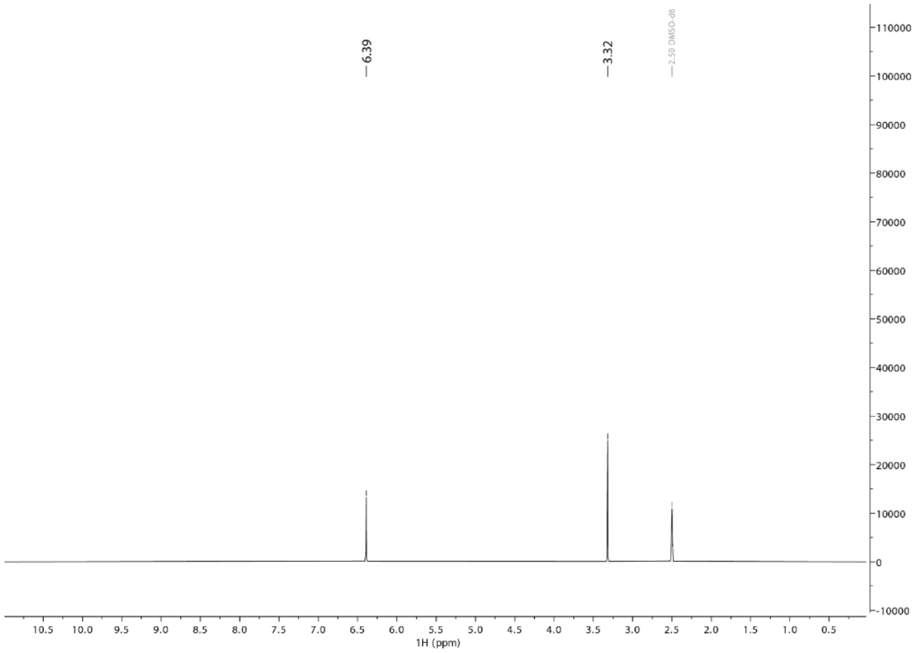

Figure S6. ^{1}H NMR of **3** in DMSO-d$_6$; residual water at $\delta = 3.32$ ppm.

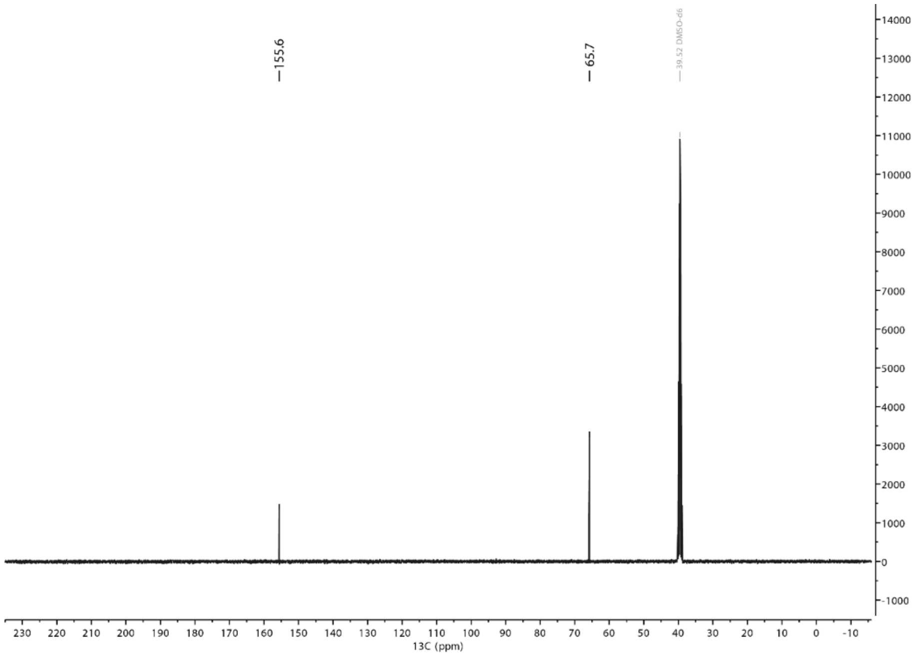

Figure S7. ^{13}C NMR of **3** in DMSO-d$_6$.

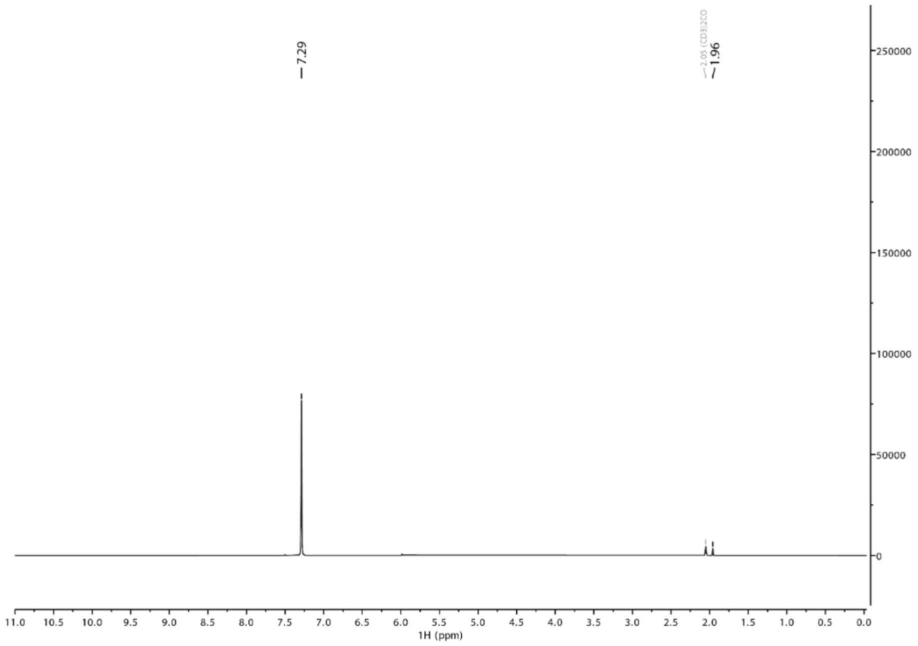

Figure S8. ^{1}H NMR of **4** in acetone-d$_6$; residual acetone at δ = 1.96 ppm.

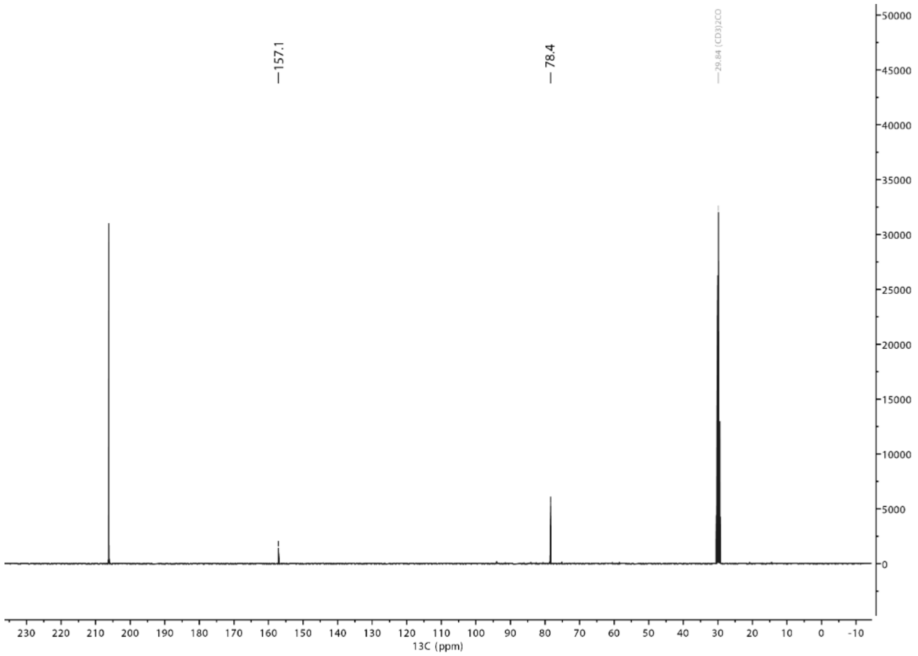

Figure S9. ^{13}C{^{1}H} NMR of **4** in acetone-d$_6$.

7.6.6 IR Spectroscopy

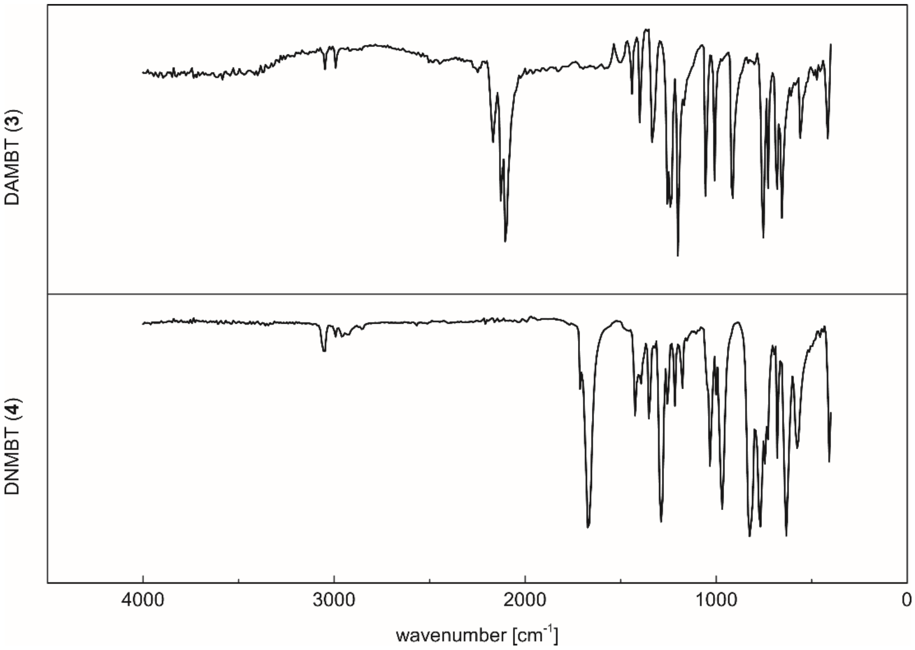

Figure S10. IR spectra of compounds **3** and **4**.

7.6.7 DTA Measurement

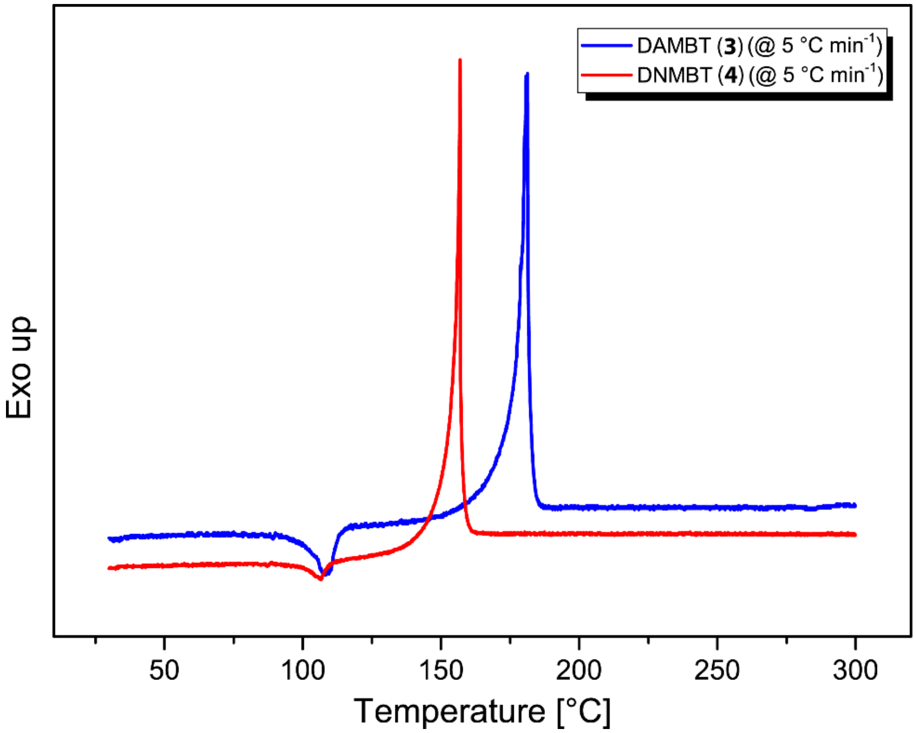

Figure S11. DTA measurement of compounds **3** and **4** with a heating rate of 5 °C min^{-1}.

7.6.8 References

S1 NATO standardization agreement (STANAG) on explosives, impact sensitivity tests, no. 4489, 1st ed., Sept. 17, **1999**.

S2 WIWEB-Standardarbeitsanweisung 4-5.1.02, Ermittlung der Explosionsgefährlichkeit, hier der Schlagempfindlichkeit mit dem Fallhammer, Nov. 8, **2002**.

S3 BAM, http://www.bam.de, (accessed March **2021**).

S4 NATO standardization agreement (STANAG) on explosive, friction sensitivity tests, no. 4487, 1st ed., Aug. 22, **2002**.

S5 WIWEB-Standardarbeitsanweisung 4-5.1.03, Ermittlung der Explosionsgefährlichkeit oder der Reibeempfindlichkeit mit dem Reibeapparat, Nov. 8, **2002**.

S7 OZM, http://www.ozm.cz, (accessed March **2021**).

S8 UN Model Regulation: Recommendations on the Transport of Dangerous Goods – Manual of Tests and Criteria, section 13.4.2.3.3, **2015**.

S9 Impact: insensitive > 40 J, less sensitive ≥ 35 J, sensitive ≥ 4 J, very sensitive ≤ 3 J; Friction: insensitive > 360 N, less sensitive = 360 N, sensitive < 360 N and > 80 N, very sensitive ≤ 80 N, extremely sensitive ≤ 10 N. According to the UN Recommendations on the Transport of Dangerous Goods, 5th ed., **2009**.

S10 M. Sućeska, EXPLO5 Version 6.05 User's Guide. Zagreb, Croatia: OZM; **2018**.

S11 M. J. Frisch, G. W. Trucks, H. B. Schlegel, G. E. Scuseria, M. A. Robb, J. R. Cheeseman, G. Scalmani, V.Barone, B. Mennucci, G. A. Petersson, H. Nakatsuji, M. Caricato, X. Li, H.P. Hratchian, A. F. Izmaylov, J. Bloino, G. Zheng, J. L. Sonnenberg, M. Hada, M. Ehara, K. Toyota, R. Fukuda, J. Hasegawa, M. Ishida, T. Nakajima, Y. Honda, O. Kitao, H. Nakai, T. Vreven, J. A. Montgomery, Jr., J. E. Peralta, F. Ogliaro, M. Bearpark, J. J. Heyd, E. Brothers, K. N. Kudin, V. N. Staroverov, R. Kobayashi, J. Normand, K. Raghavachari, A. Rendell, J. C. Burant, S. S. Iyengar, J. Tomasi, M. Cossi, N. Rega, J. M. Millam, M.Klene, J. E. Knox, J. B. Cross, V. Bakken, C. Adamo, J. Jaramillo, R. Gomperts, R. E. Stratmann, O. Yazyev, A. J. Austin, R. Cammi, C. Pomelli, J. W. Ochterski, R. L. Martin, K. Morokuma, V. G. Zakrzewski, G. A. Voth, P. Salvador, J. J. Dannenberg, S. Dapprich, A. D. Daniels, O. Farkas, J.B. Foresman, J. V. Ortiz, J. Cioslowski and D. J. Fox, Gaussian 09 A.02, Gaussian, Inc., Wallingford, CT, USA, **2009**.

S12 J. W. Ochterski, G. A. Petersson, J. A. Montgomery Jr., *J. Chem. Phys.* **1996**, *104*, 2598.

S13 CrysAlisPRO (Version 171.33.41), Oxford Diffraction Ltd., **2009**.

S14 A. Altomare, G. Cascarano, C. Giacovazzo, and A. Guagliardi, *J. Appl. Crystallogr.* **1992**, ***26***, 343.

S15 A. Altomare, G. Cascarano, C. Giacovazzo, A. Guagliardi, A. G. G. Moliterni, M. C. Burla, G. Polidori, M. Camalli and R. Spagna, SIR97, **2003**.

S16 A. Altomare, M. C. Burla, M. Camalli, G. L. Cascarano, C. Giacovazzo, A. Guagliardi, A. G. G. Moliterni, G. Polidori and R. Spagna, *J. Appl. Crystallogr.* **1999**, *32*, 115.

S17 G. M. Sheldrick, SHELXL-97, University of Göttingen, Germany, **1997**.

S18 G. M. Sheldrick, *Acta Crystallogr. Sect. A* **2008**, *64*, 112.

S19 G. M. Sheldrick, *Acta Cryst. A* **2015**, *71*, 3–8.

S20 A. L. Spek, PLATON, Utrecht University, The Netherlands, **1999**.

S21 L.J. Farrugia, *J. Appl. Cryst.* **2012**, *45*, 849.

S22 Empirical absorption correction using spherical harmonics, implemented in SCALE3 ABSPACK scaling algorithm (CrysAlisPro Oxford Diffraction Ltd., Version 171.33.41, **2009**).

S23 APEX3, Bruker AXS Inc., Madison, Wisconsin, USA.

S24 J. A. Montgomery Jr., M. J. Frisch, J. W. Ochterski and G. A. Petersson, *J. Chem. Phys.* **2000**, *112*, 6532–6542.

S25 L. A. Curtiss, K. Raghavachari, P. C. Redfern and J. A. Pople, *J. Chem. Phys.* **1997**, *106*, 1063–1079.

S26 E. F. C. Byrd and B. M. Rice, *J. Phys. Chem. A* **2006**, *110*, 1005–1013.

S27 B. M. Rice, S. V. Pai and J. Hare, *Comb. Flame* **1999**, *118*, 445–458.

S28 P. J. Lindstrom and W. G. Mallard, NIST Standard Reference Database Number 69, http://webbook.nist.gov/chemistry/, (accessed March **2021**).

S29 M. S. Westwell, M. S. Searle, D. J. Wales and D. H. Williams, *J. Am. Chem. Soc.* **1995**, *117*, 5013–5015.

S30 F. Trouton, *Philos. Mag.* **1884**, *18*, 54–57.

S31 Equation for volumetric expansion: $\rho_{298K} = \frac{\rho_T}{1+\alpha_V(298-T)}$; $\alpha_V = 1.5 \times 10^{-4} K^{-1}$.

8 1,5-Dimethyltetrazole as a Ligand in Energetic 3d^5 to 3d^{10}-Metal Coordination Compounds

Moritz Kofen, Alexander G. Harter, Thomas M. Klapötke, Jörg Stierstorfer

Published in *Energetic Materials Frontiers*, 2022.

DOI: 10.1016/j.enmf.2022.07.004

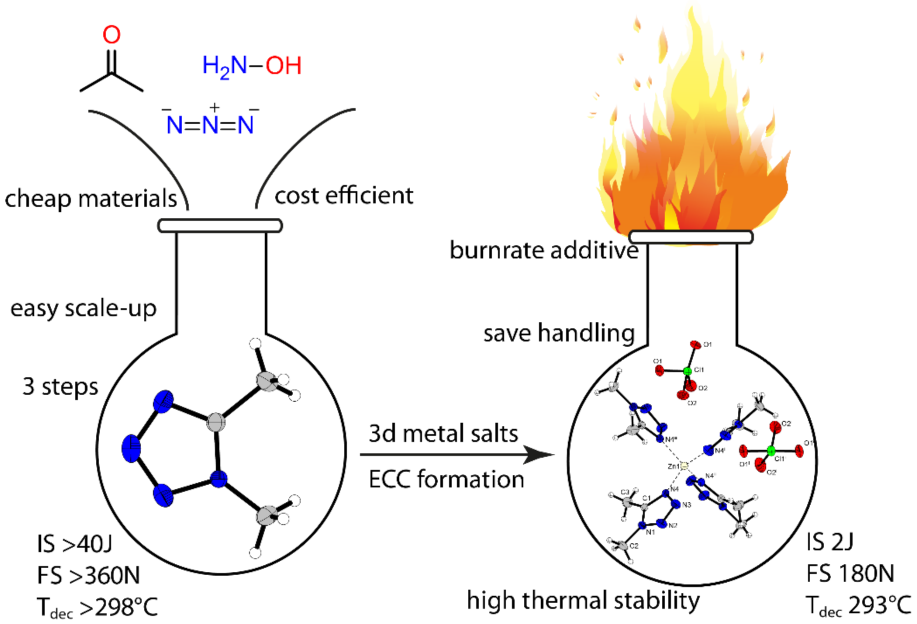

Abstract: During the last decade, energetic coordination compounds gained considerable attention due to the simple adjustments in their physicochemical properties. By combining different metal cations, energetic anions, and ligands, those compounds can be adapted for their intended use. This study used 1,5-dimethyltetrazole (**3**) as a highly endothermic, easily accessible, and insensitive ligand. It is a structural isomer to 1-ethyltetrazole (1-ETZ), which was recently described as a suitable ligand. 1,5-Dimethyltetrazole was synthesized using two different methods: (1) reaction of acetone with azido (trimethyl) silane and (**2**) reaction of acetoxime benzenesulfonate with sodium azide. Subsequently, 1,5-dimethyltetrazole was reacted with the perchlorate salts of different 3d metals (e.g., Mn, Fe, Co, Ni, Cu, Zn) to obtain new energetic coordination compounds (ECCs). In addition, copper (II) complexes with 2,4,6-trinitro-phenolate anions were synthesized. The resultant complexes were investigated through low-temperature, single crystal diffraction experiments complemented by elemental analysis, infrared spectroscopy, and differential thermal analysis. Moreover, sensitivities towards impact and friction were investigated. In this study, all

ECCs exhibited impact sensitivities between 2–10 J, friction sensitivities between 128–360 N, and thermal stabilities of up to 360 °C.

8.1 Introduction

Owing to their physical and chemical properties, coordination compounds are critical to various applications, such as spin-crossover systems[1,2], metal-organic frameworks[3], and energetic materials.[4] Most specifically, metal-organic frameworks have recently gained significant attention as hypergolic solid fuels for aerospace applications.[5-7] ECCs typically contain a 3d metal cation, are coordinated by a nitrogen-rich ligand, and gain charge balance with an oxidizing (e.g., ClO_4^-, ClO_3^-) or reducing (e.g., N_3^-) anion. Additionally, the concept of ECC formation expands many traditional synthetic approaches into new energetic materials, offering a broad range of further tuning the energetic properties towards their intended applications.[8,9] Nevertheless, the synthesis of ligands themselves is subjected to the introduction of explosophores[10-11], increasing enthalpy of formation by incorporating high amounts of nitrogen or oxygen in the molecule[11] or introducing a high strain.[11,12] The use of azoles[13,14] as ligands is highly desirable as they provide broad chemical diversity with high energy content due to their endothermic enthalpy of formation.[11] Furthermore, tetrazoles[15-18] have been proven to be promising energetic compounds that are suitable to be applied as ligands in energetic coordination compounds.[19-20] Their energetic properties can be easily modified by altering their functional groups or substitution patterns, as shown in Fig. 1. 1,5-Dimethyltetrazole (DMT, **3**) is an easily accessible, small, neutral, and nitrogen-rich molecule, which makes it a potent candidate as an energetic ligand. Although the compound looks trivial, it has never been used as a ligand; however, it offers a surprisingly high positive heat of formation. In this study, **3** was synthesized using different procedures from existing literature and further reacted with different 3d metal (e.g., Mn, Fe, Co, Ni, Cu, Zn) salts to form energetic coordination compounds. Besides their energetic properties, the change in the coordination of the ligand around the central metal was investigated. Finally, the influence of structural isomers was studied by comparing the ligands 1,5-dimethyltetrazole and 1-ethyltetrazole.

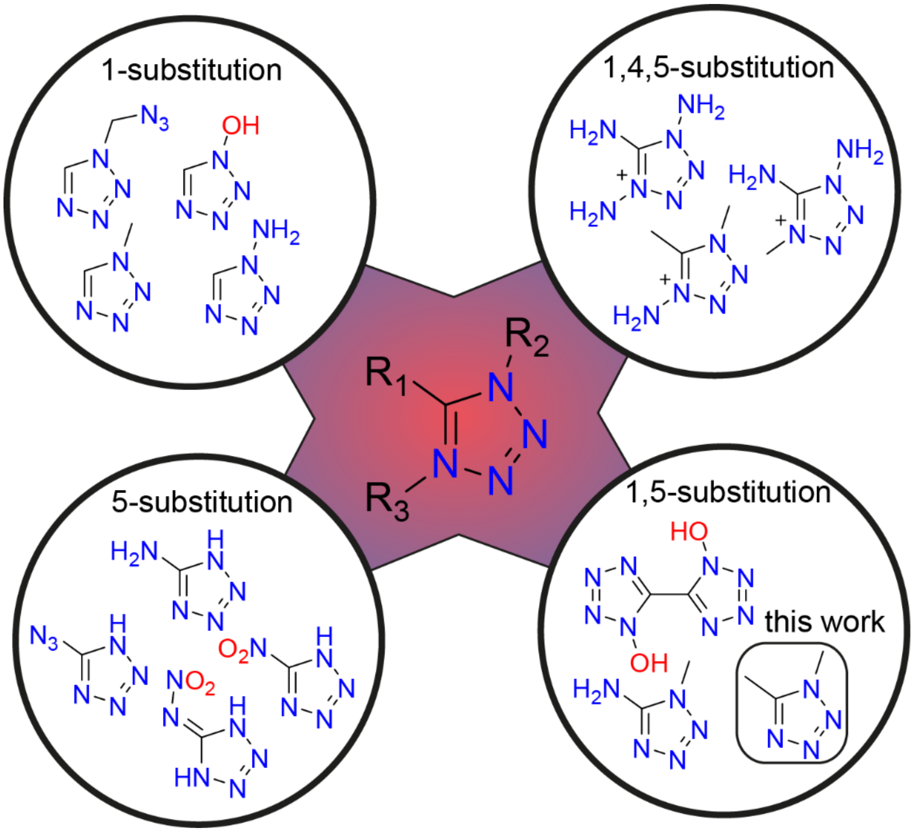

Fig. 1. Possible substitution patterns of 1,2,3,4-tetrazole, which highlight the chemical diversity.[17,18, 21-26]

8.2 Results and Discussion

8.2.1 Synthesis

1,5-Dimethyltetrazole (DMT, **3**) can be synthesized by different routes according to relevant literature[27-29] (Scheme 1). A straightforward method is the reaction of acetone with azidotrimethylsilane, which yields **3** in a one-step synthesis.[30] Another synthesis route starts with the reaction of acetone with hydroxylamine hydrochloride in water to form acetone oxime, followed by the reaction of acetone oxime with benzene sulfonyl chloride to form acetoxime benzenesulfonate, which acts as a leaving group in the final step of the reaction with sodium azide. The ring closure starts with a nucleophilic attack of the azide on the imine, accompanied by a [1,2]-rearrangement of one methyl group. Although the first synthesis procedure of applying trimethylsilylazide is more economical in terms of atoms, reaction time, and cost, the second procedure was preferred for the synthesis of **3** on a 10–20 g scale since it has a slightly higher yield of 42% than the first one (34%). **3** can be obtained as a colorless solid in the form of blocky crystals through recrystallization from water.

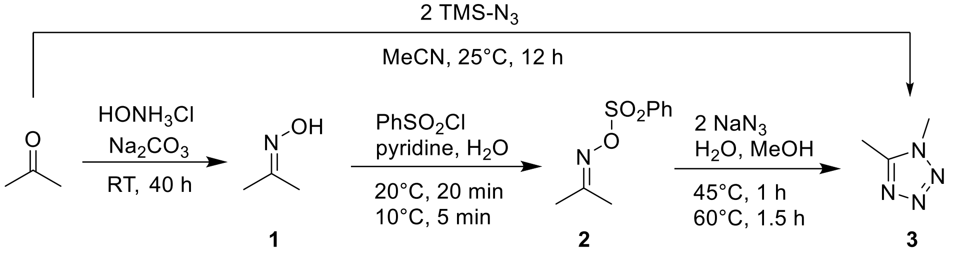

Scheme 1. Synthetical pathways towards 1,5-DMT starting from acetone

ECCs **4**–**12** were synthesized by combining aqueous solutions of corresponding metal salts with stoichiometric amounts of **3** at elevated temperatures (60–80 °C; Scheme 2). Because of the unavailability of copper (II) nitroaromatic salts, their aqueous solutions were obtained by suspending basic copper (II) carbonate in water, adding corresponding free acid, and stirring at high temperatures until the solids dissolved. For compounds **4**, **8**, **9**, **10**, **11,** and **12,** crystals suitable for single crystal X-ray diffraction experiments were obtained. For compounds **5**–**7**, the evaporation of the solvent resulted in glass-like residues, from which single crystals started to grow under a high vacuum. After crystal structures of these compounds were obtained, further analysis was impossible – even by recrystallization from different solvents. When the aqueous solution of **3** was combined with that of copper (II) styphnate, solids began to precipitate immediately. This solid was insoluble and filtered off, and the resulting clear solution was left to crystallize. The growing crystals were collected and analyzed through single crystal X-ray diffraction as compound **11a**. Elemental analysis proved that the solid formed initially was compound **11b**, for which single crystals cannot be obtained. In the synthesis of compound **12**, needle-like (**12a**) and block-like (**12b**) crystals began to precipitate, and **12a** was consumed due to the formation of **12b** after several days. Therefore, **12b** was the main product. Complex **12a** contained deprotonated nitrophenol anions, one of which was coordinating and one was non-coordinating. The copper (II) cation in complex **12a** was further coordinated by two aqua ligands and two molecules of **3**. By contrast, the copper (II) cation in **12b** was coordinated by two double deprotonated anions, bridging different metal centers. Each center was also coordinated by two molecules of **3**, with no inclusion of water.

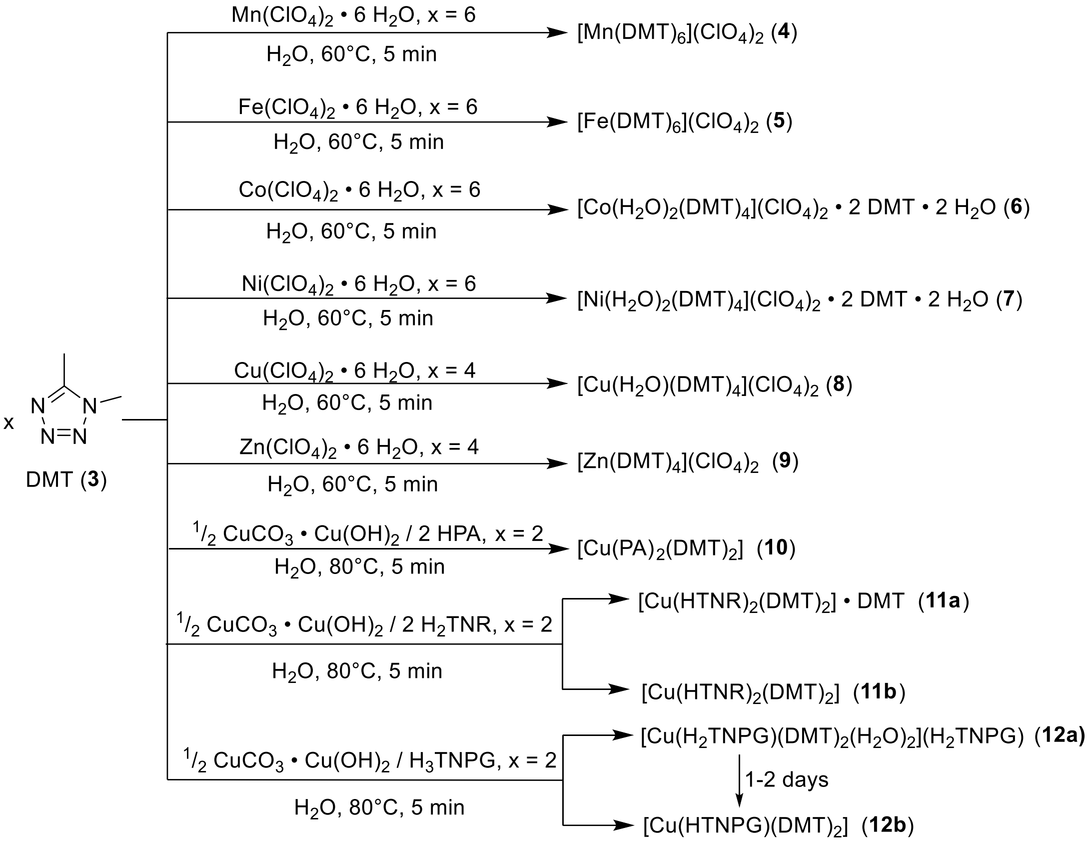

Scheme 2. Synthesis of energetic coordination compounds **4**–**12**.

8.2.2 Crystal Structures

Compound **3** and all ECCs were characterized through low-temperature single-crystal X-ray diffraction. The crystal density of all structures was recalculated to values at room temperature (298 K) for the sake of comparison. The datasets of all compounds (except for **7)** were uploaded to the CSD database and can be accessed for free with CCDC 2169296 (**3**), 2163674 (**4**), 2163667 (**5**), 2163668 (**6**), 2163673 (**8**), 2163675 (**9**), 2163671 (**10**), 2163670 (**11a**), 2163672 (**12a**), and 2163669 (**12b**). The obtained crystals of **7** had poor quality, rendering proper measurement and refinement impossible. Nonetheless, an insight into the compound's composition and the coordination of the nickel (II) cation can be obtained. The depiction of the obtained structure is provided in the supporting information (Fig. S1). Compound **3** crystallizes in the orthorhombic space group *Pnma* with four formula units per cell and a density of 1.31 g cm^{-3}. While the bond lengths are in the same range as those of comparable 1- or 5-methyltetrazoles, **3** exhibits a mirror axis (σ_v) due to a C/N disorder (Fig. 2). This causes a difficult distinction between the C1 and N1 atoms, which is intensified by a simultaneous sharing of the atoms' positions. The crystal packing of **3** along the *b* axis (Fig. 2b) represents the stacking in sets of perpendicular but rotated against molecules of **3** (red/blue). The packing along the *c* axis (Fig. 2b) shows that these sets exhibit an offset and are not face-on with each other, thereby presenting a screw-axis of **3** along the *b* axis.

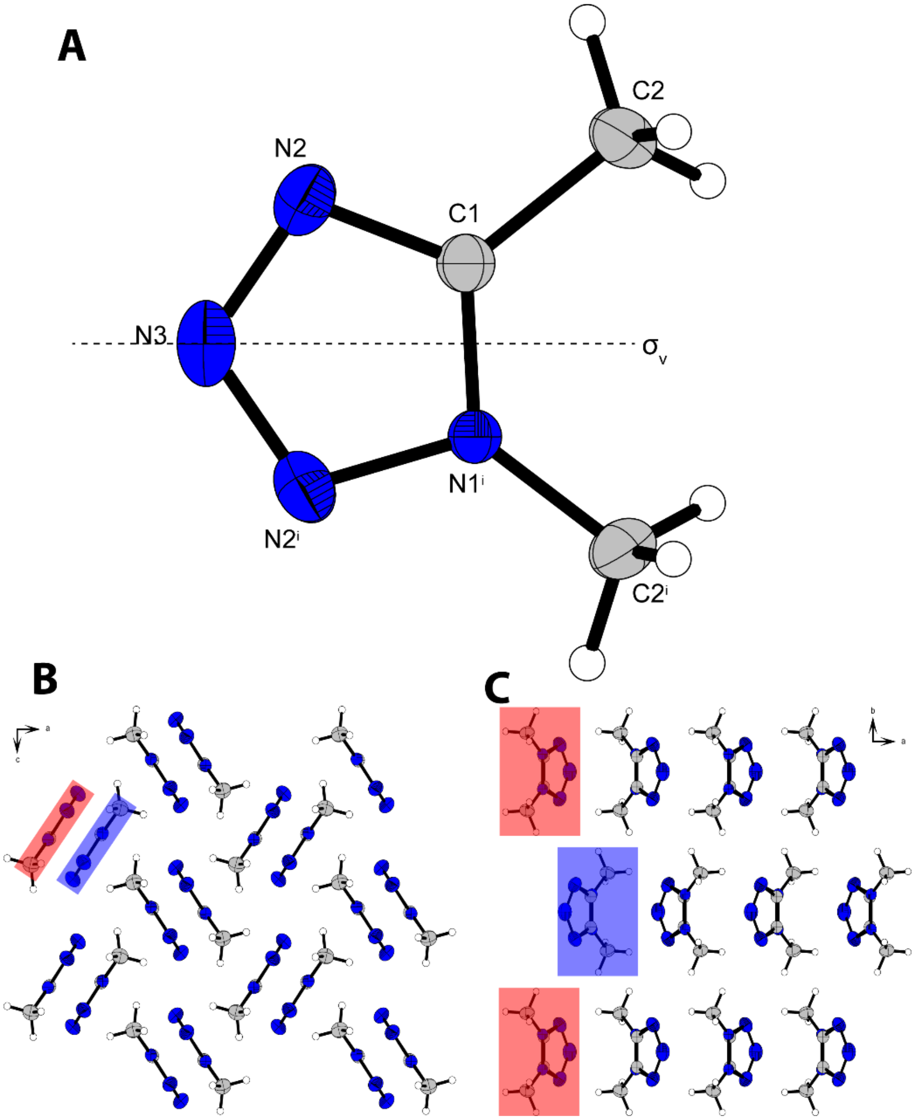

Fig. 2. (a) Molecular structure of 1,5-dimethyltetrazole (**3**); (b) crystal packing of **3** along *b*-axis; (c) crystal packing of **3** along *c*-axis. Selected bond lengths [Å]: N1–N2 1.350(6), N1–C2 1.414(6), N2–N3 1.325(14), N2–C1 1.319(7), C1–C2 1.529(7); All ellipsoids are depicted with a probability of 50%. Symmetry codes: i) +*x*, 3/2−*y*, +*z*.

Compounds **4** and **5** crystallize in the triclinic space group, *P*–3, and their calculated density is 1.53 g cm^{-3} and 1.55 g cm^{-3}, respectively, with one formula unit per cell. The manganese (II) cation of **4** (Fig. 3, top) shows sixfold coordination by 1,5-DMT ligands, forming a nearly perfect octahedron. Thus, only minor deviation angles of 0.06° from the perfect octahedron and M–L bond lengths of 2.303 Å for all six ligands can be observed. Accordingly, the manganese (II) cation with an electron configuration of $[Ar]3d^5 4s^0$ is in its high-spin state. Additionally, the iron cation of **5** (Fig. 3, bottom) also shows sixfold coordination by 1,5-DMT ligands, forming an octahedron with an angle deviation of only 0.65° from the perfect octahedron. The distortion is caused by the electron configuration of [Ar]3d^6 for a high-spin (hs) Fe (II) cation, leading to one fully filled t_{2g} orbital (Fig. 4). Since the t_{2g} orbitals do not participate in the building of σ-bonds and the π-back bonding is weak, the overall M–L bond lengths are not influenced by this distortion. Accordingly, a bond length of 2.238 Å is found in all six ligands, which is comparable to that of other hs-Fe (II) coordination compounds. By comparing the ion radii of hs-Mn (0.830 Å[31]) with hs-Fe (0.780 Å[31]) cations, the difference of 0.050 Å is found to suit the observed change in M–L bond length of –0.065 Å from Mn (II) to Fe (II), supporting the assumption of a *high spin* Fe (II) compound. Furthermore, unlike previously reported ECCs of iron (II) perchlorate[32], compound **5** shows no thermochromic effect, which would derive from a change from hs-Fe (II) to low spin (ls)-Fe (II) when cooling crystals for low-temperature X-ray diffraction experiments. This effect is known for coordination compounds exhibiting sufficient ligand field splitting of *d*-orbitals. Cooling such coordination compounds results in an increase in ligand field splitting of the *d*-orbitals, ultimately enabling a spin-crossover from hs- to ls-state.[32] Overall, this observation leads to the classification of 1,5-DMT as a weak field ligand.

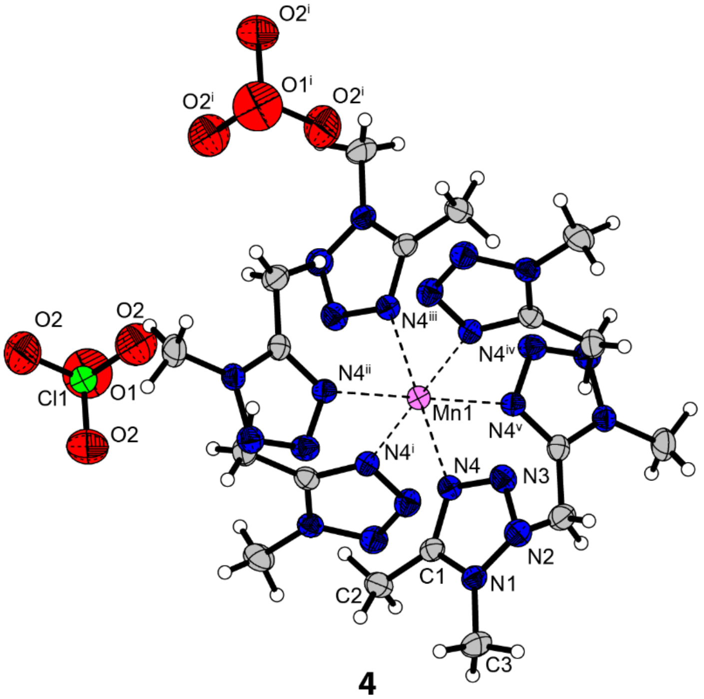

4

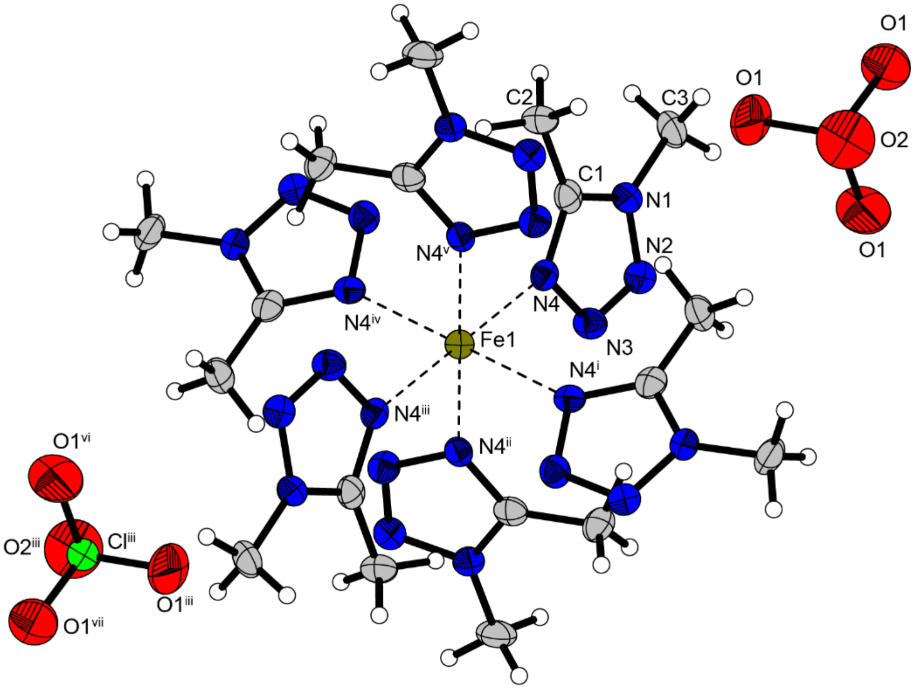

5

Fig. 3. Molecular structures of ECCs **4** and **5** in the crystalline state, displaying the coordination of the metal cation centers by 1,5-DMT. Selected bond lengths [Å]: Mn1–N4 2.303(2), Fe1–N4: 2.238(5).

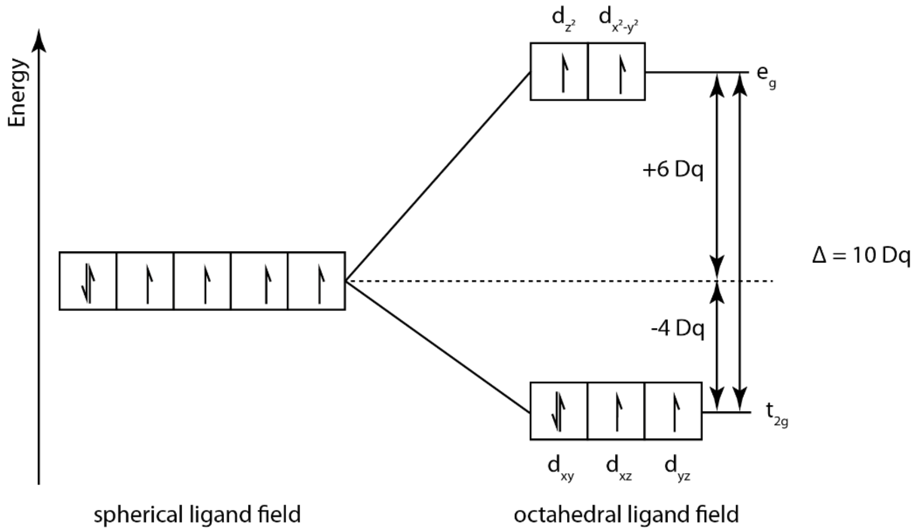

Fig. 4. Electronic configuration of a Fe (II) cation and the splitting of *d*-orbitals due to an octahedral coordination.

Compounds **6** (Fig. 5) and **7** (Fig. S1) crystallize in the monoclinic space group $P2_1/n$ and have calculated densities of 1.54 g cm^{-3} and 1.55 g cm^{-3}, respectively. The cobalt cation in **6** is coordinated by four molecules of 1,5-DMT and two water molecules, forming a slightly distorted octahedron co-crystallized by one additional 1,5-DMT and one water molecule. The angle deviations from the perfect octahedron are smaller than those in **5** due to three different M–L bond lengths. Besides the M–O bond of the axial standing aqua ligands, there are two different M–N bonds built by two pairs of 1,5-DMT ligands. One pair of opposite standing ligands coordinate via N4 of the tetrazole ring, whereas the other pair coordinate via N3 of the tetrazole ring. Among all the ligands, the highest difference in bond length is found between Co1–O6 and Co1–N7, with a *Δ* of 0.12 Å, which appears to be too small for *Jahn Teller*-like [33] distortions. Since oxygen atoms have π-basic character due to their lone pair and thus do not increase the gap difference of the t_{2g}- and e_g-orbitals, the cobalt (II) cation is in its high spin state, where significant *Jahn-Teller* effects are not expected. Consequently, steric effects between the DMT ligands and maintenance of a good *π*-orbital overlap cause the deviation from a perfect octahedron. Compound **7** shows the same coordination around the Ni (II) cation (Fig. S1) while being co-crystallized by two 1,5-DMT and two water molecules. Since the nickel cation has an electronic configuration of [Ar]3d^8 and the e_g orbital does not degrade, the slight deviations from the perfect octahedron are also caused by steric effects.

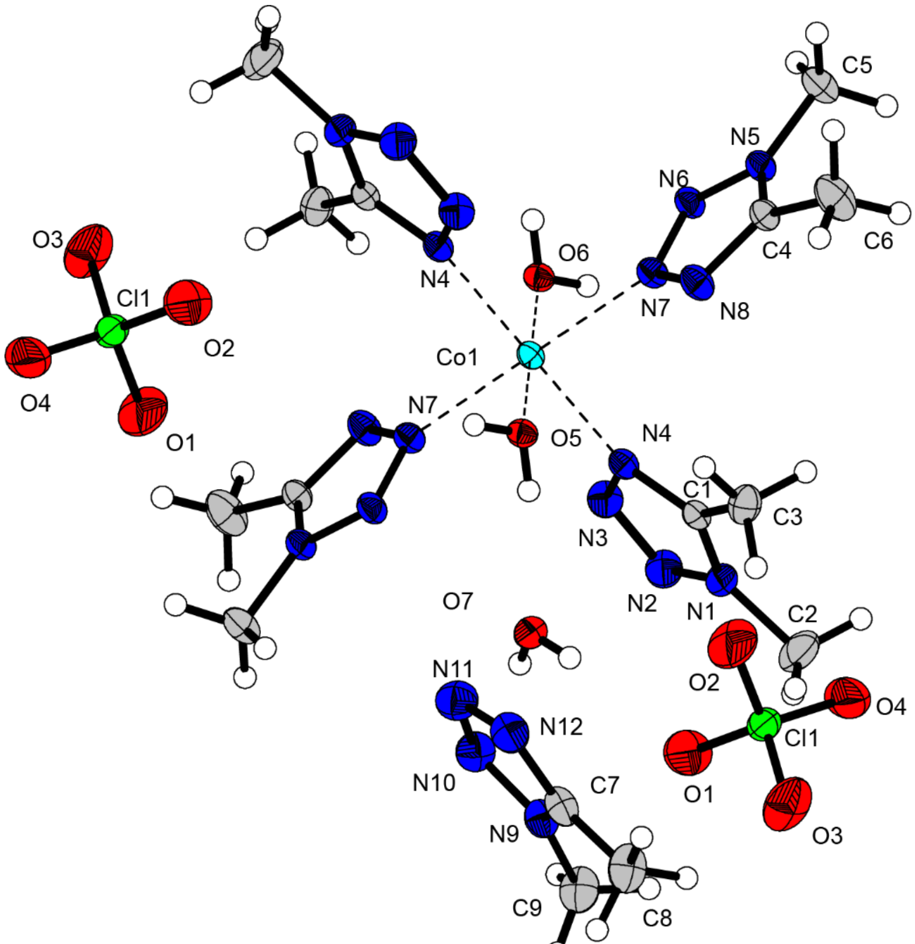

6

Fig. 5. Crystal structures of ECC **6** representing the coordination of the cobalt cation by four molecules of 1,5-DMT and two aqua ligands. Selected bond lengths [Å]: Co1–N4 2.139(2), Co1–N7 2.176(2).

Like in compound **6**, the nickel cation of **7** is coordinated by two pairs of opposite standing DMT ligands and coordinates via N3 and N4 of the tetrazole rings, resulting in small differences in the M–L bond lengths. Compound **8** (Fig. 6, top) crystallizes in the orthorhombic space group *Pbca* and has a calculated density of 1.67 g cm^{-3}.

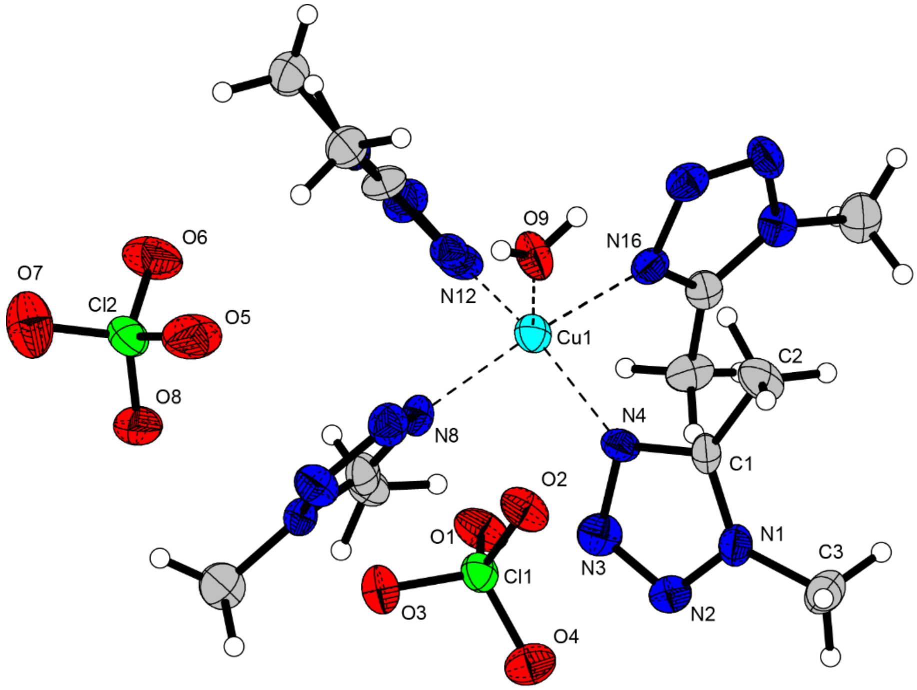

8

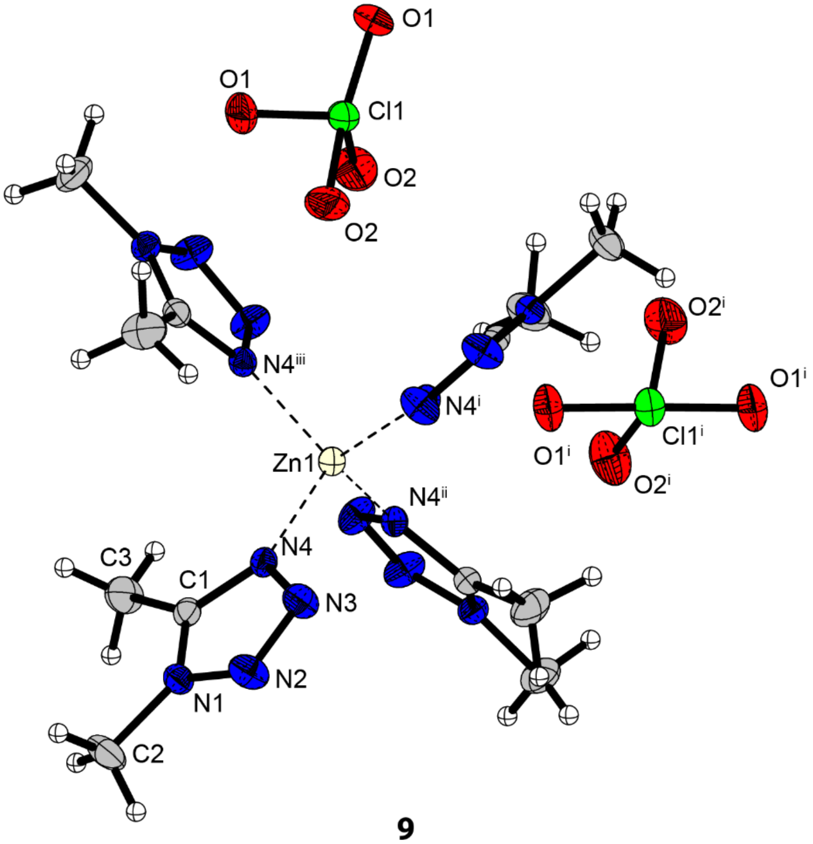

9

Fig. 6. Crystal structures of ECCs **8** and **9**, showing the coordination of the metal cation centers by 1,5-DMT. Selected bond lengths [Å]: Cu1–N4 1.995(7), Cu1–N8 2.016(7), Cu1–N12 1.991(6), Cu1–N16 2.010(7), Zn1–N4 1.990(2).

The copper (II) cation is coordinated and distorted pentagonal by four 1,5-DMT ligands and one aqua ligand. All four M–N bond lengths are equal within the error interval, with a value of around 2.00 Å. The M–O bond length of 2.144 Å can be explained by the degradation of the z^2- over the x^2–y^2-orbital for a d^9-metal in a square-pyramidal ligand field. This structure perfectly aligns with a previously suggested square-pyramidal coordination of Cu (II) cations in an aqueous solution [34] rather than the more classical *Jahn-Teller* distorted octahedral sixfold coordination. Compound **9** (Fig. 6, bottom) crystallizes in the tetragonal space group $P4_12_12$ with a density of 1.63 g cm^{-3}. The zinc (II) cation is coordinated by four molecules of **3**, forming a nearly perfect tetrahedron with M–L bond lengths of 1.990 Å for all four ligands. Throughout the series of first-row transition metals (**4**–**9**), a decrease in the metal-ligand bond length from 2.30(2) Å to 1.99(2) Å was observed, thus causing a strong contraction of the polyhedron and disfavoring the octahedral coordination of Cu (II) and Zn (II) cations by **3**. Additionally, the decreasing metal-ligand bond length indicates a decreasing radius of the corresponding metal cation. Fig. 7 shows the cation radii for first-row transition metals starting from manganese according to *Shannon & Prewitt*[31, 35]. As shown in this figure, the radii of the cations, which have a coordination number (CN) of six, decrease from Mn (II) to Ni (II) and then increase (blue dotted line) for Cu (II) and Zn (II). However, this phenomenon was not observed in this study. Owing to the change in the coordination number for Cu (II) (CN = 5) and Zn (II) (CN = 4), the effective ion radii do not follow this trend. As concluded by *Shannon & Prewitt*, Cu (II) and Zn (II) cations exhibit a decreasing effective ion radius with a decrease in the coordination number. Therefore, the change in coordination, due to a decreased metal-ligand bond length, leads to a steady decrease in cation radii throughout the whole series of **4**–**9**.

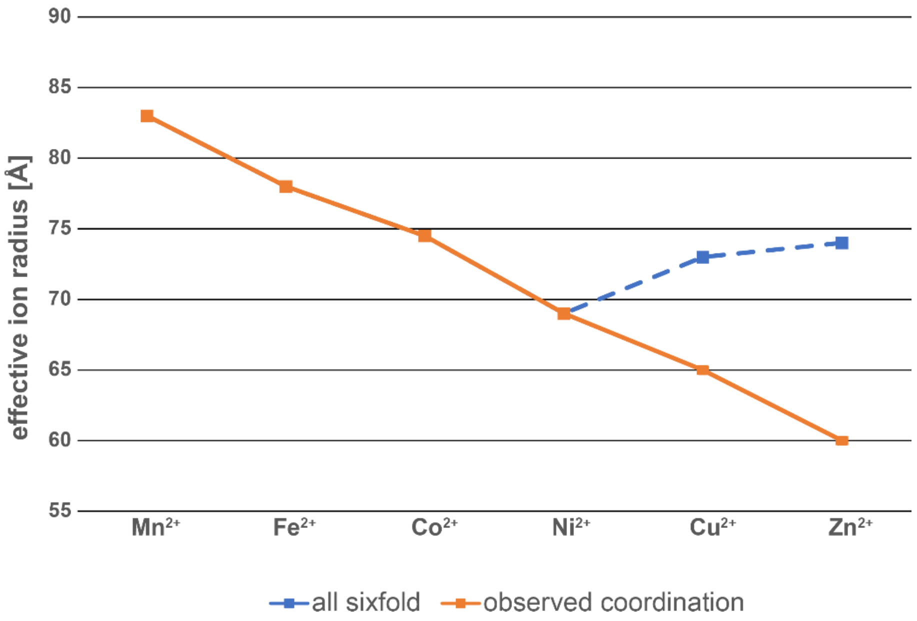

Fig. 7. Effective ion radii of first row transition metals from Mn (II) to Zn (II). The dotted blue line shows the effective ion radii for all sixfold coordination of the metal cations. The orange line shows the effective ion radii while considering their coordination numbers.

Compound **10** (Fig. 8) crystallizes in the monoclinic space group $P2_1/n$ with eight formula units per cell and a calculated density of 1.67 g cm^{-3}. Like in comparable ECCs[9], the picrate anions coordinate. Therefore, the copper (II) cation in compound **10** is sixfold coordinated by two picrate anions and two molecules of **3,** forming a highly distorted square bipyramid. Ultimately, the deprotonated hydroxy groups and the 1,5-DMT ligands are positioned in the equatorial plane with bond lengths between 1.935(3) Å (Cu1–O1) and 1.995(3) Å (Cu1–N8). Additionally, the oxygen atoms of the two coordinating nitro groups are in axial position with bonds Cu1–O9 and Cu1–O8 with lengths of 2.372(3) Å 2.420(3), respectively. While the angles within the equatorial plane differ only marginally (0.781°) from a perfect 90°, the axial positions are bent by 17.015° from the perfect 180° due to the rigidity of the anions. Compound **11a** (Fig. 9) crystallizes in the triclinic space group $P{-}1$ with one formula unit per unit cell and a density of 1.65 g·cm^{-3}. Like in **10**, the copper (II) cation in compound **11a** is also sixfold coordinated. The deprotonated hydroxy groups and the nitrogen atoms of the 1,5-DMT ligands are positioned in an equatorial plane, and the oxygen atoms of the coordinating nitro groups are axially positioned. Like those in **10**, the bond lengths and angles of compound **11a** range between 1.941 Å (Cu1–O9) and 2.014 Å (Cu1–N4) within the equatorial plane and 2.286 Å (Cu1-O13) and 2.301 Å (Cu1–O3) at axial positions. Additionally, the axial positions are strongly bent by 17.5° from the perfect 180° also due to the high rigidity of the anions. Compound **12a** (Fig. 10) crystallizes in the monoclinic space group

$P2_1/c$ with four formula units per cell and a calculated density of 1.77 g cm^{-3}, the highest among all investigated compounds. Like in **10** and **11a**, the copper (II) cation in **12a** is sixfold coordinated by two molecules of **3**, two aqua ligands, and one deprotonated trinitro phloroglucinolate anion. Owing to the rigidity of the anion occupying two coordination sites, a strongly distorted square bipyramid is formed. Meanwhile, an equatorial plane is formed by the deprotonated hydroxy group, the two 1,5-DMT ligands, and one aqua ligand with bond lengths between 1.983(1) Å (Cu1–O3) and 2.025(1) Å (Cu1–O1). Unlike to **10** and **11a**, the bond lengths of the axially positioned atoms of **12a** are 2.210(1) Å (Cu1–O2) and 2.433(1) Å (Cu1–O7), ultimately distorting the bipyramid in its axial expansion. Interestingly, **12a** is the only nitroaromatic compound in which the 1,5-DMT ligands are in a *trans* position towards each other, while they are in a cis position in **10** and **11a**. Additionally, the axis O1–Cu1–O7 in **12a** is strongly bent to an angle of 168.65°, which is comparable to that of axes in **10** and **11a**. Compound **12b** (Fig. 11) crystallizes in the monoclinic space group $P2_1/n$ with four formula units per cell and a calculated density of 1.72 g cm^{-3}. The copper (II) cation in **12b** is sixfold coordinated by two 1,5-DMT molecules and two deprotonated trinitro phloroglucinolate anions, which bridge two copper centers. While compound **12b** is free of water, the ligands form a distorted square bipyramid like in **12a**. Like all other nitroaromatic compounds (**10**, **11a**, and **12a**), the equatorial plane of **12b** is formed by the deprotonated hydroxy groups together with the 1,5-DMT ligands, with bond lengths between 1.922(2) Å (Cu1–O1) and 2.007(2) Å (Cu1–N4) and minor angle deviations (<2.5°) from the ideal 90°. The axial positions of **12b** are also coordinated by the nitro groups of the anions, with different bond lengths (2.249 Å (Cu1–O4) and 2.407(3) Å (Cu1–O9B)) and an angle deviation of 18.5° from the perfect 180° - the highest distortion of the ideal axis observed in this study.

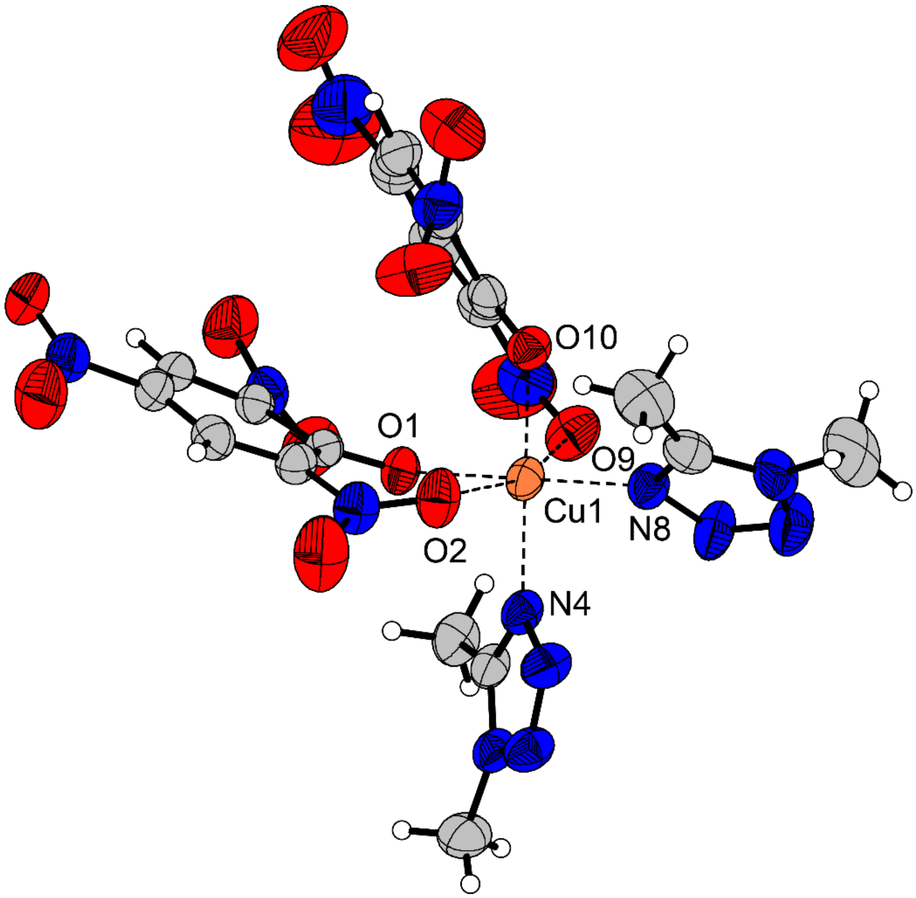

Fig. 8. Crystal structure of [Cu(PA)$_2$(DMT)$_2$] (**10**), showing two coordination picrate anions and two 1,5-DMT ligands.

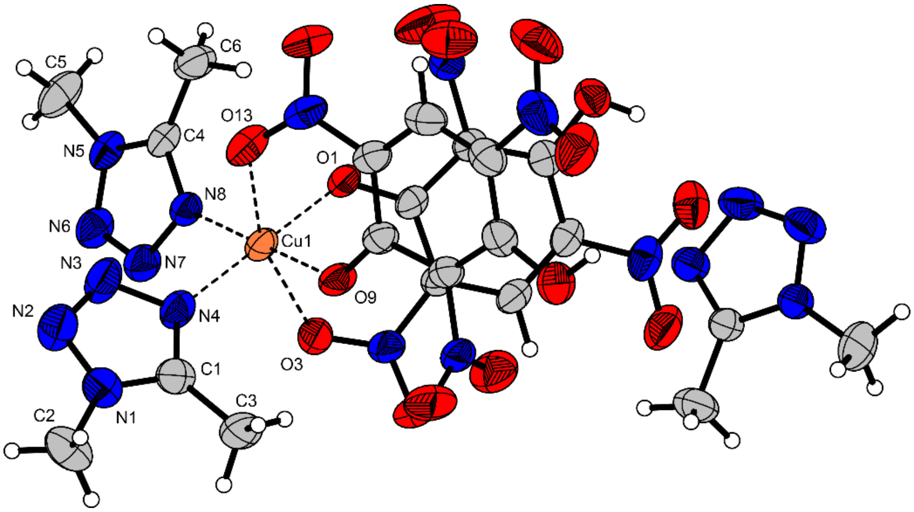

Fig. 9. Crystal structure of [Cu(HTNR)$_2$(DMT)$_2$] • DMT(**11a**), showing two coordination picrate styphnate and two 1,5-DMT ligands with one co-crystallized 1,5-DMT molecule.

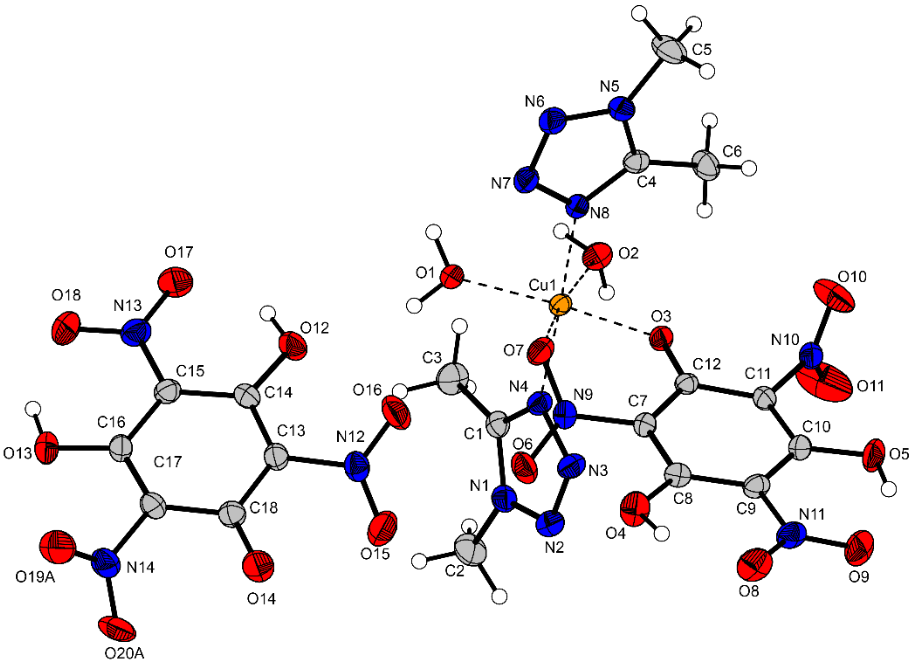

Fig. 10. Crystal structure of [Cu(H_2TNPG)(DMT)$_2$(H_2O)$_2$](H_2TNPG) (**12a**), showing one coordinating trinitro-phloroglucinolate anion, two 1,5-DMT, and two aqua ligands coordinating the copper(II) cation.

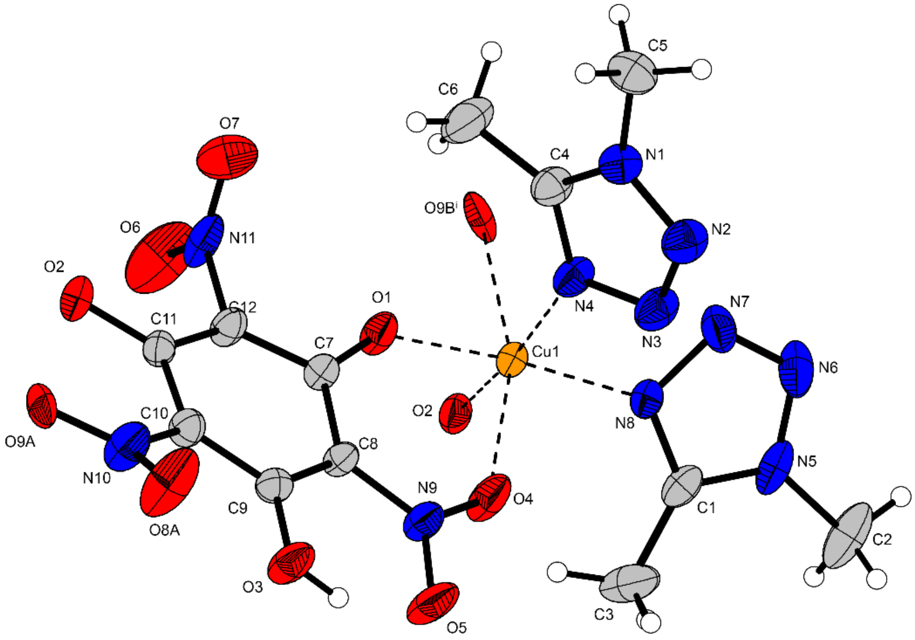

Fig. 11. Crystal structure of [Cu(HTNPG)$_2$(DMT)$_2$] (**12b**), showing two coordination trinitro-phloroglucinolate anions and two 1,5-DMT ligands. The anions bridge two copper (II) centers.

8.2.3 Infrared Spectroscopy

The infrared spectra of compounds obtained as single crystals are depicted in Fig. 12 (**3**), Fig 13 (**4**, **8**, and **9**), and S7 (**10**, **11b**, and **12b**). The spectra of the obtained ECCs pure samples were recorded according to the initially conducted elemental analysis. The IR spectra of batches produced later were compared to those of the pure batch. They were used without further purification if consensus was above 98 %. The spectrum of pure compound **3** shows asymmetric stretching vibration of the methyl groups at 2960 cm^{-1}. The broad range of 3500–3000 cm^{-1} was derived from small amounts of residual water. Additionally, strong bands at 1097, 728 cm^{-1} and 657 cm^{-1} can be attributed to the deformation vibrations of the tetrazole ring.

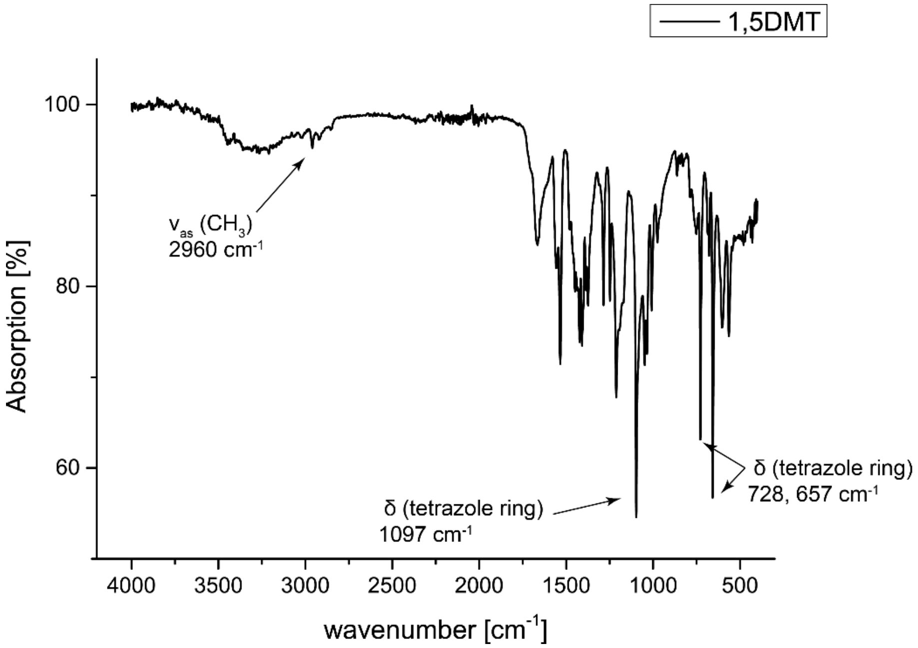

Fig. 12. IR spectrum of pure 1,5-dimethyltetrazole (**3**).

Fig. 13 depicts the IR spectra of the obtained perchlorate containing ECCs **4**, **8,** and **9**. Compound **4** shows a weak band at 2968 cm^{-1}, attributing to the asymmetric stretching vibration of the methyl groups that are slightly shifted due to coordination compared to pure **3**. The deformation vibrations of the tetrazole rings are represented by the IR bands at 729 cm^{-1} and 663 cm^{-1}. The characteristic bands of the perchlorate anions are observed at 1079 cm^{-1} and 622 cm^{-1}, which greatly agrees with the published values of non-coordinating perchlorate anions (1100 cm^{-1} and 600–700 cm^{-1}) [36]. These bands are slightly split, indicating weak hydrogen bonds between the anions and the 1,5-DMT ligands. Compounds **8** and **9** have no characteristic bands of methyl groups due to a very weak IR activity, as was already observed in pure compound **3**. Both compounds exhibit strong bands for the deformation vibrations of the tetrazole rings and the perchlorate anions, with the same range as **4**. Additionally, ECC **8** shows a broadened band with a maximum of 3421 cm^{-1}, corresponding to the vibration of the aqua ligand. Owing to the substantial overlap of bands between the ligands and the nitroaromatic anions (Fig. S7) in the fingerprint regions below

1500 cm^{-1} for compounds **10**, **11b,** and **12b**, the assignment of characteristic vibrations is quite elaborate and is not necessary for this study.

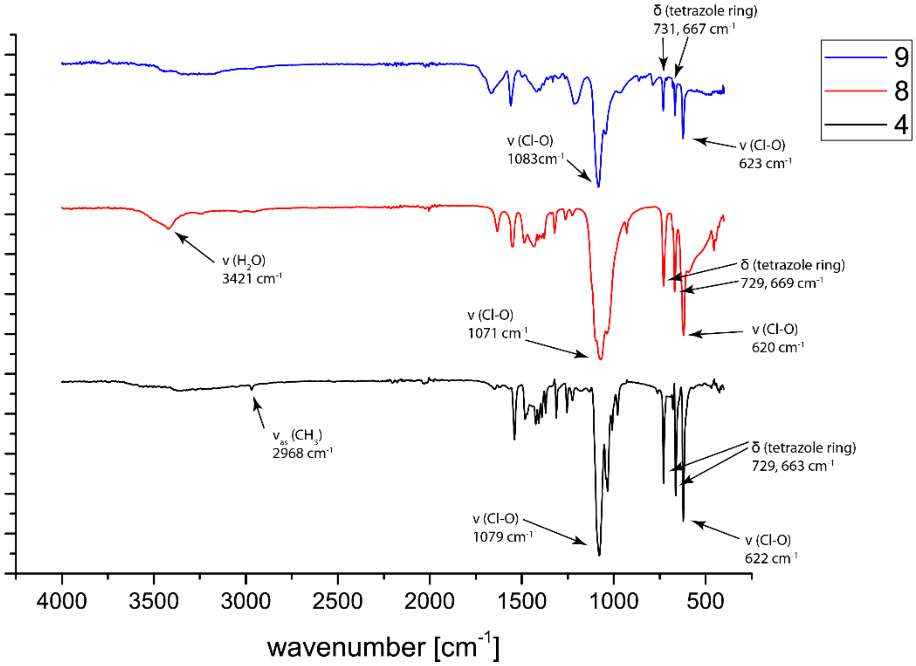

Fig. 13. IR spectra of ECCs **4**, **8,** and **9**.

8.2.4 Thermal Behavior and Sensitivities

The physiochemical properties of **3** and the complexes obtained as bulk materials are summarized in Table 1. The reported melting point of **3** at 73 °C[37] was confirmed through DTA measurements. A second endothermic event occurred at 298 °C, which was identified as the boiling point of **3** (Fig. 14). The conducted TGA measurement showed a mass loss of 96.8 % between 100–214 °C, which is related to the slow evaporation of **3** already starting at 100 °C, suggesting high vapor pressure of **3** when melting. An exothermic decomposition was not observed in **3**. Therefore, the thermal stability of 1,5-DMT is presumably above 293 °C.

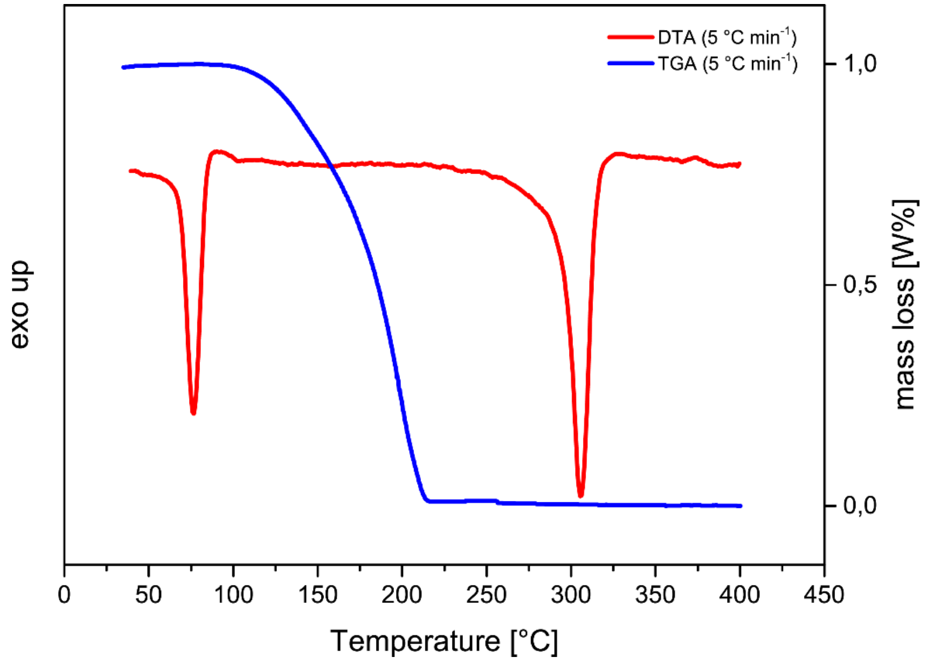

Fig. 14. DTA (red) and TGA (blue) analyses of 1,5-DMT (**3**) at a heating rate of 5 °C min^{-1}.

The thermal behavior of ECCs **4**, **8**, **9**, **10**, **11b**, and **12b** were investigated through DTA measurements at a heating rate of β=5 °C min^{-1} (Fig. 15). As shown by DTA and TGA measurements, an endothermic event was observed in compound **4** at 171 °C as a loss of ligands (weight loss: 38.8 wt%; Fig. 15), while an endothermic event was observed in **8** at 106 °C, corresponding to a loss of aqua ligands (weight loss: 2.68 wt%). Moreover, compound **9** showed an endothermic event at 292 °C, shortly followed by an exothermic event starting at 321 °C, exhibiting the highest stability observed in this study. The conducted TGA measurement (Fig. 15) did not show weight loss until 293 °C. Therefore, the endothermic peak of the DTA measurement corresponded to the decomposition temperature of **9**, which is extraordinarily high for ECCs.[38-41] As the same behavior of an endothermic event immediately evolved into an exothermic event during the DTA measurements of **10** and **11b**, no further TGA measurement was conducted for these two compounds. Additionally, since no thermal event was observed prior to the exothermic decomposition of compound **12b**, no TGA analysis was conducted. Generally, compound **10** showed a very high thermal stability of 250 °C, while **11b** and **12b** showed drastically lower yet adequate thermal stabilities of 184 °C (**11b**) and 192 °C (**12b**). Although the direct influence of anions on thermal stability cannot be deduced, the perchlorate containing ECCs (**4**, **8**, and **9**) exhibited their exothermic decomposition reaction at higher temperatures than those containing nitroaromatic anions. Indeed, it must be kept in mind that compounds **4** and **8** exhibited endothermic decompositions due to the loss of ligands before any exothermic event happened. Furthermore, the measured thermal stabilities of nitroaromatic ECCs **10**–**12b** do not allow the deduction of the direct influence of nitroaromatic anions compared to each other. Nonetheless, they agree well with previously reported ECCs[9], which also have no direct influence of anions on thermal stabilities. According to BAM standards, the sensitivities of the compounds to impact and friction have been determined and classified according to the UN recommendations on the transport of dangerous goods[42]. Accordingly, it was determined that **3** was completely insensitive to mechanical stimuli (> 40 J, > 360 N), ECCs **4**, **10**, **11b**, and **12b** were not sensitive to friction, while **5** and **6** were slightly sensitive to friction, with friction sensitivity (FS) of 128 N and 180 N, respectively. All compounds were sensitive to impact, with **4** (10 J) and **10** (8 J) showing lower impact sensitivities than **8** (3 J), **9** (3 J), **11b** (2 J), and **12b** (2 J). Therefore, ECCs **8**, **9**, **11b**, and **12b** exhibited impact sensitivities in the range of a primary explosive, whereas **4** and **10** exhibited sensitivities as typical secondary explosives, such as hexogen.[24] Although the direct influence of anions on thermal stability could not be previously deduced, their influence can be determined by comparing sensitivities. Even though the differences in sensitivities between nitroaromatic compounds are not as prominent as those between other ligand systems[8, 33], compound **10**, which incorporated the picrate anions, exhibited the lowest sensitivities, followed by compounds **11b** and **12b**. Generally, the increasing number of hydroxy functionalities from picrate to trinitrophloroglucinate also increases the sensitivities to impact and friction. Furthermore, the sensitivities of the perchlorate-containing ECCs (**4**, **8**, and **9**) are higher than those of the nitroaromatic compounds, yet they are still moderately sensitive at least to friction. Owing to their poor crystallizability, enough compounds **5**, **6,** and **7** could not be obtained. Therefore, their thermal and energetic behavior was not explored. To further investigate the energetic properties, hot plate (HP) and hot needle (HN) tests of compounds **4** and **9** were performed (Fig. 16). HP tests were conducted to determine the performance of the samples under fast heating on a copper plate, during which both compounds showed deflagration without detonation. While HP tests do not necessarily allow any conclusions on the compound’s capability as a primary explosive, the HN tests can be used to correlate deflagration with the detonation transition (DDT) capability of a compound. Therefore, HN tests were performed by fixing the sample underneath adhesive tape on a copper plate, followed by penetration with a red heated needle. A compound possesses rapid DDT if detonation occurs, which was not the case for the tested compounds.

Table 1. Sensitivities and thermal behavior of compounds **4**, **8**, **9**, and **10**–**12**.

Compound	IS [a] /J	FS [b] /N	$T_{\text{endo.}}$ [c] /°C	$T_{\text{exo.}}$ [d] /°C
3	>40	>360	73	>293
4	10	> 360	171	307
8	3	128	106	226
9	2	180	293	321
10	8	>360	–	250
11b	2	>360	–	184
12b	2	360	–	192

[a] Impact sensitivity according to the BAM drop hammer [43] (method 1 of 6). [b] Friction sensitivity according to the BAM friction tester [43] (method 1 of 6). [c] Temperature of endothermic events (onset temperatures at a heating rate of 5 °C·min^{-1}) [d] Temperature of decomposition indicated by exothermic event according to DTA (onset temperatures at a heating rate of 5 °C·min^{-1}).

Interestingly, there is a reported energetic coordination compound based on copper (II) perchlorate with 1-ethyltetrazole (1-ETZ) as ligand [4]. Given that 1,5-DMT and 1-ETZ are structural isomers and have the same empirical formula of $C_3H_6N_4$, it seems reasonable to compare both compounds as ligands. This, unfortunately, was impossible in this study since no isomeric complexes were obtained. All reported coordination compounds with 1-ETZ as ligand exhibit octahedral coordination of the copper (II) cation, whereas the obtained copper(II) complex displayed different coordination in this study. This results from higher steric demand of **3** compared to 1-ETZ. Specifically, the ethyl functionalization can easily minimize steric repulsion by rotation of the C-C bond for **3**, which is impossible for 1,5-DMT. Besides their coordinative behavior, the major difference between both compounds is their thermal behavior. 1-ETZ is a liquid at room temperature with thermal stability of up to 208 °C. Therefore, it is by far inferior to **3** in terms of thermal stability. This is also accompanied by a slight decrease in enthalpy of formation of **3** (184.1 kJ mol^{-1}) compared to 1-ETZ (224.1 kJ mol^{-1}). Thereby, higher stability of the resulting ECCs can be assumed.

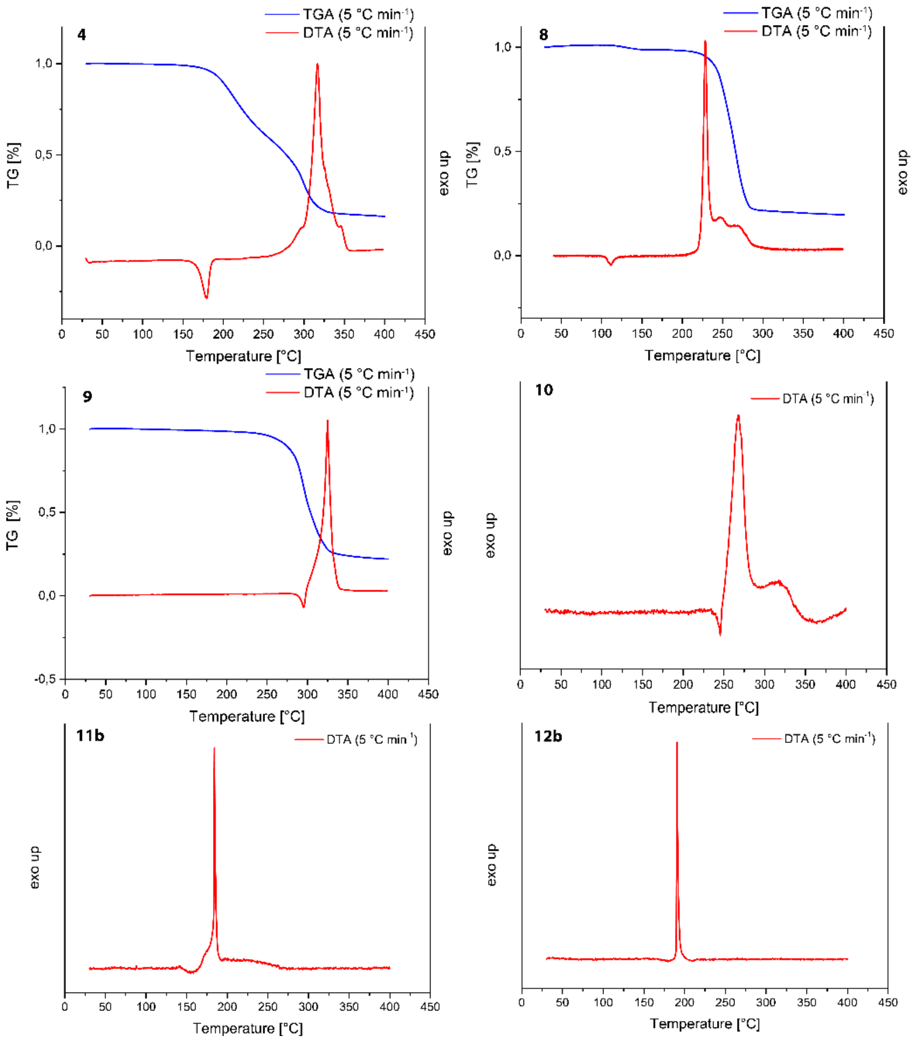

Fig. 15. Combined DTA and TGA measurements of ECCs **4**, **8,** and **9** and DTA of ECCs **10**, **11b,** and **12b** at a heating rate of 5 °C min^{-1}.

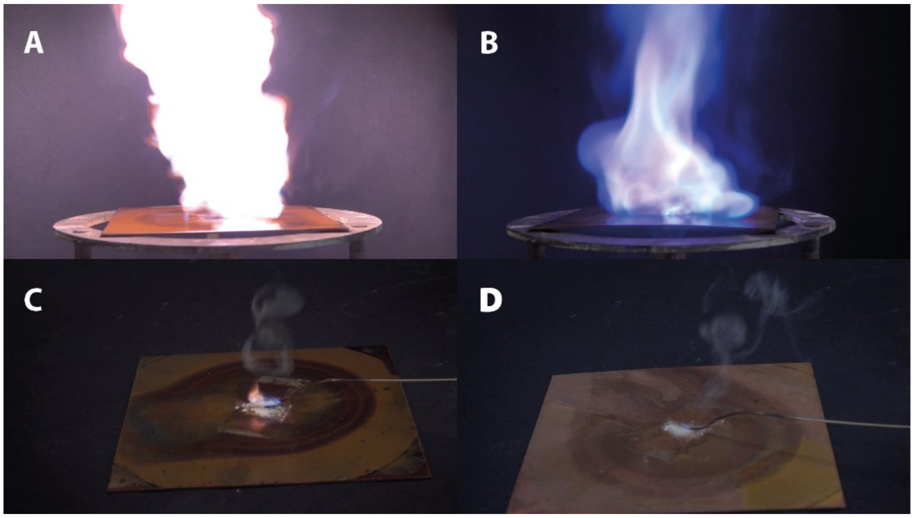

Fig. 16. HP and HN tests of compounds **4** and **9**. **a**: HP test of **4**; **b**: HP test of **9**; **c**: HN test of **1**; **d**: HN test of **6**.

8.3 Conclusion

1,5-DMT (**3**) was synthesized using a three-step procedure starting with acetone and hydroxylamine. This route was observed to be more economical than the one-step synthesis using TMS-N_3. 1,5-DMT (**3**) was fully characterized as a completely insensitive (> 360 N, > 40 J) and highly thermally stable (> 293 °C) compound with an astonishing high positive HOF of 184.1 kJ mol^{-1}. Therefore, **3** was applied as a nitrogen-rich (N = 57.1%) ligand to 11 new energetic coordination compounds of the 3d^5–3d^{10} metal (e.g., Mn, Fe, Co, Ni, Cu, Zn) perchlorate salts. The change from a sixfold (**4**, **5**) to a fourfold (**9**) coordination of the central metal cation was observed. This change was caused by a decreasing metal-ligand bond length throughout the first-row transition metals, which decreased the coordination number and ultimately led to steadily decreasing cation radii. The additional increase in steric repulsion of the ligands favors the decrease in the coordination number, supporting the change in coordination. All measured ECCs exhibited exothermic decomposition events above 184 °C (**11b**). For compound **9,** an extraordinarily high decomposition temperature of 293 °C was measured, representing the highest thermal stability investigated in this study. Hot plate tests of the most promising compounds showed a complete decomposition without detonation, while the hot needle tests indicated that none of the compounds can be classified as applicable primary explosives since no rapid DDT was observed. However, the compounds are ideal candidates for burning rate catalysts in propellant charges due to their simple and cheap syntheses and great stability.

8.4 Experimental Section

Acetone Oxime (1): Sodium carbonate (28.6 g, 0.27 mol) was added to a solution of hydroxyl ammonium chloride (15.6 g, 0.23 mol) and acetone (8.7 g, 0.15 mol) in water (300 mL). The mixture was stirred for 40 h at room temperature, and the residue was extracted with diethyl ether (4×100 mL). After washing with a saturated sodium chloride solution and drying over sodium sulfate, the solvent was removed under reduced pressure, and acetone oxime (7.7 g, 0.11 mol, 70%) was obtained as a colorless solid.

^{1}H NMR (400 MHz, $CDCl_3$): δ = 1.89 (3 H, CH_3), 1.90 (3 H, CH_3), 7.77 ppm (1 H, O*H*); **^{13}C NMR** (101 MHz, $CDCl_3$): δ = 14.8, 21.9, 155.9 ppm.

Acetoxime Benzenesulfonate (2): Acetone oxime (6 g, 0.08 mol) was dissolved in pyridine (6.5 mL, 0.08 mol), and water (16 mL) and benzene sulfonyl chloride (10.2 mL, 0.08 mol) was added dropwise with the temperature kept at 15–20 °C. A colorless solid precipitated, and the suspension was cooled to 10 °C. After filtration and washing with cold water, the solid was dried, yielding acetoxime benzenesulfonate in quantitative amounts.

^{1}H NMR (400 MHz, $CDCl_3$): δ = 1.93 (3 H, $C\mathit{H}_3$), 1.98 (3 H, CH_3), 7.54 (2 H, C*H*(3, 5)), 7.65 (1 H, C*H*(4)), 7.97 ppm (2 H, CH(2, 6)); **^{13}C NMR** (101 MHz, $CDCl_3$): δ = 17.1 ($\mathit{C}H_3$), 21.8 ($\mathit{C}H_3$), 128.9 (2 *C*H), 129.0 (2 *C*H), 133.9 (*C*H), 165.2 ppm ($H_3C\mathit{C}(N)CH_3$).

1,5-Dimethyltetrazole (3): Sodium azide (4.6 g, 0.07 mol) was dissolved in water (15 mL) and was added to a solution of acetoxime benzenesulfonate (15 g, 0.07 mol) in methanol (60 mL). The mixture was stirred for 1 h at 45 °C and later for 1.5 h at 60 °C. The solvent was removed under reduced pressure and the residue was extracted with hot benzene (4x30 mL). After evaporation of the solvent, 1,5-dimethyltetrazole (3.3 g, 0.033 mol, 48%) was obtained as a colorless solid. Recrystallization from water yields **3** as colorless block-shaped crystals.

DTA (5 °C min^{-1}) onset: 73 °C (T_{endo}), 298 °C (T_{endo}); **^{1}H NMR** (400 MHz, DMSO-d_6): δ = 2.49 (3 H, $C\mathit{H}_3$), 3.96 ppm (3 H, $C\mathit{H}_3$); **^{13}C NMR** (101 MHz, DMSO-d_6): δ = 8.1 ($CC\mathit{H}_3$), 33.2 ($NC\mathit{H}_3$), 152.4 ppm ($N_4\mathit{C}$); **IR** (ATR, $\tilde{\nu}$/cm^{-1}): 2961 (w), 1655 (w), 1533 (s), 1481 (m), 1451 (m), 1436 (m), 1423 (m), 1409 (m), 1386 (m), 1380 (m), 1374 (m), 1285 (m), 1248 (m), 1212 (m), 1097 (s), 1048 (m), 1034 (m), 1008 (m), 976 (w), 728 (s), 678 (w), 657 (vs), 605 (w), 565 (w).

Alternatively, acetone (1 g, 17 mmol, 1 eq.) was mixed with trimethylsilyl azide (5.87 g, 51 mmol, 3 eq.) and tin(II) chloride (0.322 g, 1.7 mmol, 0.1 eq.) and were stirred at 55 °C for 20 h. Extraction with benzene followed by evaporation yielded 1,5-dimethyltetrazole (0.66 g, 7.14 mmol, 42%) as a white solid.

^{1}H NMR (400 MHz, DMSO-d_6): δ = 2.49 (3 H, CH_3), 3.96 ppm (3 H, CH_3); **^{13}C NMR** (101 MHz, DMSO-d_6): δ = 8.1 (CCH_3), 33.3 (NCH_3), 152.4 ppm (N_4C).

General procedure for the preparation of complexes 4–9:

Stoichiometric amounts of the corresponding metal(II) perchlorate and **3** were individually dissolved in water, combined, and stirred for a short period at elevated temperatures. The product was obtained after crystallization at ambient conditions.

[Mn(DMT)$_6$](ClO$_4$)$_2$ (4): Compound **4** was isolated as a colorless crystalline precipitate.

DTA (5 °C min^{-1}) onset: 171 °C (T_{endo}), 307 °C (T_{exo}); **IR** (ATR, $\tilde{\nu}$ /cm^{-1}): 3346 (vw), 1540 (m), 1481 (w), 1408 (w), 1390 (m), 1370 (m), 1311 (w), 1254 (w), 1224 (w), 1079 (s), 1033 (s), 1009 (m), 979 (w), 729 (m), 678 (s), 663 (s), 622 (s); **Elemental Analysis** calcd. [%] for $C_{18}H_{36}Cl_2MnN_{24}O_8$ (842.48): C 25.66, H 4.31, N 39.90; found: C 25.31, H 4.09, N 38.93; **BAM drop hammer:** 10 J; **BAM friction tester**: >360 N.

[Fe(DMT)$_6$](ClO$_4$)$_2$ (5): Compound **5** was obtained as a brown glass-like solid. Crystals suitable for X-ray determination were obtained by subjecting a small amount to a high vacuum for several days.

[Co(H$_2$O)$_2$(DMT)$_4$](DMT)(H$_2$O)(ClO$_4$)$_2$ (6): Out of the oily red product, crystals suitable for X-ray determination of complex **6** were obtained. Owing to its consistency, only X-ray determination was possible.

[Ni(DMT)$_4$(H$_2$O)$_2$](DMT)$_2$(H$_2$O)$_2$(ClO$_4$)$_2$ (7):

Inhomogeneous solids were formed after evaporation of the solvent. From these inhomogeneous solids, small crystals of **7** suitable for X-ray determination were picked using a light microscope.

[Cu(H$_2$O)(DMT)$_4$](ClO$_4$)$_2$ (8): Complex **8** crystallized as deep blue needles suitable for X-ray determination.

DTA (5 °C min^{-1}) onset: 106 °C (loss of water), 226 °C (T_{exo}); **IR** (ATR, $\tilde{\nu}$/cm^{-1}): 3425 (w), 1554 (w), 1434 (w), 1070 (s), 727 (m), 668 (m), 619 (s); **Elemental Analysis** calcd. [%] for $C_{12}H_{26}Cl_2CuN_{16}O_{10}$ (672.89): C 21.42, H 3.69, N 33.31; found: C 21.50, H 3.74, N 33.32; **BAM drop hammer**: 3 J; **BAM friction tester**: 128 N.

[Zn(DMT)$_4$](ClO$_4$)$_2$ (9): Complex **9** was obtained as colorless crystals suitable for X-ray determination.

DTA (5 °C min^{-1}) onset: 293 °C (T_{endo}), 321 °C (T_{exo}); **IR** (ATR, $\tilde{\nu}$/cm^{-1}): 1561 (w), 1500 (w), 1331 (w), 1265 (w), 1084 (s), 1042 (m), 731 (m), 678 (w), 666 (m), 623 (s); **Elemental Analysis** calcd. [%] for $C_{12}H_{24}Cl_2ZnN_{16}O_8$ (656.71): C 21.95, H 3.68, N 34.13; found: C 21.84, H 3.46, N 33.88; **BAM drop hammer**: 2 J; **BAM friction tester**: 180 N.

[Cu(PA)$_2$(DMT)$_2$] (10): Basic copper(II) carbonate (50 mg, 226 mmol) was suspended in water (10 mL), and picric acid (104 mg, 452 mmol) was added. The mixture was stirred until all solids were dissolved and **3** (44 mg, 452 mmol) was added. After stirring for 5 min at 80 °C, the solution was left to crystallize. Compound **10** was obtained as green needles with a high yield (268 mg, 375 mmol, 83%).

DTA (5 °C min^{-1}) onset: 250 °C ($T_{\text{exo.}}$); **IR** (ATR, $\tilde{\nu}$/cm^{-1}): 3087 (w), 1741 (w), 1616 (s), 1612 (s), 1576 (s), 1533 (s), 1507 (s), 1480 (s), 1418 (s), 1361 (s), 1326 (vs), 1269 (vs), 1168 (s), 1110 (m), 1083 (m), 1047 (m), 941 (m), 916 (s), 846 (w), 824 (w), 785 (m), 743 (m), 728 (m), 704 (vs), 679 (m), 666 (s), 551 (m), 517 (m), 455 (w), 428 (w), 416 (w); **Elemental Analysis** calcd. [%] for $C_{18}H_{16}CuN_{14}O_{14}$ (715.96): C 30.20, H 2.25, N 27.39; found: C 30.31, H 2.25, N 27.58; **BAM drop hammer**: 8 J; **BAM friction tester**: >360 N.

[Cu(HTNR)$_2$(DMT)$_2$] (11b): Basic copper(II) carbonate (50 mg, 226 mmol) was suspended in water (10 mL), and trinitro resorcinol (110 mg, 452 mmol) was added. The solution was heated to 80 °C and **3** (44 mg, 452 mmol) was added. After stirring for 5 min at 80 °C, the formed precipitate of **11b** was filtered out with a high yield (267 mg, 357 mmol, 79%). The remaining solution was left to crystallize for several days, from which a few crystals of **11a** were obtained.

DTA (5 °C min^{-1}) onset: 184 °C (T_{exo}); **IR** (ATR, $\tilde{\nu}$/cm^{-1}): 3096 (w), 1628 (s), 1561 (s), 1535 (s), 1528 (s), 1476 (s), 1453 (s), 1377 (s), 1353 (s), 1319 (s), 1284 (vs), 1194 (s), 1175 (s), 1088 (s), 1049 (s), 930 (s), 828 (w), 781 (m), 762 (m), 727 (s), 713 (s), 698 (s), 681 (s), 666 (s), 641 (m), 543 (m), 462 (w), 427 (m), 417 (m); **Elemental Analysis** calcd. [%] for $C_{18}H_{16}CuN_{14}O_{16}$ (747.95): C 28.91, H 2.16, N 26.22; found: C 28.79, H 2.27, N 28.76; **BAM drop hammer**: 2 J; **BAM friction tester**: >360 N.

[Cu(HTNPG)(DMT)$_2$] (12b): Basic copper(II) carbonate (50 mg, 226 mmol) was suspended in water (10 mL), and trinitro phloroglucinol (118 mg, 452 mmol) were added. The solution was heated to 80 °C and **3** (44 mg, 452 mmol) was added. After stirring for 5 min at 80 °C, the solution was left standing to crystallize. After 1–2 d, crystals in the form of needles (**12a**) and blocks (**12b**) started to form. The initially formed **12a** started to be consumed as blocks of **12b** continued to grow. After 3–4 d, crystals of **12b** were the main product of crystallization and then were filtered out and dried. **12b** was obtained as dark blocks with a high yield (197 mg, 379 mmol, 84%).

DTA (5 °C min^{-1}) onset: 192 °C (T_{exo}); **IR** (ATR, $\tilde{\nu}$/cm^{-1}): 1736 (w), 1588 (s), 1538 (s), 1520 (vs), 1486 (s), 1455 (s), 1399 (s), 1345 (s), 1284 (vs), 1255 (vs), 1192 (s), 1175 (s), 1158 (s), 1134 (vs), 1109 (s), 1048 (s), 1027 (m), 929 (s), 837 (m), 825 (m), 806 (m), 792 (s), 708 (vs), 681 (s), 665 (vs), 642 (s), 456 (m), 434 (s), 413 (s), 408 (s); **Elemental Analysis** calcd. [%] for $C_{12}H_{13}CuN_{11}O_9$ (518.85): C 27.78, H 2.53, N 29.70; found: C 27.47, H 2.53, N 28.42; **BAM drop hammer**: 2 J; **BAM friction tester**: 360 N.

8.5 Acknowledgements

This work was funded by the Ludwig-Maximilian University of Munich (LMU), the Office of Naval Research (ONR) under Grant No. ONR.N00014-16-1-2062. The authors would like to thank Stefan Huber for sensitivity measurements.

8.6 References

[1] R. Pritchard, C. A. Kilner, S. A. Barrett, M. A. Halcrow, *Inorg. Chim. Acta* **2009**, *362*, 4365–4371.

[2] R. Mohammed, G. Chastanet, F. Tuna, T. L. Malkin, S. A. Barrett, C. A. Kilner, J. F. Létard, M. A. Halcrow, *Eur. J. Inorg. Chem*. **2013**, *2013*, 819–831.

[3] T. R. Cook, Y. R. Zheng, P. J. Stang, *Chem. Rev*. **2013**, *113*, 734–777.

[4] M. H. H. Wurzenberger, M. S. Gruhne, M. Lommel, N. Szimhardt, T. M. Klapötke, J. Stierstorfer, *Chem. Asian J.* **2019**, *14*, 2018–2028.

[5] H. M. Titi, J. M. Marrett, G. Dayaker, M. Arhangelskis, C. Mottillo, A. J. Morris, G. P. Rachiero, T. Friščić, R. D. Rogers, *Sci. Adv.* **2019**, *5*, eaav9044.

[6] Q. Y. Wang, J. Wang, S. Wang, Z. Y. Wang, M. Cao, C. L. He, J. Q. Yang, S. Q. Zang, T. C. W. Mak, *J. Am. Chem. Soc*. **2020**, *142*, 12010–12014.

[7] C. Wang, Y. J. Wang, C. L. He, Q. Y. Wang, S. Q. Zang, *JACS Au* **2021**, *1*, 2202–2207.

[8] M. H. H. Wurzenberger, M. S. Gruhne, M. Lommel, V. Braun, N. Szimhardt, J. Stierstorfer, *Inorg. Chem*. **2020**, *59;* 17875–17879.

[9] M. H. H. Wurzenberger, B. R. G. Bissinger, M. Lommel, M. S. Gruhne, N. Szimhardt, J. Stierstorfer, *New J. Chem*. **2019**, *43*, 18193–18202.

[10] J. Wilbrand, *Justus Liebigs Annalen der Chemie* **1863**, *128*, 178–179.

[11] T. M. Klapötke, *Chemistry of High-Energy Materials*. 5th ed. Berlin/Boston: DeGruyter, **2019**.

[12] R. L. Simpson, P. A. Urtiew, D. L. Ornellas, G. L. Moody, K. J. Scribner, D. M. Hoffman, *Propellants Explos. Pyrotech*. **1997**, *22*, 249–255.

[13] O. N. Verkhozina, V. N. Kizhnyaev, L. I. Vereshchagin, A. V. Rokhin, A. I. Smirnov, *Russ. J. Org. Chem*. **2003**, *39*, 1792–1796.

[14] D. Kumar, Y. Tang, C. He, G. H. Imler, D. A. Parrish, J. n. M. Shreeve, *Chem. Eur. J.* **2018**, *24*, 17220–17224.

[15] M. L. Gettings, M. T. Thoenen, E. F. C. Byrd, J. J. Sabatini, M. Zeller, D. G. Piercey, *Chem. Eur. J.* **2020**, *26*, 14530–14535.

[16] D. R. Wozniak, M. Zeller, E. C. Byrd, D. G. Piercey, *Z. Anorg. Allg. Chem*. **2022**, *648*, e202100333.

[17] N. Szimhardt, M. H. H. Wurzenberger, L. Zeisel, M. S. Gruhne, M. Lommel, J. Stierstorfer, *J. Mater. Chem. A* **2018**, *6*, 16257–16272.

[18] T. M. Klapötke, M. Kofen, L. Schmidt, J. Stierstorfer, M. H. H. Wurzenberger, *Chem. Asian J.* **2021**, *16*, 3001–3012.

[19] M. H. H. Wurzenberger, S. M. J. Endraß, M. Lommel, T. M. Klapötke, J. Stierstorfer, *ACS Appl. Energy Mater.* **2020**, *3*, 3798–3806.

[20] J. Fronabarger, A. Schuman, R. Chapman, W. Fleming, W. Sanborn, T. Massis. *Chemistry and development of BNCP, a novel DDT explosive (deflagration-to-detonation). 31st Joint Propulsion Conference and Exhibit*, AIAA, July, **1995**.

[21] D. Moderhack, M. Noreiks, *Heterocycles*, **2004**, *63*, 2605–2614.

[22] T. M. Klapötke, D. G. Piercey, J. Stierstorfer, *Eur. J. Inorg. Chem*. **2012**, *2012*, 5694–5700.

[23] P. Sharon, M. Afri, S. Mitlin, L. Gottlieb, B. Schmerling, D. Grinstein, S. Welner, A. A. Frimer, *Polyhedron* **2019**, *157*, 71–89.

[24] T. M. Klapötke, *Energetic Materials Encyclopedia*. 2nd ed. Berlin/Boston: De Gruyter, **2021**.

[25] N. Fischer, D. Fischer, T. M. Klapötke, D. G. Piercey, J. Stierstorfer, *J. Mater. Chem*. **2012**, *22*, 20418–20422.

[26] T. M. Klapötke, J. Stierstorfer, *J. Am. Chem. Soc*. **2009**, *131*, 1122–1134.

[27] H. Langhals, G. Range, E. Wistuba, C. Rüchardt, *Chem. Ber*. **1981**, *114*, 3813–3830.

[28] M. Kamuf, F. Rominger, O. Trapp, *Eur. J. Org. Chem*. **2012**, *2012*, 4733–4739.

[29] KNOLL AG, Deutsches Reich, *Verfahren zur Darstellung von Tetrazolen*, **1926**.

[30] A. A. S. El-Ahl, S. S. Elmorsy, H. Soliman, F. A. Amer, *Tetrahedron Lett*. **1995**, *36*, 7337–7340.

[31] R. Shannon, *Acta Crystallogr. A* **1976**, *32*, 751–767.

[32] V. Braun, M. H. H. Wurzenberger, V. Weippert, J. Stierstorfer, *New J. Chem*. **2021**, *45*, 11042–11050.

[33] M. Kofen, M. Lommel, M. H. H. Wurzenberger, T. M. Klapötke, J. Stierstorfer, *Chem. Eur. J.* **2022**, e202200492.

[34] P. Frank, M. Benfatto, R. K. Szilagyi, P. D'Angelo, S. Della Longa, K. O. Hodgso, *Inorg. Chem*. **2005**, *44*, 1922–1933.

[35] R. D. Shannon, C. T. Prewitt, *Acta Crystallogr. B* **1969**, *25*, 925–946.

[36] D. L. Lewis, E. D. Estes, D. J. Hodgson, *J. Mol. Struct.* **1975**, *5*, 67–74.

[37] A. Xie, Q. Zhang, Y. Liu, L. Feng, X. Hu, W. Dong, *J. Heterocycl. Chem*. **2015**, *52*, 1483–1487.

[38] N. Szimhardt, M. S. Gruhne, M. Lommel, A. Hess, M. H. H. Wurzenberger, T. M. Klapötke, J. Stierstorfer, *Z. Anorg. Allg. Chem*. **2019**, *645*, 354–361.

[39] N. Szimhardt, J. Stierstorfer, *Chem. Eur. J.* **2018**, *24*, 2687–2698.

[40] N. Szimhardt, M. H. H. Wurzenberger, T. M. Klapötke, J. T. Lechner, H. Reichherzer, C. C. Unger, J. Stierstorfer, *J. Mater. Chem. A* **2018**, *6*, 6565–6577.

[41] M. Joas, T. M. Klapötke, N. Szimhardt, *Eur. J. Inorg. Chem*. **2014**, *2014*, 493–498.

[42] UN, in Recommendations on the Transport of Dangerous Goods: Model Regulations 19th ed., New York, **2015**.

[43] BAM, http://www.bam.de, (accessed April **2022**).

8.7 Supporting Information

8.7.1 Overview of Compounds

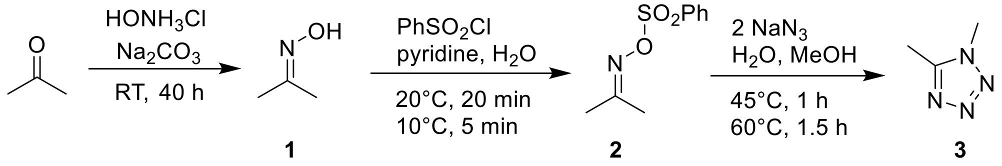

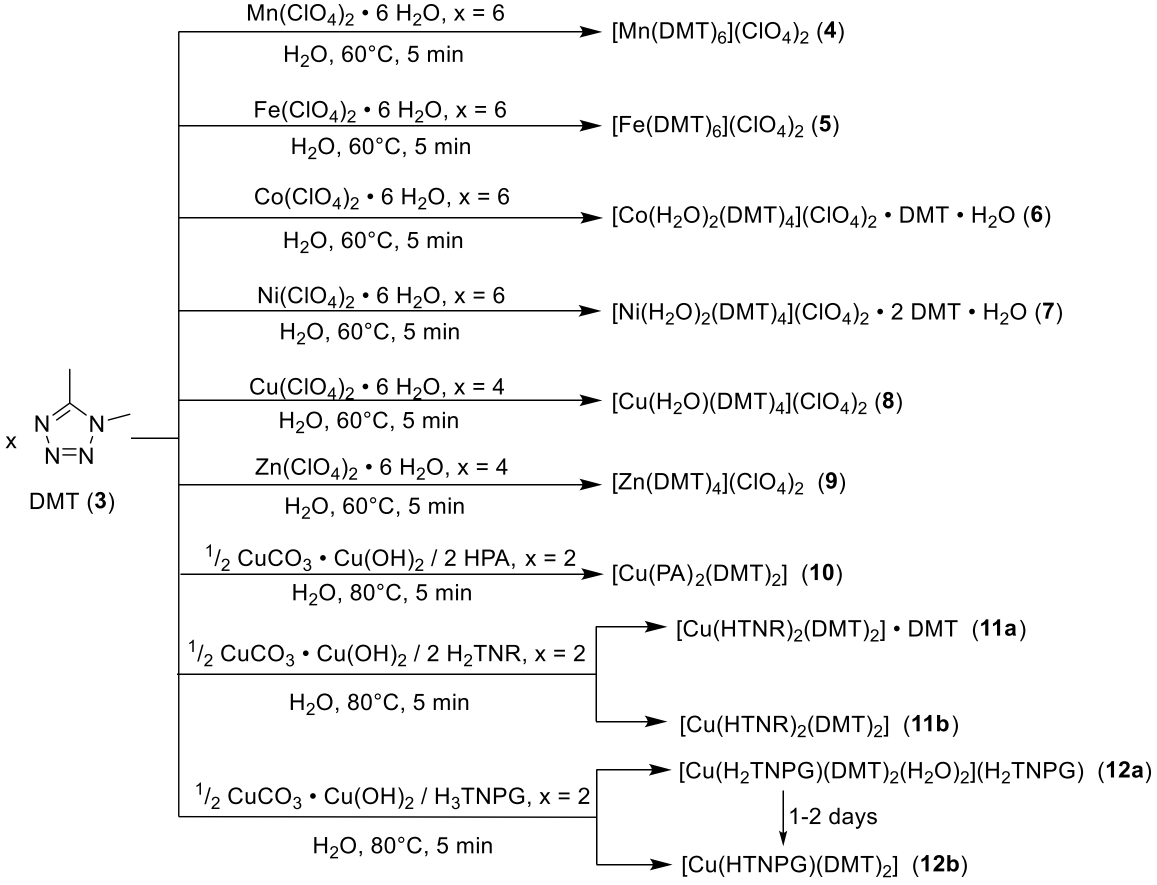

8.7.2 Single Crystal X-Ray Diffraction

For all crystalline compounds, an Oxford Xcalibur3 diffractometer with a CCD area detector or Bruker D8 Venture TXS diffractometer equipped with a multilayer monochromator, a Photon 2 detector, and a rotating-anode generator were employed for data collection using Mo-K_α radiation (λ = 0.7107 Å). On the Oxford device, data collection and reduction were carried out using the CrysAlisPRO software.[S1] On the Bruker diffractometer, the data were collected with the Bruker Instrument Service v3.0.21, the data reduction was performed using the SAINT V8.18C software (Bruker AXS Inc., 2011). The structures were solved by direct methods (SIR-92,[S2] SIR-97,[S3,S4] SHELXS-97[S5,S6] or SHELXT[S7]), refined by full-matrix least-squares on *F*2 (SHELXL[S5,S6]) and finally checked using the PLATON software[S8] integrated in the WinGX[S7,S9] or Olex2[S8] software suite. The non-hydrogen atoms were refined anisotropically and the hydrogen atoms were located and freely refined. The absorptions were corrected by a SCALE3 ABSPACK or SADABS Bruker APEX3 multi-scan method.[S11,S12] All DIAMOND2 plots are shown with thermal ellipsoids at the 50% probability level and hydrogen atoms are shown as small spheres of arbitrary radius.

Table S1. Crystallographic data and structure refinement details for compounds **3**, **4**, and **9.**

	3	**4**	**5**
Formula	$C_3H_6N_4$	$C_{18}H_{36}MnN_{24}Cl_2O_8$	$C_{18}H_{36}FeN_{24}Cl_2O_4$
FW [g mol^{-1}]	98.12	842.55	843.46
Crystal system	orthorhombic	trigonal	trigonal
Space group	*Pnma* (No. 62)	*P*-3 (No.147)	*P*-3 (No.147)
Color / Habit	colorless block	colorless platelet	colorless needles
Size [mm]	0.05 x 0.10 x 0.18	0.07 x 0.13 x 0.57	0.06 x 0.08 x 0.35
a [Å]	7.9923(5)	12.0103(8)	11.9258(17)
b [Å]	11.3058(7)	12.0103(8)	11.9258(17)
c [Å]	5.3980(3)	7.2015(6)	7.1630(12)
α [°]	90	90	90
β [°]	90	90	90
γ [°]	90	120	120
V [Å^3]	487.76(5)	899.63(16)	882.3(3)
Z	4	1	1
$\rho_{calc.}$ [g cm^{-3}]	1.336	1.555	1.587
μ [mm^{-1}]	0.096	0.593	0.658
F(000)	208	435	436
$\lambda_{MoK\alpha}$ [Å]	0.71073	0.71073	0.71073
T [K]	173	153	133
θ Min-Max [°]	4.2, 27.1	3.4, 26.4	3.5, 26.3
Dataset	-10: 10 ; -14: 14 ; -6: 6	-15: 15 ; -13: 15 ; -9: 7	-14: 14; -14: 14; -8: 8
Reflections collected	7550	5923	6811
Independent refl.	563	1225	1205
R_{int}	0.036	0.061	0.171
Observed reflections	507	896	708
Parameters	45	83	83
R_1 (obs)[a]	0.0361	0.0466	0.0708
wR_2 (all data)[b]	0.0995	0.1160	0.1801
S [c]	1.18	1.09	1.00
Resd. dens [e Å^{-3}]	-0.15, 0.22	-0.34, 0.48	-0.48, 0.99
Device type	Bruker D8 Venture TXS	Oxford Xcalibur3	Oxford Xcalibur3
Solution	SHELXT	SHELXT	SHELXT
Refinement	SHELXL-2018	SHELXL-2018	SHELXL-2018
Absorption correction	multi-scan	multi-scan	multi-scan

[a]$R_1 = \Sigma||F_0|-|F_c||/\Sigma|F_0|$; [b]$wR_2 = [\Sigma[w(F_0^2-F_c^2)^2]/\Sigma[w(F_0)^2]]^{1/2}$; $w = [\sigma c^2(F_0^2)+(xP)^2+yP]^{-1}$ and $P=(F_0^2+2F_c^2)/3$; [c]$S = \{\Sigma[w(F_o^2-F_c^2)^2]/(n-p)\}^{1/2}$ (n = number of reflections; p = total number of parameters).

Table S2. Crystallographic data and structure refinement details for compounds **3**, **4**, and **9.**

	6	**8**	**9**
Formula	$C_{18}H_{44}CoN_{24}O_{12}Cl_2$	$C_{12}H_{26}CuN_{16}O_9Cl_2$	$C_{12}H_{24}N_{16}ZnCl_2O_8$
FW [g mol^{-1}]	918.60	672.93	656.74
Crystal system	monoclinic	orthorhombic	tetragonal
Space group	$P2_1/n$ (No. 14)	*Pbca* (No. 61)	$P4_22_12$ (No. 94)
Color / Habit	rose block	blue platelet	colorless platelet
Size [mm]	0.14 x 0.24 x 0.57	0.06 x 0.12 x 0.75	0.12 x 0.18 x 0.38
a [Å]	11.6339(4)	18.761(6)	11.3468(2)
b [Å]	7.0276(3)	14.286(4)	11.3468(2)
c [Å]	24.2339(10)	19.482(5)	10.0931(3)
α [°]	90	90	90
β [°]	93.894(4)	90	90
γ [°]	90	90	90
V [Å^3]	1976.75(14)	5222(3)	1299.49(6)
Z	2	8	2
$\rho_{calc.}$ [g cm^{-3}]	1.543	1.712	1.679
μ [mm^{-1}]	0.654	1.118	1.222
F(000)	954	2760	672
$\lambda_{MoK\alpha}$ [Å]	0.71073	0.71073	0.71073
T [K]	124	130	118
θ Min-Max [°]	2.0, 30.5	3.3, 26.4	3.2, 26.4
Dataset	-14: 16 ; -6: 9 ; -33: 32	-13: 23 ; -15: 17 ; -24: 12	-14: 14 ; -14: 14 ; -12: 12
Reflections collected	14030	14591	10299
Independent refl.	5386	5331	1328
R_{int}	0.040	0.166	0.043
Observed reflections	3996	2210	1234
Parameters	265	377	112
R_1 (obs)[a]	0.0462	0.0814	0.0238
wR_2 (all data)[b]	0.1060	0.1820	0.0594
S [c]	1.05	0.95	1.06
Resd. dens [e Å^{-3}]	-0.34, 0.41	-0.79, 0.82	-0.20, 0.28
Device type	Oxford Xcalibur3	Oxford Xcalibur3	Oxford Xcalibur3
Solution	SHELXT	SHELXT	SHELXT
Refinement	SHELXL-2018	SHELXL-2018	SHELXL-2018
Absorption correction	multi-scan	multi-scan	multi-scan

[a] $R_1 = \Sigma||F_0|-|F_c||/\Sigma|F_0|$; [b] $wR_2 = [\Sigma[w(F_0^2-F_c^2)^2]/\Sigma[w(F_0)^2]]^{1/2}$; $w = [\sigma c^2(F_0^2)+(xP)^2+yP]^{-1}$ and $P=(F_0^2+2F_c^2)/3$; [c] $S = \{\Sigma[w(F_o^2-F_c^2)^2]/(n-p)\}^{1/2}$ (n = number of reflections; p = total number of parameters).

Table S3. Crystallographic data and structure refinement details for compounds **3**, **4**, and **9.**

	10	**11a**
Formula	$C_{18}H_{16}CuN_{14}O_{14}$	$C_{60}H_{60}Cu_{3}N_{50}O_{48}$
FW [g mol^{-1}]	715.99	2440.20
Crystal system	monoclinic	triclinic
Space group	$P2_1/n$ (No. 14)	P-1 (No. 2)
Color / Habit	green rod	green block
Size [mm]	0.03 x 0.03 x 0.10	0.05 x 0.06 x 0.07
a [Å]	17.6292(9)	10.3830(7)
b [Å]	11.2830(5)	15.8679(12)
c [Å]	28.5934(13)	16.3150(11)
α [°]	90	116.042(2)
β [°]	90.412(2)	90.788(2)
γ [°]	90	90.416(3)
V [Å^3]	5687.4(5)	2414.6(3)
Z	8	1
$\rho_{calc.}$ [g cm^{-3}]	1.672	1.678
μ [mm^{-1}]	0.862	0.779
F(000)	2904	1241
$\lambda_{MoK\alpha}$ [Å]	0.71073	0.71073
T [K]	304	173
θ Min-Max [°]	2.3, 25.4	2.4, 26.4
Dataset	-21: 21 ; -13: 13 ; -34: 34	-12: 12 ; -19: 19 ; -20: 20
Reflections collected	93558	40595
Independent refl.	10411	9841
R_{int}	0.060	0.047
Observed reflections	7562	7902
Parameters	855	738
R_1 (obs)[a]	0.0505	0.0395
wR_2 (all data)[b]	0.1300	0.1084
S [c]	1.05	1.04
Resd. dens [e Å^{-3}]	-0.33, 0.43	-0.39, 0.90
Device type	Bruker D8 Venture TXS	Bruker D8 Venture TXS
Solution	SHELXT	SHELXT
Refinement	SHELXL-2018	SHELXL-2018
Absorption correction	multi-scan	multi-scan

[a] $R_1 = \Sigma||F_0|-|F_c||/\Sigma|F_0|$; [b] $wR_2 = [\Sigma[w(F_0^2-F_c^2)^2]/\Sigma[w(F_0)^2]]^{1/2}$; $w = [\sigma c^2(F_0^2)+(xP)^2+yP]^{-1}$ and $P=(F_0^2+2F_c^2)/3$; [c] $S = \{\Sigma[w(F_o^2-F_c^2)^2]/(n-p)\}^{1/2}$ (n = number of reflections; p = total number of parameters).

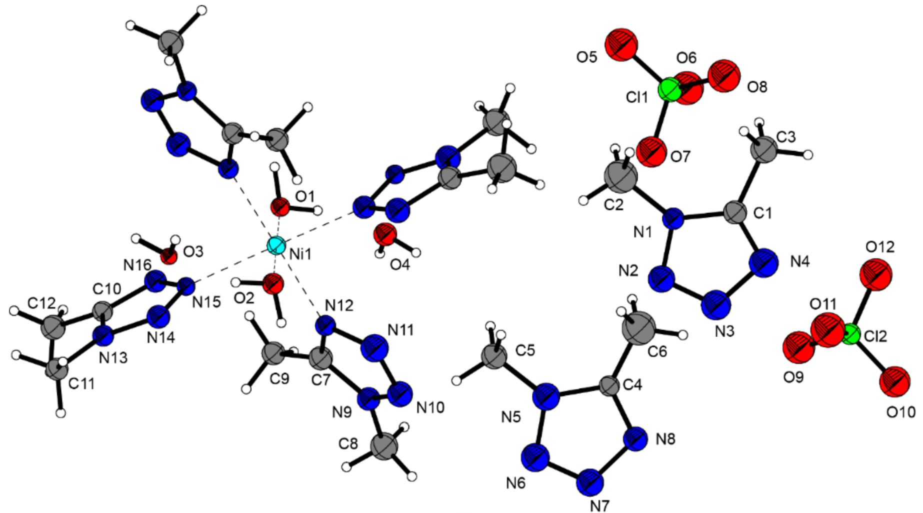

7

Figure S1. Depiction of obtained structure of compound 7.

8.7.3 NMR Spectroscopy

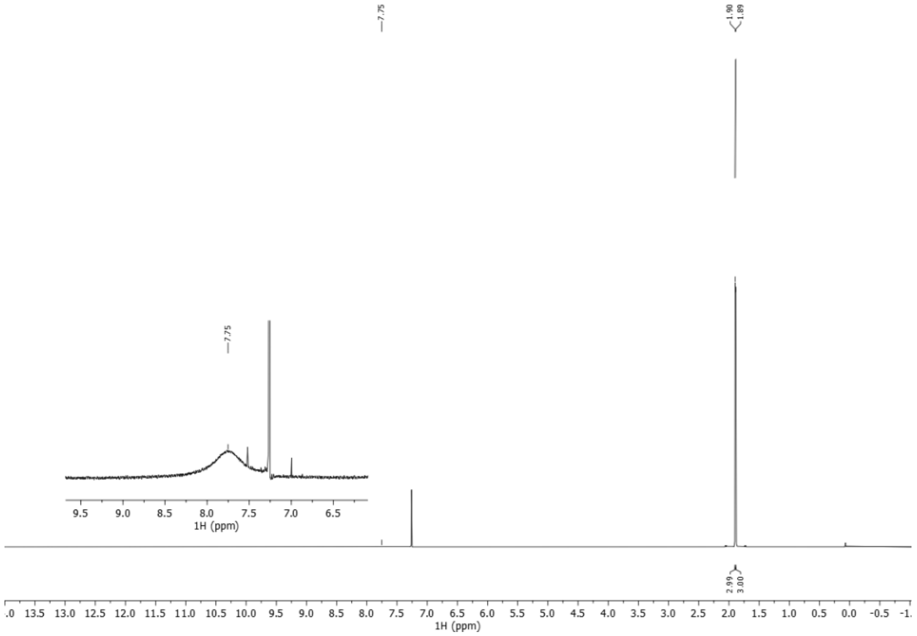

Figure S2. ^{1}H NMR of **1** in $CDCl_3$

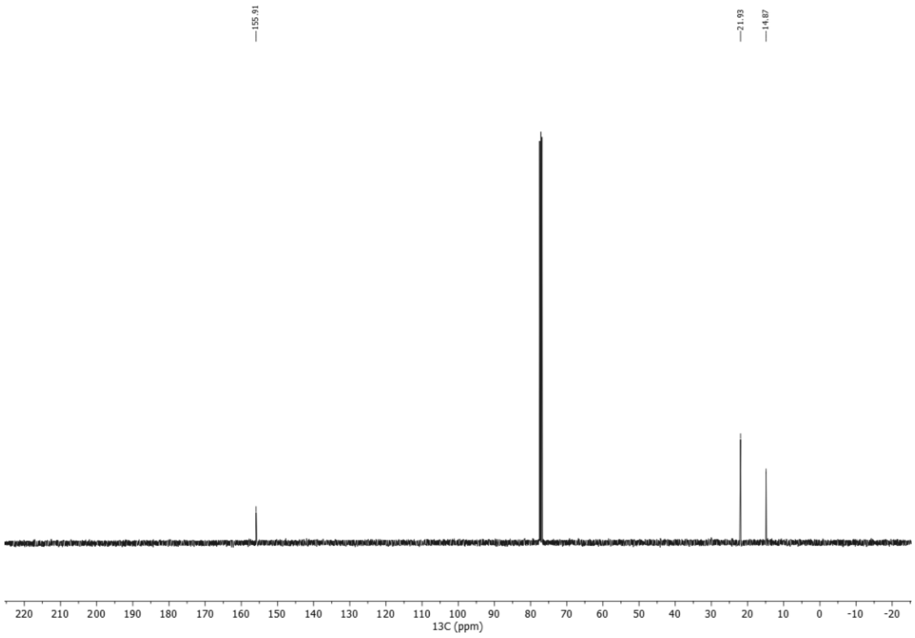

Figure S3. ^{13}C NMR of compound **1** in CDCl$_3$.

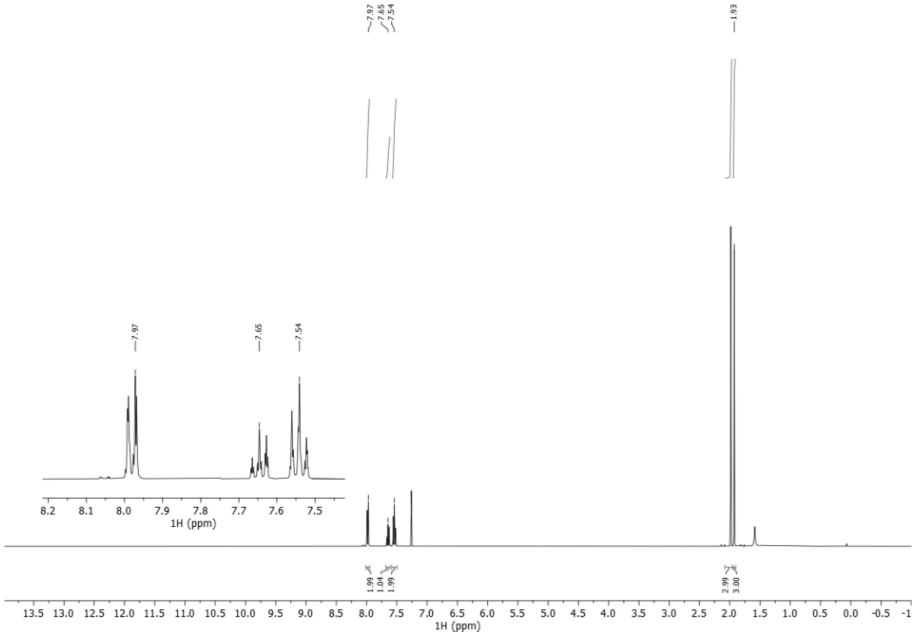

Figure S4. ^{1}H NMR of compound **2** in CDCl$_3$.

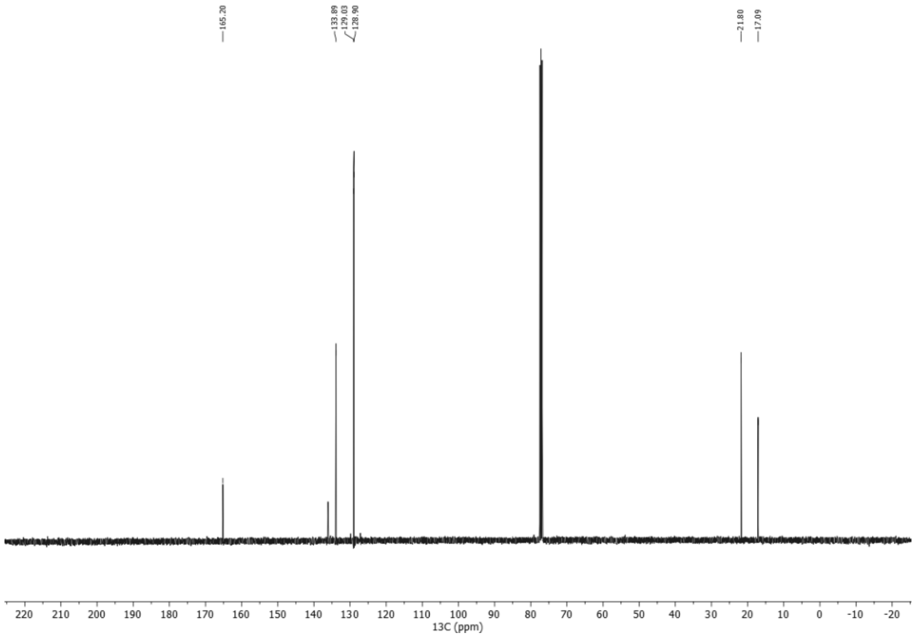

Figure S5. ^{13}C NMR of compound **2** in CDCl$_3$.

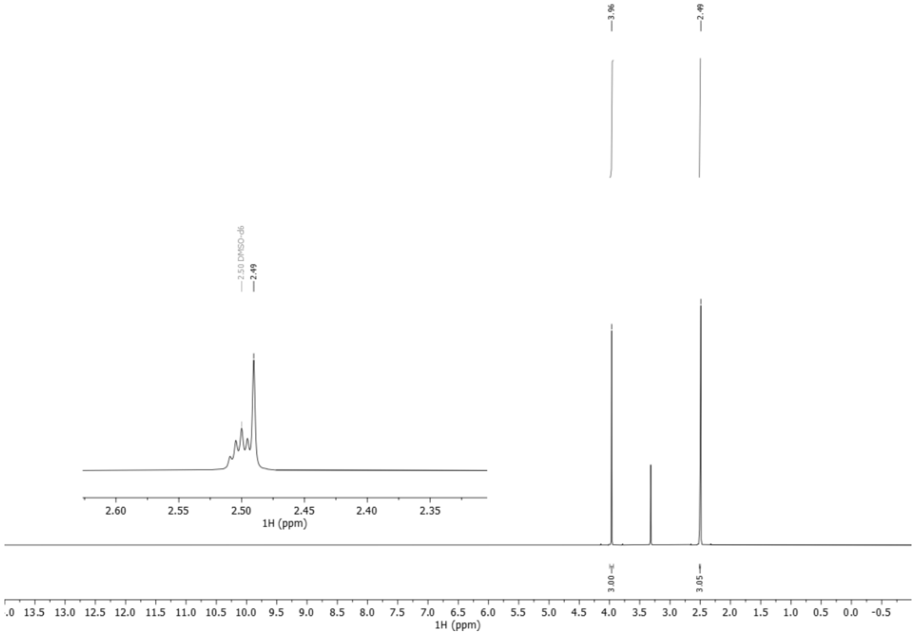

Figure S6. ^{1}H NMR of compound **3** in DMSO-d$_6$.

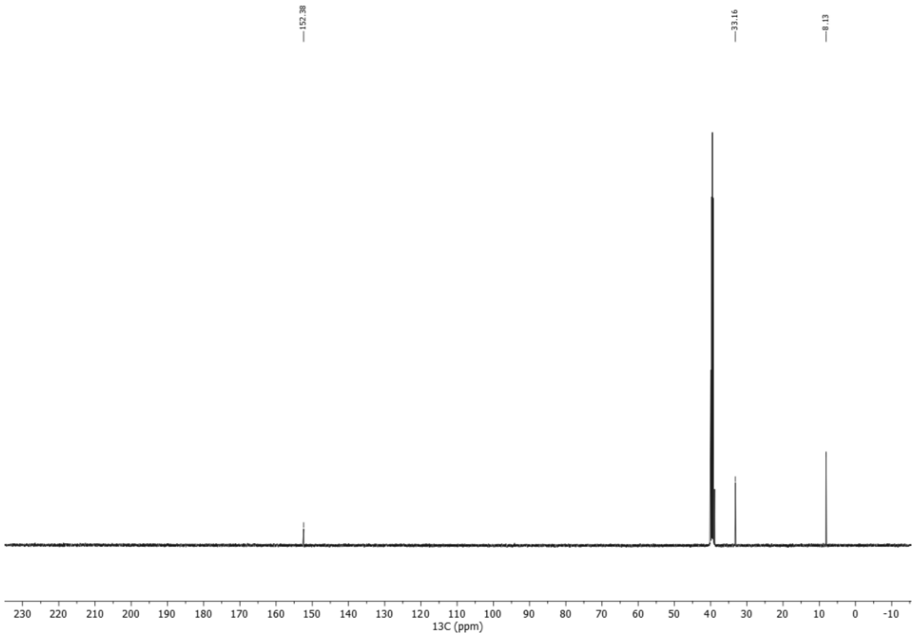

Figure S7. ^{13}C NMR of compound 3 in DMSO-d_6

8.7.4 General Methods

All chemicals and solvents were employed as received (Sigma-Aldrich, Fluka, Acros, ABCR). ^1H, $^{13}C\{^1H\}$, ^{14}N, $^{15}N\{^1H\}$ spectra were recorded at ambient temperature using a JEOL Bruker 27400, Eclipse 270, JEOL EX 400 or a JEOL Eclipse 400 instrument. The chemical shifts quoted in ppm in the text refer to typical standards such as tetramethylsilane (^1H, ^{13}C) nitromethane (^{14}N,^{15}N) in DMSO-d_6, D_2O or acetone-d_6 as the solvent. Endothermic and exothermic events of the described compounds, which indicate melting, loss of crystal water or decomposition, are given as the extrapolated onset temperatures. The samples were measured in a range of 25–400 °C at a heating rate of 5 °C min^{-1} through differential thermal analysis (DTA) with an OZM Research DTA 552-Ex instrument. Infrared spectra were measured with pure samples on a Perkin-Elmer BXII FT-IR system with a Smith DuraSampler IR II diamond ATR. Determination of the carbon, hydrogen, and nitrogen contents was carried out by combustion analysis using an Elementar Vario El (nitrogen values determined are often lower than the calculated ones' due to their explosive behavior). Impact sensitivity tests were carried out according to STANAG 4489[S13] with a modified instruction[S14] using a BAM (Bundesanstalt für Materialforschung) drophammer.[S15] Friction sensitivity tests were carried out according to STANAG 4487[S17] with a modified instruction[S18] using the BAM friction tester.[S15,16] The classification of the tested compounds results from the "UN Recommendations on the Transport of Dangerous Goods".[S19,20]

8.7.5 References

S1 CrysAlisPRO (Version 171.33.41), Oxford Diffraction Ltd., **2009**.

S2 A. Altomare, G. Cascarano, C. Giacovazzo, and A. Guagliardi, *J. Appl. Crystallogr.* **1992**, *26*, 343.

S3 A. Altomare, G. Cascarano, C. Giacovazzo, A. Guagliardi, A. G. G. Moliterni, M. C. Burla, G. Polidori, M. Camalli and R. Spagna, SIR97, **2003**.

S4 A. Altomare, M. C. Burla, M. Camalli, G. L. Cascarano, C. Giacovazzo, A. Guagliardi, A. G. G. Moliterni, G. Polidori and R. Spagna, *J. Appl. Crystallogr.* **1999**, *32*, 115.

S5 G. M. Sheldrick, SHELXL-97, University of Göttingen, Germany, **1997**.

S6 G. M. Sheldrick, *Acta Crystallogr. Sect. A* **2008**, *64*, 112.

S7 G. M. Sheldrick, *Acta Cryst. A* **2015**, *71*, 3–8.

S8 A. L. Spek, PLATON, Utrecht University, The Netherlands, **1999**.

S9 L.J. Farrugia, *J. Appl. Cryst.* **2012**, *45*, 849.

S10 O. V. Dolomanov, L. J. Bourhis, R. J. Gildea, J. A. K. Howard and H. Puschmann, *J. Appl. Cryst*. **2009**, *42*, 339–341.

S11 Empirical absorption correction using spherical harmonics, implemented in SCALE3 ABSPACK scaling algorithm (CrysAlisPro Oxford Diffraction Ltd., Version 171.33.41, **2009**).

S12 APEX3, Bruker AXS Inc., Madison, Wisconsin, USA.

S13NATO standardization agreement (STANAG) on explosives, impact sensitivity tests, no. 4489, 1st ed., Sept. 17, **1999**.

S14 WIWEB-Standardarbeitsanweisung 4-5.1.02, Ermittlung der Explosionsgefährlichkeit, hier der Schlagempfindlichkeit mit dem Fallhammer, Nov. 8, **2002**.

S15 BAM, http://www.bam.de, (accessed April **2022**).

S16 OZM, http://www.ozm.cz, (accessed April **2022**).

S17 NATO standardization agreement (STANAG) on explosive, friction sensitivity tests, no. 4487, 1st ed., Aug. 22, **2002**.

S18 WIWEB-Standardarbeitsanweisung 4-5.1.03, Ermittlung der Explosionsgefährlichkeit oder der Reibeempfindlichkeit mit dem Reibeapparat, Nov. 8, **2002**.

S19 UN Model Regulation: Recommendations on the Transport of Dangerous Goods – Manual of Tests and Criteria, section 13.4.2.3.3, **2015**.

S20 Impact: insensitive > 40 J, less sensitive ≥ 35 J, sensitive ≥ 4 J, very sensitive ≤ 3 J; Friction: insensitive > 360 N, less sensitive = 360 N, sensitive < 360 N and > 80 N, very sensitive

≤ 80 N, extremely sensitive ≤ 10 N. According to the UN Recommendations on the Transport of Dangerous Goods, 5th ed., **2009**.

9 Summary and Conclusion

Within the work for this thesis, several new compounds based on the 1*H*-tetrazole scaffold were synthesized and applied as either ligand for ECCs or as anions for energetic salts. The results are summarized in chapters **2**–**8**. All chapters represent independent publications in peer-reviewed scientific journals.

All compounds within this work were extensively characterized including standard techniques such as Elemental Analysis, Infrared Spectroscopy, Differential Thermal Analysis, Thermogravimetric Analysis, multinuclear (^{1}H, ^{13}C, ^{14}N, ^{15}N, ^{19}F) NMR Spectroscopy, and single-crystal X-ray diffraction experiments. Additionally, all compounds were analyzed toward the typical properties of energetic materials including the measurement of sensitivities toward external stimuli (impact, friction, and electrostatic discharge), and trends of different derivatives were analyzed and explained by Hirshfeld surface and fingerprint analysis. Corresponding ECCs or salts were investigated by Hot Plate (HP) and Hot Needle (HN) tests to initially assess their energetic behavior as well as their applicability as primary explosives.

9.1 Summary of Chapter 2

The synthesis of 1-hydroxytetrazole (HTO) and bis-(1-hydroxytetrazol-5-yl)triazene (Figure 1) is presented. Applying a procedure called *Dediazonization*, to 1-hydroxy-5-aminotetrazole (5-ATO), proved to be a good strategy to obtain synthetical access to the otherwise elaborately obtained tetrazole derivate. HTO exhibits good thermal stability (186 °C), impact sensitivity (10 J), and a high detonation velocity (8405 m s^{-1}). Bis-(1-hydroxytetrazol-5-yl)triazene monohydrate, exhibits reduced thermal stability (100 °C), combined with high sensitivities toward mechanical stimuli (< 1 J, 4 N), satisfactory density (1.8 g cm^{-3}), and outstanding detonation velocity of 9433 m s^{-1}.

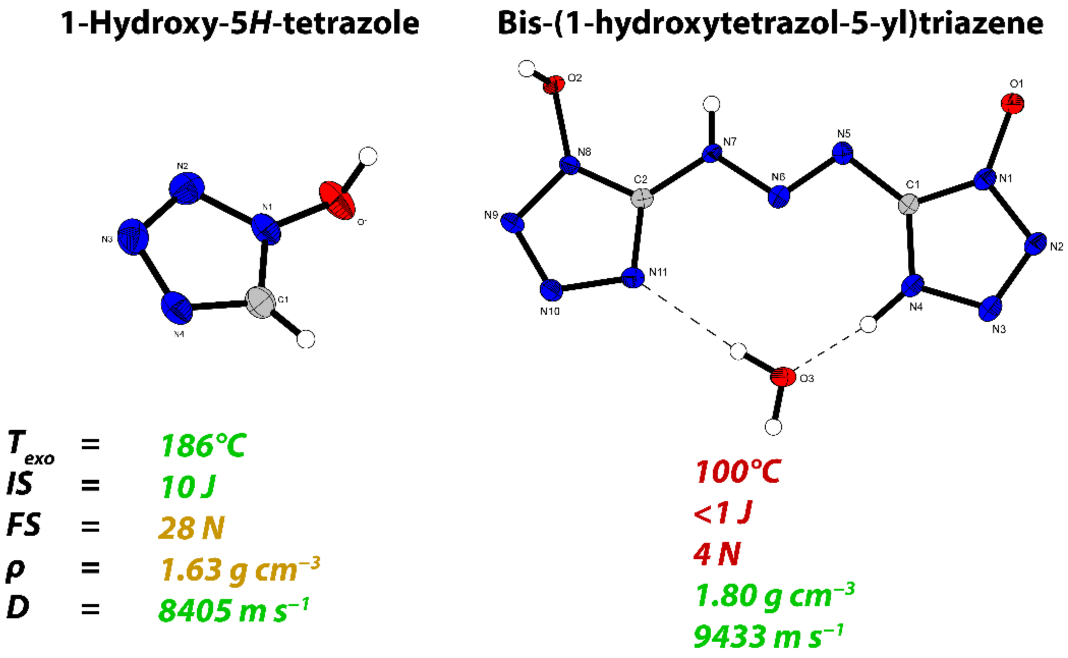

Figure 1. Comparison of 1-hydroxytetrazole (HTO) and bis-(1-hydroxytetrazol-5-yl)triazene.

To further tune the energetic properties of both compounds, several alkali and nitrogen-rich salts were synthesized and presented. For HTO, the most promising compounds are the nitrogen-rich salts of hydroxylamine and hydrazine, both showing sensitivities in an adequate range (IS > 6 J, FS > 240 N) together with good thermal stabilities of up to 213 °C and detonation velocities of 9284 m s^{-1} and 9437 m s^{-1}, respectively. Additionally, the silver salt of HTO proved to be a primary explosive (IS < 1 J, FS < 1 N) with good thermal stability of 211 °C and the capability of initiating PETN. The alkali salts of bis-(1-hydroxytetrazol-5-yl)triazene include up to six molecules of water, drastically decreasing the performance. Nonetheless, the nitrogen-rich salt of hydroxylamine is free of water and exhibits the highest detonation velocity within this chapter (9663 m s^{-1}) combined with sensitivities in the range of a typical booster explosive (IS = 4 J, FS = 128 N). The triple guanidinium salt is also free of water and exhibits ideal properties (IS > 40 J, FS > 360 N) to be applied as a gas generator as it releases a large volume of gaseous products upon ignition at a temperature above 222 °C.

9.2 Summary of Chapter 3

The syntheses of 1-(fluoromethyl)tetrazole (1-FMT), 2-(fluoromethyl)tetrazole (2-FMT), 1-(fluoromethyl)-5-aminotetrazole (1-FMAT), and 2-(fluoromethyl)-5-aminotetrazole) (2-FMAT) are presented. All compounds are accessible via a classical substitution reaction of 5*C*-functionalized 1*H*-tetrazole and fluoroiodomethane. Generally, the introduction of fluorine as a functional group drastically lowers the melting and boiling point compared to the CH_3-analogous. While the heat of formation is also slightly lowered by the introduction of the CH_2F moiety, the detonation parameters are generally improved. Further, all four compounds are applied as ligands for ECCs. Here, the 2*N*-isomers exhibit poor coordination abilities, and the 5-amino derivatives act as reducing agents, resulting in the formation of amorphous Cu(I) species. Nonetheless, 1-FMT proves to be well-coordinating and no reducing ability is observed. Therefore, the copper(II) chlorate and perchlorate ECCs are synthesized. Like for the pure ligands, drastically decreased thermal stabilities (80–184 °C), compared to the ECCs of 1-methyltetrazole (159–211 °C), are observed. Additionally, the fluorine-containing ECCs exhibit higher sensitivities (IS < 1 J, FS = 24 N) than their methyl-analogous.

9.3 Summary of Chapters 4–6

The syntheses of the three methylene-bridged ligands 1-(azidomethyl)tetrazole (AzMT), 1-(nitratomethyl)tetrazole (1-NAMT) and 1-(nitromethyl)tetrazole (1-NMT) are presented (Figure 3).

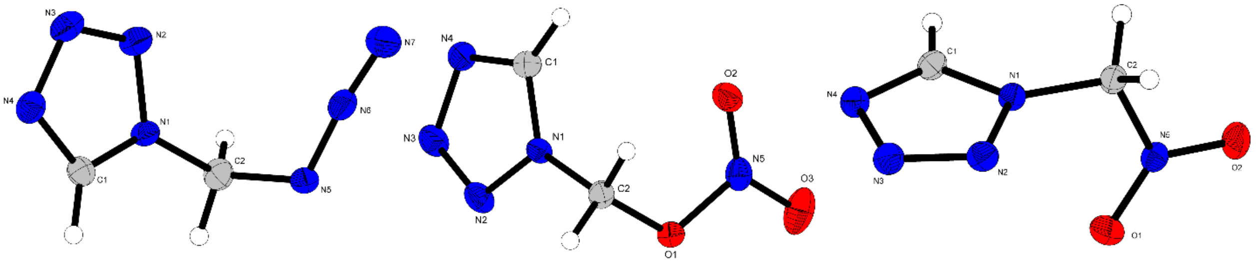

		1-(Azidomethyl)-5*H*-tetrazole	**1-(Nitratomethyl)-5*H*-tetrazole**	**1-(Nitromethyl)-5*H*-tetrazole**
IS	=	**2 J**	**<1 J**	**>40 J**
FS	=	**1 N**	**9 N**	**>360 N**
T_{exo}	=	**167 °C**	**119 °C**	**145 °C**
V_{det}	=	**8124 m s^{-1}**	**8294 m s^{-1}**	**7952 m s^{-1}**
$\Delta_f H^0$	=	**+655 kJ mol^{-1}**	**+187 kJ mol^{-1}**	**+253 kJ mol^{-1}**
ρ	=	**1.55 g cm^{-3}**	**1.68 g cm^{-3}**	**1.62 g cm^{-3}**

Figure 3. Comparison of 1-(Azidomethyltetrazole, 1-(Nitratomethyl)tetrazole, and 1-(Nitromethyl)tetrazole.

Chapter 3 & 4. The crucial step toward the synthesis of AzMT and 1-NAMT is the synthesis of 1-(hydroxymethyl)tetrazole (HMT) as a precursor compound. The breakthrough toward a successful synthesis of HMT was the use of catalytic amounts of sodium hydroxide for the addition of formaldehyde to 1*H*-tetrazole. After further functionalization, AzMT and 1-NAMT are obtained in overall good (AzMT, 30%) to moderate (1-NAMT, 13%) yields. Ultimately, AzMT and 1-NAMT exhibit sensitivities in the range of highly sensitive primary explosives (IS ≤ 2 J, FS ≤ 9 N) combined with the performance of secondary explosives. With an outstanding and highly endothermic enthalpy of formation (+655 kJ mol^{-1}), AzMT is the most endothermic ligand, ever included in ECCs in our working group so far. Due to the high enthalpy of formation, AzMT exhibits a good detonation velocity of 8124 m s^{-1}, which is surpassed by 1-NAMT due to a significantly higher density of the nitro ester (1.68 g cm^{-3}) over the azide moiety (1.55 g cm^{-3}). Further, AzMT and 1-NAMT were applied as ligands for several ECCs of transition metal chlorates, perchlorate, nitrate, azides, fulminates, and nitroaromatics like picrate, styphnate, and trinitrophloroglucinate. Generally, the trend toward an increased sensitivity of the ECCs compared to the pure ligand is confirmed. Therefore, the ECCs of both ligands are extremely sensitive compounds, some compounds (Figure 4) don't even possess a no-fire level. Additionally, most of the coordination compounds exhibit thermal stabilities between 120–160 °C and for most of the AzMT-containing complexes a positive PETN initiation was tested, which was not successful for all 1-NAMT-containing ECCs. This supports the introduction of the *energy density* [J cm^{-3}] as a critical parameter for ligands applied in ECCs, which is significantly higher for AzMT (8109 J cm^{-3}) over those of 1-NAMT (2348 J cm^{-3}).

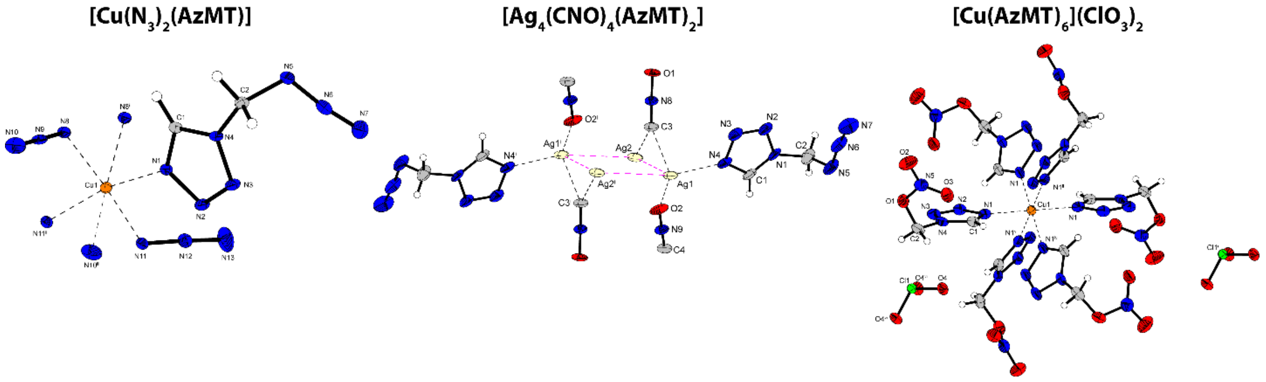

Figure 4. Structures of AzMT containing ECCs [Cu(N$_3$)$_2$(AzMT)], [Ag$_4$(CNO)$_4$(AzMT)$_2$], [Cu(AzMT)$_6$](ClO$_3$)$_2$ without a no-fire limit.

Chapter 5. The challenge of producing 1-NMT and 2-NMT was the complex optimization of nitration, which was necessary to prevent double or even triple nitration of the acetonyl function of the starting material. Both compounds are nearly completely insensitive to mechanical stimuli (IS > 40 J, FS ≥ 328 N), which was against our expectations based on the results of AzMT and 1-NAMT. While 1-NMT combines a higher enthalpy of formation than 1-NAMT with a significantly higher density than AzMT, it exhibits a slightly lower detonation velocity (7952 m s^{-1}). 1-NMT and 2-NMT are of significant academic interest as they embody the fourth and fifth ever reported azoles that contain the *N*-nitromethyl moiety. This functionality shows promising properties for the design of new insensitive and high-performing secondary explosives, especially for melt-castable explosives. Further, 1-NMT applied as a ligand for ECCs of copper(II) nitrate, chlorate, and 3d metal perchlorates verifies the general trend toward an increase in sensitivity upon ECC formation. All ECCs exhibit high impact sensitivities (IS < 1 J) and moderate friction sensitivities between 14–80 N. Furthermore, almost all ECCs improve the comparatively low thermal stability of 1-NMT (145 °C), reaching thermal decomposition onset temperatures of up to 217 °C. While several ECCs of 1-NMT undergo DDT when ignited by a single-pulsed laser and during the HN test, none of the ECCs can initiate PETN.

9.4 Summary of Chapter 7

The introduction of an *N*-hydroxymethyl moiety via the addition of formaldehyde is also feasible for the 5,5'-bistetrazole backbone, and the resulting bis-(hydroxymethyl)-5,5'-bistetrazole compounds are further functionalized toward 2,2'-bis(nitratomethyl)-5,5'-bistetrazole (DNMBT) and 2,2'-bis(azidomethyl)-5,5'-bistetrazole (DAMBT). Both compounds (Figure 5) are extremely sensitive toward mechanical stimuli in the range of primary explosives and exhibit performances (V_{det} = 8155–8377 m s^{-1}) in the range of secondary explosives.

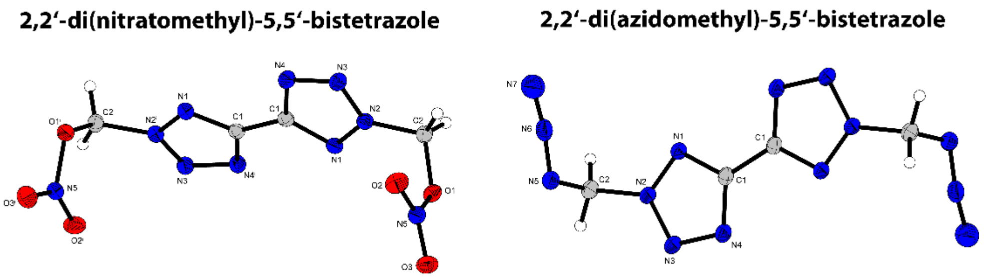

IS	=	**<1 J**	**2 J**
FS	=	**0.3 N**	**<0.1 N**
$T_{endo/exo}$	=	**100 °C/ 150 °C**	**102 °C/ 177 °C**
V_{det}	=	**8377 m s^{-1}**	**8155 m s^{-1}**
$\Delta_f H^0$	=	**+441 kJ mol^{-1}**	**+1258 kJ mol^{-1}**
ρ	=	**1.69 g cm^{-3}**	**1.62 g cm^{-3}**

Figure 5. Comparison of 2,2'-bis(nitratomethyl)-5,5'-bistetrazole (DNMBT) and 2,2'-bis(azidomethyl)-5,5'-bistetrazole (DAMBT).

Further, DAMBT exhibits an enormously high enthalpy of formation of +1258 kJ mol^{-1}, the highest within this thesis. DNMBT exhibits melting at 100 °C and exothermic decomposition at 150 °C with a violent detonation. DAMBT, on the other hand, melts at 102 °C and is thermally stable up to 177 °C, corresponding to a liquid range of almost 80 °C, which is necessary for the application as a melt-castable explosive. The possibility to melt and drip DAMBT on a secondary explosive is tested and is, thus far, the only example of a melt-castable primary explosive.

9.5 Summary of Chapter 8

While 1,5-dimethyltetrazole (DMT) is already known in the literature, a full characterization including the crystal structure and thermal behavior is yet missing. Therefore, the synthesis and characterization of 1,5-dimetyltetrazole (1,5-DMT) as well as several ECCs of 1,5-DMT and $3d^5$–$3d^{10}$ transition metals are presented (Figure 6).

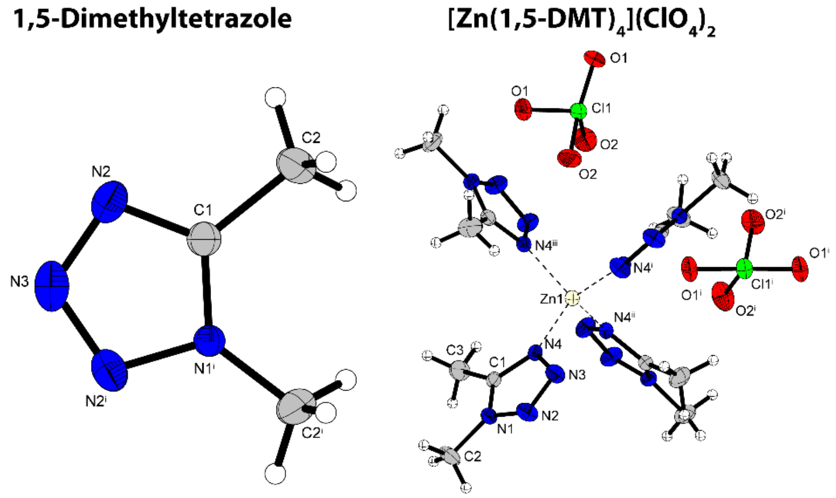
1,5-Dimethyltetrazole **$[Zn(1,5\text{-}DMT)_4](ClO_4)_2$**

IS	=	>40 J	2 J
FS	=	>360 N	180 N
T_{exo}	=	>293°C	293°C
Δ_fH^0	=	+184 kJ mol^{-1}	n.d.

Figure 6. Molecular structure of 1,5-dimethyltetrazole and $[Zn(1,5\text{-}DMT)_4](ClO_4)_2$.

1,5-DMT exhibits a high endothermic enthalpy of formation together with a complete insensitivity toward mechanical stimuli. Additionally, it exhibits thermal stability of over 293 °C, extrapolated as no exothermic decomposition is observed until the boiling at 293 °C. This high thermal stability is also observed for the zinc(II) perchlorate complex, exhibiting an exothermic decomposition temperature of 293 °C, which is one of the highest ever reported for ECCs. Additionally, all ECCs of 1,5-DMT exhibit sensitivities toward impact (2–10 J) and friction (128–360 N) in the range between a primary explosive and a booster explosive. While they don’t exhibit a DDT upon ignition by an SII, they are applicable as burn rate modifiers and possible solid-state hypergolic fuels for rocket engines.